

**In Search of an Ideal Modulator for Comprehensive Two-
Dimensional Gas Chromatography**

by

Haleigh Boswell

A thesis

presented to the University of Waterloo

in fulfillment of the

thesis requirement for the degree of

Doctor of Philosophy

in

Chemistry

Waterloo, Ontario, Canada, 2019

© Haleigh Boswell 2019

Examining Committee Membership

The following served on the Examining Committee for this thesis. The decision of the Examining Committee is by majority vote.

External Examiner

John Dimandja
Senior Scientist
Office of Regulatory Affairs
Food and Drug Administration
Atlanta, GA

Supervisor

Tadeusz Górecki
Professor
Department of Chemistry
University of Waterloo

Internal Member

Susan Mikkelsen
Professor
Department of Chemistry
University of Waterloo

Internal Member

Terrance McMahon
Professor
Department of Chemistry
University of Waterloo

Internal – external Member

Ken Stark
Professor
Department of Kinesiology
University of Waterloo

Author's Declaration

This thesis consists of material all of which I authored or co-authored: see Statement of Contributions included in the thesis. This is a true copy of the thesis, including any required final revisions, as accepted by my examiners.

I understand that my thesis may be made electronically available to the public.

Statement of Contributions

The introduction and literature review presented in the first chapter were searched and written by the author of this thesis. The second chapter contains prior work that was completed by Matthew Edwards, a previous group member of the Górecki group. Planning and experimental work presented in chapter 2, as well as the data analysis, interpretation of the results and writing were performed by the author of the thesis. The work presented in the third, fourth and fifth chapters including the experimental planning and design, experimental work conducted in the laboratory, data analysis, interpretation of results and writing were performed by the author of the thesis. The work presented in the sixth chapter was suggested by Matthew Edwards and the experimental work, data analysis, interpretation of the results and writing were performed by the author of the thesis. Planning and performing experimental work presented in chapter 7, as well as data analysis, interpretation of the results and writing were performed by the author of the thesis. The work presented in the eighth- and ninth chapters including planning, experimental work, data analysis, interpretation of results and writing were performed by the author of the thesis. Parts of the experimental procedures in the laboratory were performed by undergraduate student Kieran Tarazona.

Abstract

Gas chromatography has been a prevailing technique to separate different mixtures of volatile and semi-volatile compounds in order to qualitatively and quantitatively identify each individual component. With more complex mixtures, co-elutions can occur, leading to misidentification or an inadequate separation. This led to the need of a more complex instrumentation that could confront the challenges of one-dimensional gas chromatography. In 1991, Phillips successfully completed the first comprehensive two-dimensional gas chromatographic analysis. By implementing two columns of differing stationary phases, more complex samples can be separated without co-elutions occurring. In order to connect the two columns, an interface or modulator must preserve the primary column separation and refocus the analytes before re-injecting them into the secondary column. To make this technique available to a wide range of scientists, it must be cost-effective, user-friendly, and applicable to a wide range of applications and samples. Due to the many available commercial and experimental modulators, deciding which one is the ideal platform can be daunting. Understanding the operational capabilities, as well as the advantages and disadvantages of each platform is crucial for the desired application. In this thesis, various modulator platforms were optimized, evaluated and improved upon in search of the ideal modulator for GC×GC. The UW consumable-free, thermal modulator is a heater-based platform that performs modulation by trapping and focusing analytes through the cooling of a sorbent material within a metal capillary, which is subsequently released through an electrical discharge event. Various treatments were applied to determine the parameters to achieve an optimized coating within the trapping capillary. An optimized phase was obtained that allowed proper trapping of analytes, without breakthrough, and complete desorption. Two sections within the trapping capillary of different adsorptivity were beneficial in

obtaining adequate separation with active and passive cooling at lower modulation voltages. Base oils, an extremely complex matrix, were chosen to challenge the UW thermal modulator and a commercial flow modulator. Neither model was found superior to the other and both platforms achieved comprehensive separation of the specific classes of compounds and allowed differentiation of the oils. A commercial flow modulator was further improved upon by adding a cryogen-free focusing mechanism to test a proof of concept hybrid interface. Thinner film traps of 0.5 and 3.0 μm provided significant focusing while operating under 2D flow rates compatible with mass spectrometric detection. Finally, a commercial thermal modulator was evaluated by determining the operational capabilities and its ability to analyze bitumen. The platform successfully achieved adequate separations of two standard mixtures of different volatilities and polarities, providing an affordable option to achieve GC \times GC separation without the need for consumables. Total group and biomarker classification were also successfully performed to differentiate homologous compounds within a bitumen sample. The work presented in this thesis provides a better understanding of the benefits and limitations of various modulator designs, which is vital in the search of an ideal modulator for GC \times GC.

Acknowledgements

First, I would like to thank my supervisor, Professor Tadeusz Górecki, for giving me the opportunity to be part of his research group. I have been very fortunate to work under his supervision, gaining knowledge and experience from a leader in the field of comprehensive two-dimensional gas chromatography. I am sincerely grateful for being given the opportunity to participate in diverse projects and for having been allowed to attend important scientific conferences and meetings where I could present my work and meet fellow scientists within the field of analytical chemistry.

I would like to thank my committee members, Professor Susan Mikkelsen and Professor Terrance McMahon for the time and efforts they have spent reading my thesis, and for their guidance and advice throughout my journey as a PhD candidate. I would also like to thank my external examiner, Dr. John Dimandja, and my internal examiner, Professor Ken Stark, for being a part of the evaluation committee of my work and examining my thesis.

I would also like to thank the staff of the Department of Chemistry, especially Cathy Van Esch, for her continuous help. My sincere thanks are expressed to the Science Shop of the University of Waterloo, especially Hiruy Haile for his guidance and assistance in the creation of several aspects of instrumentation included in my thesis. I would like to thank the University of Waterloo WAT Lab for their assistance and service in acquiring the SEM and EDX data. I would also like to extend my gratitude to my colleagues, John Chow, Faten Salim and Alshymaa Aly for their help and support.

Lastly, my deepest gratitude and appreciation to my parents for their love, support and continuous encouragement throughout my entire graduate career. Thank you for always pushing me to reach for the stars and never give up on dreams.

Dedication

I dedicate this thesis to my parents, Victor and Donna Boswell.

Table of Contents

Examining Committee Membership.....	ii
Author's Declaration.....	iii
Statement of Contributions.....	iv
Abstract.....	v
Acknowledgements.....	vi
Dedication.....	viii
List of Figures.....	xiv
List of Tables.....	xxv
List of Abbreviations.....	xxvii
Chapter 1. Introduction.....	1
1.1 Comprehensive two-dimensional gas chromatography.....	1
1.1.1 Principles of gas chromatography.....	1
1.1.2 Principles of two-dimensional gas chromatography.....	2
1.1.3 GC×GC modulator.....	3
1.1.4 Interpretation of GC×GC data.....	7
1.1.5 Two-dimensional column selection & detectors.....	10
1.2 GC×GC modulators.....	13
1.2.1 Thermal modulation.....	13
1.2.1.1 Heater-based interfaces.....	14
1.2.1.2 Cryogenic-based interfaces.....	16
1.2.1.3 Other thermal interface designs.....	20
1.2.1.4 Thermal modulation optimization.....	24
1.2.2 Flow & valve-based modulation.....	26
1.2.2.1 Flow & valve-based interfaces.....	28
1.2.2.2 Other flow and valve designs.....	36
1.2.2.3 Flow & valve modulation optimization.....	44
1.2.3 Compare & contrast.....	47
1.2.4 Applications.....	52
1.3 Prior work.....	55
1.4 Thesis objective.....	63
Chapter 2. Optimization of treatment and characterization of the stationary phase previously used within trapping capillaries.....	65
2.1 Introduction.....	65
2.1.1 Experimental parameters for GC×GC analysis.....	69
2.2 Treatment parameters and chromatographic results obtained for MXT-1 #1 and #2.....	70
2.3 Imagining the stationary phase within the trapping capillary	75

2.4 SEM images of the MXT-1 #1.....	77
2.5 SEM images of MXT-1 #1 with treatment plan D	79
2.6 EDX results for MXT-1 #1	80
2.7 Results for various sections of the MXT-1 #1 trapping capillary.....	82
2.8 MXT-1 #3 results	85
2.9 Summary	89
Chapter 3. Alternative sources of the trapping capillaries.....	92
3.1 Alternative stationary phases	92
3.2 Instrumental parameters for the analysis of diesel.....	93
3.3. Extreme treatment of MXT-1 #3	93
3.4 Alternative Restek stationary phases	95
3.5 Agilent columns	98
3.5.1 Treatment plan	102
3.5.2 Performance results.....	104
3.5.3 SEM and EDX results	106
3.6 Various voltage treatments of Agilent columns.....	112
3.6.1. Performance results.....	114
3.6.2. SEM and EDX results.....	120
3.7. Treatment plans for treating sections of the trapping capillary	127
3.7.1. Performance results.....	129
3.7.2. SEM and EDX results.....	143
3.8 Summary	155
Chapter 4. Improvement of modulator design.....	159
4.1 Introduction.....	159
4.2 Experimental	159
4.3 Modified ceramic cooling pads.....	160
4.3.1 Design	161
4.3.2. Performance evaluation	161
4.4 Removal of deactivation phase from within the unions.....	163
4.4.1 Performance results.....	164
4.5 Summary	170
Chapter 5. Diagnostic measurements of new stationary phase within trapping capillary	172
5.1 Introduction.....	172
5.2 Determination of the trapping capillary temperature during the treatment process	173
5.3 Determination of trapping capillary temperature within the ceramic cooling pads.....	177
5.4 Determination of ceramic cooling pads temperature with varying oven temperature ramps	181

5.5 Summary	184
Chapter 6. Comparison of thermal and flow-based modulation in comprehensive two-dimensional gas chromatography –time-of-flight mass spectrometry (GC×GC -TOFMS) for the analysis of base oils	186
6.1 Introduction.....	186
6.2 Experimental.....	192
6.2.1 Base oil samples.....	192
6.2.2 GC×GC instrumentation	193
6.2.3 Thermal modulation.....	196
6.2.4 Flow modulation	196
6.3 Results and discussion	197
6.3.1. Ion source tailing.....	197
6.3.2. Group type identification	200
6.3.3. Thermal modulation vs. flow modulation.....	203
6.3.4. Identification of antioxidants through soft-ionization	208
6.3.5 Resolution from UCM	212
6.4 Conclusions.....	213
Chapter 7. Modified flow modulator: A proof of concept hybrid interface	215
7.1 Introduction.....	215
7.2 Experimental.....	218
7.2.1 Sample.....	218
7.2.2 Modulator design	218
7.3 Instrumental setup.....	226
7.4 Results and discussion	227
7.4.1 Time delay of the jet	227
7.4.2 Septa within column holder	229
7.4.3 Cooling trap film thickness comparison and reproducibility evaluation	230
7.4.3.1 0.5 µm cooling trap.....	232
7.4.3.1 0.5 µm cooling trap reproducibility evaluation.....	235
7.4.3.3 3.0 µm cooling trap.....	236
7.4.3.4 3.0 µm cooling trap reproducibility evaluation.....	239
7.3.4.5 5.0 µm cooling trap.....	240
7.4.4 Insulating cooling air line	244
7.4.4.1 0.5 µm cooling trap.....	245
7.4.4.2 3.0 µm cooling trap.....	248
7.5 Conclusions.....	251
Chapter 8. Evaluation of the operational capabilities of a solid-state thermal modulator in comprehensive two-dimensional gas chromatography-time-of-flight mass spectrometry (GC×GC -TOFMS).....	252
8.1 Introduction.....	252

8.2 Experimental	255
8.2.1 Samples	255
8.2.2 Solid state modulation.....	256
8.3 Instrumental setup	258
8.4 Results and discussion	261
8.4.1. MRP standard mix separation.....	261
8.4.2 FA standard mix separation	262
8.4.3 Retention time repeatability	263
8.4.4 Peak area reproducibility	267
8.4.5 Second dimension evaluation	269
8.4.5.1 Injection bandwidth at half height.....	269
8.4.5.2 Second dimension peak width.....	271
8.4.5.3 Peak capacity in the 2D.....	275
8.5 Conclusions.....	275
Chapter 9. Characterization of bitumen using cryogen-free thermal modulation based comprehensive two-dimensional gas chromatography time – of – flight mass spectrometry (GC×GC -TOFMS).....	277
9.1 Introduction.....	277
9.2 Experimental	281
9.2.1 Samples	281
9.2.2 Solid state modulator	281
9.2.3 Analysis conditions	282
9.3 Results and discussion	283
9.3.1 Group-type identification.....	283
9.3.2 Biomarker analysis.....	285
9.3.3 Biomarker identification	288
9.3.4 Differences between extraction solvents	293
9.4 Conclusions.....	294
Chapter 10. Summary and future work	296
10.1 Summary.....	296
10.2 Future work.....	301
References.....	304
APPENDIX.....	319
Appendix A.....	319
Chapter 3 Supplementary material.....	319
Appendix B	347
Chapter 6 Supplementary information.....	347
Appendix C	349

Chapter 7 Replicate data	349
Modified flow modulator: A proof of concept hybrid interface	349
Appendix D	361
Chapter 8 Supplementary data	361
Appendix E	386
Chapter 9 Supplementary data	386

List of Figures

Figure 1.1 Block diagram of a GC×GC system based on reference [2]. (1) Injector; (2) first dimension; (3) modulator (GC×GC Interface); (4) second dimension; (5) detector.....	3
Figure 1.2 The importance of the GC×GC interface, based on reference [2]. As analytes separated in the 1D enter the 2D directly (A), they can come together and co-elute as a single band (B). Analytes can also change elution order based on the interactions with the stationary phase in the 2D (C). In a comprehensive two-dimensional analysis, an interface is placed between the 1D and 2D (D). As the analytes move from the 1D, the first band is trapped within the interface (E). Refocusing occurs and the analyte is then re-injected into the 2D as a narrow band, while the following band is trapped by the interface to prevent coelution (F). Analytes that co-elute from the 1D may be separated in the 2D owing to the orthogonal nature of the two columns (G).....	4
Figure 1.3 Different phases of modulation in GC×GC. (A) In-phase modulation, (B) 180° out-of-phase modulation, and (C) any other phase modulation. (Based on Ref. [11])	6
Figure 1.4 Interpretation of GC×GC data. (A) Raw GC×GC chromatogram consisting of short second dimension chromatograms. The injections to the second dimension are indicated by t_1 , t_2 , t_3 . (B) The injection times are used to slice the original signal into multiple individual chromatograms by the computer. (C) They are then aligned on a two-dimensional plane with the primary retention on the X axis, the secondary retention on the Y axis and the signal intensity as the Z axis. (D) Color-coded spots create a visual representation of peaks when viewed from above. Reprinted with permission from Ref. [2].	9
Figure 1.5 Schematic of thermal desorption modulator, based on reference [6].	14
Figure 1.6 Schematic of longitudinally modulated cryogenic system, based on reference [25]. .	16
Figure 1.7 Schematic of the two-stage, quad jet cryogenic modulator, based on Ref. [26]. (A) As the analytes elute from the 1D, the upstream cold jet would trap and focus them in the first trapping stage. (B) The upstream hot jet would then initiate, remobilizing the trapped analytes to the second stage where the downstream cold jet would focus the band of analytes. (C) The upstream cold jet would activate to trap the next fraction of analytes. (D) The downstream jet would remobilize the band of analytes focused in the second stage, injecting them into the 2D for further separation.	17
Figure 1.8 Schematic of the dual jet loop modulator based on Ref. [29]. (A) The cold jet ran continuously, providing two cold spots, one in the upstream and one in the downstream portion of the loop. (B) The hot jet was initiated intermittently, temporarily diverting the cold jet away from the loop and heating the cold spot to remobilize the trapped analytes.....	19
Figure 1.9 Schematic of a miniaturized dual stage thermal modulator for μ GC x μ GC [31].	21
Figure 1.10 Schematic of the Solid-State Modulator, based on Ref. [34].	23

Figure 1.11 Schematic of the differential flow modulator, based on reference [43].	29
Figure 1.12 Schematic of the simple fluidic modulator. The fill state (A) and flush state (B) are displayed. Based on Ref [45].	31
Figure 1.13 The two states of the Deans switch modulator are (A) bypass state and (B) inject state. Based on Ref [39].	34
Figure 1.14 Schematic of valve-based differential flow modulator, based on reference [51].	36
Figure 1.15 The flow paths for the (A) Fill cycle and (B) Flush cycle of the reverse fill/flush modulator. Based on Ref. [54].	40
Figure 1.16 Schematic design of the three possible operational modes of the multi-mode modulator: (A) the divert stage for low-duty cycle and full transfer modes, (B) the inject state for the low-duty cycle and (C) the inject state for the full transfer mode. Based on Ref [39].	43
Figure 1.17 Schematic of dual-stage, consumable-free thermal modulator [78].	56
Figure 1.18 Schematic of dual-stage trapping capillary (A) and improved single-stage trapping capillary (B) [81].	57
Figure 1.19 Schematic of single-stage, consumable-free thermal modulator [84].	59
Figure 1.20 SEM image of 0.53mm ID MXT-1 (3 μ m) trapping capillary before treatment.	60
Figure 1.21 SEM image of 0.53mm ID MXT-1 (3 μ m) trapping capillary after treatment	61
Figure 1.22 Zoomed SEM image of 0.53mm ID MXT-1 (3 μ m) trapping capillary after treatment	61
Figure 2.1 Schematic of the setup used for thermal treatment of the metal trapping capillaries.	66
Figure 2.2 Raw 2D chromatogram of alkane ladder analysis utilizing MXT-1 #2 (0.25 mm ID x 0.25 μ m) trapping capillary with treatment parameters of ten minutes of 800 $^{\circ}$ C increase, followed by two five-minute treatments at 680 $^{\circ}$ C.	72
Figure 2.3 Raw 2D chromatogram of the alkane ladder analysis using MXT-1 #2 (0.25 mm ID x 0.25 μ m) trapping capillary with continuous air supply and a treatment of ten minutes at 800 $^{\circ}$ C and two minutes at 680 $^{\circ}$ C.	73
Figure 2.4 Raw 2D chromatogram of the alkane ladder analysis utilizing MXT-1 #1 (0.28 mm ID x 1 μ m) trapping capillary with continuous air supply and a treatment of ten minutes at 800 $^{\circ}$ C and four minutes at 680 $^{\circ}$ C.	74

Figure 2.5 Chromatographic analysis of n-alkane ladder utilizing treatment D (MXT-1 #1), treated for five minutes at 655 °C followed by five minutes at 550 °C (raw 2D chromatogram).	75
Figure 2.6 Aluminum jig used to open the trapping capillaries.....	77
Figure 2.7 SEM images Edwards MXT-1 traps (A) before and (C) after treatment compared to treatment plan 1 images of MXT-1 trap #1 (B) before and (D) after treatment.	79
Figure 2.8 SEM images of treatment D applied to MXT-1 #1 trapping capillary. Treatment included five minutes at 655 °C followed by five minutes at 550 °C with continuous air supply.	80
Figure 2.9 Raw 2D chromatograms for the analysis of n-alkane ladder utilizing (A) MXT-1 #1E and (B) MXT-1 #1M trapping capillaries.....	83
Figure 2.10 SEM results for MXT-1 #1E (A) before and (C) after treatment and MXT-1 #1M (B) before and (D) after treatment.....	84
Figure 2.11 Raw 2D chromatogram for the analysis of n-alkane ladder with the treated capillaries (A) MXT-1 #3F and (B) MXT-1 #3M.....	86
Figure 2.12 SEM results of trapping capillaries MXT-1 #3F and MXT-1 #3M. MXT-1 #3F from before (A) and after (C) treatment. MXT-1 #3M from before (B) and after (D) treatment.	87
Figure 3.1 Diesel analysis utilizing the extreme treatment MXT-1 #3 (0.28 mm ID x 1 µm) trapping capillary	94
Figure 3.2 Diesel separation using MXT-5 trapping capillary #4	96
Figure 3.3 Analysis of diesel using MXT guard column trapping capillary #5	97
Figure 3.4 Analysis of diesel using MXT guard column trapping capillary #6	98
Figure 3.5 Analysis of diesel with an untreated DB-PS1 trapping capillary with active cooling and a modulation voltage of 50 V.....	101
Figure 3.6 Analysis of diesel with an untreated DB-PS2887 trapping capillary with active cooling and a modulation voltage of 40 V.....	102
Figure 3.7 Analysis of diesel with a treated DB-PS1 #1 trapping capillary with modulation voltages of (A) 30 V, (B) 50 V, (C) 55 V.....	105
Figure 3.8 Analysis of diesel with a treated DB-PS2887 #2 trapping capillary with modulation voltages of (A) 30 V, (B) 45 V, and (C) 60 V.	106
Figure 3.9 SEM images of DB-PS1 #1 (A) 500x magnification untreated, (B) 500x magnification treated, (C) 20,000x magnification untreated, and (D) 20,000x magnification treated.....	107

Figure 3.10 SEM images of DB-PS2887 #2, (A) 100x magnification untreated, (B) 100x magnification treated, (C) 20,000x magnification untreated, and (D) 20,000x magnification treated..... 109

Figure 3.11 EDX comparison of the untreated DB-PS1 and treated DB-PS1 #1 capillaries. 111

Figure 3.12 EDX comparison of the untreated DB-PS2887 and treated DB-PS2887 #2 capillaries. 112

Figure 3.13 Comparison of the performance of a treated DB-PS1 #9 trapping capillary at various modulation voltages with active (A - C) and passive cooling (D - F) in the analysis of diesel. The deactivation layer was present within the unions at the front and back end of the trapping capillary. Modulation voltages were 35 V (A and D), 50 V (B and E) and 55 V (C and F). 116

Figure 3.14 Comparison of the performance of the DB-PS2887 #17 trapping capillary at various modulation voltages with active (A - C) and passive cooling (D - F) in the analysis of diesel. The deactivation layer was present within the unions at the front and back end of the trapping capillary. Modulation voltages were 25 V (A and D), 45 V (B and E), 50 V (F) and 55 V (C). 118

Figure 3.15 SEM images of DB-PS1 #9, (A) 500x magnification treated, (B) 2,000x magnification treated, (C) 10,000x magnification treated, and (D) 20,000x magnification treated. 121

Figure 3.16 EDX results for DB-PS1 #9 for three separate areas compared to the spectrum obtained for the untreated DB-PS1. 123

Figure 3.17 SEM images of DB-PS2887 #17, (A) 100x magnification treated, (B) 5,000x magnification treated, (C) 10,000x magnification treated, and (D) 20,000x magnification treated. 124

Figure 3.18 EDX results of DB-PS2887 #17 for two separate areas compared to the spectra obtained for the untreated DB-PS2887. 126

Figure 3.19 Comparison of the performance of the DB-PS1 #40 trapping capillary at various modulation voltages with active (A - C) and passive cooling (D - F) in the analysis of diesel. The deactivation layer was present within the unions at the front and back end of the trapping capillary. Modulation voltages were 35 V (A and D), 45 V (B and E) and 50 V (C and F). 130

Figure 3.20 Comparison of the performance of the DB-PS1 #41 (Configuration A) trapping capillary at various modulation voltages with active (A - C) and passive cooling (D - F) in the analysis of diesel. The deactivation layer was present within the unions at the front and back end of the trapping capillary. Modulation voltages were 30 V (A and D), 40 V (B and E), 45 V (F) and 50 V (C)..... 132

Figure 3.21 Comparison of the performance of the DB-PS1 #41 (Configuration B) trapping capillary at various modulation voltages with active (A - C) and passive cooling (D - F) in the analysis of diesel. The deactivation layer was present within the unions at the front and back end of the trapping capillary. Modulation voltages were 35 V (A and D), 40 V (B and E), 45 V (F), and 50 V (C)..... 133

Figure 3.22 Comparison of the performance of DB-PS1 #32 trapping capillary at various modulation voltages with active (A - C) and passive cooling (D - F) in the analysis of diesel. The deactivation layer was present within the unions at the front and back end of the trapping capillary. Modulation voltages were 25 V (A and D), 35 V (B and E), and 45 V (C and F). 135

Figure 3.23 Comparison of the performance of the DB-PS1 #42 (Configuration A) trapping capillary at various modulation voltages with active (A - C) and passive cooling (D - F) in the analysis of diesel. The deactivation layer was present within the unions at the front and back end of the trapping capillary. Modulation voltages were 25 V (A and D), 35 V (B and E), and 50 V (C and F). 137

Figure 3.24 Comparison of the performance of the DB-PS1 #42 (Configuration B) trapping capillary at various modulation voltages with active (A - C) and passive cooling (D - F) in the analysis of diesel. The deactivation layer was present within the unions at the front and back end of the trapping capillary. Modulation voltages were 25 V (A and D), 35 V (B and E) and 50 V (C and F). 139

Figure 3.25 Comparison of the performance of the DB-PS2887 #39 trapping capillary at various modulation voltages with active cooling (A - C) present for the analysis of diesel. The deactivation layer was present within the unions at the front and back end of the trapping capillary. Modulation voltages were 25 V (A), 40 V (B) and 55 V (C). 140

Figure 3.26 Comparison of the performance of the DB-PS2887 #35 (Configuration A) trapping capillary at various modulation voltages with active (A - C) and passive cooling (D - F) in the analysis of diesel. The deactivation layer was present within the unions at the front and back end of the trapping capillary. Modulation voltages were 25 V (A and D), 30 V (B and E) and 40 V (C and F). 141

Figure 3.27 Comparison of the performance of the DB-PS2887 #35 (Configuration B) trapping capillary at various modulation voltages with active cooling (A - C) in the analysis of diesel. The deactivation layer was present within the unions at the front and back end of the trapping capillary. Modulation voltages were 25 V (A), 35 V (B) and 40 V (C). 143

Figure 3.28 SEM images of DB-PS1 #41 (Treated Half), (A) 100x magnification treated, (B) 5,000x magnification treated, (C) 10,000x magnification treated, and (D) 20,000x magnification treated..... 144

Figure 3.29 EDX results of DB-PS1 #41 (Treated Half) for three separate areas compared to the spectra obtained for the untreated DB-PS1..... 145

Figure 3.30 SEM images of DB-PS1 #32, (A) 500x magnification treated, (B) 2,000x magnification treated, (C) 10,000x magnification treated, and (D) 20,000x magnification treated.	146
Figure 3.31 EDX results of DB-PS1 #32 for two separate areas compared to the spectra obtained for the untreated DB-PS1.....	147
Figure 3.32 SEM images of DB-PS1 #42 (Half 40 V/35 V), (A) 100x magnification treated, (B) 5,000x magnification treated, (C) 10,000x magnification treated, and (D) 20,000x magnification treated.....	149
Figure 3.33 EDX results of DB-PS1 #42 (Half 40 V/35 V) for three separate areas compared to the spectra obtained for the untreated DB-PS1.....	150
Figure 3.34 SEM images of DB-PS1 #42 (Half 45 V/40 V), (A) 100x magnification treated, (B) 5,000x magnification treated, (C) 10,000x magnification treated, and (D) 20,000x magnification treated.....	151
Figure 3.35 EDX results of DB-PS1 #42 (Half 45 V/40 V) for three separate areas compared to the spectra obtained for the untreated DB-PS1.....	152
Figure 3.36 SEM images of DB-PS2887 #35 (Half 40 V/35 V), (A) 500x magnification treated, (B) 2,000x magnification treated, (C) 10,000x magnification treated, and (D) 20,000x magnification treated.	154
Figure 3.37 EDX results of DB-PS2887 #35 (Half 40 V/35 V) for three separate areas compared to the spectra obtained for the untreated DB-PS1.....	155
Figure 4.1 Schematic of the (A) original rectangular ceramic cooling pads, and (B) newly designed, trapezoidal ceramic cooling pads. The new design provided complete coverage independently of the length of the trapping capillaries.....	161
Figure 4.2 Analysis of diesel using MXT-5 #4 trapping capillary with 65 V modulation voltage for remobilization. The top contour plot employed the new trapezoidal ceramic cooling pads, while the bottom contour plot employed the old rectangular ceramic cooling pads	162
Figure 4.3 Schematic of the trapping capillary placed within the cooling pads, connected to the 1D and 2D columns by unions at the front and back end. The red circles where the trapping layer was removed (within the unions at the front and back end of the trapping capillary).....	163
Figure 4.4 Analysis of diesel utilizing the trapping capillary DB-PS1 #9 with active cooling employed and a modulation voltage of 45 V. The adsorbent was removed from the segments of the capillary within the unions in the top contour plot, while it was still present in the bottom contour plot.	165

Figure 4.5 Analysis of diesel utilizing the trapping capillary DB-PS1 #32 with active cooling employed and a modulation voltage of 35 V. The adsorbent was removed from the segments of the capillary within the unions in the top contour plot, while it was still present in the bottom contour plot.	166
Figure 4.6 Analysis of diesel utilizing the trapping capillary DB-PS1 #41 (Treated Half) with passive cooling employed and a modulation voltage of 35 V. The adsorbent phase was removed from the segments of the capillary within the unions in the top contour plot, while it was still present in the bottom contour plot.	167
Figure 4.7 Analysis of diesel utilizing the trapping capillary DB-PS1 #40 with active cooling employed and a modulation voltage of 45 V. The adsorbent phase was removed from the segments of the capillary within the unions in the top contour plot, while it was still present in the bottom contour plot.	168
Figure 4.8 Analysis of diesel utilizing the trapping capillary DB-PS1 #40 with passive cooling employed and a modulation voltage of 45 V. The adsorbent phase was removed from the segments of the capillary within the unions in the top contour plot, while it was still present in the bottom contour plot.	169
Figure 4.9 Analysis of diesel utilizing the trapping capillary DB-PS1 #42 (Configuration B) with active cooling employed and a modulation voltage of 35 V. The adsorbent phase was removed from the segments of the capillary within the unions in the top contour plot, while it was still present in the bottom contour plot.	170
Figure 5.1 Instrumental set-up for the determination of trap temperature increase during treatment at various discharge voltages.	174
Figure 5.2 Temperature increase for DB-PS1 during treatment at various discharge voltages with both air on (circles) and air off (squares).	176
Figure 5.3 Temperature increase for DB-PS2887 during treatment at various discharge voltages with both air on (circles) and air off (squares).	177
Figure 5.4 Determination of trapping capillary temperature between the cooling pads of the modulator.	178
Figure 5.5 DB-PS1 trap temperature within cooling pads with active cooling (TECs and fans on)	180
Figure 5.6 DB-PS1 trap temperature within cooling pads with passive cooling (TECs off and fans on).....	181
Figure 5.7 Instrumental set-up to determine the temperature of cooling pads with varying oven temperature ramps.....	182

Figure 5.8 Temperature of the cooling pads with active cooling (TECs and fans on) with various oven temperature ramps.	183
Figure 5.9 Temperature of cooling pads with passive cooling (no TECs, fans on).....	184
Figure 6.1 Design of the single-stage, consumable-free thermal modulator from the University of Waterloo [84]. Reprinted from Journal of Chromatography A, 1391, Muscalu et al., Evaluation of single-stage, consumable-free modulator for comprehensive two-dimensional gas chromatography: Analysis of polychlorinated biphenyl, organochlorine pesticides and chlorobenzenes, 93-101, Copyright (2016), with permission from Elsevier.	196
Figure 6.2 (a) Flow path of the fill stage of the Insight RFF flow modulator and (b) flow path of the flush stage of the Insight RFF flow modulator [58]......	197
Figure 6.3 Unprocessed, one-dimensional linear chromatograms of (a) a TOF trace for the flow-based platform; (b) a FID trace for the flow-based platform; (c) a TOF trace for the thermal-based platform; and (d) a FID trace for the thermal-based platform.	198
Figure 6.4 Unprocessed, partially zoomed-in one dimensional linear chromatograms of (a) a TOF trace for the flow-based platform; (b) a FID trace for the flow-based platform; (c) a TOF trace for the thermal-based platform; and (d) a FID trace for the thermal-based platform.	199
Figure 6.5 Unprocessed, contour plots of (a) a TOF trace for the flow-based platform; (b) a FID trace for the flow-based platform; (c) a TOF trace for the thermal-based platform; and (d) a FID trace for the thermal-based platform.	200
Figure 6.6 Group analysis of a conventional oil from Brand A with viscosity 5W-20 illustrating the separation with (a) a flow-based modulator platform; and (b) a thermal based modulator platform. The colors presented correspond to the following groups accordingly: blue for paraffins and isoparaffins, green for alkylbenzenes, orange for mononaphthenes, yellow for dinaphthenes, red for trinaphthenes, and purple for naphthalenes.....	203
Figure 6.7 GC×GC-TOF-MS contour plots of (a) conventional oil from Brand A with viscosity 10W-30; (b) conventional oil from Brand B with viscosity 10W-30; (c) conventional oil from Brand A with viscosity 5W-20; and (d) conventional oil from Brand B with viscosity 5W-20; illustrating the separation with the thermal-based modulator platform.	204
Figure 6.8 GC×GC-TOF-MS contour plots of (a) conventional oil from Brand A with viscosity 10W-30; (b) conventional oil from Brand B with viscosity 10W-30; (c) conventional oil from Brand A with viscosity 5W-20; and (d) conventional oil from Brand B with viscosity 5W-20; illustrating the separation with the flow-based modulator platform.	206
Figure 6.9 GC×GC-TOF-MS contour plots of (a) synthetic oil from Brand A with viscosity 10W-30; (b) synthetic oil from Brand B with viscosity 10W-30; (c) synthetic oil from Brand A with viscosity 5W-20; and (d) synthetic oil from Brand B with viscosity 5W-20; illustrating the separation with the thermal-based modulator platform.	207

Figure 6.10 GC×GC-TOF-MS contour plots of (a) synthetic oil from Brand A with viscosity, 10W-30; (b) synthetic oil from Brand B with viscosity 10W-30; (c) synthetic oil from Brand A with viscosity 5W-20; and (d) synthetic oil from Brand B with viscosity 5W-20; illustrating the separation with the flow-based modulator platform.	208
Figure 6.11 GC×GC-TOFMS mass spectra of (a) diphenylamine with the flow-based platform and (b) diphenylamine with the thermal-based platform.	210
Figure 6.12 GC×GC-TOF-MS mass spectra comparison of hard and soft ionization for the identification (a) monononyl-diphenylamine with the flow-based platform; (b) dinonyl-diphenylamine with the flow-based platform; (c) monononyl-diphenylamine with the thermal-based platform; and (d) dinonyl-diphenylamine with the thermal-based platform.	212
Figure 7.1 Schematic of the hybrid system.	219
Figure 7.2 Close up images of compressed air line, jet, flow modulator, cooling trap and column holder.	222
Figure 7.3 Various cooling times in comparison to flow modulation parameters for two modulation periods.	223
Figure 7.4 Cooling jet design used for all experimental analyses.	224
Figure 7.5 Column holder without (A) and with (B) the septa.	226
Figure 7.6 Chromatograms displaying the effect of cooling jet time delay on injection band widths; (A) absence of cooling (Jet off), (B) 2.6 s cooling with 0.028 min delay, (C) 2.6 s cooling with 0.05 min delay.	229
Figure 7.7 Chromatograms comparing the results obtained with the septum absent (A) or present (B) within the column holder.	230
Figure 7.8 Chromatograms comparing the various cooling times applied to the 0.5 μm cooling trap. (A) Absence of cooling (Jet off), (B) 1500 ms cooling, (C) 2000 ms cooling, (D) 2600 ms cooling, and (E) 3000 ms cooling.	233
Figure 7.9 Chromatograms comparing the various cooling times applied to the 3.0 μm cooling trap. (A) Absence of cooling (Jet off), (B) 1000 ms cooling, (C) 1500 ms cooling, (D) 2000 ms cooling, (E) 2600 ms cooling, (F) 3000 ms cooling.	237
Figure 7.10 Chromatograms comparing the various cooling times applied to the 5.0 μm cooling trap. (A) Absence of cooling (Jet off), (B) 1000 ms cooling, (C) 1500 ms cooling, (D) 2000 ms cooling, (E) 2600 ms cooling, (F) 3000 ms cooling.	241
Figure 7.11 Insulated copper tubing for compressed airline.	244

Figure 7.12 Chromatograms comparing the presence and absence of insulation on the copper tubing which provides compressed air for the jet nozzle with the 0.5 μm cooling trap.	246
Figure 7.13 Chromatograms comparing the presence and absence of insulation on the copper tubing which provides compressed air for the jet nozzle with the 3.0 μm cooling trap.	249
Figure 8.1 Diagram of the solid-state modulator (based on Ref. [39]).....	257
Figure 8.2 Diagram of dual-stage thermal modulation in the SSM (based on Ref. [39]).....	258
Figure 8.3 GC \times GC-TOF-MS contour plots of triplicate analyses of MRP standard mixture using the SSM platform. The chromatograms have been shifted to display all peaks within the same modulation period.	262
Figure 8.4 GC \times GC-TOF-MS contour plots of triplicate analyses of FA standard mixture using the SSM platform. The chromatograms have been shifted to show all peaks within the same modulation period.	263
Figure 8.5 GC \times GC-TOFMS contour plots of triplicate analysis of MRP standard mixture illustrating wraparound in the second dimension.	265
Figure 8.6 GC \times GC-TOF-MS contour plots of triplicate analysis of FA standard mixture illustrating wraparound in the second dimension.	265
Figure 8.7 One-dimensional trace of Isodrin comparing all three replicates (A) and one-dimensional trace of Estragole comparing all three replicates (B).	267
Figure 8.8 GC \times GC-TOF-MS contour plot displaying the three siloxane peaks chosen for the analysis of re-injection bandwidths at half height.	270
Figure 8.9 Placement of peaks chosen in five retention bands to properly evaluate the second-dimension peak width and second dimension peak capacity of the MRP analysis. The color and marker type correspond to the retention bands as follows: red circle band 1, orange square band 2, yellow diamond band 3, green triangle band 4, and blue dash band 5.	272
Figure 8.10 Placement of peaks chosen in six retention bands to properly evaluate the second-dimension peak width and second dimension peak capacity of the FA analysis. The color and marker type correspond to the retention bands as follows: red circle band 1, orange square band 2, yellow diamond band 3, green triangle band 4, blue dash band 5 and purple cross band 6. ..	273
Figure 8.11 GC \times GC chromatograms utilizing the SSM displaying the n-alkane C ₉ using modulation column average linear velocities of (A) 30 cm/s, (B) 25 cm/s, (C) 15 cm/s and (D) 13 cm/s. Reprinted with permission from [139].	274
Figure 9.1 Group type identification of bitumen oil sands extracted with (A) toluene and (B) cyclohexane. The various colored boxes correspond to specific groups: paraffins (orange), alkylated steranes (red), terpanes (green) and hopanes (purple).....	284

Figure 9.2 Biomarker analysis of bitumen oil sands extracted with (A) toluene and (B) cyclohexane. The colored boxes correspond to various biomarker groups: C2 & C3 alkylated steranes (orange), C4 & C5 alkylated steranes (purple), C6 alkylated steranes (green), cyclic terpanes (white), diasteranes (pink), monoaromatic steranes (yellow), triaromatic steranes (blue), methyl hopanes (red) and methyl steranes (teal). 288

Figure 9.3 Tentative identification of three characteristic biomarkers in the biomarker region of the toluene extract. The compounds (A) 24-ethyl-5 α (H)-14 β (H), 17 β (H)-20R-cholestane (C₂₉ $\alpha\beta\beta$ -20), (B) 17 α (H)-22,29,30-trisnorhopane (T_m), and (C) 17 α (H)-21 β (H)-hopane (H30) were identified by EIC and molecular ion peak..... 291

Figure 9.4 Mass spectrum of a C31 late-eluting terpane found in (A) toluene bitumen oil sands extract and (B) cyclohexane bitumen oil sands extract. 292

Figure 9.5 Aromatic hydrocarbons found within the cyclohexane extract of bitumen oil sands. The colored boxes correspond to various aromatic groups: 4-ring aromatics (red), 5-ring aromatics (blue) and 6-ring aromatics (green)..... 294

List of Tables

Table 1.1 Comparison of advantages and disadvantages of various modulators	51
Table 1.2 Atomic percentages of the elements in the MXT-1 capillary coating before treatment, determined by EDX	62
Table 1.3 Atomic percentages of the elements in the MXT-1 capillary coating before and after treatment, determined by EDX	63
Table 2.1 Treatment plans for trapping capillaries	70
Table 2.2 Treatment plan for trapping capillaries with shorter treatment times for MXT-1 #1 ...	74
Table 2.3 EDX results for the MXT-1 #1 under treatment plans 1 and D.....	82
Table 2.4 EDX results for MXT-1 #1E and MXT-1 #1M before and after treatment	85
Table 2.5 EDX results of MXT-1 #3F and MXT-1 #3M before and after treatment plan 1	88
Table 3.1 Various treatment plans for DB-PS1 and DB-PS2887.....	114
Table 3.2 Treatment plan for different sections of Agilent trapping capillaries.....	129
Table 6.1 Different compound groups and their corresponding mass fragments	201
Table 6.2 Resolution from the UCM for monononyl DPA for both the flow-based and thermal-based platforms.	213
Table 7.1 Equations used to determine proper fill and flush times	221
Table 7.2 Comparison of re-injection band widths (ms) with 2000 and 2600 ms cooling for 0.5 μm cooling trap.....	234
Table 7.3 Reproducibility data for 0.5 μm cooling trap	236
Table 7.4 Comparison of re-injection bandwidths (ms) with 2000 and 2600 ms cooling for 3.0 μm cooling trap.....	238
Table 7.5 Reproducibility data for 3.0 μm cooling trap	240
Table 7.6 Re-injection bandwidths (ms) for 1000 and 1500 ms of cooling with 5.0 μm cooling trap	242
Table 7.7 Unfocused bandwidths (ms) of 0.5, 3.0, and 5.0 μm cooling traps with the absence of cooling (Jet Off).....	243

Table 7.8 Comparison of peak width at half height (ms) for insulated vs. not insulated copper tubing with the 0.5 μm cooling trap.....	247
Table 7.9 Comparison of peak widths at half height (ms) for insulated vs. non-insulated cooling line for the 3.0 μm cooling trap	250
Table 8.1 Chromatographic and modulator conditions for the analysis of MRP and FA standards mix	260

List of Abbreviations

$1D$	First Dimension
1D	One-dimensional
2α MH C31	2α -methyl-hopane C31
$2D$	Second Dimension
2D	Two-Dimensional
ADPA	Alkylated Diphenylamine
APCI	Atmospheric Pressure Chemical Ionization
API	American Petroleum Institute
$C_{29}\alpha\beta\beta$ -20	24-ethyl-5 α (H)-14 β (H), 17 β (H)-20R-cholestane
CFT	Capillary Flow Technology
CI	Chemical Ionization
DFM	Differential Flow Modulator
DPA	Diphenylamine
DVM	Diaphragm Valve Modulator
ECD	Electron Capture Detector
EI	Electron Ionization
EIC	Extracted Ion Chromatogram
EPC	Electronic Pressure Controller
F ₁	$1D$ Flow
F ₂	$2D$ Flow
F _A	Auxiliary Flow
FA	Fragrance Allergens Standards

FAME	Fatty acid methyl ester
FI	Field Ionization
FID	Flame Ionization Detector
GC	Gas Chromatography
GC×GC	Comprehensive Two-dimensional gas chromatography
μGC×μGC	Micro-GC x Micro-GC
H30	17α(H)-21β(H)-hopane
HRTOFMS	High resolution Time-of-Flight Mass Spectrometry
ISCC	International Symposium on Capillary Chromatography
LMCS	Longitudinally modulated cryogenic system
Matecs	Modulation and Timed Events Control Software
MMM	Multi-mode Modulator
MS	Mass Spectrometry
Mr	Modulation ratio
MRP	Multiresidue Pesticide Standards
NC	Normally Closed
NCD	Nitrogen Chemiluminescence Detector
NIST	National Institute of Standards and Technology
NO	Normally Open
NP	Nanoparticles
PAO	Poly-alpha-olefin
PDMS	Polydimethylsiloxane
PI	Photoionization

PIONA	Paraffins, Isoparaffins, Olefins, Naphthalenes and aromatics
PITTCON	Pittsburgh Conference on Analytical Chemistry and Applied Spectroscopy
P _M	Modulation period
QMS	Single Quadrupole Mass Spectrometer
RFF	Reverse fill/flush
RSD	Relative Standard Deviation
RT	Retention Time
RTM	Rotating Thermal Modulator
SAE	Society of Automotive Engineers
SCD	Sulfur Chemiluminescence Detector
SEM	Scanning electron microscope
S/N	Signal-to-noise ratio
SSM	Solid-State Modulator
STS	Science Technical Services
TEC	Thermoelectric Cooling
TDM	Thermal Desorption Modulator
TIC	Total Ion Chromatogram
TiM	Thermally Independent Modulator
T _m	17 α (H)-22,29,30-trisnorhopane
T _s	18 α (H)-22,29,30-trisnorneohopane
UCM	Unresolved Complex Mixture
μ TM	Micro-Thermal Modulator
TOFMS	Time-of-Flight Mass Spectrometry

VOC	Volatile Organic Compounds
VUV	Vacuum ultraviolet
WATLab	Waterloo Advanced Technology Laboratory
w _b	Peak width at the base
w _h	Peak width at half-height

List of Abbreviations

¹ D	First Dimension
1D	One-dimensional
2 α MH C31	2 α -methyl-hopane C31
² D	Second Dimension
2D	Two-Dimensional
ADPA	Alkylated Diphenylamine
APCI	Atmospheric Pressure Chemical Ionization
API	American Petroleum Institute
C ₂₉ $\alpha\beta\beta$ -20	24-ethyl-5 α (H)-14 β (H), 17 β (H)-20R-cholestane
CFT	Capillary Flow Technology
CI	Chemical Ionization
DFM	Differential Flow Modulator
DPA	Diphenylamine
DVM	Diaphragm Valve Modulator
ECD	Electron Capture Detector
EI	Electron Ionization
EIC	Extracted Ion Chromatogram
EPC	Electronic Pressure Controller
F ₁	¹ D Flow
F ₂	² D Flow
F _A	Auxiliary Flow

FA	Fragrance Allergens Standards
FAME	Fatty acid methyl ester
FI	Field Ionization
FID	Flame Ionization Detector
GC	Gas Chromatography
GC×GC	Comprehensive Two-dimensional gas chromatography
μGC×μGC	Micro-GC x Micro-GC
H30	17α(H)-21β(H)-hopane
HRTOFMS	High resolution Time-of-Flight Mass Spectrometry
ISCC	International Symposium on Capillary Chromatography
LMCS	Longitudinally modulated cryogenic system
Matecs	Modulation and Timed Events Control Software
MMM	Multi-mode Modulator
MS	Mass Spectrometry
M _R	Modulation ratio
MRP	Multiresidue Pesticide Standards
NC	Normally Closed
NCD	Nitrogen Chemiluminescence Detector
NIST	National Institute of Standards and Technology
NO	Normally Open
NP	Nanoparticles
PAO	Poly-alpha-olefin
PDMS	Polydimethylsiloxane

PI	Photoionization
PIONA	Paraffins, Isoparaffins, Olefins, Naphthalenes and aromatics
PITTCON	Pittsburgh Conference on Analytical Chemistry and Applied Spectroscopy
P _M	Modulation period
QMS	Single Quadrupole Mass Spectrometer
RFF	Reverse fill/flush
RSD	Relative Standard Deviation
RT	Retention Time
RTM	Rotating Thermal Modulator
SAE	Society of Automotive Engineers
SCD	Sulfur Chemiluminescence Detector
SEM	Scanning electron microscope
S/N	Signal-to-noise ratio
SSM	Solid-State Modulator
STS	Science Technical Services
TEC	Thermoelectric Cooling
TDM	Thermal Desorption Modulator
TIC	Total Ion Chromatogram
TiM	Thermally Independent Modulator
T _m	17 α (H)-22,29,30-trisnorhopane
T _s	18 α (H)-22,29,30-trisnorneohopane
UCM	Unresolved Complex Mixture
μ TM	Micro-Thermal Modulator

TOFMS	Time-of-Flight Mass Spectrometry
VOC	Volatile Organic Compounds
VUV	Vacuum ultraviolet
WATLab	Waterloo Advanced Technology Laboratory
w_b	Peak width at the base
w_h	Peak width at half-height

Chapter 1. Introduction

1.1 Comprehensive two-dimensional gas chromatography

1.1.1 Principles of gas chromatography

Gas chromatography (GC) has been a leader in the field of separating mixtures of volatile and semi-volatile compounds due to its multiple capabilities of achieving both high selectivity and resolution with a broad dynamic concentration range and high sensitivity [1]. One-dimensional (1D) gas chromatography requires four main instrumental components: injector, column, oven, and detector. In the simplest terms, the analytes are vaporized within the injector, and then passed through the analytical column by the carrier gas until they reach the detector, which then produces a chromatogram displaying the separation. The separation within the column is accomplished due to the variation in partitioning of the analytes between the mobile phase (carrier gas) and the stationary phase [2]. With the vast array of stationary phase coatings available on the market, a specific column can be chosen to produce an optimal separation. In an ideal separation, each individual analyte would be separated without co-elutions. This would allow complete analysis of a mixture in which each analyte could be identified and quantified with ease.

An important fundamental concept to consider within any chromatographic separation is the peak capacity, or the number of individual analytes that can be placed side by side within the available separation space [3]. Because of random peak distribution in real samples, the peak capacity of the column used should vastly surpass the number of individual analytes within a mixture. However, in most cases, this is difficult due to the complexity of real-world samples. As

a result, the overall separation quality is compromised, leading to the demand for a separation technique that can address the drawbacks of 1D chromatography.

1.1.2 Principles of two-dimensional gas chromatography

To address the low resolution of 1D chromatographic separations, Giddings introduced the concept of multidimensional separations, in which analytes could be subjected to several different separation mechanisms in order to increase the selectivity and peak capacity [4]. The peak capacity of a multidimensional separation is the sum of the peak capacities of each individual separation dimensions within the system. The original concept of a multidimensional GC separation, or ‘heart cutting’, involved sampling a fraction of the effluent from the initial column and injecting it into a second column with a different stationary phase. Despite the increase in peak capacity, this approach only improved the separation of a portion of the entire sample. Giddings also described a concept in which the entire sample was subjected to both dimensions of separation, termed comprehensive multidimensional chromatography [4]. This concept required that the separations accomplished in each dimension had to be preserved until the analysis was complete, and that the entire effluent from the first separation dimension had to be transferred and subject to separation in the second dimension. As a first approximation, the peak capacity of such a comprehensive multidimensional separation is the product of the peak capacities of each individual dimension within the system [5]. In 1991, Phillips was the first to demonstrate a comprehensive gas chromatographic separation, termed GC×GC [6]. Constantly evolving, GC×GC is rapidly becoming one the dominant separation techniques for volatile and semi-volatile analytes owing to its increased peak capacity, resolution, selectivity and sensitivity. The most important concept in GC×GC is the transfer of the entire effluent from the first dimension (¹D) to the second dimension (²D), while maintaining the separation achieved in the

¹D [2]. In order to accomplish this, an interface called a modulator is needed. The basic GC×GC instrument includes five components: injector, ¹D column, modulator, ²D column, and detector, as seen in Fig. 1.1. The modulator connects the ¹D column to the ²D column, allowing a comprehensive two-dimensional analysis.

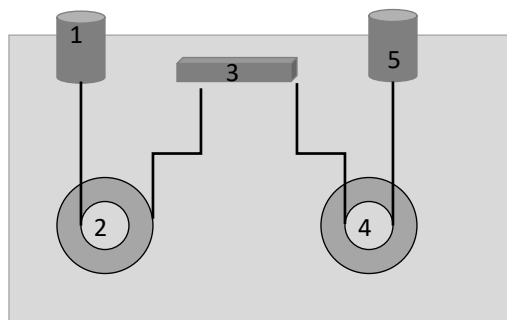


Figure 1.1 Block diagram of a GC×GC system based on reference [2]. (1) Injector; (2) first dimension; (3) modulator (GC×GC Interface); (4) second dimension; (5) detector.

1.1.3 GC×GC modulator

The modulator is the ‘heart’ of a GC×GC system, as it allows a multidimensional comprehensive gas chromatographic separation to occur. The three main functions of the modulator include: trapping or sampling the ¹D effluent, refocusing the effluent into a narrow band, and injecting the focused band into the ²D [7]. Without the modulating interface between the ¹D and ²D, the initial separation may be compromised due to co-elutions occurring in the ²D separation (Figure 1.2 A-C).

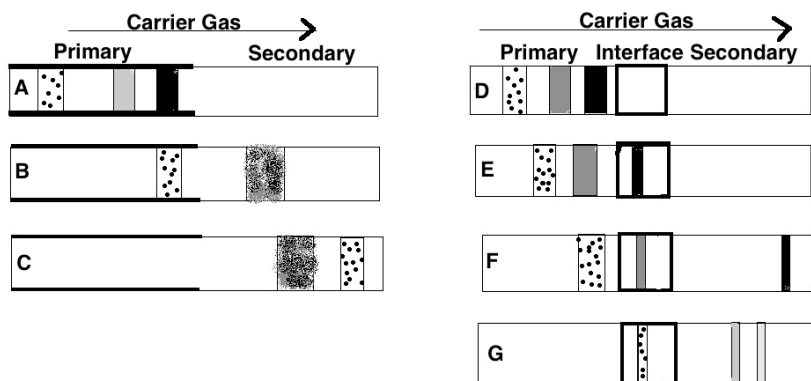


Figure 1.2 The importance of the GCxGC interface, based on reference [2]. As analytes separated in the ¹D enter the ²D directly (A), they can come together and co-elute as a single band (B). Analytes can also change elution order based on the interactions with the stationary phase in the ²D (C). In a comprehensive two-dimensional analysis, an interface is placed between the ¹D and ²D (D). As the analytes move from the ¹D, the first band is trapped within the interface (E). Refocusing occurs and the analyte is then re-injected into the ²D as a narrow band, while the following band is trapped by the interface to prevent coelution (F). Analytes that co-elute from the 1D may be separated in the ²D owing to the orthogonal nature of the two columns (G).

Modulation must occur frequently and throughout the entire analysis to ensure the primary separation is preserved and further separation within the ²D can occur properly (Figure 1.2 D-G). The frequency of the modulation ultimately determines how well the ¹D separation is preserved. According to Murphy *et al.*, each peak eluting from the ¹D should be sampled three to four times before entering the ²D [8]. Choosing the correct sampling frequency, or modulation period, is fundamental in obtaining a two-dimensional separation. The modulation period can be more effectively described by the term modulation ratio (M_R) [9]. The term is defined as in equation 1.1,

$$M_R = \frac{4\sigma}{P_M} = \frac{w_b}{P_M} = \frac{w_h \times 1.6985}{P_M} \quad (1.1)$$

where the peak width at base (w_b), defined as 4 times the ¹D peak standard deviation (σ) or 1.6985 times the width at half-height of the peak (w_h), is divided by the modulation period (P_M).

It has been suggested to utilize an M_R value of at least three for quantitative analysis of trace compounds, while an M_R of 1.5 is sufficient for semi-quantitative analysis of major components [9]. However, these suggestions did not take into consideration the preservation of the 1D separation, as previously defined by Murphy *et al.* Furthermore, the phase of modulation affects the degree of resolution and reconstructed peak width of an analyte eluting from the 1D [10]. The phase of modulation is defined as the difference between the centroid of the first-dimension peak and the mean of the peak region sampled by the modulator. There are two extreme scenarios, in-phase and 180° out-of-phase modulation, as seen in Fig. 1.3A and 1.3B, respectively. In-phase modulation gives a symmetric pulse sequence with a single maximum peak and a number of side peaks, while 180° out-of-phase modulation gives two equal symmetric maxima [11]. Due to the random nature of peaks eluting from the 1D , any phase between the two limiting cases may be observed in an actual two-dimensional separation, as seen in Fig. 1.3C [10]. Since this parameter cannot be altered to obtain the desired modulation phase, it is recommended to utilize the sum of the peak areas as a quantitative measure of response since it is independent of the modulation phase [11].

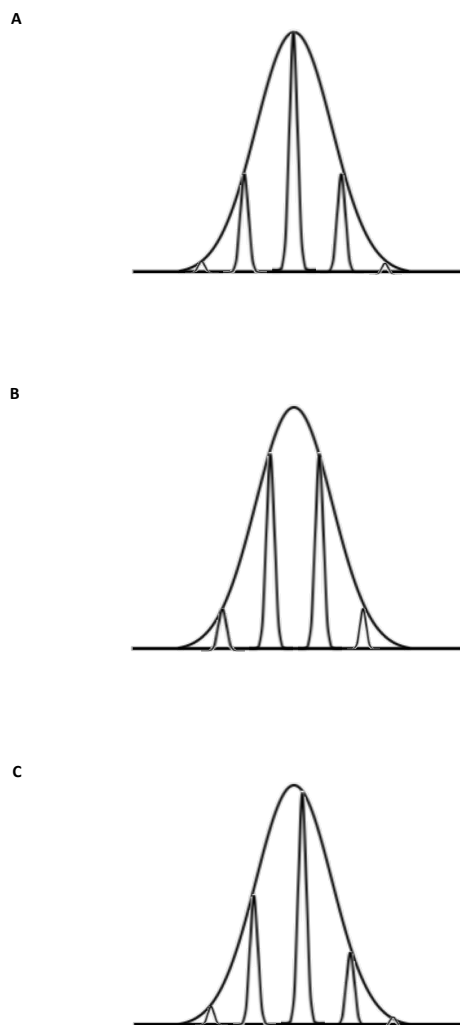


Figure 1.3 Different phases of modulation in GCxGC. (A) In-phase modulation, (B) 180° out-of-phase modulation, and (C) any other phase modulation. (Based on Ref. [11])

Two other important phenomena that might occur during comprehensive two-dimensional chromatographic analysis are peak wraparound and breakthrough. Peak wraparound occurs when analytes are retained strongly within the 2^D , ultimately eluting during the subsequent modulation period [3]. This can lead to potential co-elutions with compounds within subsequent fractions and incorrect location within the two-dimensional chromatogram. To the untrained eye, these wrap-around peaks could be misidentified due to their misleading locations,

altering the structured order of a two-dimensional chromatogram. The latter problem, breakthrough, occurs when the analytes eluting from the ¹D are not completely trapped and reach the ²D as an unfocused band [7]. Breakthrough compromises the integrity of the ²D separation by creating broad peaks that could potentially compromise the quantitation and identification of other analytes. Peak tailing may also occur because of breakthrough.

An important characteristic of a modulator is the widths of the second-dimension peaks it generates [2]. With a limited separation space in the second dimension, narrower injection bands allow more peaks to fit side-by-side, increasing the peak capacity [12]. As peaks become narrower, they become inherently taller, increasing the signal intensity and sensitivity of the separation. As the modulation period is increased, the ¹D resolution is compromised due to fewer, larger fractions being collected. While this leads to more intense ²D peaks, it also results in more “chemical noise” (*e.g.* solvent tail, column bleed) from the ¹D separation being collected. However, the overall sensitivity is improved, as the ²D column separates the analyte signal from the chemical noise of the ¹D separation [2]. On the other hand, decreasing the modulation period increases the risk of peak wraparound [3].

1.1.4 Interpretation of GC×GC data

As the refocused analytes travel from the ¹D to the ²D column, the raw data is collected as a one-dimensional chromatogram consisting of a sequence of “slices,” representing the short individual ²D separations (Fig. 1.4A). In order to fully interpret the data and identify the analytes, computer software is necessary to create a proper two-dimensional chromatogram. The computer software recognizes the individual sections of each ²D separation based on the modulation period. Aligning these “slices” side by side allows the viewer to visualize the entire

separation in a three-dimensional plane with the first dimension along the x-axis, the second dimension along the y-axis and the signal intensity along the z-axis [2] (Fig. 1.4C). Compounds that were co-eluting within the one-dimensional chromatogram can be seen as separate entities within the second-dimension separation. The three-dimensional plot can be converted into a contour plot by converting to a top-down view with the first dimension along the x-axis, the second dimension along the y-axis, and the signal intensity indicated by color (Fig. 1.4D).

A two-dimensional chromatographic analysis has a higher resolving power, better selectivity and higher peak capacity than a one-dimensional analysis due to the use of two orthogonal columns. The columns are considered orthogonal when the two stationary phases chosen provide independent separation mechanisms [13]. A single 2D analysis consists of two individual one-dimensional analyses using differing stationary phases [14]. Identification of analytes is thus more reliable since it is based on two retention times. The structured nature of two-dimensional plots allows tentative identification based on the clear homologous groups that appear as bands within the contour plot [15]. This unique feature can be used to identify patterns and even analytes without known standards simply through visual examination of the contour plot.

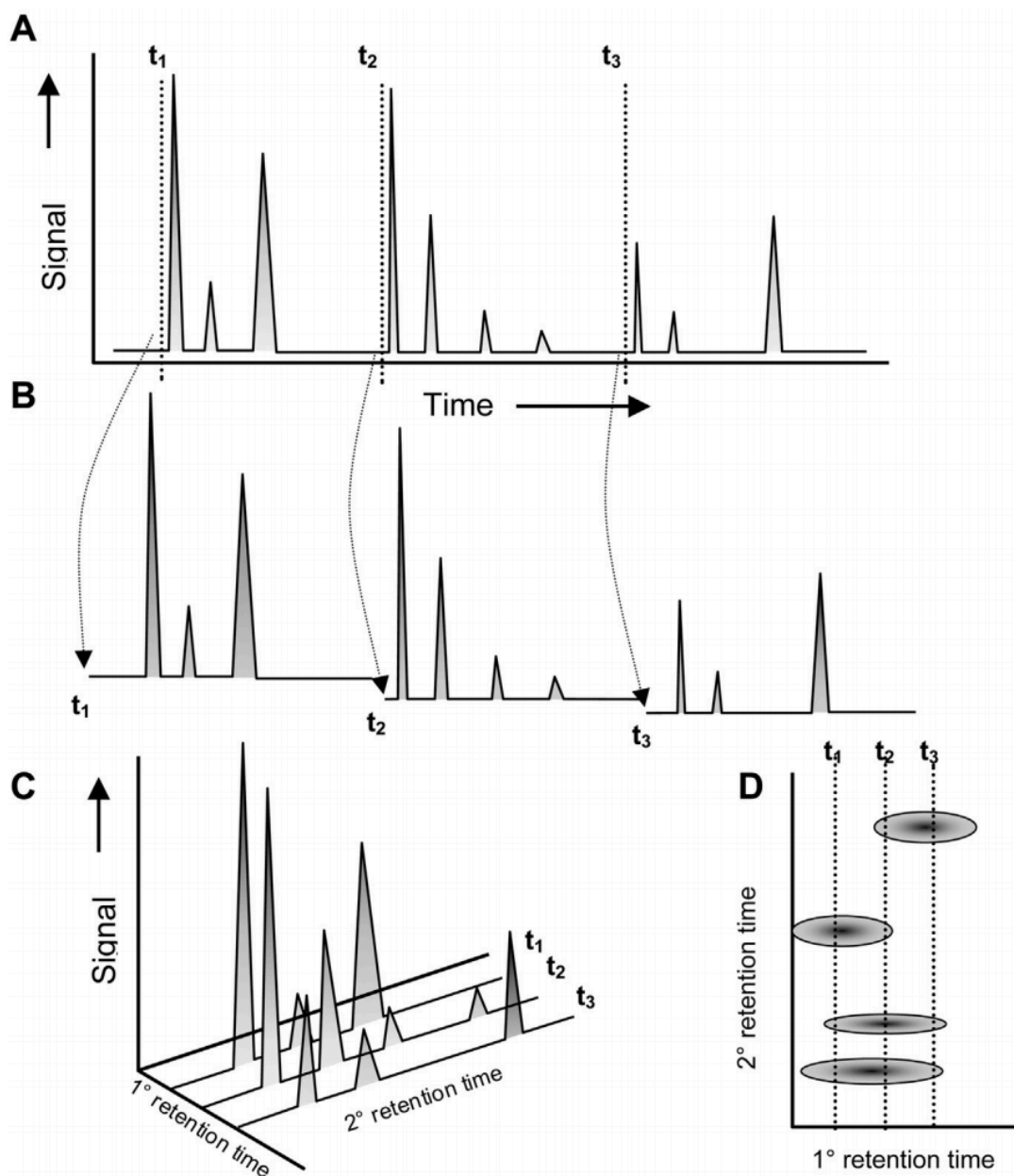


Figure 1.4 Interpretation of GCxGC data. (A) Raw GCxGC chromatogram consisting of short second dimension chromatograms. The injections to the second dimension are indicated by t_1 , t_2 , t_3 . (B) The injection times are used to slice the original signal into multiple individual chromatograms by the computer. (C) They are then aligned on a two-dimensional plane with the primary retention on the X axis, the secondary retention on the Y axis and the signal intensity as the Z axis. (D) Color-coded spots create a visual representation of peaks when viewed from above. Reprinted with permission from Ref. [2].

1.1.5 Two-dimensional column selection & detectors

Many of the components used with traditional one-dimensional gas chromatography can also be used for two-dimensional analysis. With the appropriate components, essentially any GC analysis can be converted to a two-dimensional analysis. One of the main factors that must be considered when trying to achieve a GC×GC separation is the column selection. Two columns with differing stationary phases must be chosen that will allow the ¹D separation to be preserved and further enhanced within the second dimension. One of the benefits of employing orthogonal stationary phases is the structured nature of the two-dimensional chromatograms. This feature is extremely beneficial for homologous compounds, which elute in similar regions, but do not have known standards for positive identification. There are two types of column set-ups, often referred to as “normal” and “reverse”. In the normal setup, the first dimension column is coated with a non-polar stationary phase, such as 100% polydimethylsiloxane (PDMS) or 95%/5% methyl/phenylpolysiloxane. These characteristics allow for a ¹D separation based on volatility (for non-polar compounds only). The second-dimension column is customarily coated with a more polar stationary phase, such as 50%/50% phenyl/methyl or a polyethylene glycol-based phase. This allows the ²D separation to be based primarily on analyte polarity. In the reverse setup, the polar stationary phase is the first dimension, while the non-polar phase is the second dimension. Recently, M.S. Klee *et al.* showed that having the same inner diameter for both the ¹D and ²D would enable the highest ²D peak capacity [16]. Internal column diameter of 0.25 mm was also shown to be the smallest diameter to achieve acceptable sharp reinjection pulses.

The fast nature of the ²D separation results in narrow peak widths at the baseline, 100 milliseconds or less, which require a detector with a high data acquisition rate to ensure the two-dimensional chromatogram can be properly reconstructed [14]. Flame-ionization detector (FID)

was the first detector applied to a GC×GC analysis due to its ability to detect the fast, narrow peaks eluting off the ²D [3]. With acquisition rates up to 500 Hz, FID is a very logical choice that is extremely robust, user friendly, reliable with good sensitivity and a wide linear dynamic range. These characteristics make this detector an ideal choice for quantitative analysis. However, this detector lacks the selectivity and structural information that a mass spectrometer can provide. In order to properly identify unknown compounds, authentic standards are required to compare both ¹D and ²D retention times.

Other detectors such as an electron capture detector (ECD), sulfur chemiluminescence detector (SCD) and nitrogen chemiluminescence detector (NCD) have also been used for specialty applications. As a selective and sensitive detector towards halogenated compounds, an ECD is extremely popular for the analysis of environmental samples. The μ -ECD has a reduced internal volume of 150 μ L and an acquisition rate of 50 Hz, making it a suitable detector for GC×GC. The SCD and NCD are sensitive and selective to sulfur and nitrogen compounds, respectively. However, the rather large internal volume and slow response of both detectors may lead to broad peaks when coupled with GC×GC [17, 18].

A detector that has been more recently coupled with GC×GC is the vacuum ultraviolet (VUV) detector, which can collect VUV absorption data between 115-240 nm [19]. The detector offers higher sensitivity when compared to classical UV detection, and provides structural and isomer-selective information [20]. In combination with the structured order of a GC×GC chromatogram, the VUV detector offers group-specific spectral information for the determination of compound classes [20]. The VUV detector can provide complementary information on isobaric compounds to supplement the structural information from a mass spectrometer, ultimately making identification easier.

A mass spectrometer (MS) is the most informative detector for GC×GC due to its ability to provide structural information. Software assists in performing deconvolution of spectra of unresolved peaks, allowing the system to be used for a wide range of analytes and applications. Amongst the many possible MS detectors, the time-of-flight mass spectrometer (TOFMS) is the most common in this type of analysis [21]. With the acquisition rate of up to 500 spectra per second, it has the ability to produce a full spectrum for every pulse of ions from the source [3]. With the high data acquisition rate, spectral deconvolution and high sensitivity, low-resolution TOFMS has proven to be a vital tool in combination with GC×GC. A high resolution TOFMS (HRTOFMS) provides higher resolution and mass accuracy when compared to the low-resolution TOFMS, but at the cost of a reduced data acquisition rate. Despite lower acquisition speeds of 200 Hz, the HRTOFMS provides the opportunity to analyze highly complex samples. Single quadrupole and triple quadrupole mass spectrometers have also been used with GC×GC, however, each has its limitations. Older models of single quadrupole mass spectrometers (QMS) did not have the necessary acquisition speed for quantitative analysis. In order to couple a QMS with GC×GC, a compromise between the mass range and acquisition rate is required. For a wider mass range, a low acquisition rate is needed; conversely, when a narrow mass range is used, a higher acquisition rate can be used. With the development of more advanced designs, rapid-screening QMS are commercially available that can generate an acquisition speed over 30 Hz. The greatest advantage of the QMS is the lower instrument cost when compared to the LRTOFMS.

1.2 GC×GC modulators

As the key component within a GC×GC instrument, the modulator quickly evolved after its inception, but there are several recent developments to improve the design. Overall, modulators can be divided into three basic categories: thermal, valve and flow-based. Thermal modulators can be further separated into heater-based and cryogenic-based. Heater-based interfaces rely on collecting analyte bands from the ¹D at or slightly below the oven temperature, and then releasing them through an increase in temperature. Cryogenic based interfaces rely on collecting analyte bands at very low temperatures with the use of cryogenics, and then releasing them at or slightly above the oven temperature. Valve-based interfaces utilize a short collection loop to collect fractions of the ¹D column effluent, which are subsequently flushed onto the head of the ²D column. They can be classified as flow diversion or low duty cycle platforms. Flow-based interfaces are similar in design to valve-based, however, two independent carrier gas flows are coupled to perform modulation. These platforms are classified as differential flow, flow switching or full transfer.

1.2.1 Thermal modulation

To achieve effective trapping and remobilization of the analytes, the retention factors are altered. In thermal modulator platforms this is achieved by heating and/or cooling, in relation to the GC-oven temperature. Historically, trapping of analytes has been achieved using a thick stationary phase, intense cooling, or a combination of both. The greatest advantage of thermal modulation over valve and flow-based modulation is the focusing effect. Thermal modulation focuses analytes in space, not in time, during trapping to create very narrow re-injection bands on the head of the ²D column. This focusing effect results in a reconcentration of the analyte bands during the trapping phase for an order of magnitude gain in S/N [22]. In order to maintain

the narrow reinjection bands, rapid remobilization of the trapped analytes is necessary. This is achieved through direct heating or rapid equilibration with the GC oven temperature possible due to the low thermal mass of capillary columns. Without these remobilization techniques, the focusing effect could be lost due to band broadening.

1.2.1.1 Heater-based interfaces

Phillips introduced and implemented the first two-stage thermal desorption modulator (TDM) in 1991 [6]. The design included a segment of a column coated with electrically conductive gold paint that was placed in between the ¹D and the ²D (Figure 1.5). This interface was looped outside the oven to remain at room temperature. Electrical leads (1, 2, and 3) were placed on the column to supply electric current to either stage one (leads 1 and 2) or stage two (leads 2 and 3) of the interface.

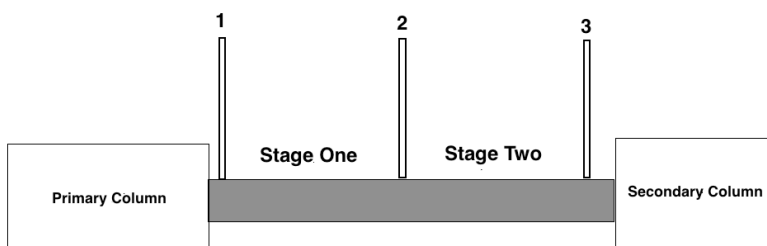


Figure 1.5 Schematic of thermal desorption modulator, based on reference [6].

As the ¹D effluent entered the coated segment of the ²D column, the stationary phase kept at ambient temperature would trap the analytes. Electric current was then applied to stage one to rapidly heat the capillary to force the analytes out of the stationary phase and into the carrier gas to be swept downstream and be trapped again. As this occurred, stage one would have cooled down to continue trapping, and the second stage was heated to inject the trapped analytes as a

narrow band to the ²D column. Even though this interface was revolutionary in providing the very first truly comprehensive GC×GC analysis, the gold paint was not robust and required constant replacement.

In 1996, Phillips and Ledford presented a new design of a so-called “rotating thermal modulator” (RTM) [23]. It was commercialized in 1999 [24]. This first commercially available modulator was known as the ‘sweeper.’ As analytes exited the ¹D column, they would accumulate within the thick stationary phase of the modulator capillary. Computer control would engage the RTM cycle by causing a slotted heater to begin to rotate. The heater was typically kept at least 100 °C above the GC oven temperature when it would move over the upstream portion of the capillary. By rapidly heating a zone that moved along the capillary at the speed of the heater’s rotation in the direction of the carrier gas, the trapped analytes would be forced into the carrier gas. This moving heating zone created a thin slice of analytes that would be trapped and refocused again within a section of the capillary that was not yet exposed to the rotating heater. With each continuous rotation, the moving heat zone drove the focused bands into the ²D. The high temperature differential required for the heater made the analysis of high boiling point analytes difficult because the oven had to be kept at a temperature lower by 100 °C than the upper limit of the columns used. Under specific conditions the modulator could be used for an analysis range between C₄ and C₄₀, but typically it was limited to 100 °C below the oven temperature [25]. The rotating thermal modulator is now considered inferior and is no longer commercially available.

1.2.1.2 Cryogenic-based interfaces

Unlike the TDM and RTM, cryogenic interfaces rely on cryogens in order to trap analytes eluting from the 1D at temperatures far below that of the GC oven. Marriott applied this theory to his longitudinally modulated cryogenic system (LMCS), the first cryogenic modulator [26]. The interface included two steel tubes of differing lengths in which the inside diameters formed a cavity for the cryogen to be pumped in and out. Liquid carbon dioxide (CO_2) was then pumped through the trap while compounds were being eluted off of the 1D . In order to release the trapped analytes as a focused band, the cryotrap was moved upstream, allowing the cooled capillary to return to oven temperature. For proper modulation, the trap was moved longitudinally along the column towards the detector to trap analytes and then away from the detector to release the focused band of analytes (Figure 1.6). Arguably the biggest innovation in modulator technology since the RTM, the LMCS proved to be a superior interface in many ways. Despite the benefits, the LMCS used moving parts and did not use the cryogens in an efficient manner.

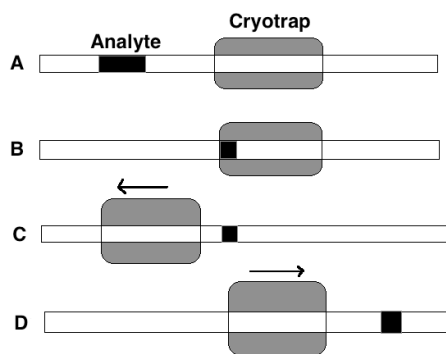


Figure 1.6 Schematic of longitudinally modulated cryogenic system, based on reference [25].

To alleviate the downfalls of the LMCS, several different cryogenic designs emerged between the years of 2000 and 2003. Ledford first presented the two-stage, dual jet liquid nitrogen and heated air system in 2000 at the 23rd International Symposium on Capillary

Chromatography (ISCC) [27] (Fig. 1.7). In order to trap and focus the analytes, two cool jets alternately directed nitrogen gas cooled with liquid nitrogen (N_2) onto the inlet of the 2D column. To remobilize the trapped analytes, two hot jets would alternately heat the previously cooled spots to reinject the trapped compounds into the 2D as narrow pulses. Zoex Corporation commercialized the quad-jet dual stage liquid nitrogen modulator. LECO Corporation also commercialized this design with a secondary oven under license from Zoex Corporation, which is still sold with the GC \times GC-TOFMS system. A consumable-free model is also available, which uses a closed loop chiller instead of liquid nitrogen to cool the heat exchanger [62].

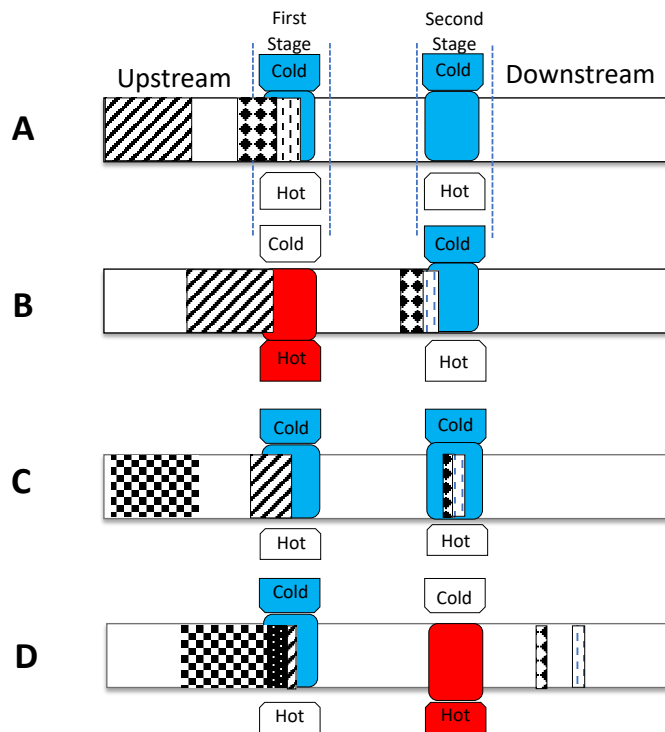


Figure 1.7 Schematic of the two-stage, quad jet cryogenic modulator, based on Ref. [26]. (A) As the analytes elute from the 1D , the upstream cold jet would trap and focus them in the first trapping stage. (B) The upstream hot jet would then initiate, remobilizing the trapped analytes to the second stage where the downstream cold jet would focus the band of analytes. (C) The upstream cold jet would activate to trap the next fraction of analytes. (D) The downstream jet would remobilize the band of analytes focused in the second stage, injecting them into the 2D for further separation.

Despite achieving comparable modulation with no moving parts, drawbacks still occurred in this new design. The cost of the cryogenic agent, liquid N₂, was the biggest disadvantage. Only a year later in 2001, Beens *et al.* developed a similar design that used a simple, dual stage cryojet system with no moving parts [28]. Instead of nitrogen, liquid CO₂ was used within the cool jets, and no hot jets were included. Two jets would alternately spray a stream of liquid CO₂ onto small segments of the ²D column, cooling the effluent from the ¹D to form narrow pulses. The surrounding hot oven air would then heat the column to reinject the band into the ²D once the cold jet was shut off. Overall, the design struggled with stability and robustness due to the high flow of cold CO₂ sprayed directly onto the column and rather large CO₂ consumption. Harynuk and Górecki were amongst the firsts to develop a cryogenic based modulator with no moving parts [29]. The interface used Silcosteel capillaries, housed within a cryochamber that was cooled with liquid N₂. The cryogenic agent would trap and freeze the analytes eluting from the ¹D. Resistively heating the Silcosteel capillaries would reinject the analytes into the second dimension in either single or dual stage modes. With proper placement of the cryogen nozzle and appropriate heating pulse, very narrow injection bands were achieved [28].

Ledford would further improve upon the quad jet, dual stage modulator by designing a loop modulator, which was presented in 2002 at the Pittsburgh Conference on Analytical Chemistry and Applied Spectroscopy (PITTCON) [30] (Fig. 1.8). This modulator employed a delay loop between the two cold stages of modulation formed by a single cold jet. As the ¹D effluent reached the first cold stage, the cold jet trapped the analytes momentarily. The hot jet then released the analytes into the delay loop. As the effluent reached the end of the delay loop, the cold jet was activated again to trap the analytes in the second cold stage. The hot jet was turned on again to release the refocused, narrow band to the ²D. The cold jet remained on during

the entire analysis, while the hot jet deflected the cold jet from the delay loop. Optimization had to be performed for the length of the loop and velocity of the carrier gas for each modulation period [30]. This design is also commercially available with liquid nitrogen cooling or as a consumable free model, which uses a refrigeration unit [63].

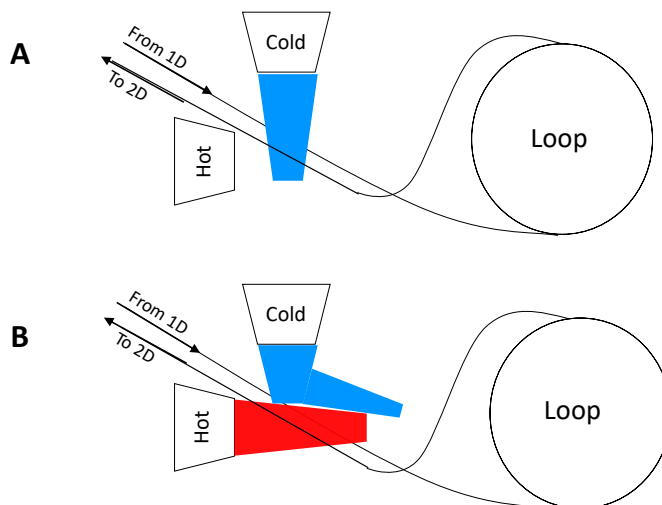


Figure 1.8 Schematic of the dual jet loop modulator based on Ref. [29]. (A) The cold jet ran continuously, providing two cold spots, one in the upstream and one in the downstream portion of the loop. (B) The hot jet was initiated intermittently, temporarily diverting the cold jet away from the loop and heating the cold spot to remobilize the trapped analytes.

Harynuk and Górecki developed another cryogenic system based on the loop interface by Ledford [31]. A delay loop with a single jet was used to achieve dual stage modulation. The main goal of this design was to deliver liquid N₂ rather than cooled nitrogen gas to the jet that could be turned on or off quickly, while also decreasing the consumption of liquid N₂. As the analytes exited the ¹D, they entered a deactivated fused silica capillary. Alternating cold and hot jets would trap and launch the analytes into the delay loop and eventually the ²D. A system of two cryogenic solenoid valves was used to help consistently deliver liquid N₂ to the jet, with excess liquid nitrogen recycled back to a Dewar. With the liquid N₂ cooling, this interface could

trap propane in a deactivated capillary for one minute without breakthrough. For the analysis of volatile organic compounds (VOCs), liquid N₂ was superior due to its ability to reach significantly lower temperatures when compared to liquid CO₂ or cooled N₂. Harynuk and Górecki were also able to minimize the daily consumption of liquid N₂ to about 30 L per day, but the operational cost of the modulator still remained rather high.

1.2.1.3 Other thermal interface designs

In order to appeal to the growing field and further popularize the use of comprehensive GC×GC analysis, the instrumentation needs to be robust, simple, affordable without any consumables and applicable to a wide range of analytes. Further development of interfaces without the need of expensive consumables would be the most effective way to make the comprehensive technique more affordable for industrial and routine laboratories. More recent developments in heater-based and flow-based interfaces have led to promising techniques that require no consumables and have wide applicability. Kim *et al.* was able to miniaturize a dual stage thermal based modulator (Figure 1.9) for use in micro-GC x micro-GC (μ GC x μ GC) [32]. Voltage to microheaters attached to the top portions of the microchannels provided the heat necessary to allow the transfer of the analytes. Thermoelectric cooling (TEC) throughout the entire analysis rapidly cooled and trapped the analytes while also preventing breakthrough of the analytes during desorption. Alternating the cooling and heating allowed the analytes to be first trapped, then desorbed and refocused again within the second trapping stage. This ensured the analytes were injected into the 2D as a narrow, focused band. Ultimately, it was successful in trapping VOCs at low temperatures without the use of expensive consumables. Serrano *et al.* was the first to implement the micro-thermal modulator (μ TM) and perform a comprehensive

GC×GC separation [33]. The μ TM was able to produce fast GC×GC separations without the use of consumables such as cryogenic fluids. [33].

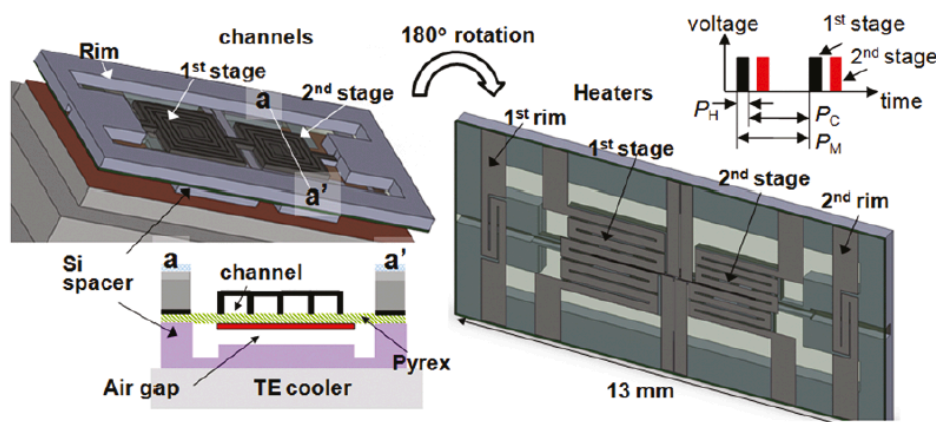


Figure 1.9 Schematic of a miniaturized dual stage thermal modulator for μ GC x μ GC [31].

Originally introduced in 2016 as the thermal independent modulator (TiM) [34], J&X Technologies now commercially produces the Solid State Modulator (SSM), as seen in Figure 1.10 [35]. The modulator platform operated outside the GC oven and featured thermally independent heating and cooling zones. Micathermic heaters allowed temperature programming from ambient to greater than 350 °C for remobilization within the two aluminum heating chambers (entry and exit zones). A pair of three-stage thermoelectric coolers allowed temperature programming from -50 °C to 50 °C within the trapping zone. The entry and exit hot zones were connected to the cold zone with a copper tube. To ensure the zone operated in an independent manner, the cold zone contained an insulation septum, placed snugly on the enclosure wall. Two separate copper tubes, located in the entry and exit hot zones, transferred the ends of the modulation column into the GC oven to connect the 1D and 2D , respectively. Dual stage modulation was achieved by mechanically moving the modulator column back and forth in a similar principle to the LMCS system. However, instead of moving the cold trap along the column, like in the LMCS system, the modulation column moved in and out of the cold zone.

Actuation of a solenoid valve swung a column gripper left and right to drive the column back and forth between the hot and cold zones by 30 mm. A graphite roller was placed in each heating chamber to facilitate the movement of the modulation column and reduce the wear of the polyimide exterior coating. As the analytes eluted off the ¹D, they were trapped in the segment of column exposed to the cooled zone. As the modulator column moved into the entry hot zone, the analytes were remobilized due to the elevated temperature. With this movement of the modulator column, the downstream segment was exposed to the cooling zone. As the remobilized analytes traversed the modulation column, they were exposed to the cooling zone and trapped during the second stage. Movement of the modulator column towards the exit zone exposed the previously trapped analytes once again to an elevated temperature for injection into the ²D. Simultaneously, the upstream portion of the modulation column was exposed to the first stage of trapping once again. The entry hot zone was set at a lower temperature than the exit hot zone to prevent the possibility of analyte breakthrough. The modulator column consisted of two pieces of capillary connected with an SGE Siltite μ -Union. The front half (placed within the entry hot zone) was coated with a proprietary phase, while the back half (placed within the exit hot zone) was uncoated. This design was to prevent peak broadening of the analyte bands, as well as improve the bandwidths within the second dimension. This modulator platform has four series of modulator columns available based on various boiling point ranges in order to choose accordingly to the specific application and analytes of interest. The four options include EV, HV, SV and DV columns. The EV series has a modulation range from C₂ to C₁₂, which is suitable for volatile organic compound analyses. The HV series has a modulation range between C₅ to C₃₀, which is applicable to fragrances/allergens, petrochemical and organic environmental pollutant analysis. The SV series covers the range from C₇ to C₄₀, while the DV series ranges from C₉ to

C₄₀₊. Both of these modulator columns are applicable for mineral and crude oils, PAHs and pesticides. As a consumable-free system, the SSM provided a viable option for a wide variety of analyses. However, the movement of the modulation column requires maintenance due to the possible breakage that could occur after successive modulation periods. The graphite rollers used as column guides within the heating zones require replacement after every 100,000 modulations. The movement of the modulation column also limits the lifetime of the column to approximately 500,000-1,000,000 modulations, which requires users to change the column for preventative maintenance.

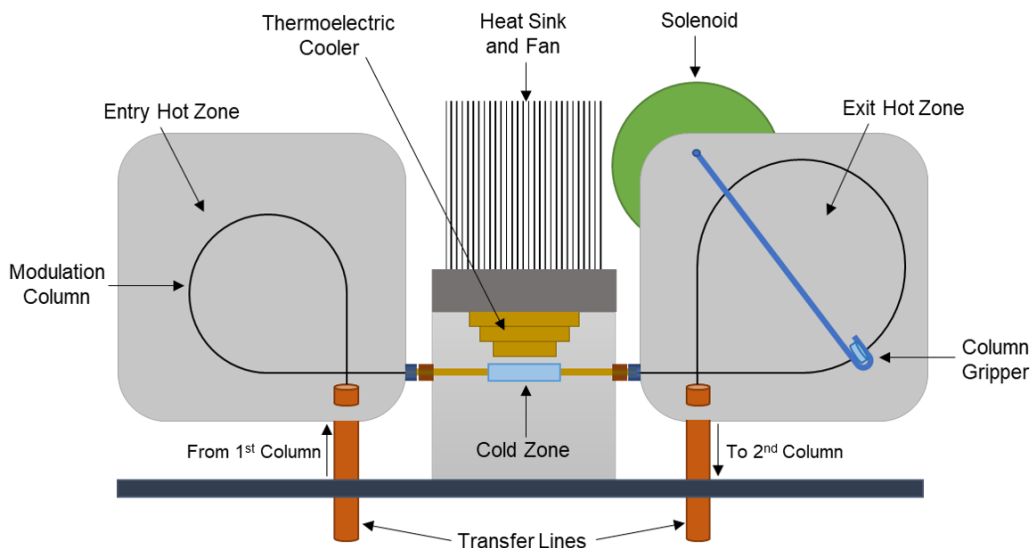


Figure 1.10 Schematic of the Solid-State Modulator, based on Ref. [34].

The Górecki group has developed several different designs of a consumable-free thermal modulator, which will be further elaborated on in detail in Section 1.3.

1.2.1.4 Thermal modulation optimization

When optimizing a GC×GC separation, the type of modulator platform can directly affect the resolution in both dimensions. The width of the reinjection band produced by the modulator affects the maximum peak capacity increase achievable, so careful consideration is needed [16]. While each design is unique, the main optimization component of all thermal modulators is the modulation period. For the majority of commercially available thermal modulators, optimization tools or recommendations are provided. Simply GC×GC, a free online tool from the LECO Corporation, allows users to optimize a GC×GC method based on the parameters of their Pegasus instruments [36]. Other platforms must rely on altering the temperature offset for the heating and/or cooling, along with the modulation period to achieve an adequate GC×GC separation.

As previously discussed in Section 1.1.3, the modulation ratio directly affects the number of times a peak from the ¹D is sampled. A shorter modulation period results in a greater possibility of peak wrap around; however, a longer modulation period can significantly degrade the preservation of the ¹D separation. Peak wraparound can possibly disrupt the structure of a two-dimensional chromatogram, but as long as the analytes elute within the void time of the second dimension, the structure is not affected. The void time is the unused space within the second-dimension chromatogram which is determined by the dead time of the least retained compound in ²D. This space can be used for further separation of compounds, in which case wraparound is not necessarily a negative when performing method optimization.

For thermal modulator platforms that employ a temperature offset and hot pulse for a specific duration of time, such as the quad jet thermal modulator from LECO, it is important to optimize these parameters for an optimal separation. For quick and efficient remobilization, the

temperature offset is vital to the release of the analytes from the trapping phase within the modulator. When the temperature offset is too low or too high, the remobilization can be greatly affected. In the prior situation, high boiling compounds may be inefficiently injected onto the head of the ²D column. In the latter case, the separation between analytes in the second dimension can be reduced due to the increased temperature in the ²D [3]. The injection efficiency and trapping performance can be affected by the duration of the hot pulse for the high boiling and low boiling compounds, respectively. The timing of the hot pulse and correspondingly cold pulse are directly related to one another, equaling half of the modulation period. When the hot pulse timing is increased, the cold pulse time must be reduced. There must be a balance between the hot and cold pulse timing. The hot pulse must be long enough to efficiently remobilize the high boiling point analytes into the ²D, while not reducing the cold pulse to a time that would insufficiently trap the low boiling point compounds. Very short hot pulses have been found to degrade the separation achieved in the first dimension [37].

Interfaces that employ a delay loop, such as the Zoex dual jet loop modulator, require optimization of the delay loop length, which must provide a delay longer than the period required to cool and heat the modulation area [38]. This is to prevent analyte breakthrough so the remobilized analyte from the first cold zone does not reach the second modulation stage before the second cold zone is restored. Thus, the length of the delay loop is dependent on the linear velocity of the carrier gas through the delay loop [38]. With these considerations it is clear there is a necessary minimum length of the delay loop; however, if the loop is too long, the analytes may reach the second modulation stage during the desorption phase. Thus, the analytes will reach the ²D without refocusing. This can also occur when the modulation period is adjusted.

When compared to the quad jet platforms, the dual jet delay loop platforms require thorough optimization that can be difficult when changes are made to the instrumental setup.

J&X Technologies provides a GC×GC flow calculator to assist in performing method optimization when utilizing the SSM [39]. The program allows for all chosen parameters to be entered including the carrier gas, pressure unit, initial oven temperature, all dimensions of the ¹D and ²D (length, inner diameter and film thickness), detector type and dimensions of any transfer lines to detector(s). The pressures at the inlet and connections, as well as the ¹D and ²D hold up times are then calculated for the user. The final equivalent ¹D length from the inlet to the detector is also determined in order to be entered into the GC method for proper operational flows and pressures. For insufficient primary dimension separation, it is recommended to lower either the oven temperature ramp rate, lower ¹D flow rate, lower initial oven temperature, increase the ¹D length or increase the ¹D film thickness. If excessive wraparound occurs, the ²D flow rate can be increased by introducing an auxiliary flow or the modulation period can be increased. The ²D length could alternatively be decreased. The ²D stationary phase may also not be an appropriate choice if excessive wraparound or insufficient ²D separation occurs. Also, the ²D length can be increased to assist in achieving sufficient ²D separation. J&X Technologies also provides their users with recommended GC×GC methods and parameters for a variety of instrumental setups.

1.2.2 Flow & valve-based modulation

Both flow and valve-based modulators typically operate in two modes, a divert and inject mode. The divert stage can be used to store sampled analytes from the ¹D effluent or send an excess effluent to an exhaust line. The inject mode is used to send the sampled fractions of ¹D effluent onto the head of the ²D column for further separation. These interfaces may seem to

have similar operating principles; however, the possible paths the ¹D effluent might take during the divert stage differ with each platform. When most of the ¹D effluent is directed to an exhaust pathway during the divert stage, ultimately never reaching the ²D, the modulator is considered low duty cycle [40]. On the other hand, when the ¹D effluent is directed to be stored during the divert stage, which is then subsequently injected onto the ²D during the inject stage, the modulator is considered a full transfer model [40]. Flow diversion modulators are inherently low duty cycle platforms, while differential flow modulators are full transfer models. As a low duty cycle platform, flow diversion modulators direct only a small portion of the ¹D effluent to the ²D column, whereas differential flow modulators are full transfer due to the complete transfer of the ¹D effluent to the ²D, sampling all analytes [41]. There has been deliberation on whether low duty cycle valve modulators qualify as comprehensive due to their operational mode of sampling only small portions of the ¹D effluent. However, a consensus was reached that as long as enough of the ¹D effluent is sampled to be representative of the sample, then the technique can be considered comprehensive [2]. Due to the differing operational capabilities, it is clear that the differential flow, full transfer modulators have an advantage of sampling the entire ¹D effluent before reinjection onto the ²D column. Thus, trace analysis is easier. However, in order to achieve full transfer modulation, high ²D flows are necessary, leading to elevated pressures and difficulties with evacuated detectors, such as a mass spectrometer [41]. Typically, a splitter is implemented to split the excess ²D flow between an FID or ECD and a mass spectrometer. On the other hand, a low-duty cycle, flow diversion modulator can be directly coupled to an evacuated detector, such as a mass spectrometer, without the need for effluent splitting [40]. Despite this clear advantage over differential flow, full transfer platforms, these modulator platforms are not well suited for trace analysis [42].

1.2.2.1 Flow & valve- based interfaces

Flow-based interfaces were rather different from heater and cryogenic based interfaces in that they used valves to periodically vent the majority of the ¹D effluent, while a small fraction of it was injected into the ²D column. Bruckner *et al.* successfully applied the first valve-based interface, the diaphragm valve modulator (DVM), to GC×GC analysis in 1998 [43]. A 6-port diaphragm valve was placed within the oven between a wide-bore, PDMS coated ¹D and narrow bore, polyethylene glycol coated ²D column. Only 4 of the 6 ports of the valve were used to operate in two states: (1) sampling and (2) venting. In the sampling mode, the diaphragm was activated twice per second for a short time to allow a small fraction of the effluent from the ¹D to travel to the ²D. The venting mode occurred while the separation took place within the ²D. This mode simply vented the rest of the ¹D effluent into the atmosphere. Due to the rapid activation of the diaphragm, narrow peaks of ¹D effluent entered the ²D column; however, 80 to 90 % of the sample was vented into the atmosphere, resulting in significant analyte loss. Since only about 10 % of the ¹D effluent was sampled, this interface was unsuitable for trace analysis. The valve modulator also had severe thermal limitations so only VOCs could be analyzed efficiently.

A few years later, Seeley *et al.* developed an interface which used all 6 ports of a diaphragm valve [44]. The differential flow modulator (DFM) was based on the same concept as the DVM, but it was capable of transferring a significantly larger amount of the ¹D effluent to the ²D. All ports of the valve were used through the addition of a sampling loop that was kept outside the oven and maintained hot by heater blocks. This design also involved two different stages: (1) collection and (2) injection (Figure 1.11). The sample loop was filled by the ¹D effluent before being vented into the atmosphere. As the collection of the effluent was completed, it was physically compressed before entering the ²D by high flow of carrier gas from

an auxiliary source. The high flow in the ²D produced a narrow injection band allowing a fast separation to occur, but required a long ²D column.

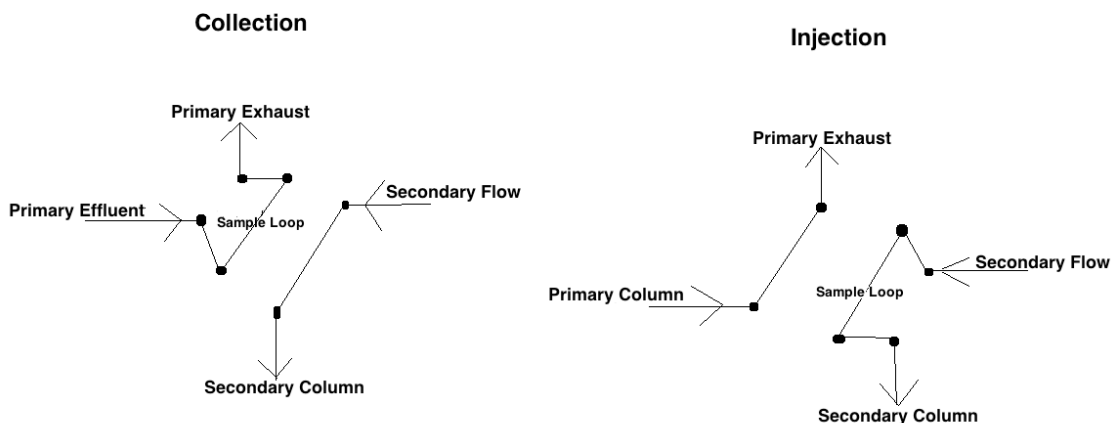


Figure 1.11 Schematic of the differential flow modulator, based on reference [43].

Despite the increase in transfer efficiency, the thermal limitations were not resolved in this design. Seeley *et al.* later developed a flow switching modulator that contained no valves within the oven and was made of materials suitable for a wider range of temperatures [45]. This interface was also the first flow based one to enable 100% transfer from the ¹D to the ²D due to the removal of the ¹D effluent vent. This revolutionary design is now known as the pulsed flow modulator.

The simple fluidic modulator was introduced by Seeley *et al.* as an alternative to the flow switching platform in 2006 [46]. The design included two stainless steel tee unions, deactivated fused silica tubing and a three-port solenoid valve, which was positioned outside the oven. To connect the outlet ports of the valve to the tee-unions, a 250 μm ID fused silica tubing was used. The normally closed and normally open ports of the valve were connected to the upper and lower tee union, respectively. A sample loop, constructed of a 15 cm x 450 μm ID piece of fused silica

capillary tubing, connected the two tee unions. The ¹D effluent entered the modulator interface at the upper tee union, while auxiliary flow of the carrier gas (20 mL/min) entered at the common port of the valve. Modulation occurred in two stages: fill and flush, as seen in Figure 1.12. In the fill state, the primary effluent was directed toward the bottom union. Analytes were collected within the sample loop as the ¹D effluent flowed from the top union to the bottom union. Prior to the effluent reaching the bottom union, the valve was actuated to begin the flush state. To flush the contents of the sample loop onto the ²D column, auxiliary carrier gas traveled from the top union to the bottom union with a substantially greater flow than that employed in the ¹D. The pressure pulse from the actuation of the valve also caused the flow of the carrier gas at the outlet of the ¹D to momentarily stop, or even slightly reverse, which prevented breakthrough. Compared to previously developed diaphragm valve modulators, the simple fluidic platform provided similar two-dimensional separations with a wide temperature range while maintaining optimal performance over a wider range of differential flow ratios. With a simple design that was easy to implement, the modulator would eventually lead to several future designs [47].

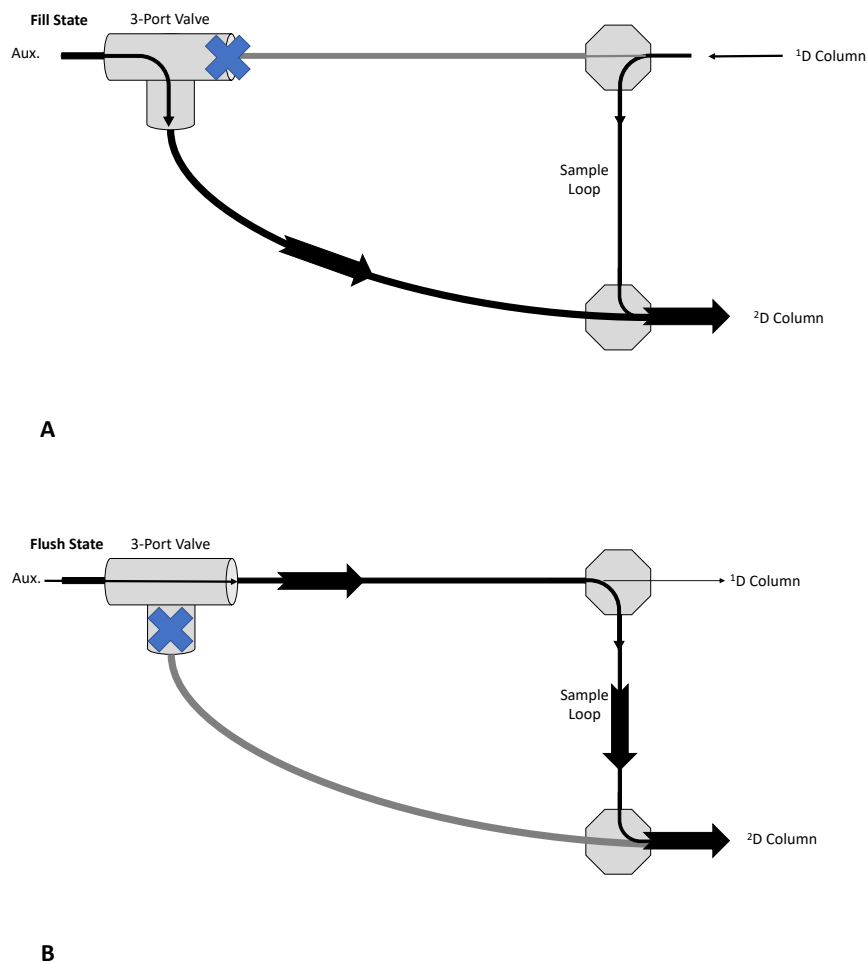


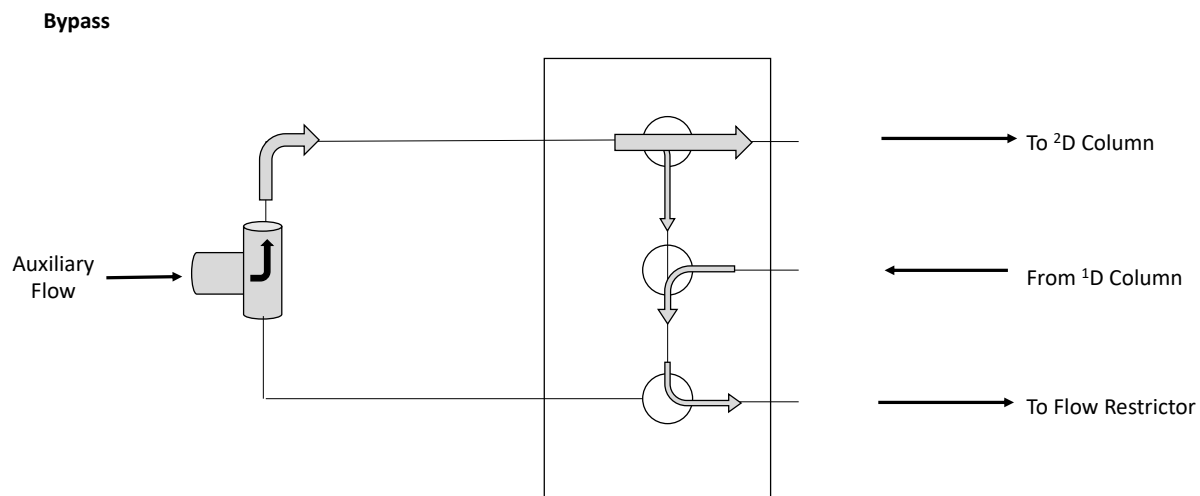
Figure 1.12 Schematic of the simple fluidic modulator. The fill state (A) and flush state (B) are displayed. Based on Ref [45].

In 2007, a Deans switch was implemented by Seeley as a low-duty or flow diversion modulator [41]. Originally introduced in the 1960's by David Deans, the platform used a microfluidic flow switching device to perform heart cutting to transfer a few select groups of compounds from the ¹D to the ²D [48]. To complete the Deans switch modulator, a three-port solenoid valve was added to the standard Agilent microfluidic Deans switch five-port manifold. The manifold was placed within the GC oven, while the solenoid valve was placed outside of it. Modulation was completed in two stages by either directing the ¹D effluent to the ²D or to a flow

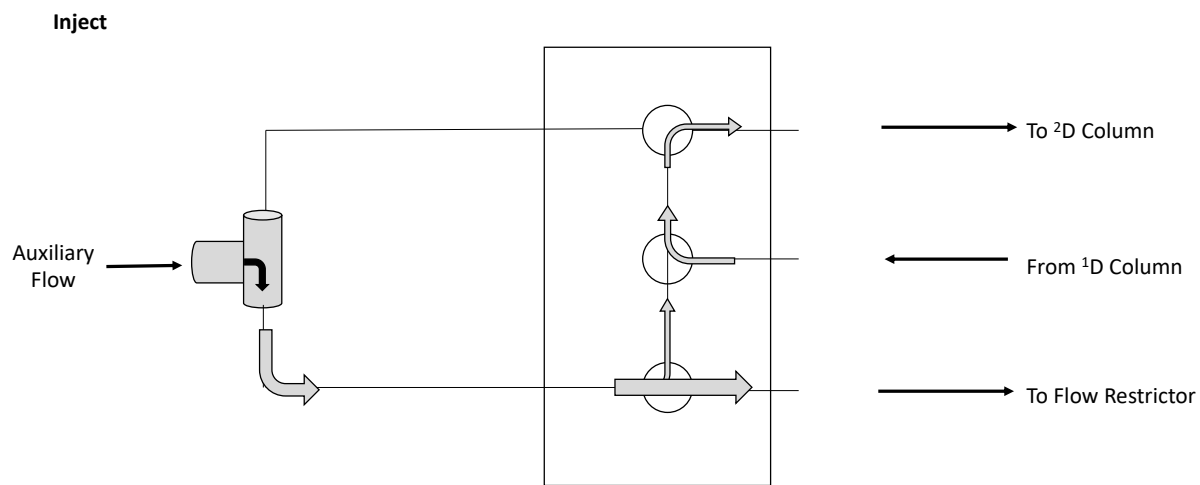
restrictor. The flow restrictor consisted of an uncoated deactivated fused silica column with the same length and internal diameter as that of the ²D column. The solenoid valve provided an auxiliary carrier gas to either of the two outer ports to determine the state of the modulator, as seen in Figure 1.13. In the “bypass” state, the ¹D effluent was directed towards the flow restrictor, while the auxiliary flow was directed to the end of the manifold connected to the ²D where it was split, with a fraction exiting through the ²D column and the rest combining with the ¹D effluent to exit through the flow restrictor. With actuation of the solenoid valve, the “inject” state was initiated. The auxiliary flow was directed towards the flow restrictor end of the manifold in which the flow was split, with a part exiting through the flow restrictor and the rest combining with the ¹D effluent to enter the ²D column. Similarly to Seeley’s previous fluidic design [46], an auxiliary flow greater than that of the ¹D flow was needed for proper operation. However, since it was a low-duty cycle modulator, only a small portion of the ¹D effluent was sampled, resulting in a signal intensity decrease. This had the greatest consequences for trace analysis. Despite the shortcomings of the low-duty platform, the Deans switch was able to produce GC×GC chromatograms that were somewhat similar to those produced by thermal and differential flow modulation. The wide injection bands, limited length of the modulation period and low intensity of peaks hindered the Deans switch from achieving analogous separations to thermal and differential flow platforms. Analyses could be performed over a wide range of temperatures, making it suitable for semi-volatile compounds.

The advantages of the Deans switch were explored by several commercial manufacturers to further advance the technology for new designs that could be used for heart cutting and back-flushing purposes. By expanding upon the pre-existing capillary flow technology (CFT), Agilent Technologies produced a device created by photolithography and diffusion bonding techniques

to integrate all junctions and conduits inside a single inert metal base [49]. The updated design provided low void volume, no moving parts, non-contact switching, high-temperature and leak-free operation, and a high degree of inertness through a deactivation/passivation process [49]. SGE Analytical Science-Trajan also produced a micro-fluidic platform available as SilFlow [49]. The chemically deactivated stainless steel micro-fluidic plate featured low dead volume, very high maximum temperature operation, high pressure capability and low thermal lag [49].



A



B

Figure 1.13 The two states of the Deans switch modulator are (A) bypass state and (B) inject state. Based on Ref [39].

Harynuk and Górecki introduced stop flow modulation in the hopes of removing the compromise between first dimension resolution and second dimension separation time. This interface was designed to stop the flow within the ¹D column to allow the separation within the second dimension to reach completion [50]. An air-actuated, six-port valve was used in order to allow the second-dimension separation of the ¹D effluent to occur independently of the length of the trapping stage. A single-stage liquid nitrogen cryojet was placed downstream of the trap to focus the components of the ¹D effluent before subsequent injection onto the ²D. Independent adjustment of the ¹D sampling time and the overall length of the modulation period helped accomplish an optimal separation. Long, efficient ²D columns could be used to increase the separation power of the analysis. By increasing the length of the ²D separation without reducing the ¹D sampling frequency, the ¹D separation was preserved. Wraparound peaks were eliminated with the use of this modulator due to the longer time allowed for the separation within the ²D. Despite the many benefits of this design, it was a rather complicated setup and required long analysis times. To further improve the stop-flow modulator, a pneumatic pressure switch was used in place of mechanical valves [51]. The removal of the in-line valves improved the robustness of the interface and eliminated temperature limits and artifacts related to the valves. Despite the clear advantages of the stop-flow technique, the approach was not widely adopted, most likely due to the added complexity and longer overall analysis time. However, the idea of momentarily stopping the flow in ¹D to accomplish modulation forms the basis of operation of the simple fluidic modulator.

Wang *et al.* developed a valve-based differential flow modulator that used two four-port, two-position switching valves that were activated electronically [52]. The author described the two stages as X and Y (Figure 1.14). In stage X, ¹D effluent entered the first valve and traveled

down a transfer line to the second valve. If the transfer line volume was exceeded, the effluent would be vented to the atmosphere and auxiliary flow would enter the second valve to sweep through the opposite transfer line, flushing its content into the ²D. Stage Y began when the valves were activated into their second position. The ¹D effluent from the transfer line would be flushed into the ²D by auxiliary flow, while the effluent leaving the ¹D would fill the opposite transfer line. Again, when the transfer line reached maximum volume, excess flow was vented to the atmosphere. Overall, 100% transfer occurred from the ¹D to the ²D and the valves were capable of withstanding temperatures of up to 350 °C. This design helped expand the range of analytes that could be analyzed by valve-based modulators.

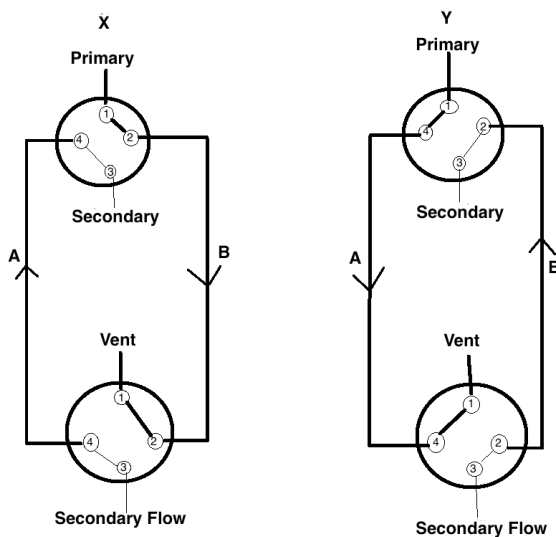


Figure 1.14 Schematic of valve-based differential flow modulator, based on reference [51].

1.2.2.2 Other flow and valve designs

The high gas flows required in the second dimension of flow-based modulators have been a constant issue. In order to address this problem, Tranchida *et al.* implemented a reduced gas flow modulator [53]. Despite the significant decrease from about 20 mL/min to about 6-8

mL/min, this system efficiently re-injected analytes into the second-dimension column by lengthening the re-injection stage (flush time) in combination with a long accumulation loop. With reduced gas flows, respectable peak shapes were maintained in the ²D. However, the reduced gas flows were still intolerable by the majority of mass spectrometers. This was the first flow-based modulator with a high duty cycle and low gas flows that could be directly coupled to a common MS detector. To further improve on previous work, the same group designed a flow-based interface which used MS-compatible second dimension flows of about 4 mL/min [54]. The design was based on the original flow modulator proposed by Seeley [46], with the addition of two MXT Y-unions and a 3-way solenoid valve, located outside the GC oven, which was controlled by an auxiliary pressure source. The MXT Y-unions consisted of a metal, low-dead volume and inert connector with leak tight connections that were operational up to oven temperatures of 350 °C. Two restrictors made of uncoated tubing were connected to the two Y-unions in order to extend the re-injection pulse. The long re-injection period was necessary to achieve efficient flushing of the accumulation loop with gas flows of ~ 4 mL/min. Ultimately, the modified flow platform allowed a complete transfer of the analytes to any commercial MS without ²D effluent splitting. However, when implementing low flows with a differential modulator interface, broad ²D peaks were inevitable, resulting in a reduced overall peak capacity.

Differential flow modulation has proven to be a simple technique applicable across the entire volatility range analyzed by GC; however, with a fixed internal loop volume, the forward flush operation can lead to overloading and streaking within the second dimension. Streaking occurs when some of the ¹D effluent enters the modulator during the flush stage, creating a substantial tail due to the loss in return to baseline between modulations. To improve upon the shortcomings of the design, Griffith *et al.* designed the reverse fill/flush differential flow

modulator [55] (Fig. 1.15), based on the simplified design by Seeley *et al.* [46]. A 2-way, non-purged splitter, 2-way purged splitter CFT plate and a 3-way solenoid valve were used to construct the modulator. The flow to the ²D column was supplied by an auxiliary electronic pressure control. In the forward fill/flush model, the ¹D column flow continued to fill the sample loop behind the portion being swept during the flush stage. Without a pressure pulse to temporarily pause the ¹D flow, the ¹D effluent would continue to fill the loop. When returning to the fill stage, a component could elute from the ¹D while flushing the sample loop, reaching the ²D as an unmodulated band, resulting in tailing. Without efficient flushing of the sample loop, the signal would not return to baseline between modulations. This negative effect was more substantial for high concentration components, ultimately altering the separation of adjacent peaks within the second dimension, especially those of differing concentrations. By reversing the flow in the flush stage, Griffith *et al.* intended on preventing the ¹D effluent from entering ²D column during the fill stage. To provide an equivalent flow to the output of the first-dimension column, a bleed line with a specific length and internal diameter was added in order to match the pressure and flow conditions of the columns used. The purpose of the bleed line was to provide a channel for the flow within the sample loop if overfilled during the fill stage, and, more importantly, to provide the reversal of flow during the flush stage. Reversing the flow during the flush state substantially decreased the baseline rise between modulations when compared to the forward flush design. Additionally, the modulator was able to handle overloading without losing resolution in the second dimension, resulting in an increase in peak capacity. A more detailed comparison between the forward and reverse fill/flush designs can be found in ref. [56]. The reverse fill/flush differential flow modulator provided superior separation and resolution while utilizing commercial CFT plates for a simple setup with a variety of column dimensions and

optional sample loop dimensions, as seen in Figure 1.15. SepSolve Analytical commercialized a similar platform which used a compact Trajan SilFlow 7-port plate and unpurged 2-way splitter to achieve reverse fill/flush modulation, known as the INSIGHT modulator [57]. The interface provided interchangeable sample loops for flexibility in method development, as well as the ability to perform heart-cutting and back flushing. An optional 2-way splitter allowed parallel detection between single-channel detectors and mass spectrometers for qualitative and quantitative analysis. With a compact design, two interfaces could be placed in a single GC oven for enhanced productivity with a dual channel configuration. A flow calculator provided the analyst with a user-friendly way to simplify method development for a variety of configurations [58].

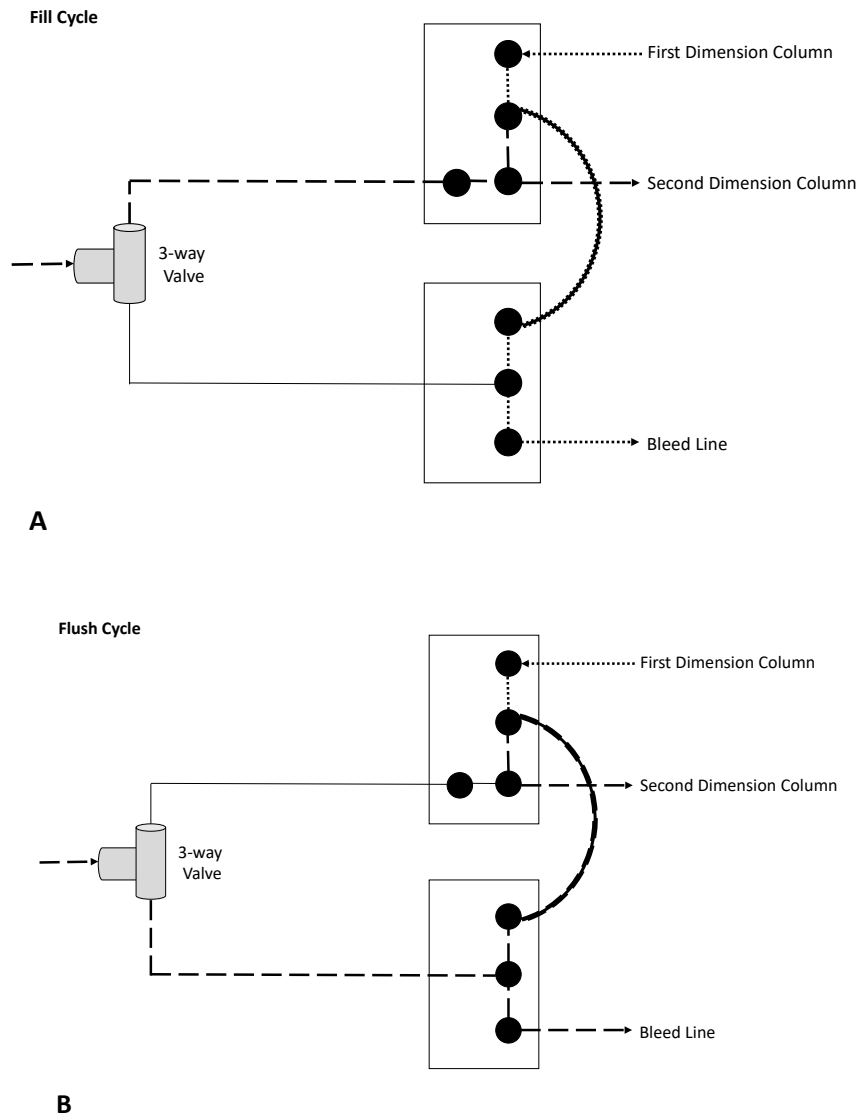


Figure 1.15 The flow paths for the (A) Fill cycle and (B) Flush cycle of the reverse fill/flush modulator. Based on Ref. [54].

Despite the improvements made to overcome the shortcomings of the various flow and valve-based platforms, a choice between a low-duty cycle and full transfer modulator still had to be made. Seeley *et al.* addressed this issue by designing a multi-mode modulator (MMM) [40]. The goal was to provide a flexible platform which could perform all modes of modulation including heart-cutting, low-duty and full transfer. Based on a previous low-duty cycle design

[59], the MMM consisted of a 3-port solenoid valve, a cross union, a T-union and a joining capillary (0.53mm ID, metal), as seen in Figure 1.16. The ¹D column was inserted through one end of the cross union and through the joining capillary, which was attached to the opposite end of the union. The other end of the joining capillary was connected to the T-union. The ²D column was inserted into the opposite end of the T-union and through the joining capillary. Within the joining capillary, the ¹D and ²D columns were kept in close proximity to one another. The distance between the two dimensions and flows implemented in ¹D and ²D determined the mode of operation of the modulator. This was vital to produce an optimal pulse shape for proper operation. The normally-closed port of the 3-way solenoid valve was connected to the cross union, while the normally-opened out port was connected to the T-union. The fourth port of the cross union was connected to a flow restrictor. Auxiliary carrier gas flow entered through the 3-port solenoid valve in order to perform flow switching and alternate between the divert and inject stages. The divert stage occurred in a similar manner for both low duty cycle and full transfer modes of modulation by directing the auxiliary flow towards the T-union and the ²D . This was achieved by employing an auxiliary flow (F_A) greater than the ²D flow (F_2) to prevent the ¹D effluent (F_1) from entering the ²D column, as seen in Figure 1.16A. The auxiliary flow met the requirements of the ²D column, while the excess traveled towards the tip of the ¹D within the joining capillary. The excess flow acted as a “curtain” to prevent the ¹D effluent from entering the ²D. The inject stage occurred by directing the auxiliary flow to the ¹D through the cross union. The value of the ²D flow in comparison to the ¹D flow determined if the MMM operated as a low duty cycle or full transfer modulator. When the ¹D flow (F_1) was greater than the ²D flow (F_2), low duty cycle modulation was achieved. As the ¹D flow exceeded the requirements for the ²D, the remainder traveled back towards the cross union. The auxiliary flow that entered

the cross union was directed towards the flow restrictor. The ¹D effluent that eluted during the previous divert stage was stored in the annular region and swept towards the flow restrictor. In this mode, narrow pulses could be generated due to the low ²D flow, however, only a fraction of the ¹D effluent reached the ²D. Additionally, in this mode the MMM could achieve heart-cutting by directing the ¹D effluent towards the flow restrictor or the ²D column. When the ¹D flow (F_1) was lower than the ²D flow (F_2), full transfer modulation was achieved. Due to insufficient flow provided by the ¹D, the auxiliary flow was directed towards the head of the ²D through the joining capillary at the cross union. As the ¹D flow entered the joining capillary, it combined with the auxiliary flow before entering the ²D column. Any ¹D effluent that was stored in the annular region from the preceding divert stage was quickly flushed into the ²D, completing full transfer. Not only was the value of the ²D flow vital for the mode of modulation desired, the placement of the ¹D and ²D within the joining capillary had to be adjusted accordingly. In the low duty cycle, the columns were placed close to one another. Due to the ¹D effluent and auxiliary flow being greater than the required ²D flow, extreme bleed of the ¹D effluent would not occur with the close positioning. However, in the full transfer mode, the ²D flow is greater than the ¹D flow, so the columns were positioned further apart to prevent ¹D effluent bleed. The greatest advantage of the MMM was the use of the joining capillary, allowing any poorly swept volumes caused by poor fittings or column connections to not hinder the performance of the modulator. The ability to operate in three different modulation modes through a single flow interface was a significant advancement towards achieving a universal platform.

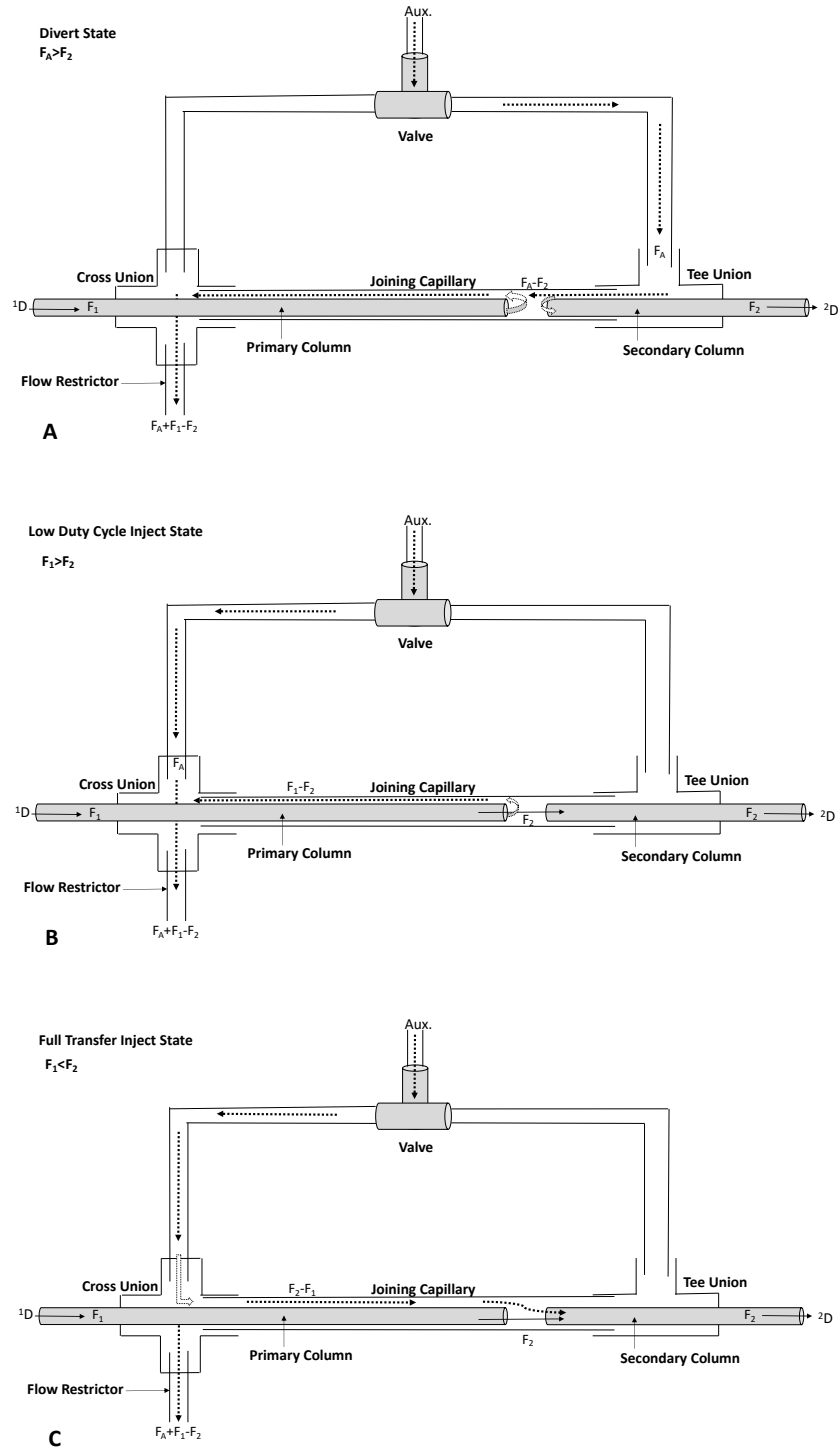


Figure 1.16 Schematic design of the three possible operational modes of the multi-mode modulator: (A) the divert stage for low-duty cycle and full transfer modes, (B) the inject state for the low-duty cycle and (C) the inject state for the full transfer mode. Based on Ref [39].

LECO Corp. recently introduced the FLUX flow modulator based on the low-duty cycle design of the MMM [60]. The main goal was to introduce a platform that was easy to implement and use, making GC×GC possible for all users. The modulator consisted of the same components as the MMM, including a tee union, a cross union, a solenoid valve and a joining capillary. The interface performed modulation by actuation of a valve to alternate between a divert and inject mode. When the auxiliary flow was directed towards the cross union and then towards the waste, the ¹D effluent was directed towards the ²D to complete the inject mode. When the valve was actuated, the divert mode would send the auxiliary flow towards the tee union and onto the ²D . As this occurred, the ¹D effluent was directed towards the waste. Unlike other flow platforms, the software package only required the selection of two parameters, ²D retention time and injection duration, to manage method development. The modulator has been implemented for a variety of complex analyses, including weathered crude oil, petroleum and fragrances. While the design is simple and robust, the modulator could not achieve the same detectability as that achievable with a quad jet thermal modulator.

1.2.2.3 Flow & valve modulation optimization

Flow and valve-based modulators require careful installation due to the many connections and numerous steps involved in method development and optimization. For proper operation it is vital to ensure all connections along the column path are leak-free, especially when coupling with a mass spectrometer. Before installation, the proper lengths of the ¹D, ²D and auxiliary or transfer lines, as well as the flows required for each stage should be determined. If the instrumental setup is not accurate, proper modulation may not be achievable. The greatest downside to optimization of flow-based platforms is that when a change is made to the setup, the

entire system must be altered accordingly. For full transfer platforms, the optimization of the stages is extremely important to ensure the sample is not being under- or oversampled. A flow calculator is typically employed to determine the correct pressures and flows for the entire setup for both the low-duty and full transfer modulators.

Determining the restrictor length and necessary pressures for the operation of a low-duty modulator such as a Deans switch are important in the optimization process [61]. The calculator allows the user to input the type of carrier gas, starting analysis temperature, primary detector type and corresponding outlet pressure, secondary detector type and corresponding outlet pressure, ¹D and ²D dimensions with corresponding flows, and restrictor diameter. The restrictor column is then determined to ensure the pneumatic resistance is the same as that of the ²D with a shorter holdup time. The ¹D column flow is chosen to be at or near the optimum of the desired column to ensure the ²D flow does not exceed the optimum to such a degree that the resolution is lost. The restrictor length is then entered into the calculator to determine the necessary ¹D pressure and the auxiliary pressure. Once all the parameters are entered, the inlet pressure and auxiliary pressure required to complete both modes of modulation for that specific setup are determined.

In a similar manner to low-duty modulators, a full transfer model must also utilize a flow calculator to achieve optimal modulation through method development. Specifically, for flow based full transfer modulators, the ratio between the ¹D and ²D flows needs to be carefully considered to achieve narrow ²D peak widths and proper gas flows [58]. A narrow ¹D helps in achieving an optimal separation with a lower flow rate; however, it is important to remember that these dimensions may require an inlet pressure which exceeds the pressure limits of the instrument when operating at higher oven temperatures. The same limitations as those discussed

for the 1^{D} may apply when choosing the 2^{D} dimensions. The high flow rates employed in the 2^{D} create a greater flow ratio between both dimensions with decreased loop flush times, ultimately creating narrow 2^{D} peak widths. However, the pressure limits of the electronic pressure control (EPC) for the auxiliary flow should not be exceeded. For reverse fill/flush flow modulators, the dimensions of the bleed line must be determined to achieve a flow that matches that of the 1^{D} flow rate. This is vital for the proper operation of the reverse flush mode. If the bleed line flow rate must be altered, the EPC pressure can be increased, or the column can be shortened. The sample loop must also be optimized to ensure the entire 1^{D} effluent is transferred to the 2^{D} . If the sample loop is overfilled, the excess 1^{D} effluent will exit through the bleed line. The FID can be used to monitor the components lost through the bleed line if desired. To prevent the loss of analytes to the bleed line, a larger volume sample loop can be employed to allow a longer collection stage. Additionally, it can provide a longer fill time and subsequently longer modulation period to eliminate any potential wraparound. However, larger volumes require a longer flush time, resulting in a broader 2^{D} injection bands. To achieve narrow bandwidths with a longer modulation period, a smaller volume sample loop with a short flush period should be used. While some 1^{D} effluent may escape through the bleed line due to the smaller sample loop overfilling, ultimately the 2^{D} resolution will be improved. For full transfer modulators that employ a bleed line, it is important to determine the equivalent 1^{D} length to account for the bleed line and its impedance in the column path. SepSolve Analytical provides a guide for all steps necessary for the calculations required for method optimization [58].

1.2.3 Compare & contrast

Due to the differences in operation, a direct comparison of flow-based and thermal modulators is difficult [62]. The separation with the two platforms cannot be carried out under identical conditions, but the final product (chromatograms) can be compared when each platform is operated under their optimal conditions. However, both types of modulators have their advantages and disadvantages in regard to the robustness, performance, analyte volatility range, limit of detection, retention time reproducibility, 2D peak widths, as well as the costs and ease of use as seen in Table 1.1.

Cooling is used in order to trap analytes eluting from 1D with thermal modulators at a temperature lower than that of the oven. In both consumable and consumable free systems, the trapping provides a re-concentration of the analytes, creating a focusing effect in space. This phenomenon results in narrow reinjection bandwidths in the 2D that are not achievable when a flow modulator is employed. A flow modulator can only physically compress the bands in time, not in space, by employing a high 2D flow. Although flow modulators can sometimes achieve 2D peak widths that are comparable to thermal platforms, the separation method is not identical in the comparison and no re-concentration occurs. The greatest advantage of the focusing effect achieved with thermal modulators is the possibility to gain about an order of magnitude increase in S/N when compared to a one-dimensional separation [22]. When compared to flow modulation, method development is rather straightforward for thermal modulation. Without a sample loop, there is one less parameter that needs to be optimized. However, the Zoex modulator with the delay loop requires the length of the loop to be optimized if flow rates are altered. For the Pegasus instruments, LECO provides their ChromaTOF software to aid in method development by achieving constant flow when different inner diameter and film

thicknesses are coupled. Their “Simply GC×GC” tool assists users in converting from 1D GC to GC×GC. For the Solid-State Modulator, J&X Technologies offers a free Flow Calculator to assist users in determining the equivalent column lengths for GC×GC. Generally, thermal modulators require fewer connections along the column train, reducing the number of potential leaks. The greatest advantage for thermal modulation platforms over flow modulation is the normal flow rate through both the ¹D and ²D. This allows direct coupling with all detectors with an acquisition rate fast enough for GC×GC, including mass spectrometers. Some flow modulation platforms require a large auxiliary flow for proper operation, ultimately hindering their ability to be directly coupled to a mass spectrometer. Cryogenic platforms provide superior performance; however, they require a large amount of cryogenics, resulting in high running costs. The cryogen-free versions help reduce the operating cost, but the modulation volatility range is reduced. For LECO’s cryogen free version a range from C₈ to C₄₀ can be modulated, and the Zoex version works for C₇ to C₄₀ [63, 64]. For the Solid-State modulator, the modulation volatility range can be optimized by choosing a proper modulation column. However, due to the limited ranges of volatilities available, it may be difficult to achieve a complete separation with a single modulation column. For example, the EV series allows for modulation from C₂ to C₁₄, while the SV series ranges from C₇ to C₄₀ [65]. With four varying modulation columns, the platform can be optimized accordingly. However, this might require the column to be changed for each application. The Solid-State modulator also requires the graphite rollers to be replaced every 100,000 modulations as preventative maintenance.

Flow based platforms provide an alternative to thermal platforms with a small, compact footprint that is easily installed within existing GC systems. With no moving parts, low thermal mass and practically no temperature limits, the setup is quite robust. However, the large number

of connections involved in most flow platforms can lead to leaks within the column path, potentially causing issues when a mass spectrometer is employed. When compared to thermal platforms, the greatest advantage of flow platforms is the cryogen-free operation, which decreases the operating costs while increasing the modulation volatility range. With essentially no temperature limit other than that of the column set, a modulation volatility range from C_1 to C_{60} is possible, allowing for both volatiles and semi-volatiles to be modulated in a single analysis. However, without the use of cryogens or a focusing step, the 2D injection bandwidths are not as narrow as those achieved with thermal modulation [66]. Even when substantial 2D differential flow is employed, the peak widths at the base are greater by about 100 milliseconds when compared to those that have been focused by a cryogenic platform [57]. The high 2D column flow helps in achieving comparable narrow re-injection bands; however, the analytes do not experience the S/N increase like in cryogenic modulation. Ultimately, the greatest issue results when coupling to a mass spectrometer due to the vacuum pumps limitations [30]. With flow rates up to 20 mL/min, a mass spectrometer cannot receive such high volumes while under vacuum. To alleviate this issue, the 2D flow must be split to a vent line or a single channel detector to decrease the flow received by the mass spectrometer. Alternatively, atmospheric pressure chemical ionization (APCI) interfaces could be used without the requirement of splitting the 2D effluent. This interface tolerates higher flow rates when compared to other designs. Thermal modulators do not require the high 2D flow for proper operation, leading to greater sensitivity than a flow-based platform when comparing the mass spectrometric data [66]. Flow modulation provides superior retention time repeatability since the electronic pressure control provides negligible discrepancies in retention times in both dimensions [57]. Commercial flow-based platforms, such as the SepSolve Insight, can provide less than 1% relative standard

deviation for both the 1D and 2D retention times. Converting from a 1D GC to a GC \times GC system can be rather challenging when a flow modulator is employed. It is rather difficult to alter the columns once installed onto the modulator plates, so it is key to determine the proper lengths and dimensions to achieve proper flows and modulation [3]. Altering the 1D flow and timing of the fill and flush stages are rather simple; however, any other modifications require a complete disassembly of the modulator [3]. When compared to thermal modulator platforms, flow-based ones are more difficult when translating a 1D separation to a GC \times GC separation [66]. Due to the operational conditions of a low 1D flow and a high 2D column flow, original GC methods are rarely used. However, for thermal modulators, transitioning between 1D GC and GC \times GC is rather easy. With the many advantages and disadvantages of both thermal and flow-based platforms, it is important to understand what is necessary for the specific application being analyzed.

Table 1.1 Comparison of advantages and disadvantages of various modulators

Category	Flow Based	Valve Based	Thermal Based
Robustness	(+) No moving parts (other than in the valves)	(-) Some valves have temperature limits	(+) LECO and Zoex no moving parts (other than in the valves) (-) Solid State has moving parts
Performance	(-) No focusing (+) Full transfer of sample from ¹ D to ² D (-) Less sensitive for trace analytes	(-) If low duty cycle, the entire sample is not transferred	(+) All types focus the trapped band before reinjection (+) Full transfer from ¹ D to ² D
Volatility Range	(+) < C ₆ , C ₁ -C ₆₀		(-) Without cryogenics C ₇ or C ₈ -C ₄₀
Retention Time Reproducibility	(+) <1% for ¹ D and ² D		(+) Good
² D Peak Width	(+) <100 ms at the base with high differential flow (-) Several hundred ms with differential flows directly compatible with MS		(+) Very narrow
Associated Costs	(+) No consumables	(+) No consumables	(-) Consumables if cryogenics are implemented
Ease of Operation	(+) Easy to install within an existing GC system (+) Small in size, can implement two within the same GC oven (-) Difficult to couple with MS (-) Difficult to optimize and make alterations to setup (-) Numerous connections (potential for leaks) (-) Difficult to convert from GC to GC×GC	(-) Can be difficult to install	(+) Easy method optimization (+) Fewer connections so fewer leaks (+) Normal flow for both ¹ D and ² D (+) Easy coupling with MS (+) Zoex and Solid State can be installed in existing instruments

1.2.4 Applications

The superior separation and resolution capabilities of GC×GC when compared to traditional one-dimensional GC allow for the analysis of highly complex mixtures. GC×GC has been used in a variety of applications including forensics, environmental, metabolomics, food and fragrances as well as petrochemical. Due to the great number of published applications, only those specific to the work presented in this thesis will be briefly reviewed. More detailed information can be found elsewhere [67, 47, 68, 69, 70, 71].

Petrochemical samples such as crude oil, bitumen, diesel, gasoline, and jet fuel, are extremely complex and contain thousands of analytes in a single mixture. The added complexity of the matrix itself increases the challenges faced when analyzing any of these samples. GC×GC has been effective in separating the unresolved complex mixture (UCM) from the various species present within these mixtures [72]. The structured nature of the chromatograms has also been beneficial in group type analysis, a key feature needed in many petrochemical processing steps to ensure the products meet industry requirements. With the application of element-specific detectors such as SCD and NPD, industries can perform analyses that provide information on undesirable components within their products.

Typically, reference methods such as EN 12916, ASTM D6591 and EN 14103, are employed for various analyses of specific compounds within several groups within distillate mixtures. However, these traditional methods require multiple analyses to be performed on a single sample, costing time and money. By employing GC×GC-TOFMS, a single analysis can be performed to obtain a complete group-type quantification of petroleum middle distillates [73]. Jennerwein *et al.* determined that the presented method was in good agreement with the reference methods, while providing higher precision and selectivity. It was also found that the

single method could provide quantification and distribution of the fatty acid methyl ester (FAME) content, which required two different analyses previously. Furthermore, Kulsing *et al.* used GC×GC with multiple detectors such as QTOFMS and flame photometric detection (FPD) to perform group-type analysis of hydrocarbons and identification of sulfur compounds in jet fuel [74]. When performing PIONA (paraffins, isoparaffins, olefins, naphthalenes and aromatics) analysis, the ASTM D2425 method is typically employed, beginning with a prefractionation step detailed in ASTM D2549. Similar results to the traditional PIONA analysis were obtained with the group-type method; however, further separation of two sulfur polarity groups (low and high) was accomplished within the applied method. The identification of sulfur heteroatoms is vital to ensure there is no performance suppression occurring or negative environmental outcomes. GC×GC allowed for a more in-depth and detailed understanding of the distribution of sulfur-containing compounds in fuel, which typically requires many time-consuming analyses. As an undesirable element within petrochemical samples, the identification of sulfur compounds has been greatly explored utilizing GC×GC. Avila *et al.* found that with no-pretreatment or fractionation required, qualitative and semi-quantitative characterization of sulfur compounds in petroleum samples could be performed by GC×GC-TOFMS [75].

Another important application in the petrochemical field is the study and comparison of various crude oils for geochemical characterization and oil spill identification. The immense complexity of crude oil samples, as well as the differences that occur due to their geographical origin and weathering that may have occurred, mean that oil spill forensics demands as much detail as possible. Traditional one-dimensional gas chromatography simply cannot separate these samples; however, with GC×GC combined with FID and HRTOFMS detection, a complete inventory of compounds in varying crude oil samples can be determined [76]. The resolving

power of GC×GC coupled with the identification capabilities of a HRTOFMS led to the identification of alkylated homologues series and individualized biomarkers. The specificity provided by the analysis showed the importance of GC×GC in its ability to differentiate similar spill sources by their individualized characteristics.

To better assist in group type analysis, a reverse column set-up is common in the analysis of petrochemical samples. Employing a polar column in the ¹D and non-polar column in the ²D provides greater resolution for less polar compounds, ultimately better utilizing the second dimension space [77]. With a non-polar column in the second dimension, the ²D retention of lower polarity compounds is increased, allowing for separation of the non-aromatic species, specifically those typically found in the UCM when utilizing a traditional normal setup.

Historically, cryogenic modulators have been employed in the analysis of petrochemical applications due to the gain in S/N from the focusing effect. However, as previously discussed, they require expensive cryogenic consumables for operation. Several comparisons have been completed to determine the capabilities of differential flow modulators in comparison to cryogenic platforms for the analysis of light cycle oil [66] and heavy petroleum cuts [62]. Semard *et al.* found that with a properly optimized system, the resolution and peak capacity of a cryogenic system could be achievable with a differential flow platform [66]. Nonetheless, if high sensitivity was required, the cryogenic platform provided better focusing when compared to the differential flow platform. It was clear that the choice of the modulator would depend on the specific needs of the application. Duhamel *et al.* found the reverse fill/flush design to be superior to the forward fill/flush design and cryogenic platform by reducing dispersion and enhancing sensitivity and peak capacity [62]. The adjustable sample loop allowed flexibility in regard to increasing the first-dimension flow rate or modulation period without overloading, allowing for a

superior separation of the heavy petrochemical sample. Overall, it is clear that GC×GC is a valuable tool in the petrochemical industry and both modulator platforms and column setups can be successfully applied.

1.3 Prior work

Previous group members Ognjen Panic, Christopher McNeish and Matthew Edwards have made significant contributions to the continuous development of the heater-based modulator within the Górecki's laboratory. Harynuk and Górecki found the use of Silcosteel® capillaries to be very promising for modulation in 2002 [29]. Earlier in 2000, Lee *et al.* used stainless steel capillaries that were coated with 3- μm polydimethylsiloxane (PDMS) and resistive heating to perform two stage thermal desorption modulation [78]. However, significantly broader peaks within the second dimension led the authors to conclude that Silcosteel was not a suitable material for a GC×GC modulator. Improvements made by the Górecki's lab proved this conclusion to be wrong. By decreasing the internal volume of the trapping capillary, the injection pulses within the second dimension would become narrower. Through the addition of a short, small ID uncoated fused silica tubing between the first column and the trap acting as a flow restrictor, the band broadening upon heating was minimized. This early design played a key role in the developments that were contributed by Ognjen Panic.

The key elements within Panic's design included a 15 cm deactivated stainless steel capillary that was looped outside the GC oven, and a cooling blower or Vortex cooler (Figure 1.17) [79]. The capillary was flattened and internally coated with PDMS at two separate trapping sections, about 3 cm in length. With no moving parts or cryogenic consumables, the device performed dual-stage modulation with the use of the cooler and a custom capacitive discharge

power supply. Within the flattened sections of the capillaries, the analytes were trapped and then thermally desorbed by the capacitive discharge.

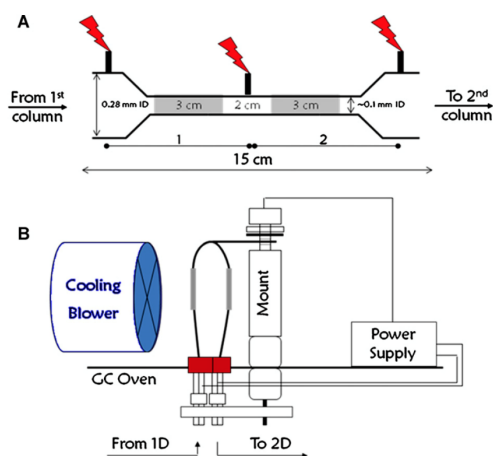


Figure 1.17 Schematic of dual-stage, consumable-free thermal modulator [78].

The device could analyze a gasoline sample with comparable peak widths to that of cryogenic modulators [80]. The device was also used in the thermal desorption aerosol comprehensive two-dimensional GC-MS system developed by Goldstein et al [81]. Panic discovered two important concepts in the development of the dual stage modulator: (1) selective conversion of the stationary phase within the capillary and (2) flattening of the capillary. Selective conversion of the stationary phase was done by thermally degrading the PDMS coating within the trapping capillary. The capacitive discharge unit was set at a voltage that would resistively heat the trap beyond the upper temperature limit of the column. For an allotted time, ranging from 10 to 30 minutes, the trap was subjected to frequent heating events, which caused the trap to glow red. By varying the thickness of the stationary phase, Panic found that analytes of lower volatility could be analyzed. The selective conversion of the stationary phase also

decreased the tailing of the peaks eluting from the modulator. Flattening of the capillary reduced the internal volume of the capillary trap, which significantly decreased the peak widths within the second dimension.

Chris McNeish further developed Panic's design in order to improve the heater-based modulator [82]. Modification for single-stage modulation was completed and ultimately proved to be more robust, but just as effective as the dual stage modulation (Figure 1.18). McNeish also discovered that with larger flattened sections of the capillary trap, even better ²D peak widths could be achieved. Decreased wall thickness also reduced the cool down time, which allowed for shorter modulation periods during the analysis.

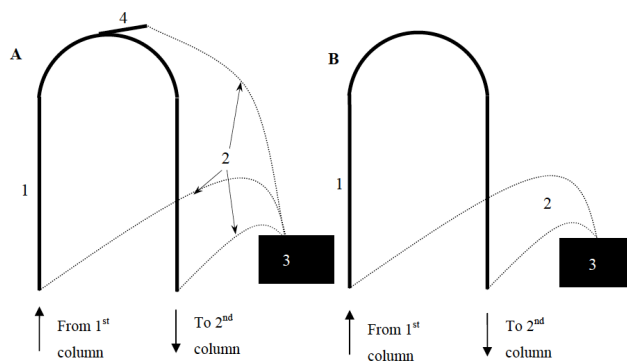


Figure 1.18 Schematic of dual-stage trapping capillary (A) and improved single-stage trapping capillary (B) [81].

Further optimization of the single stage modulator by Edwards included the addition of a thermoelectric cooling apparatus, ceramic cooling pads, and placement of the heat conduits and heat sinks outside the GC oven [83]. Kim *et al.* had previously used thermoelectric cooling (TEC) in the miniaturization of a dual stage modulator for the first time as a means of trapping analytes [25]. TEC, or Peltier cooling, occurs when an electrical current is applied to a thermoelectric material, and a temperature difference is created between opposite surfaces.

Heating or cooling effects can occur depending on the direction of the current. This design allowed for a user-friendly set-up that was easy to operate and use (Figure 1.19) [84]. As the analytes eluted from the ¹D, they entered the flattened capillary cooled with ceramic cooling pads, which were in direct contact with the capillary during the entire analysis. As the analytes traveled from the ¹D into the trapping capillary, they were trapped by sorption onto the stationary phase kept at low temperature by the cooling pads. An electrical discharge was then applied after a preordained time, around 4-6 seconds, to rapidly heat the capillary trap and drive the analytes into the ²D. The direct contact of the trap with the cooling blocks allowed the trap to rapidly return to the trapping temperature after desorption. The heat sinks outside the GC oven were used to passively remove heat from the cooling pads. Alternatively, TECs could be used for active cooling, in which case cooling fans were used to draw heat away from the unit. In both designs, the trapping capillary temperature increased during the run, lagging behind the oven temperature. This facilitated the analysis of compounds with a wide range of boiling points, from volatile to semi-volatile ones. The hydrocarbon range of this modulator was between C₆ and C₄₀.

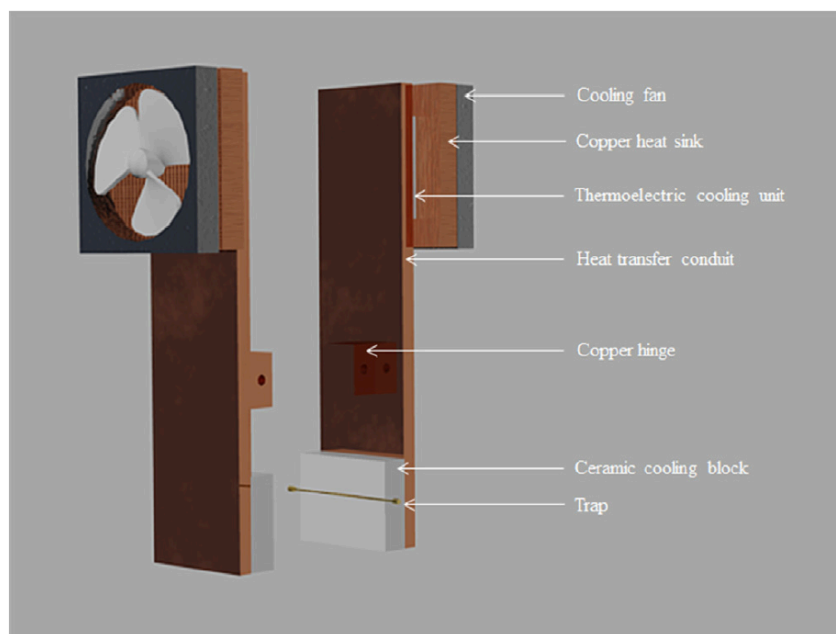


Figure 1.19 Schematic of single-stage, consumable-free thermal modulator [84].

Preliminary results provided several important conclusions: (1) less stationary phase within the trapping capillary produced narrower peaks and less tailing, (2) 10 cm capillary length proved to be as efficient as the original 15 cm, (3) higher desorption temperatures provided by the discharge power supply were necessary for efficient release of semi-volatile compounds, and (4) properly placing the capillary between the cooling pad surfaces was necessary to reduce voltage required to achieve adequate desorption [83].

Unaware of the nature of the stationary phase coating after treatment, Edwards investigated this further by performing scanning electron microscopy (SEM) and energy dispersive x-ray spectroscopy (EDX) on both treated and untreated capillary traps. SEM is a type of electron microscope that produces images of a surface's topography and composition by scanning it with a beam of electrons. Figure 1.20 displays a zoomed image of a 0.53mm ID x 3 μm film thickness MXT-1 capillary (Restek) before treatment. The PDMS coating inside appears

in the middle as a dark grey color, and the underlying stainless-steel capillary appears as a light grey color.

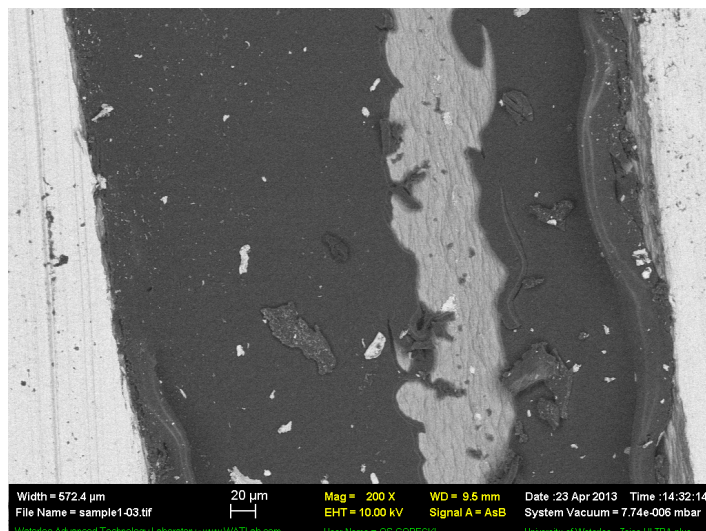


Figure 1.20 SEM image of 0.53mm ID MXT-1 (3 μm) trapping capillary before treatment

Figure 1.21 displays a zoomed image of a 0.53mm ID MXT-1 (3 μm) capillary after treatment. It is evident that the treatment creates nanoparticles (NPs) within the capillary. The porous layer of nanoparticles has a high surface area that is sorptive and “spongy” in nature (Figure 1.22).

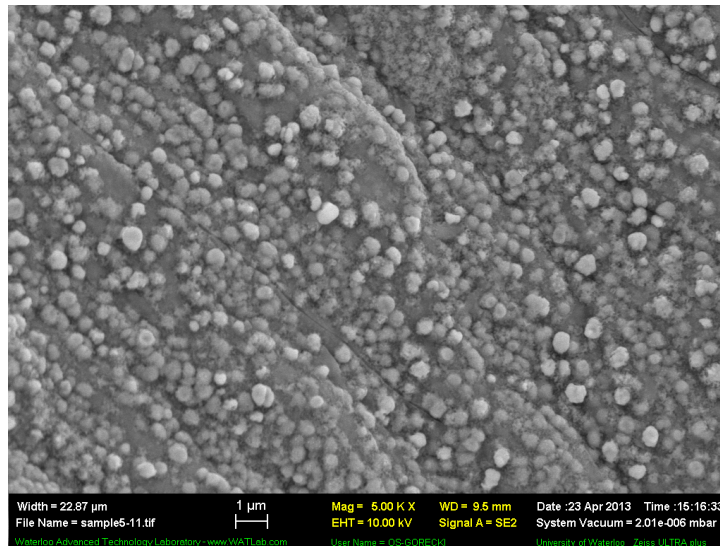


Figure 1.21 SEM image of 0.53mm ID MXT-1 (3 μm) trapping capillary after treatment

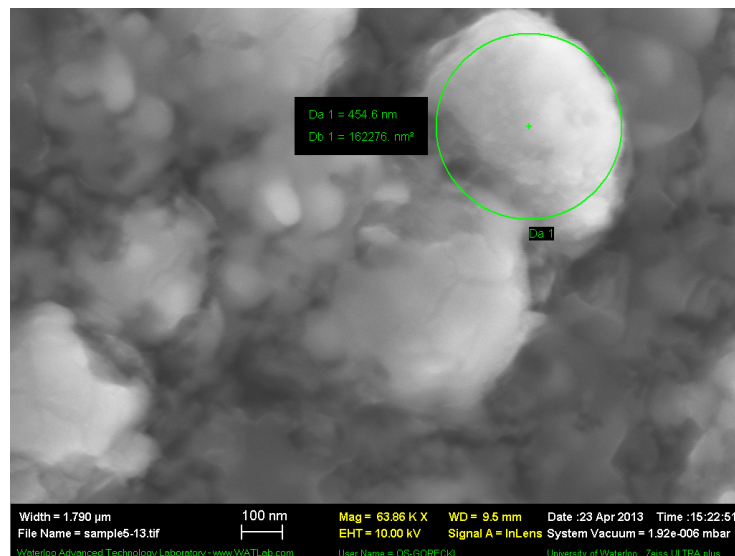


Figure 1.22 Zoomed SEM image of 0.53mm ID MXT-1 (3 μm) trapping capillary after treatment

To determine the nature of this new treated stationary phase, EDX analysis was performed. EDX is a spectroscopic technique that measures the elemental composition within a material by irradiating it with a beam of x-rays. From the data, atomic percentages of carbon (C), oxygen (O) and silicon (Si) were determined both before and after treatment. The data collected

was an average of four different areas amongst the coating. Table 1.2 displays the comparison of atomic percentages of a MXT-1 capillary before treatment, and known percentages of PDMS coating. This was done to ensure the EDX analysis was producing accurate results.

Table 1.2 Atomic percentages of the elements in the MXT-1 capillary coating before treatment, determined by EDX

Element	PDMS	Coating Before Treatment
C	50%	56%
O	25%	28%
Si	25%	21%

Table 1.3 displays the comparison of atomic percentages of the elements in the MXT-1 capillary coating before and after treatment. During the treatment process the atomic percentage of carbon decreased, while the percentage of silicon increased. It was known that some of the carbon removed during the treatment process was in the form of CO₂, but the nature of the remaining carbon was unknown. It was unclear if the carbon left were carbon particles or carbonyl carbons. As a conclusion from this analysis, the new treated stationary phase was described as carbon-doped silica.

Table 1.3 Atomic percentages of the elements in the MXT-1 capillary coating before and after treatment, determined by EDX

Element	Before Treatment	After Treatment
C	56%	29%
O	28%	18%
Si	21%	52%

1.4 Thesis objective

As the heart of a GC×GC system, the modulator is in charge of sampling the ¹D effluent, focusing the effluent into a narrow band and reinjecting the band into the ²D for further separation. Without this interface, comprehensive two-dimensional separation could not be achieved, as a direct connection of two different columns in series produces the same results as using a stationary phase being a mixture of the two phases used. The three main types of modulator interfaces include thermal, valve and flow based. Depending on the desired application, a modulator should be selected based on the operational capabilities, modulation volatility range, ease of use and costs involved. As previously presented, each interface has advantages and disadvantages, ultimately resulting in no universal modulator. The main objective of this thesis included the search for an ideal modulator for comprehensive two-dimensional gas chromatography. This goal can be divided into two lines of research: the optimization of the University of Waterloo single-stage thermal modulator, and the evaluation and possible improvement of commercial modulators.

The first goal was to further optimize the UW thermal modulator by ensuring the coating within the trapping capillary was appropriate for the analysis of a wider range of analytes. To

accomplish this, metal capillary columns were subjected to a variety of treatment parameters to achieve an optimal coating for efficient trapping of analytes and subsequent desorption during the modulation process. SEM and EDX were employed to characterize the nature of the coating within the trapping capillary before and after treatment. The design of the UW thermal modulator was also improved to eliminate poorly cooled sections of the trapping capillary. An optimal set of treatment parameters was obtained for the trapping capillary used in the UW thermal modulator.

The secondary goal of the thesis was the evaluation and possible improvement of commercial modulators. The UW thermal modulator was compared to a commercial reverse fill/flush modulator for the analysis of base oils. Neither platform was superior to the other; however, the thermal platform was more accommodating in the method optimization process. A commercial flow modulator was modified to test a proof of concept hybrid interface. A focusing trap and cooling air jet were employed and tested, while operating under mass spectrometry-compatible column flows. The hybrid interface showed promise in achieving adequate focusing and a decrease in peak widths.

The so-called solid-state modulator was evaluated on its operational capabilities through the analysis of standard reference mixtures of varying volatilities. The reproducibility of ¹D and ²D retention times, peak height, peak area, as well as the peak capacity in the ²D were determined. The modulator proved to be an adequate alternative without the need for consumable cryogenes. Furthermore, the solid-state modulator was used in the characterization of bitumen and tentative identification of potential biomarkers. Three distinguishing biomarkers were tentatively identified and group identification of specific classifications of compounds was achieved.

Chapter 2. Optimization of treatment and characterization of the stationary phase previously used within trapping capillaries

2.1 Introduction

Building off the previous work completed by Edwards, further optimization of the treatment process was to be performed to obtain an optimal trapping capillary for single stage modulation. However, when the project was initiated, the MXT-1 column that Edwards had previously used was no longer available. Edwards had used up all the material for previous experiments, requiring a new MXT-1 column of the same nominal dimensions to be used. A new MXT-1 column was obtained from Restek Corporation and was then used to perform the optimization of the treatment process. This trapping capillary will be referred to as MXT-1 #1.

Treatment of the trapping capillary was performed through pulsed heating at specific voltages to implement a desired temperature increase. This was achieved by connecting a capacitive discharge power supply to the front and back end of the metal trapping capillary via alligator clips, as seen in Fig. 2.1. The capillary was also attached to the house compressed air line to supply air during the treatment process. As previously discovered by Edwards, when temperatures above the upper temperature limit of the column were applied, the repeated resistive heating process led to thermal degradation of the PDMS coating, creating a sorptive, porous layer of nanoparticles, ideal for use in the single-stage modulator. To achieve this, the trapping capillary was subjected to ten minutes of pulsed capacitive discharge at about 68 V (~800 °C increase), followed by two five-minute periods of pulsed capacitive discharge at about 62 V (~680 °C). These treatment parameters caused the metal capillary to glow bright red with

each successive discharge. This was used as a visualization tool to confirm that the treatment process was thermally degrading the PDMS coating. The overall process of creating the carbon-doped silica after treatment of the PDMS was developed by Edwards; however, the method was not optimized and led to inconsistent performance between trapping capillaries, which received identical treatment. By utilizing the same nominal product as Edwards for the trapping capillary, the goal was to determine the optimal treatment of the stationary phase for a wider range of analytes, and to characterize the new phase after treatment. Analysis of n-alkane ladder was performed to evaluate the chromatographic performance of the different treatment processes applied to the trapping capillary. Subsequently, SEM and EDX analyses were performed to visualize the appearance and characterize the elemental composition of the phase after treatment.

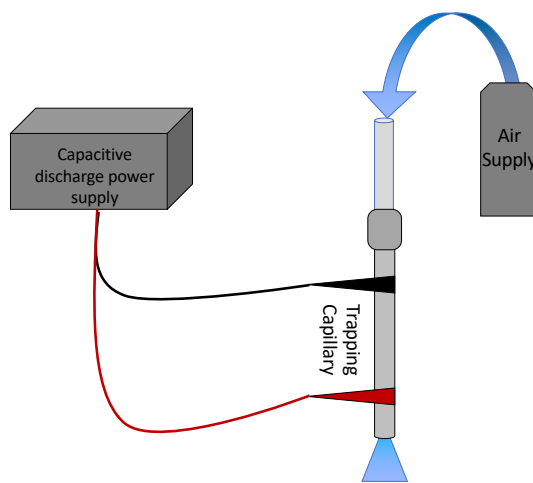


Figure 2.1 Schematic of the setup used for thermal treatment of the metal trapping capillaries.

SEM is a valuable tool that provides information on the surface's topography in fine detail due to the enhanced depth of field and superior resolution when compared to optical microscopes [85, 86]. Combined with the elemental analysis given by EDX, a full spectrum of characteristic elemental compositions can be obtained. The process of SEM involves the

specimen being scanned by a highly energetic (2 to 1000 keV) and focused electron beam, while the interactions between the electrons in the sample and electron beam are recorded [87]. By mapping the various points of different intensities, an image of the surface's topography is created [85]. Two types of primary effects occur once the electron beam interacts with the sample; inelastic and elastic scattering. In inelastic scattering, the direction of the primary electrons does not change but the energy is partially lost, while elastic scattering results in primary electrons changing their direction but the energy is retained [87]. Secondary effects, such as emitted secondary electrons, backscattered electrons and characteristic X-rays also occur outside the surface of the specimen. Secondary electrons escape the sample surface after ejection from an orbital around the atom caused by a primary electron [86]. These electrons are of utmost importance in obtaining high resolution images. Furthermore, they are very abundant since each primary electron can produce several secondary electrons. Backscatter electrons are not as abundant as secondary electrons, but they are vital in providing compositional information since they vary directly with the atomic number of the elements present [87]. They are a result of a primary electron colliding with an atom of the sample, ultimately losing energy and scattering in a backward (180°) fashion. X-rays occur when the atom of the sample de-energizes after the production of a secondary electron [87]. The inner-shell electron is displaced by the incident electron and the outer-shell electron fills the now empty orbit [86]. Subsequently, electrons move from higher to lower energy states until all states are filled. An X-ray is emitted during each transition to conserve energy. The emitted X-rays are of great analytical importance due to the direct relationship between the distinct energy and elemental composition [85]. EDX utilizes the electronic transitions to characterize the elements in a rapid manner for qualitative characterization. The X-ray energy is determined by measuring the number of electron-hole pairs

created after the X-ray penetrates a silicon crystal [86]. The number of electron-hole pairs increases with increasing X-ray energy. Elements with atomic numbers greater than 10 can be detected and reported in a complete spectrum [88]. The location of the peak within the spectrum and area under the curve indicate the element and number of atoms of the element in the selected area, respectively [88]. It is important to note that the generated signal greatly depends on the energy of the X-rays and the average atomic weight of the sample [87]. For example, X-rays from a lighter element like carbon are easily absorbed by the sample, while those emitted from a heavier element like iron are only absorbed by the sample in small amounts [89, 90, 91]. This would result in a slightly biased spectrum with easier detection of heavier elements when compared to lighter elements. For this reason, it was vital when analyzing the spectra for all analyzed trapping capillaries that the presence of the exterior metal capillary before and after the treatment process be taken into consideration. For all analyses, the complete spectrum was acquired which included carbon, oxygen, silicon, iron and chromium. Carbon, oxygen and silicon were the components of the stationary phase within the capillary, while iron and chromium made up the exterior metal capillary. The atomic percentages reported for the EDX analyses could differ depending on the elements selected. Carbon, oxygen and silicon were always selected; however, in some cases iron and chromium were also selected. When the atomic percentages of the metals present in the exterior capillary were not documented in the analysis, the total atomic percentage of the selected area did not add up to 100% due to the exclusion of these metals. As a result, for the interpretation of all EDX analyses, statements on the trends of the presence of carbon, oxygen and silicon in regard to the metals present before and after treatment will be made. The reported atomic percentages of specific elements may be misleading, resulting in an incorrect conclusion if the presence of the metals was not taken into

consideration. The results obtained by SEM and EDX will be used as a tool to decipher the changes that occurred during the various treatment processes.

2.1.1 Experimental parameters for GC×GC analysis

The alkane ladder consisted of several lower molecular weight n-alkanes (Sigma Aldrich, Oakville, ON, Canada) including C₆, C₈, C₁₀, and C₁₂, each at a concentration of 1000 ppm in carbon disulfide. The GC×GC system used for the analysis consisted of an Agilent 6890 gas chromatograph (Agilent Technologies, Santa Clara, CA, USA) equipped with a split/splitless injector and FID detector. The column configuration included a 30 m x 0.25 mm ID x 0.25 μm Rxi-5MS (Restek Corp.) as the ¹D and a 0.5 m x 0.25 mm ID x 0.25 μm Rxi-17MS (Restek Corp.) as the ²D. An Agilent 7683 series injector was used to make a 1 μL injection of the alkane ladder using the split/splitless injector at a split ratio of 100:1. The inlet temperature was set at 300 °C with a 4 mm ID Precision split liner with quartz wool (Restek Corp.). Hydrogen gas with a purity of 99.999% purity (Praxair) was used as the carrier gas at a constant flow of 1.5 mL/min. The oven temperature program was 40 °C to 120 °C at 8 °C/min, followed by 20 °C/min to 280 °C, which was held for 10 minutes. The FID was operated at 300 °C with flows of 40 mL/min, 400 mL/min and 45 mL/min for H₂, air and N₂, respectively. The UW single-stage, consumable-free thermal modulator was employed as the modulator interface. A modulation period of 4 seconds was used. A more detailed description on the operation can be found in section 1.3. Active cooling was employed including thermoelectric coolers, heat sinks and fans.

2.2 Treatment parameters and chromatographic results obtained for MXT-1 #1 and #2

Several different treatment parameters were chosen to be investigated during the treatment process, such as capacitive discharge versus continuous heating, presence versus absence of oxygen, time of treatment and temperature of the heating stage. The chromatographic performance was then assessed by analyzing a wide range of analytes before characterization through SEM and EDX. The treatment plan maintained the same three stages of heating, a ten-minute phase with a higher voltage followed by two five-minute phases with a lower voltage, the setting originally used by Edwards. Four different levels of heating were chosen with applied voltages producing temperatures differing by about 100 °C, as shown in Table 2.1. These temperature increase values were arbitrarily chosen in hopes to obtain a wide range of possible trapping phases after the treatment process. The temperature increase values were pre-determined by Edwards based on previous experimentations performed on the MXT-1 (0.28mm ID x 1.0 µm) trapping capillaries during the treatment process.

Table 2.1 Treatment plans for trapping capillaries

Treatment ID	1 st Stage (10 min)		2 nd Stage (5 min)		3 rd Stage (5 min)	
	Temp Increase (°C)	Voltage (V)	Temp Increase (°C)	Voltage (V)	Temp Increase (°C)	Voltage (V)
1	800	68	680	62	680	62
2	655	61	550	55	550	55
3	500	52	430	48	430	48
4	400	46	340	42	340	42

The MXT-1 #1 was chosen due to the belief that the material within the capillary column was the same as that used previously by Edwards. However, the dimensions of this capillary, 0.28 mm ID, were not as user-friendly due to their limited contemporary use and unavailable necessary consumables, such as ferrules. Alongside the MXT-1 #1, another capillary column was chosen to use as a trapping capillary in an effort to make the overall modulator more available for commercialization. MXT-1 was also available with dimensions of 0.25 mm ID x 0.25 μ m film thickness, which were more common dimensions and the consumables were readily available. This MXT-1 capillary with 0.25 mm ID will be referred to as MXT-1 #2. Even though the inner diameter was 0.03 mm smaller than that of the 0.28 mm column and it contained a significantly thinner film of 0.25 μ m versus 1 μ m, the treatment conditions presented in Table 2.1 were applied for a direct comparison. Both MXT-1 #1 and #2 were treated utilizing treatment plan 1 (Table 2.1), which included a ten-minute phase of 800 °C temperature increase, followed by two five-minute phases of 680 °C temperature increase with air on for all three treatment phases. The preliminary result obtained from the analysis of n-alkane ladder after treatment of the MXT-1 #2 (0.25mm ID x 0.25 μ m) trapping capillary can be seen in Fig. 2.2. The upper chromatogram displayed four separate components of the mixture, with the third peak highlighted. The chosen peak was further zoomed in, as displayed in the lower chromatogram. The modulated peak displayed two peaks with fronting at the leading edge, emphasizing the breakthrough occurring within the trap. Similar results were obtained with MXT-1 #1 and the analytes were not properly trapped during the modulation process.

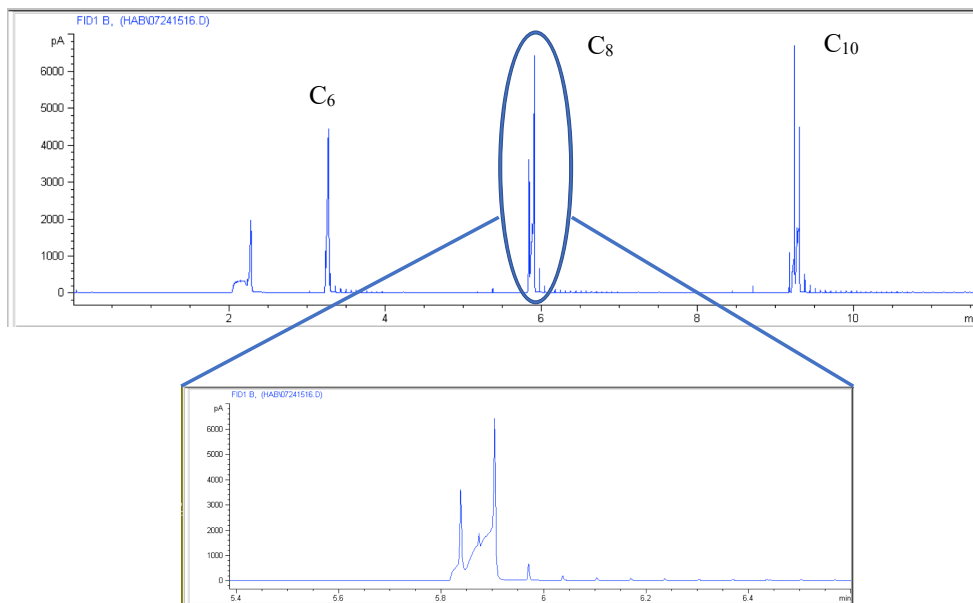


Figure 2.2 Raw 2D chromatogram of alkane ladder analysis utilizing MXT-1 #2 (0.25 mm ID x 0.25 μ m) trapping capillary with treatment parameters of ten minutes of 800 $^{\circ}$ C increase, followed by two five-minute treatments at 680 $^{\circ}$ C.

In an attempt to create a less adsorbent material, treatment plan 1 (Table 2.1) was applied in two-minute increments. After each treatment was applied, a chromatographic analysis of n-alkane ladder was performed to determine if the treatment had created an improved phase without breakthrough. Figure 2.3, displays a sample chromatogram of treatment plan 1 for ten minutes with an 800 $^{\circ}$ C temperature increase and only two minutes with 680 $^{\circ}$ C with a continuous air supply for MXT-1 #2. The treatment was too severe, creating a sub-par stationary phase that could not properly trap analytes, resulting in breakthrough.

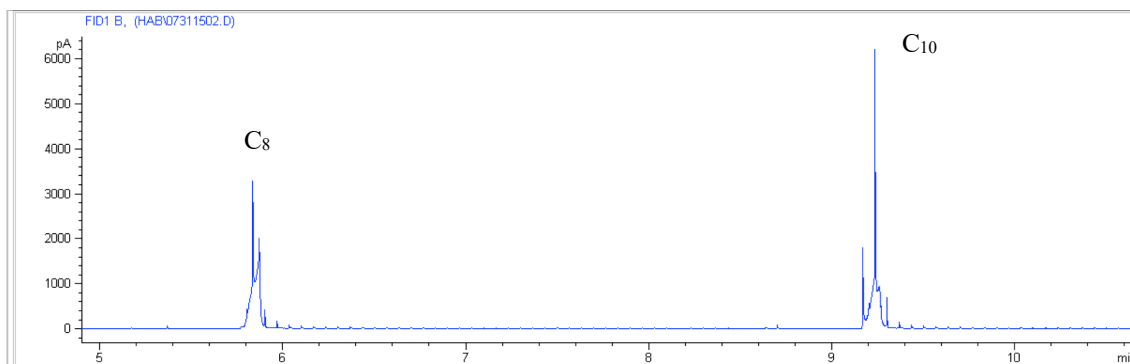


Figure 2.3 Raw 2D chromatogram of the alkane ladder analysis using MXT-1 #2 (0.25 mm ID x 0.25 μ m) trapping capillary with continuous air supply and a treatment of ten minutes at 800 $^{\circ}$ C and two minutes at 680 $^{\circ}$ C.

Unsure if this treatment plan was not functioning due to the dimensions of the MXT-1 #2 trapping capillary, MXT-1 #1 was also subjected to two-minute increment treatments utilizing treatment plan 1 (Table 2.1). Figure 2.4 displays a sample chromatogram obtained with the MXT-1 #1 trapping capillary treated with continuous air supply for ten minutes at 800 $^{\circ}$ C followed by four minutes at 680 $^{\circ}$ C. The chromatography was still sub-par with breakthrough and inefficient trapping of analytes, hence it was concluded that the treatment plan was too severe.

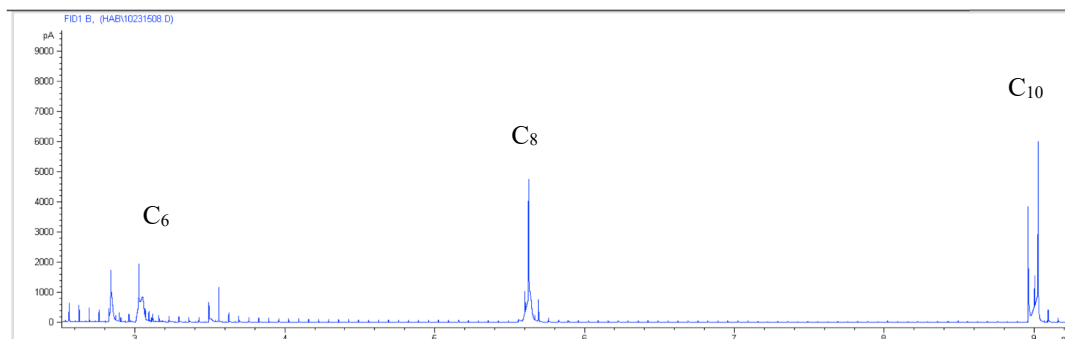


Figure 2.4 Raw 2D chromatogram of the alkane ladder analysis utilizing MXT-1 #1 (0.28 mm ID x 1 μ m) trapping capillary with continuous air supply and a treatment of ten minutes at 800 °C and four minutes at 680 °C.

To address the issues encountered with the treatment plan 1, an alternative plan was designed for MXT-1 #1. Table 2.2 displays the four possibilities of treatment chosen for MXT-1 #1, which included shorter treatment time for each phase and smaller temperature changes between each level. Treatment D included a temperature increase of 655 °C for five minutes followed by a temperature increase of 550 °C for five minutes with a continuous air supply.

Table 2.2 Treatment plan for trapping capillaries with shorter treatment times for MXT-1 #1

Treatment ID	1 st Stage (5 min)		2 nd Stage (3 min)		3 rd Stage (2 min)	
	Temp Increase (°C)	Voltage (V)	Temp Increase (°C)	Voltage (V)	Temp Increase (°C)	Voltage (V)
A	800	68	683	62	683	62
B	755	66	630	60	630	60
C	700	63	575	57	575	57
D	655	61	550	55	550	55

Figure 2.5 displays the sub-par chromatography when utilizing treatment plan D for the analysis of n-alkane ladder with MXT-1 #1. After testing several combinations of treatment temperatures and times, it was clear that both the MXT-1 #1 and #2 were not producing the desired stationary phase for efficient trapping of analytes. To compare the composition of the stationary phase before and after treatment that was achieved by Edwards, MXT-1 #1 and #2 had to be opened and analyzed by SEM and EDX.

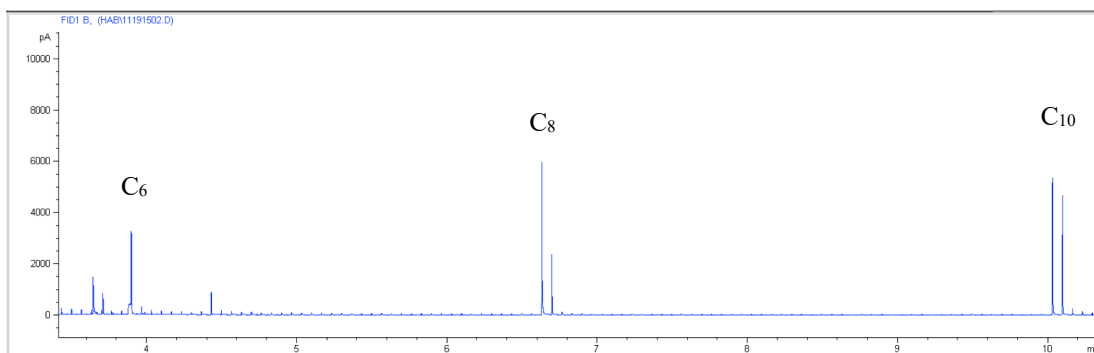


Figure 2.5 Chromatographic analysis of n-alkane ladder utilizing treatment D (MXT-1 #1), treated for five minutes at 655 °C followed by five minutes at 550 °C (raw 2D chromatogram).

2.3 Imaging the stationary phase within the trapping capillary

Once the trap was treated with the chosen set of parameters and its chromatographic performance was analyzed, the capillary was opened in order to image the stationary phase coating within the capillary. Previously, the outer metal wall of the trapping capillary was filed or sanded down to expose the stationary phase within the capillary for imaging. However, this method risked damaging the stationary phase and took a considerable amount of time for each capillary. To alleviate these issues, a reproducible mechanism was created to open the flattened, treated trap to perform SEM and EDX analyses. An aluminum jig was created at the University of Waterloo Science Technical Services Machine Shop, as seen in Figure 2.6. The jig consisted of two aluminum blocks that were held together by two screws. The screws were long enough to

go through both blocks without protruding from the backside. This ensured the jig would lay even and flat once placed in the end mill to open the trapping capillary. A small slot, measuring about half the width of the flattened capillary, was placed on one edge of the jig. The trapping capillary was then placed within the jig and securely fastened, while a portion of the flattened edge protruded past the end. The jig was then placed within the end mill in order to slice off the protruding edge of the flattened capillary with a carbide drill bit. This bit was chosen to assist in creating a fast and clean cut. Once one edge was removed from the trapping capillary, it was removed from the jig and flipped so the other flattened edge could be removed. After both edges of the trap were removed, a ceramic column cutter was used to make a precise cut at one end of the trapping capillary. With both flattened edges removed, the cut along the trap allowed the capillary to be easily peeled apart, exposing the inside with the thermally treated stationary phase coating. The jig ensured the trapping capillary remained stationary while both sides were removed, keeping the stationary phase intact and unaltered. Exposing the stationary phase in this manner was time efficient and easy due to the precision and fast nature of the end mill. The manner in which the trapping capillary was opened was extremely beneficial for SEM and EDX analyses, allowing simple sample preparation and imaging due to the completely flat surface, with no rounded edges. This was a vital component to achieve accurate results due to the nature of operation of SEM and EDX. Both analyses utilize an electron beam in order to interact with the surface and atoms present in the sample to visualize the surface topography and determine atomic composition, respectively. Any rounded edges of the outer metal capillary caused an obstruction for the electron beam resulting in inaccurate or unattainable readings.



Figure 2.6 Aluminum jig used to open the trapping capillaries

2.4 SEM images of the MXT-1 #1

SEM was chosen as a tool to visually inspect the structure and topography of the inner stationary phase. The stationary phase in a GC column is chemically bonded to the underlying deactivation layer, creating a robust and stable surface for the analytes to interact with as they travel through the capillary [92-97]. As shown in Section 1.3, Figure 1.11 supported this previous knowledge and provided an example for future comparisons. To directly compare the trapping capillaries produced by Edwards, MXT-1 #1 trapping capillaries before and after treatment were opened and visualized by SEM. Treatment plan 1 consisted of the same parameters that Edwards had previously used; ten minutes at a temperature increase of 800 °C, and two phases of five minutes at a temperature increase of 680 °C, with continuous air flow. Figure 2.7 displays the before and after treatment images of both the Edwards trap and the MXT-1 #1. When comparing the before treatment topography of the Edwards trap (A) and MXT-1 #1 (C), the differences were quite apparent. The Edwards trap had a consistent underlying deactivation layer (light grey section in middle) onto which the stationary phase (dark grey) was

completely bonded. In the MXT-1 #1, the deactivation layer was several microns thick with holes and ridges. The stationary phase on top was only adhering to the underlying layer locally, leaving holes and openings. Overall, the starting structure of the deactivation layer and stationary phase were completely different from the Edwards trap. Similarly, when comparing the after-treatment topography of the Edwards trapping capillary (B) and MXT-1 #1 trapping capillary (D), they were very different. Due to the chemical bonding between the stationary phase and the deactivation layer in the Edwards trap before treatment, an efficient conversion to the sorptive, porous layer of nanoparticles could be achieved. The “spongy” material with a high surface area provided an active trapping mechanism for analytes traveling through the modulator. After treatment plan 1 was applied to MXT-1 #1, only the areas in which the stationary phase was locally adhering to the deactivation layer were converted to nanoparticles. However, there were large gaps left within the final phase due to the uneven nature of the deactivation layer. The gaps within the phase created a less efficient sorptive material, ultimately causing breakthrough from inefficient trapping of analytes. After examination by SEM, it was apparent that the starting material that was used by Edwards and the material present in MXT-1 #1 were vastly different from one another. The inability to obtain the same chromatographic results previously achieved by Edwards was due to the change in the starting material, even though the two columns were nominally the same.

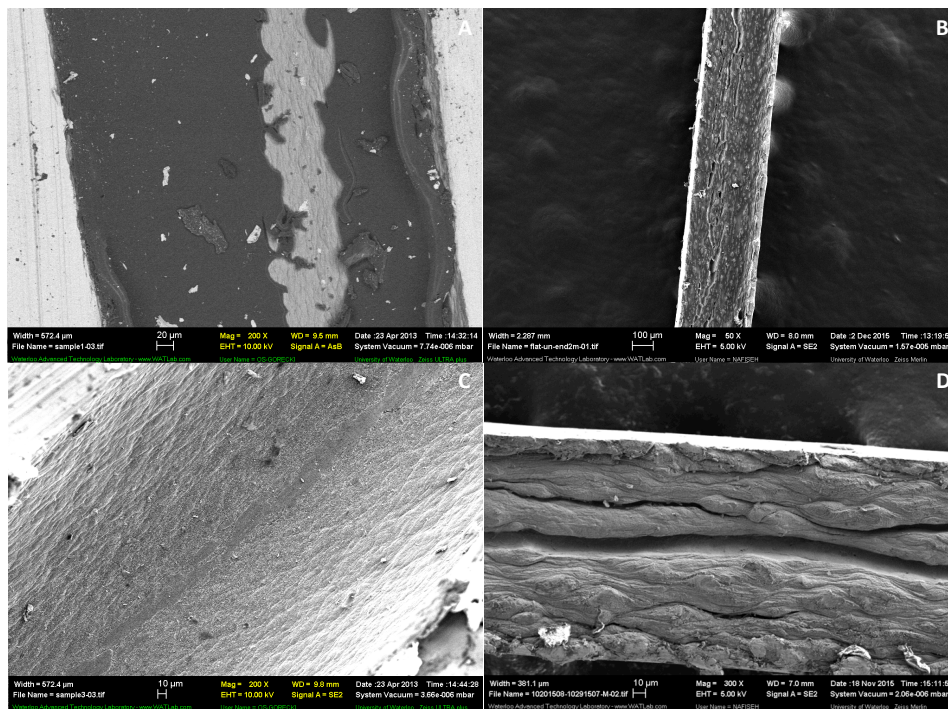


Figure 2.7 SEM images Edwards MXT-1 traps (A) before and (C) after treatment compared to treatment plan 1 images of MXT-1 trap #1 (B) before and (D) after treatment.

2.5 SEM images of MXT-1 #1 with treatment plan D

Treatment plan D (MXT-1 #1), which included five minutes at a temperature increase of 655 °C and five minutes at a temperature increase of 550 °C with continuous air flow, was also opened to be imaged by SEM. Figure 2.8 displays two magnifications of the trapping phase after treatment. The top image shows the same topography as previously discussed, a thick deactivation layer with ridges and gaps, exposing the underlying metal capillary wall. The lower image shows a closer look at the nanoparticles that were created during treatment on the areas of the deactivation layer in which the stationary phase locally adhered. Overall, the surface was not smooth or consistent, resulting in poor adsorptivity for the analytes.

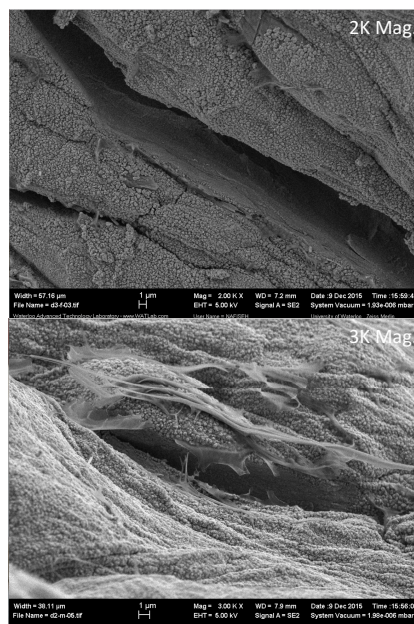


Figure 2.8 SEM images of treatment D applied to MXT-1 #1 trapping capillary. Treatment included five minutes at 655 °C followed by five minutes at 550 °C with continuous air supply.

2.6 EDX results for MXT-1 #1

EDX was chosen as a tool to investigate the changes in atomic composition of the main three components that are incorporated in a 100% PDMS stationary phase: carbon, oxygen and silicon. The percentages of the three elements in PDMS are well known [98], permitting a full evaluation of the starting material before treatment and subsequently what happens to the material after treatment. The EDX results for the trapping capillary used by Edwards before and after treatment are found in Table 1.2. The atomic percentages of C, O and Si began at about 55%, 27% and 18%, respectively. According to the literature, these values were comparable to the elemental distribution within a commercially available 100% PDMS stationary phase. After the treatment was completed, the atomic percentage of C decreased significantly, while that of Si increased substantially. The O also decreased by about 10%, not as drastic as the changes which occurred to the other two elements. With a prior understanding of how the atomic composition

of the stationary phase changed during the treatment process acquired by Edwards, EDX was also performed MXT-1 #1 trapping capillaries to better comprehend why their chromatographic performance was sub-par. Table 2.3 displays the atomic percentages of the coating components in the traps before and after treatment for both the treatment plan 1 and D. As previously shown in the comparison of the SEM images, the starting material of the trapping capillary used by Edwards was visually different from MXT-1 #1. The atomic percentages of C, O and Si before treatment of MXT-1 #1 were about 39%, 15% and 16%, respectively. These values were significantly lower than the atomic percentages of those found in Edwards untreated capillary, as well as the known distribution for a 100% PDMS stationary phase. It should be noted that these values did not add up to 100% due to the large gaps within the deactivation layer and subsequent stationary phase, which left the underlying metal capillary exposed for the EDX analysis.

Treatment plan 1 of MXT-1 #1 included the same parameters as those used by Edwards; ten minutes at a temperature increase of 800 °C followed by two five-minute phases at a temperature increase of 680 °C with continuous air flow. Despite receiving identical treatments, MXT-1 #1 did not change in a similar manner. After treatment plan 1, the atomic percentages of C and Si decreased, while the O increased. This was due to the differences in the starting material of MXT-1 #1 when compared to that used by Edwards, which was confirmed previously in the SEM images. Comparable results were also obtained for treatment plan D, which included five minutes at 655 °C followed by five minutes at 550 °C with continuous air flow. The observation supported the results of SEM imaging by confirming that the stationary phase that was not chemically bonded to the deactivation layer because of the non-uniform structure of that layer was lost during treatment, instead of being converted to nanoparticles as before. Ultimately, the combined results of the SEM imaging and EDX atomic readings explain the poor modulation

previously observed with MXT-1 #1. They also confirm that the material present in MXT-1 #1 was vastly different from that previously used by Edwards, resulting in a completely different phase after treatment.

Table 2.3 EDX results for the MXT-1 #1 under treatment plans 1 and D

Element	Untreated (Atomic %)	Treatment Plan 1 (Atomic %)	Treatment Plan D (Atomic %)
C	39%	---	20%
O	15%	14%	78%
Si	16%	6%	2%

2.7 Results for various sections of the MXT-1 #1 trapping capillary

Due to the insufficient performance by MXT-1 #1 treated with both treatment plans 1 and D, different sections of the total MXT-1 #1 column were investigated to ensure it was not a non-uniformity issue. The original column was divided into several sections labeled front, middle and end. Trapping capillaries were made from both the middle and the end of the MXT-1 #1 column, referred to as MXT-1 #1M and #1E, respectively. Treatment plan 1 with continuous air flow was applied to both trapping capillaries. Figure 2.9 shows the chromatographic comparison of the analysis of n-alkane ladder between (A) MXT-1 #1E and (B) MXT-1 #1M. MXT-1 #1M behaved in a similar manner to MXT-1 #1E. Again, trapping of analytes was inefficient, resulting in breakthrough. To visually compare the topography before and after treatment, the trapping capillaries were opened and analyzed through SEM imaging.

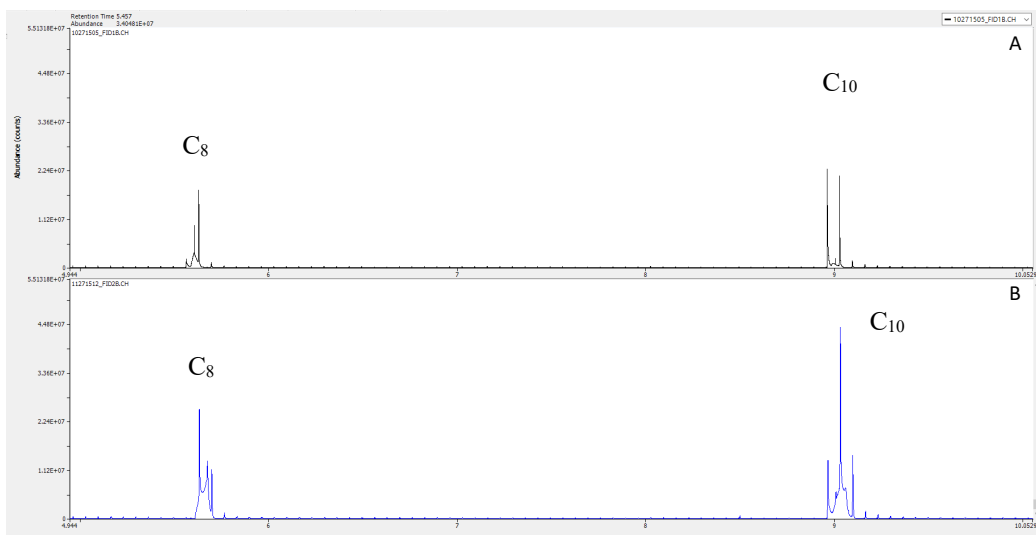


Figure 2.9 Raw 2D chromatograms for the analysis of n-alkane ladder utilizing (A) MXT-1 #1E and (B) MXT-1 #1M trapping capillaries

As seen in Figure 2.10, MXT-1 #1M and MXT-1 #1E were visually very similar both before and after treatment. There were still gaps within the deactivation layer, causing a poor conversion to the nanoparticle material after treatment.

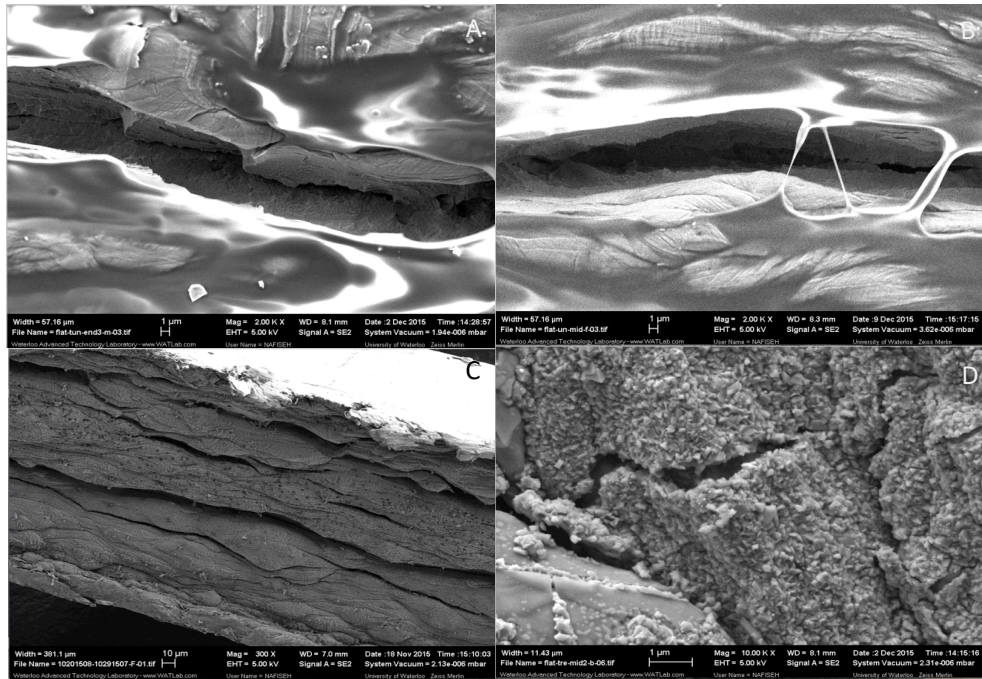


Figure 2.10 SEM results for MXT-1 #1E (A) before and (C) after treatment and MXT-1 #1M (B) before and (D) after treatment.

Table 2.4 shows the EDX results for the untreated, starting material of MXT-1 #1M and MXT-1 #E. There appeared to be inconsistencies in the silicon present within the untreated MXT-1 #1M and MXT-1#E. When comparing the individual spectra from MXT-1 #1M and MXT-1 #1E the presence of the underlying metal from the exterior capillary was rather similar. However, the silicon presence was substantially greater in MXT-1 #1E than MXT-1 #1M. This was due to the non-uniform layer of stationary phase that was only locally adhered to the underlying deactivation layer. Even though MXT-1 #1E appeared to have a greater amount of silicon, this was most likely a misleading outcome. This was a result of the specific area chosen for analysis. The area for MXT-1 #1E may have had more stationary phase present than the area selected for MXT-1 #1M, resulting in a more prominent presence of silicon when in reality, the presence of silicon was most likely similar from MXT-1 #1E to MXT-1 #1M. After treatment,

MXT-1 #1E had a very large increase in the atomic percentage of metals. Even though there appeared to be a decrease in silicon for MXT-1 #1E, there was most likely the same or only a slightly lower presence of silicon after treatment due to the increase in metals. After treatment, MXT-1 #1M had an increased presence of oxygen due to the decomposition of the stationary phase, exposing more of the underlying deactivation layer. With only local adherence of the stationary phase to the underlying deactivation layer and poor transformation after treatment of MXT-1 #1M and MXT-1 #1E, as well as the poor trapping capabilities, a brand new MXT-1 (0.28 mm ID x 1.0 μm) column was purchased.

Table 2.4 EDX results for MXT-1 #1E and MXT-1 #1M before and after treatment

Element	MXT-1 #1E Untreated (Atomic %)	MXT-1 #1E Treatment Plan 1 (Atomic %)	MXT-1 #1M Untreated (Atomic %)	MXT-1 #1M Treatment Plan 1 (Atomic %)
C	39%	---	41%	17%
O	15%	14%	53%	63%
Si	16%	6%	7%	19%

2.8 MXT-1 #3 results

The new MXT-1 column will be referred to as MXT-1 #3. It was divided into three five-meter sections labeled as front, middle and end. Trapping capillaries were created from the front and middle sections and will be referred to as MXT-1 #3F and MXT-1 #3M, respectively. They were both treated using treatment plan 1 with continuous air flow and subsequently tested chromatographically by analyzing n-alkane ladder. Figure 2.11 shows the results for both (A) MXT-1 #3F and (B) MXT-1 #3M. The chromatography was slightly better than previously obtained with MXT-1 #1; however, some breakthrough and tailing still occurred.

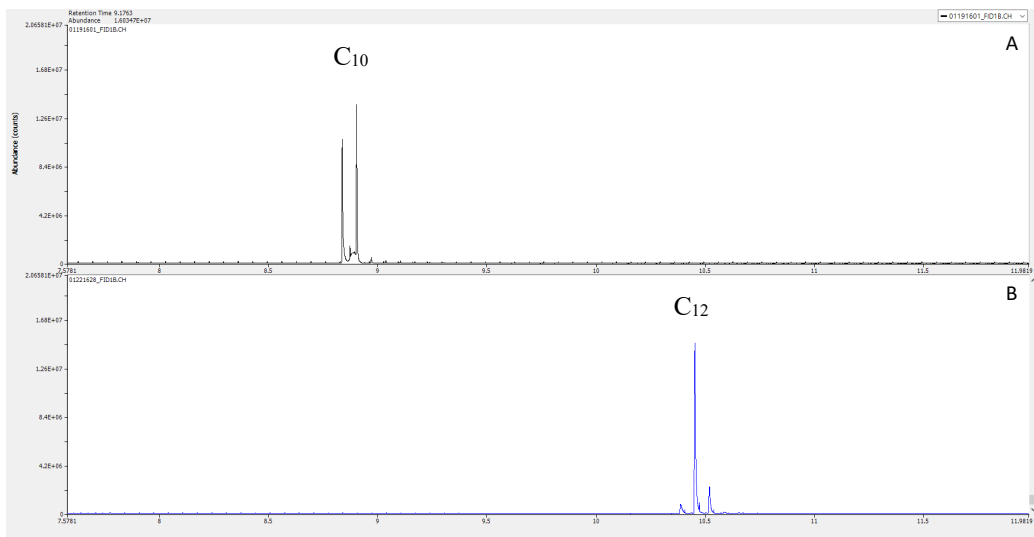


Figure 2.11 Raw 2D chromatogram for the analysis of n-alkane ladder with the treated capillaries (A) MXT-1 #3F and (B) MXT-1 #3M

Once opened and examined by SEM, the untreated MXT-1 #3 column had fewer gaps in the deactivation layer, allowing for better coverage of the overlying stationary phase as seen in Figure 2.12. Thus, the images of the MXT-1 #3 treated with plan 1 showed fewer cracked areas, allowing for better trapping of analytes with the sorbent nanoparticle surface.

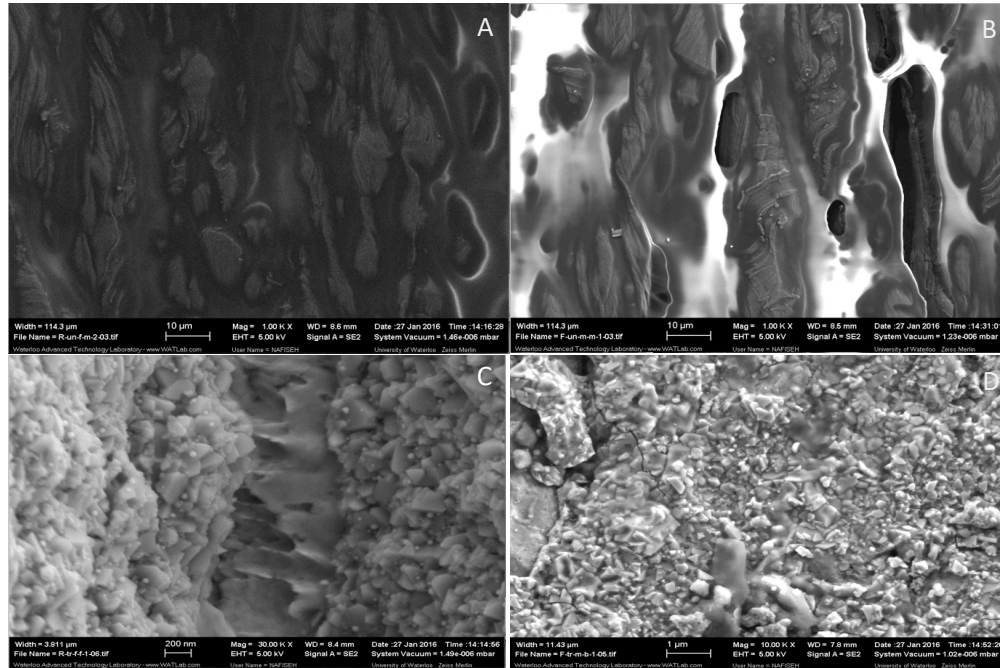


Figure 2.12 SEM results of trapping capillaries MXT-1 #3F and MXT-1 #3M. MXT-1 #3F from before (A) and after (C) treatment. MXT-1 #3M from before (B) and after (D) treatment.

MXT-1 #3F and #3M were also analyzed by EDX to determine their elemental compositions, as seen in Table 2.5. The untreated distributions of the C, O and Si were comparable from MXT-1 #3F and #3M with atomic percentages of about 50%, 35% and 15%, respectively. Before treatment, the presence of the underlying exterior metal capillary was evident for both MXT-1 #3F and #3M. After treatment, similar trends were seen from the MXT-1 #3F and #3M with the presence of the exterior metal capillary increasing. This was due to the treatment process decomposing and removing stationary phase material, resulting in a thinner material and exposing more of the exterior metal capillary. When the increase of metals was taken into consideration it was concluded that the oxygen increased, while the silicon remained the same or decreased only slightly after treatment with both MXT-1 #3F and #3M. The silicon also increased after treatment with the trapping capillary used by Edwards. However, due to the

drastic differences in the starting material used by Edwards and that within MXT-1 #3, the phase created after the same treatment process was not the same.

Table 2.5 EDX results of MXT-1 #3F and MXT-1 #3M before and after treatment plan 1

Element	MXT-1 #3F Untreated (Atomic %)	MXT-1 #3F Treatment Plan 1 (Atomic %)	MXT-1 #3M Untreated (Atomic %)	MXT-1 #3M Treatment Plan 1 (Atomic %)
C	50%	18%	45%	16%
O	35%	77%	37%	77%
Si	15%	6%	18%	7%

Ultimately, after investigating different sections of both MXT-1 #1 and #3 columns, the manufacturer was contacted to enquire about the changes made in the manufacturing of these columns. It was confirmed that the deactivation process had changed; however, the chromatographic performance of the columns still met manufacturing specifications. Despite the columns meeting all the manufacturer requirements, they were not producing a good quality sorbent after treatment as previously discovered. Due to the change in the deactivation process, the sorptive nanoparticle material first observed by Edwards could not be produced with the same yield. Since no other material had been used in the past, alternative stationary phases and other treatments were then investigated as possible solutions. Further investigation of continuous heating and absence of air during treatment were not analyzed with the Restek MXT-1 columns due to the poor performance under the previously ideal treatment conditions.

2.9 Summary

Recreation of the sorptive surface with carbon-doped silica nanoparticles originally created by Edwards was attempted. Chromatographically, the phase created with MXT-1 #1 performed poorly in comparison to that produced by Edwards, resulting in inefficient modulation and analyte breakthrough. Through examination by SEM, clear differences in the untreated and treated MXT-1 #1 trapping capillaries compared to those previously achieved by Edwards were quite apparent. Formerly, the untreated capillary used by Edwards had a consistent underlying deactivation layer allowing the stationary phase to be completely chemically bonded. On the other hand, the untreated capillary of MXT-1 #1 had a thick deactivation layer with gaps and ridges, only allowing the stationary phase to be bonded locally. After the same treatment process, the Edwards trapping capillary effectively converted the phase to a nanoporous material for effective modulation. In comparison, MXT-1 #1 had holes within the locally adhered stationary phase which left gaps within the converted phase after treatment, resulting in a less efficient sorptive material. It was clear that the starting material that was used by Edwards was different from that of MXT-1 #1. EDX was performed to differentiate the atomic percentages of carbon, oxygen and silicon before and after treatment in MXT-1 #1. The amount present in the untreated capillary MXT-1 #1 was lower than that found in the Edwards untreated capillary. With the Edwards trapping capillaries, the treatment process decreased the amount of carbon and oxygen, while increasing the silicon. For treatment plan 1, the carbon also decreased. However, the oxygen and silicon behaved in an opposite manner, increasing and decreasing, respectively, after treatment of MXT-1 #1. To overcome this issue, an alternative plan was implemented which included less treatment time and lower discharge voltages. Similar results to treatment plan 1 were obtained.

Different portions of MXT-1 #1 were used to create trapping capillaries to ensure it was consistent throughout. The MXT-1 #1M and #1E performed chromatographically the same and had similar topographies before and after treatment plan 1 was applied. Before treatment, MXT-1 #1M and #1E had different presence of silicon. It was concluded that due to the inconsistent nature of the stationary phase and the local adherence to the deactivation layer, that compositions of similar material could result in different results. This was due to the specific areas chosen for analysis. If an area was chosen with more adherence of the stationary phase to the deactivation layer, it would result in a higher presence of silicon. After treatment plan 1 was applied to both MXT-1 #1M and #1E, slightly different trends were achieved. MXT-1 #1M had a drastic increase in oxygen due to the removal of the stationary phase, leaving the underlying deactivation layer exposed. On the other hand, MXT-1 #1E had the same or slightly lower presence of silicon due to only the partial removal of the stationary phase in the specifically analyzed area. MXT-1 #3 was purchased to validate the results previously obtained and several portions across the entire column were tested (MXT-1 #3F and #3M). The modulation was slightly better with limited breakthrough and the SEM displayed fewer gaps in the deactivation layer before treatment. The sorptive nanoparticle surface was created with fewer gaps, permitting more efficient trapping. Atomic percentages from MXT-1 #3F and #3M were consistent before treatment. After treatment, both MXT-1 #3F and #3M revealed more of the exterior metal capillary, increased presence of oxygen and a similar or slight decrease in silicon. A similar trend was seen in the change of elemental composition produced by the treatment process on the trapping capillary used by Edwards; however, due to the differences in the starting material between Edwards and MXT-1 #3 the phases after treatment were not the same. Due to the change in the manufacturing process of the Restek MXT-1 deactivation layer, an alternative

column from a separate manufacturer would need to be investigated as the source of the trapping capillaries.

Chapter 3. Alternative sources of the trapping capillaries

3.1 Alternative stationary phases

The MXT-1 column used by Edwards provided an excellent starting material that allowed efficient trapping and complete desorption of analytes during single-stage modulation after the thermal treatment. However, unknowingly to us, the manufacturer of the deactivated tubing changed the deactivation process, and consequently the previous material became unavailable. After applying the treatment process established by Edwards to the new product, which nominally was the same column as that used by Edwards, it became clear that the product had changed drastically, resulting in a material that was no longer effective after treatment. In an effort to find an appropriate starting material that would produce an effective trapping material after treatment, various alternative columns from Restek and other manufacturers were evaluated. The goal was to find a good starting material that would be commercially available and easy to handle. After various treatment settings were applied, the trapping capillaries were used to perform a diesel analysis to test the chromatographic performance with active or passive cooling. Various modulation voltages were applied to determine the optimal range for effective remobilization of analytes with active or passive cooling. The instrumental and method parameters for the diesel analysis for all trapping capillaries can be found in Section 3.2. Following the analysis of diesel, the trapping capillaries were opened utilizing the aluminum jig described in Section 2.3 for imaging and evaluation of the topography and elemental composition by SEM and EDX, respectively.

3.2 Instrumental parameters for the analysis of diesel

Diesel was acquired from a local gas station within Waterloo, ON in order to analyze as a standard mixture. The sample was not diluted before injection into the analytical system. The GCxGC system used for analysis consisted of an Agilent 6890 gas chromatograph (Agilent Technologies, Santa Clara, CA, USA) equipped with a split/splitless injector and FID detector. The column configuration included a 30 m x 0.25 mm ID x 0.25 μ m Rxi-5MS (Restek Corp.) as the ¹D and a 0.5 m x 0.25 mm ID x 0.50 μ m MXT-WAX as the ²D. An Agilent 7683 series injector was used to make a 1 μ L injection of diesel using the split/splitless injector at a 300:1 split ratio. The inlet temperature was set at 280 °C with a 4 mm ID Precision split liner with wool (Restek Corp.) Helium gas with a purity of 99.999% was used as the carrier gas at a constant flow of 1.8 mL/min. The oven temperature program was 40 °C to 240 °C at 8 °C/min, followed by 20 °C/min to 260 °C, which was then held for 5 minutes. The FID was operated at 280 °C with an acquisition rate of 100 Hz and a ratio of 40 mL/min H₂ : 450 mL/min air. The UW single-stage, consumable-free thermal modulator was employed as the interface. A modulation period of 8 seconds was used. A more detailed description on the modulator operation can be found in Section 1.3. Both passive and active cooling were evaluated for the analysis of diesel.

3.3. Extreme treatment of MXT-1 #3

Prior to testing other stationary phases, the newly acquired MXT-1 column (0.28 mm ID x 1 μ m) previously labeled as #3, was exposed to an extreme treatment which included a sixty-minute phase at a temperature increase of 800 °C, followed by a second sixty-minute phase at a temperature increase of 680 °C. Previously, the trapping capillary had been treated with a variety

of temperature increases and phase times; however, due to the poor results obtained, all possibilities had to be examined.

After treatment, the trap was used to test a diesel sample, a ‘standard’ in GC×GC, to assess the ability to achieve an adequate separation. Figure 3.1 shows both the (A) two-dimensional chromatogram and (B) one-dimensional trace. Overall, this trapping capillary produced unsatisfactory modulation, in which some analytes seemed to have been retained too strongly to the active sites on the surface, only eluting once the oven temperature increased (Figure 3.1B). This resulted in the “streaking” present in Figure 3.1A. Due to the unsatisfactory results obtained with both the standard treatments and the extreme treatment, other columns were explored.

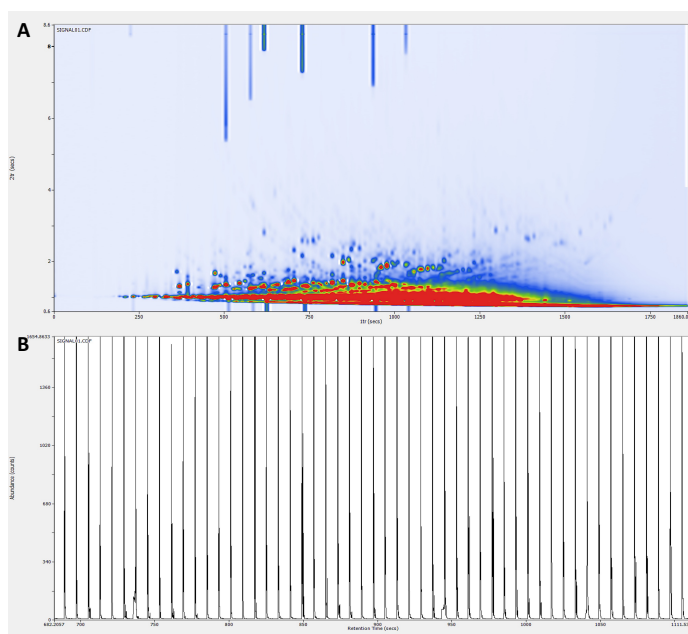


Figure 3.1 Diesel analysis utilizing the extreme treatment MXT-1 #3 (0.28 mm ID x 1 μm) trapping capillary

3.4 Alternative Restek stationary phases

Three separate starting materials were investigated as alternative options for the trapping capillary: an MXT-5 column with a 3 μm thick film of 95 % PDMS/5% phenyl referred to as #4, an older model MXT-Guard column referred to as #5, and a newly acquired MXT-Guard column referred to as #6. It is important to note the metal guard columns used contain a deactivation layer within the capillary. This phase is too thin to provide separation; however, there is enough of a deactivation layer present to be converted to a trapping material after the treatment process. Guard column #5 originated from the period when the original deactivation technology was used, which was the reason it was tested. All three traps were treated with a ten-minute phase at a temperature increase of 800 $^{\circ}\text{C}$, followed by two five-minute phases at a temperature increase of 680 $^{\circ}\text{C}$ with continuous air flow. The MXT-5 column contains a very similar stationary phase to the MXT-1, except for 5% phenyl present on the backbone. Despite this addition, the stationary phase is still considered low-polarity. In theory, the phase should behave similarly to the MXT-1 column that was previously used. As seen in Figure 3.2, the two-dimensional chromatogram of diesel utilizing the MXT-5 trap #4 produced adequate modulation with reasonable separation in the second dimension. All compounds visible in the chromatogram were modulated, as there are no streaks present. There is a normal distribution of hydrocarbons in diesel. There was minor tailing present within the second dimension, but no streaking within the ^2D . Streaking might occur in a chromatogram due to the amount injected from overloading or the concentration of the compound. Overall, the MXT-5 trap #4 was determined to be insufficient due to excessive trap bleed, hindering the separation of the compounds within the lower eluting band.

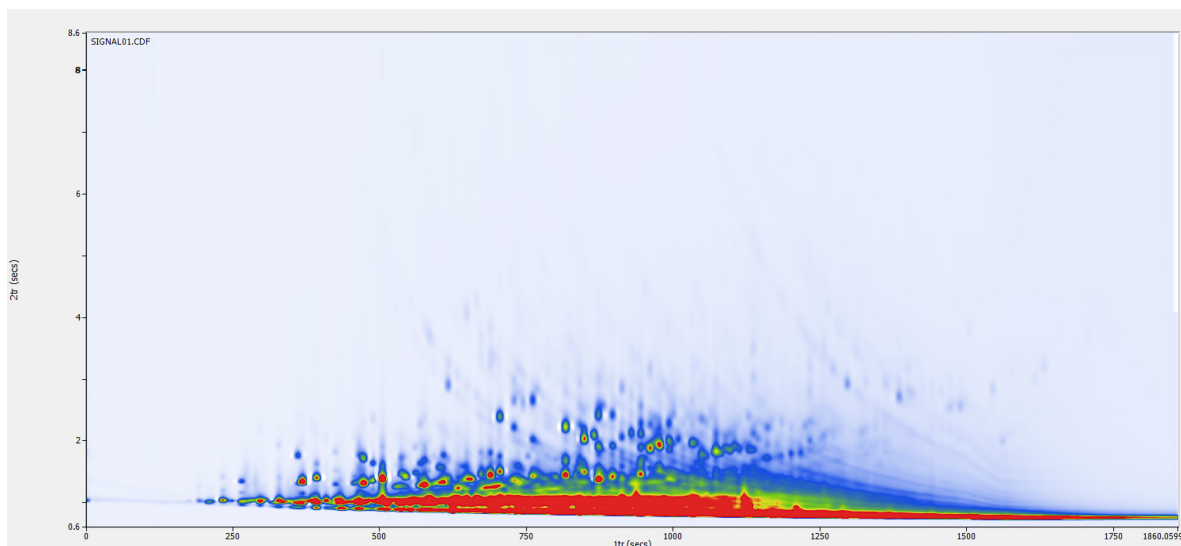


Figure 3.2 Diesel separation using MXT-5 trapping capillary #4

With only a very thin deactivation layer present, the guard columns should have theoretically been a poor choice for the modulation traps. However, guard column #5 showed promising results, as seen in Figure 3.3. The separation was similar to that obtained by MXT-5 trap #4. The peak widths in the $2D$ were comparable due to similar modulation. However, the early eluting compounds were most likely not trapped properly. Interestingly, the MXT guard columns #5 and #6 did not behave in a similar manner when subjected to the same treatment parameters.

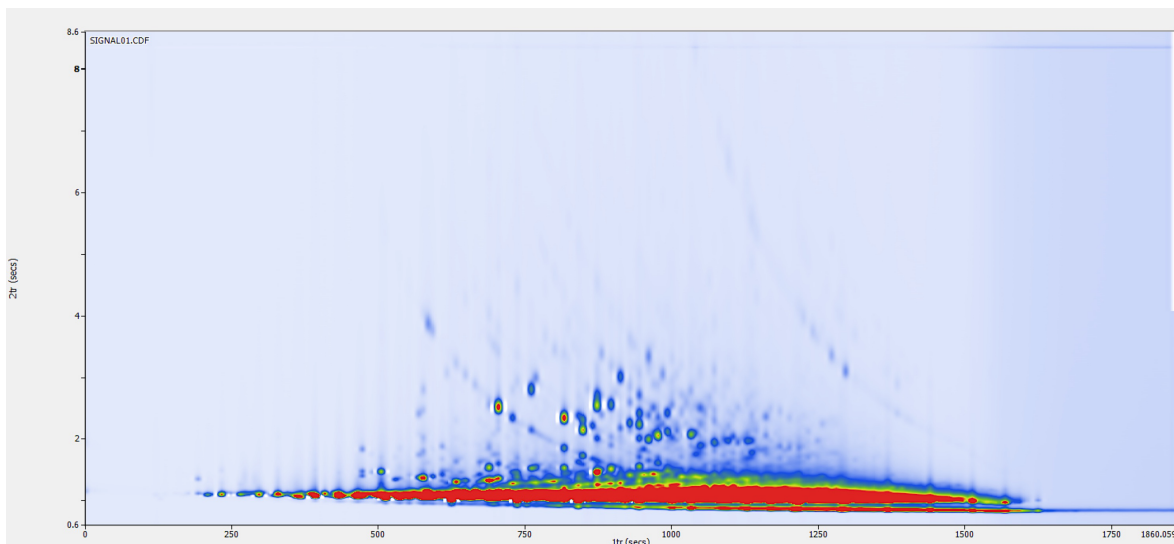


Figure 3.3 Analysis of diesel using MXT guard column trapping capillary #5

The guard column #6, as seen in Figure 3.4, performed extremely poorly, probably by retaining compounds too strongly on the active sites within the trap. This was emphasized in the one-dimensional chromatogram (Figure 3.4B), in which the peaks did not return to baseline. The capacity of the trap was possibly very low and compounds at slightly elevated concentration were only partially modulated, resulting in significant breakthrough. The partially modulated peaks appeared as streaks, as seen on the two-dimensional chromatogram (Figure 3.4A). The small amount of stationary phase present within the guard column justified the chromatographic results.

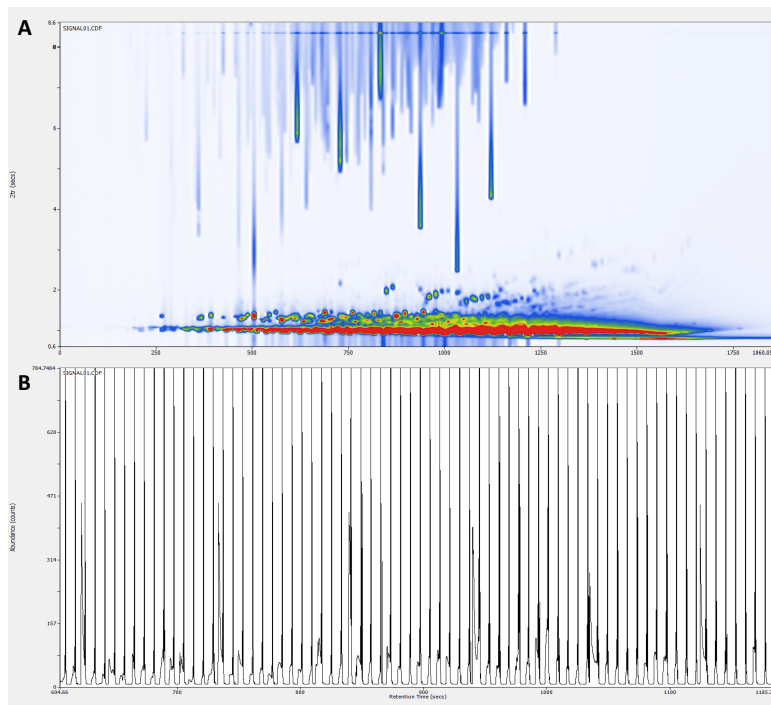


Figure 3.4 Analysis of diesel using MXT guard column trapping capillary #6

Overall, the MXT-5 column #4, as well as guard columns #5 and #6 were deemed inadequate for efficient modulation. Due to the change in the deactivation process for the tubing used by Restek, the results obtained previously by Edwards could not be recreated. Rather than performing further optimization on the Restek products, the project was shifted towards finding a new product which could provide a material that was robust, with accessible commercial consumables and able to perform effective modulation after treatment.

3.5 Agilent columns

Utilizing metal columns as a trap within the modulator is a vital requirement due to the use of capacitive discharge to rapidly heat the trap to reinject the analytes onto the second dimension. Due to the unreliable results obtained with the various Restek MXT products that were previously employed, an alternative manufacturer of metal columns was searched for.

Agilent Technologies Inc. is a highly respected and recognized manufacturer of GC columns that began manufacturing metal capillaries under the name ProSteel (PS). With a reputable history in the column market, they were a wise choice as source of an alternative starting material for the trapping capillaries. Despite the well-known processes used in the manufacturing of the Restek MXT Silcosteel and Siltek columns [92, 99], there is little public knowledge on the Agilent ProSteel products. The online catalogue simply states that the metal capillary is deactivated with a “special process treatment formula” which provides inertness [100]. The stationary phase in PS series columns is bonded and cross-linked and ideal for high temperature analysis. These properties and commercial availability made the Agilent ProSteel columns a potential alternative to the Restek MXT columns.

Two stationary phases were chosen due to their similar composition to that of the Restek 100 % PDMS MXT-1 phase. Agilent produces a DB-PS1 and DB-PS2887, both of which contain a non-polar, 100 % PDMS phase. The latter is specifically designed for a simulated distillation for the characterization of petroleum products and fractions. In accordance with the ASTM method D 2887, the boiling range distribution and boiling point order of hydrocarbons can be determined using this column. The ProSteel (PS) line utilizes a standard megabore column dimension of 0.53 mm ID, therefore traditional consumables can be used during installation and maintenance. However, the overall dimensions available in the metal capillary from Agilent differ drastically from the previously used 0.28 mm ID x 1 μm capillary. The DB-PS1 is available with the dimensions 0.53 mm ID x 0.15 μm film thickness, while the DB-PS2887 is available with the dimensions 0.53 mm ID x 3 μm film thickness. Despite the stationary phases being similar, each manufacturer utilizes their own deactivation, bonding and cross-linking technologies when manufacturing GC columns. While they behave in a comparable

manner when used for traditional GC analysis, the results obtained after thermal treatment could not be predicted.

First, untreated segments of DB-PS1 and DB-PS2887 columns were used as trapping capillaries for the analysis of diesel using the experimental parameters discussed in Section 3.2. Various discharge voltages were applied to determine the optimal voltage for remobilization. Understanding the capabilities of the untreated trapping capillaries was important to determine if they would be appropriate as an alternative option. As seen in Fig. 3.5, the separation achieved with the untreated DB-PS1 capillary was reasonably good. There was clear differentiation of the various homologous groups and good separation of early eluting compounds from the unresolved complex mixture at the beginning of the ²D. However, the ²D separation near the end of the run was not as good, with ²D peaks getting progressively wider. A relatively high capacitive discharge of 50 V was applied to completely release the trapped analytes in a quick manner. At lower modulation voltages, broad streaking occurred in the ²D. The streaks were caused by the analytes not being released sufficiently fast during desorption. By increasing the modulation voltage, the remobilization speed was increased, but at a cost of more pronounced bleed from the stationary phase in the trap, visible clearly in Figure 3.5. While the untreated DB-PS1 column performed reasonably well as a trapping capillary, treated traps previously prepared by Edwards performed significantly better. Thus, to improve the separation achieved, thermal treatment was applied to create an adsorbent material for improved trapping and desorption during modulation.

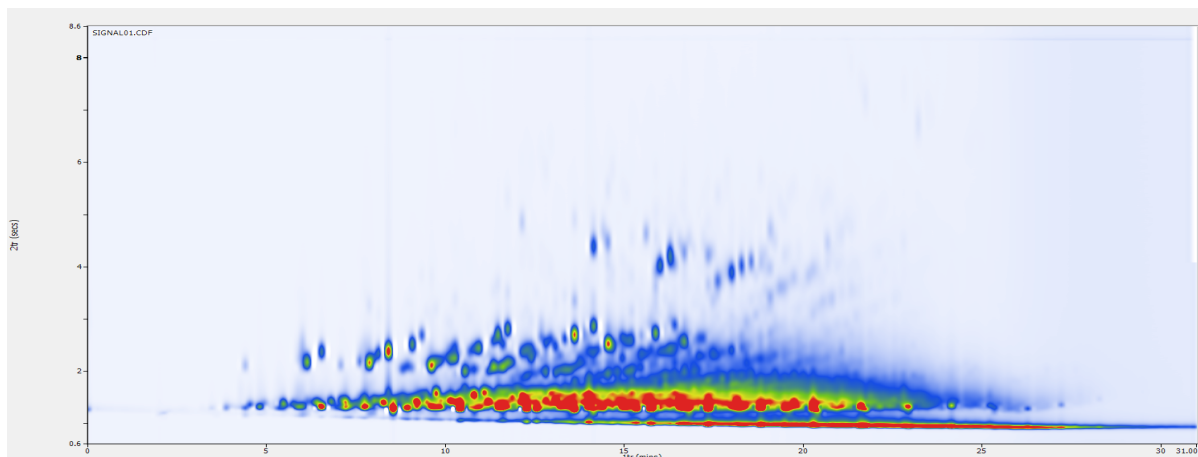


Figure 3.5 Analysis of diesel with an untreated DB-PS1 trapping capillary with active cooling and a modulation voltage of 50 V.

DB-PS2887 was also tested as a trapping capillary with no treatment applied to assess the capabilities of the untreated phase. Fig. 3.6 displays the separation of diesel obtained with DB-PS2887. Similarly, to untreated DB-PS1 the DB-PS2887 also provided adequate separation with differentiation of the various groups. Minor streaking of the lighter weight compounds was observed together with lower resolution of the heavier compounds, consistent with slower analyte remobilization from the thicker film of the stationary phase. The stationary phase bleed was significantly more pronounced, extending throughout nearly the entire run even though a lower capacitive discharge voltage of 40 V was applied to achieve remobilization of the trapped analytes. Streaking was significant when lower capacitive discharge voltages were used. As before, it was assumed that the thermal treatment would help improve trapping and release of the analytes.

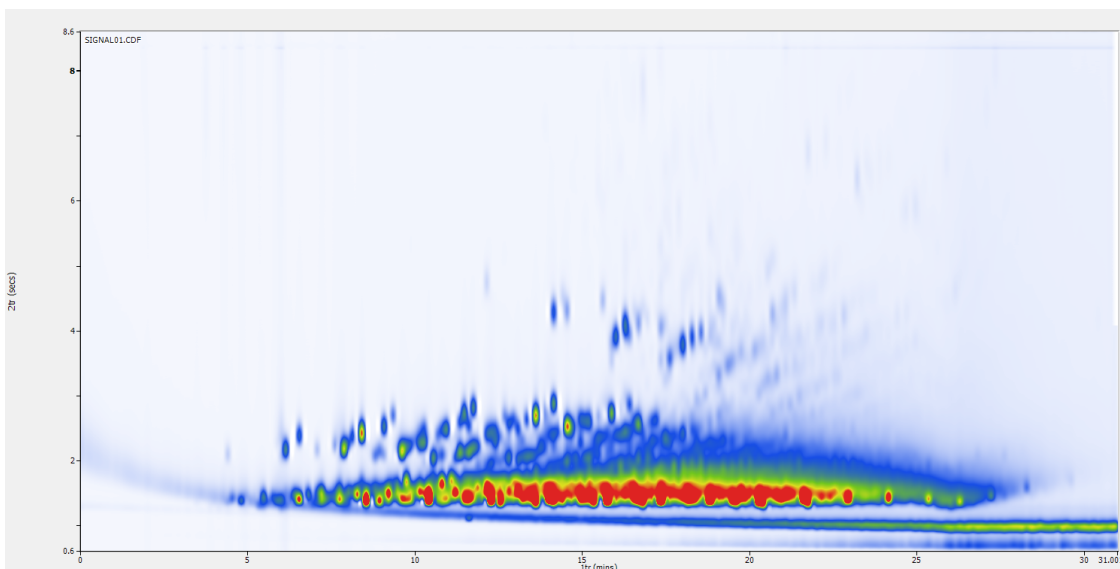


Figure 3.6 Analysis of diesel with an untreated DB-PS2887 trapping capillary with active cooling and a modulation voltage of 40 V.

3.5.1 Treatment plan

Originally, to maintain analogous treatment conditions to those previously used on the Restek MXT-1 capillaries, the same treatment times and voltages were used. However, after initial inspection of the Agilent ProSteel capillaries, it became clear that the composition of the exterior metal tubing was different from the Restek material. The Agilent metal tubing was extremely pliable and soft when compared to the rigid material used by Restek. The original treatment parameters included a ten-minute phase at a temperature increase of 800 °C and two five-minute phases at a temperature increase of 680 °C. The temperature increase values were specific to the Restek MXT-1 capillary with corresponding applied voltages of 68 V and 62 V, respectively. When the preliminary voltage of 68 V was applied to both the DB-PS1 and DB-PS2887 capillaries for treatment, they immediately broke due to excessive current. When the original treatment of 68 V was applied to the MXT-1 capillary, it would glow bright red for each

successive capacitive discharge. This was an important visualization tool in the treatment process to ensure the decomposition of the original material was occurring. To determine the voltage required to obtain a glowing red capillary without breakage, the capacitive discharge was lowered from 68 V. The DB-PS1 and DB-PS2887 trapping capillaries were subjected to maximum capacitive discharge voltages during treatment of 55 V and 60 V, respectively. However, these values still caused occasional breakage of the capillary. The voltages were steadily decreased until the entire treatment process could be completed, while maintaining the red glow. Temperature increase values similar to those used with the Restek MXT-1 tubing could not be achieved with either DB-PS1 or DB-PS2887 columns due to the limitations of the metal tubing material. The same capacitive discharge voltages were selected for both DB-PS1 and DB-PS2887 columns due to the presence of the red glow without breakage during the total treatment time, even though (as explained later) the maximum temperature values during the treatment were not identical. It was decided that it was more important to treat the DB-PS1 and DB-PS2887 capillaries at voltages that would maintain the red glow during treatment without breakage rather than aiming at the same temperature increase and risking frequent failures.

The treatment plan consisted of a ten-minute phase with 50 V discharge applied, followed by two five-minute phases at 45 V with continuous air flow throughout. The DB-PS1 and DB-PS2887 had varying temperature increase values at the same applied capacitive discharge due to the different specific resistance of the tubing. For an applied capacitive discharge of 50 V and 45 V, the DB-PS1 had corresponding temperature increases of 530 °C and 440 °C, while the DB-PS2887 had corresponding temperature increases of 650 °C and 545 °C. DB-PS1 was treated for ten minutes at 50 V followed by two five-minute phases at 45 V and will be referred to as DB-PS1 #1. DB-PS2887 was also treated for ten minutes at 50 V followed by two five-minute phases

at 45 V and will be referred to as DB-PS2887 #2. It is important to note that the temperature increase values during treatment for DB-PS1 and DB-PS2887 were not identical, so the products cannot be directly compared with regard to their structure and performance after treatment. However, it was decided that keeping the treatment protocol as simple as possible would be advantageous in the long run. As long as the red glow was observed during the treatment process, the stationary phase was above the decomposition temperature, and previous knowledge obtained by Edwards indicated that exact temperature control is not required for the creation of the desired adsorbent material. The method for determining the temperature increase values for each applied voltage will be discussed in Chapter 5.

3.5.2 Performance results

Due to the unknown nature of the Agilent capillaries used as traps within the modulator, the voltage applied during modulation was also investigated. Multiple analyses were completed with a starting value of 25 V applied during modulation for the analysis of a diesel sample. The voltage was increased at 5 V increments, while the overall separation and modulation capabilities were monitored. The experimental parameters for the analysis of diesel were described in Section 3.2. The treated DB-PS1 trapping capillary #1 results for the analysis of diesel at three different applied voltages are presented side by side in Figure 3.7. When 30 V was applied for modulation (Figure 3.7A), adequate separation was achieved in the second dimension; however, streaking was present at the top of the secondary space. With a low voltage, some analytes were strongly sorbed to the active sites within the trap and were not released rapidly enough. They instead remained sorbed until the temperature of the oven increased during the run, allowing them to be mobilized as a broad band creating a streak within the secondary space. When the

modulation voltage was increased to 50 V (Figure 3.7B), the separation improved, but streaking was still present in the secondary space. Applying a voltage of 55 V (Figure 3.7C) led to the decomposition of some analytes due to pyrolysis within the trap. 50 V was determined to be an appropriate modulation voltage for proper modulation when utilizing the DB-PS1 trapping capillary #1.

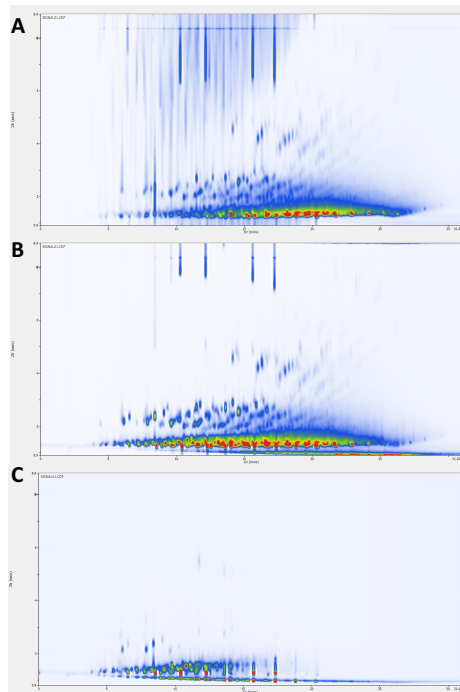


Figure 3.7 Analysis of diesel with a treated DB-PS1 #1 trapping capillary with modulation voltages of (A) 30 V, (B) 50 V, (C) 55 V.

The treated DB-PS2887 trapping capillary #2 results for the analysis of diesel at three different applied voltages are overlaid in Figure 3.8. Poor modulation and extreme streaking were present when 30 V was applied (Figure 3.8A) for the same reasons as explained above. Increasing the modulation voltage to 45 V (Figure 3.8B) slightly improved the separation, eliminating some streaking within the chromatogram. However, the stationary phase bleed was more pronounced. At an applied voltage of 60 V, pyrolysis of the analytes occurred, eliminating

some compounds from the chromatogram (Figure 3.8C). Since a voltage of 60 V was too extreme, 50 V was decided to be a suitable modulation voltage for the modulation when using the DB-PS2887 #2 trapping capillary.

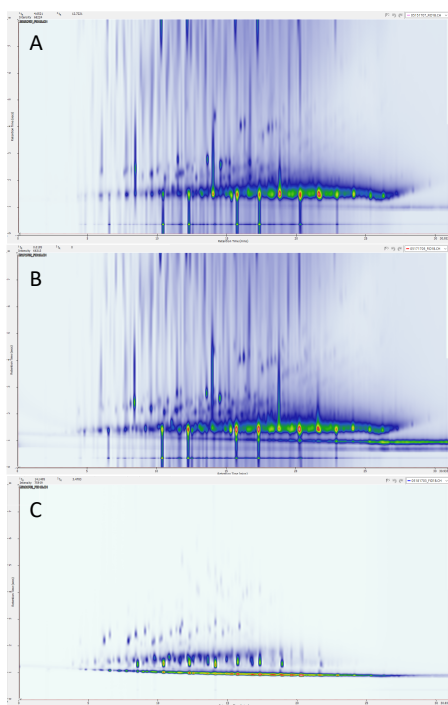


Figure 3.8 Analysis of diesel with a treated DB-PS2887 #2 trapping capillary with modulation voltages of (A) 30 V, (B) 45 V, and (C) 60 V.

3.5.3 SEM and EDX results

To better understand the Agilent DB-PS1 #1 and DB-PS2887 #2 materials as trapping capillaries before and after treatment, both SEM and EDX were employed. Several magnifications were evaluated to visualize all aspects of the surface. The untreated DB-PS1 trap images at magnifications of 500x and 20,000x can be seen in Figures 3.9A and 3.9C, respectively. Initially, it was seen that the stationary phase was completely bonded to the deactivation phase with no gaps present in the untreated state. Further inspection of the zoomed

SEM image displayed a flakey texture in which small cracks or ridges were present within the stationary phase. Nevertheless, the ridges were small in comparison to those found within the Restek columns. It was critical that the stationary phase was completely bound to the underlying deactivation phase without any gaps, similarly to that observed by Edwards. After treatment, the DB-PS1 #1 trap images at magnifications of 500x and 20,000x can be found in Figures 3.9B and 3.9D, respectively. The overall texture after treatment was different from the untreated capillary. It was evident that the stationary phase had been decomposed, leaving a uniform deactivation phase exposed. Most importantly, the treatment process created nanoparticles, which were vital for proper modulation.

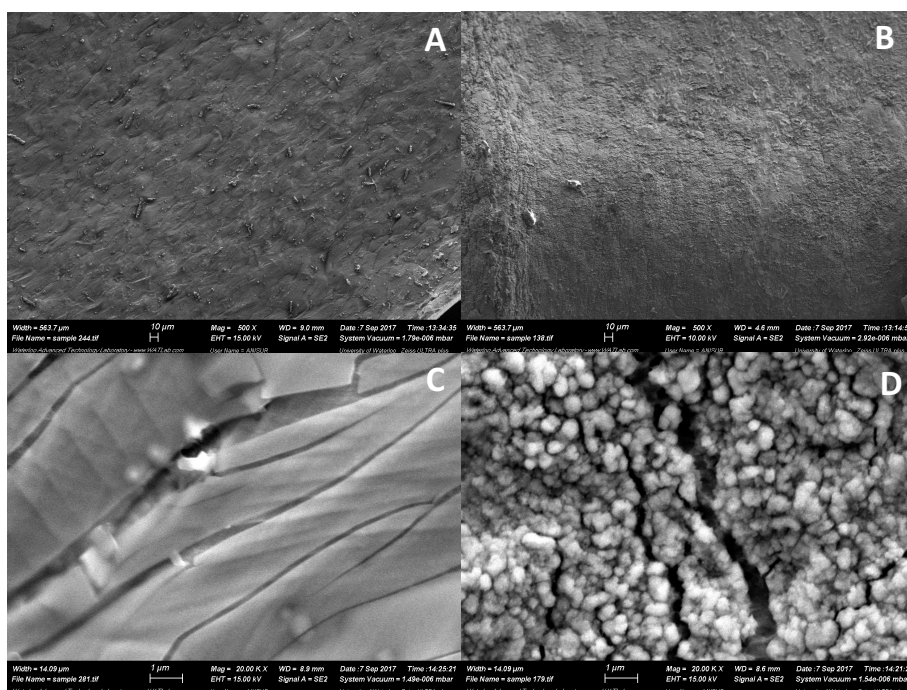


Figure 3.9 SEM images of DB-PS1 #1 (A) 500x magnification untreated, (B) 500x magnification treated, (C) 20,000x magnification untreated, and (D) 20,000x magnification treated.

The SEM images of the DB-PS2887 #2 trapping capillary can be seen in Figure 3.10. The untreated DB-PS2887 #2 at magnifications of 100x and 20,000x are shown in Figures 3.10A and

3.10C, respectively. Initial inspection showed that the stationary phase appeared to be completely bonded to the underlying deactivation layer (Figure 3.10A). Under higher magnification, it appeared the stationary phase had small gaps present and the sections that were bonded were uniform with no flaking present (Figure 3.10C). The untreated DB-PS2887 had to be gold coated (~20 nm) in order to properly image under higher magnifications. Without the gold coating present, the surface became excessively charged with a large accumulation of electrons, which resulted in a blurred image. Even though the gold coating helped with the imaging process, it also covered the majority of the minor features present on the untreated surface. Due to the very smooth surface and minimal detail, the image after gold coating does not present valuable information about the topography. After treatment, the texture of the surface changed in comparison to the untreated surface (Figure 3.10B). Upon closer magnification, less

cracking was present in the deactivation phase when compared to the DB-PS1 #1 treated surface. Nanoparticles along the surface were also created during the treatment process (Figure 3.10D).

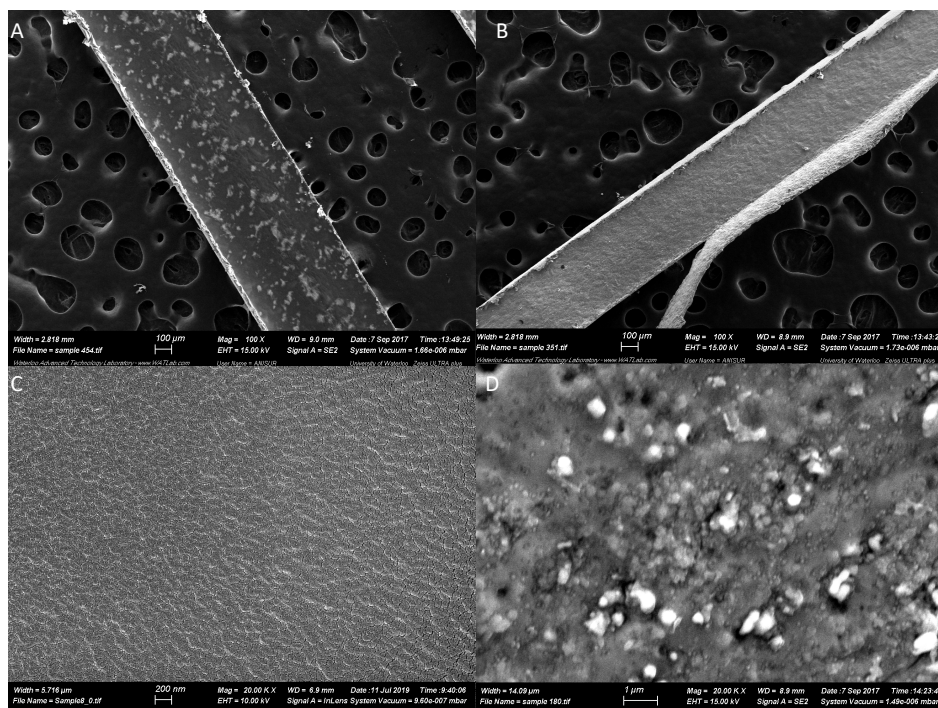


Figure 3.10 SEM images of DB-PS2887 #2, (A) 100x magnification untreated, (B) 100x magnification treated, (C) 20,000x magnification untreated, and (D) 20,000x magnification treated.

EDX analysis was performed to determine the changes in the elemental composition of the stationary phase within the modulator traps before and after treatment. Polydimethylsiloxane stationary phase is composed of carbon (C), silicon (Si) and oxygen (O) at specific atomic percentages [98]. By comparing the untreated and treated Agilent capillaries, the transformation of the stationary phase could be further understood. It is important to note that due to the operational capabilities of EDX, the thickness of the material present within the trapping capillary could affect the detection of metals from the column tubing. The metals present in the exterior capillary were identified as iron and chromium. To compare the Agilent capillaries

before and after treatment, the relative ratios of carbon, oxygen and silicon with respect to iron and chromium were examined. Absolute intensities of the individual peaks could not be used for comparison due to the possible variability in results when analyzing the same sample caused by the geometry or angle of the beam and voltage applied. The location of the peak on the x-axis corresponds to a specific energy of the x-ray emitted, which helps identify the element. Carbon, oxygen and silicon energies were 0.277, 0.523 and 1.740 (keV), respectively. Iron was found at values of 0.705 and 6.403, while chromium was found at values of 0.573 and 5.414 (keV) [4].

EDX spectrum of the DB-PS1 #1 treated capillary was compared to the spectrum of the untreated capillary, as seen in Fig. 3.11. Carbon, oxygen and silicon were clearly identified in both spectra. Iron and chromium were present at their designated x-ray emission energies but were not labeled. The peaks in both spectra were similar; however the relative ratios of oxygen to silicon and to the metals present were different. Silicon was the most abundant peak in both spectra, but the iron and chromium increased significantly after treatment in comparison to the untreated capillary. This was most likely due to the removal of the stationary phase and possibly some of the deactivation layer, revealing more of the underlying exterior metal capillary. The only other possible explanation would be that the amount of silicon was reduced while the intensity of the metal bands remained the same. However, this is rather unlikely, as no volatile silicon species should be formed during thermal decomposition of PDMS in the presence of oxygen. What is certain is that oxygen signal increased after the treatment relative to silicon. This is consistent with the conversion of PDMS to silica. In addition, metal oxides could have been formed during treatment.

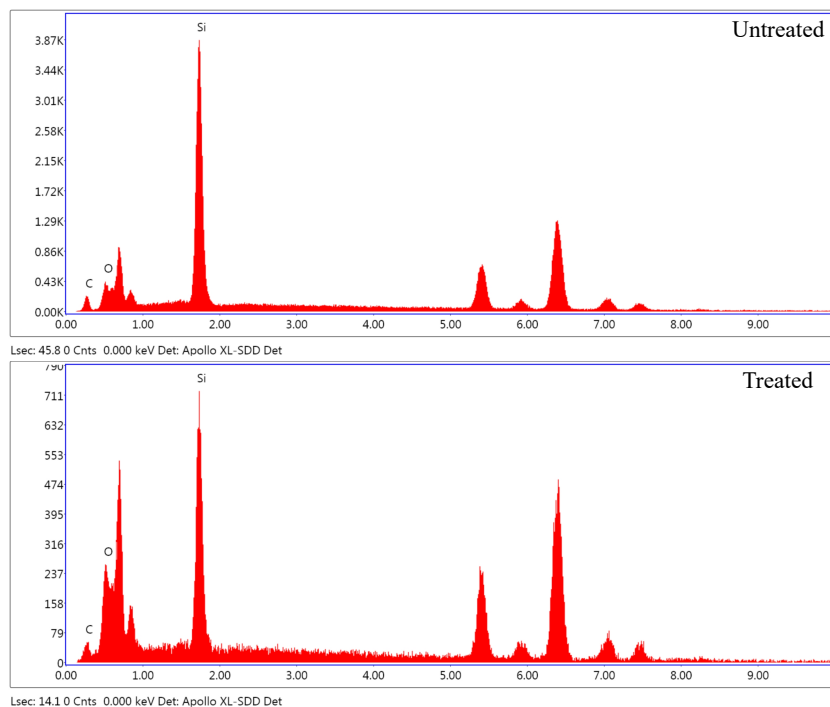


Figure 3.11 EDX comparison of the untreated DB-PS1 and treated DB-PS1 #1 capillaries.

EDX spectrum of the DB-PS2887 #2 trapping capillary was compared to the spectrum of the untreated DB-PS2887 capillary, as seen in Fig. 3.12. The same elements were identified as before. In the spectrum of the untreated capillary, the intensities of the metals were very small in comparison to the carbon, oxygen and silicon. This was due to the thick stationary phase, shielding the underlying metal capillary. The intensity of silicon significantly decreased after treatment in comparison to the untreated capillary. However, this must be compared to the relative ratio of metals present before and after treatment. After treatment, the intensity of iron and chromium increased dramatically due to the decomposition of the stationary phase during treatment, exposing the underlying exterior metal capillary. As before, oxygen increased after treatment due to the conversion of PDMS to silica and possibly the exposure of the deactivation layer and the metal capillary.

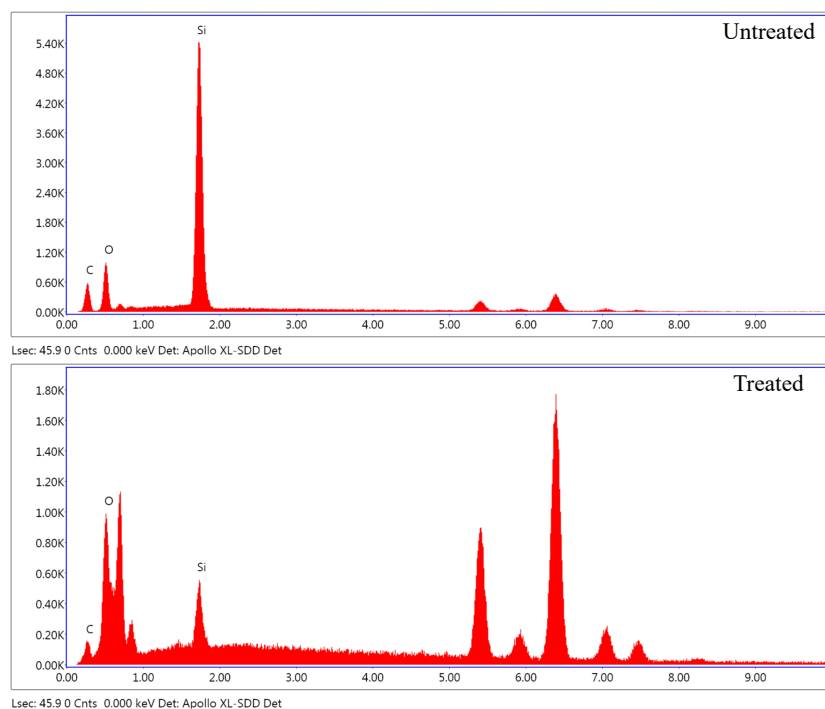


Figure 3.12 EDX comparison of the untreated DB-PS2887 and treated DB-PS2887 #2 capillaries.

3.6 Various voltage treatments of Agilent columns

Initially, the chromatographic performance of the DB-PS1 #1 and DB-PS2887 #2 trapping capillaries showed promising results. The SEM images showed a stationary phase more uniformly bonded to the underlying deactivation layer, which was previously determined to be vital in the proper conversion to an adsorbent material after treatment. The EDX results showed that with both capillaries the treatment process decomposed the stationary phase and exposed more of the underlying exterior metal capillary. To further optimize their performance as a trapping capillary, various voltages during treatment were investigated. As seen in Table 3.1, both DB-PS1 and DB-PS2887 were treated using similar capacitive discharge voltages that were greater than or less than the treatment of 50 V followed by 45 V. The previously established time

of treatment, a ten-minute phase with a higher voltage followed by two five-minute periods with a slightly lower voltage remained the same. Air was provided during the treatment process for all scenarios. The corresponding temperature increase for each capacitive discharge setting was determined using an in-house built calculator, which will be described in Chapter 5. As seen in the chart, the corresponding temperature values for the lower voltage settings of 40 V and 30 V differed for the DB-PS1 and DB-PS2887 columns because of different resistance of the tubing. This could have been due to different wall thicknesses of the tubing or different alloys used. The DB-PS2887 column was capable of handling a higher discharge voltage when compared to DB-PS1. When 60 V was applied to the DB-PS1 trapping capillary during treatment, it instantly snapped since it could not withstand such a high temperature increase. A maximum capacitive discharge of 55 V was achievable for this column. Due to the different temperature increases obtained at similar voltages, the Agilent columns were not treated under the same temperature increases. This makes the two columns incomparable; however, obtaining the glowing red capillary during treatment was more important to ensure the conversion of the stationary phase occurred. From the initial voltages of 50V and 45V, a similar voltage increase or decrease was performed. It is also important to note that DB-PS 1 #11 and DB-PS2887 #25 were tested below the decomposition temperature and did not have a red glow during treatment. These plans were tested to have a complete understanding of how the Agilent stationary phases transformed when any voltage was applied during treatment.

Table 3.1 Various treatment plans for DB-PS1 and DB-PS2887

ID#	Column	1 st stage (10 min)		2 nd stage (5 min)		3 rd stage (5 min)	
		Temp. Increase (°C)	Voltage (V)	Temp. Increase (°C)	Voltage (V)	Temp. Increase (°C)	Voltage (V)
27	DB-PS1	640	55	530	50	530	50
9	DB-PS1	355	40	280	35	280	35
11	DB-PS1	215	30	160	25	160	25
22	DB-PS2887	900	60	770	55	770	55
17	DB-PS2887	450	40	365	35	365	35
25	DB-PS2887	290	30	222	25	222	25

3.6.1. Performance results

To assess the performance of the newly treated Agilent trapping capillaries, they were first used in the analysis of diesel. The instrumental parameters and method employed for the analysis were the same as those discussed in Section 3.2. The pattern of diesel in GC×GC chromatograms is well known, permitting an easy evaluation of each set of treatment parameters for both DB-PS1 and DB-PS2887. Similarly to the assessment of the original treatment parameters of 50 V followed by 45 V, the capacitive discharge voltage applied during modulation was also varied. This voltage during modulation has a drastic effect on the chromatographic performance, so it was vital to establish an appropriate range for efficient remobilization for each set of voltage treatment parameters. Voltages ranging from 25 V to 55 V were applied at 5 V increments.

DB-PS1 #9 was treated at 40 V and 35 V and subsequently used for the analysis of diesel. Various modulation voltages were applied with both active and passive cooling, as seen in Fig 3.13. Active cooling (A-C) was compared to passive cooling (D-F) at similar modulation voltages. When a low voltage of 35 V was applied, incomplete remobilization of analytes occurred with both active (A) and passive (C) cooling, indicated by broad streaks within the second dimension. The broad streaks were caused by strong sorption by select analytes that were not efficiently remobilized due to the combination of a strong sorbent and a low modulation voltage. An increase in modulation voltage to 50 V greatly improved the chromatographic performance with active (B) and passive (E) cooling. In the latter case, the streaking was completely eliminated, resulting in a clear separation of all groups in the second dimension, but some analytes were pyrolyzed as evidenced by their disappearance from the chromatogram. Increasing the modulation voltage to 55 V caused further pyrolysis of the sample for both active (C) and passive (F) cooling. A more detailed, quantitative characterization of the trap performance is planned for the future. Compared to DB-PS1 #1, which was treated at 50 V followed by 45 V, it appeared the 40 V and 35 V treatment performed reasonably well for passive cooling only. For active cooling, a slightly higher treatment voltage above 40 V was necessary to achieve adequate two-dimensional separation without streaking artifacts. After visually examining the chromatographic performance of the trapping capillary, SEM and EDX analyses were performed.

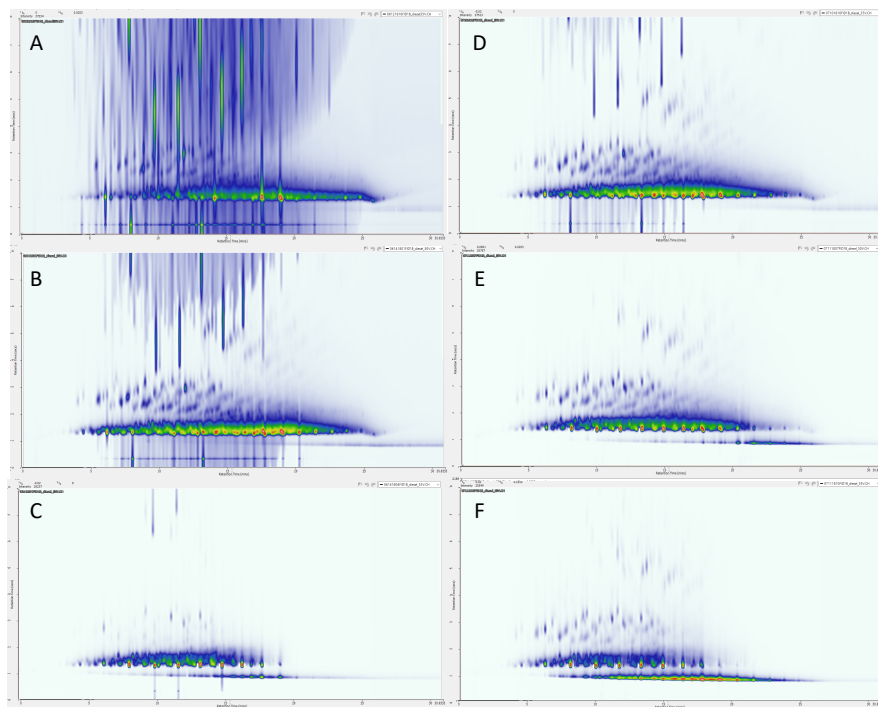


Figure 3.13 Comparison of the performance of a treated DB-PS1 #9 trapping capillary at various modulation voltages with active (A - C) and passive cooling (D - F) in the analysis of diesel. The deactivation layer was present within the unions at the front and back end of the trapping capillary. Modulation voltages were 35 V (A and D), 50 V (B and E) and 55 V (C and F).

DB-PS1 #27 and #11 were also used for the analysis of diesel to evaluate the chromatographic performance with active or passive cooling at various modulation voltages. The results were found to be inferior to DB-PS1 #9 and DB-PS1 #1 since efficient trapping and remobilization could not be achieved. Further discussion of these results can be found in Appendix A.

After full investigation of a variety of treatment voltages for the DB-PS1 phase, it can be concluded that a range between 40 V to 50 V for the initial ten-minute phase is the most suitable in providing an adsorbent phase to assist in trapping and efficient remobilization of the analytes for single-stage modulation. Voltages above 50 V would be detrimental in the production process, possibly wasting an expensive consumable for little to no improvement in

chromatographic performance. Due to the excessive discharge applied during the treatment process, these parameters typically led to breakage of the metal capillary without completion of the desired treatment time. Voltages of 40 V and below performed better with passive cooling in comparison to active cooling. However, in an effort to create a universal material that could be used with either mode of cooling, with little to no modifications or maintenance of the modulator setup, it would be advantageous to not perform treatment below 40 V. If passive cooling was all that was required of extremely high-molecular weight analytes which require little cooling for trapping, lower treatment voltages might be appropriate. A more complete evaluation of the stationary phase characteristics would be performed by SEM and EDX.

The same treatment parameters were also applied to the DB-PS2887 phase, except for the voltage settings greater than 50 V. The different resistance of the PS2887 tubing allowed the use of a treatment voltage of 60 V for 10 minutes, followed by two five-minute phases at 55 V. The same analytical instrumentation and method parameters were implemented in the analysis of diesel to examine the chromatographic performance of all voltage treatments of DB-PS2887. Various modulation voltages ranging from 25 V to 50 V at 5 V increments were tested as before. Both active and passive cooling were tested.

Treatment voltages of 40 V and 35 V were also applied to DB-PS2887 #17 and used in the analysis of diesel with active and passive cooling at various modulation voltages, as seen in Fig. 3.14. Applying a low voltage of 25 V with active (A) and passive (D) cooling resulted in similar chromatographic results. With lower treatment voltages, the DB-PS2887 #17 phase behaved more closely to that of the DB-PS1 #9 phase. Clear differentiation of the various groups was achieved with the roof-tile effect across the entire secondary space. Under further inspection, the active cooling had slightly more tailing occurring than the passive cooling. By

increasing the modulation voltage to 45 V, both the active (B) and passive (E) cooling produced slightly better separation of analytes from the unresolved complex mixture eluting at the bottom of the secondary space, but trap bleed became more pronounced. Pyrolysis occurred at voltages of 55 V and 50 V, for active (C) and passive (D) cooling, respectively. Compared to the original treatment parameters of 50 V and 45 V, the lower treatment voltages obtained significantly improved chromatographic performance. There were no broad streaking bands in the 2D , which signified the phase was sorptive enough to trap the analytes, but not too strong of a sorbent to prevent efficient release of the trapped analytes.

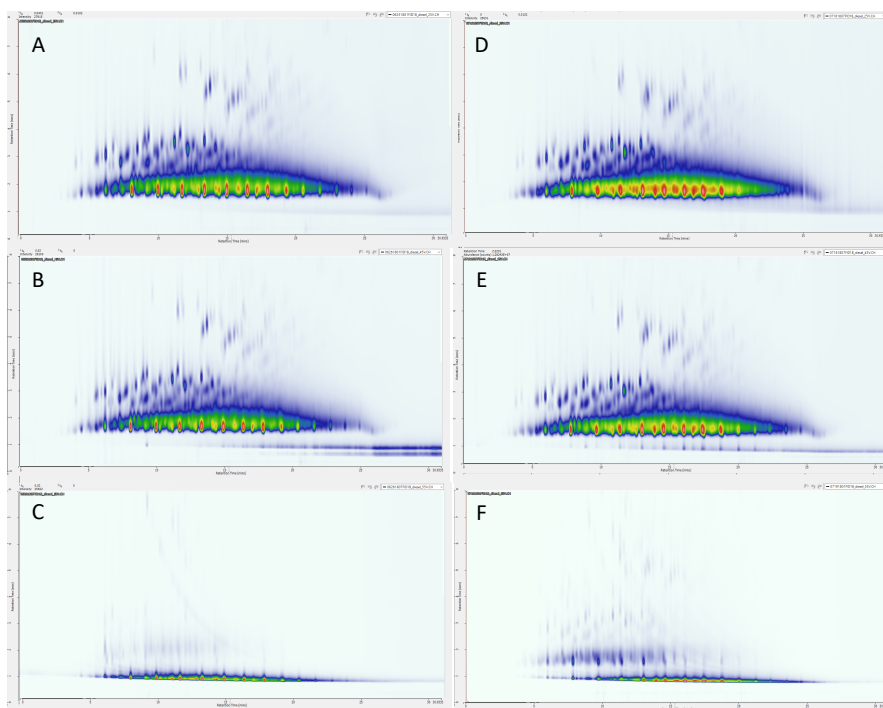


Figure 3.14 Comparison of the performance of the DB-PS2887 #17 trapping capillary at various modulation voltages with active (A - C) and passive cooling (D - F) in the analysis of diesel. The deactivation layer was present within the unions at the front and back end of the trapping capillary. Modulation voltages were 25 V (A and D), 45 V (B and E), 50 V (F) and 55 V (C).

DB-PS2887 #22 and #25 were also tested in the analysis of diesel to evaluate their chromatographic performance. The results were found to be inferior to DB-PS2887 #17 and DB-

PS2887 #2 since efficient trapping and remobilization could not be achieved. Further discussion on these results can be found in Appendix A.

After full evaluation of various treatment voltages to the DB-PS2887 trapping capillary, it was concluded that parameters of 40 V followed by 35 V achieved the best chromatographic performance. A modulation voltage of 45 V provided the best separation; however, lower voltages could be applied adequately depending on the sample analyzed. Higher voltages of 50 V and 60 V in the treatment process resulted in undesirable broad bands within the second dimension and poor separation from the early eluting unresolved complex band. This set of treatment voltages created excessively strong sorbent, resulting in poor remobilization of the trapped analytes. Also, the entire treatment process was rarely completed without breakage under these high discharge voltages, ultimately wasting material. Lower voltages were inadequate in providing satisfactory chromatography when active cooling was applied. Passive cooling produced satisfactory chromatographic performance but would only be appropriate for the analysis of higher molecular weight compounds which do not require active cooling for trapping. DB-PS2887 #17 performed significantly better with both active and passive cooling when compared to DB-PS1 #9. However, all other treatment plans of DB-PS2887 were ultimately determined inferior in comparison to the DB-PS1 phase. This was due to the insufficient separation of the early eluting compounds from the large unresolved complex mixture. Further evaluation by SEM and EDX was performed to characterize the stationary phases within the trapping capillaries.

3.6.2. SEM and EDX results

After chromatographic evaluation was completed, the trapping capillaries were further characterized by SEM and EDX analyses. DB-PS1 #9 was treated at a lower set of voltages compared to DB-PS1 #27. A value of 40 V was implemented for ten-minutes, followed by two five-minutes phases at 35 V. Fig. 3.15 displays the SEM images at various magnifications. The visual appearance of the phase after treatment was vastly different from previous treatment parameters. A magnification of 500 times shows a large area of the treated phase (A). It appeared cracked and rough with an uneven surface. Under closer inspection of 2,000 (B) and 10,000 (C) magnification, three different types of surfaces were apparent. The light-colored flakes were the decomposed PDMS stationary phase and the dark underlying layers were stationary phase that has been slightly broken down. The stationary phase had been partially decomposed in the treatment process, but the lower treatment voltages had not resulted in a complete conversion to the desired adsorbent. Only a few small, round nanoparticles could be observed on top of the dark stationary phase. Chromatographically, this treatment process produced better separation with passive cooling compared to active cooling. Thus, the material was an efficient sorbent for proper trapping with minimal cooling. Ultimately, this would signify a stronger sorbent material than previously achieved by Edwards.

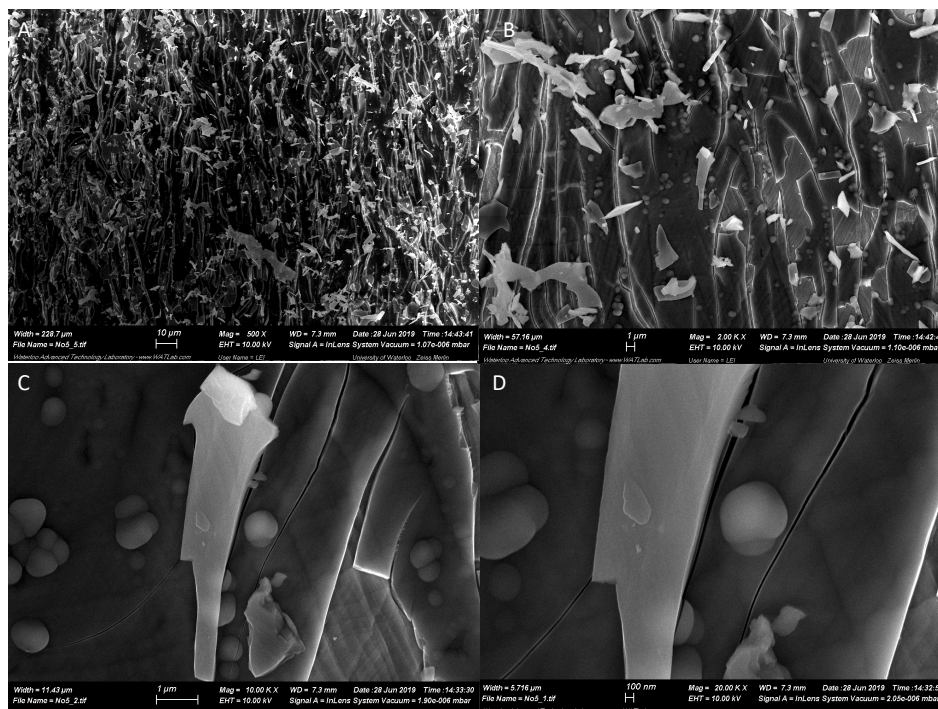


Figure 3.15 SEM images of DB-PS1 #9, (A) 500x magnification treated, (B) 2,000x magnification treated, (C) 10,000x magnification treated, and (D) 20,000x magnification treated.

Due to the drastically different surfaces present, each was individually analyzed by EDX for better understanding. Fig. 3.16 shows the image that was used to select the three specific areas for the analysis. The corresponding spectra are also displayed and labeled with their designated area number. The spectrum for the untreated DB-PS1 was placed above the three examined areas for easy comparison. It is important to note the scales on the x-axis are different for the untreated DB-PS1 compared to three areas for DB-PS1 #9. Despite the difference in scales, carbon, oxygen, silicon, iron and chromium were all identified at their corresponding x-ray emission energies. Area 1 corresponded to the nanoparticle that was adhered to the dark stationary phase underneath. Area 2 corresponded to the light stationary phase flake that was loosely adhered to the dark stationary phase. Area 3 corresponded to the dark stationary phase layer that was partially decomposed, revealing the underlying deactivation layer. Compared to

the untreated spectrum, the presence of iron and chromium decreased significantly for all three areas examined. The material formed after treatment must have shielded the underlying metal surface better, as the signals for metals decreased relative to that of silicon. The apparent increase in the relative magnitude of the silicon signal could have been due only to better shielding of the underlying metal, or to more of the silicon-based deactivation layer being exposed. Carbon and oxygen were present at very low relative intensities in all three spectra. In comparison to the untreated spectrum, it was apparent that the signals for carbon and oxygen decreased relative to silicon after treatment, possibly because more of the deactivation layer became exposed. There was a weak oxygen signal (not labeled) in the nanoparticles, noted as area 1. Carbon decreased after treatment, resulting in a surface dominated by silicon for all three areas examined. Based on the appearance and trends in elemental spectra, it can be concluded that the treatment process broke down the stationary phase which was cross-linked and chemically bound to the underlying deactivation layer. When this occurred, light flakes started to peel off the dark stationary phase, possibly representing an intermediate stage of the transformation to silica nanoparticles. As the conversion reached completion, the flakes created nanoparticles on the surface. SEM and EDX analyses were also performed on DB-PS1 #27 and #11 to further understand their inferior chromatographic performance. Further discussion can be found in Appendix A.

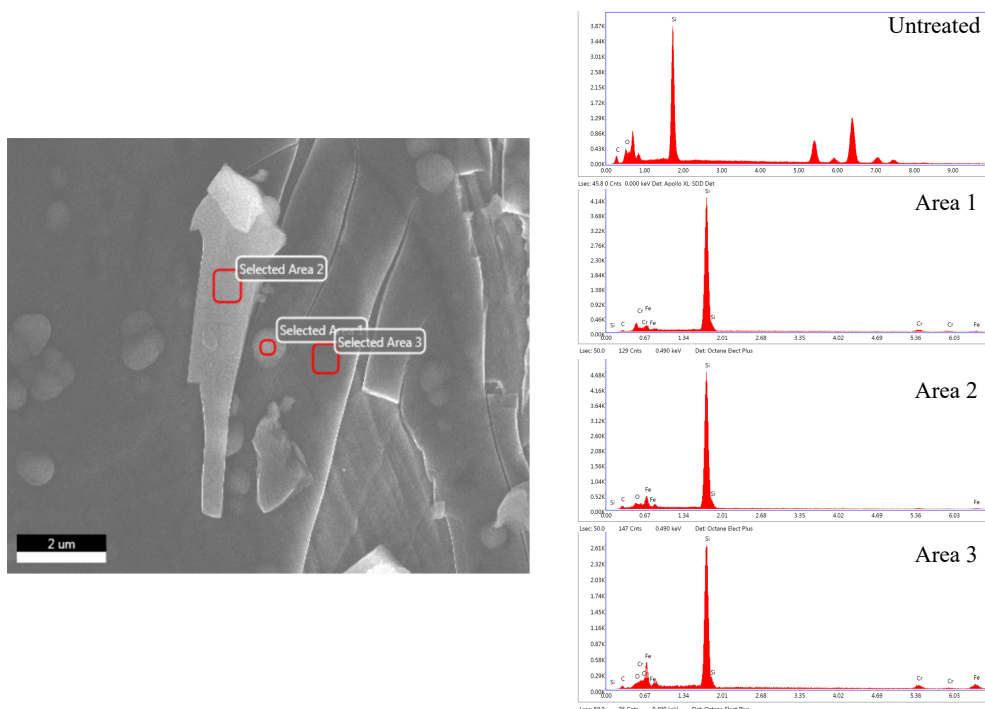


Figure 3.16 EDX results for DB-PS1 #9 for three separate areas compared to the spectrum obtained for the untreated DB-PS1.

DB-PS2887 # 17 was treated for ten minutes at 40 V, followed by two five-minute phases at 35 V. This treatment produced superior chromatographic performance compared to all other treatments of the DB-PS2887 phase. To perform SEM, this phase was gold coated with a thickness of approximately 20 nm. Due to the higher energy produced by the electron beam interacting with the DB-PS2887 stationary phase, images were difficult to capture and often blurry without gold coating. Applying this coating did not alter the topography of the surface; it only served to improve SEM imaging of it. Fig. 3.17 shows SEM images of multiple magnifications of the DB-PS2887 #17 trapping capillary. The lower magnification, ~100 times, showed uneven, cracked surface along the entire treated capillary (A). Closer magnification of 5,000 (C) and 20,000 (D) revealed a more discernible surface. The stationary phase had several gaps and holes from where it was only locally adhered to the underlying deactivation layer.

Within the gaps, the underlying deactivation layer was intact and undisturbed. The gaps revealed the thickness of the stationary phase on top of the deactivation layer. When comparing the images to those shown in Figure 3.10, it is evident that the stationary phase was at the early stages of thermal decomposition with no sorbent nanoparticles created yet, as previously seen with other DB-PS2887 capillaries that were treated at higher voltages. It seems that this partial decomposition of the much thicker stationary phase film of the DB-PS2887 column struck the right balance between strong sorption and efficient release of the analytes, as these treatment parameters were chromatographically superior to all others for this stationary phase.

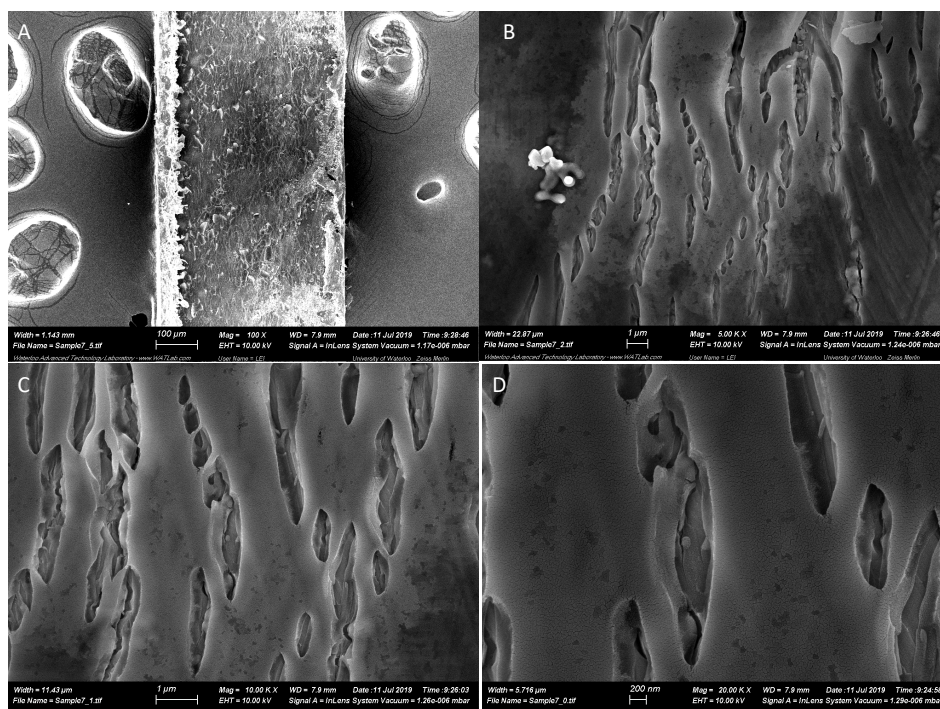


Figure 3.17 SEM images of DB-PS2887 #17, (A) 100x magnification treated, (B) 5,000x magnification treated, (C) 10,000x magnification treated, and (D) 20,000x magnification treated.

EDX analysis was performed on the two distinct surfaces within the DB-PS2887 #17 trapping capillary, as seen in Fig. 3.18. It is important to note that due to the gold coating process, gold was present within the EDX spectra. Gold signals occurred at x-ray emission

energies of 2.120 and 9.712 [4]. Again, the x-axis scale of the untreated capillary spectrum was different from those of both areas analyzed for DB-PS2887 #17. Area 1 corresponded to the stationary phase that had been slightly cracked during the treatment process. The surface was relatively smooth with no alterations and no nanoparticles present. Area 2 corresponded to the underlying deactivation layer that was exposed after the treatment process through the gaps in the stationary phase. The relative intensities of the iron and chromium signals in Area 1 were lower than their average intensities in the untreated capillary, indicating that the slightly decomposed stationary phase still effectively prevented the detection of the underlying metal capillary. The relative intensities of the iron and chromium signals in Area 2 were higher than in untreated capillary indicating that the deactivation layer only did not shield the underlying metal as effectively after treatment. Oxygen signal increased relative to silicon in Area 1, which is consistent with the onset of thermal decomposition of PDMS in the presence of oxygen. Carbon signal remained roughly the same relative to silicon after treatment, again pointing to early stages of decomposition. SEM and EDX analyses were also performed on DB-PS2887 #22 and #25 to further understand their inferior chromatographic performance. Further discussion can be found in Appendix A.

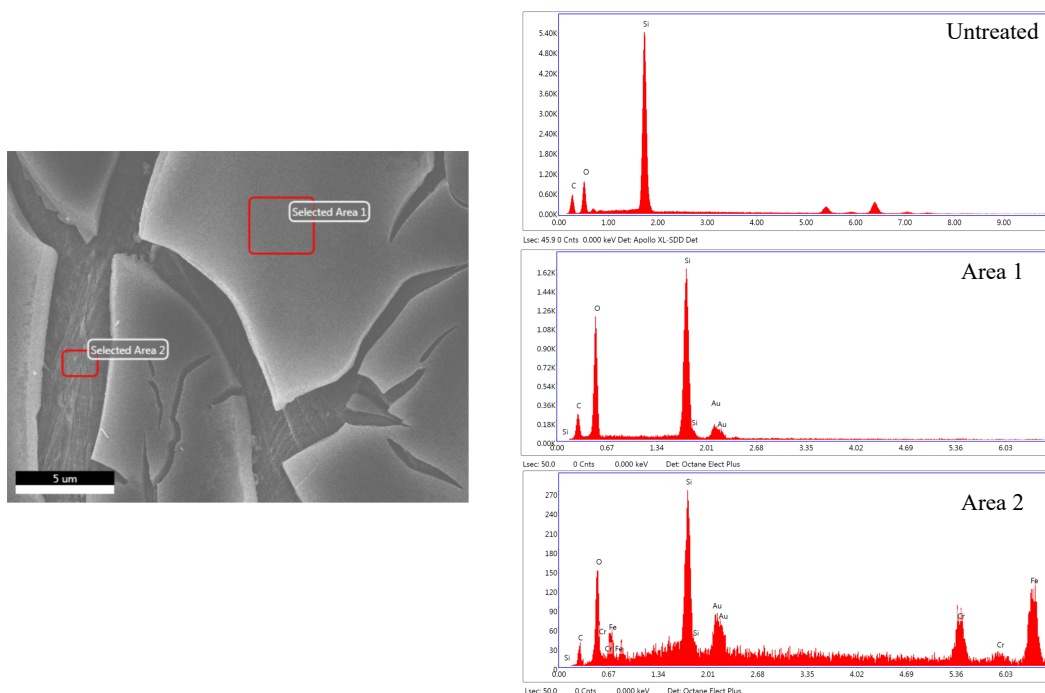


Figure 3.18 EDX results of DB-PS2887 #17 for two separate areas compared to the spectra obtained for the untreated DB-PS2887.

After the evaluation of the various voltage treatments applied to both DB-PS1 and DB-PS2887, it was concluded that the former column with a much thinner film of the stationary phase (0.15 μm) requires that the strong nanoparticle sorbent be formed after treatment for proper chromatographic performance. A treatment plan between 40 V and 50 V for DB-PS1 resulted in the best chromatographic separation and produced the desired nanoparticle trapping material. The DB-PS2887 column coated with a much thicker film of the stationary phase (3 μm) required only partial thermal decomposition of the stationary phase to produce good chromatographic results. The combination of chromatographic analysis, SEM and EDX allowed a comprehensive characterization of the results obtained with each set of treatment parameters.

3.7. Treatment plans for treating sections of the trapping capillary

Evaluation of the Agilent DB-PS1 and DB-PS2887 trapping capillaries at various treatment voltages provided a better understanding of the parameters necessary to achieve an effective coating for proper single-stage modulation. In the next step, it was decided to thermally treat individual sections of the trapping capillaries to see if a better product can be obtained. As previously mentioned, the key in the treatment process was the presence of red glow during the treatment. This same principle was applied when selecting the temperatures applied during the partial treatment process. Table 3.2 shows the ranges of voltages applied to specific sections of the trapping capillary. It was assumed that the untreated sections or sections subject to less aggressive treatment would be less adsorbent, which should facilitate rapid remobilization of the previously trapped bands. As previously seen in Section 3.2, the untreated DB-PS1 and DB-PS2887 produced adequate separations of diesel except for the heavier analytes. The untreated material was adsorbent enough to trap and desorb analytes without extreme streaking in the 2D , but efficient remobilization required high modulation temperatures that led to pronounced trap bleed. Ideally, the combination of a treated and untreated section would reduce or eliminate the streaking previously often seen within the secondary space, caused by an imbalance between a trapping phase that was too strong and an inefficient remobilization process. Ultimately, this would create smaller secondary injection bandwidths. The sections selected for treatment were the middle of the capillary and one half of it. In addition, the two halves of the trapping capillary were treated at different temperatures to create one half that was more adsorbent than the other. The length of the treated sections was 3 cm in each case. The treatment plans that included two differing temperatures on each half also used 3 cm treatment areas; however, there was a slight

overlap of the two treatments in the middle of the capillary to ensure there was no material left untreated.

Another possible source of secondary streaking was the untreated section of phase left within the unions at the front and back ends of the trapping capillary. The treatment process involved treating the capillary for the length of the cooling pads within the modulator. Unions were then placed at the front and back ends of the trapping capillary to connect it to the ¹D and ²D columns. This left the area within the unions untreated, creating “cold spots” along the column train. These spots in fact remained at the oven temperature; however, they were colder in relation to the rest of the trapping capillary during the discharge for remobilization. Due to the large thermal mass of the metal unions, the areas within the unions did not heat up from the capacitive discharge like the rest of the trapping capillary. This scenario could potentially lead to sorption of analytes within the cooler areas. As the oven temperature increased, the analytes trapped within these spots would slowly elute onto the second dimension as broad bands. To test this theory, the entire trap including the sections within the unions at the front and back of the trapping capillary were treated.

Table 3.2 Treatment plan for different sections of Agilent trapping capillaries

			1 st stage (10 min)	2 nd stage (5 min)	3 rd stage (5 min)
ID#	Column	Section Treated	Voltage (V)	Voltage (V)	Voltage (V)
40	DB-PS1	Entire trap & unions	50	45	45
41	DB-PS1	Half	50	45	45
32	DB-PS1	Middle	50	45	45
43	DB-PS1	Half	50	45	45
		Half	40	35	35
42	DB-PS1	Half	45	40	40
		Half	40	35	35
39	DB-PS2887	Entire trap & unions	50	45	45
35	DB-PS2887	Half	40	35	35
36	DB-PS2887	Middle	40	35	35

3.7.1. Performance results

Each trapping capillary was first used for the analysis of diesel to evaluate the chromatographic performance. The same experimental parameters were used as described in Section 3.2. A range of modulation voltages between 25 V and 55 V were implemented at 5 V increments to determine the appropriate value for efficient remobilization of the analytes.

Fig. 3.19 displays the results obtained using DB-PS1 #40 trap for the analysis of diesel with active and passive cooling at various modulation voltages. The treatment of the area within the unions clearly had a negative effect on the chromatography under all conditions. It led to the creation of a stronger adsorbent within the unions, resulting in stronger sorption within the “cold spots” at the front and back of the trapping capillary. This resulted in a substantial increase in streaking in ²D due to more analytes being strongly sorbed and not quickly released from the

areas within the unions. A low voltage of 35 V produced extreme streaking within the secondary space with both active (A) and passive (D) cooling. Increasing the voltage to 45 V reduced the streaking more with active cooling (B) than with passive cooling (E). The various groups within the second dimension were more visible; however, the broad bands persisted in the 2D , hindering the identification of later eluting analytes due to co-elutions. Maximum voltages of 50 V and 55 V were applied for active and passive cooling, respectively. Even though the increase in modulation voltage decreased the streaking within the 2D , it was evident they could not be eliminated. Higher voltages were not applied due to the possibility of breaking the trapping capillary. In conclusion, these treatment parameters for DB-PS1 were deemed unsuitable.

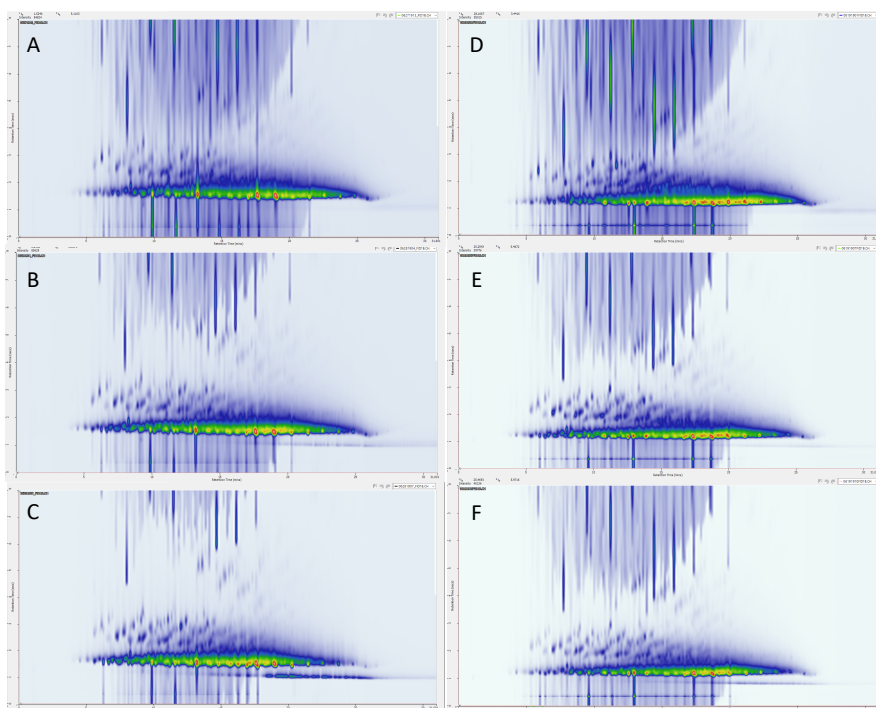


Figure 3.19 Comparison of the performance of the DB-PS1 #40 trapping capillary at various modulation voltages with active (A - C) and passive cooling (D - F) in the analysis of diesel. The deactivation layer was present within the unions at the front and back end of the trapping capillary. Modulation voltages were 35 V (A and D), 45 V (B and E) and 50 V (C and F).

The trapping capillaries with different sections treated were tested chromatographically in two configurations within the column train: the front half treated and the back half treated. In the former configuration, the analytes eluted off the ¹D and entered the trapping capillary, exposed to the treated section with more sorptive material first. As they traversed the trap, they were exposed to the untreated section of less sorptive section at the back half, before re-injection onto the ²D. Herein this will be referred to as configuration A. Alternatively, when the trap was placed in the opposite configuration, the analytes were exposed to the untreated section before traversing the trap towards the treated half. This will be referred to as configuration B.

The results of diesel analysis using DB-PS1 #41 capillary in configuration A at various modulation voltages with active and passive cooling are displayed in Fig. 3.20. Modulation voltage of 30 V led to significantly improved chromatography for both active (A) and passive (D) cooling compared to previous results. Streaking within the second dimension was more pronounced with passive cooling. On the other hand, passive cooling had narrower peaks. Increasing the modulation voltage to 40 V improved the separation notably with passive cooling (E). Streaking was also decreased within the ²D. At the maximum voltages of 50 V and 45 V applied for active (C) and passive (F) cooling the onset of pyrolysis was clearly visible, and streaking was not completely eliminated. In this configuration, active cooling with modulation voltage of 40 V performed the best. Overall, though, placing the treated section in configuration A was detrimental to effective release of the trapped analytes. The untreated, or less adsorbent section at the downstream end of the modulator caused broadening of previously focused bands from the treated section within the front half of the capillary.

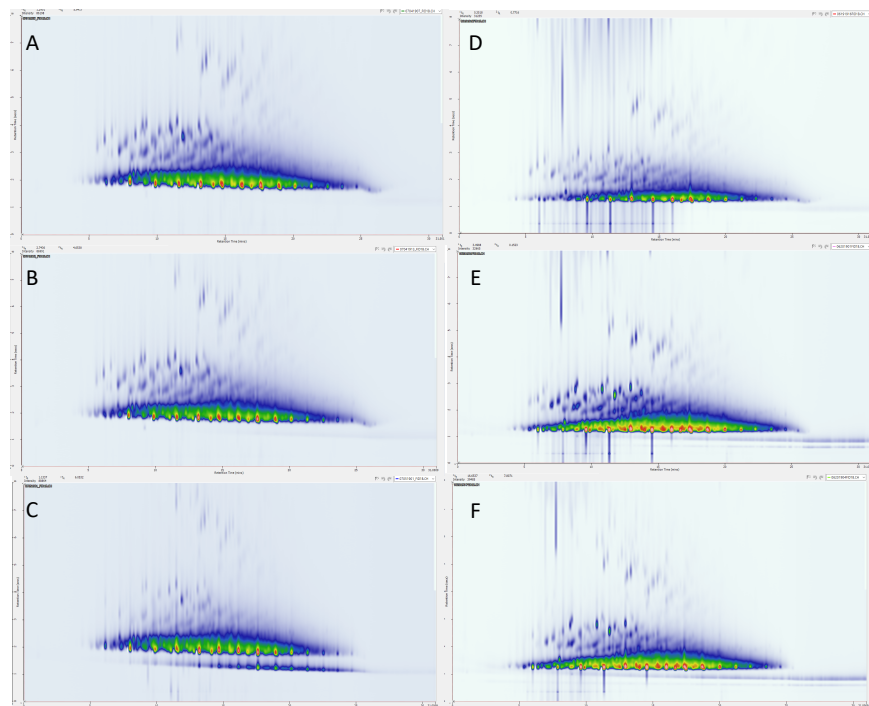


Figure 3.20 Comparison of the performance of the DB-PS1 #41 (Configuration A) trapping capillary at various modulation voltages with active (A - C) and passive cooling (D - F) in the analysis of diesel. The deactivation layer was present within the unions at the front and back end of the trapping capillary. Modulation voltages were 30 V (A and D), 40 V (B and E), 45 V (F) and 50 V (C).

By placing DB-PS1 #41 in configuration B, the chromatography was greatly improved for passive cooling, as seen in Fig. 3.21 (D – F). The separation achieved with active cooling (Fig 3.21 A-C) was similar to that obtained with the treated section in the front end of the trapping capillary. Streaking within the ²D with passive cooling was essentially eliminated in this configuration. Modulation voltages of 30 V and 40 V adequately remobilized analytes with both active and passive cooling. Increasing the voltage by 10 V had no effect on the minimal streaking present within the ²D for passive cooling. The combination of two different sections proved to be beneficial in efficient modulation with active and passive cooling at a lower modulation voltage. The ability to utilize lower modulation voltages to achieve the same

separation which was previously achieved with higher voltages was beneficial in prolonging the life of the trapping capillary and eliminating the risk of pyrolysis. This set of treatment parameters with configuration B provided versatility in modulation settings with good separation obtained in all scenarios. With configuration B, a less adsorbent material assisted in the trapping of analytes, while the more adsorbent material further focused those trapped bands, resulting in narrower injection bands in the 2D . Quick and efficient remobilization of trapped analytes was achieved in this configuration.

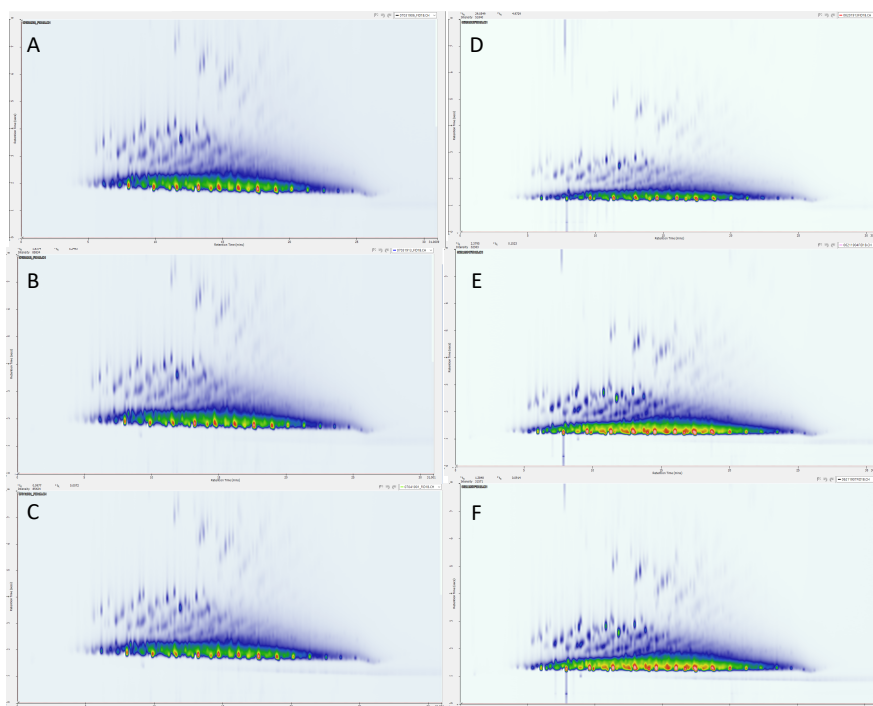


Figure 3.21 Comparison of the performance of the DB-PS1 #41 (Configuration B) trapping capillary at various modulation voltages with active (A - C) and passive cooling (D - F) in the analysis of diesel. The deactivation layer was present within the unions at the front and back end of the trapping capillary. Modulation voltages were 35 V (A and D), 40 V (B and E), 45 V (F), and 50 V (C).

DB-PS1 #32 was treated with settings of 50 V followed by 45 V; however, only the center section was treated, leaving small sections at the front and back end of the trapping

capillary untreated. The results of analysis of diesel at various modulation voltages with active and passive cooling are seen in Fig. 3.22. A low modulation voltage of 25 V for active (A) cooling provided adequate separation. There was more streaking within the ²D with passive cooling (D). Increasing the modulation voltage by 10 V greatly improved the separation with passive cooling (E) by eliminating the majority of the ²D streaking. Despite the increase, the minimal streaking in the ²D remained with active cooling (B). Another 10 V increase resulted in the onset of pyrolysis with both active (C) and passive (F) cooling. Interestingly, the treatment of only the center section of the trap allowed the modulation voltages to be significantly decreased. Compared to DB-PS1 #41 with the front half treated and the back half untreated, a similar trend of pronounced ²D streaking with passive cooling was present. This was caused by the presence of an untreated section at the back of the trapping capillary leading to broadening of the previously focused bands. This was more pronounced with DB-PS1 #41 due to the larger section left untreated when compared to the center treated DB-PS1 #32 trapping capillary. When the shorter untreated sections were on both the front and back end of the trapping capillary, the ²D streaking was reduced. Treating only the middle section of the trapping capillary yielded a good product. Lower modulation voltages could be applied, extending the life of the trap and reducing the risk of pyrolysis with both active and passive cooling. Overall, DB-PS1 #41 with the back half treated and DB-PS1# 32 with the center section treated performed superior to previous treatments which included treatment of the entire trap.

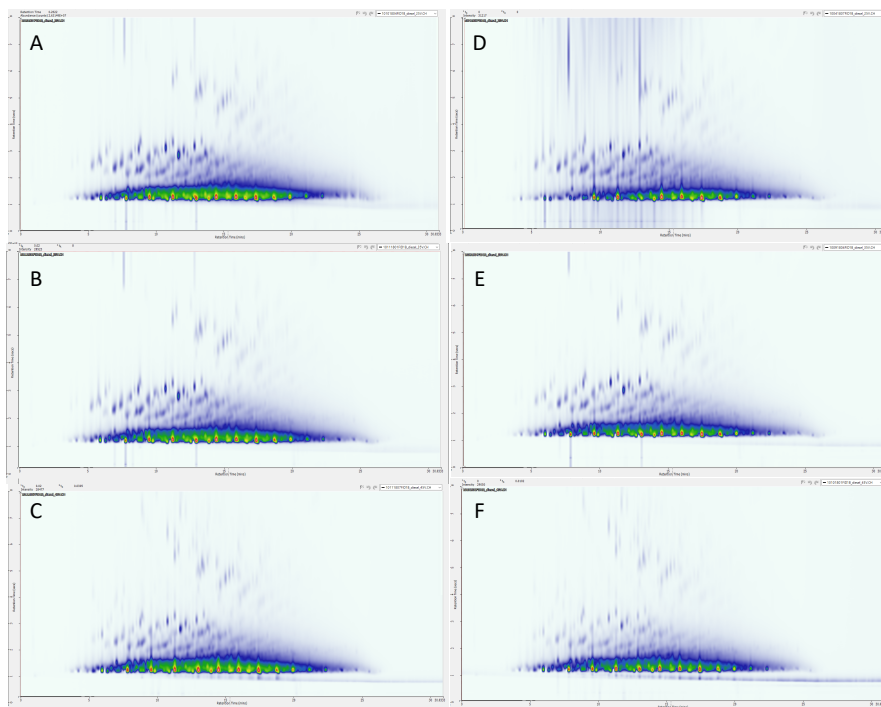


Figure 3.22 Comparison of the performance of DB-PS1 #32 trapping capillary at various modulation voltages with active (A - C) and passive cooling (D - F) in the analysis of diesel. The deactivation layer was present within the unions at the front and back end of the trapping capillary. Modulation voltages were 25 V (A and D), 35 V (B and E), and 45 V (C and F).

Treatment of specific sections of the trapping capillary yielded promising results for effective single-stage modulation. Building on the idea of utilizing sections of differing treatments within a single trap, DB-PS1 #43 and #42 were created using the processes described in Table 3.2. Both trapping capillaries were entirely treated with no area left untreated, but one half was treated with a slightly higher set of voltages when compared to the other half. DB-PS1 #43 was treated for ten minutes at 50 V, followed by two five-minute phases at 45 V on one half, while the other half was treated for ten minutes at 40V, followed by two five-minutes phases at 35 V. DB-PS1 #42 was treated for ten minutes at 45 V, followed by two five-minutes phases at 40 V on one half, while the other half was treated for ten minutes at 40 V, followed by two five-minute phases at 35 V. The traps were tested for the analysis of diesel at various modulation

voltages with active and passive cooling. As previously described, two trapping capillary configurations within the column train were evaluated. Configuration A had the more sorptive material at the exit of the ¹D and the less sorptive material at the entrance of the ²D. Conversely, configuration B had the less sorptive material at the exit of the ¹D and the more sorptive material at the entrance of the ²D.

Fig. 3.23 displays the results of the analysis of diesel at various modulation voltages with active and passive cooling using DB-PS1 #42 in configuration A. With a modulation voltage of 25 V, the separation achieved with active (A) and passive (D) cooling was very good. Clear differentiation of all groups and separation from the early eluting unresolved mixture was obtained. There was no streaking present within the ²D for either cooling option; however, there was some tailing in the ²D. The tailing was caused by the slightly more adsorbent material being placed in the front of the modulator. This resulted in releasing of the trapped analytes into the less sorptive region, which caused slight tailing. Similar results were achieved with a modulation voltage of 35 V with active (B) and passive (E) cooling. Pyrolysis onset was observed with passive cooling at a modulation voltage of 50 V (F), but did not occur under active cooling (C). Achieving a successful GC×GC separation at lower modulation voltages was advantageous in preserving the lifetime of the trapping capillary and reducing the potential for pyrolysis. The ability to obtain similar separations at various voltages brings about versatility in optimizing the separation according to the range of compounds within the sample matrix analyzed.

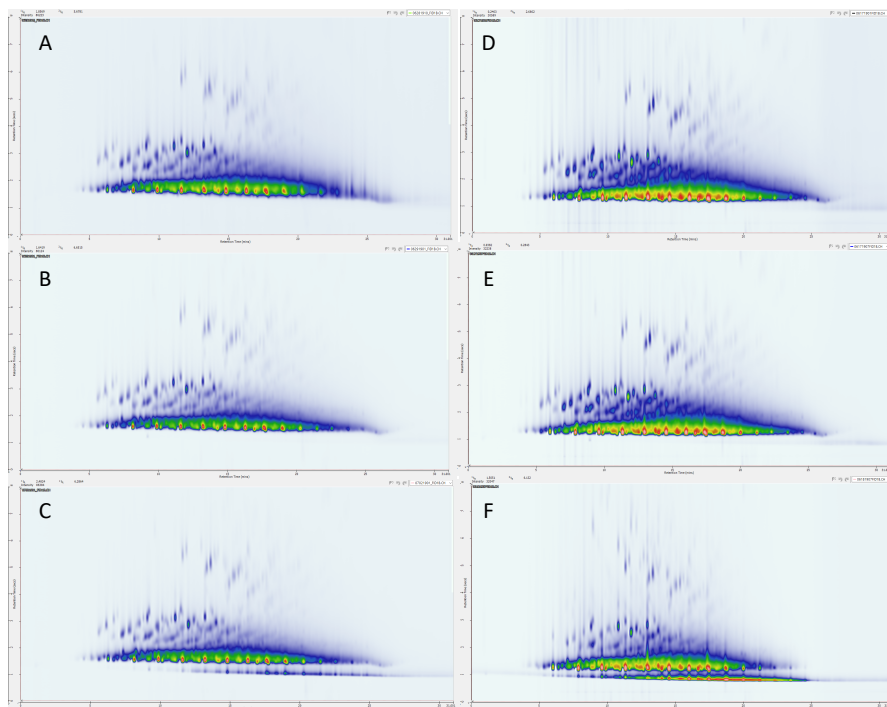


Figure 3.23 Comparison of the performance of the DB-PS1 #42 (Configuration A) trapping capillary at various modulation voltages with active (A - C) and passive cooling (D - F) in the analysis of diesel. The deactivation layer was present within the unions at the front and back end of the trapping capillary. Modulation voltages were 25 V (A and D), 35 V (B and E), and 50 V (C and F).

DB-PS1 #42 was also analyzed in configuration B with the section treated at higher voltages at the entrance of the ²D column, while the lower voltage section was at the exit of the ¹D column. The results of diesel analysis at various modulation voltages with active and passive cooling are displayed in Fig. 3.24. It is important to note the longer ²D retention times in the chromatograms with passive cooling (D-F). This was later traced to a small leak in the trapping capillary connections. Due to this difference, the comparison between active and passive cooling was not quite exact. The separations obtained with active cooling at 25 V (A) and 35 V (B) were similar to those previously obtained with the DB-PS1 #42 trap in the opposite configuration. On the other hand, the separation achieved with passive cooling was slightly worse with 25 V modulation voltage (D), as more tailing was present for the late eluting compounds. By

increasing the modulation voltage to 35 V, the separation achieved with passive cooling was significantly improved (E). The resolution from unresolved mixture for late eluting compounds was enhanced in comparison to the opposite configuration of DB-PS1 #42 thanks to less peak tailing. At modulation voltages of 50 V, active (C) and passive (F) cooling achieved similar results to those of the opposite configuration. Pyrolysis was much more pronounced with passive cooling. A trend similar to that observed for DB-PS1 #41 was achieved when the more adsorbent material was placed downstream. Configuration B allowed effective trapping and quick release of the analytes.

Overall, similar chromatographic results were obtained with DB-PS1 #42 in both configurations within the modulator for the analysis of diesel. Configuration B improved the separation of the early eluting compounds from the unresolved mixture, as well as the late eluting compounds in the ²D. Independently of the configuration of the trapping capillary, good separation with no streaking in ²D was achieved at low modulation voltages, extending the lifetime of the trap. The combination of a less adsorbent phase and a more adsorbent phase in configuration B created a trapping capillary that could effectively trap the analytes and release them in a quick and efficient manner. DB-PS1 #43 was chromatographically evaluated and deemed unsatisfactory. Further discussion can be found in Appendix A.

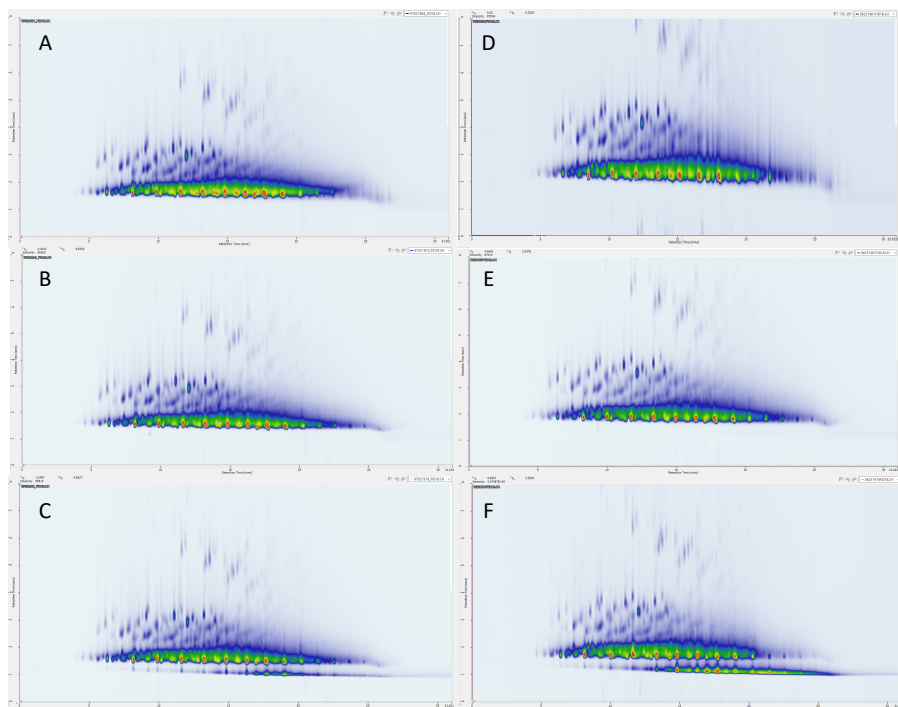


Figure 3.24 Comparison of the performance of the DB-PS1 #42 (Configuration B) trapping capillary at various modulation voltages with active (A - C) and passive cooling (D - F) in the analysis of diesel. The deactivation layer was present within the unions at the front and back end of the trapping capillary. Modulation voltages were 25 V (A and D), 35 V (B and E) and 50 V (C and F).

Partial treatment of DB-PS2887 was also investigated. In an effort to reduce the streaking in the ²D, treatment of the entire trap and areas within the unions was also performed on the DB-PS2887. Analyses of diesel with active cooling at various modulation voltages are displayed in Fig. 3.25. Similar results were obtained as those acquired with DB-PS1 #40. When a low modulation voltage of 25 V (A) was used, extreme streaking in the ²D occurred. Analytes were strongly sorbed to the new phase within the trap and could not be efficiently remobilized with the low modulation voltage. Increasing the voltage to 40 V (B) decreased the streaking within the ²D only marginally. A modulation voltage of 55 V helped in further reducing the streaking within the ²D, but overall the inadequate separation was not improved. Risk of breakage was a concern when utilizing a modulation voltage of 55 V. The treatment of the entire trap and unions was

thus deemed unsatisfactory and not investigated further due to the strong sorption within the “cold” spots of the unions, which did not experience the same temperature increase during the remobilization event.

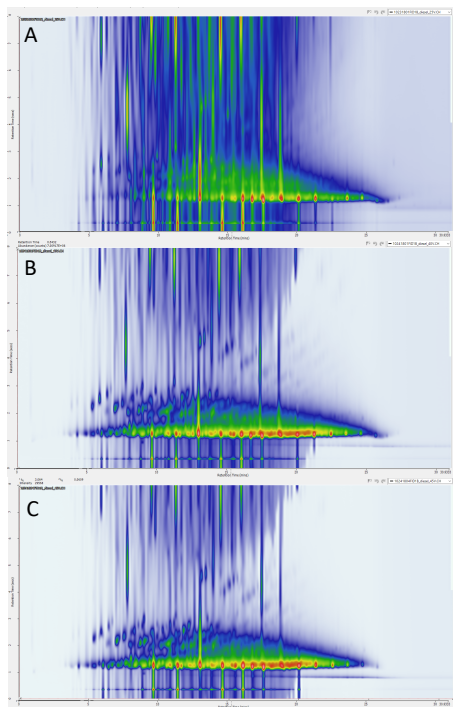


Figure 3.25 Comparison of the performance of the DB-PS2887 #39 trapping capillary at various modulation voltages with active cooling (A - C) present for the analysis of diesel. The deactivation layer was present within the unions at the front and back end of the trapping capillary. Modulation voltages were 25 V (A), 40 V (B) and 55 V (C).

Treatment of select sections of DB-PS2887 trapping capillaries was performed in a similar manner to that of DB-PS1 with the voltages of 40 V and 35 V. DB-PS2887 #35 was a capillary with one half subjected to the treatment process while the other half was left untreated. Configurations A and B were evaluated for the analysis of diesel. Fig. 3.26 displays results for various modulation voltages with active and passive cooling in configuration A. No streaking was present in the ²D when a low modulation voltage of 25 V was applied with active (A) and

passive (D) cooling. The prior provided better resolution of compounds from the unresolved mixture. Increasing the modulation voltage by 5 V produced very similar separations with both active (B) and passive (E) cooling. A modulation voltage of 40 V produced significant stationary phase bleed with both active (C) and passive (F) cooling with no substantial improvement in chromatographic performance. In addition, pyrolysis onset was clear with passive cooling. In comparison to the previously superior treatment parameters of 40 V and 35 V for the entire trap, this configuration was determined to be inferior because of the broader peaks it produced. In configuration A, tailing occurred with both active and passive cooling. The untreated section led to broadening of the injection bands.

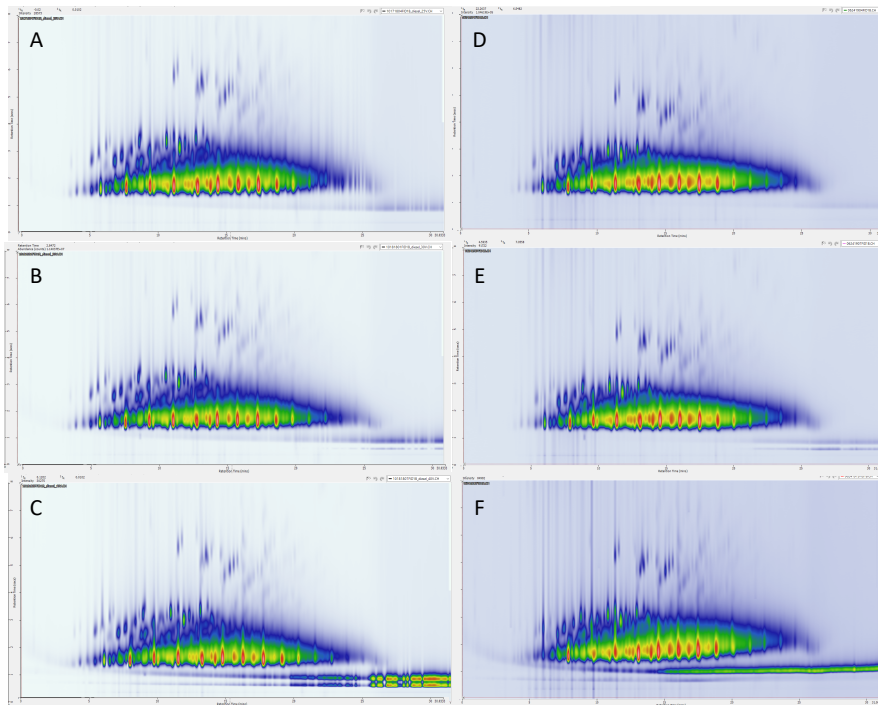


Figure 3.26 Comparison of the performance of the DB-PS2887 #35 (Configuration A) trapping capillary at various modulation voltages with active (A - C) and passive cooling (D - F) in the analysis of diesel. The deactivation layer was present within the unions at the front and back end of the trapping capillary. Modulation voltages were 25 V (A and D), 30 V (B and E) and 40 V (C and F).

After placing the trapping capillary in configuration B, the chromatography was greatly improved, as seen in Fig. 3.27. Analysis of diesel with active cooling at low modulation voltages of 25 V (A) and 30 V (B) provided clear differentiation of the homologous groups within the ²D. Similar to the previous results obtained with configuration B, no streaking was observed. The tailing that was previously seen with the opposite configuration was resolved due to the adsorbent material quickly releasing the trapped analytes. The resolution of analytes from the unresolved mixture was superior compared to configuration A. With a more adsorbent material placed at the head of the ²D column, the previously trapped analytes within the less adsorbent material were further focused. They were then subsequently completely released in a quick manner as a narrow re-injection band. A modulation voltage of 40 V did not cause pyrolysis of the diesel sample; however, it led to significant trap bleed. Treating one half of the DB-PS2887 trapping capillary at 40 V followed by 35 V was concluded to be an effective option when placed in configuration B. In comparison to the previously optimized treatment parameters of 40 V and 35 V for the entire DB-PS2887 trap, these parameters produced similar chromatographic results.

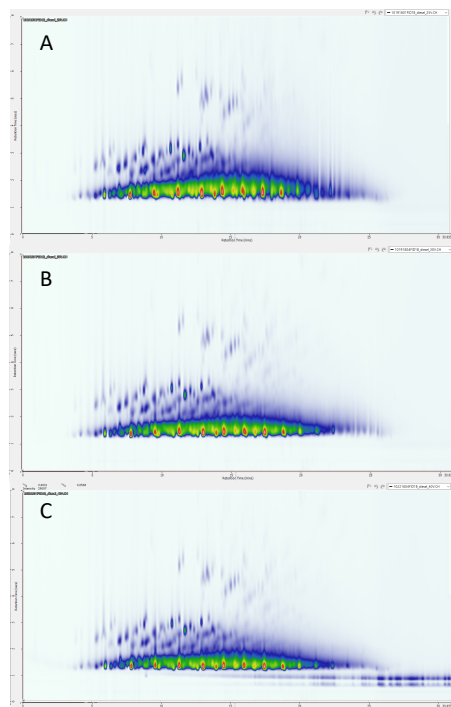


Figure 3.27 Comparison of the performance of the DB-PS2887 #35 (Configuration B) trapping capillary at various modulation voltages with active cooling (A - C) in the analysis of diesel. The deactivation layer was present within the unions at the front and back end of the trapping capillary. Modulation voltages were 25 V (A), 35 V (B) and 40 V (C).

3.7.2. SEM and EDX results

SEM and EDX were employed as tools to image and characterize the elemental composition of the trapping capillaries in which treatment was only applied to specific sections. Each section was individually characterized by SEM and EDX to understand the similarities and differences in the varying sections. DB-PS1 #41 was treated under voltages of 50 V and 45 V for half of the trapping capillary, while the other half was left untreated. SEM images of the treated section at various magnifications are displayed in Fig. 3.28. The surface of the phase was rough and uneven, as seen in Fig. 3.28A. With higher magnification, it was evident how different this phase was from previous results. Compared with other trapping capillaries, the new phase was

extremely cracked and decomposed with crystal-like structures rather than nanoparticles. This was a result of much higher temperatures applied during treatment. The lighter colored flakes corresponded to the intermediate stage of the decomposed stationary phase. Differentiating the underlying deactivation layer was rather difficult due to the many layers of cracked material. By treating only half the trapping capillary the topography drastically changed due to the extreme temperature increase within a shorter treatment distance. Despite the low-abundance of nanoparticles, DB-PS1 #41 performed well chromatographically when placed in configuration B.

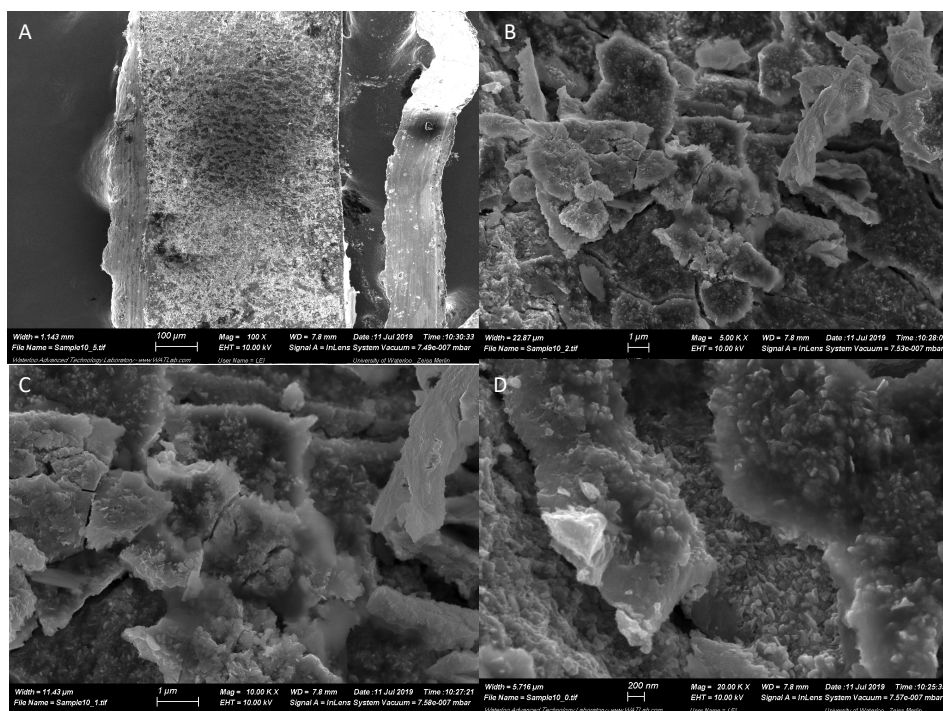


Figure 3.28 SEM images of DB-PS1 #41 (Treated Half), (A) 100x magnification treated, (B) 5,000x magnification treated, (C) 10,000x magnification treated, and (D) 20,000x magnification treated.

EDX was used to further evaluate the atomic ratios of carbon, oxygen and silicon present in the varying surfaces in DB-PS1 #41, as seen in Fig. 3.29. It is important to note the difference in x-axis scale of the spectrum of the untreated capillary when compared to the spectra of the

selected areas of the treated section. Three different areas were analyzed to understand the differences in their appearance. Area 1 corresponded to a darker segment with less prominent crystals. Area 2 corresponded to the light-colored flakes of decomposed stationary phase. Area 3 was similar to area 1 in appearance, a darker material with crystal like structures. Before treatment iron and chromium signals were quite prominent, but after treatment their intensity decreased substantially. This showed that the treatment process built up the material within the capillary, creating a thicker phase that was not exposing the underlying metal capillary as much. The behavior of the silicon and oxygen was also similar across all three selected areas. After treatment there was a substantial decrease in the relative intensity of silicon present. There was also a considerable increase in the relative amount of oxygen after treatment. This is consistent with the conversion of PDMS to carbon-doped silica. This material apparently better shielded the underlying metal tubing, which led to reduced signals of iron and chromium.

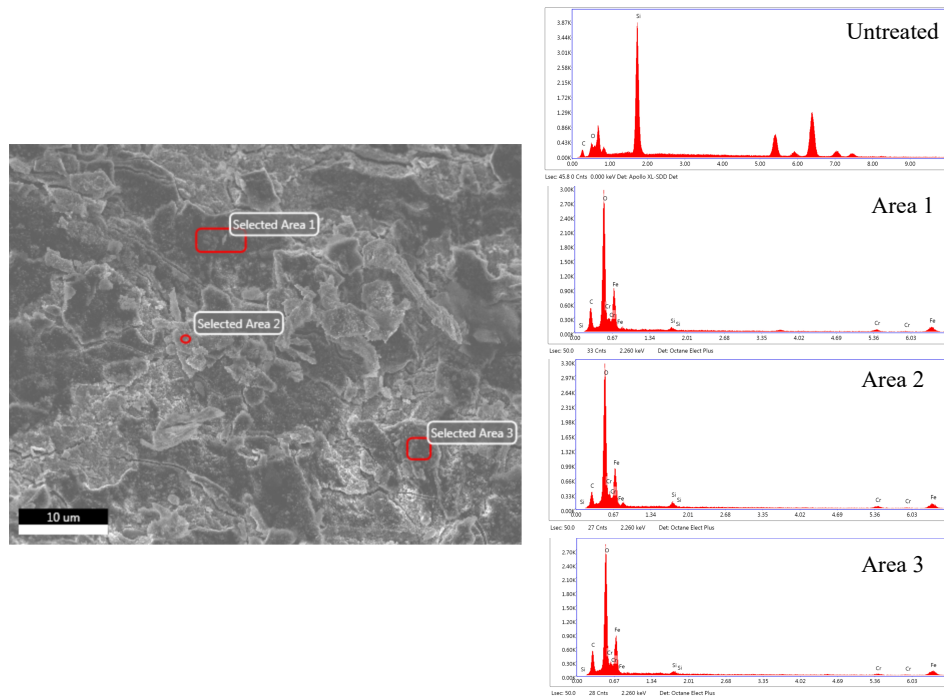


Figure 3.29 EDX results of DB-PS1 #41 (Treated Half) for three separate areas compared to the spectra obtained for the untreated DB-PS1.

DB-PS1 #32 had similar treatment voltages as DB-PS1 #41, but only the center section was treated, leaving sections of untreated material at the front and back end of the modulator trapping capillary. Treating the center section at these voltages allowed for efficient trapping and remobilization of analytes at lower modulation voltages. The treated section of the trap was analyzed by SEM to visualize the surfaces topography, as seen in Fig. 3.30. Overall, the surface was very similar to that of DB-PS1 #41, which is understandable considering that the treated sections were subject to identical treatment. The irregularly shaped crystal-like structures were present on every surface as well as within the cracks and gaps in the phase. The surface was extremely textured and uneven, with flakes of stationary phase adhering locally.

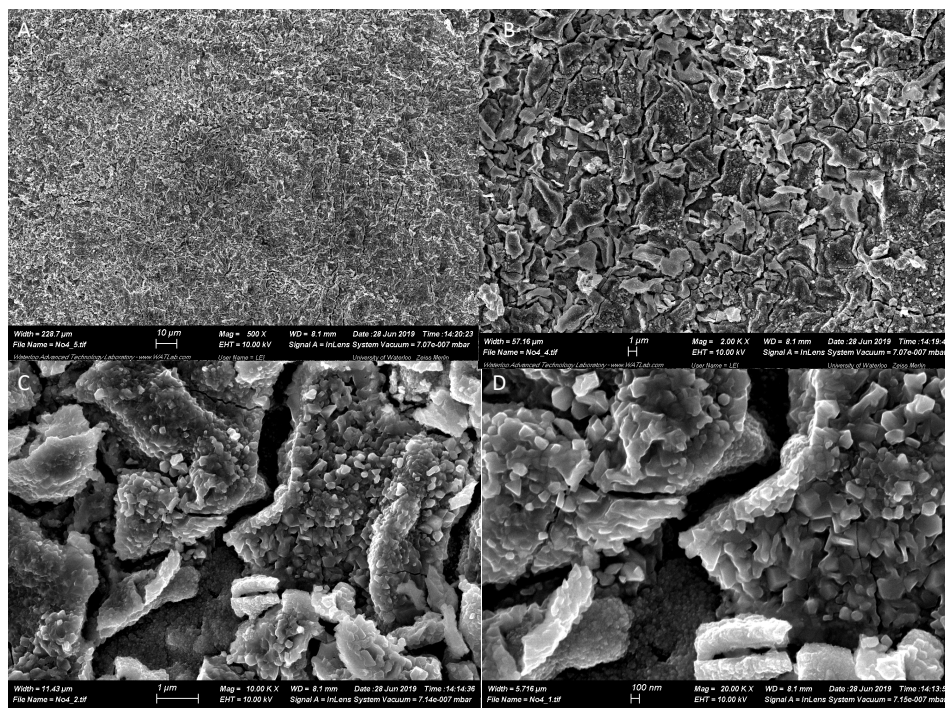


Figure 3.30 SEM images of DB-PS1 #32, (A) 500x magnification treated, (B) 2,000x magnification treated, (C) 10,000x magnification treated, and (D) 20,000x magnification treated.

Evaluation of the two distinct areas was completed by EDX analysis, as seen in Fig. 3.31. Area 1 corresponded to the stationary phase which had adhered to the deactivation layer to create irregularly shaped crystal-like structures. Area 2 corresponded to the underlying deactivation layer within the cracks of the decomposed stationary phase. Compared to the spectrum of the untreated capillary, the presence of iron and chromium decreased after treatment in both selected areas as before. However, there was a slightly higher intensity of metals in area 2 when compared to area 1. This was understandable due to the thicker nature of area 1. The relative increase of the oxygen signal was consistent with conversion of PDMS to silica. Overall, the results were very similar to those obtained for DB-PS #41.

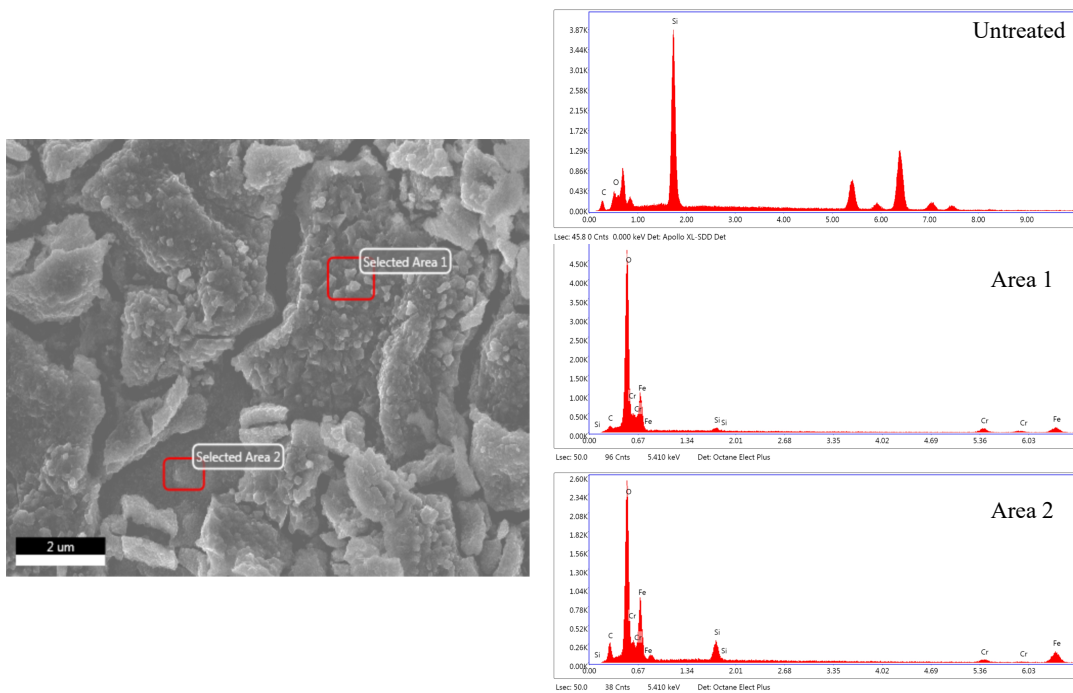


Figure 3.31 EDX results of DB-PS1 #32 for two separate areas compared to the spectra obtained for the untreated DB-PS1.

DB-PS1 #42 was treated at different temperatures in each half of the trapping capillary. One half was treated with voltages of 40 V and 35 V, while the other half was treated with 45 V and 40 V. The SEM images of the half treated with 40V and 35V are displayed in Fig. 3.32. A magnification of 5,000 times (B) displayed a cracked and uneven surface. There was more underlying deactivation layer exposed with nanoparticles and flakes of stationary phase attached. Closer magnification of 10,000 (C) and 20,000 (D) displayed a significant number of nanoparticles formed from the decomposed stationary phase adhering to the deactivation layer. Overall, the topography resembled that of DB-PS1 #9 trap, with a clear onset of the conversion of PDMS to carbon-doped silica nanoparticles. The most efficient trapping was obtained with DB-PS1 #42 when placed in configuration B. This material was adsorbent enough to trap the analytes effectively but not too strongly, which would prevent their quick and complete release.

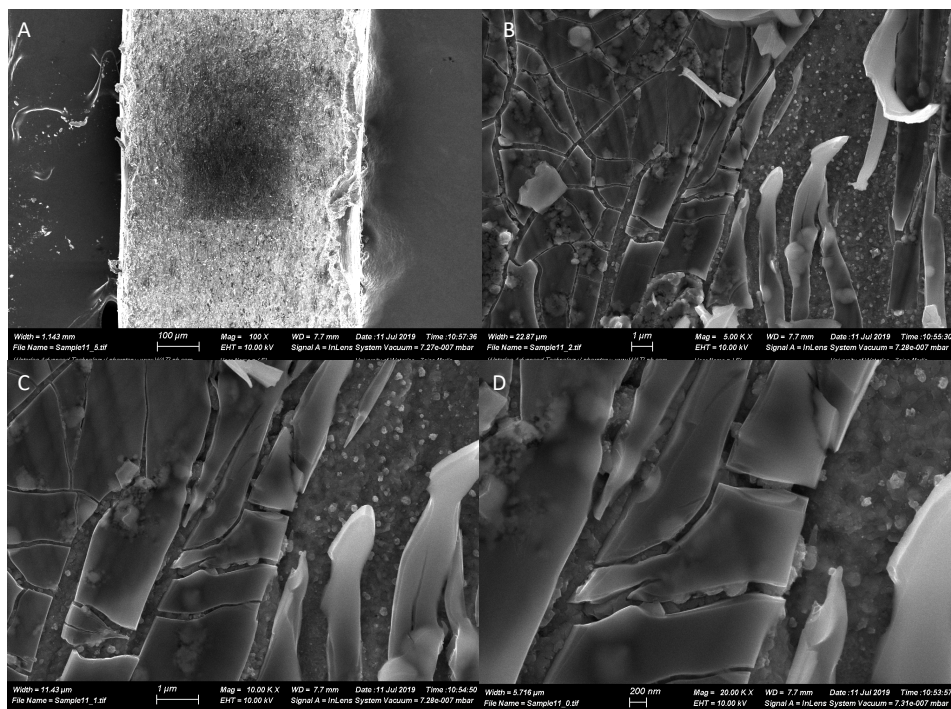


Figure 3.32 SEM images of DB-PS1 #42 (Half 40 V/35 V), (A) 100x magnification treated, (B) 5,000x magnification treated, (C) 10,000x magnification treated, and (D) 20,000x magnification treated.

The EDX results of three selected areas on the surface of DB-PS1 #42 that was treated at 40V and 35V are displayed in Fig. 3.33. Area 1 corresponded to the deactivation layer with a large number of small nanoparticles. Area 2 corresponded to the smooth partially decomposed stationary phase with underlying nanoparticles. Area 3 corresponded to a loosely attached light-colored flake of stationary phase. Relative intensities of the iron and chromium signals in the untreated capillary were higher than in the three areas, indicating that the treatment process led to slightly better shielding of the underlying metal capillary. The intensity of iron and chromium signals was higher in area 1 compared to the other two areas due to the full exposure of the underlying deactivation layer, which was a thin material once the stationary phase had been removed. Significant increase of the oxygen signal relative to that of silicon in all three areas points to conversion of PDMS to silica. The incomplete decomposition and creation of

nanoparticles in the half of DB-PS1 #42 that was treated at lower temperature settings confirmed why this half was beneficial in configuration B. The incomplete transition of the phase created a less adsorbent trapping material, which was advantageous in achieving enough sorption but not too much to hinder the quick release of trapped analytes.

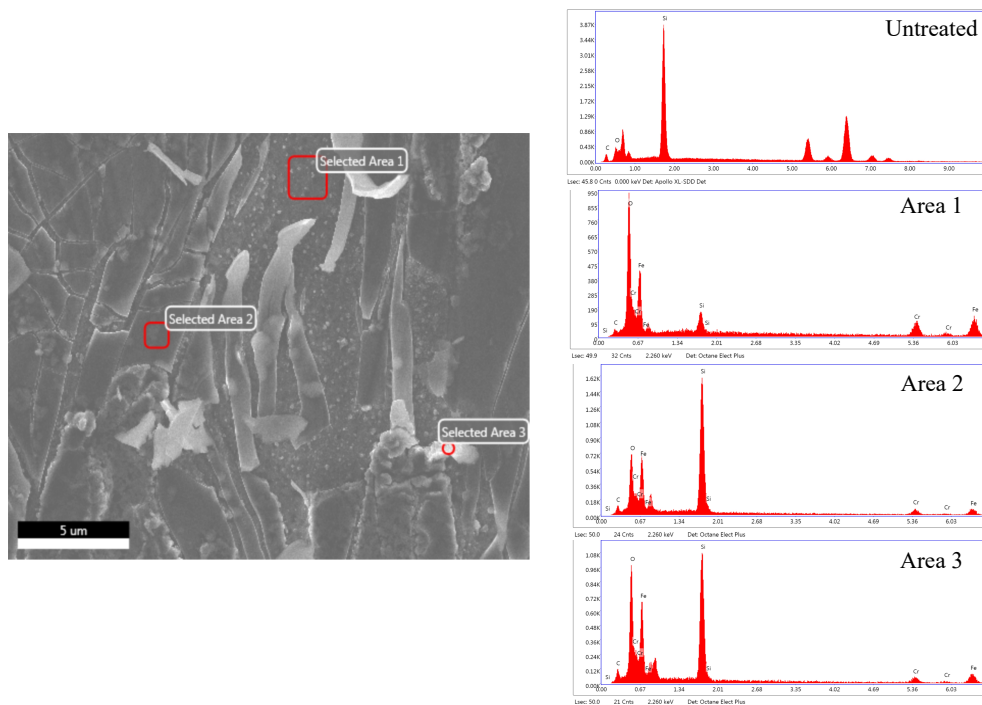


Figure 3.33 EDX results of DB-PS1 #42 (Half 40 V/35 V) for three separate areas compared to the spectra obtained for the untreated DB-PS1.

The other half of DB-PS1 #42 was treated at 45 V followed by 40 V, which was a set of voltages that had not been tested previously. The SEM images of this half of DB-PS1 #42 are displayed in Fig. 3.34. Under low magnification of 100 times (A) the appearance was very smooth when compared to previous treatments of 50 V and 40 V. There appeared to be fewer cracks within the new phase. Higher magnification of 5,000 (B) and 10,000 (C) displayed a surface entirely covered in spongy like particles with few cracks in the surface. There was no apparent stationary phase or flakes left on the surface. Complete decomposition of the stationary

phase and adherence to the underlying deactivation phase occurred. Magnification of 20,000 (D) showed the phase covered with nanoparticles even within the visible crack. There was a uniform consistency in the surface's topography that had not been seen in any of the previous treatments. Placing this material at the back of the modulator performed the best, providing efficient trapping and quick desorption.

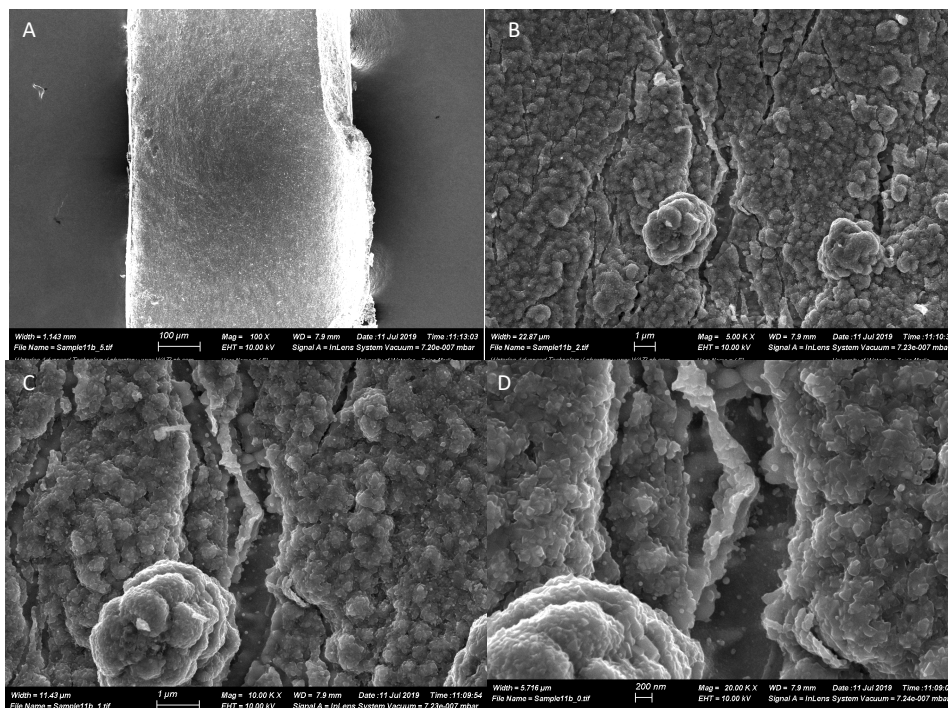


Figure 3.34 SEM images of DB-PS1 #42 (Half 45 V/40 V), (A) 100x magnification treated, (B) 5,000x magnification treated, (C) 10,000x magnification treated, and (D) 20,000x magnification treated.

EDX was also performed on the half of DB-PS1 #42 that was treated at 45 V followed by 40 V, as seen in Fig. 3.35. Three specific areas were analyzed based on their varying appearances. Spot 1 corresponded to the space within one of the cracks in the surface. Area 1 corresponded to a large and spongy nanoparticle on the surface. Area 2 corresponded to a flatter area of surface with smaller nanoparticles present. As expected, spot 1 had a drastic increase in the iron and chromium signals. Areas 1 and 2 had very similar spectra, with a significant increase

in oxygen signal relative to Si in both spectra when compared to the spectrum of the untreated capillary. This clearly pointed to conversion of PDMS to silica nanoparticle sorbent.

Applying these temperature treatment parameters created a phase that was highly adsorbent with a large surface area, which was beneficial in focusing the trapped analytes when placed in configuration B. Furthermore, this phase provided a consistent material that was present along the entire capillary with minimal gaps to allow quick and efficient desorption of trapped analytes. This allowed proper trapping of analytes, without breakthrough, and complete desorption at lower modulation voltages. Further discussion on the evaluation of DB-PS # 40, #43 and the untreated section of #41 by SEM and EDX can be found in Appendix A.

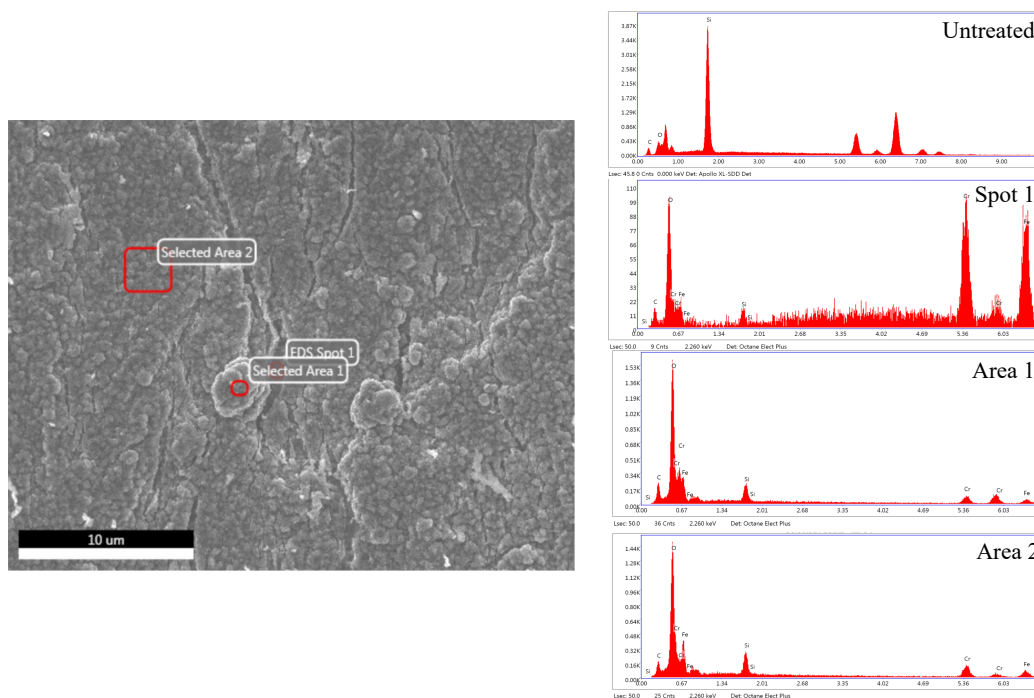


Figure 3.35 EDX results of DB-PS1 #42 (Half 45 V/40 V) for three separate areas compared to the spectra obtained for the untreated DB-PS1.

Even though the DB-PS2887 treated capillaries were established to be inferior to the DB-PS1 treated capillaries, SEM and EDX was performed to fully characterize the topography and

elemental composition of the phase after treatment. This was performed in order to understand the characteristics which defined an inferior trapping capillary. DB-PS2887 #35 was treated with 40 V followed by 35 V for only half of the trapping capillary. When placed in configuration B, limited streaking occurred in the ²D and improved separation from the unresolved mixture was obtained compared to other DB-PS2887 trapping capillaries. Similar to other DB-PS2887 trapping capillaries, #35 was gold coated to enhance the quality of the images under higher magnification. SEM images of the treated section are displayed in Fig. 3.36. At a low magnification of 500 times (A), the surface was consistent and appeared to contain only the deactivation layer. Closer magnification (C & D) revealed a large number of nanoparticles on the surface with very little deactivation phase exposed. The nanoparticles were present in various sizes and shapes. The deactivation phase that was exposed was smooth and flat, with minor cracks present. Nanoparticles were also present within the cracks and along the walls.

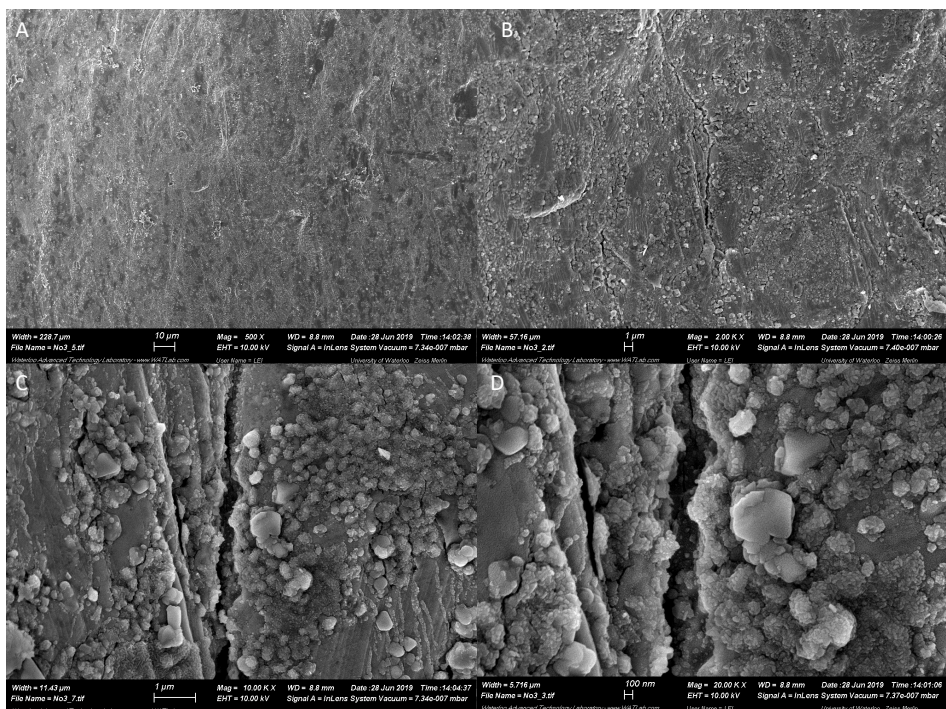


Figure 3.36 SEM images of DB-PS2887 #35 (Half 40 V/35 V), (A) 500x magnification treated, (B) 2,000x magnification treated, (C) 10,000x magnification treated, and (D) 20,000x magnification treated.

EDX was performed on three separate areas of differing appearance within DB-PS2887 #35, as seen in Fig. 3.37. The spectra acquired for each area were compared to the spectrum obtained for the untreated DB-PS2887 capillary. Area 1 corresponded to a large nanoparticle on the surface. Area 2 corresponded to a crack in the deactivation layer where no nanoparticles were present. Area 3 contained many small nanoparticles along the surface. The spectrum of the untreated capillary appeared different from the untreated DB-PS1 due to the thicker starting material within the capillary. Relative signal intensities for iron and chromium were lower compared to silicon. The spectra in all three treated areas resembled closely those obtained for DB-PS1 #42, with a significant increase of the oxygen signal relative to silicon, again indicating complete conversion of PDMS to carbon-doped silica.

The treatment applied to the center of the trapping capillary produced the nanoparticle sorbent across the surface. This phase was adsorbent enough to efficiently trap analytes but did not hinder the quick and complete release of those trapped analytes. The evaluation of DB-PS2887 #39 by SEM and EDX can be found in Appendix A.

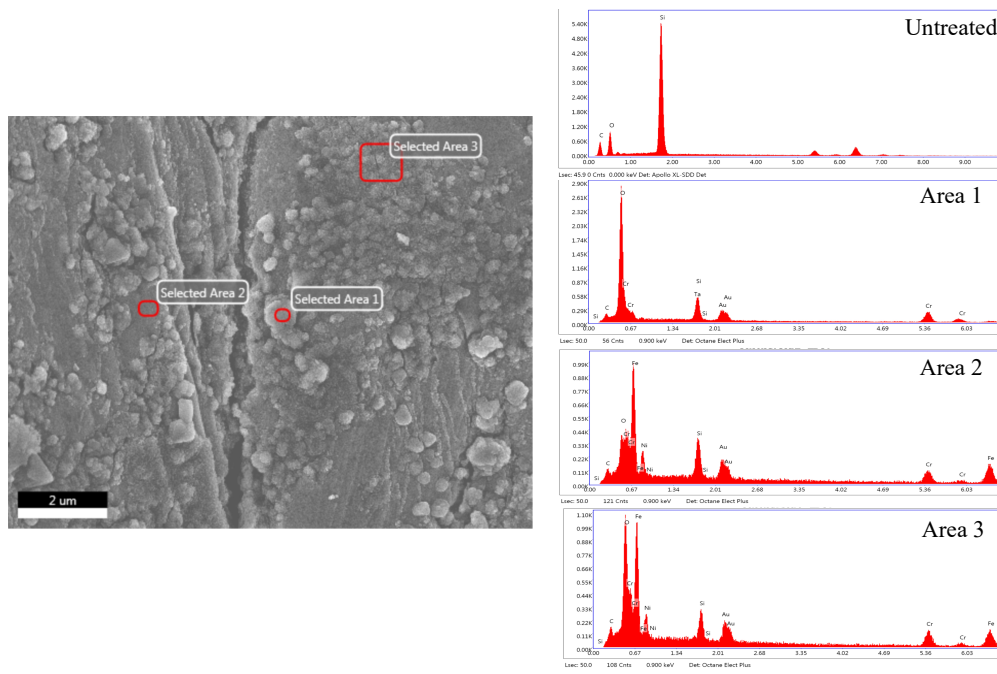


Figure 3.37 EDX results of DB-PS2887 #35 (Half 40 V/35 V) for three separate areas compared to the spectra obtained for the untreated DB-PS1.

3.8 Summary

Various alternative stationary phases and treatments were evaluated in search of an optimal material for the trapping capillaries. Extreme treatment of two sixty-minute phases at temperature increases of 800 °C followed by 680 °C was applied to MXT-1 #3. This treatment process did not lead to desired results. The material obtained that was too strong an adsorbent, hampering the rapid release of the trapped analytes. Three alternative stationary phases from

Restek were treated at 50 V for ten minutes followed by two five-minute phases at 45 V. MXT guard column #5 performed the best and provided adequate separation of diesel; however, all three phases were deemed unsatisfactory.

Two 100% PDMS-coated columns from Agilent Technologies, DB-PS1 and DB-PS2887, were evaluated as alternatives to overcome the shortcomings encountered with the new deactivation process employed by Restek Corporation. Both DB-PS1 #1 and DB-PS2887 #2 were treated at 50 V for ten minutes followed by two five-minute phases at 45 V. DB-PS1 #1 provided a satisfactory separation of diesel. Minor streaking was present in the ²D from analytes adsorbing too strongly to the active sites within the phase. The untreated phase was evaluated by SEM and appeared smooth with the stationary phase bound to the underlying deactivation layer. Nanoparticles were created after the treatment process was applied. DB-PS2887 #2 also provided adequate separation of diesel; however, it was worse compared to DB-PS1 #1. After treatment, nanoparticles were also created across its surface. Based on the results obtained from the chromatographic evaluation, as well as SEM and EDX analyses, the Agilent DB-PS1 and DB-PS2887 phases were deemed acceptable alternatives.

Various treatment plans were applied to determine the appropriate range of voltages required for optimal performance for both DB-PS1 and DB-PS2887. A range of 40 V to 50 V as the higher voltage applied during treatment was concluded to be the most suitable for the DB-PS1 column based on the results obtained for DB-PS1 #1 and #9. Voltages above 50 V were detrimental to the performance, while voltages below 40 V were only beneficial when passive cooling was applied. Treatment voltages beginning at 40 V followed by 35 V were the most appropriate for DB-PS2887. The higher voltage treatment plans resulted in severe streaking in the ²D and poor separation of early eluting compounds from the unresolved mixture, while lower

voltages produced poor chromatography when active cooling was employed. The treatment of the entire capillary for both DB-PS1 and DB-PS2887 resulted in a material that was too strong a sorbent, leading poor chromatographic performance.

Various sections of the trapping capillary were subjected to treatment with both the DB-PS1 and DB-PS2887 columns in search of improved chromatographic performance. In addition, the entire trap including the areas within the unions at the front and back of the trapping capillary were treated. Treating the entire trap had a negative effect on the chromatography by causing substantial streaking in the ²D for both phases. This was due to the strong adsorbent material created within the unions. These areas did not experience the same temperature increase as the trapping capillary during the capacitive discharge, which resulted in strong sorption of analytes within the unions.

Having two sections within the trap of different adsorptivity proved beneficial for DB-PS1 and DB-PS2887 as it allowed obtaining adequate separation with active and passive cooling at lower modulation voltages. Ultimately, this would prolong the life of the trapping capillary over multiple analyses and reduce the odds of pyrolysis. Both DB-PS1 and DB-PS2887 produced better chromatography when the more adsorbent phase was placed in configuration B. This allowed rapid and efficient remobilization. In comparison to the DB-PS1 phase, DB-PS2887 performed slightly worse. For DB-PS1, traps #41 and #32 provided the best chromatographic performance. They were both treated at 50 V for ten minutes, followed by two five-minute phases at 45 V. DB-PS1 #41 was superior when placed in configuration B, while DB-PS1 #32 had the treated section within the center of the trapping capillary. The treated sections of DB-PS1 #41 and #32 produced similar SEM and EDX results. The optimal phase created was DB-PS1 #42 which contained one half treated at 45 V for ten minutes followed by two five-minutes

phases at 40 V, while the other half was treated at 40 V for ten minutes followed by two five-minutes phases at 35 V. When placed in configuration B, the separation of diesel was superior to all other phases. This was due to the more adsorbent material effectively trapping and completely releasing the analytes in a quick manner. The half treated at lower temperatures contained few sorbent nanoparticles. The higher temperature half was completely covered in spongy silica nanoparticles. Configuration B proved to be the optimal phase for efficient trapping and complete desorption at lower modulation voltages with both active and passive cooling.

An optimal set of treatment parameters was obtained for an alternative material. Agilent DB-PS1 #42, which was treated at 45 V followed by 40 V on one half of the trapping capillary and 40 V followed by 35 V on the other half of the trapping capillary, produced very promising results when placed in configuration B. However, further evaluation of the treatment time and temperature, as well as other treatment parameters, is warranted in search of the optimal trapping capillary.

Chapter 4. Improvement of modulator design

4.1 Introduction

Establishing a treatment plan to apply to an appropriate starting material to create an adsorbent trapping capillary was vital in achieving efficient modulation with the single-stage consumable-free modulator. Alongside the trapping capillary, there were other components of the design that could be further improved to produce an optimum modulator. As previously discussed in Chapter 3, many of the tested treatments performed adequate separation through trapping and remobilization of analytes; however, there was a reoccurring theme of streaking in the ²D and pyrolysis of the sample at high discharge voltages. These phenomena were explored through alterations of the modulator and trapping capillary design. A diesel analysis was performed before and after the alterations were made to evaluate their performance. The instrumental parameters for the diesel analysis for the alteration of the modulator and trapping capillary design can be found in Section 4.2.

4.2 Experimental

Diesel was obtained from a local gas station in Waterloo, ON to analyze as a standard. The GC×GC system consisted of an Agilent 6890 gas chromatograph (Agilent Technologies, Santa Clara, CA, USA) equipped with a split/splitless injector and FID detector. The column configuration included a 30 m x 0.25 mm ID x 0.25 μm Rxi-5MS (Restek Corp.) as the ¹D and a 0.5 m x 0.25 mm ID x 0.50 μm MXT-WAX as the ²D. An Agilent 7683 series injector was used to make a 1 μL injection of undiluted diesel at a 300:1 split ratio. The inlet temperature was set

at 280 °C and a 4 mm ID Precision split liner with wool (Restek Corp.) was used. Helium gas with a purity of 99.999% (Air Liquide, Kitchener, ON, Canada) was used as the carrier gas at a constant flow of 1.8 mL/min. The oven temperature program was 40 °C to 240 °C at 8 °C /min, followed by 20 °C/min to 260 °C, which was then held for 5 minutes. The FID was operated at 280 °C with an acquisition rate of 100 Hz and a ratio of 40 mL/min to 400 mL/min of H₂ to Air, respectively. The UW single-stage, consumable-free thermal modulator was employed as the modulator interface. A modulation period of 8 seconds was used. A more detailed description of the operation of this modulator can be found in Section 1.3.

4.3 Modified ceramic cooling pads

The ceramic cooling pads are a vital component in effectively cooling the modulator column to trap analytes below the oven temperature before being reinjected onto the head of the secondary column for further separation. They should cover the entire modulator trapping capillary in order to cool actively by thermoelectric coolers or passively by heat sinks and fans. With the original rectangular design (Fig. 4.1A), the cooling pads fit within the copper heat conduits that are used to transfer heat away from the pads to the thermoelectric coolers. The heat is then dissipated via heat sinks and fans. However, with small variances in the length of the modulator trap, small segments of the trap can lie outside the cooling pads. These spots are detrimental to the modulator operation since they are not effectively cooled. The exposed areas might become extremely hot from the capacitive discharge, which might lead to pyrolysis of certain compounds.

4.3.1 Design

To overcome this issue, a new trapezoidal pad design was implemented. This shape allowed for complete coverage of modulator trapping capillaries of varying lengths by adjusting their position between the pads, as seen in Fig 4.1B. With complete coverage within the cooling pad, the entire trap could be efficiently cooled, thus minimizing pyrolysis.

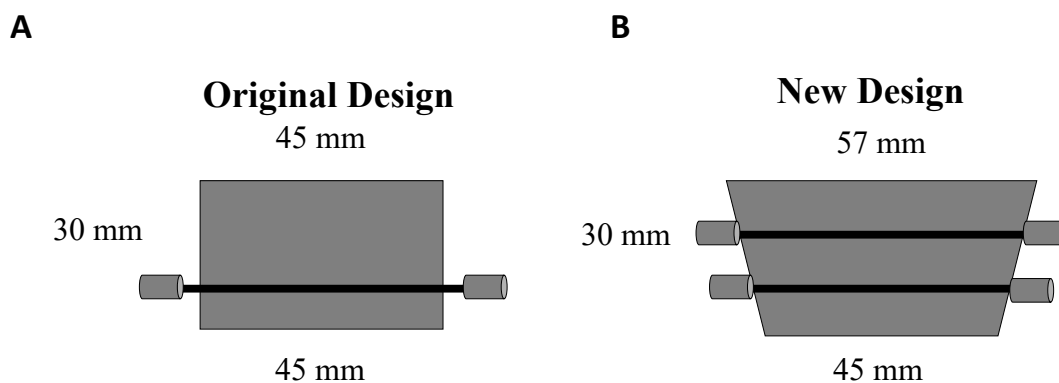


Figure 4.1 Schematic of the (A) original rectangular ceramic cooling pads, and (B) newly designed, trapezoidal ceramic cooling pads. The new design provided complete coverage independently of the length of the trapping capillaries.

4.3.2. Performance evaluation

Originally tested as an alternative stationary phase to the MXT-1 #1, #2, and #3 evaluated in Chapter 2, MXT-5 #4 was considered an option before the assessment of the Agilent DB-PS1 and DB-PS2887 trapping capillaries. MXT-5 #4 was employed to evaluate the difference in cooling achieved with the two designs of ceramic cooling pads. As seen in Fig. 4.2, the separation of diesel was performed with MXT-5 #4 with the old and new ceramic cooling designs at a high discharge voltage of 65 V. With the old, rectangular design, the areas of the trapping capillary that were left exposed to the oven temperature were not properly cooled,

which resulted in pyrolysis of some diesel sample components. This decomposition of the sample likely occurred within the hot portions of the trapping capillary, which lied outside the ceramic cooling pads. When the newly designed trapezoidal ceramic cooling pads were used, the entire trap was cooled more efficiently, preventing (or at least reducing) pyrolysis of the sample. This was evidenced by somewhat higher abundance of late-eluting compounds observed in the chromatogram.

Preventing analyte decomposition was vital in optimizing the performance of the modulator design. The trapezoidal design allowed for more complete coverage of the trapping capillary for proper cooling of its entire length. Also, this allowed for increased flexibility when testing trapping capillaries of different lengths without alterations to the modulator design.

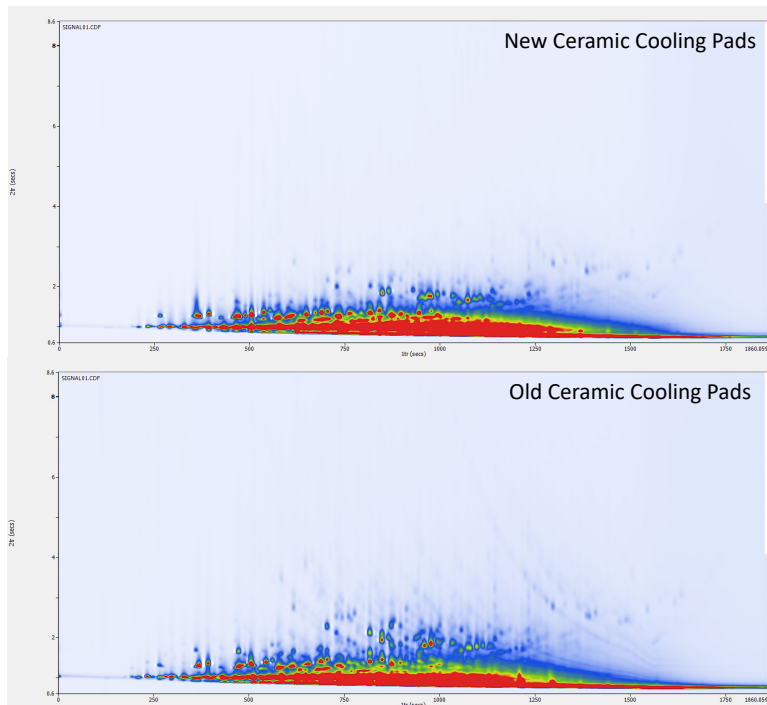


Figure 4.2 Analysis of diesel using MXT-5 #4 trapping capillary with 65 V modulation voltage for remobilization. The top contour plot employed the new trapezoidal ceramic cooling pads, while the bottom contour plot employed the old rectangular ceramic cooling pads

4.4 Removal of deactivation phase from within the unions

Streaking within the two-dimensional chromatograms was a recurring problem, creating broad secondary peaks that had the potential of co-eluting with other compounds, possibly making identification difficult. These streaks were likely caused by analytes being strongly sorbed within the unions at the front and back end of the modulator trapping capillary. The analytes within the unions did not elute off as easily as those within the trap during the discharge event since the unions were not heated to any significant extent during the capacitive discharge. Instead, they remained at the temperature of the oven and as the oven temperature program ramped up, the increasing temperature allowed these analytes within the unions to be released. However, they eluted as a broad band, ultimately creating a streak within the chromatogram.

To alleviate this problem, the adsorbent phase was removed from within the unions at the front and back end of the modulator trapping capillary. By removing this layer, the active material was no longer present for the analytes to strongly adsorb to, allowing more efficient desorption. The phase was removed by using an appropriately sized drill bit to manually scraping the capillary portion that was positioned within the union, noted by the red circles in Fig. 4.3.

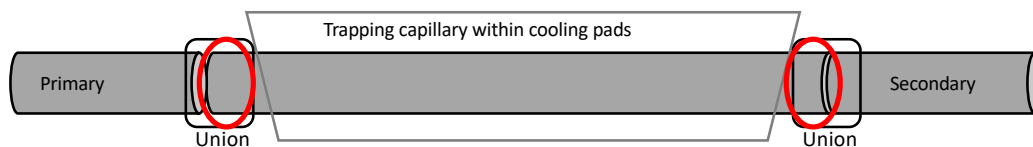


Figure 4.3 Schematic of the trapping capillary placed within the cooling pads, connected to the ¹D and ²D columns by unions at the front and back end. The red circles where the trapping layer was removed (within the unions at the front and back end of the trapping capillary).

4.4.1 Performance results

Due to the large number of trapping capillaries that were previously evaluated in Chapter 3, only those deemed acceptable will be discussed. DB-PS2887 trapping capillaries will also be excluded from discussion since they were found inferior to the DB-PS1 trapping capillaries. DB-PS1 #9 was treated at 40V for ten minutes followed by two five-minute phases at 35V. The treatment process created an ideal adsorbent material for efficient trapping; however, there was substantial streaking present in the ²D with active cooling. The streaking was less prominent with passive cooling due to the less effective cooling method. This was slightly decreased by applying a higher discharge voltage, but the issue remained with active cooling. As seen in Fig. 4.4, the removal of the adsorbent layer within the unions at the front and back of the trapping capillary significantly decreased the streaking present in the ²D. The overall separation and identification of later eluting compounds was no longer hindered.

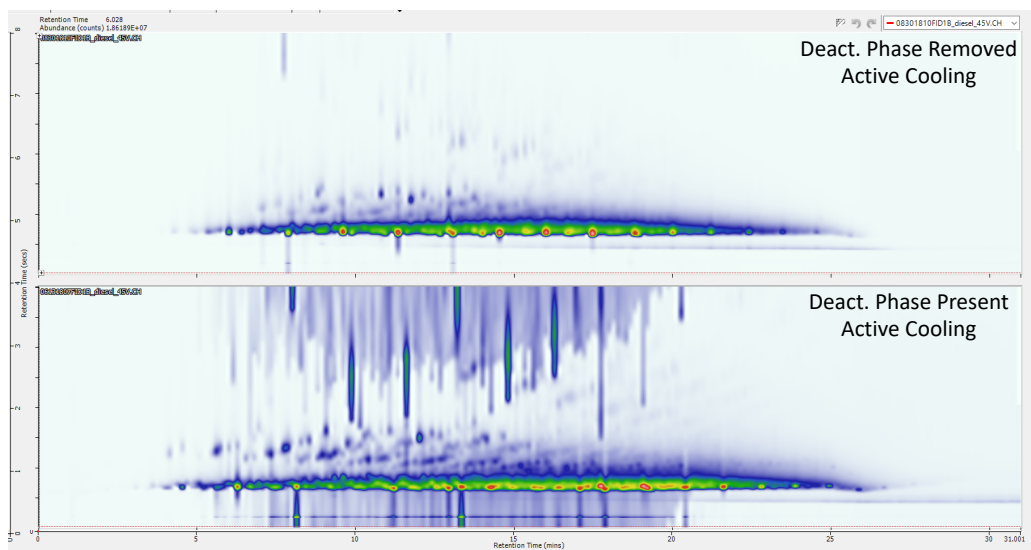


Figure 4.4 Analysis of diesel utilizing the trapping capillary DB-PS1 #9 with active cooling employed and a modulation voltage of 45 V. The adsorbent was removed from the segments of the capillary within the unions in the top contour plot, while it was still present in the bottom contour plot.

DB-PS1 #32 was treated at 50V for ten minutes followed by two five-minute phases at 45V for only half of the trapping capillary, while the other half was left untreated. By treating only a portion of the trapping capillary, superior separation was achieved with lower discharge voltages. There was still minor streaking present with both active and passive cooling. Similarly, to DB-PS1 #9, the streaking was eliminated with passive cooling by increasing the discharge voltage. Removing the adsorbent layer within the unions at the front and back end of the trapping capillary helped in removing some of the streaking present, as seen in Fig. 4.5. There was still minimal streaking present due to the unoptimized method of removal of the adsorbent layer. Manual scrapping of the remaining phase within the small openings of the capillary within the unions was not completely removing all the adsorbent present.

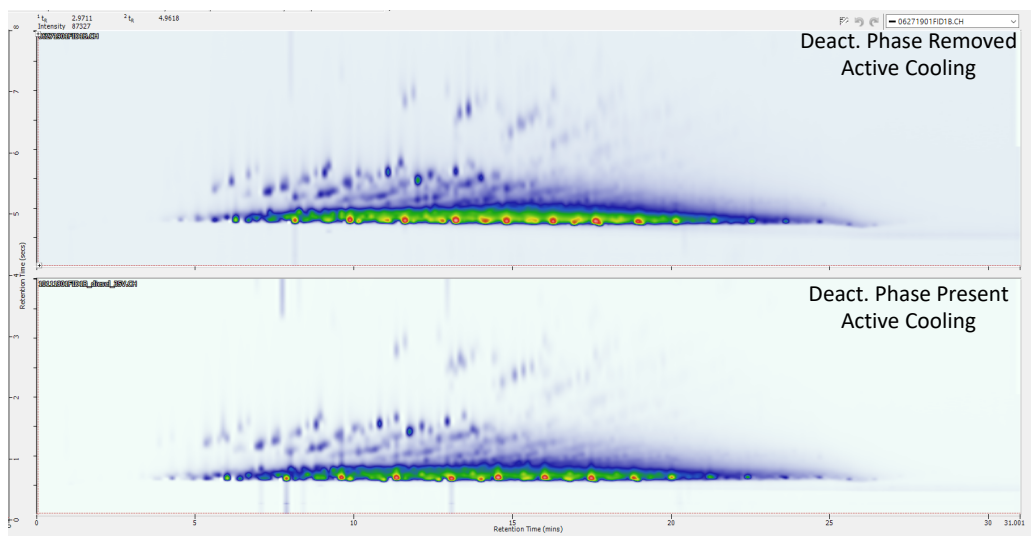


Figure 4.5 Analysis of diesel utilizing the trapping capillary DB-PS1 #32 with active cooling employed and a modulation voltage of 35 V. The adsorbent was removed from the segments of the capillary within the unions in the top contour plot, while it was still present in the bottom contour plot.

DB-PS1 #41 was treated in a similar manner to DB-PS1 #32, with a ten-minute phase at 50V, followed by two five-minute phases at 45 V; however, one half was treated instead of the center portion. This left the other half of the trapping capillary untreated, allowing for two possible configurations within the modulator. Configuration B was deemed a better option due to the streaking present in the ²D when placed in configuration A. After removal of the adsorbent phase from within the unions, the streaking was completely eliminated, as seen in Fig. 4.6. This process greatly improved the applicability of DB-PS1 #41. Before the removal of the adsorbent phase, it only performed efficient modulation when placed in configuration B and active or passive cooling was employed. If placed in configuration A, only active cooling could be successfully employed to achieve a separation without streaking. After the removal of the adsorbent layer from the unions, DB-PS1 #41 could be placed in either configuration with active or passive cooling and achieve adequate separation at lower discharge voltages.

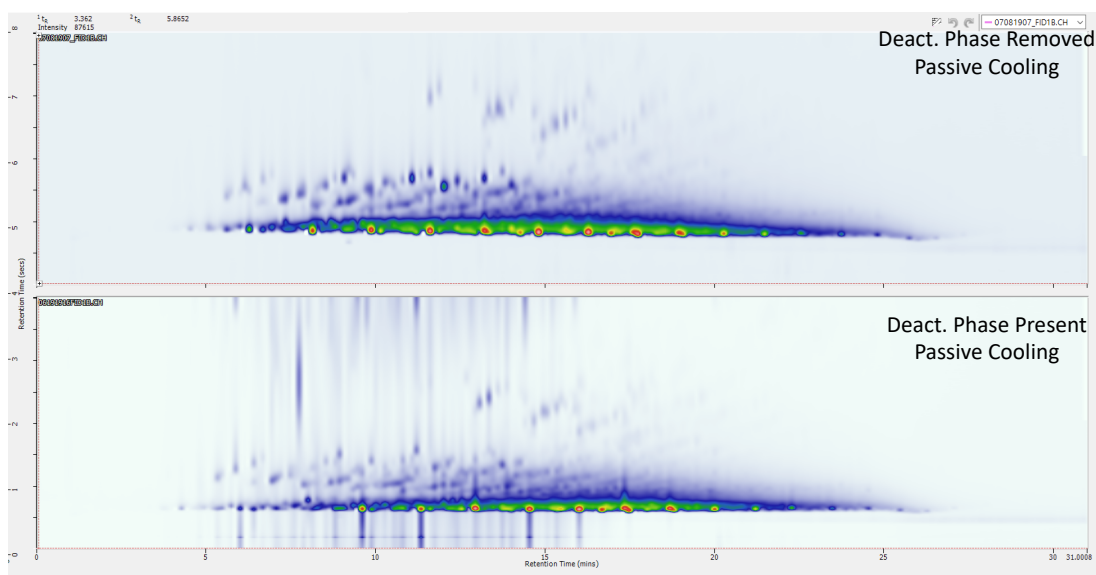


Figure 4.6 Analysis of diesel utilizing the trapping capillary DB-PS1 #41 (Treated Half) with passive cooling employed and a modulation voltage of 35 V. The adsorbent phase was removed from the segments of the capillary within the unions in the top contour plot, while it was still present in the bottom contour plot.

DB-PS1 #40 was treated at 50 V for ten minutes followed by 45 V for two five-minute phases for the entire length of the trap, as well as the area within the unions. This initially was performed to eliminate the streaking in the ²D; however, the opposite effect was achieved. A substantial increase in streaking in the ²D occurred with both active and passive cooling. Increasing the discharge voltage eliminated the streaking marginally, but the separation of the later eluting compounds was continually hindered by co-elutions. After removal of the active layer from the unions at the front and back of the trapping capillary the separation was greatly improved with both active and passive cooling, as seen in Fig. 4.7 and 4.8, respectively. The elimination of streaking in the ²D was greater with active cooling, but minor streaking remained with both types of cooling. With active cooling, the majority of the streaking was present within the void time, lowering the possibility of co-elutions with later eluting compounds in the ²D space.

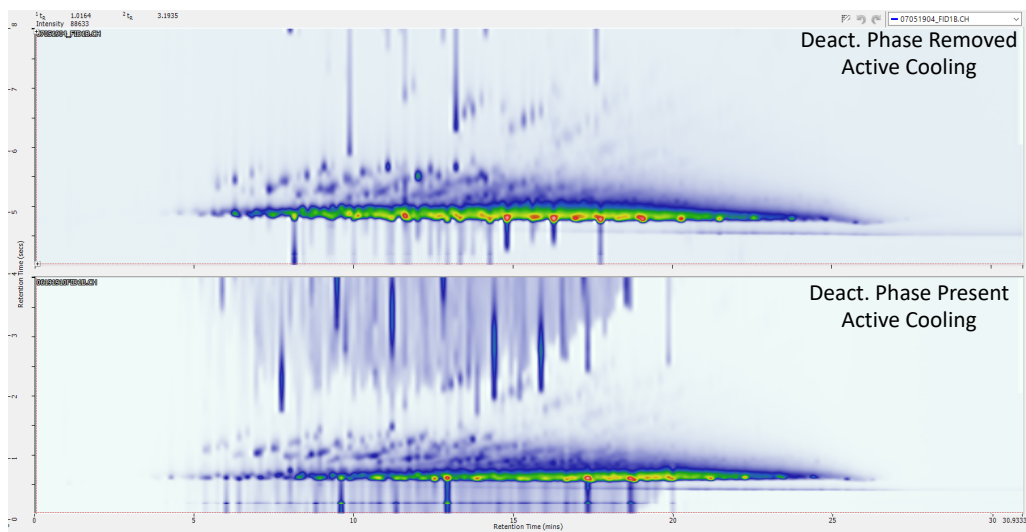


Figure 4.7 Analysis of diesel utilizing the trapping capillary DB-PS1 #40 with active cooling employed and a modulation voltage of 45 V. The adsorbent phase was removed from the segments of the capillary within the unions in the top contour plot, while it was still present in the bottom contour plot.

There was more streaking present with passive cooling; however, the bands occurred at the end of the 2^2D space, clearly depicting the later eluting compounds unhindered. Despite the removal of the adsorbent layer improving the separation achieved with DB-PS1 #40, the treatment process was concluded inferior to the treatments performed on portions of the capillaries of DB-PS1 #41 and #32.

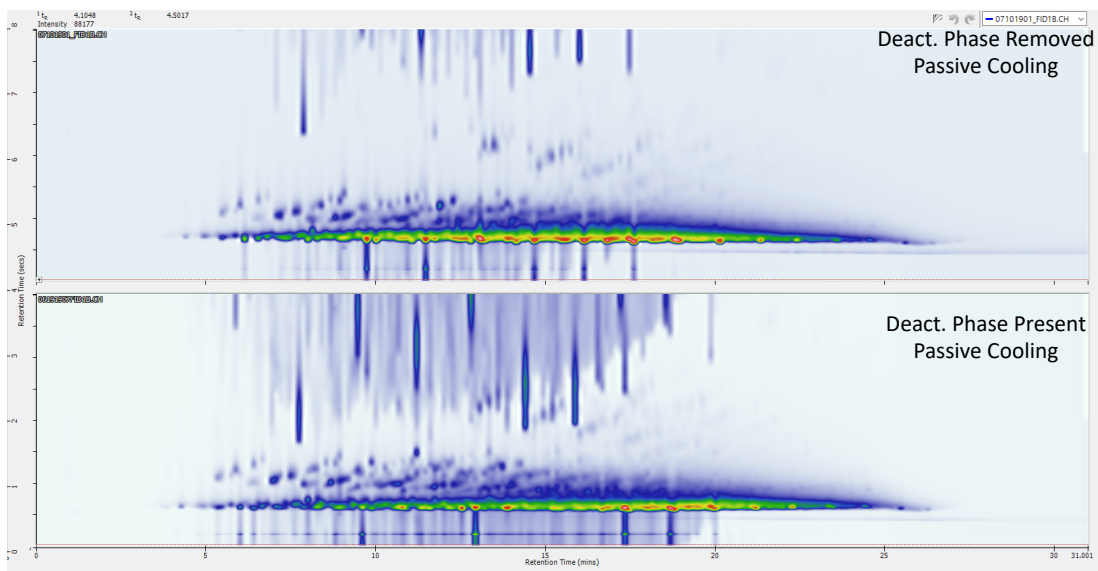


Figure 4.8 Analysis of diesel utilizing the trapping capillary DB-PS1 #40 with passive cooling employed and a modulation voltage of 45 V. The adsorbent phase was removed from the segments of the capillary within the unions in the top contour plot, while it was still present in the bottom contour plot.

DB-PS1 #42 was treated with two ranges of voltages, 45 V followed by 40 V was used on one half, while 40 V and 35 V were used on the other half of the trapping capillary. The chromatographic performance of the traps obtained using these treatment parameters was superior to all other tested traps. The combination of a more adsorbent portion and less adsorbent material efficiently trapped and completely desorbed analytes with lower discharge voltages. There was no streaking present in any of the tested discharge voltages with either active or passive cooling. The adsorbent phase was removed from within the unions at the front and back of the trapping capillary to ensure there was no negative effect on the chromatography. As seen in Fig. 4.9, the same separation of diesel was achieved with the adsorbent present or removed with active cooling employed. This further supports the claim that DB-PS1 #42 in configuration B is the optimal trapping capillary for single-stage modulation.

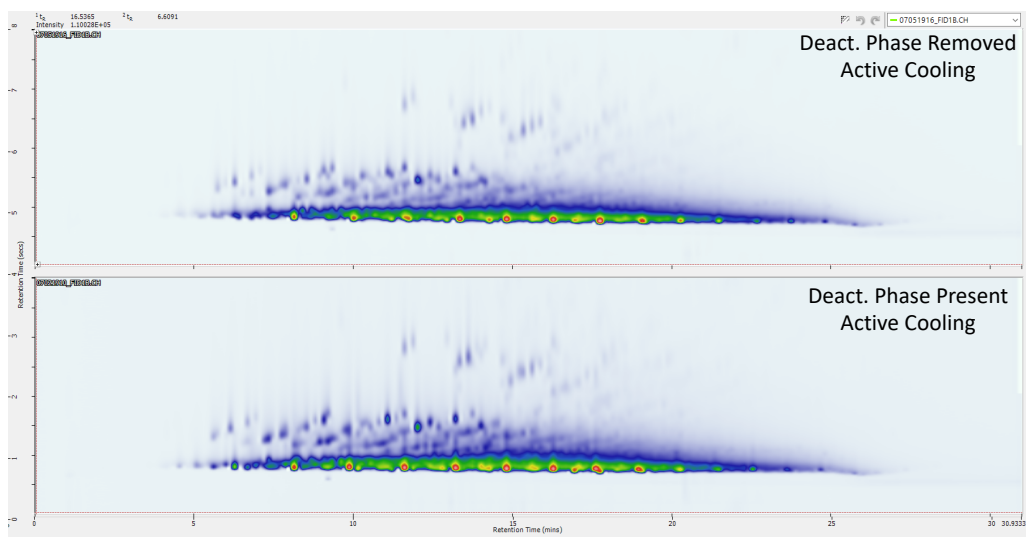


Figure 4.9 Analysis of diesel utilizing the trapping capillary DB-PS1 #42 (Configuration B) with active cooling employed and a modulation voltage of 35 V. The adsorbent phase was removed from the segments of the capillary within the unions in the top contour plot, while it was still present in the bottom contour plot.

In conclusion, the removal of the adsorbent phase from within the unions at the front and back end of the trapping capillary helped in decreasing or even eliminating streaking within the 2D chromatograms for some capillaries. Ultimately, this improved the overall separation and reduced co-elutions in the 2D. This process was beneficial with both active and passive cooling, making previously established treatment processes more applicable to all scenarios, without the need to increase the discharge voltage to undesirably high values. However, to be practical, the method of adsorbent phase removal would need to be further developed for consistent results.

4.5 Summary

The new trapezoidal design of the ceramic cooling pads helped provide effective cooling to the entire length of the trapping capillary. In addition, this new design was accommodating

towards varying lengths of trapping capillaries. The previous rectangular design left portions of the trapping capillary exposed to the oven in some cases, creating hot spots that led to pyrolysis and decomposition of some sample components during analysis. Complete coverage of the trapping capillary within the ceramic cooling pads eliminated pyrolysis by leaving no portion exposed to the oven.

Removal of the adsorbent layer from the portions of the trapping capillary located within the unions at the front and back end decreased and/or eliminated the streaking in the 2D for some capillaries. Even though the streaking was not completely eliminated in some cases, the decrease drastically improved the separation of late eluting compounds due to fewer co-elutions. The removal was beneficial with both active and passive cooling. It allowed the DB-PS1 trapping capillaries treated with previously tested processes to be more widely applicable at lower discharge voltages. However, the removal process of the adsorbent layer was not reproducible, leading to sometimes inconsistent results. Further improvements to the technology should be pursued unless the need for the treatment is eliminated, as was the case for the DB-PS1 #42 trapping capillary.

Chapter 5. Diagnostic measurements of new stationary phase within trapping capillary

5.1 Introduction

As previously discussed in Chapter 3, thermal degradation of the polydimethylsiloxane (PDMS) stationary phase and its subsequent conversion to the adsorbent phase played a key role in creating a sorptive material necessary for efficient single stage modulation. Since the thermal depolymerization temperature for PDMS is known to be greater than 350 °C [101], it was important to determine the corresponding temperatures for an applied voltage during the treatment process and within the ceramic cooling pads of the thermal modulator for analysis. Despite the Restek MXT and Agilent DB-PS both containing a 100% PDMS phase within a metal capillary, each manufacturer utilizes different technology to prepare their metal tubing, deactivate the tubing and coat the stationary phase. Ultimately, this results in a completely different product in regard to the malleability of the metal capillary, its robustness and modification during treatment. When comparing the Restek and Agilent products, it is clear that the prior is a more sturdy and rigid metal, while the latter feels softer and more malleable. Although the materials used in creating the metal exterior are proprietary, it was evident they were quite different. The corresponding temperature increase for a wide range of applied voltages had previously been determined for the Restek column, but due to the apparent differences in the Agilent column, these diagnostic measurements had to be repeated.

5.2 Determination of the trapping capillary temperature during the treatment process

To determine the actual temperature of the trapping capillary during the treatment process, several instruments were required. The treatment set-up remained the same, as previously discussed in Chapter 2 (Fig. 2.1). Briefly, two alligator clips were attached to the trapping capillary to provide the capacitive discharge from the power supply. The clips were placed at a distance from one another that corresponded to the length of the cooling pads of the modulator. The trapping capillary was also connected to the house compressed air supply to provide air during treatment, if necessary. Additional instrumentation for the measurement of the temperature included a K-type thermocouple (0.5mm diameter, Omega), an in-house amplifier (UW Science Shop) and an oscilloscope (Hameg). The thermocouple was spot-welded onto the center of the trapping capillary. It was connected to an amplifier and subsequently an oscilloscope, as seen in Figure 5.1. As the capacitive discharge power supply applied a specified voltage to rapidly heat the trap, the thermocouple produced a reading which was amplified 100 times and displayed on the oscilloscope, as seen in Figure 5.1. The peak increase corresponded to the maximum temperature, while the decrease in signal reflected the cooling time required to return to baseline. Both Agilent DB-PS1 and DB-PS2887 capillaries were used to establish the actual temperature increase at various applied discharge voltages with both air on and off during treatment. For both capillaries, the capacitive discharge was applied at six second intervals.

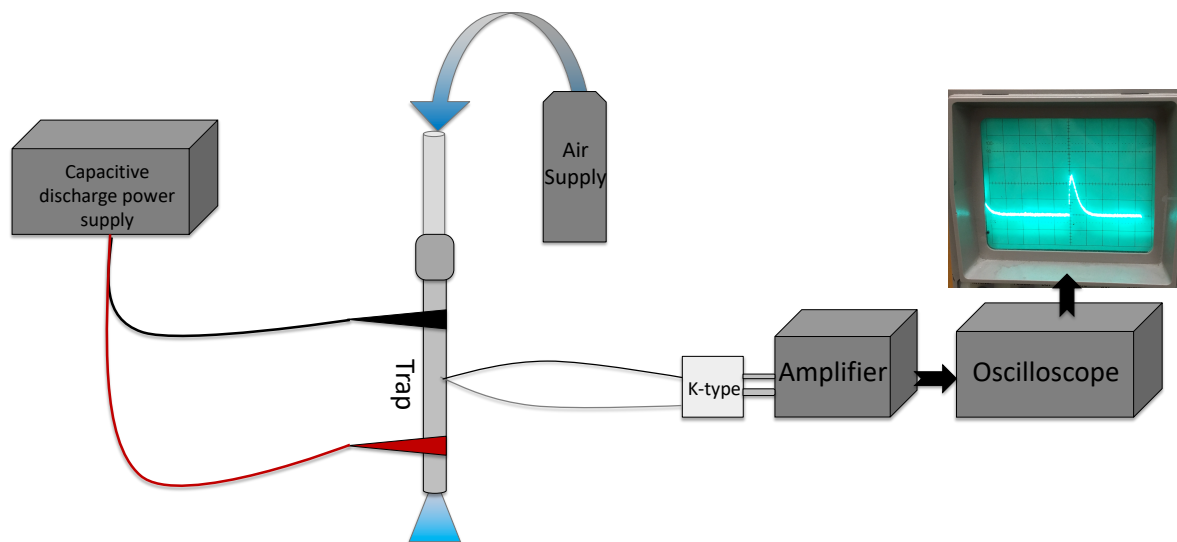


Figure 5.1 Instrumental set-up for the determination of trap temperature increase during treatment at various discharge voltages.

Further data processing was required once the mV increase and cooling time readings were acquired. First, the mV increase determined from the oscilloscope reading had to be divided by a factor of 100 due to the amplifier. Thereafter, the corresponding temperature increase ($^{\circ}\text{C}$) was determined by substituting the mV increase value into the K-type thermocouple equation, as seen in Equation 1. The equation was rearranged to solve for x, the temperature increase, by substituting the mV increase value for y. The calculated temperature increase value was then added to $20\text{ }^{\circ}\text{C}$ to account for the ambient temperature within the room (which was the temperature of the cold junction of the thermocouple). Ultimately, the trapping capillary temperature increase at various discharge voltages was used to create a calculator. The discharge voltages applied were plotted on the x-axis, with the corresponding trap temperature increase on the y-axis for all scenarios. Polynomial relationships, as seen in Fig. 5.2 and 5.3, were used to determine the trap temperature increase at any chosen discharge voltage during treatment.

(1)

$$y = -0.0417x - 0.1522$$

$$R^2 = 0.99994$$

The comparison between air on and off during treatment for the Agilent DB-PS1 trap is displayed in Fig. 5.2. The circle data points correspond to the scenario with the air on during treatment, while the square data points correspond to the scenario with the air off during treatment. The plots display the corresponding polynomial equations for the line of best fit and R-squared values for both scenarios. The polynomial trend was similar for both scenarios; however, the greatest temperature increase occurred while the air was off during treatment. The air off scenario also drastically increased in temperature when more than 50 V of capacitive discharge were applied. The air on scenario better fitted the polynomial model, based on the R-squared value, when directly compared to the air off scenario. Also, when comparing the air on and air off scenarios, the prior helps in cooling the trapping capillary during treatment, as seen by the smaller temperature differential when higher voltages are applied. Thermal degradation of PDMS occurs at 350 °C, corresponding to a value of at least 35 V when the air is off and 40 V when the air is on during treatment of the thin film DB-PS1 trapping capillary. Based on the optimal treatment of a DB-PS1 ranging from 40 V to 50 V, the trapping capillary is subject to an estimated increase in temperature from approximately 350 °C to 600 °C. Overall, both equations were used to create a universal temperature increase calculator for the DB-PS1 trapping capillary.

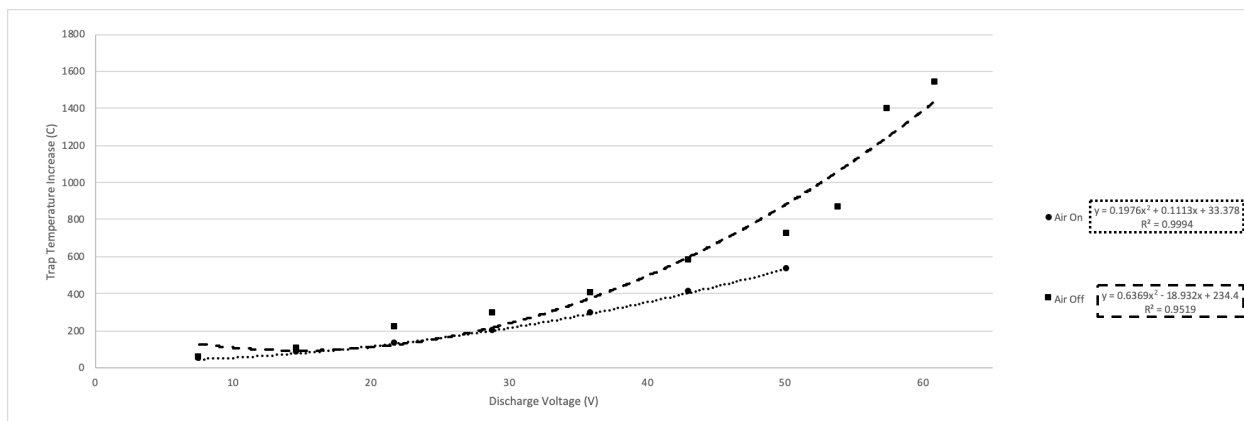


Figure 5.2 Temperature increase for DB-PS1 during treatment at various discharge voltages with both air on (circles) and air off (squares).

The comparison between air on and air off during treatment for the Agilent DB-PS2887 is displayed in Fig. 5.3. As in the plot for DB-PS1, the circle data points correspond to the air on scenario, while the square data points correspond to air off. Again, as expected, the greatest temperature increase occurred while the air was off during treatment. However, the trends of the air on and air off scenarios were more similar for the DB-PS2887 trapping capillary than they were for the DB-PS1 trapping capillary. Similarly to the DB-PS1 trapping capillary, the air on scenario helped provide cooling during treatment, resulting in smaller temperature increase compared to the air off scenario. It is important to note that the metal tubing was different between the DB-PS1 and DB-PS2887 columns. As a result, DB-PS2887 could be treated at significantly higher voltages than the DB-PS1. Thermal degradation begins at approximately 30 V when the air is off and approximately 35 V when the air is on. Both polynomial equations were used to create a calculator to determine the temperature increase of the trapping capillary during treatment when a certain voltage was applied. Due to the differences in the tubing material between DB-PS1 and DB-PS2887, the temperature increase of the trapping capillary during treatment differed when the same capacitive discharge voltage was applied.

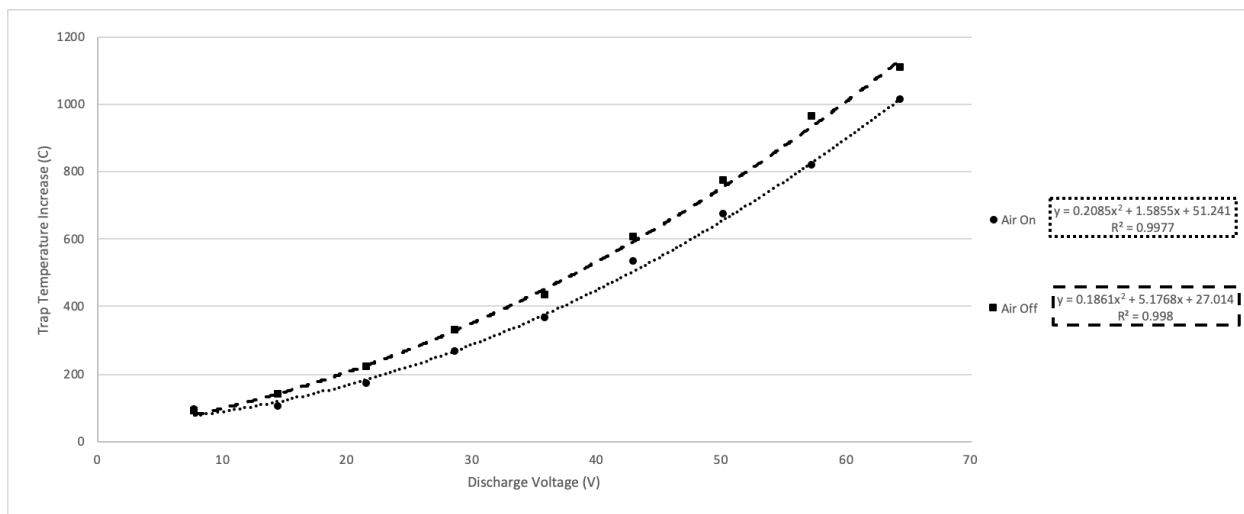


Figure 5.3 Temperature increase for DB-PS2887 during treatment at various discharge voltages with both air on (circles) and air off (squares).

5.3 Determination of trapping capillary temperature within the ceramic cooling pads

The temperature of the trapping capillary while between the cooling pads of the modulator was also determined. A similar instrumental set-up as that discussed in Section 5.2 was used; however, a separate component was required, as seen in Figure 5.4. A home-made K-type thermocouple was spot welded onto the trapping capillary before it was placed within the cooling pads. The thermocouple was connected to the amplifier and subsequently the oscilloscope. A second K-type thermocouple was placed between the cooling pads to determine their temperature at various GC oven temperatures. This measurement was important to determine the temperature of the cooling pads at any time during the run. By design, the cooling pads lag behind the GC oven to facilitate the desorption of high-boiling point compounds eluting from the ¹D at higher temperatures. The thermocouple was placed within the center of the cooling pads without touching the trapping capillary. The capacitive discharge power supply was

connected to the nuts on the front and back end of the trapping capillary, positioned just outside the cooling pads of the modulator. As the power supply applied a voltage to rapidly heat the trap, the thermocouple signal was amplified and displayed on the oscilloscope.

Compared to the readings acquired for the uncompressed trap during the treatment phase, there was more noise present, resulting in greater uncertainty in the readings taken from the oscilloscope, as seen in Figure 5.2. The mV increase readings were taken at various discharge voltages at 5 V increments at a set oven temperature. This was repeated at four separate oven temperatures, (40 °C, 100 °C, 200 °C, 300 °C) to simulate common values reached during an analytical run with a set oven temperature ramp. Both active cooling (thermoelectric coolers (TECs) and fans on) and passive cooling (TECs off with fans on) were also tested to assess every possible scenario.

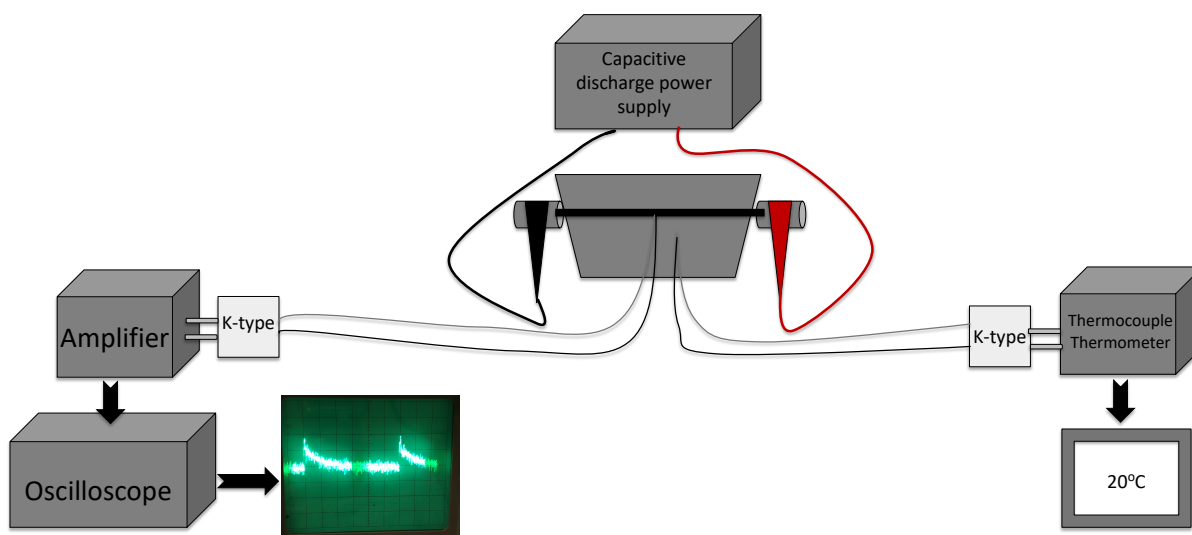


Figure 5.4 Determination of trapping capillary temperature between the cooling pads of the modulator.

Similarly to the determination of temperature increase of the trapping capillary during the treatment process, further data processing was required to determine the temperature of the trap within the cooling pads. The K-type thermocouple equation was used to determine the temperature from the signal displayed on the oscilloscope. After determining the trap temperature from the voltage, the temperature of the cooling pads for each chosen oven temperature was added to determine the actual temperature of the trapping capillary. The various discharge voltages were then plotted on the x-axis, and the corresponding trap temperatures were plotted on the y-axis. The polynomial relationships for each oven temperature with active cooling were then overlaid on a single plot for better visualization, as seen in Fig. 5.5. All four trends show a polynomial relationship between the discharge voltage applied and actual temperature of the trap, with R-squared values above 0.98. The greatest temperature increase occurred while the oven was at the lowest temperature of 40 °C (diamond markers), while the lowest temperature increase occurred while the oven was at the highest temperature of 300 °C (circle markers). At an oven starting temperature of 40 °C, there was a temperature increase from 40 °C to 500 °C, which was an increase of 460 °C. On the other hand, at the oven temperature of 300 °C, the trapping capillary increased to 650 °C, which was an increase by 350 °C. As previously seen in Chapter 3, pyrolysis of the sample typically occurred when extremely high discharge voltages, such as 50 V or 55 V, were applied during analysis. The actual trap temperature at an oven temperature of 300 °C was the greatest, ranging from approximately 450 °C to 650 °, when a high discharge voltage was applied. This confirmed the possibility of degradation and loss of the sample by pyrolysis. It is important to note, when determining the necessary discharge voltage for analysis, that as the temperature of the oven increases, the actual temperature of the trap also increases. Voltages between 30 V and 40 V were more suitable due

to the trap temperature remaining below the pyrolysis temperature. Also, these voltages should prolong the life of the trapping capillary and the sorbent material within due to a maximum temperature of approximately 400 °C.

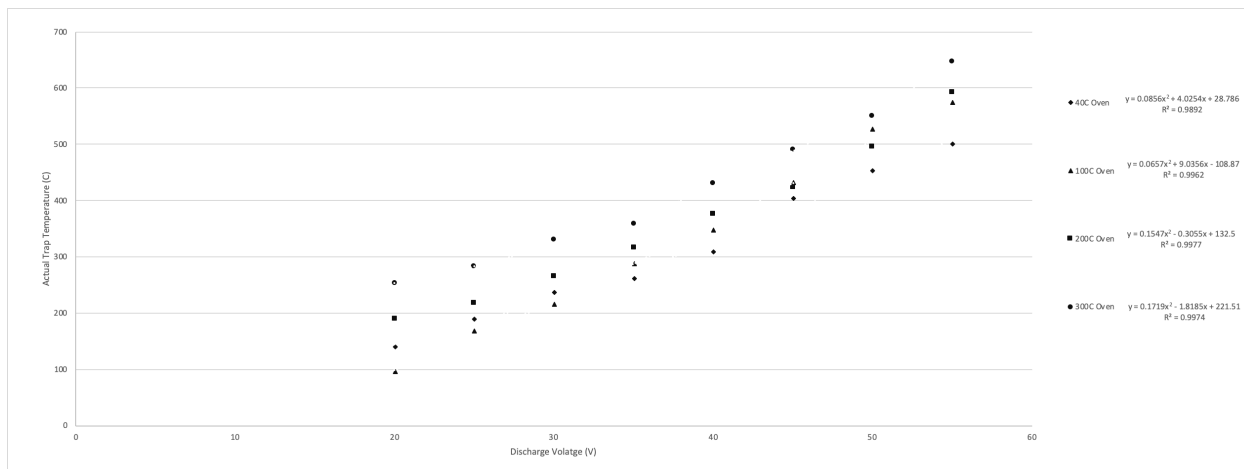


Figure 5.5 DB-PS1 trap temperature within cooling pads with active cooling (TECs and fans on)

The polynomial relationships for each oven temperature with passive cooling were also overlaid on a single plot for better visualization, as seen in Fig. 5.6. Similarly, the greatest temperature increase occurred while the oven was at the lowest temperature (diamond markers) and the lowest temperature increase occurred while the oven was at the highest temperature (circle markers). At a starting oven temperature of 40 °C, there was a temperature increase of 40 °C to approximately 650 °C, which was an increase of approximately 610 °C. At the oven temperature of 300 °C, the trapping capillary increased to approximately 750 °C, which was an increase of 450 °C.

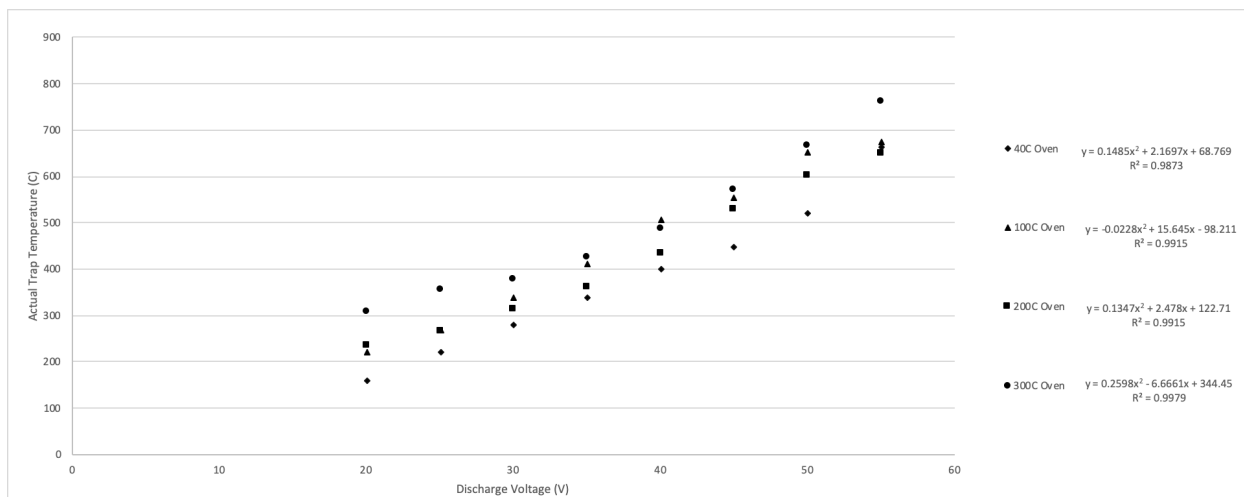


Figure 5.6 DB-PS1 trap temperature within cooling pads with passive cooling (TECs off and fans on).

5.4 Determination of ceramic cooling pads temperature with varying oven temperature ramps

With new ceramic cooling pads that were designed for more efficient cooling, they needed to be evaluated on their actual temperatures as the GC oven temperature increased with varying temperature ramps. The instrumental set-up required a K-type thermocouple and a thermocouple thermometer to read the temperature within the cooling pads, as seen in Figure 5.7. The custom-made K-type thermocouple was placed within the center of the ceramic cooling pads, assuring that it did not touch the trapping capillary. The GC oven was set for three separate temperature ramps: 3 °C/min, 6 °C/min, and 9 °C/min to represent the commonly used values. Once the GC was started, the cooling pads temperature was read every ten degrees to obtain the data points.

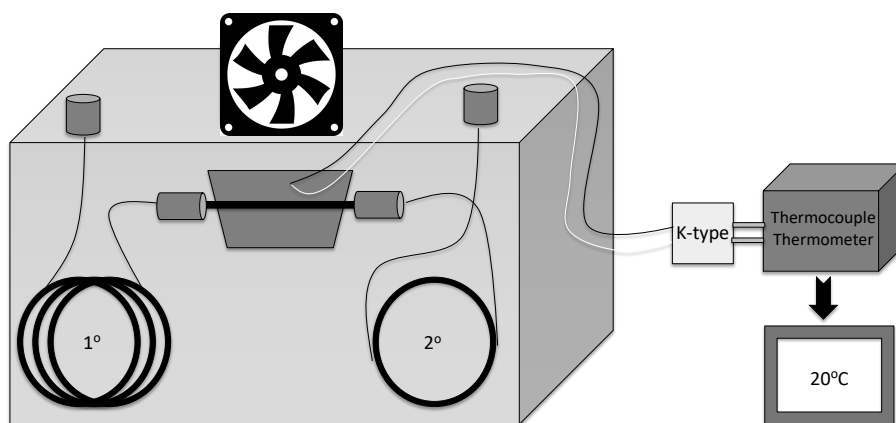


Figure 5.7 Instrumental set-up to determine the temperature of cooling pads with varying oven temperature ramps

This was performed with both active and passive cooling to determine the temperature differential of the ceramic pads. The oven temperature was plotted on the x-axis while the corresponding cooling pad temperature was plotted on the y-axis. The three oven ramp scenarios with active cooling are overlaid for easy comparison in Fig 5.8. The linear relationship between the oven and cooling pads temperatures was consistent over all three oven ramps, with similar trend lines. As the oven temperature increased, the cooling pads lagged behind, facilitating the analysis of semi-volatile compounds. Should the cooling pads be excessively cold, a high discharge voltage would be necessary to properly remobilize the trapped analytes, which could lead to their pyrolysis. As the oven temperature increased, the temperature differential between the cooling pads and the oven became greater. This allowed efficient trapping of heavier compounds while making their release easier. The cooling pads maintained a maximum temperature below 150 °C when the oven temperature was at 300 °C. The oven temperature program was stopped at 300 °C due to the temperature limit of the thermoelectric coolers. The ceramic pads were able to achieve efficient cooling with a wide range of oven ramps from

relatively slow to rather quick, without any drastic variation.

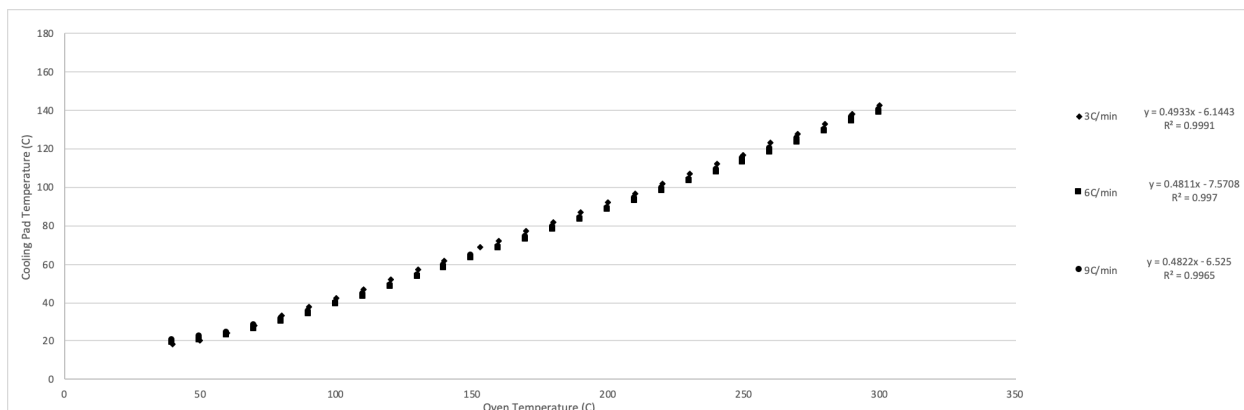


Figure 5.8 Temperature of the cooling pads with active cooling (TECs and fans on) with various oven temperature ramps.

The three oven ramp scenarios with passive cooling were overlaid for easy comparison in Fig. 5.9. As previously seen with the active cooling, there was a linear relationship between the oven temperature and cooling pad temperature for all three temperature ramps. Also, the trends for the different temperature ramps were very similar. With passive cooling, the cooling pads also lagged behind the oven temperature, assisting in the analysis of semi-volatiles. However, in comparison to active cooling, the temperature differential between the oven and the cooling pads was smaller. The maximum temperature of the cooling pads remained below the maximum oven temperature by about 15 °C. The oven temperature program was able to reach values greater than 300 °C since the Peltier coolers were removed from the modulator platform. At the beginning of the oven temperature ramp, the differential for active cooling was approximately 30 °C, while passive cooling only achieved a differential of about 1 °C. Half-way through the temperature ramp, active cooling achieved a differential of approximately 100 °C, while passive cooling achieved approximately a 10 °C differential. At the end of the temperature program, there was a differential of approximately 150 °C for active cooling and only 15 °C for passive cooling.

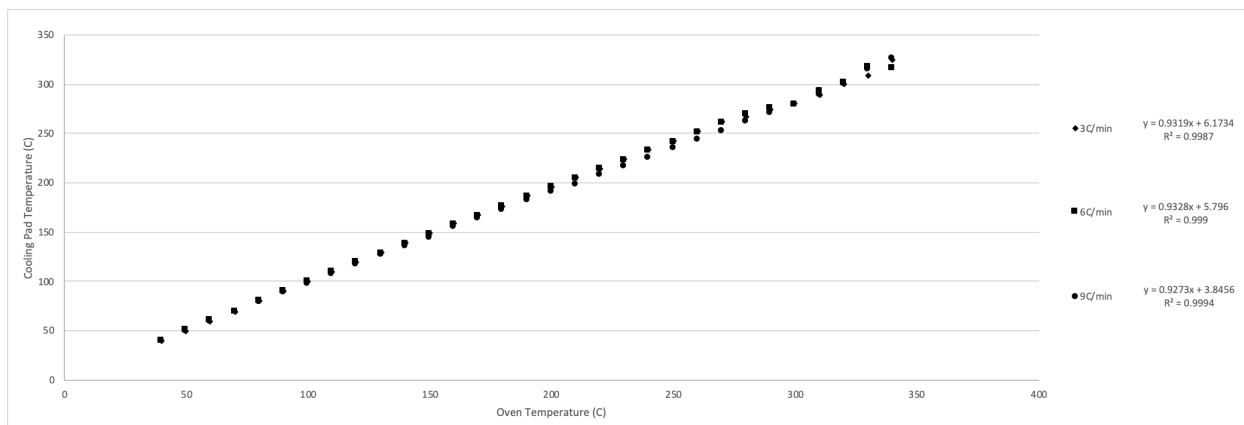


Figure 5.9 Temperature of cooling pads with passive cooling (no TECs, fans on)

5.5 Summary

The trap temperature increase during treatment of DB-PS1 and DB-PS2887 columns was determined. Both scenarios of air on and off during treatment were analyzed for both trapping capillaries. A calculator was then created in order to understand the temperature increase at any applied discharge voltage. As expected, the air on scenario resulted in lower temperature increases when compared to the air off scenario for both trapping capillaries. The DB-PS2887 could be treated with higher discharge voltages because of different resistance of the metal tubing it was made of. The temperature of the trapping capillary when placed within the modulator was also determined with both active and passive cooling. Potential for pyrolysis of the analytes was confirmed by the measured temperature increases that occurred with both active and passive cooling at the highest discharge voltages. An appropriate voltage could be determined to avoid pyrolysis during analysis based on the data collected. With passive cooling, a lower voltage was required to avoid pyrolysis compared to active cooling.

The temperature of the cooling pads with active and passive cooling during various temperature ramps was measured. With both scenarios, the temperature of the cooling pads

lagged behind the oven temperature, allowing for easier analysis of semi-volatile compounds.

There was a linear relationship between the oven temperature and the cooling pads temperature for both scenarios. Active cooling achieved a greater temperature differential from the oven when compared to passive cooling.

Chapter 6. Comparison of thermal and flow-based modulation in comprehensive two-dimensional gas chromatography –time-of-flight mass spectrometry (GC×GC -TOFMS) for the analysis of base oils

6.1 Introduction

Evaluation of the UW single-stage, consumable-free thermal modulator was previously completed by Edwards. To further evaluate the separational capabilities of the UW modulator, a comparison to a commercially available flow modulator was performed. Due to the different operational principles of the two modulation platforms, a direct comparison under identical conditions was not possible, hence each modulator was tested under its optimal conditions. An extremely complex matrix, base oils, that have not been analyzed much within literature were selected to challenge the modulator platforms. As a major component of lubricating greases, engine oils and metal processing fluids, base oils are encountered in both industry and everyday life. They are produced by refining crude oil or chemical synthesis, using typical processes of distillation, cracking, hydrogenation and dewaxing [102,103]. Originating from heavy crude oil, the hydrocarbons in base oils range between 18-40 carbon atoms with a boiling point range between 288 °C and 566 °C [102]. To differentiate the levels of refinement, the American Petroleum Institute (API) classifies these oils into five groups. Group 1 contains the least refined, conventional petroleum base oils. Group 2 has a better grade of petroleum when compared to

group 1, partially produced by hydrocracking. Group 3 contains the best grade of petroleum that is fully produced by hydrocracking. The synthetic oils and poly-alpha-olefins (PAOs) are placed in group 4. Finally, any other types that were not previously mentioned are placed in group 5.

Engine oils' main functions include lubrication of the moving parts, cleaning, inhibiting corrosion, and helping cool the engine by removing heat from the moving parts [104]. These oils can be further differentiated by their base stock and viscosities, which define their working capability. Base stocks are separated into three groups: synthetic, semi-synthetic and mineral. This classification is an important quality control measure used for identification of adulteration [105]. The Society of Automotive Engineers (SAE) defines two kinematic viscosities for engine oils; one at a low and one at a high temperature. The value that is directly followed by a "W" refers to the winter, or low temperature kinematic viscosity value (SAE 0W, 5W, 10W and 20W) [105]. The values that do not contain a letter refer to the high temperature kinematic viscosity value (SAE 20, 30, 40 and 50) [105]. These viscosities determine the "thickness" of the oil, with larger numbers denoting thicker consistencies due to the increased amount of time it takes to flow when compared to the smaller values. For example, SAE 5W-30 is designed for temperature conditions below -18 °C, providing good low temperature performance and fuel economy [104]. On the other hand, SAE 20W-50 is designed for temperature conditions above -7 °C, providing performance for high temperatures such as driving in the desert and towing heavy loads for a long time [104].

Continual testing throughout the production process is vital to ensure the oils are performing to their necessary regulations and requirements. When analyzed by conventional one-dimensional gas chromatography (1D-GC), a large raised baseline region due to unresolved complex mixture (UCM) is observed, making it difficult to separate co-eluting compounds and

differentiate the complex nature of the oil matrix [106]. This shortcoming of 1D-GC drives the search for more capable methods. Comprehensive two-dimensional gas chromatography (GC×GC) has become an established method for the analysis of complex mixtures since its inception in the 1990's. In fact, one of the first GC×GC applications was the investigation of petroleum [107]. By implementing two separate stationary phases, the sample in GC×GC is subjected to an orthogonal separation according to both polarity and volatility. A so-called 'roof tile effect' is a common visual characteristic of GC×GC chromatograms of petroleum fractions that allows differentiation of various chemical classes in which compounds from similar homologous groups are arranged together in sequential order by their carbon number [108]. This effect is extremely useful when performing a group type separation, specifically PIONA (Paraffins, Isoparaffins, Olefins, Naphthenes and Aromatics) [107]. Owing to enhanced resolution when compared to 1D-GC, GC×GC allows an in-depth investigation of trace components, such as biomarkers and chemical additives within petrochemical samples. Biomarkers are a vital investigative tool for forensic purposes when an identification of an oil source and maturity are needed in regard to an environmental pollution event [108].

Chemical additives and antioxidants are typically added to an oil or lubricant to enhance its performance, alleviate adverse properties and prevent oxidation [109, 110]. Antioxidants are added to eliminate or slow down the oxidation processes that hydrocarbons are prone to at high temperatures. In this way, the oils and lubricants are protected from the harmful effects of oxidation, which include the formation of harmful species and deterioration of the lubricant [110]. The two main classes of antioxidants are alkylated diphenylamines and sterically hindered phenolic compounds. The composition of these additives within engine oils is constantly evolving to meet the requirements of the continuous engine operation modifications [111].

GC×GC aids in separating and identifying these compounds that may be at trace levels, hidden within the UCM within a 1D-GC chromatogram. Identification of these compounds is vital in distinguishing brands, blends and kinematic viscosities (low vs. high temperature) of oils.

So-called “normal” GC×GC column configuration includes a non-polar column in the first dimension and a semi-polar/polar column in the second dimension. However, this is not an advantageous configuration in regard to the hydrocarbons found within engine oils. By employing a polar column in the first dimension and a non-polar column in the second dimension, a reverse column set-up takes advantage of the operating mechanism of GC×GC to give an enhanced separation of samples with similar compositions to that of engine oils [112, 113, 114, 115, 116]. The reverse column configuration specifically aids in group-type analysis by increasing the resolution of the straight chain and branched alkanes from the aromatic hydrocarbons [117]. The aromatic species elute at a shorter ²D retention time (lower in ²D space), while the saturated alkanes elute at a longer ²D retention times (higher in ²D space), creating distinct bands [117]. In a comparison of both column configurations, Tran *et al.* found that the normal set-up used the two-dimensional space poorly, while the reverse set-up improved the separation of the non-polar compounds [118]. With a polar ¹D column, the alkanes elute at lower temperatures, resulting in a higher retention factor on the non-polar ²D column [118]. Ultimately, this increases the non-polar peak resolution due to the greater retaining power. On the other hand, polar compounds are strongly retained on the polar ¹D column, resulting in a higher elution temperature and a shorter ²D retention time [118].

To ensure the sample is properly transferred from the ¹D column to the head of the ²D column, a modulator must be employed. As the ‘heart’ of GC×GC, the modulator must collect the components of or sample the entire ¹D column effluent and create a narrow band to be

injected onto the ²D column while preserving the previous separation achieved on the ¹D column. To preserve the separation accomplished in ¹D, the modulator must sample each ¹D peak at least three to four times [8]. The commercially available modulators can be separated into two classes: thermal modulators and flow modulators. Detailed reviews of the history and operating principles of the various modulator designs can be found elsewhere [2, 7, 12, 42, 47, 119]. Also, several publications have previously compared cryogenic and flow modulators for the analysis of petroleum products [62, 66]. When comparing the Agilent differential flow modulator and the liquid N₂ modulator for the analysis of light cycle oil, Semard *et al.* concluded the quality of separation and separation space obtained by the cryogenic modulator was reproduced by the flow modulator [66]. The cryogenic modulator did obtain an increase in sensitivity by a factor of 2.5 due to the focusing effect when compared to the differential flow modulator [66]. Ultimately, they determined that the performance (resolution and peak capacity) of the cryogenic modulator could be matched by the flow modulator when operated under optimal conditions [66]. Similarly, a comparison of the reverse fill/flush differential flow modulator and the CO₂ dual jet cryogenic modulator for the analysis of heavy petroleum cuts determined that the separation space used was similar for both platforms [62]. Duhamel *et al.* also found that the reverse fill/flush differential flow modulator increased the peak capacity by a factor of 3 due to the employment of a longer ²D column, due to the independent flow rates used in both dimensions [62]. However, it is important to note that it is impossible to apply strictly identical analytical conditions when a specific platform is employed, due to the different operating principles [62]. For example, thermal modulation focuses the ¹D effluent band in space, while flow modulation only focuses it in time [120]. Despite both platforms' ability to

achieve similarly narrow peak widths within the second dimension, thermal modulation is superior in regard to providing increased sensitivity and high-resolution separations [120].

Mass spectrometry is commonly employed to assist in identifying analyte peaks. Typically, time-of-flight mass spectrometers are the model of choice for GC×GC due to their fast acquisition speed and full scan range capabilities. However, if there are no standard reference materials or compounds are not included in the mass spectral library, not all of the compounds can be identified. Positive identification of a compound can only occur with an authentic standard. Classical electron ionization (EI) employs 70 eV energy. Since most molecules have significantly lower ionization energies, the mass spectra contain an abundance of small fragment ions, often leaving the molecular ion barely visible or absent [121]. To better assist in providing a more definitive identification, soft ionization can be implemented. This technique utilizes a lower energy to ionize the compound, resulting in less fragmentation [121]. The spectra typically contain a molecular ion in greater abundance and fewer but more distinctive fragmentation ions. Some available soft ionization techniques include chemical ionization (CI), photoionization (PI) and field ionization (FI). Some limitations of these techniques include a different ion-source configuration with a reagent gas, weak ion currents, and limited sample applicability, respectively. Previously, GC×GC-PI-TOF-MS was used for the molecular characterization of base oil hydrocarbons and identification of isomers; however, extensive fragmentation pattern analysis and comparison to EI spectra were required [122]. Alternatively, variable ionization energy-TOFMS (Select-eV) addresses these issues by performing both hard and soft ionization ranging between 70 and 10 eV on a single mass spectrometer, without the need for reagent gases, pressure adjustments, or alterations to the ion source [121, 123]. The identification of specific isomers within motor oil samples was successfully accomplished by utilizing the low and high

ionization energy mass spectra in combination with the separation power and resolution of GC×GC [121].

The goal of this project was to compare a single-stage, consumable-free thermal modulator and a commercially available reverse fill/flush differential flow modulator on their separation capabilities of various engine oils. The oils differed in regard to their blend, viscosities and brand. The modulator platforms were evaluated in terms of their ability to provide group type separation, resolution from the UCM and identification of additives through soft-ionization. Similarities and differences between the samples based on their varying characteristics were also investigated.

6.2 Experimental

6.2.1 Base oil samples

A total of 8 different motor oils were acquired from a local Canadian Tire retail company differing in brand, viscosity (two different cold and high temperature performance values) and blend. SAE 10W-30 and SAE 5W-20 were selected in both conventional and synthetic blends from Brand A and Brand B for the analyses. Each sample was diluted by adding 0.4 mL of oil to a 1 mL volumetric flask and filling to the mark with CS₂ (Sigma-Aldrich, Oakville, ON, Canada). An aliquot of each sample solution was transferred to 2.0 mL glass GC vials with PTFE-lined silicone septa (Chromatographic Specialties, Brockville, ON, Canada) for analysis by GC×GC-TOFMS/FID, as described in Section 6.2.2.

6.2.2 GC×GC instrumentation

Due to the operational mechanisms of flow and thermal modulation, a direct comparison cannot be accomplished. Therefore, both systems were used under their optimal conditions to achieve the best separation possible. Instrumental conditions, such as column dimensions and column flow rates were not the same; however, other parameters, such as the oven temperature program, injection split ratio and detector settings were kept the same. Both platforms were set-up with a reverse column set utilizing the same ¹D and ²D column stationary phases.

The GC×GC system used for analysis consisted of an Agilent 6890 gas chromatograph (Agilent Technologies, Santa Clara, CA, USA) equipped with a split/splitless injector and a second split/splitless injector used as an auxiliary pressure source. A Bench-TOF-Select mass spectrometer (Markes International, Llantrisant, UK) and an FID detector were employed simultaneously by placing a two-way splitter (SepSolve Analytical Ltd., Peterborough, UK) at the end of the ²D column. An Agilent 7683 series injector was used to make 1 µL injections of each sample using 30:1 split ratio. The inlet temperature was set at 300 °C with a 4 mm ID precision split liner with wool (Restek Corp., Bellefonte, PA, USA). Helium gas (Praxair, Kitchener, ON, Canada) with a purity of 99.999% was used as the carrier gas. The oven temperature program was 40 °C to 340 °C at 5 °C/min with a 15-minute hold. The FID was operated at 300 °C with an acquisition rate of 200 Hz and a ratio of 40 mL/min H₂ (Praxair) : 450 mL/min Air (Praxair). The TOF-MS transfer line and ion source were operated at 250 °C. The TOF-MS scan speed was 50 Hz with a mass range of 50 to 600 m/z. Ionization energies of both 14 eV and 70 eV were explored for the engine oil samples. ChromSpace (Markes International) was used for data acquisition and processing of the TOF-MS data. ChemStation (Agilent

Technologies) and ChromSpace (Markes International) were used for data acquisition and processing of the FID data, respectively.

The thermal modulation platform consisted of the University of Waterloo single-stage, consumable-free thermal modulator[84]. The column configuration consisted of a 20 m x 0.18 mm x 0.18 μm Mega 17-MS from MEGA (Legnano, Italy) in the first dimension and a 70 cm x 0.15 mm x 0.15 μm Rxi-1MS from Restek (Bellefonte, PA, USA) in the second dimension. A 5.0 cm x 50 μm deactivated restrictor column from Molex (Lisle, Illinois, USA) was placed after the ¹D dimension column as a pressure restriction before the trapping capillary. The trapping capillary contained a proprietary stationary phase. It was placed within the cooling pads of the modulator. The ¹D column length entered into the software was 30.8 m x 0.15 mm x 0.15 μm to account for the entire column train from the ¹D dimension through the ²D dimension. An Agilent two-way purged splitter was placed after the second-dimension column in order to split the column effluent between the FID and TOF-MS detectors. An Agilent splitter calculator was used to determine the necessary transfer line dimensions with a flow ratio of 1:1 between detector 1 (FID) and detector 2 (TOF-MS). A 1.64 m x 0.15mm transfer line was employed to the FID, and a 2.19 m x 0.15 mm transfer line was employed to the TOFMS. A total length of 3.83 m x 0.15 mm was programmed into the software as the second-dimension column in order to employ a makeup flow of 4.4 mL/min from the back inlet (Auxiliary pressure control). A flow of 2.0 mL/min was used in the ¹D dimension and a flow of 3.0 mL/min was accomplished in each the FID and TOF after auxiliary flow was added. This achieved hold up times of 0.014 minutes and 0.016 minutes for the FID and TOF, respectively. A modulation period of 8 seconds was used. All connections on the Agilent splitter were made with Agilent Ultimetal Plus Flexible Metal Ferrules from Agilent Technologies (Mississauga, ON, Canada). Connections between the ¹D

column and the restrictor, and subsequently the restrictor and the trapping capillary, were made with Siltite Double Taper Ferrule/Micro-union and Siltite Mini Ferrule (Trajan, Victoria, Australia), respectively.

The flow modulation platform consisted of the INSIGHT Reverse Fill/Flush Flow Modulator from SepSolve Analytical Ltd. (Peterborough, UK) [58]. The column configuration consisted of a 20.0 m x 0.18 mm x 0.18 μm Mega 17MS from MEGA (Legnano, Italy) in the first dimension and a 9.1 m x 0.25 mm x 0.25 μm Rxi-1 from Restek (Bellefonte, PA, USA) in the second dimension. A 10.0 m x 100 μm of deactivated silica tubing (Trajan Scientific, Melbourne, Australia) was used as the bleed line. A two-way-non-purged splitter from SepSolve Analytical Ltd. (Peterborough, UK) was used to divide the ²D column effluent between the FID and the TOF-MS. With a constant flow of 0.5 mL/min in the ¹D dimension and a constant flow of 21.3 mL/min in the ²D dimension, the SepSolve flow calculator assisted in determining the necessary auxiliary pressure to apply in order to achieve the correct flow through the bleed line, as well as the proper transfer line dimensions for both the FID and TOF-MS. An auxiliary pressure of 45 psig was needed to achieve a flow of 0.5 mL/min within the bleed line to match the flow in the first dimension at the starting oven temperature. Transfer lines of deactivated fused silica tubing with dimensions of 0.8 m x 0.32 mm and 1.0 m x 0.18 mm (SGE Analytical, Australia) were employed for the FID and the TOFMS, respectively. These dimensions gave identical hold up times of 0.0039 minutes for both the FID and the TOF. The two-way splitter employed a 4:1 split between the FID and TOF-MS with flows of 16.56 mL/min and 4.78 mL/min, respectively. All connections to the necessary ports were made with SilFlow Ferrules from Trajan (Victoria, Australia). A modulation period of 4 seconds with a 100-millisecond flush was used.

6.2.3 Thermal modulation

The single-stage, consumable-free thermal modulator shown in Figure 6.1 was described elsewhere [84]. A more detailed description of the operational parameters can be found in Section 1.3. For the analysis of base oils, only passive cooling was used due to the high boiling points of the analytes. In both designs, the trapping capillary temperature would lag behind the oven temperature during the run, assisting in the analysis of semi-volatiles.

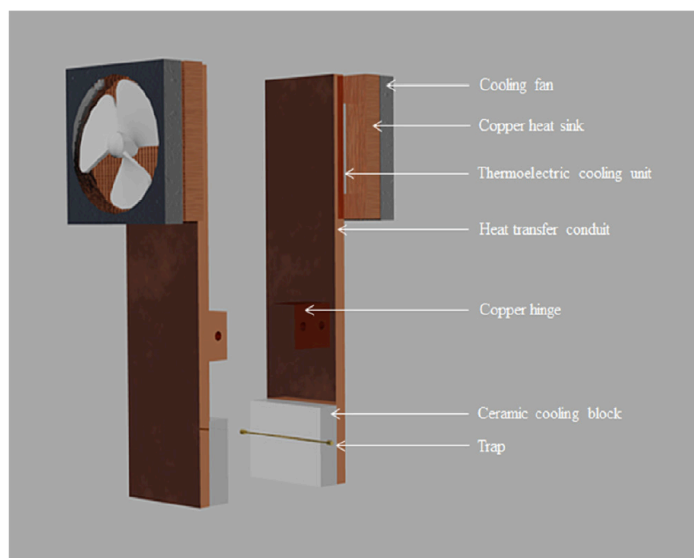


Figure 6.1 Design of the single-stage, consumable-free thermal modulator from the University of Waterloo [84]. Reprinted from *Journal of Chromatography A*, 1391, Muscalu *et al.*, Evaluation of single-stage, consumable-free modulator for comprehensive two-dimensional gas chromatography: Analysis of polychlorinated biphenyl, organochlorine pesticides and chlorobenzenes, 93-101, Copyright (2016), with permission from Elsevier.

6.2.4 Flow modulation

As seen in Fig. 6.2, the INSIGHT reverse fill/flush flow modulator consisted of a single microchannel plate with 7 ports and a complementary two-way non-purged splitter with 3 ports

for coupling to a mass spectrometer and a single-channel detector [58]. A more detailed description of the operation of the modulator can be found in Section 1.2.2.2.

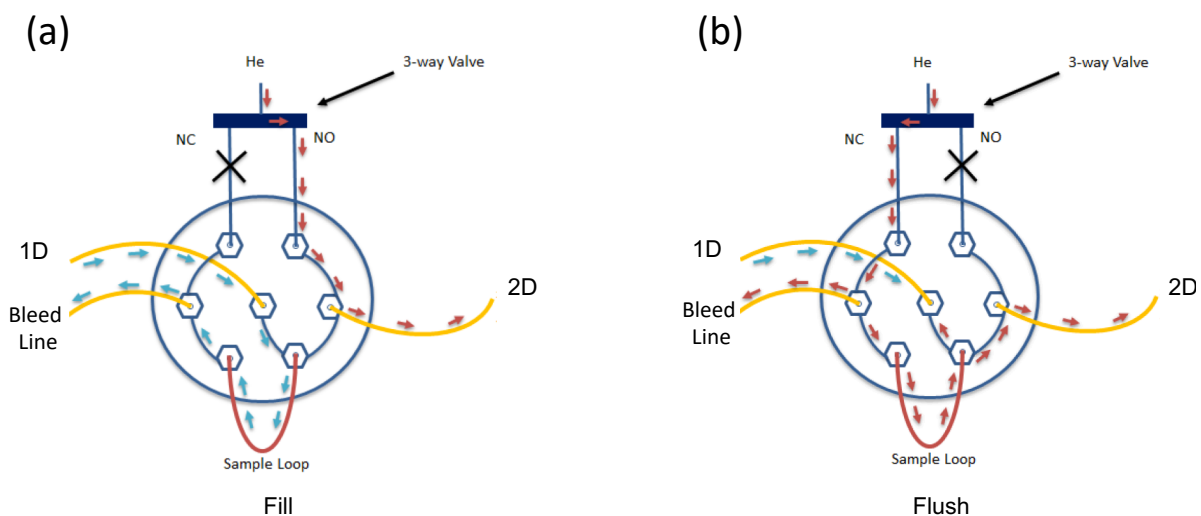


Figure 6.2 (a) Flow path of the fill stage of the Insight RFF flow modulator and (b) flow path of the flush stage of the Insight RFF flow modulator [58].

6.3 Results and discussion

6.3.1 Ion source tailing

As previously mentioned, the ^2D column effluent was split for dual detection to the FID and TOF-MS for both modulator platforms. However, the thermal platform required an additional auxiliary flow via a purged two-way splitter to reduce the ion source tailing. When comparing the split flow ratios for both platforms, the proportion of the sample directed towards the TOF-MS varied significantly. For the flow modulator, the ^2D effluent was split 1:4, with about 4 mL/min directed to the MS and the remaining 16 mL/min directed to the FID. For the thermal modulator with the auxiliary flow, the ^2D effluent was split 1:1, with 3 mL/min directed to the MS and 3 mL/min directed to the FID. Due to the different operational principle of each

platform, it was not possible to achieve the exact same flow to both detectors. The analytes introduced into the ion source after flow modulation had significantly higher concentration, producing a pronounced tail due to the high 2D flow with the flow-based platform. This was strictly an issue with the ion source of the TOF-MS, not the thermal modulator platform itself, as the FID trace showed no 2D tailing. The closed design of the Benchtop Select-eV ion source made it difficult for the higher molecular weight compounds to diffuse out of the source in a timely fashion, ultimately creating tailing. As seen in Figs. 6.3a and 6.3c, the unprocessed linear chromatogram displayed large baseline rise for the TOF trace, while the FID trace returned completely to baseline (Fig. 6.3b and 6.3d).

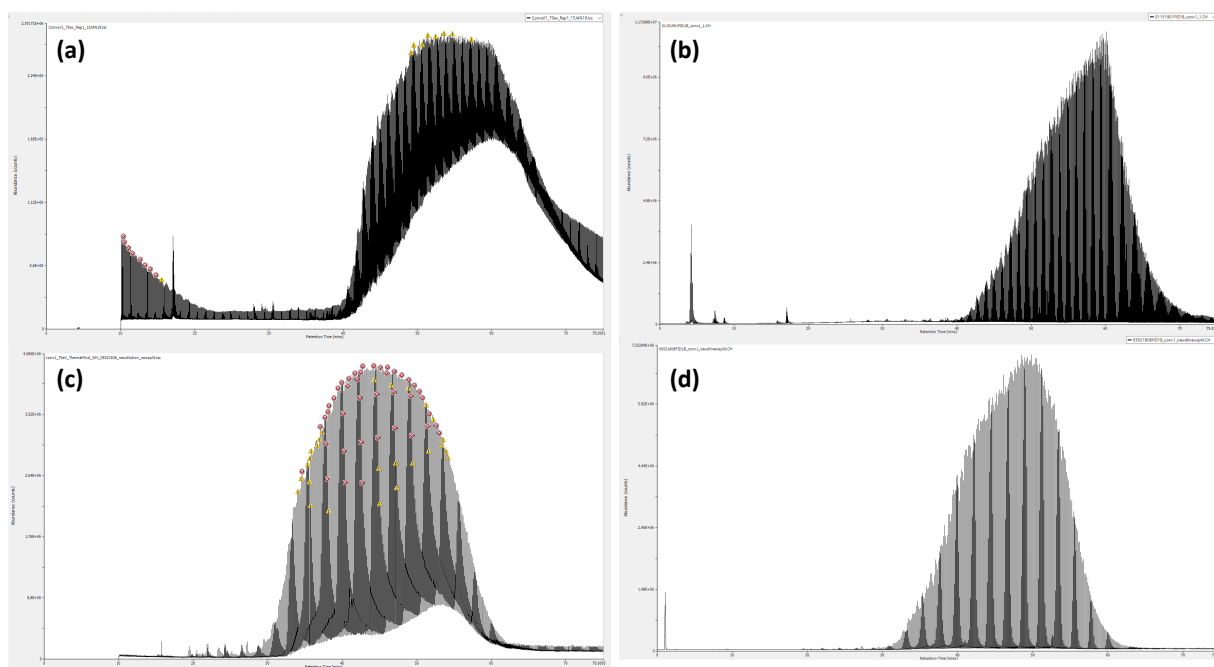


Figure 6.3 Unprocessed, one-dimensional linear chromatograms of (a) a TOF trace for the flow-based platform; (b) a FID trace for the flow-based platform; (c) a TOF trace for the thermal-based platform; and (d) a FID trace for the thermal-based platform.

Fig. 6.4a and 6.4c show zoomed-in chromatograms illustrating the tailing observed with the TOFMS, while the FID trace again shows Gaussian peaks which return to baseline (Fig. 6.4b and 6.4d).

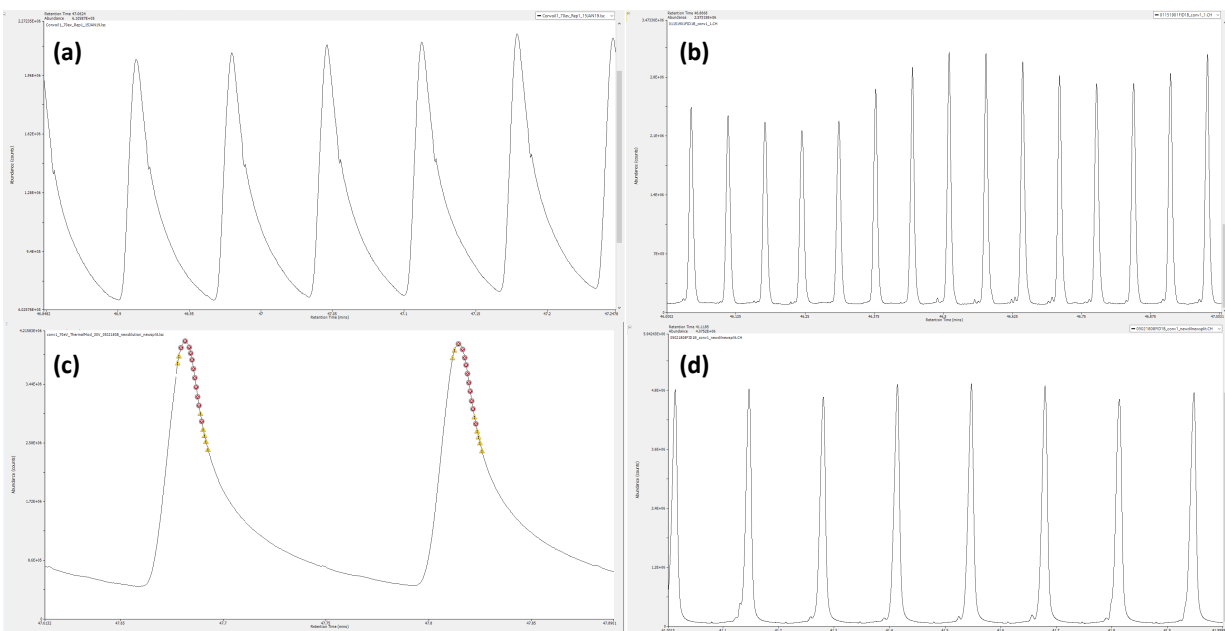


Figure 6.4 Unprocessed, partially zoomed-in one dimensional linear chromatograms of (a) a TOF trace for the flow-based platform; (b) a FID trace for the flow-based platform; (c) a TOF trace for the thermal-based platform; and (d) a FID trace for the thermal-based platform.

The ion source tailing is extremely prominent in the unprocessed two-dimensional chromatograms, as seen in Fig. 6.5a and 6.5c. The heavy compounds within the UCM created a broad band across the entire two-dimensional space, making it almost impossible to detect any trace analytes. Baseline correction and data processing were required in order to achieve a two-dimensional chromatogram with distinguishable peaks. Unprocessed two-dimensional chromatograms acquired with the FID showed no tailing, with clear distinction of groups surrounding the UCM (Fig. 6.5b and 6.5d). Overall, the combination of the closed source design, heavy sample matrix and lower flow entering the ion source led to substandard peak shapes. As a

result, data processing was required for the chromatograms acquired with the TOF-MS to produce a discernible separation. All TOF-MS chromatograms presented herein for both platforms were processed in this way to distinguish trace analytes.

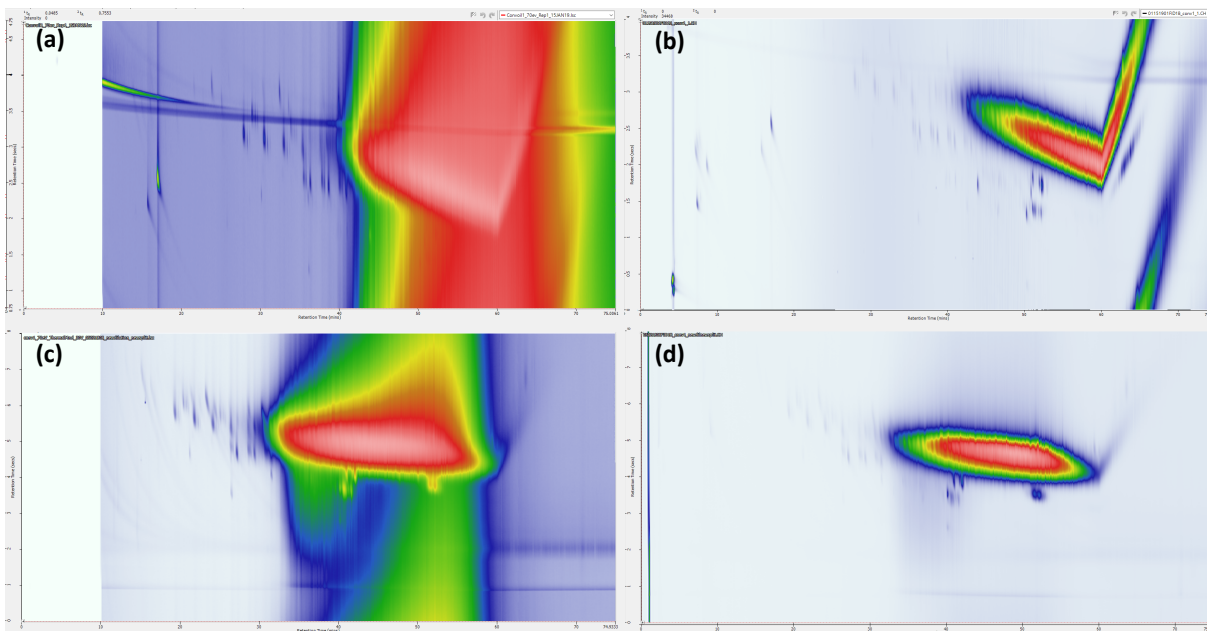


Figure 6.5 Unprocessed, contour plots of (a) a TOF trace for the flow-based platform; (b) a FID trace for the flow-based platform; (c) a TOF trace for the thermal-based platform; and (d) a FID trace for the thermal-based platform.

6.3.2. Group type identification

Group-type identification of hydrocarbons is a vital tool for petrochemical samples due to the complexity of the sample matrix and numerous compounds present. Instead of identifying each individual compound, group classifications based on placement within the chromatographic region and mass spectral properties can be used [124]. Each group contains specific compounds which provide a chemical characteristic and impart specific properties to the petroleum-based

sample [124]. This type of separation and identification allows obtaining a more complete picture of the chemical makeup, while saving time and providing an easier data processing workflow. With the ²D column used, aromatic hydrocarbons eluted at shorter ²D retention times, followed by branched alkanes and subsequently straight-chain alkanes with the latest elution band located at a longer ²D retention time [117]. Due to the use of a non-polar column in ²D, the elution range of these compounds was ‘stretched’, allowing better differentiation between the various alkane series [118]. Alongside the preliminary estimation of location of the various groups, summed extracted ion chromatograms of characteristic ions and fragments are used to help in the identification, as seen in Table 6.1 [73, 125].

Table 6.1 Different compound groups and their corresponding mass fragments

Class	Mass Fragments
Paraffins and Isoparaffins	43 + 57 + 71 + 85 + 99 + 113 +127 + 141 + 155 +169
Alkylbenzenes	91 + 92 + 106 + 119 + 120 + 133 +134 +147 +148 + 161 + 162 + 175 +176
Mononaphthenes	67 + 67 + 83 + 97 + 111 + 125 + 139 + 153 + 167
Dinaphthenes	81 + 95 + 109 + 123 + 137 + 151 + 165 + 179 + 193
Trinaphthenes	67 + 79 + 93 + 107 +121 + 135 + 149 + 163 + 177 +191 + 205 + 219 + 233 + 247
Naphthalenes	141 + 142 + 155 + 156 + 169 +170 + 183 +184 + 197 + 198 + 211 + 212 + 225 +226 + 239 + 240

The stencil feature within the ChromSpace software allows the user to manually draw around a specific region within the chromatogram, save the template, and apply it to further samples. The saved stencil is applied to the same chromatographic region based on the retention areas (both ¹D and ²D) that are chosen by the user. Once the summed extracted ion

chromatograms are completed for each group, a stencil is drawn, and saved to a specific color. This is repeated for each individual group with varying colors for easy visualization. In this work, the following colors were used: blue for paraffins and isoparaffins, green for alkylbenzenes, orange for mononaphthenes, yellow for dinaphthenes, red for trinaphthenes, and purple for naphthalenes. To ensure that the stencils were correctly identifying the specific groups, summed extracted ion chromatograms were applied to confirm the stencil location. As seen in Fig. 6.6, the overall location of the groups was relatively similar, with varying concentrations of paraffins and substituted naphthenes across all samples. It is important to note that there was no clear separation between each group, with several overlaps between them. Due to the overlap between groups, FID could not be used for group quantitation. Alternatively, the TOF-MS could be used for semi-quantitation by analyzing standards belonging to each group because the analytes have different response factors on the TOF-MS [73].

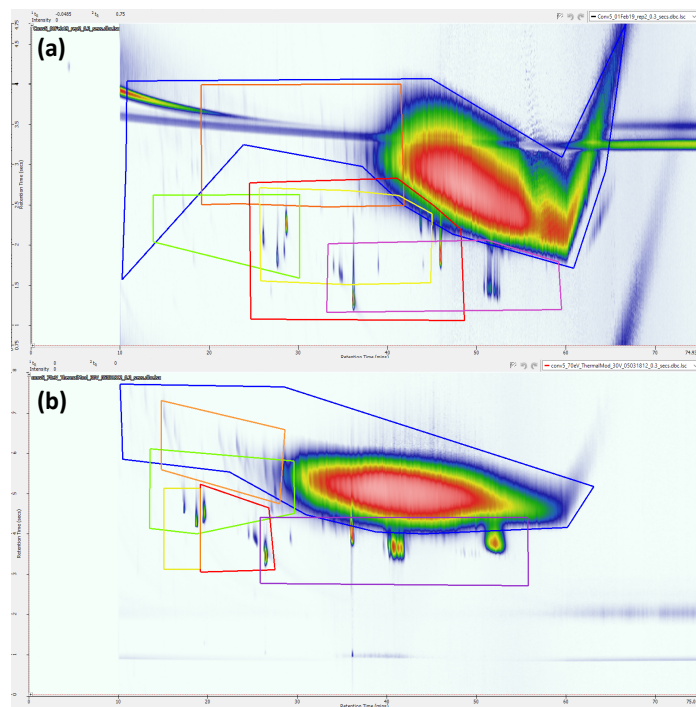


Figure 6.6 Group analysis of a conventional oil from Brand A with viscosity 5W-20 illustrating the separation with (a) a flow-based modulator platform; and (b) a thermal based modulator platform. The colors presented correspond to the following groups accordingly: blue for paraffins and isoparaffins, green for alkylbenzenes, orange for mononaphthenes, yellow for dinaphthenes, red for trinaphthenes, and purple for naphthalenes.

6.3.3. Thermal modulation vs. flow modulation

To best compare the conventional and synthetic samples for each modulation platform, the GC×GC-TOF-MS chromatograms were placed one on top the other. Fig. 6.7 shows the conventional oil separations for the thermal modulator platform. Each chromatogram displays several homologous groups, a large UCM and two distinct groups eluting from the UCM (indicated with the black circles). The main differences were observed in the nature of the alkanes eluting late in the 2D, as well as the distribution of hydrocarbons within the UCM. Specifically, in Fig. 6.7a, the brand A 10W-30 conventional oil contained significantly more

straight-chain alkanes when compared to the three other conventional samples (b-d). Brand A 5W-20 conventional oil (Fig. 6.7c) contained a higher concentration of di- and tri- substituted naphthenes when compared to the other conventional samples (a, b, and d). When comparing the distribution of compounds within the UCM of the four conventional samples, it could be seen that each blend was slightly different from each another. Brand A 10W-30, as seen in Fig. 6.7a, had a relatively consistent distribution of hydrocarbons within the UCM. Brand B 10W-30 conventional oil (Fig. 6.7b) had a distribution that extended further towards heavier hydrocarbons. Brand A and B 5W-20 oils contained lower concentration of high-molecular weight hydrocarbons, which explains their lower viscosity at low temperatures. A key similarity in all four samples was the presence of two distinct groups (indicated by the black circles) separated from the UCM at about 40 minutes and 50 minutes. Further investigation of these groups will be discussed in Section 6.3.4.

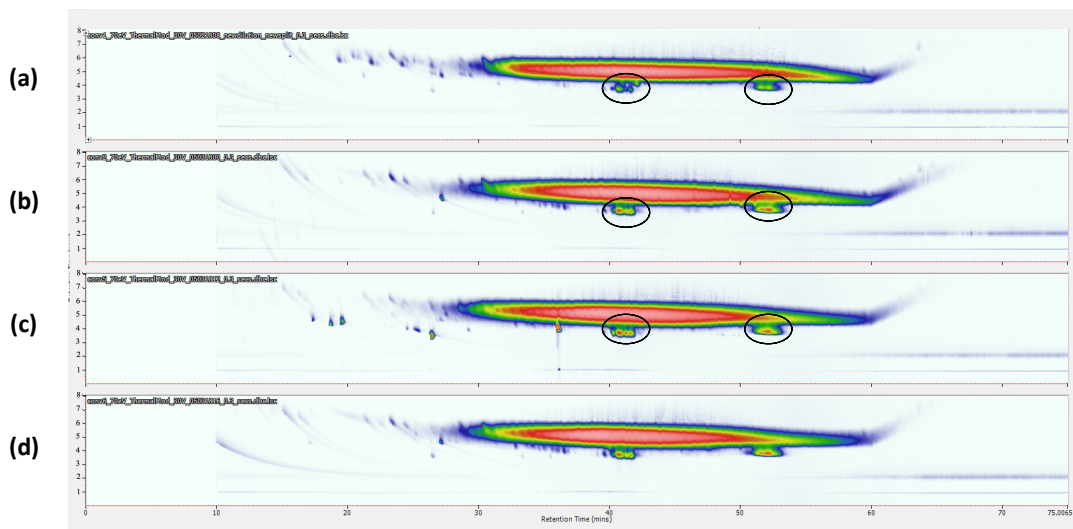


Figure 6.7 GCxGC-TOF-MS contour plots of (a) conventional oil from Brand A with viscosity 10W-30; (b) conventional oil from Brand B with viscosity 10W-30; (c) conventional oil from Brand A with viscosity 5W-20; and (d) conventional oil from Brand B with viscosity 5W-20; illustrating the separation with the thermal-based modulator platform.

The conventional oil separations for the flow modulation platform with TOF mass spectrometric detection can be seen in Fig. 6.8. When comparing these chromatograms to those in Fig. 6.7, the differences are obvious. It is important to note that with the thermal modulator platform, the length of the second-dimension column was optimized and a longer modulation period was used to avoid wraparound and excessive retention in the second dimension. Due to the operational constraints of the flow modulator, such as the required lengthy ²D column and short modulation period, this optimization process was not possible. This resulted in wraparound of the isothermal hold region of the analysis within the chromatograms when utilizing the flow modulator platform. The two distinct groups (indicated by black circles), previously distinguished with the thermal modulator were also separated with the flow modulator. These groups were located at approximately 50 and 65 minutes. The abundance of the latter group was lower when compared to that obtained with the thermal platform.

The distribution of paraffinic compounds within Brand A 10W-30, as seen in Fig. 6.8a, was found to be very similar when utilizing the flow modulator platform. The di- and tri- substituted naphthenes in Brand A 5W-20 were also apparent when utilizing the flow modulator platform, as seen in Fig. 6.8c. Brand A 10W-30 conventional oil, as seen in Fig. 6.8a, had a large presence of lower molecular weight hydrocarbons that eluted before the UCM when compared to the other conventional samples. Fig. 6.8b, Brand B 10W-30 conventional oil, had a rather even distribution of hydrocarbons in the UCM. Fig. 6.8d, Brand B 5W-20 conventional oil, had a smaller region of mid-weight molecular range hydrocarbons when compared to the 10W-30 variety from the same brand. The ¹D and ²D retention times of the compounds varied between both platforms due to differences in the ¹D and ²D flow rates and ²D column dimensions.

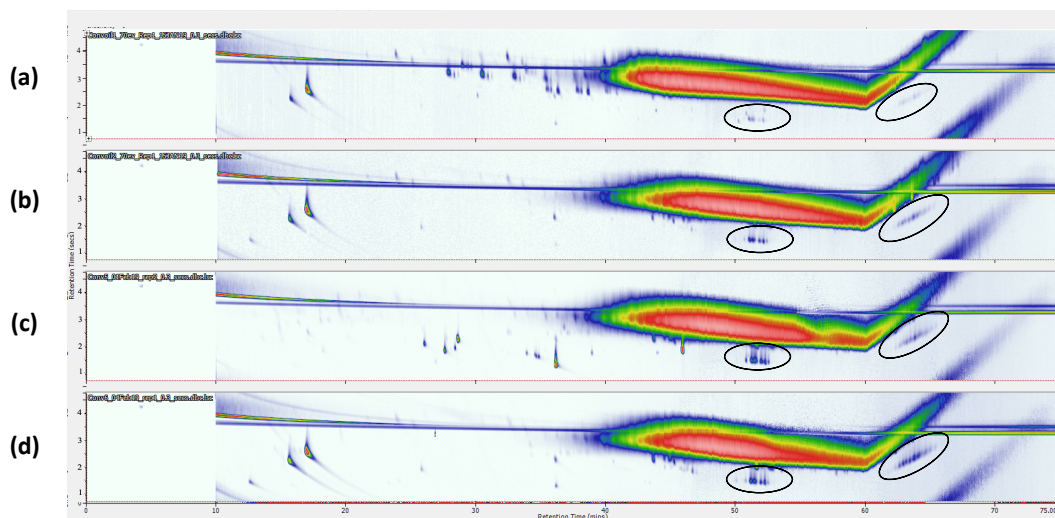


Figure 6.8 GCxGC-TOF-MS contour plots of (a) conventional oil from Brand A with viscosity 10W-30; (b) conventional oil from Brand B with viscosity 10W-30; (c) conventional oil from Brand A with viscosity 5W-20; and (d) conventional oil from Brand B with viscosity 5W-20; illustrating the separation with the flow-based modulator platform.

The synthetic oil chromatograms obtained with the thermal modulator looked quite different from one another, as seen in Fig. 6.9. The distribution of hydrocarbons within the UCM clearly differentiated each synthetic oil. In Brand A 10W-30 oil (Fig. 6.9a), the distribution was relatively uniform throughout from the lighter to heavier molecular weight hydrocarbons. However, the UCM of Brand B 10W-20 oil (Fig. 6.9b) was very different. The heavier hydrocarbons spanned a larger range than in the other oils. The distribution of the hydrocarbons was also more uniform, with the widest range of hydrocarbons overall. The distribution peaked roughly in the middle of the UCM. Fig. 6.9c displays the chromatogram of Brand A 5W-20 synthetic oil, with a large concentration of middle weight hydrocarbons, and more lighter hydrocarbons than heavier. Finally, Brand B 5W-20 (Fig. 6.9d) also contained high concentration of middle weight hydrocarbons, with lower concentrations of heavy and light compounds. On the other hand, the distribution of analytes before the UCM was similar between

brands. As seen in Fig. 6.9a and 6.9c, there was a higher concentration of di- and tri- substituted naphthenes and a trace number of paraffinic compounds for Brand A, while Brand B (Fig. 6.9b and 6.9d) contained higher concentration of paraffinic compounds, as well as a third group that was differentiated from the UCM. The two distinct groups (indicated with black circles) that were present within the conventional samples were also present within the synthetic samples with the same corresponding 1D retention times of approximately 40 and 50 minutes.

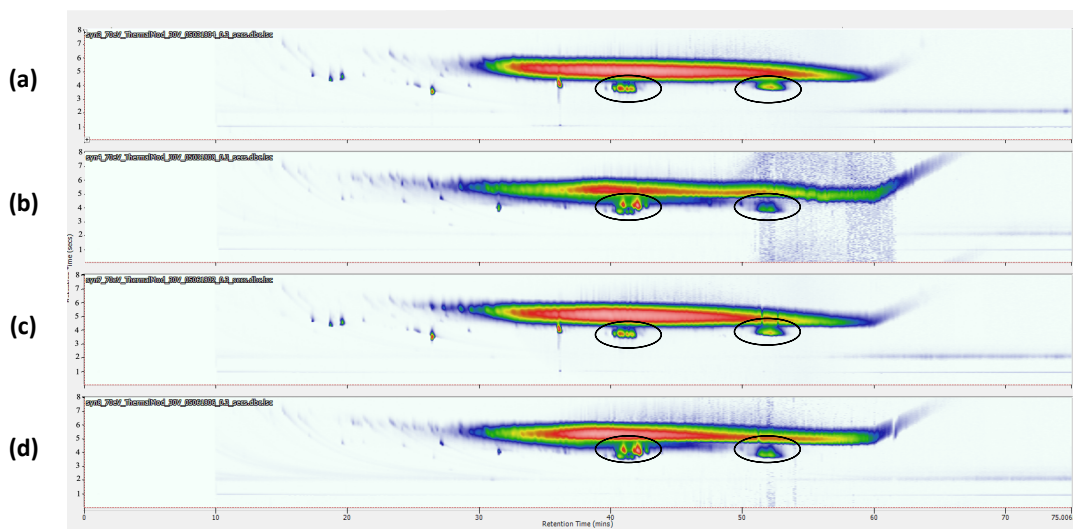


Figure 6.9 GCxGC-TOF-MS contour plots of (a) synthetic oil from Brand A with viscosity 10W-30; (b) synthetic oil from Brand B with viscosity 10W-30; (c) synthetic oil from Brand A with viscosity 5W-20; and (d) synthetic oil from Brand B with viscosity 5W-20; illustrating the separation with the thermal-based modulator platform.

As previously seen in the synthetic oil chromatograms obtained with the thermal modulator platform, similarities were observed in the distribution of the di- and tri- substituted naphthenes for the different viscosities of Brand A analyzed with the flow platform (Fig. 6.10a and Fig. 6.10c). The observed distribution of the hydrocarbons within the UCM was also quite distinct for each sample analyzed using flow modulation. It mirrored the results obtained with the thermal platform. The two distinct groups (as indicated with black circles) were present in each of the

four synthetic samples when utilizing the flow-based modulator platform. The second group, however, was again less prominent when compared to the thermal modulator platform. On the other hand, two new groups separated from the UCM (indicated by black squares) were observed with the flow-based platform for Brand B oils that have not been previously separated, as seen in Fig. 6.10b and Fig. 6.10d, respectively.

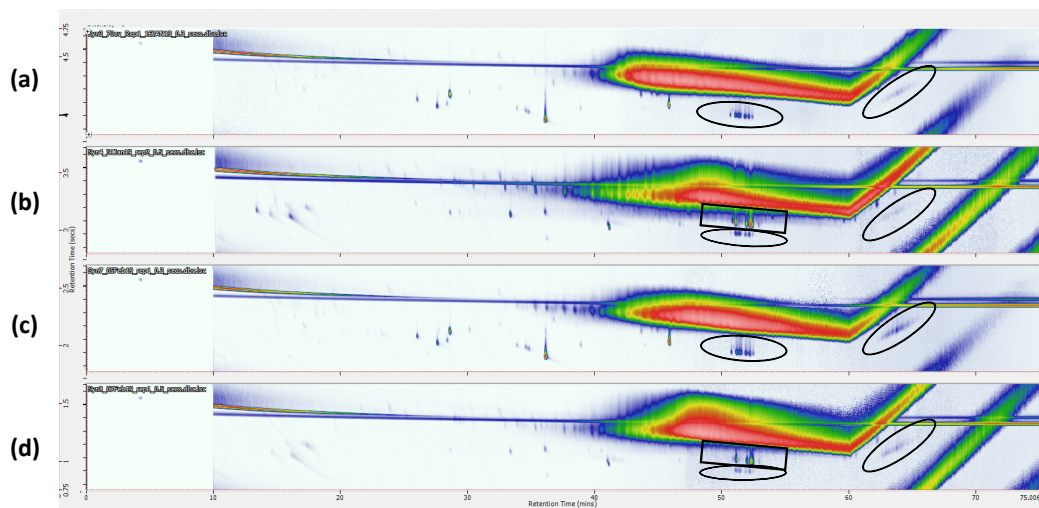


Figure 6.10 GCxGC-TOF-MS contour plots of (a) synthetic oil from Brand A with viscosity, 10W-30; (b) synthetic oil from Brand B with viscosity 10W-30; (c) synthetic oil from Brand A with viscosity 5W-20; and (d) synthetic oil from Brand B with viscosity 5W-20; illustrating the separation with the flow-based modulator platform.

6.3.4 Identification of antioxidants through soft-ionization

Preventing oxidation of lubricants within the operational machinery is a vital part of ensuring no harmful species are generated, eventually compromising the life and functionality of the lubricant. An antioxidant additive is a key component in protecting the lubricant from oxidation, allowing the oil to perform optimally [126]. Alkylated diphenylamines (ADPAs) have been used for this purpose for over two decades, providing higher reactivity than unsubstituted

diphenylamine [126]. Mono-ADPA are more effective than di-ADPA due to the additional alkylation decreasing the amount of diphenylamine per unit weight [126]. Identification of ADPAs is an important part of engine oil characterization. Due to their aromatic nature, they should appear lower in the two-dimensional space with shorter ²D retention times due to their strong retention in the ¹D column and subsequently higher ¹D elution temperature.

Diphenylamine was tentatively identified in each sample with both thermal and flow modulation by comparing the experimental spectrum with NIST library spectrum, as seen in Fig. 6.11a and 6.11b, respectively. However, identification of the components of the two prominent groups separated from the UCM within each sample proved more problematic, as the agreement between library hits and experimental spectra was poor. The molecular ion in each case was barely visible, making identification difficult.

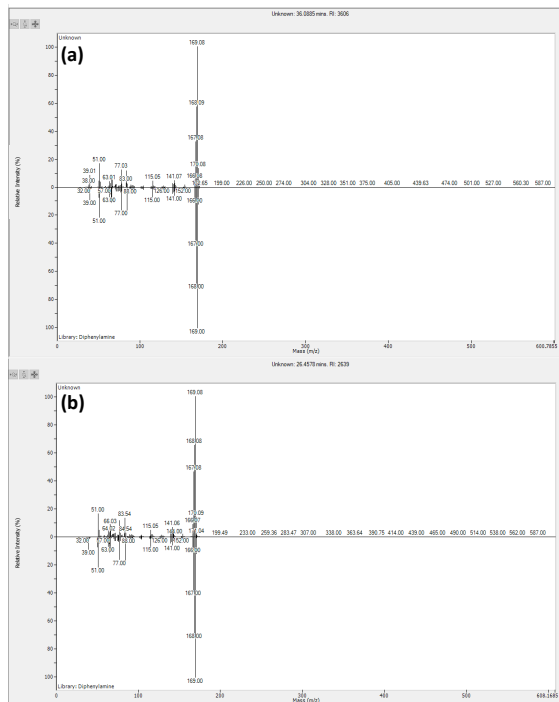


Figure 6.11 GCxGC-TOFMS mass spectra of (a) diphenylamine with the flow-based platform and (b) diphenylamine with the thermal-based platform.

To overcome these limitations, soft-ionization was implemented to reduce fragmentation and increase the abundance of the molecular ion. Figs. 6.12a-6.12d compare the mass spectra obtained for the two distinct groups from the UCM at 14 and 70 eV. The groups were previously noted at ¹D retention times of 40 and 50 minutes with the thermal modulator and 50 and 65 minutes with the flow modulator. It is apparent that the soft ionization technique created more prominent molecular ions while reducing overall fragmentation and increasing the abundance of higher-mass fragments to assist in the identification process. The poor agreement between the experimental and library spectra for the unknowns suggested that the latter were not included in the NIST library. The only available ADPA spectrum within the NIST library is the dioctyl substituted diphenylamine. As seen in Fig. 6.B.1. of Appendix B, the mass spectrum of the

dioctyl substituted diphenylamine displayed the molecular ion of 393 m/z with two C₈H₁₇ alkyl substitutions off the diphenylamine backbone. Despite there being no exact match within the NIST library for the unknown species eluting from the UCM, the soft ionization technique enhanced the molecular ions, which were used for comparison to the known mass of the dioctyl ADPA. The first unknown displayed a molecular ion of 296 m/z, located at ¹D retention times of about 50 min and 40 min for the flow modulator and thermal modulator, respectively. Based on this information, a preliminary identification of monononyl diphenylamine was made.

The second unknown displayed a molecular ion of 422 m/z, located at a ¹D retention times of about 65 min and 50 min for the flow modulator and thermal modulator, respectively. Based on this information, a preliminary identification of dinonyl diphenylamine was made. It is important to note the differences in the spectra obtained for dinonyl diphenylamine with the flow modulator (Fig. 6.12b) and thermal modulator (Fig. 6.12d). The quality of the spectrum obtained with the flow modulator had lower quality due to the low abundance of the peak. The larger mass fragments obtained with soft ionization assisted in further confirming the tentative identification of these unknowns through a comparison with mass spectral data obtained for known standards by Lu *et al.* [127]. In this paper, substituted diphenylamine antioxidants were identified within urban creeks of Canada utilizing tandem mass spectrometry [127]. Table 6.B.1. in Appendix B displays the multiple reaction monitoring diagnostic transitions used by Lu *et al.*, which were subsequently used for comparison with the soft ionization mass spectral data and tentative identification of the unknown ADPAs present within the oils. Nonetheless, analysis of authentic standards is required for a positive identification of both the monononyl and dinonyl diphenylamines.

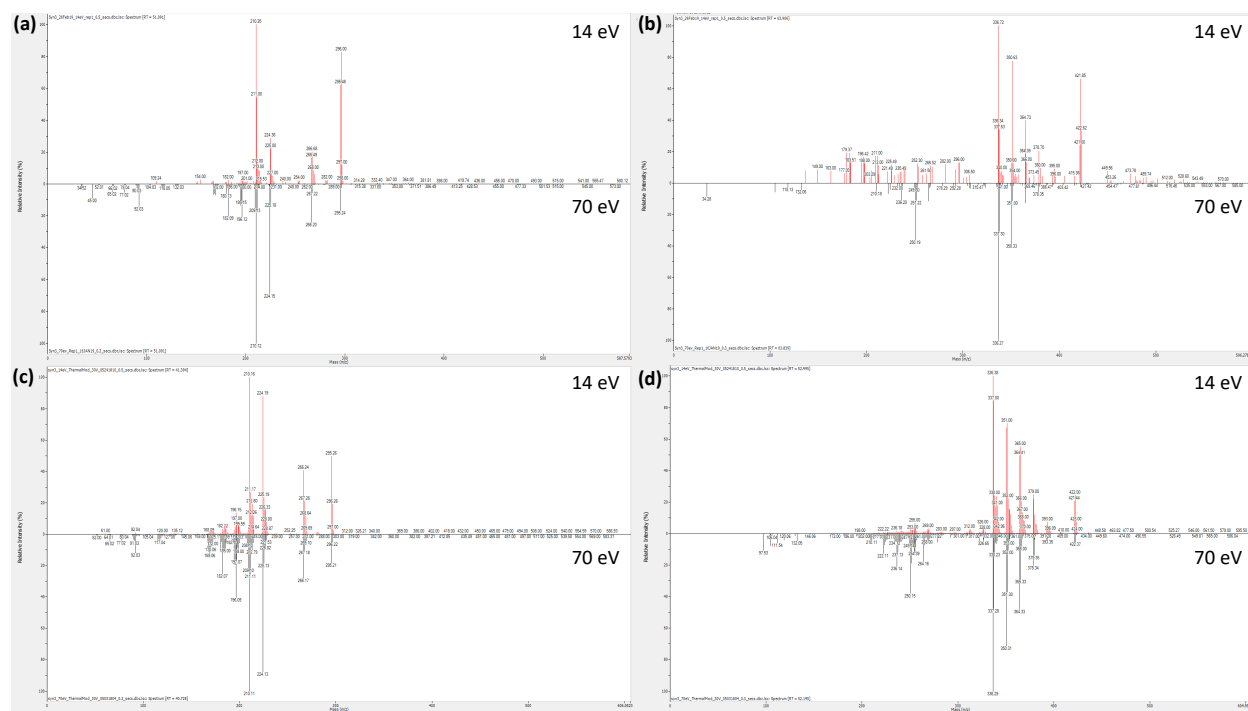


Figure 6.12 GCxGC-TOF-MS mass spectra comparison of hard and soft ionization for the identification (a) mononyl-diphenylamine with the flow-based platform; (b) dinonyl-diphenylamine with the flow-based platform; (c) mononyl-diphenylamine with the thermal-based platform; and (d) dinonyl-diphenylamine with the thermal-based platform.

6.3.5 Resolution from UCM

Determining the resolution of the identified ADPA species from the UCM helps compare the separation capabilities of both modulator platforms. Differentiating the ADPA species from the UCM allows confident identification thanks to clean mass spectra. For this application, the resolution from UCM were performed for the FID trace to avoid the issues encountered with ion source tailing. The flow modulator platform provided a better overall resolution for mononyl DPA from the UCM when compared to the thermal modulator, as seen in Table 6.2. This was most likely due to the longer ²D column used. When directly compared to the thermal modulator, the flow modulator provided better resolution for synthetic samples 3 and 7 and conventional

samples 2, 5 and 6. It should be noted that the resolution values listed for synthetic samples 4 and 8 for the flow modulator were not the resolution values from the UCM. They were instead the resolution from a new set of compounds eluting from the UCM that the thermal modulator platform could not separate. When comparing the resolution for the dinonyl DPA for the flow and thermal platforms, it was difficult to determine the values due to the low abundance of this compound in the FID trace.

Table 6.2 Resolution from the UCM for monononyl DPA for both the flow-based and thermal-based platforms.

Sample	Compound	Flow Modulator	Thermal Modulator
Conventional 1	Monononyl DPA	0.91	1.3
Conventional 2	Monononyl DPA	1.8	1.5
Synthetic 3	Monononyl DPA	3.3	1.4
Synthetic 4	Monononyl DPA	0.99	1.2
Conventional 5	Monononyl DPA	2.1	1.7
Conventional 6	Monononyl DPA	2.0	1.7
Synthetic 7	Monononyl DPA	2.0	1.6
Synthetic 8	Monononyl DPA	1.4	1.6

6.4 Conclusions

A reverse fill/flush flow modulator and single-stage, consumable free thermal modulator were compared for the separation of several conventional and synthetic engine oils of various viscosities and brands with dual detection. The closed design of the select ionization TOF-MS was detrimental in obtaining baseline resolution of the heavier molecular weight compounds and UCM, in comparison to the FID. Appropriate data processing was necessary to differentiate and

visualize minor components separated from the UCM when using TOF. Overall, both brands of engine oils had similar compositions. Upon closer inspection, differences were found based on the distribution of hydrocarbons within the UCM. When both platforms were optimized accordingly to their operational parameters, the thermal modulator and flow modulator performed comparably in the separation of analytes from the UCM. The thermal platform produced less wraparound of the isothermal portion of the analysis when compared to the flow platform thanks to a longer modulation period that was possible with this platform. It was concluded that the flow modulator platform was more constrained in the optimization process.

Stencils based on characteristic ions and position in the 2D space allowed easy identification of various compound groups within the engine oils. Soft ionization was used to enhance the molecular ion and larger mass fragments to aid in identification of unknown compounds. It proved vital in tentative identifications of monononyl and dinonyl diphenylamines in all samples with the flow and thermal based platforms. Supplementing traditional ionization of 70 eV with soft ionization techniques should be performed more frequently when compounds of similar nature are investigated. Both flow and thermal modulation provided adequate resolution of the monononyl diphenylamine from the UCM. Neither model was superior to the other and a direct comparison between two modulators of different operating principles was not possible. Both flow modulation and thermal modulation achieved comprehensive separation of specific compound classes and allowed differentiation of engine oils.

Chapter 7. Modified flow modulator: A proof of concept hybrid interface

7.1 Introduction

In the search of an ideal modulator, a commercial flow modulator was improved upon to test a proof of concept hybrid interface. Theoretically, by augmenting the design of a reverse fill/flush modulator through the addition of a cryogen-free focusing mechanism, lower flow rates in the ²D could be employed for direct coupling to a mass spectrometric detector, while also achieving adequate secondary re-injection band widths.

Cryogenic models, such as the quad jet and loop modulators from LECO and Zoex, respectively, are often considered superior due to their focusing effect [64, 128, 129]. This leads to very narrow injection bands in ²D and to an increase in the signal-to-noise ratio when compared to a one-dimensional separation, hence these modulators offer greater resolution for highly complex samples and lower limits of detection for trace analytes [23]. Compatibility with mass spectrometric detectors adds to the abilities of cryogenic models, making both targeted and untargeted trace analysis possible. Despite the many advantages, cryogenic liquids are an expensive consumable. Consumable-free cryogenic models are available; however, the volatility range is narrower for them [130]. Heater based models have become increasingly more popular due to their comparable performance to cryogenic models without the need for cryogenics. The Solid-State Modulator (SSM) from J&X Technologies and Single Stage, consumable free thermal modulator from the University of Waterloo utilize Peltier coolers for trapping, while the

prior uses aluminum block heaters and the later uses resistive heating for remobilization [65, 84]. Similarly, to the cryogenic models, the focusing effect helps increase the S/N and they can be coupled with a mass spectrometer without issue. The SSM requires preventative maintenance for specific components due to the moving modulator column [65]. There are also various modulation columns for specific volatility ranges, making it difficult to perform an analysis of a sample covering wide range of volatilities with a single setup [65].

Flow based models, such as the SepSolve Insight and LECO Flux, utilize an auxiliary flow in order to switch between an inject and a sample mode [57, 60]. The SepSolve model operates under differential flow conditions, sampling the primary effluent within a sample loop at a low ¹D flow and using a high auxiliary flow to flush the bands of analytes onto the secondary column in a reverse direction. Switching between the modes is accomplished by actuating a solenoid valve, controlled by an electronic control board, resulting in good secondary retention time reproducibility. With essentially no volatility limitations except for the limitations of the column set employed, and no cryogenics required, this model has great potential. However, the high secondary flow rates makes it impossible to directly couple a mass spectrometer without splitting the secondary effluent to a vent line and/or a single-channel detector. This reduces the amount of secondary effluent being sent to the mass spectrometer, resulting in a decrease in S/N. The LECO Flux model is new to the market and operates under a low-duty cycle design, similar to the Multi-mode modulator from Seeley. Without the requirement of a high secondary flow rate for proper operation, this model can be directly coupled to a mass spectrometer. However, the entire primary effluent is not sent to the secondary column for further separation; when not in the inject mode, a large fraction of the primary effluent is directed to a waste line. This makes this modulator poorly suitable for trace analysis.

The greatest disadvantage of all flow-based modulators is their inability to create a focusing effect, making them inferior to thermal models.

Incompatibility of full transfer, differential flow modulators with mass spectrometers has previously been addressed by the Mondello Group at the Univeristà de Messina [53, 54, 131]. By increasing the re-injection period or flush time and decreasing the secondary column flow, an equivalent setup can be achieved as that of the traditional short flush time and high secondary flow rate. However, it is important to note, if the flush time is too long, the primary column flow conditions will not be maintained, consequently allowing primary effluent to enter the sample loop before the end of the previous flush cycle. With a secondary flow rate of about 6-8 mL/min, they were only able to achieve a sub-standard peak width at base of 780 milliseconds (ms) for the highest modulated peak [53]. When increasing the re-injection period, it is vital that the peak shape is not negatively altered due to the loss of primary dimension separation [132]. By increasing the length of the sample loop, a double accumulation or re-injection step can occur, allowing for the peak shape to be preserved [131]. To further improve upon this concept, an even longer re-injection period and lower secondary flow rate of about 4 mL/min were successfully employed [54], but at the cost of even wider ²D peaks.

With the advantages and disadvantages outlined, it is clear that there is no universal modulator. This led to the idea of creating a novel design, in which the advantages of both the thermal and flow-based platforms would be combined. By implementing the focusing effect of a thermal modulator without the necessity for cryogenics and maintaining retention time reproducibility of the flow modulator while operating under mass spectrometric column flows, a hybrid system can be achieved. The phases of the design process and operational capabilities of this novel modulator will be outlined.

7.2 Experimental

7.2.1 Sample

A saturated alkane mixture (Product number 49452-U) was obtained from Millipore Sigma (Oakville, Ontario, Canada). The mixture contained a total of 33 alkanes from C₇ to C₄₀. Each component was present at a concentration of 1000 µg/mL in hexane.

7.2.2 Modulator design

A reverse fill/flush modulator, compressed airline, jet nozzle and thick film cooling trap were employed in the design. The features that were considered when determining what was necessary to complete the hybrid system included the flow modulator parameters, the jet which provided the compressed air for cooling, a cooling trap to help in the focusing step, and a column holder or stabilizer to ensure the column remained motionless during cooling, as seen in Fig. 7.1.

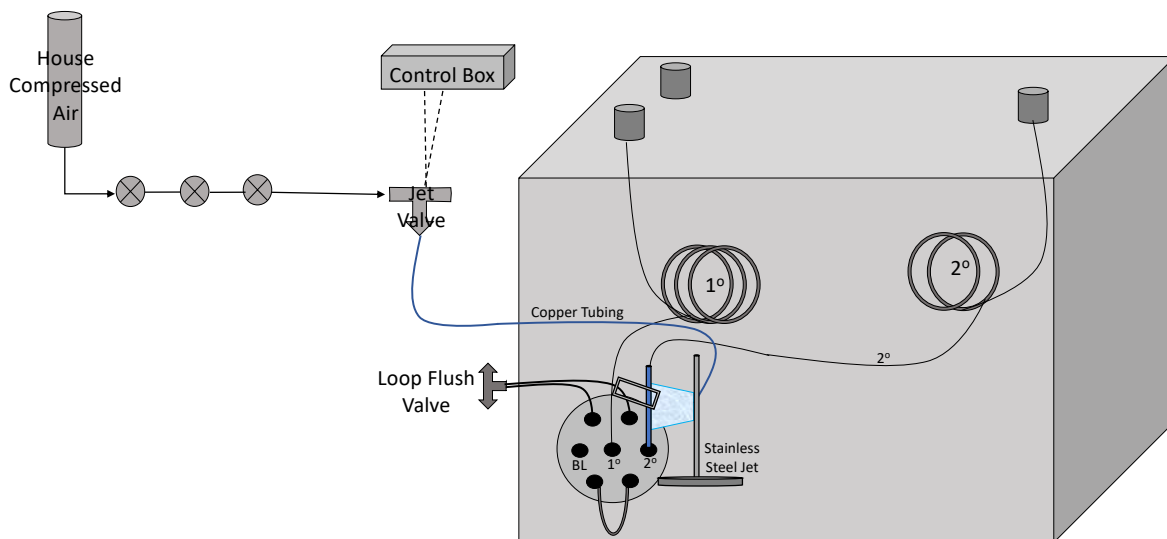


Figure 7.1 Schematic of the hybrid system.

A SepSolve Insight reverse fill/flush modulator was employed to perform the sampling of the primary column effluent and re-injection onto the secondary column. In a conventional set-up, the modulator utilizes high secondary flows (~ 20 mL/min) to quickly flush the sample loop as a compressed band onto the head of the secondary column. In order to accommodate an appropriate column flow in the second dimension for direct coupling to a mass spectrometer, the fill and flush parameters had to be adjusted accordingly. The manufacturer recommends setting the fill capacity to 75% of the volume of the selected sample loop, with a subsequent flush of 1.5 loop volumes for full transfer mode [58]. As previously mentioned, a larger sample loop is beneficial when utilizing a lower secondary flow rate [131], however, a larger sample loop and longer flush period results in broader secondary injection bandwidths [58]. A sample loop of 22.66 cm length was implemented for a total fill volume of $50 \mu\text{L}$. To determine the necessary dimensions of the secondary column and bleed line that would allow a low secondary flow rate, a flow calculator was used [58]. A 20 m x 0.18 mm ID x $0.18 \mu\text{m}$ Rxi-5MS primary column and

2.0 m x 0.15 mm ID secondary guard column were used. With a primary flow of 0.7 mL/min, a bleed line of 1.78 m x 0.1 mm ID was necessary to receive matching flow rates, which is necessary for proper reverse flush operation of the modulator. The resulting secondary flow rate was 3.2 mL/min. A guard column without any stationary phase was chosen as the secondary column in order to determine the actual re-injection bandwidths of the components after the hybrid modulation occurred. By employing a column that has no retention properties, the resulting analyte peak widths, height and area represent the result of the modulation process. With a significant decrease in the second-dimension flow, the injection bands will inherently be wider due to the loss of compression resulting from the typically high secondary flow rate. This will be counteracted by the thermal components of the hybrid system, which will allow focusing of the wider bands.

The flow calculator provided by SepSolve Analytical not only helps in determining the tubing lengths and carrier gas flows for proper operation, but it also provides additional information that was used to determine the appropriate fill and flush settings to fill the sample loop to 75% capacity and flush the loop by 1.5 loop volumes [58]. The calculator allows for many input values, such as the starting oven temperature, secondary dimensions (length and internal diameter), bleed line dimension (length and internal diameter), loop length, primary flow and secondary flow. The pressure control monitor allows for the input pressure to be adjusted to receive a corresponding bleed line flow which matches that of the desired primary column flow rate. The resulting information includes the loop volume, and the primary and secondary average linear velocity. These three parameters were then used to create an in-house calculator to determine the necessary fill and flush times, as seen in Table 7.1. By using equations (3) and (4), the fill volume for a specific fill time was determined. This value was then compared to the result

of equation (1) to ensure the fill volume was just below the 75% capacity. Similarly, equations (5) and (6) were used to determine the flush volume for a specific flush time. This was then compared to the result of equation (2) to ensure the flush volume was equal to or just greater than the 1.5 loop volume amount. To fill the sample loop to 75% capacity or 37 μL , 3.0 seconds (s) was necessary. To flush 1.5 loop volumes, or 76 μL , 1.3 s was necessary. To determine the length of the modulation period, the fill and flush time were added, resulting in 4.3 s.

Table 7.1 Equations used to determine proper fill and flush times

Equation	Result
(1) = Loop volume * 0.75	75% capacity
(2) = Loop Volume * 1.5	1.5 loop volumes
(3) = Fill (s) * ¹ D avg. linear velocity	Fill Length
(4) = (Loop volume/Loop length) * Fill Length	Fill Volume
(5) = Flush (s) * ² D avg. linear velocity	Flush Length
(6) = (Loop volume/Loop length) * Flush Length	Flush Volume

Incorporating compressed air cooling (without cryogenics) required additional hardware (cooling jet) to be added to the system. A 1/16" copper tubing was placed within the GC oven, through the same opening through which the auxiliary lines for the flow modulator entered, as seen in Fig. 7.2. The copper tubing was malleable, allowing it to be directed towards the flow modulator set-up. To control the timing of the compressed air jet, a three-way solenoid valve and Insight control board were used, as seen in Fig. 7.1. The copper tubing was placed at the normally closed (NC) port of the solenoid valve, and the normally open (NO) port was closed

with a blank ferrule. The solenoid valve was then connected to the house compressed air line. To control the timing of the solenoid valve, it was connected to a second valve terminal on the Insight control board. Matecs (Modulation and Timed Events Control Software) software (Markes International) was used to configure the valve as a GCxGC valve, allowing for complete control of when the jet was on or off.

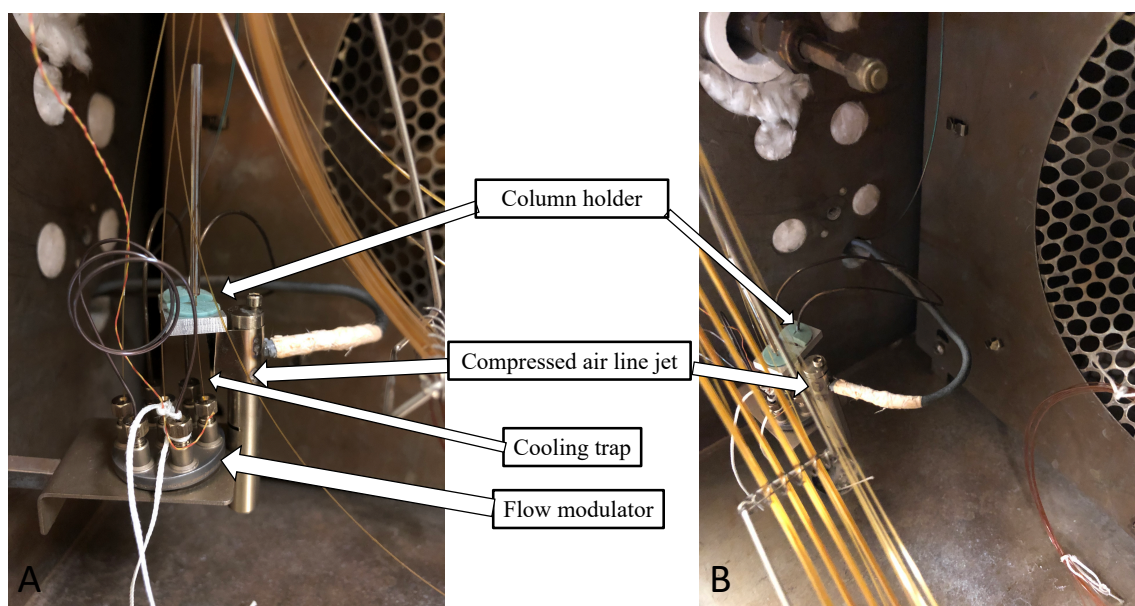


Figure 7.2 Close up images of compressed air line, jet, flow modulator, cooling trap and column holder.

The timing of the jet in regard to the flush of the sample loop was an important consideration in the design phase. The jet had to be initiated prior to or simultaneously with the flush stage in order to produce a cold section for the wide band to be focused. The Matecs software allowed for the control of the modulation period and flush time; it then subsequently determined the fill time by subtracting the flush time from the total modulation period. Matecs allowed valve operating parameters to be programmed separately. The first valve was programmed for the fill/flush operation of the modulator, and the second valve was programmed

for the timing of the cooling jet. With various cooling times, the initiation of the jet in regard to the flow modulator fill and flush parameters can be seen in Fig. 7.3.

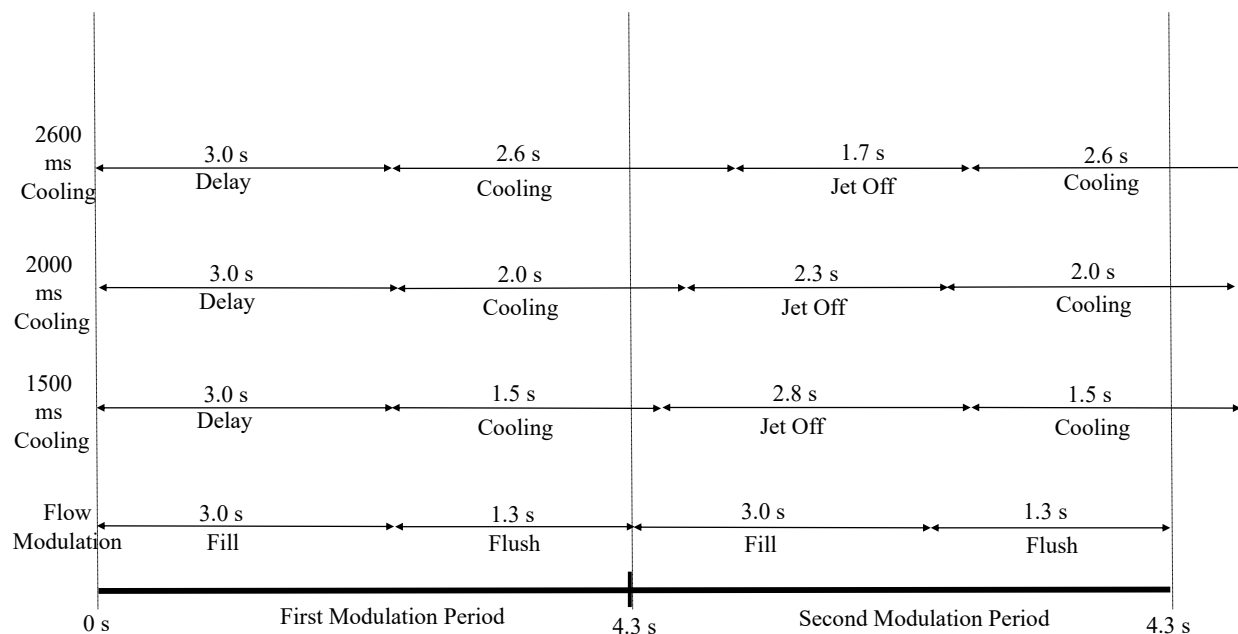


Figure 7.3 Various cooling times in comparison to flow modulation parameters for two modulation periods.

Several versions of the jet were made to accommodate necessary changes that occurred during the design process. The original design was inspired by the non-moving dual stage liquid CO₂ jet modulator by Beens *et al.* [28]. All designs implemented a stainless-steel rod, which was attached via a slot at the bottom of the rod to the flow modulator plate holder, with an opening for copper tubing to direct compressed air through a narrow slit which ran parallel to the capillary. The slot directed cool compressed air towards the head of the secondary column, as seen in Fig. 7.4. A small screw at the top of the stainless-steel rod ensured the tubing did not move while the jet was initiated. This design allowed for movement of the jet along the flow modulator plate holder, ultimately making it easier to direct the air flow. In the next iteration of

the design, a longer and narrower slit was used to provide a cool air flow to a larger section of the secondary column. However, in order to create this new slit, a larger opening where the copper tubing is inserted was required. As a result, most of the air escaped out the back of the stainless-steel rod, instead of through the slit. The final design (Fig. 7.4) worked off the previous one by adding a stainless steel strip at the back in order to cover the large opening, so air could not escape. A hole was placed in the stainless steel cover for the copper tubing to be inserted into the stainless-steel rod. The remainder of the strip was then wrapped around the edges of the rod and silver soldered on either side. The ends were trimmed to create “guides” to better direct the air escaping the narrow slit towards the secondary column.

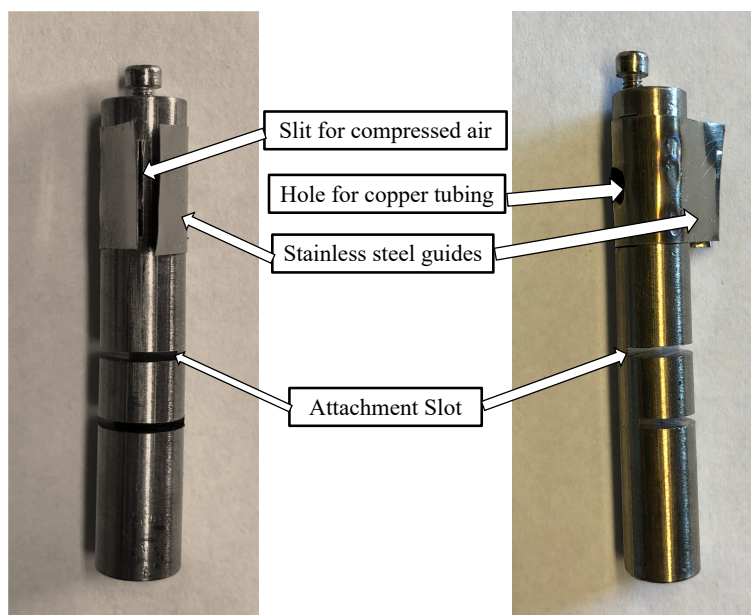


Figure 7.4 Cooling jet design used for all experimental analyses.

Thermal modulators utilize a thick stationary phase or an adsorbent phase for sorption of analytes at or below ambient temperatures. This same theory was employed in this hybrid system

through the addition of a thick film segment of a column, placed at the head of the secondary column, to be used as a “focusing trap” at which the compressed air jet was directed. A short section was placed in the second-dimension location of the flow modulator 7-port plate and subsequently connected to the secondary column by a press-fit column connector. With the low secondary flow rates employed, the injection bands are inherently wide. It was hypothesized that the thick film cooling trap would allow these wide bands to be trapped and properly focused by the cool compressed air, which would then be desorbed by the elevated oven temperature when the jet was turned off. The thicker the film used, the more retentive it is, causing an increase in retention of the analyte [133]. In some cases, too much retention can occur when too thick a film is employed [133]. It is important to note that if too much cooling is produced, a hot jet would be necessary to remobilize the analytes due to insufficiently high oven temperature. Various film thicknesses were tested to determine the optimal dimensions for creating narrow re-injection bands.

The final component of the hybrid system was a holder, placed on the cooling trap in order to stabilize the column from movement created by the force of the compressed air jet. This was necessary to alleviate any potential issues of column breakage, as well as ensuring the jet was consistently directed at the column during each modulation period. The key consideration when designing the holder was the material implemented and an open, lightweight design to ensure there were no cold spots along the column or added weight. A piece of aluminum and two inlet septa were combined to create the holder. The septa are a common consumable used in gas chromatography, capable of withstanding temperatures up to 350 °C. An aluminum rectangle was created that was small enough in size to ensure the primary column and sample loop were not obstructed. The interior was then milled out in order to place two septa beside one another

within cut-outs, as seen in Fig. 7.5. This design allowed the septa to hold the weight of the aluminum holder while also attached to two columns. The back septum was cut to fit around a metal auxiliary line, acting as a stationary component to stabilize the cooling trap column. The cooling trap column was fed through the front septum.

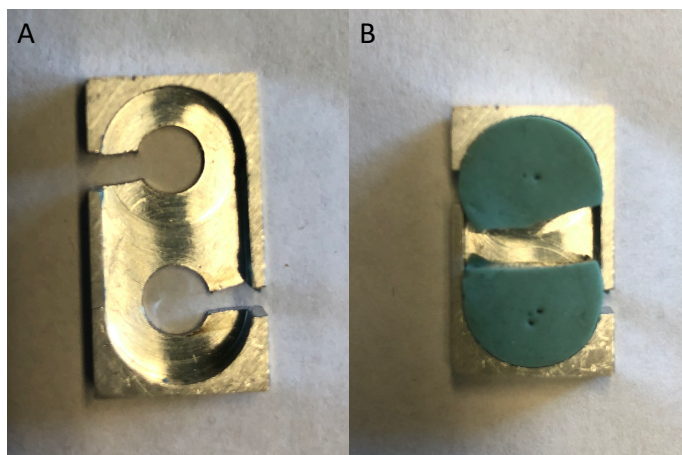


Figure 7.5 Column holder without (A) and with (B) the septa.

7.3 Instrumental setup

An Agilent 6890 gas chromatograph with a split/splitless inlet, an Agilent 7683 auto-sampler and FID were used for all analyses. The column configuration used for all analyses included a 20 m, 0.18 mm ID, 0.25 μm film thickness BPX-5 from SGE Analytical as the primary column; a 1.78 m, 0.1 mm ID guard column from Restek Corporation as the bleed line, and a 2.0 m, 0.15 mm ID guard column from Restek Corporation as the secondary column. Three different cooling trap columns of varying film thicknesses were used at the head of the secondary column: (1) Rxi-5MS 0.25 mm ID, 0.5 μm from Restek Corporation, (2) SPB-1 0.25 mm ID, 3.0

μm from Supelco, (3) HP-1 0.32 mm ID, 5.0 μm from Agilent Technologies. Connections between the cooling trap column and secondary column were made using Restek Corporation press-fit connectors. One microliter samples were injected into the split/splitless injector, operated in split mode with a 4-mm ID single taper inlet liner with quartz wool. Helium gas (Air Liquide, Cambridge, ON, Canada) with a purity of 99.999% was used as the carrier gas with a flow rate of 0.7 mL/min in the primary dimension, and 3.2 mL/min in the secondary dimension. The oven temperature program began at 50 °C for 1 minute, then ramped to 320 °C at a rate of 10 °C /min (held 5 minutes). The FID was operated at an acquisition rate of 100 Hz with a flow ratio of 40 mL/min : 400 mL/min H₂:Air. ChemStation software was used for data acquisition and instrument control, and ChromSpace (Markes International, Llantrisant, UK) was used for data processing.

7.4 Results and discussion

7.4.1 Time delay of the jet

The timing of the compressed air jet in regard to the flush stage of the flow modulator was a vital consideration to ensure the most efficient cooling was applied. The thick film within the trap assisted in trapping the wide injection bands with the help of the room temperature compressed air. If the trap was cooled during the fill stage, the trap would rapidly return to oven temperature once the jet was turned off, resulting in a non-cooled trap during the flush stage. With a fill time of 3.0 s, two different delays were implemented for the initiation of the compressed air jet, 0.028 min (1.68 s) and 0.05 min (3.0 s). The shorter delay would initiate the

jet halfway through the fill stage and remain on for part of the flush cycle. When longer jet times are implemented, cooling will remain on during the entire flush stage. The longer delay would initiate the jet to start once the first fill stage was completed, ensuring the jet remained on during the entire flush stage. As seen in Figure 7.6, the longer delay improved the cooling over the shorter delay, especially with the higher molecular weight compounds. When comparing the jet off experiment (Fig. 7.6A) to the 0.028 min delay (Fig. 7.6B), focusing of the bands begins at approximately 22 min. With an even longer time delay, as seen in Fig. 7.6C, the analytes have been focused even more and tailing has been significantly reduced. By increasing the initial time delay, the cold jet was initiated at the beginning of the flush period and remained on during the entire stage. As subsequent modulation cycles occurred, the cooling jet remained off during the fill stage and was initiated at the beginning or slightly after the initiation of the flush cycle, depending on the total time of the cooling.

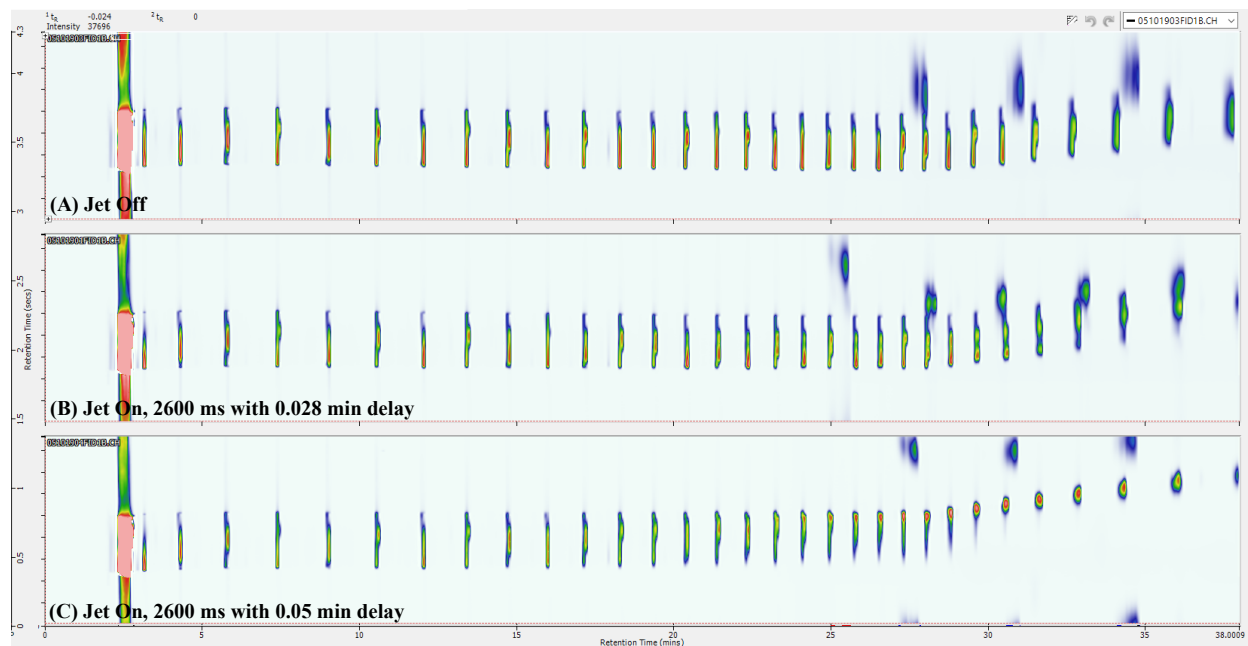


Figure 7.6 Chromatograms displaying the effect of cooling jet time delay on injection band widths; (A) absence of cooling (Jet off), (B) 2.6 s cooling with 0.028 min delay, (C) 2.6 s cooling with 0.05 min delay.

7.4.2 Septa within column holder

Despite utilizing a typical septum with the column holder that is employed in all GC systems, there was still a concern that its presence could cause a cold spot along the column train, leading to an adverse effect in regard to analyte remobilization by the GC oven. To test this theory, a comparison was completed with and without the septum present in the column holder. The cooling jet was turned off for this test to ensure the column would not break when there were no septa present. As seen in Fig. 7.7, there was no substantial difference between the septum being absent (Fig. 7.7A) and with the septum present (Fig. 7.7B). The streaking present within both chromatograms was due to analyte sorption within the focusing trap in the absence of cooling. As the temperature of the oven increased, the higher molecular weight compounds

were poorly remobilized and eluted off the thick film cooling trap as a streak in the 2D . It was concluded that the septum within the column holder was a suitable choice in order to help stabilize the cooling trap and prevent potential column breakage due to the force created by the compressed air jet during the cooling process.

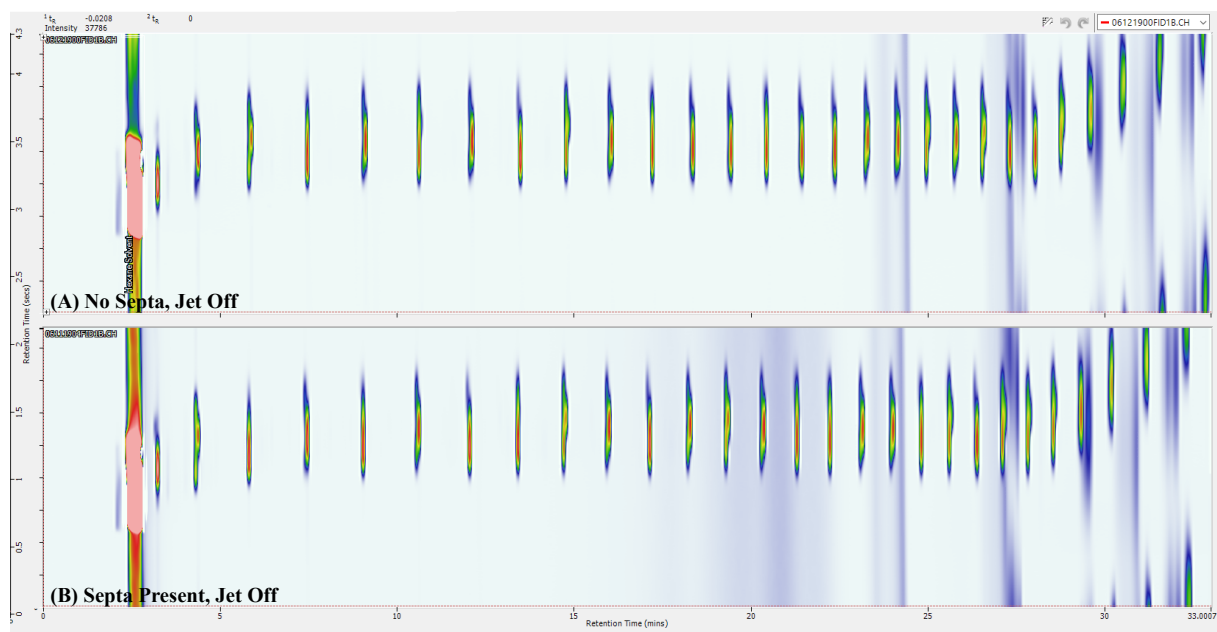


Figure 7.7 Chromatograms comparing the results obtained with the septum absent (A) or present (B) within the column holder.

7.4.3 Cooling trap film thickness comparison and reproducibility evaluation

Once the suitable time delay of the cooling jet was determined, the total amount of time the cooling jet was on also had to be optimized. Due to the low secondary column flow, a longer flush period was required for the flow modulator to operate properly. Consequently, the re-injection bands were inherently wider, requiring a cooling jet time that was equivalent or longer

than the flush period. A range of cooling times from 1000 ms (1.0 s) to 3000 ms (3.0 s) were employed to the three cooling trap thicknesses and the re-injection bandwidths were measured for all alkane compounds to determine which one provided the greatest focusing effect. To measure the analyte re-injection bandwidths, the “slicer” tool within the ChromSpace software was used. This feature allows the user to visualize the individual slices of each compound created in the modulation process. However, the software does not report the peak width at half height; it only reports the peak width at base for each slice. To eliminate any bias caused by tailing, the peak width at half height was determined manually. The peak width at half height was reported as the re-injection bandwidth for the tallest slice of each analyte. The total area of the compound, including all slices, as well as the height of the tallest slice and the primary and secondary retention times were recorded. From visual comparison of the chromatograms obtained using various cooling times and peak width at half height calculations, the optimal cooling times for each cooling trap film thickness were determined.

Triplicate analyses were also performed with the jet off and at the optimal cooling time for 0.5 and 3.0 μm cooling traps to evaluate the reproducibility of the hybrid system. This was not performed for the 5.0 μm cooling trap due to poor performance, which will be discussed further in section 7.4.3.5. The percent relative standard deviation (%RSD) for the peak widths at half height, primary and secondary retention times, peak height of the tallest slice and total peak area are reported. The reproducibility of a modulator platform is extremely important for consistent results over multiple replicates. As previously discussed, flow platforms typically have low %RSD for secondary retention times due to the use of an electronic pressure control (EPC), which controls the gas flows. For cryogenic platforms, secondary retention time shifts can occur, resulting in cumbersome and time-consuming data processing. By adding a thermal

component to the flow modulator to create this hybrid system, the capabilities had to be evaluated to ensure the modulator operated with acceptable repeatability. The average peak widths at half height, narrowest achievable peak width at half height, average decrease in peak width with cooling and the greatest decrease in peak width with cooling were also determined from the triplicate analyses.

7.4.3.1 0.5 μm cooling trap

As seen in Fig. 7.8, the total time of cooling drastically altered the focusing effect on the re-injection bandwidths when using the 0.5 μm cooling trap. Times of 2000 ms and 2600 ms proved to be far superior to 1500 ms. The shorter time of 1500 msec did not provide enough cooling when compared to the jet not being employed, as seen in Fig 7.8A and 7.8B, respectively. The longest time of 3000 ms provided sufficient cooling, however, it was not until C_{25} , resulting in tailing of the mid-molecular weight compounds when compared to the times of 2000 ms and 2600 ms. When comparing the time of 2000 ms to 2600 ms, the focusing effect appears to be very similar, beginning around C_{20} . Ultimately, the lower value of 2000 ms provided the best overall focusing effect across the entire range of compounds. Furthermore, this cooling time caused less tailing with the mid-molecular weight compounds, ranging from C_{16} to C_{22} , when compared to 2600 ms. Table 7.2 lists the peak widths at half height for each compound in the absence and presence of cooling. The peak widths at half height were measured from the tallest slice of each compound. As seen in Table 7.2, some peak widths appeared rather narrow. In some cases, there were more than one slice per compound and the tallest was extremely narrow. For the compounds that eluted before approximately 22 min, only partial

focusing occurred resulting in peaks that were more focused than others. For the compounds that eluted after approximately 22 min, complete focusing occurred. Generally, 2000 ms of cooling provided optimal results. The average peak width at half height when 2000 ms of cooling was applied was 495 ms, a 38% decrease compared to no cooling.

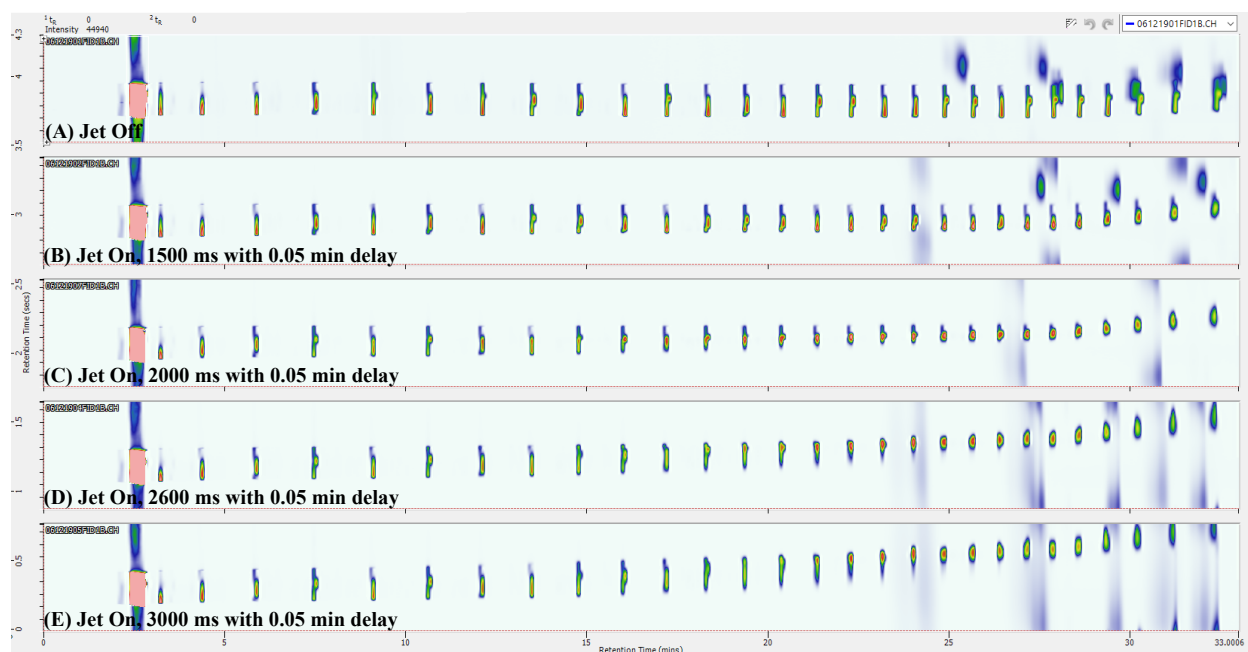


Figure 7.8 Chromatograms comparing the various cooling times applied to the 0.5 μ m cooling trap. (A) Absence of cooling (Jet off), (B) 1500 ms cooling, (C) 2000 ms cooling, (D) 2600 ms cooling, and (E) 3000 ms cooling.

Table 7.2 Comparison of re-injection band widths (ms) with 2000 and 2600 ms cooling for 0.5 μm cooling trap

Peak Width at Half Height (ms)							
Compound	Jet Off	2000	2600	Compound	Jet Off	2000	2600
C7	282	272	255	C21	337	247	326
C8	405	496	520	C22	320	226	296
C9	484	598	526	C23	676	244	330
C10	558	276	284	C24	696	242	356
C11	628	619	684	C25	231	240	315
C12	635	260	293	C26	289	255	346
C13	696	650	661	C27	760	222	379
C14	361	649	716	C28	653	291	427
C15	558	181	731	C29	821	281	401
C16	543	193	361	C30	759	303	448
C17	665	449	785	C31	774	320	522
C18	632	171	224	C32	314	390	627
C19	585	314	723	C33	792	489	776
C20	599	162	626	C34	363	574	924
				Avg	550	343	495

7.4.3.2. 0.5 μm cooling trap reproducibility evaluation

Based on the results determined in Section 7.4.3.1, the optimal condition of 2000 ms cooling was used to evaluate the reproducibility of the 0.5 μm cooling trap. As seen in Table 7.3, the cooling jet on for 2000 ms produced the best results overall. The peak width at half height and secondary retention time RSD values were 2.2% and 0.8%, respectively. In the absence of cooling, ^2D peak width reproducibility was acceptable, but the ^2D retention times were characterized by large %RSD values. Without any cooling present, the change in partition coefficients within the thick film trap was the only process responsible for trapping and focusing the compounds. With a thicker film, the retention of compounds increases in comparison to when a thin film is employed. The %RSD for the peak heights and total area for all parameters were adequate and below 5%.

The average peak width at half height with no cooling was 608 ms. The narrowest peak width with 2000 ms cooling was for a heavier compound, C_{18} , at 163 ms. The average decrease in peak width at half height was 218. The greatest decrease in peak width was 519 ms for C_{25} with 2000 ms cooling. The average percent difference of all replicates between absence and presence of cooling applied at 2000 ms was 43%. The triplicate data for the 0.5 μm cooling trap including peak width at half height (ms), ^1D and ^2D retention times, peak height and total peak area can be found in Tables 7.C.1., 7.C.2., 7.C.3., 7.C.4., 7.C.5., respectively, in Appendix C.

Table 7.3 Reproducibility data for 0.5 μm cooling trap

	% RSD Avg				
	Peak Width at Half Height	Primary Retention Time	Secondary Retention Time	Tallest Slice Peak Height	Total Peak Area
Jet Off	4.6	0.01	1.9	3.2	2.0
Jet On 2000 ms	2.2	0.01	0.8	3.6	1.0

7.4.3.3 3.0 μm cooling trap

Similarly to the results for the 0.5 μm film, the 3.0 μm film thickness saw the same trend of requiring a longer cooling time to efficiently focus the trapped analytes, as seen in Fig. 7.9. The shorter times of 1000 ms (Fig. 7.9B.) and 1500 ms (Fig. 7.9C.) provided little to no focusing when compared to the jet remaining off (Fig. 7.9A.) during the analysis. The more appropriate choices were cooling times of 2000 ms, 2600 ms and 3000 ms. Focusing effect began at approximately C_{12} , substantially lower than that achieved with 0.5 μm cooling trap. However, the longest cooling time (Fig. 7.9F.) created tailing for the high molecular weight compounds ($+C_{30}$) due to excessive retention. The oven could not remobilize the components sufficiently fast from the cooling trap for proper re-injection into the secondary column. Due to the shortcomings of the oven in this scenario, a hot jet would have to be employed for efficient remobilization. Alternatively, the cooling air temperature could be altered to increase throughout the analysis. With a higher temperature of cooling air, remobilization would be accomplished more easily. When comparing times of 2000 ms (Fig. 7.9D.) and 2600 ms (Fig. 7.9E.), similar focusing effect was achieved. However, the longer time of 2600 ms created narrower re-injection bands over a wider range of compounds, as seen in Table 7.4. Generally, the 2600 ms cooling time provided the best focusing effect. The average peak width at half height when 2600 ms of cooling was

applied was 591 ms, a 29% decrease compared to an absence of cooling. When compared to the 0.5 μm cooling trap, the 3.0 μm cooling trap did not provide as much of a focusing effect.

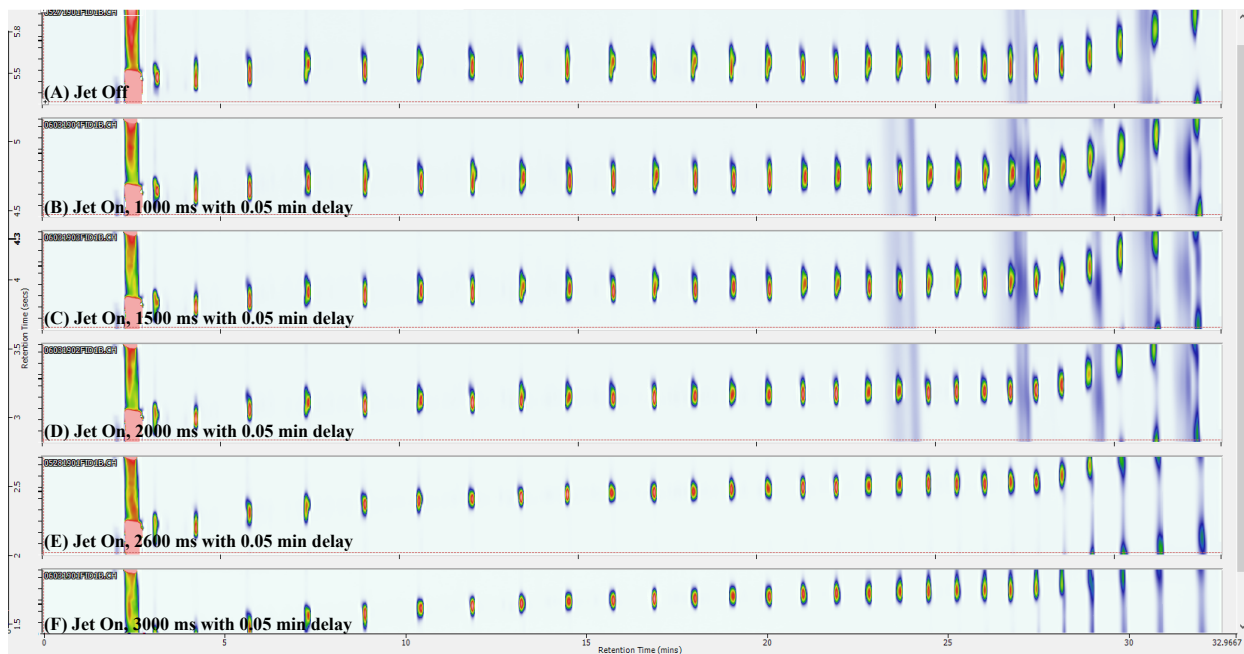


Figure 7.9 Chromatograms comparing the various cooling times applied to the 3.0 μm cooling trap. (A) Absence of cooling (Jet off), (B) 1000 ms cooling, (C) 1500 ms cooling, (D) 2000 ms cooling, (E) 2600 ms cooling, (F) 3000 ms cooling.

Table 7.4 Comparison of re-injection bandwidths (ms) with 2000 and 2600 ms cooling for 3.0 μm cooling trap

Peak Width at Half Height (ms)							
Compound	Jet Off	2000	2600	Compound	Jet Off	2000	2600
C7	390	1212	419	C21	978	607	478
C8	669	535	893	C22	982	570	507
C9	711	573	739	C23	730	557	504
C10	574	456	420	C24	759	553	543
C11	740	527	480	C25	971	566	556
C12	564	485	396	C26	988	613	560
C13	771	513	413	C27	825	575	628
C14	966	623	441	C28	974	602	605
C15	989	490	405	C29	1058	585	695
C16	610	512	424	C30	1023	684	754
C17	764	550	466	C31	1051	804	889
C18	652	521	423	C32	1112	999	1024
C19	521	598	480	C33	1051	1065	1317
C20	684	542	492	C34	1250	1643	N/A
				Avg	834	663	591

7.4.3.4 3.0 μm cooling trap reproducibility evaluation

The reproducibility of the 3.0 μm cooling trap was only analyzed for the jet off and optimal cooling time of 2600 ms (Table 7.5). When comparing the absence to presence of cooling, the latter produced significantly lower %RSD for the peak width at half height. The cooling provided by the jet helped increase reproducibility from approximately 8% to 4% RSD due to the focusing effect. The secondary retention time reproducibility was essentially equivalent at 1.5% RSD. The reproducibility peak heights of the tallest slices and total peak area for both parameters were adequate at about 6% RSD.

The average peak width at half height for no cooling was 801 ms, significantly larger than that obtained by the 0.5 μm cooling trap. The average peak width with 2600 ms cooling was 654 ms. The narrowest peak was C₁₃ (415 ms) with an overall average decrease in peak width of 248 ms. The greatest decrease in peak width was 506 ms for C₁₈ with 2600 ms of cooling. The average percent difference of the replicates in peak widths at half height between the absence and presence of cooling applied for 2600 ms was 18.3%. This was an adequate improvement in peak width; however, the thicker film cooling trap did not decrease peak widths substantially in comparison to the 0.5 μm cooling trap. The results of triplicate analysis for the 3.0 μm cooling trap with the absence and presence of cooling applied for 2600 ms including the peak widths at half height (ms), ¹D and ²D retention times, peak height and total peak area can be found in in Tables 7.C.6., 7.C.7., 7.C.8., 7.C.9., 7.C.10., 7.C.11., respectively, in Appendix C.

Table 7.5 Reproducibility data for 3.0 μm cooling trap

	% RSD Avg				
	Peak Width at Half Height	Primary Retention Time	Secondary Retention Time	Tallest Slice Peak Height	Total Peak Area
Jet Off	8.2	0.04	1.6	5.7	5.4
Jet On 2600 ms	4.0	0.07	1.5	5.3	5.5

7.3.4.5 5.0 μm cooling trap

As expected, the thickest film, 5.0 μm , required significantly less cooling to achieve a focusing effect, as seen in Fig. 7.10. Cooling times of 2000, 2600 and 3000 ms (Fig. 7.10D, 7.10E, and 7.10F, respectively) provided too much cooling in combination with a thick film, resulting in excess tailing in the second dimension due to the analytes not being desorbed from the cooling trap efficiently. As previously discussed with the 3.0 μm trap, oven heating only is not sufficient to release the trapped analytes as a narrow-focused band. A hot jet would be necessary to properly remobilize the compounds that are trapped within the thicker film and cooled for longer time periods. Alternatively, the cooling air temperature could be higher to decrease the strong trapping that occurred within the thicker film when longer cooling periods were used. Since the thick film has an added trapping capacity when compared to the thinner films, a shorter cooling time was required to obtain the desired focusing effect. Cooling times of 1000 and 1500 ms (Fig. 7.10B and 7.10C.) provided very similar narrow re-injection bands, as seen in Table 7.6. It is important to note that with a thick film trap, the bands were inherently wider in the absence of cooling when compared to the 0.5 μm and 3.0 μm traps, as seen in Table 7.7. Another important factor to consider was the difference in the diameters of the 5 μm cooling trap and 2D. The cooling trap had an inner diameter of 0.32 mm, while the 2D had an inner

diameter of 0.25 mm. As the analytes traveled from a larger diameter tubing to a smaller diameter tubing, the chromatographic band width physically increased. Ultimately, the larger ID thick film cooling trap was determined to be an unsuitable choice for this hybrid setup and the reproducibility evaluation was not completed.

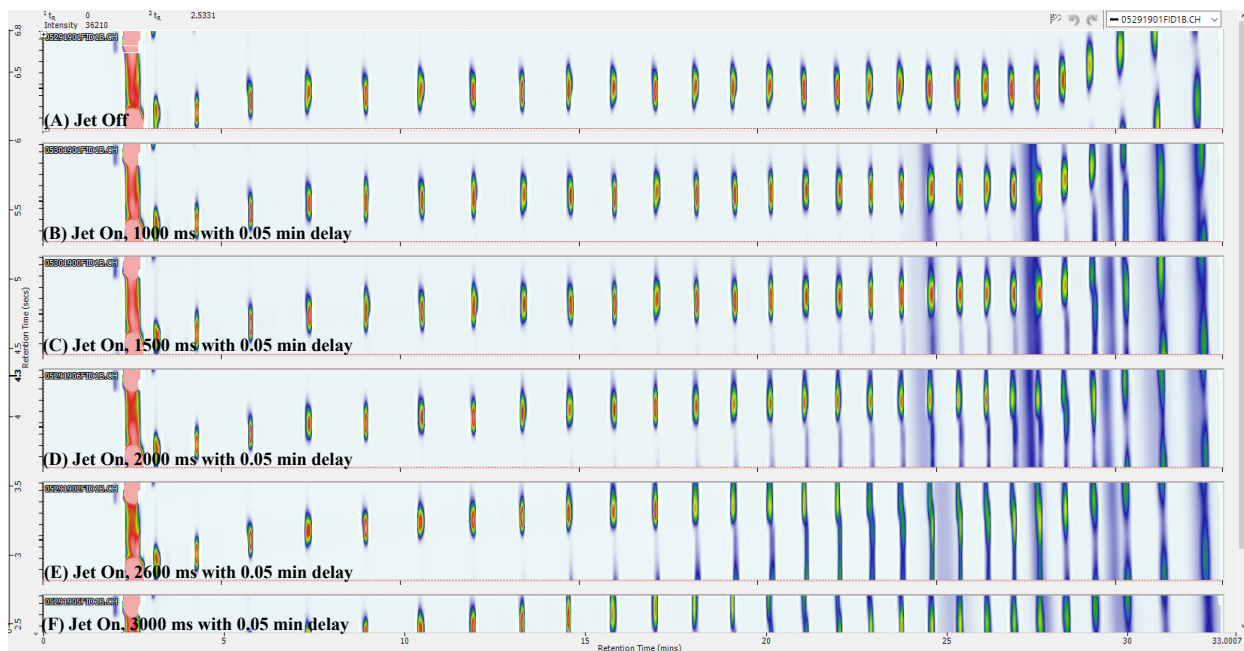


Figure 7.10 Chromatograms comparing the various cooling times applied to the 5.0 μm cooling trap. (A) Absence of cooling (Jet off), (B) 1000 ms cooling, (C) 1500 ms cooling, (D) 2000 ms cooling, (E) 2600 ms cooling, (F) 3000 ms cooling.

Table 7.6 Re-injection bandwidths (ms) for 1000 and 1500 ms of cooling with 5.0 μ m cooling trap

Peak Width at Half Height (ms)							
Compound	Jet Off	1000	1500	Compound	Jet Off	1000	1500
C7	1217	1195	554	C21	992	950	975
C8	748	771	868	C22	986	969	964
C9	848	882	832	C23	1210	1117	1048
C10	741	841	858	C24	1209	1068	1071
C11	923	1119	1145	C25	1033	990	999
C12	1211	939	945	C26	1021	1005	998
C13	914	1134	1142	C27	940	1211	1118
C14	969	841	873	C28	1006	1021	1009
C15	1166	951	957	C29	1022	1021	1022
C16	824	976	1005	C30	1118	1063	1098
C17	965	869	864	C31	1374	1284	1446
C18	803	1017	1017	C32	1521	N/A*	1921
C19	1161	1022	1011	C33	1723	2780	2215
C20	844	1073	1056	C34	2031	N/A	N/A
				Avg	1090	1081	1074

*N/A = non-modulated peak

Table 7.7 Unfocused bandwidths (ms) of 0.5, 3.0, and 5.0 μm cooling traps with the absence of cooling (Jet Off)

Compound	0.5 μm	3.0 μm	5.0 μm	Compound	0.5 μm	3.0 μm	5.0 μm
C7	282	390	1217	C21	337	978	992
C8	405	669	748	C22	320	982	986
C9	484	711	848	C23	676	730	1210
C10	558	574	741	C24	696	759	1209
C11	628	740	923	C25	231	971	1033
C12	635	564	1211	C26	289	988	1021
C13	696	771	914	C27	760	825	940
C14	361	966	969	C28	653	974	1006
C15	558	989	1166	C29	821	1058	1022
C16	543	610	824	C30	759	1023	1118
C17	665	764	965	C31	774	1051	1374
C18	632	652	803	C32	314	1112	1521
C19	585	521	1161	C33	792	1051	1723
C20	599	684	844	C34	363	1250	2031
				Avg	550	834	1090

7.4.4 Insulating cooling air line

Since the copper tubing which provides the compressed air to the jet nozzle was exposed to the increasing GC oven temperature during analysis, there was concern that this feature could have an adverse effect on the cooling process. The copper line was therefore insulated with GC oven insulation material, and the results were compared to those obtained with an uninsulated copper line for the optimal cooling times for the 0.5 and 3.0 μm traps. As seen in Fig. 7.11, the entire copper line was wrapped with the insulating material, which was then securely tied to the tubing to ensure it did not move when the GC fan was operating. This was not performed with the 5.0 μm cooling trap since it was previously determined that excessive cooling with a thick film trap resulted in broad bands due to insufficient remobilization of the analytes.



Figure 7.11 Insulated copper tubing for compressed airline.

7.4.4.1 0.5 μm cooling trap

As seen in Fig. 7.12, the addition of insulation to the copper line improved the focusing effect, especially with the mid-range molecular weight alkanes. There was also a reduction in tailing that occurred when there was no insulation on the copper line. However, the heavy molecular weight compounds C_{30} to C_{34} were slightly wider with the insulation present on the copper tubing. The lower cooling air temperature thanks to the insulation caused the focused bands to slightly widen upon remobilization. Overall, the insulation did not provide a decrease in average peak widths, as seen in Table 7.8. The uninsulated copper line provided a narrower average peak width due to the peak widths for the heavy compounds. If the heavy compounds were excluded, a slightly smaller average peak width with the insulated line was achieved. This emphasized the fact that allowing the cooling air to follow the oven temperature during the analysis would be beneficial.

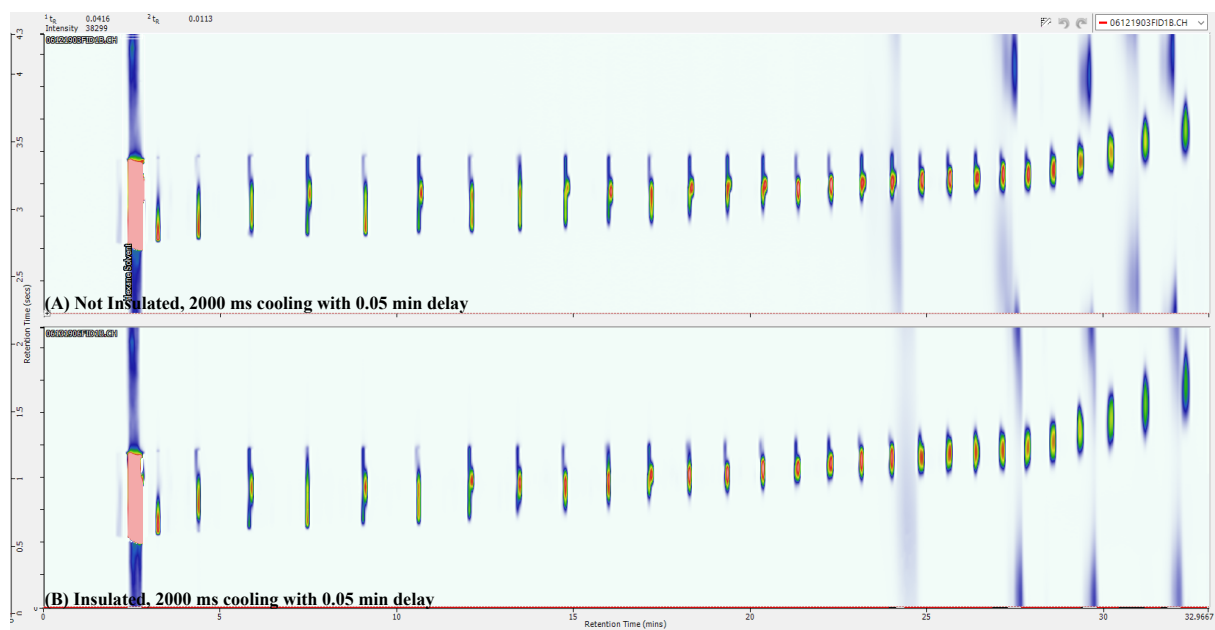


Figure 7.12 Chromatograms comparing the presence and absence of insulation on the copper tubing which provides compressed air for the jet nozzle with the 0.5 μm cooling trap.

Table 7.8 Comparison of peak width at half height (ms) for insulated vs. not insulated copper tubing with the 0.5 μm cooling trap

Compound	Jet Off	Insulated	Not Insulated	Compound	Jet Off	Insulated	Not Insulated
C7	282	334	272	C21	337	234	247
C8	405	494	496	C22	320	245	226
C9	484	319	598	C23	676	300	244
C10	558	717	276	C24	696	332	242
C11	628	308	619	C25	231	287	240
C12	635	663	260	C26	289	313	255
C13	696	201	650	C27	760	390	222
C14	361	271	649	C28	653	364	291
C15	558	365	181	C29	821	374	281
C16	543	371	193	C30	759	417	303
C17	665	207	449	C31	774	517	320
C18	632	251	171	C32	314	536	390
C19	585	250	314	C33	792	718	489
C20	599	258	162	C34	363	808	574
				Avg	550	387	343

7.4.4.2 3.0 μm cooling trap

In comparison to the 0.5 μm cooling trap, the insulation was not beneficial to the 3.0 μm cooling trap. As seen in Fig. 7.13, the insulation on the copper tubing provided too much cooling with the mid-heavier molecular weight compounds, leading to excessive tailing from inefficient remobilization. A hot jet would be required in order to properly remobilize the focused analytes within the thicker film trap. With no hot jet being employed in this hybrid setup, the insulation is not recommended. Alternatively, increasing the cooling air temperature during the analysis would allow for proper remobilization of the higher molecular weight compounds, which do not require as much cooling for trapping. Overall, the non-insulated copper line provided narrower peak widths, as seen in Table 7.9.

The insulation of the copper line provided too much cooling for the mid-heavier molecular weight compounds, resulting in excessive tailing. Alternatively, the cooling air temperature should increase with the oven temperature during an analysis since the heavier compounds do not require substantial cooling for trapping. On the other hand, more efficient cooling was important for the more volatile, lighter molecular weight compounds. Even though the insulation of the cooling line did not substantially decrease the peak widths of the lighter compounds, alternative cooling options could be applied without the use of consumable cryogenics. A vortex cooler or a multi-stage thermoelectric cooler could be used to decrease the cooling air temperature by 20 °C or 50 °C, respectively.

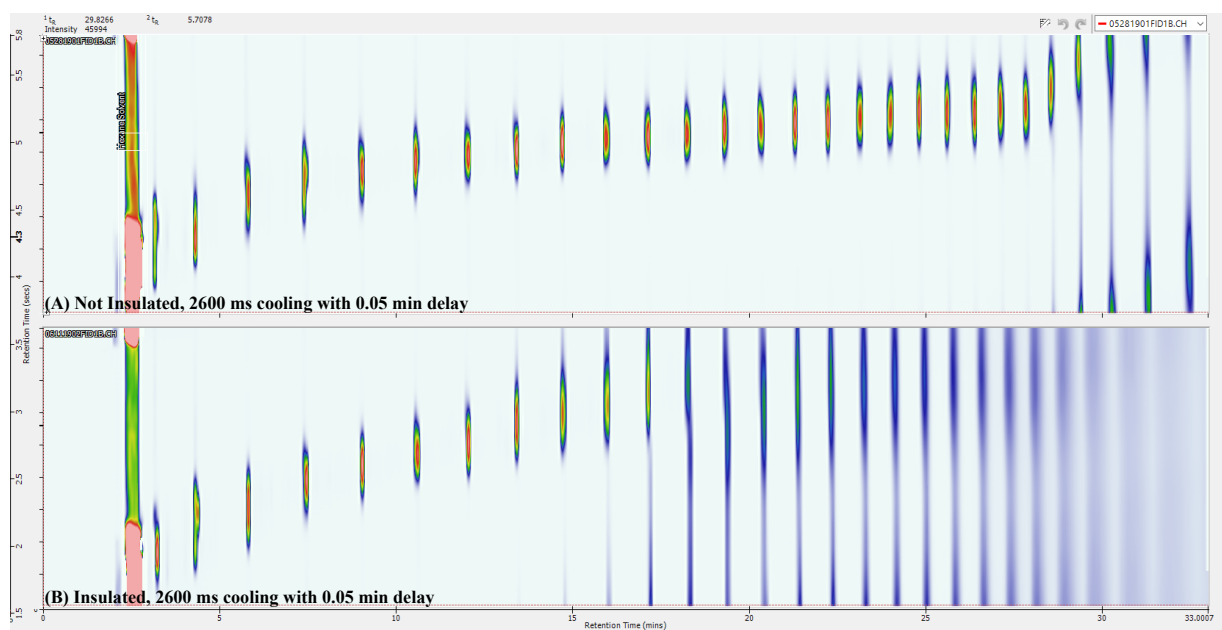


Figure 7.13 Chromatograms comparing the presence and absence of insulation on the copper tubing which provides compressed air for the jet nozzle with the 3.0 μm cooling trap.

Table 7.9 Comparison of peak widths at half height (ms) for insulated vs. non-insulated cooling line for the 3.0 μm cooling trap

Compound	Jet Off	Insulated	Not Insulated	Compound	Jet Off	Insulated	Not Insulated
C7	390	456	419	C21	978	1791	478
C8	669	400	893	C22	982	1986	507
C9	711	757	739	C23	730	2077	504
C10	574	471	420	C24	759	2234	543
C11	740	496	480	C25	971	2463	556
C12	564	478	396	C26	988	2661	560
C13	771	542	413	C27	825	3025	628
C14	966	674	441	C28	974	3641	605
C15	989	744	405	C29	1058	N/A*	695
C16	610	802	424	C30	1023	N/A	754
C17	764	990	466	C31	1051	N/A	889
C18	652	1552	423	C32	1112	N/A	1024
C19	521	2013	480	C33	1051	N/A	1317
C20	684	1660	492	C34	1250	N/A	N/A
				Avg	834	1451	591

*N/A = non-modulated peak

7.5 Conclusions

A hybrid system that employed the advantages of both a thermal and flow-based platform has been designed and employed. The reproducibility of a reverse fill/flow modulator combined with a thick film trap that was cooled while operating under a total column flow compatible with a mass spectrometer proved to be a promising design. Three cooling trap thicknesses were evaluated. The 0.5 and 3.0 μm film traps proved to be superior to the 5.0 μm trap, providing significant focusing for narrow re-injection bands. The 3.0 μm trap provided too much retention in comparison to the 0.5 μm one. A phase thickness of 1.0 μm may be a possible compromise solution for the proper amount of retention needed to trap the analytes without causing too much broadening, ultimately allowing the cooling process to perform optimally. The jet nozzle design was helpful in providing cooling for analyte focusing. A method of measuring the temperature of the cooling air would be beneficial in ensuring significant cooling occurs throughout an entire analysis. Insulating the copper line, which provided the compressed air for cooling, was not advantageous for both cooling traps. The peak widths at half height and secondary retention times reproducibilities were below 5% RSD when the cooling jet was implemented. The greatest decrease in peak width for the 0.5 and 3.0 μm traps was 519 ms and 506 ms, respectively. Overall, the 0.5 and 3.0 μm traps provided an average percent decrease in peak width of 43% and 18%, respectively.

Chapter 8. Evaluation of the operational capabilities of a solid-state thermal modulator in comprehensive two-dimensional gas chromatography-time-of-flight mass spectrometry (GC×GC - TOFMS)

8.1 Introduction

The comparison of the UW thermal modulator and a commercial reverse fill/flush flow modulator for the analysis of a complex mixture has previously been discussed. Both modulator platforms achieved separation of conventional and synthetic engine oils and obtained satisfactory group analysis. To further improve upon a commercial fill/flush flow modulator, a proof of concept hybrid interface was created. A thermal focusing mechanism was added to allow the direct coupling to a mass spectrometer with lower ²D flow rates, which achieved adequate ²D re-injection band widths. In order to find an ideal modulator for GC×GC, the evaluation of a recently introduced commercial thermal modulator was completed.

With the many commercial platforms available on the market, it may be difficult to determine which one suits the desired application. The advantages and disadvantages of all platforms need to be understood. Thermal platforms are straightforward when converting from traditional one-dimensional gas chromatography (1D), making method optimization relatively easy. Most designs have a simple setup, leading to a limited number of column connections and

possible sources of leaks. More importantly, thermal platforms are directly compatible with mass spectrometric detectors, without the need to split or vent the ^2D flow. Despite the advantages of thermal platforms, they also have disadvantages. The analyte volatility range is typically limited (C_4 to C_{40+} at the maximum) due to the limited ability to trap very volatile compounds and problems with efficient desorption of high-boiling compounds. Some models might suffer from slight retention time shifts that can occur over large data sets, making data processing more time consuming. For example, for cryogenic models, frost formation might occur in humid environments, causing issues with the cold jets. The most significant disadvantage of cryogenic platforms is the use of expensive and cumbersome cryogenic liquids [119]. Consumable-free cryogenic modulators are available, but the volatility range with these platforms is narrower. Flow modulator platforms do not require cryogenic consumables, which results in low operating costs. Since they collect fractions of the entire ^1D effluent rather than trapping its components, flow platforms have no volatility limits [134]. The only limitation is the upper temperature limit of the column set that is used. For most platforms, flow switching accomplished through actuation of a 3-way valve is used to transfer the fractions of the ^1D effluent to the ^2D column. This results in good reproducibility of the ^2D retention times. However, the overall design of flow modulators can be quite complex, requiring multiple column connections, leading in turn to higher potential for leaks. Translating from a 1D to a 2D separation can be quite difficult and any alterations to the modulator setup make method optimization rather challenging. An important disadvantage for most flow modulator platforms is the incompatibility with mass spectrometers [47]. Since most models employ high ^2D flow rates to perform modulation, the ^2D effluent must be split to a single channel detector or vented when a mass spectrometer is needed. This ultimately leads to less sample being introduced into the MS, making trace analysis difficult.

However, when comparing thermal and flow modulators, the greatest advantage to thermal platforms is the focusing effect that is created by thermal modulation. Very narrow injection bands are created within the modulator by focusing the analytes in space, ultimately increasing the S/N ratio and lowering the limits of detection [23]. In comparison, the flow modulator platforms create narrow bands by physically compressing the ¹D fractions collected through the use of high pressure in ²D, but this focuses them in time only, not in space. Despite the narrow secondary peak widths that are achieved with both platforms, there is typically little to no increase in the S/N ratio with flow platforms. This disadvantage often makes thermal based platforms the preferred choice, especially in trace analysis. Nevertheless, cryogenics are a significant long-term cost and potential safety issue. To overcome the necessity of an expensive consumable, the University of Waterloo developed a single-stage consumable-free, thermal modulator, which trapped, focused and re-injected analytes into the ²D column without the need for cryogenic consumables [84].

The solid-state thermal modulator (SSM) was first described by Luong *et al.* in 2016 as the thermally independent modulator (TiM) [34]. The design was based on the same concept as the longitudinally modulated cryogenic system (LMCS), except cooling was achieved with thermoelectric coolers (TECs) rather than a moving cryochamber. It was later commercialized by J&X as the Solid-State Modulator (SSM); an alternative cryogen free platform with the ability to perform independent modulation without the use of consumables for trapping [39]. The retention time (RT) reproducibility reported in this paper was 0.009% and 0.008% RSD for the ¹D and ²D RT, respectively, for simple compounds such as benzene, toluene, ethyl benzene and xylenes [34]. Reported peak widths at half height were below 120 ms for the aromatic compounds within a diesel sample [34]. Overall, the modulator performed satisfactorily for a volatility range of *n*C₆

to nC_{24} . The ability to analyze atmospheric volatiles from C_2 to C_{12} was also achieved using the solid-state modulator [135], demonstrating that a consumable free, low resource GC×GC system could be implemented for routine volatile organic compound monitoring in real world samples. This study expands on previous evaluations to determine the operational capabilities of the solid-state thermal modulator to analyze standard mixtures of different volatility and polarity, including pesticides, fragrances and allergens. The modulator platform was assessed based on the retention time reproducibility in 1D and 2D , peak area reproducibility, 2D peak widths at half height and peak capacity in the second dimension. Significant co-elutions within the complex mixtures of analogous compounds were evaluated to determine the separation capabilities of the modulator. It was demonstrated that mixtures of complex nature can be analyzed utilizing the solid-state modulator for GC×GC-TOFMS.

8.2 Experimental

8.2.1 Samples

GC multiresidue pesticide standards kit (MRP) and fragrance allergens standards kit (FA) were obtained from Restek Corporation (Bellefonte, PA, USA). The MRP kit contained nine individual standard mixtures, which were combined and used for the analysis of a comprehensive MRP mixture, for a total of 203 compounds. The FA kit contained three individual standard mixtures, which were combined and used for the analysis of a comprehensive FA mixture, for a total of 31 compounds. All compounds within the MRP mixture were present at a concentration of 100 ng/mL, dissolved in toluene. All compounds within the FA mixture were present at a

concentration of 400 ng/mL, dissolved in methyl *tert*-butyl ether. The three individual FA standards each contained an internal standard, 1-fluornaphthalene, at a concentration of 20 ng/mL.

8.2.2 Solid state modulation

Solid state modulation was implemented for all analyses. The operating principles of the SSM are described elsewhere in detail [34, 35, 39]. The modulator platform consisted of two heating zones, one cold zone, a solenoid valve, heat sink with fan, column gripper, and two copper tube transfer lines, as seen in Fig. 8.1. The SSM was mounted on top of the GC oven, placed over the back inlet to avoid interference with the front inlet autosampler. The SSM could achieve temperatures up to +350 °C within the two heating zones and a range of -50 °C to 50 °C in the cold zone without any consumables.

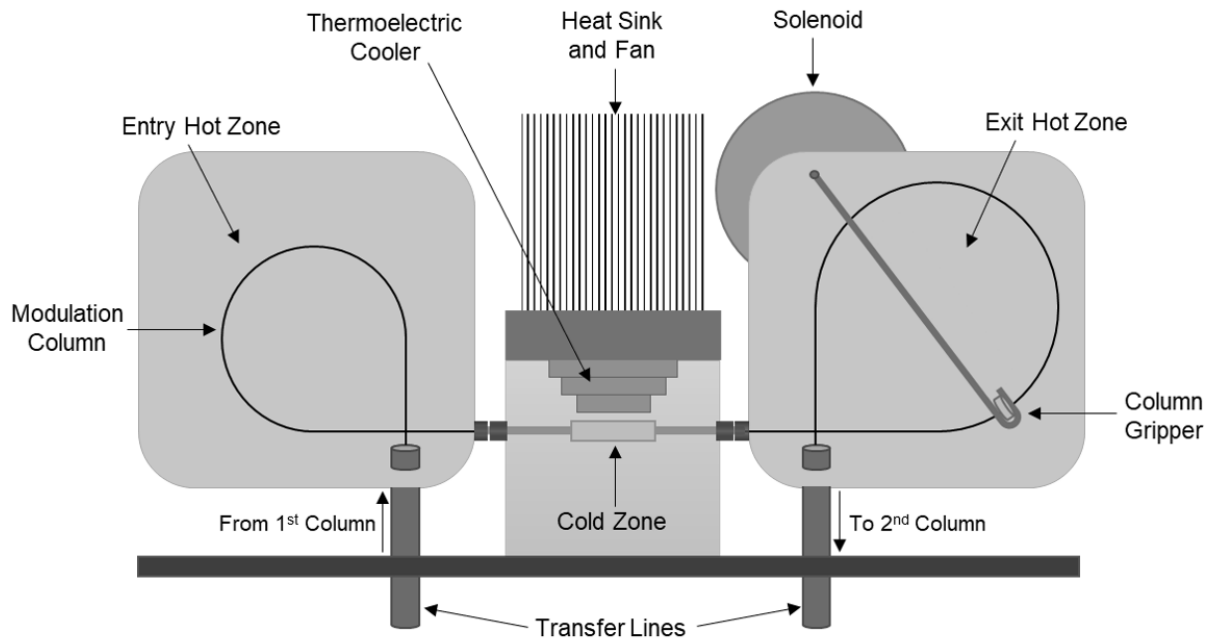


Figure 8.1 Diagram of the solid-state modulator (based on Ref. [39]).

Thermal modulation was achieved by moving the modulation column between the heating and cooling zones, as seen in Fig. 8.2. When the column was driven into the entry hot zone (top), the segment of the column previously within the cold zone was exposed to an elevated temperature to remobilize the trapped black band. Simultaneously, with this movement, the segment of the column previously in the exit hot zone entered the cold zone to trap the grey band. When the column was driven toward the exit hot zone (bottom), the segment previously in the entry hot zone entered the cold zone to trap the black band. Concurrently, the previously trapped grey band moved into the exit hot zone to remobilize onto the secondary column for further separation. Continuous movement back and forth between the heating and cooling zones achieved dual stage modulation. To minimize the possibility of analyte breakthrough, the entry hot zone was set at a lower temperature than the exit hot zone. The modulator column consisted of two separate pieces of capillary connected with an SGE Siltite μ -Union. The front half (within

the entry hot zone) of the modulation column was coated with a proprietary phase, while the back half (within the exit hot zone) was uncoated and had a smaller internal diameter. This specific design was to prevent broadening of the analyte bands, as well as improve the bandwidths in the second dimension. Four different modulation column types are available for various boiling point ranges. The EV series has a modulation range from C₂ to C₁₂, useful for volatile organic compounds analysis. The HV series can modulate between C₅ to C₃₀, which is applicable for petrochemical, fragrances/allergens and organic environmental pollutant analysis. The SV series has a modulation range from C₇ to C₄₀, while the DV series has a modulation range from C₉ to C₄₀₊. These column series are applicable for mineral and crude oils, PAHs and pesticides.



Figure 8.2 Diagram of dual-stage thermal modulation in the SSM (based on Ref. [39]).

8.3 Instrumental setup

An Agilent 6890 gas chromatograph (Agilent Technologies, Wilmington, Delaware, USA) equipped with a split/splitless injector, an Agilent 7683 auto-sampler and a LECO Pegasus TOFMS (St. Joseph, MI, USA) were used. The following column configuration was used for all analyses: a 30 m, 0.25 mm i.d., 0.25 μ m film thickness Rxi-5MS from Restek Corporation as the ¹D column, and a 1.0 m, 0.25 mm i.d., 0.25 μ m film thickness Rxi-17MS from Restek Corporation as the ²D column. An HV series modulation column, with a modulation range between C₅ to C₃₀ (b.p. 36 °C – 450 °C), was used for all analyses. Connections between the first

dimension, modulation column and second dimension were made using Restek Corporation Pressfit Connectors for 0.25 columns. One microliter samples were injected into the split/splitless injector, operated in split mode with a 4 mm i.d. single taper inlet liner with fused silica wool. Helium gas (Air Liquide, Cambridge, Ontario, Canada) with a purity of 99.999% was used as the carrier gas with a flow rate of 3.0 mL/min for all analyses. The TOF-MS was operated at an acquisition rate of 200 Hz. ChromaTOF software (LECO Corporation) was used for data acquisition, SSCenter software (J&X Technologies) was used for the control of the SSM platform, and ChromSpace (Markes International, Llantrisant, UK) was used for data processing. Table 8.1 lists the chromatographic and modulator conditions used for the analyses.

Table 8.1 Chromatographic and modulator conditions for the analysis of MRP and FA standards mix

	Multiresidue Pesticide Standards Mix	Fragrance Allergens Standards Mix
Inlet	200 °C, 5:1 split ratio	250 °C, 50:1 split ratio
Oven program	120 °C hold for 2 min, 10 °C/min ramp to 320 °C hold for 3 min	40 °C hold for 1 min, 4 °C/min ramp to 220 °C hold for 1 min
Modulator entry hot zone	+30 °C offset, capped to 320 °C	+30 °C offset, capped to 260 °C
Modulator exit hot zone	+120 °C offset, capped to 320 °C	+120 °C offset, capped to 320 °C
Modulator cold zone	9 °C, -50 °C/min ramp to -51 °C/min, hold for 3.8 min, 20 °C/min ramp to 9 °C, hold for 17 min	9 °C, -50 °C/min ramp to -51 °C/min, hold for 27.3 min, 20 °C/min ramp to 9 °C, hold for 18 min
Modulation period	3 sec, with releasing time 1 sec	4 sec, with releasing time 1 sec
Scan mass range	50-600 amu	45-600 amu
Mass spectrometer temperature	225 °C source, 250 °C transfer line	250 °C source and transfer line

8.4 Results and discussion

8.4.1. MRP standard mix separation

The MRP standard mixture was analyzed in triplicate, achieving an overall adequate separation. As seen in Fig. 8.3, the analysis sufficiently used the second-dimension space to separate the mixture. The majority of the compounds eluted within the middle region of the contour plot. Wraparound was allowed in order to achieve a full separation of all components of the mixture. Column bleed was observed in all replicates due to the high temperature implemented at the end of the GC analysis. An additional bleed band located above the regular column bleed band was observed and was believed to be the result of the movement of the modulation column within the modulator. As the modulation column moves into the cold trapping zone, siloxanes from ¹D stationary phase decomposition are trapped and focused together with the analytes, and are then remobilized into the ²D column. The second bleed band is likely due to siloxanes originating from the modulation column itself.

Of the total 203 compounds within the MRP mixture, only 186 were identified. The nine individual standard mixtures within the total MRP mixture were analyzed individually in order to tentatively identify each component by primary and secondary retention times. Match factors greater than 650 were used for peak identification by comparison to the NIST database. Detailed information on the compounds identified in the combined MRP standard mixture is presented in Table 8.D.1. of Appendix D. Of the 17 missing compounds, there were 5 significant co-elutions present, as listed in Table 8.D.2 of Appendix D.

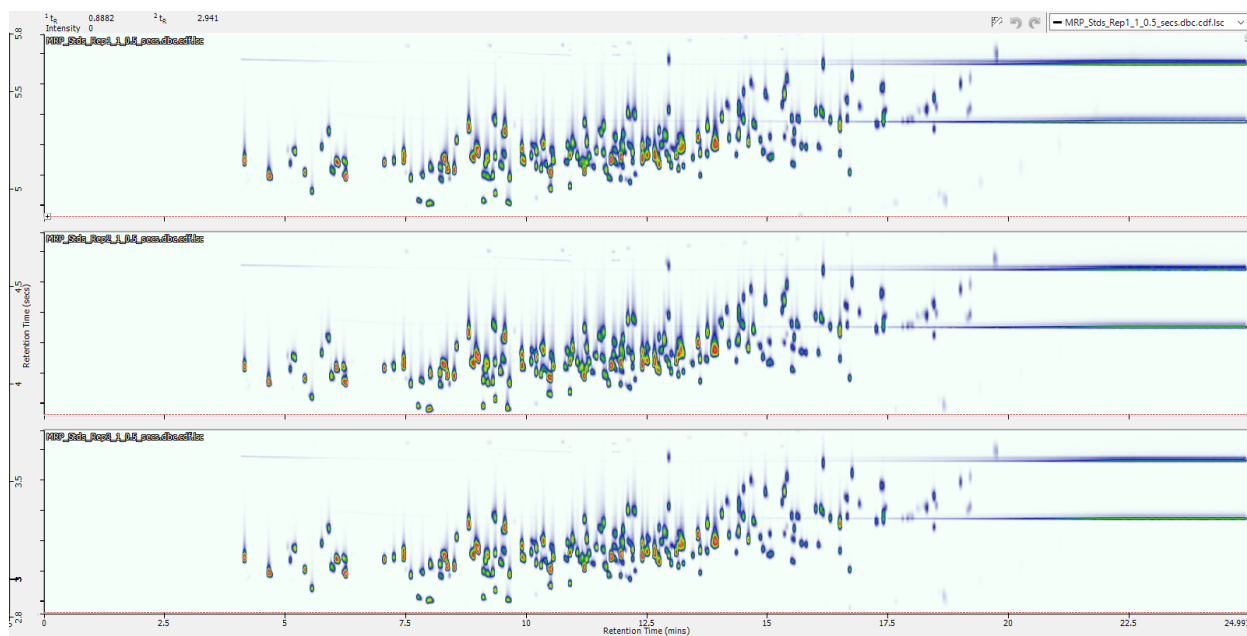


Figure 8.3 GCxGC-TOF-MS contour plots of triplicate analyses of MRP standard mixture using the SSM platform. The chromatograms have been shifted to display all peaks within the same modulation period.

8.4.2 FA standard mix separation

The FA standard mixture was analyzed in triplicate, achieving an overall separation of all 31 compounds. As illustrated in Fig. 8.4, the analytes were baseline resolved from one another. The second-dimension space was fully used in order to separate components with the same ¹D retention times, and wraparounds were allowed. In comparison to the MRP mixture, a shorter secondary column could have been used for further optimization. However, utilizing the same column configuration in both dimensions was deemed important in achieving as direct a comparison as possible. The ¹D column and modulation column bleed bands were not present within the FA mixture contour plots due to the lower temperature programs implemented in the GC oven and modulator exit zone. The three individual standard mixtures within the total FA mixture were analyzed individually in order to tentatively identify each component by primary

and secondary retention times. Match factors greater than 600 were used for peak identification by comparison to the NIST database. The detailed information on the compounds identified in the total FA standard mixture is presented in Table 8.D.3 of Appendix D.

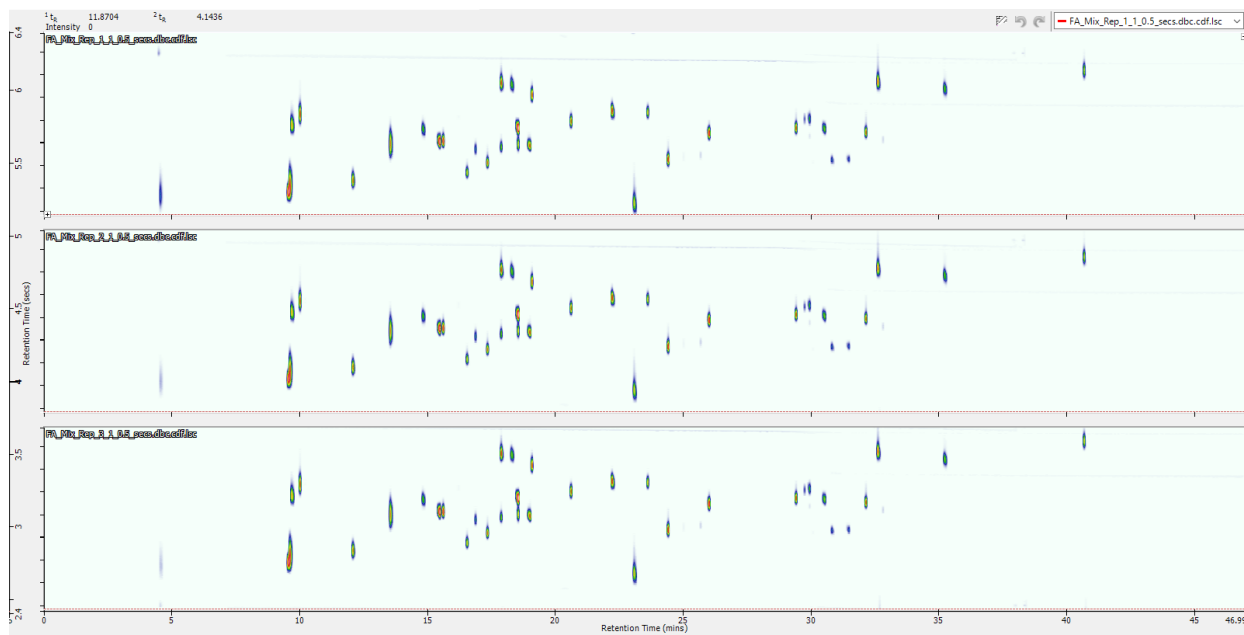


Figure 8.4 GCxGC-TOF-MS contour plots of triplicate analyses of FA standard mixture using the SSM platform. The chromatograms have been shifted to show all peaks within the same modulation period.

8.4.3 Retention time repeatability

Retention time repeatability in both the primary and secondary dimensions was evaluated for each identified compound in the MRP and FA standards mixtures. The reproducibility data for the MRP and FA standards mixtures can be found in Tables 8.D.4 and 8.D.5, respectively in Appendix D. Dependable modulation and injection of analytes into the 2^{D} is necessary for analyte identification with non-selective detectors. Retention time shifts can complicate data processing, ultimately making the identification process difficult and time-consuming.

In order to acquire the retention time of each compound from the ChromSpace software, the ‘slicer tool’ was used. The tool allows the user to visualize all “slices” of the compound, ensuring that each slice has the same mass spectrum. The ¹D time displayed within the tool dictated the original time of a typical one-dimensional separation, while the ²D time displayed was an average of all slices of the individual compound. However, wraparound within the triplicates had to be taken into account. Figs 8.5 and 8.6 illustrate the variation of second dimension retention times over the three replicate analyses for wrapped-around peaks within both the MRP and FA mixtures, respectively. In Fig. 8.5, the wraparound compounds that eluted within the dead time of the contour plot in the first and third replicates eluted earlier in the second replicate producing split peaks. In Fig. 8.6, a wraparound compound that eluted within the dead time is present in the third replicate. However, in the first and second replicates it was present in the previous modulation period. Wraparound of those peaks found within the dead time of the chromatogram had to be manually adjusted to correct the ²D retention times of the peaks. A dead time of 1.2 sec and 1 sec were identified for the MRP and FA standards mixtures, respectively. Whenever the ²D retention time was less than the dead time, the modulation period (3 sec and 4 sec for MRP and FA Standards mix, respectively) was added to the recorded retention time. This correction was important to evaluate the reproducibility of the second-dimension retention time.

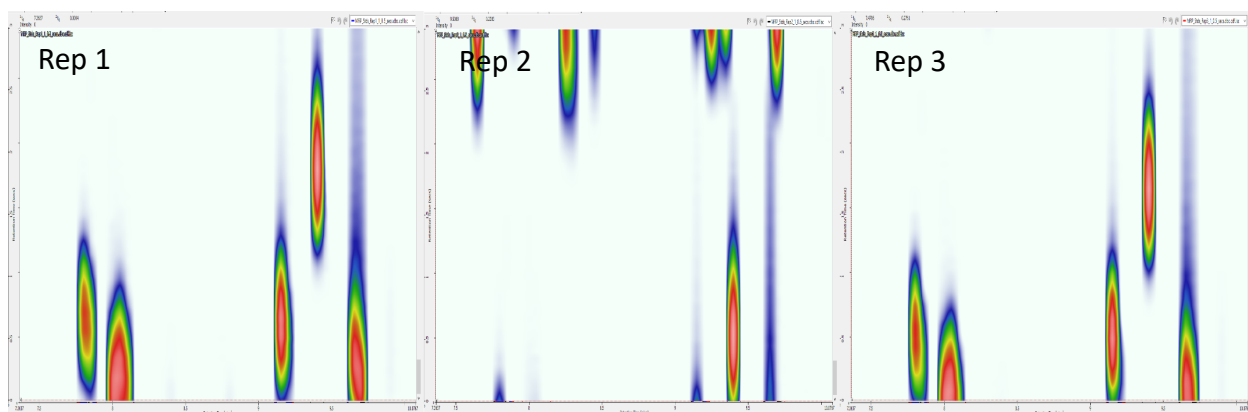


Figure 8.5 GC×GC-TOFMS contour plots of triplicate analysis of MRP standard mixture illustrating wraparound in the second dimension.

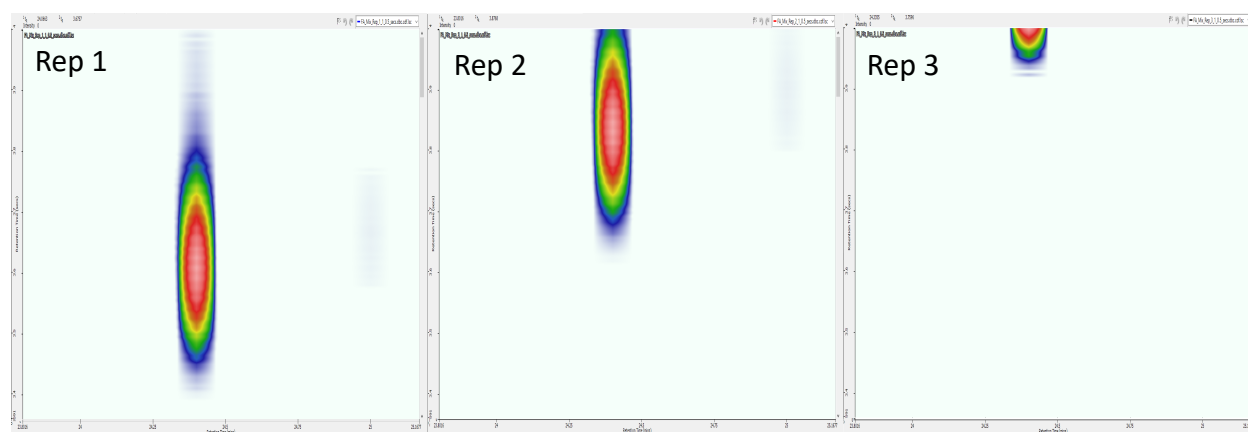


Figure 8.6 GC×GC-TOF-MS contour plots of triplicate analysis of FA standard mixture illustrating wraparound in the second dimension.

The average relative standard deviations (%RSD) of the ¹D retention times for the MRP and FA standard mixture components were 0.08% and 0.09%, respectively. The average %RSD of the ²D retention time for both mixtures were 2.4% and 8.6%, respectively. The detailed data on the repeatability of the ¹D and ²D retention times for all replicates for both the MRP and FA mixtures can be found in Tables 8.D.4 and 8.D.5, respectively. The reproducibility of the ²D retention time was not satisfactory, as it could create problems when acquiring data with non-

selective detectors. The variations in ²D retention times was most likely caused by the modulator internal clock and the GC clock not being synchronized. Initiation of the GC analysis activated the actuation of the modulation, however, without proper synchronization, the beginning of the modulation period in each replicate analysis was not exactly the same. Fig. 8.7 presents 1D traces of single compounds from each mixture, illustrating the difference between the replicates. Fig. 8.7A show the three replicates of compound Isodrin from the MRP mixture. Fig. 8.7B show the three replicates of compound Estragole form the FA mixture. When each replicate was overlaid, the difference in retention times was quite apparent. Of the three replicates, the minimum ²D retention time was subtracted from the maximum ²D retention time to determine the greatest difference between all replicates. The greatest difference in ²D retention times over all three replicates was calculated to be 132 msec and 534 msec for Isodrin and Estragole, respectively. The average difference between the maximum and minimum ²D retention times for all compounds of the MRP and FA mixtures were 129 msec and 528 msec, respectively. Despite the large differences between replicates of a single compound, the difference in ²D retention time across all components of each mixture was similar. This showed that the modulation process of the SSM was operating consistently within a single analysis for all compounds, affecting the ²D retention time of each compound equally. The greater issue lies in the synchronization of the modulation process with the GC start time. In order to ensure the modulation period begins consistently with the GC analysis, the modulator needs to match the GC internal clock. With this correction, the reproducibility of the ²D retention times could be improved.



Figure 8.7 One-dimensional trace of Isodrin comparing all three replicates (A) and one-dimensional trace of Estragole comparing all three replicates (B).

8.4.4 Peak area reproducibility

Peak area reproducibility was evaluated for both the MRP and FA mixtures. The triplicate data is presented in Tables 8.D.6 and 8.D.7 for MRP and FA mixtures, respectively, in Appendix D. This measurement assessed the total peak area of all slices of each analyte for the summation in both the primary and secondary dimensions. The ability to obtain reproducible peak area across multiple replicates is vital for quantitative purposes in regard to determining the concentration of species as well as limits of detection and quantitation. The ChromSpace software automatically took into account each slice of an analyte to acquire the total area. The average %RSD for all compounds for the MRP and FA mixtures were 24.3 % and 39.9%, respectively.

A major issue with the peak area data obtained was due to the use of the ChromaTOF software for acquisition and ChromSpace software for data processing. The raw files were transferred into the ChromSpace software due to compatibility issues encountered with the ChromaTOF software and the SSM platform. The baseline correction feature and integration in

ChromSpace may have not obtained the same quality data that ChromaTOF could produce due to differences in the underlying software algorithms. Inconsistencies in the second-dimension retention time, as discussed previously in Section 8.4.3, can lead to a different number of slices per analyte over multiple replicates. Although this should not affect the total area of the analyte peak, the integration process applied in data processing can be affected. This can result in a peak being improperly integrated, resulting in irreproducible peak area.

With the issue previously stated in regard to reproducibility of the ²D retention time, it is important to understand how this could affect the phase of modulation. Marriott and Shellie define modulation phase as the difference between the center of the primary peak and the mean of the peak sampled by the modulator [10]. There are two limiting scenarios, in-phase and 180° out-of-phase modulation. In-phase contains a single, central peak with a symmetrical pulse distribution, while 180° out-of-phase contains two peak maxima [10]. Any phase between the two limiting phases is possible and occurs at random due to the uncontrolled and random nature of a peak as it enters the modulator. It has been suggested that deviations in timing of the modulation start time could possibly vary the sampling pattern of a one-dimensional peak by obtaining different modulation phases [9]. Over replicate analyses, the slices obtained for each one dimensional peak may differ due to differences in the intensity of the peak, phase of modulation and S/N parameters within software for detection [9]. Ultimately, 100% of the total peak response is not guaranteed, and 75% or less may only be recovered [9]. To accurately determine an analyte's concentration, the full peak area response is necessary. Peak area underestimation due to peak detection omitting slices below a S/N threshold, or overestimation due to a baseline that is set too low, will directly affect analyte quantitation [136]. However, manual integration is time consuming and inaccuracies could occur in measuring smaller slices

at the extremities of an analyte peak area distribution and identifying peaks at the extremities with the same secondary retention time using a non-specific detector [136]. It has been shown that using the relative modulated area (based on the two or three most intense peaks) reduces the overestimation of peak area and provides an adequate estimation for determining the concentration of species [136, 137]. Furthermore, the main advantage of utilizing the relative modulated area method was the independence from the timing of the modulation and modulation phase [136].

Following the initial integration results, the peak areas were re-evaluated to ensure the integration was performed properly. Within the slicer tool, the analytes were manually integrated to ensure each peak was measured in its entirety, and that no peaks were improperly omitted. The revised peak area reproducibility for the MRP and FA mixtures were 19.3 % and 11.5 %, respectively. The detailed information on all replicates for the MRP and FA mixtures can be found in Tables 8.D.6 and 8.D.7, respectively.

8.4.5 Second dimension evaluation

8.4.5.1 Injection bandwidth at half height

To properly evaluate the modulator capabilities, the peak widths at half height of unretained compounds were evaluated. The three circled peaks in Fig. 8.8 represent siloxane peaks that were evaluated. The peak widths at half height were manually measured within the ChromSpace 'slicer tool'. Peaks 1, 2, and 3 had peak widths of 58, 53 and 52 msec, respectively. The overall average injection bandwidth at half height was 54 msec with a 3.6% RSD. The

narrow reinjection bandwidths show the focusing capabilities of the SSM with comparable values to other thermal modulator platforms. This measurement was important because of the presence of wraparound peaks in the analysis of both the MRP and FA mixtures. With longer residence time within the ²D column peaks broaden significantly, obscuring the capabilities of a modulator platform. The injection bandwidths at half height should be kept in mind when evaluating the peak widths at half height, which will be discussed in Section 8.4.5.2.

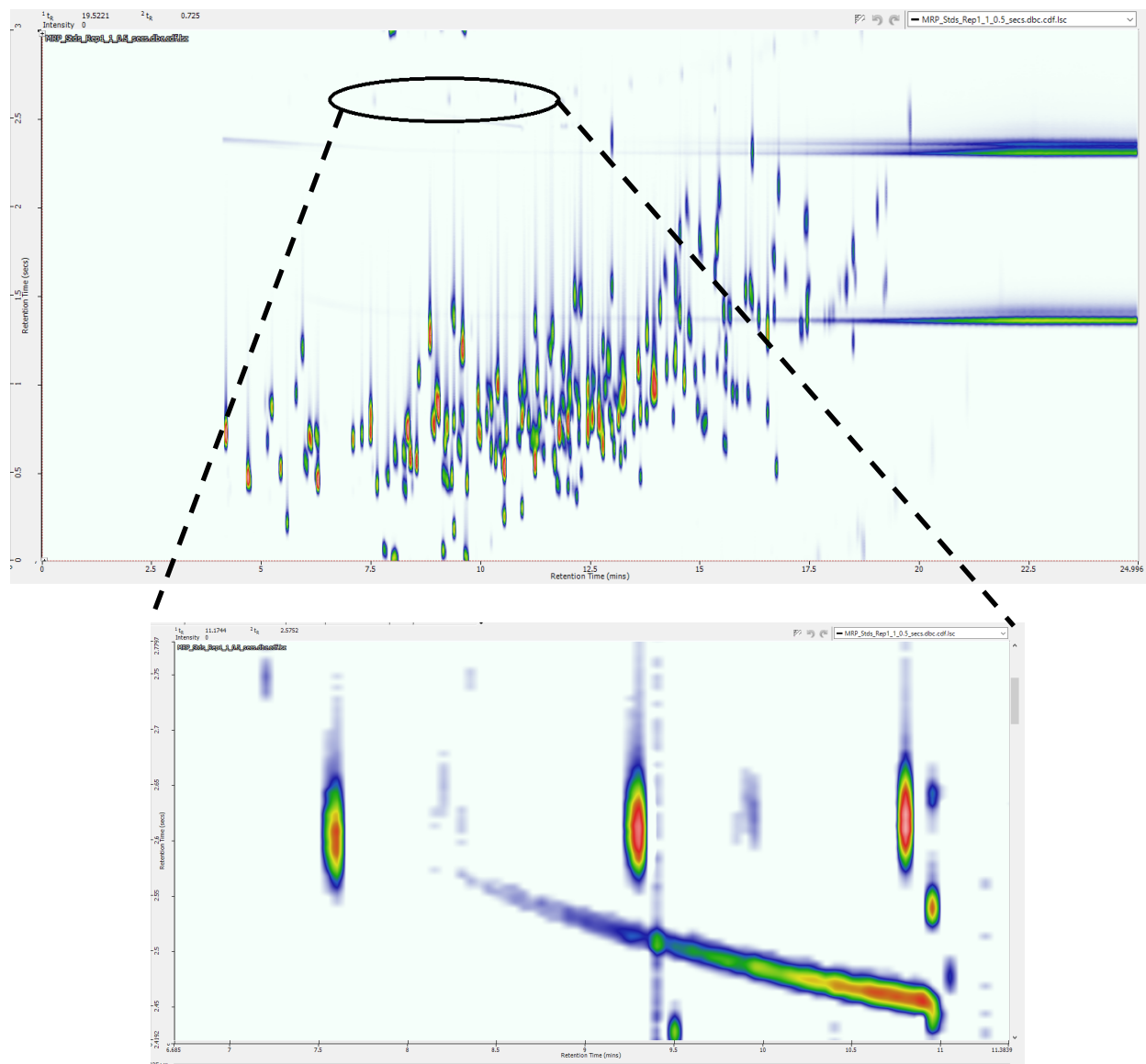


Figure 8.8 GCxGC-TOF-MS contour plot displaying the three siloxane peaks chosen for the analysis of re-injection bandwidths at half height.

8.4.5.2 Second dimension peak width

Second dimension peak width is a vital component of the evaluation of a modulator platform. This measurement evaluates the peak width at the outlet of the secondary column and the ability of the modulator to focus the band from the primary column. Widths determined from half height are of more value than those at the baseline due to the elimination of possible issues with baseline resolution as well as fronting and tailing nature of non-Gaussian peaks. Within the ChromSpace software, the 'slicer tool' allowed for precise determination of the secondary peak width of the largest slice per compound. However, the actual peak width was measured manually due to the software only reporting peak width at the base. In order to determine the peak width at half height, the half-height was determined from the total height provided in the software. At exactly half height, the retention times of the tail end and front end of the peak were recorded, and the peak width was calculated. The secondary retention time of the largest slice was then determined by taking the average value of the retention times recorded from the front and tail of the peak. The second-dimension retention time of the largest slice was required for the determination of the peak capacity in the second dimension, which will be discussed in Section 8.4.5.3.

To ensure the average second dimension peak width contained an appropriate representation of compounds across the entire secondary space, it was divided into several secondary retention bands of equal distance from one another. As the second-dimension retention time increases, the peak widths become greater due to the nature of chromatographic separation. In order to obtain an average peak width that is not biased, several peaks within each

retention band were chosen to represent the entire second dimension space. The spacing between the secondary retention bands was kept equal across the entire space. The distributions of peaks chosen for the MRP and FA mixtures are seen in Figs. 8.9 and 8.10, respectively. The second-dimension peak widths at half height for the MRP standard mixture ranged from 65 msec to 160 msec. The early eluting compounds, located in band 1 of the chromatogram, maintained a peak width below 75 msec, while the late eluting compounds, located in band 5, maintained a peak width greater than 120 msec. The average peak width at half height for the MRP standard mixture was 104 msec with an average %RSD of 3.9 % for the selected compounds of the five retention bands, as seen in Fig. 8.9.

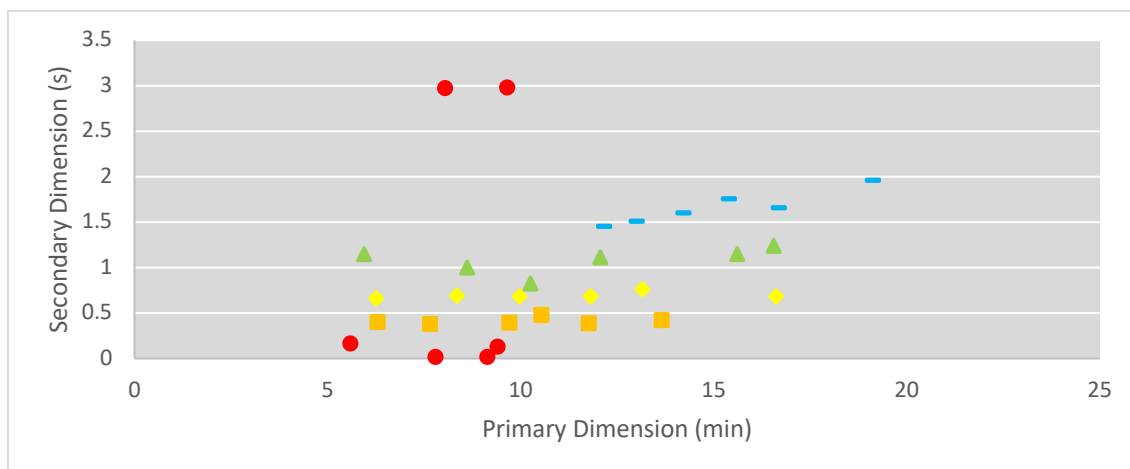


Figure 8.9 Placement of peaks chosen in five retention bands to properly evaluate the second-dimension peak width and second dimension peak capacity of the MRP analysis. The color and marker type correspond to the retention bands as follows: red circle band 1, orange square band 2, yellow diamond band 3, green triangle band 4, and blue dash band 5.

The second-dimension peak widths at half height for the FA standard mixture ranged from 112 msec to 450 msec. In comparison to the MRP standard mixture, the peak widths for the FA standard mixture were larger. With the substantial wraparound within the FA mixture, the

overall peak widths were inherently wider than those within the MRP mixture. The early eluting compounds, located in band 1 of the chromatogram, maintained a peak width below 150 msec, while the late eluting compounds, located in band 6, maintained a peak width greater than 250 msec. The average peak width at half height for the FA standard mixture was 196 msec with an average %RSD of 2.5% for the selected compounds of the six retention bands, as seen in Fig. 8.10. For complete optimization, a shorter secondary column could have been implemented to alleviate the excessive wraparound. With this alteration, the peak widths for the FA mixture should have smaller values. Although the peak widths for this analysis appear wide, it is important to remember the re-injection bandwidths were determined to be about 50 msec, as previously discussed in Section 8.4.5.1.

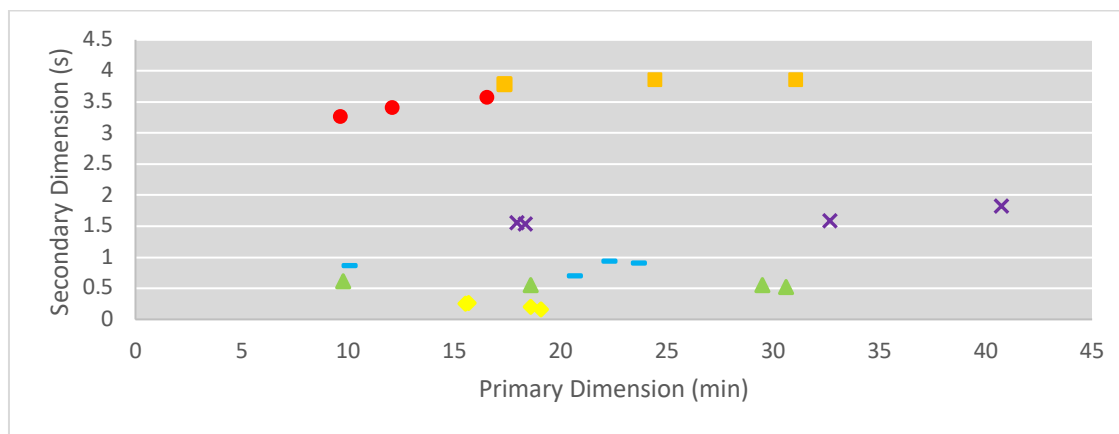


Figure 8.10 Placement of peaks chosen in six retention bands to properly evaluate the second-dimension peak width and second dimension peak capacity of the FA analysis. The color and marker type correspond to the retention bands as follows: red circle band 1, orange square band 2, yellow diamond band 3, green triangle band 4, blue dash band 5 and purple cross band 6.

Zoccali *et al.* found a profound effect on SSM performance when evaluating the change of intra-modulation column gas velocity and modulation column inner diameter dimensions [138]. The previous study found that a higher intra-modulation column gas velocity led to

incomplete trapping of analytes, causing breakthrough of lower molecular weight compounds, as seen in Fig. 8.11A [138]. More efficient trapping of lower molecular weight compounds was found with a lower intra-modulation column gas velocity, but at the cost of inferior chromatographic performance, as seen in Fig. 8.11D [138]. A similar trend was found with the lower molecular weight FA compounds. With a higher intra-modulation column gas flow, the analytes were trapped, however, the focusing within the modulation column and injection bandwidths on the secondary column were not consistent. Some compounds tended to broaden within the modulator column, causing them to be injected as a wide band when lower intra-modulation column gas flow was used.

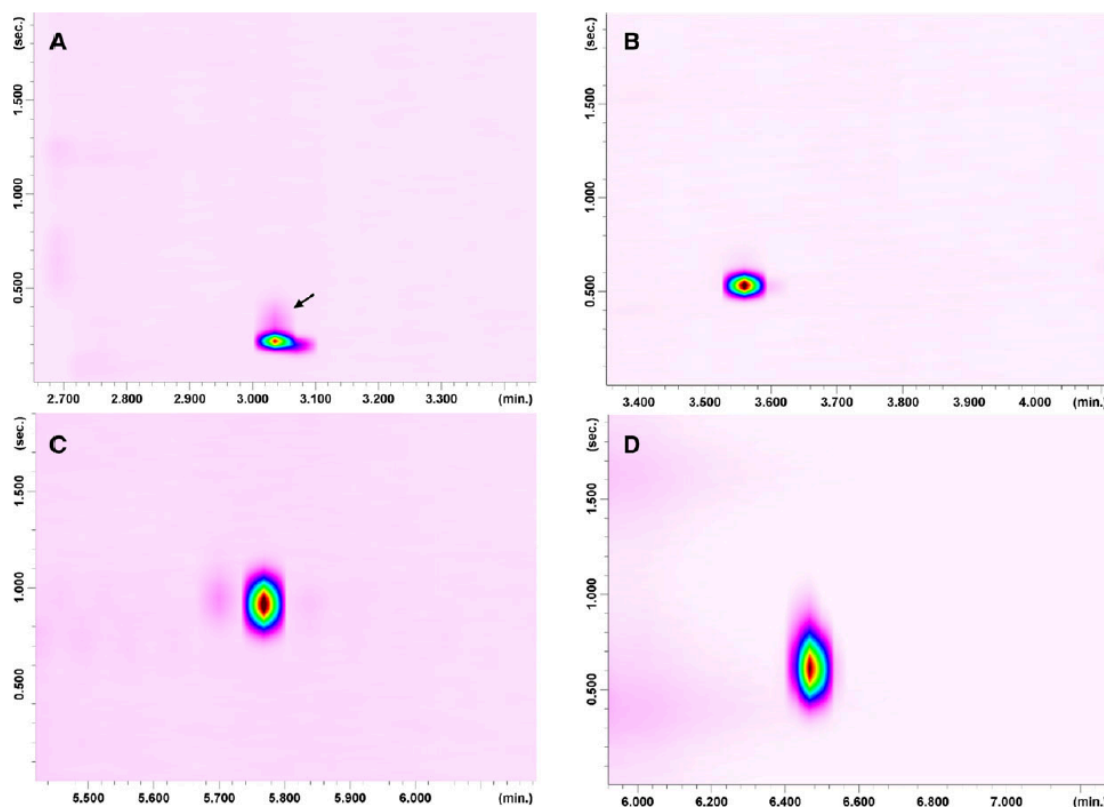


Figure 8.11 GC \times GC chromatograms utilizing the SSM displaying the n-alkane C₉ using modulation column average linear velocities of (A) 30 cm/s, (B) 25 cm/s, (C) 15 cm/s and (D) 13 cm/s. Reprinted with permission from [138].

8.4.5.3 Peak capacity in ²D

The peak widths at the base are required to determine the peak capacity of the second dimension. In lieu of utilizing the peak widths at the base provided by the ChromSpace software, the manually measured peak widths at half height were converted to peak widths at the base using the following relationship [139]:

$$w_b = \frac{(w_1 \times 4)}{2.35}$$

This process reduces uncertainties in peak widths caused by asymmetrical peaks.

Similar to the methodology employed for the determination of the peak widths at half height, specific compounds within secondary retention bands were used for the average peak width determination at the base. Peak capacity was then calculated by dividing the modulation period, or available separation space, by the average peak widths at base. With a modulation period of 3 seconds, the MRP standard mixture had a peak capacity of 17 in the second dimension. With a modulation period of 4 seconds, the FA standard mixture had a peak capacity of 12 in the second dimension.

8.5 Conclusions

A consumable-free thermal modulator platform was used for the analysis of a wide range of analytes and complex mixtures. Several criteria were chosen in order to evaluate the capabilities of the modulator, such as overall separation, primary and secondary retention time repeatability, peak area reproducibility, second dimension peak widths and second dimension

peak capacity. The modulator platform was successful in achieving adequate separation of a multiresidue pesticide mixture and fragrance allergens mixture. A summary of the evaluation criteria for both MRP and FA mixtures is presented in Table 8.D.8 of Appendix D. The retention time reproducibility was sufficient in the ¹D dimension. The overall timing of the initiation of the modulation process in regard to the GC analysis was poorly synchronized, causing irreproducible ²D retention times. The internal clock of the SSM should be in-tune with the GC clock in order to alleviate this problem. The peak area reproducibility was below 20% RSD for both mixtures. The secondary peak widths at half height were consistent with other thermal modulator platforms available on the market with secondary re-injection band widths of ~50 msec. The fragrance allergen mixture produced wider second dimension peaks when compared to the multiresidue pesticide mixture due to the long ²D column. A shorter ²D column could have been used to eliminate the wraparound; however, the direct comparison of both standard mixtures was more important. As a result, the secondary peak capacity for the pesticide mixture was greater than for the fragrance allergen mixture. Overall, with the ease of use and without the need for consumable cryogenics, the platform provides an affordable option for any user to achieve acceptable GC×GC by separating complex mixtures with sufficiently narrow second dimension peak widths.

Chapter 9. Characterization of bitumen using cryogen-free thermal modulation based comprehensive two-dimensional gas chromatography time – of – flight mass spectrometry (GC×GC - TOFMS)

9.1 Introduction

The solid-state modulator was previously evaluated on the operational capabilities to separate two standard mixtures. The platform was assessed based on the retention time reproducibility in ¹D and ²D, peak area reproducibility, ²D peak widths at half height and peak capacity in the ²D. The evaluation of the same modulator was expanded upon through the analysis of a complex mixture, such as bitumen. This platform has not been used for the analysis of bitumen previously. As a new application for the solid-state modulator, the platform was assessed on its ability to characterize bitumen, identify specific groups of compounds and identify any distinguishing biomarkers. Bitumen is a low grade of crude oil, made up of heavy hydrocarbons, that can be found in oil reservoirs [140]. Present as a thick, viscous fluid within oil reservoirs, it must be extracted from the ground. It is also the main fossil fuel component of oil sands, a natural mixture of sand, water and bitumen [141]. Drilling wells are used to recover the heavy bitumen, which cannot flow on its own. As a by-product of petroleum exploration and drilling, it is mainly used in the construction industry for paving and roofing [140]. Added as a

binder in asphalt, bitumen is used in paving roads, runways and parking lots. Also, it is used in roofing as a waterproofing compound to help seal and insulate.

As a highly complex mixture, bitumen contains a very large number of compounds belonging to many chemical compound classes. This leads to numerous co-elutions when utilizing traditional one-dimensional gas chromatography (1D GC). Comprehensive two-dimensional gas chromatography (GC×GC) coupled to time-of-flight mass spectrometry (TOFMS) has the ability to reduce the severity of these limitations by employing two different dimensions of separation and fast, full scanning capabilities of the TOFMS. Furthermore, GC×GC has the ability to identify biomarkers within crude oil or bitumen samples. Biomarkers are organic molecules that show resistance to chemical change and can assist in determining geological origin and environmental transformations [142, 143]. These compounds can assist in connecting crude oils to their source, indicate the maturity of the oil, as well as help identify the company responsible for the oil spill. Typically, the classes of primary biomarkers of interest in petroleum geochemistry include hopanes, terpanes, steranes and aromatic steroids [143].

GC×GC -TOFMS has successfully been employed for the qualitative and quantitative identification of biomarkers in various crude oil and bitumen samples. Aguiar et al. performed both group and individual biomarker characterization in Brazilian oils using GC×GC -TOFMS [142]. GC×GC allowed for greater separation compared to 1D GC, which allowed terpanes and steranes which usually co-elute to be separated. Hopanes and steranes, which share a similar fragment of 217 m/z, showed no overlap within the two-dimensional space. The C₃₀ hopane and C₃₀R demethylated homohopane, which typically co-elute in 1D GC, were separated with GC×GC. Also, for the first time in Brazilian oil samples, the demethylated tri- and tetracyclic terpanes were identified.

As the first study to separate hopane and 2 α -methylhopane with tentative spectral identification within Ceara Basin Oils from Brazil, this was a breakthrough in oil analysis [143]. Hopane and 2 α -methylhopane elute very close to one another when an apolar methylsilicone column is employed. Identification of these compounds are usually completed by GC-MS selective ion monitoring or GC-MS/MS transitions; however, both procedures do not provide mass spectra. Due to the coelution and identification problems, GC \times GC -TOFMS was used. The improved separation and enhanced response of GC \times GC -TOFMS allowed for the tentative identification of these compounds. Silva *et al.* employed GC \times GC -TOFMS to quantify biomarkers in oils from Colombia [144]. The ability to quantify the identified biomarkers is important for determining the origin of the petroleum, thermal maturity, biodegradation level and source correlations. The identification or absence of the biomarker is not a sufficient evidence for the identification of geochemical location or thermal maturity, hence the biomarker ratios must be provided. Silva *et al.* used the ratios in order to compare whether the oils have similar thermal maturity levels. GC \times GC -TOFMS proved again to be an appropriate tool by resolving typical 1D GC co-elutions and providing spectral deconvolution. Biomarker identification by GC \times GC -TOFMS was also shown as a powerful tool in studying the chemical attributes of asphaltene [145]. By studying the biomarkers and biomarker ratios, the thermal maturity was determined. More recently, GC \times GC coupled to a flame ionization detector (FID) and high-resolution time-of-flight mass spectrometer (HR-TOFMS) were employed to compare two crude oil spills in the Gulf of Mexico, Ixtoc I and Deepwater Horizon. Groups of chemicals and some individual species were positively identified by accurate mass spectra. The two oil spills of similar origin/type could be differentiated through GC \times GC environmental fingerprinting techniques. Furthermore, information on the degradation and weathering gained from post-spill

monitoring of Ixtoc I could be implemented for predicting the long-term outcomes of the Deepwater Horizon spill.

The identification of biomarkers has been shown to be important for petrochemical, geochemical and environmental industries; however, it is not an easy task due to the low concentrations of the biomarkers in highly complex matrices. In GC×GC, the choice of the modulator interface is a key consideration in obtaining the desired separation and identification of trace compounds. Typically, cryogenic thermal modulators are employed due to their superior focusing effect, resulting in an increase in S/N when compared to a 1D separation. This gain is very beneficial when analyzing trace compounds, making their identification not as challenging. However, some of these modulators require expensive cryogenic consumables. As an alternative to expensive cryogenic platforms, there are consumable-free models to decrease the costs involved. Also, heater-based thermal modulators offer a similar focusing effect without the need for cryogenes. The recently commercialized Solid-State Modulator (SSM) has shown promise in separating various mixtures. It has been employed among others to the analysis of kerosene, light cycle oil and diesel [146, 147, 148]. However, this platform has not been used yet to analyze very complex mixtures such as bitumen. The aim of this study was to implement the SSM for the analysis of bitumen by GC×GC -TOFMS for the first time. Group analysis was employed for a full characterization of bitumen. Furthermore, characteristic biomarker identification from extracted ion chromatograms was performed.

9.2 Experimental

9.2.1 Samples

An oil sand sample was obtained from Alberta (Canada). Solvent extraction was performed based on a previously established protocol for bitumen from oil sand [149]. Briefly, a ratio of solvent/oil sand of 5:3 (mL/g) was stirred at a velocity of 500 rpm for 30 minutes at a temperature of 50-60 °C. The extract was then evaporated to dryness. Two different solvents were used for the extraction process, cyclohexane and toluene. It is important to choose a solvent that promotes the bitumen to dissolve and a low boiling point, to allow easy solvent recovery [150]. Wang *et al.* studied various solvents to determine the best choice for bitumen recovery and asphaltene content determination in regard to their solubility parameter [149]. The solubility parameter is the dissolving capacity of a substance in a given solvent [149]. Cyclohexane was found to be an appropriate choice due to its medium solubility parameter and medium bitumen recovery, while toluene offered a slightly higher bitumen recovery and solubility parameter [149]. Despite the higher bitumen recovery, toluene has a higher boiling point than cyclohexane, and a lower boiling point is beneficial for the solvent extraction process [150].

9.2.2 Solid state modulator

Solid-state, thermal modulation was implemented for all analyses using SSM1810 thermal modulator from J&X Technologies (Shanghai, China) [39]. A more detailed description on the operational parameters of the SSM can be found in section 1.2.1.3.

9.2.3 Analysis conditions

An Agilent 6890 gas chromatograph (Agilent Technologies, Wilmington, Delaware, USA) with a split/splitless injector, an Agilent 7683 auto-sampler and LECO Pegasus III TOFMS (St. Joseph, MI, USA) were used for all analyses. A normal column configuration was used, which included a 30 m x 0.25 mm x 0.25 μm Rxi-5MS from Restek Corporation (Bellefonte, PA, USA) as the ¹D, and a 1.0 m x 0.25 mm x 0.25 μm Rxi-17MS from Restek Corporation as the ²D. HV series modulation column, capable of a modulation range from C₅ to C₃₀, was used for all analyses. The oven temperature program began at 100 °C for 5 minutes, then ramped to 200 °C at a rate of 2 °C/min and to 320 °C (held for 5 minutes) at a rate of 4 °C/min. All connections between the primary column, the modulation column and the ²D column were made using Pressfit Connectors for 0.25 mm columns (Restek Corporation). One microliter sample was injected into the injector operated in split mode with a 4-mm i.d. single taper inlet liner with fused silica wool. Helium gas (Praxair) with a purity of 99.999% was used as the carrier gas with a flow rate of 1.5 mL/min for all analyses. The TOF-MS was operated at an acquisition rate of 200 Hz and scanned from 35-600 amu. ChromaTOF software (LECO Corporation) was used for data acquisition, SSCenter software (J&X Technologies) was used for controlling the SSM platform, and ChromSpace (Markes International, Llantrisant, UK) was used for data processing. A different software package was used for data processing since the ChromaTOF software only acquired raw, one-dimensional data and was incapable of creating a two-dimensional chromatogram. The entry hot zone of the SSM was set at a +30°C offset, following the oven temperature program and capped to 320 °C. The exit hot zone was set at a +120 °C offset, following the oven temperature program and capped to 320 °C. The cold zone began at 9 °C, then ramped down to -50 °C for 28.8 minutes at a rate of 50 °C/min, then ramped

back to 9 °C for 57 minutes at a rate of 20 °C/min. A 6 s modulation period and 1 s desorption time were used for all analyses.

9.3 Results and discussion

9.3.1 Group-type identification

One of the key features of the two-dimensional contour plots is the “roof-tile” effect created by the placement of homologous groups within the two-dimensional space. With a non-polar ¹D stationary phase, the separation of non-polar compounds is based on volatility, while the semi-polar ²D stationary phase separates analytes based on their polarity. A reverse column set-up could also be used for greater separation of the non-polar compounds with the use of a non-polar ²D stationary phase. As compounds of similar nature and chemical composition elute in a contour plot, they appear in similar regions, allowing for group type identification to be completed. Total ion and extracted ion chromatograms were analyzed to perform a broad group type analysis using m/z 85 (paraffins), m/z 177 and 191 (demethylated terpanes and cyclic terpanes, respectively), m/z 191 (hopanes), and m/z 217 (alkylated steranes) [142, 151, 152]. Despite the same characteristic m/z, terpanes and hopanes were differentiated from one another based on their position within the ²D space. With a normal column configuration, terpanes elute before hopanes within the ²D [142]. As seen in Fig. 9.1, the bitumen samples have been separated into four general groups based on EICs. The paraffins (orange) could be found at the bottom of the separation space, eluting first within the second-dimension space. Due to their non-polar like nature, they did not have significant retention when analyzed on a semi-polar column.

The terpanes (green), steranes (red) and hopanes (purple) had similar retention on the non-polar ¹D column, making identification with 1D GC difficult. Each group had more retention on the semi-polar secondary column, allowing for clear distinction between the groups within the second-dimension space. This ordered nature is advantageous for homologous groups, especially when reference standards are limited or not available for positive identification. Bitumen extraction with toluene (Fig. 9.1A) and cyclohexane (Fig. 9.1B) produced similar results with very few differences. The elution patterns of the four main groups of compounds were comparable in both separations; however, the cyclohexane extract (Fig. 9.1B) contained more aromatic species, which will be discussed in Section 9.3.4.

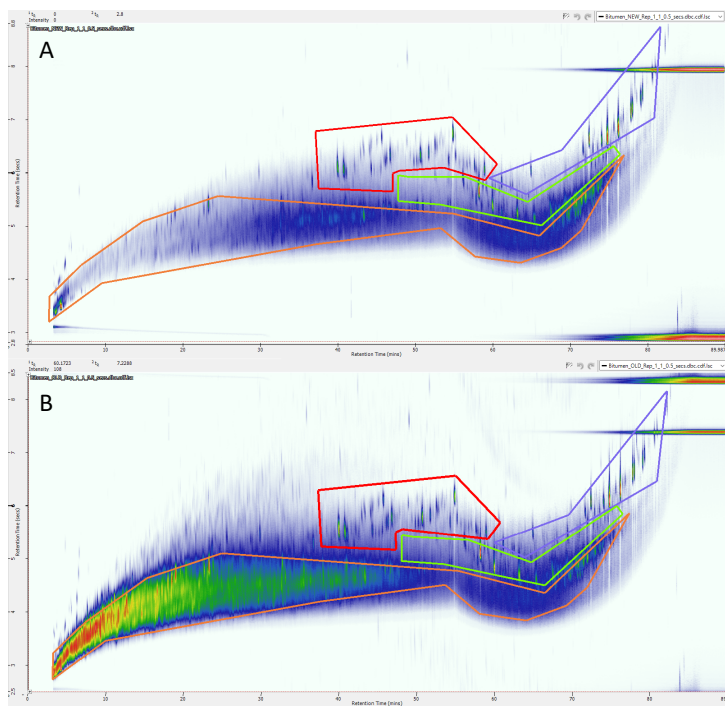


Figure 9.1 Group type identification of bitumen oil sands extracted with (A) toluene and (B) cyclohexane. The various colored boxes correspond to specific groups: paraffins (orange), alkylated steranes (red), terpanes (green) and hopanes (purple).

9.3.2 Biomarker analysis

The exploration and identification of biomarkers is an increasingly popular task in geochemical and petrochemical analyses. Their complex structure provides details on the parent organic molecules due to the little to no change in structure that occurs in sediments, rocks and crude oils over time, which helps determine the origin and maturity [153]. Understanding the origin and biochemistry of these biomarkers is important to distinguish the different life forms and environmental habitats that contribute to the source rock, sediment and petroleum [153]. There are three domains of life which distinguish the origin of the biomarker: archaea, eubacteria and eukarya [153]. Archaea and eubacteria are classified as prokaryotes, characterized by their biochemistry and habitats in which they grow and further classified based on their simple morphology. Eukarya is classified as eukaryotes, characterized by their morphology. Prokaryotes consist of millions of unicellular species [153]. Eukaryotes contain a membrane-bound nucleus and complex organelles [153]. Examples of eukaryotes include algae, protozoa, and fungi. Another important distinction between prokaryotes and eukaryotes are the type of lipid membrane [153]. Prokaryotes use hopanoids within the lipid membrane, while eukaryotes utilize steranes. This accounts for the large presence of steranes and hopanes in petroleum. Ultimately, lipids are the principle source of many compounds in petroleum, including the common saturated biomarkers [153].

To further break down the general groups identified in Section 9.3.1, EIC's specific to characteristic biomarkers were used to tentatively identify homologous groups. Three series of alkyl steranes, (1) C₂ & C₃, (2) C₄ & C₅ and (3) C₆ were identified in both extracted samples, indicated by the orange, purple and green boxes in Fig. 9.2, respectively. Specifically, m/z 245 and 246 (C₂ & C₃), m/z 287 and 288 (C₄ & C₅) and m/z 301 and 302 (C₆) were used. These

compounds were of relatively high abundance within the chromatogram and easy to identify visually since they were not at trace levels. Typically, these compounds are at low abundance and difficult to detect due to co-elutions with other steranes and methyl steranes [151]. Their presence can be used for oil-source rock correlations for origin determination [151, 154]. Cyclic terpanes, including tri-, tetra- and penta- series, were tentatively identified with m/z 191, noted as the white box in Fig. 9.2 [142, 151]. As a late eluting group in the first dimension and an early eluting group in the second dimension, the compounds correspond with having a relatively non-polar nature. This allowed for differentiation of the terpanes from the hopanes based on the roof-tile effect. These compounds were found in high abundance in both extracts, as seen in Fig. 9.2A and 9.2B. All species contribute to the terpane fingerprint in order to relate source rocks to oil samples, as well as to evaluate the thermal maturity and biodegradation of the oil [154]. It is suggested that most terpanes in petroleum samples originate from prokaryotic bacteria [154]. Methyl steranes are differentiated from alkyl steranes by monitoring the m/z 231, noted as the teal box in Fig. 9.2 [143, 151]. Found at trace levels, these compounds were not easy to identify in the TIC. The EIC assisted in making their presence more prominent. Methyl steranes have been suggested to assist in differentiating the presence of marine versus non-marine bacteria [154]. Diasteranes were identified by m/z 259, marked as the pink box in Fig. 9.2 [142, 153]. As seen in Fig. 9.2, these compounds lie within a section labeled as cyclic terpanes. Even with GC \times GC, the separation of diasteranes from the cyclic terpanes was not achieved. By using EIC with diagnostic ions, these two groups were identified, showing the power of the additional dimension of information that TOFMS brings to the analysis. A high diasteranes/sterane ratio within crude oils has been shown to be the result of high thermal maturity and/or high biodegradation [154]. Monoaromatic steranes stencils used m/z 253 (yellow box), while

triaromatic steranes stencils used m/z 231 (blue box) as seen in Fig. 9.2 [152, 153]. The monoaromatic steranes were found in slightly higher amounts than the triaromatic steranes. The latter species were difficult to visualize in the TIC, and EIC was required to confirm their presence within the sample. Due to biodegradation, the monoaromatic and triaromatic steranes are found in smaller quantities when compared to methylhopanes [152]. The monoaromatic species have been connected to determining the type of eukaryotic bacteria that was input in deposition environment of the oil sample [154]. Also, the triaromatic species are said to be more sensitive to thermal maturity since they originate from aromatization of monoaromatic species, which causes them to lose a methyl group [154]. The final group, methyl hopanes were identified with m/z 205 (red) [145]. These compounds were found in high abundance and easily identified. These compounds are helpful in determining the type of prokaryotic source input of the deposition environment [154].

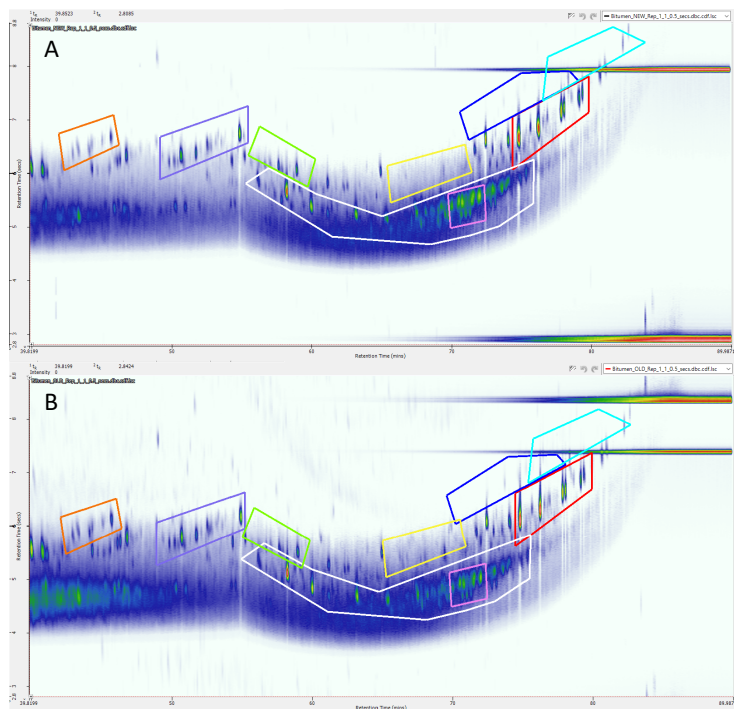


Figure 9.2 Biomarker analysis of bitumen oil sands extracted with (A) toluene and (B) cyclohexane. The colored boxes correspond to various biomarker groups: C2 & C3 alkylated steranes (orange), C4 & C5 alkylated steranes (purple), C6 alkylated steranes (green), cyclic terpanes (white), diasteranes (pink), monoaromatic steranes (yellow), triaromatic steranes (blue), methyl hopanes (red) and methyl steranes (teal).

9.3.3 Biomarker identification

Tentative identification of three specific established biomarkers; 24-ethyl-5 α (H)-14 β (H), 17 β (H)-20R-cholestane (C₂₉ $\alpha\beta\beta$ -20), 17 α (H)-22,29,30-trisnorhopane (T_m) and 17 α (H)-21 β (H)-hopane (H30), was carried out based on EIC and confirmation of the molecular ion peak. All three biomarkers were identified in both the toluene and cyclohexane extract bitumen oil sands samples. As seen in Fig. 9.3A, C₂₉ $\alpha\beta\beta$ -20, located at a primary retention time of about 71 minutes, was initially identified when evaluating the m/z 217 for steranes in the group analysis. The compound identity was confirmed based on an analogous mass spectrum found in the literature [145]. EICs assisted in extracting the individual compounds since cyclic terpanes and

diasteranes were found in low abundance and overlapping within the biomarker region.

Typically, the $C_{29}\alpha\alpha\alpha-20$ isomer ratios are specific for the immature-to-mature range and will increase proportionally with thermal maturity [145]. However, it is suggested that the $C_{29}\alpha\beta\beta-20$ can be used in combination with the $C_{29}\alpha\alpha\alpha-20$ to determine the levels of thermal maturity [145]. Also, the ratio of diasteranes to steranes has been used in distinguishing crude oil from carbonate and shale source rocks.

Fig. 9.3B displays the mass spectra for the characteristic hopane T_m , based on the EIC for m/z 191 and corresponding mass spectra found in the literature [145]. This compound is of great significance due to its use in determining the thermal maturity based on the ratio between T_m and $18\alpha(H)-22,29,30$ -trisorneohopane (T_s). When the ratio $T_s/(T_s+T_m)$ increases, the oil is determined to be more mature due to the greater thermal stability of T_s compared to T_m [145, 155]. A high ratio may also be indicative of bitumen from a hypersaline source rock [154]. The T_m species was extremely prominent in the bitumen oil sands; however, the T_s species was not detected. This may suggest a relative immaturity of the oil; however, an authentic standard or further mass spectral investigation would be required to ensure T_s was not present.

The final compound, H30, was tentatively identified utilizing the same EIC m/z 191 as T_m ; however, the molecular ion was different, as seen in Fig. 9.3C [145]. Upon further investigation, this compound was tentatively identified as one of three petroleum biomarkers, namely $17\beta-21\beta$ -hopane and $17\beta-21\alpha(H)$ -hopane, within a stereoisomeric series of hopanes ranging from C27-C35 [154]. H30 is characteristic of greater thermodynamic stability when compared to the other series and the $\beta\beta$ series are typically not found in petroleum due to their thermal instability during catagenesis [153]. The presence of H30 was distinct within the bitumen oil sands and was identified based on the corresponding mass spectra published in the

literature [145]. This compound is indicative of bacteriohopanetetrol and bacteriohopanes as precursors in source rocks and crude oil [153]. However, this compound is similar in nature to Gammacerane, a non-hopanoid triterpane, which contains the same formula ($C_{30}H_{52}$), molecular ion of m/z 412 and diagnostic fragment ion of m/z 191 [153]. This compound has been found to be more resistant to biodegradation than hopanes and highly specific to water-column stratification during source-rock deposition [154]. When large amounts of Gammacerane are present in crude oil, it is indicative of hypersaline conditions during deposition [154]. Without an authentic standard, positive identification of this compound could not be confirmed. The tentative identification of 24-ethyl-5 α (H)-14 β (H), 17 β (H)-20R-cholestane ($C_{29}\alpha\beta\beta$ -20), 17 α (H)-22,29,30-trisnorhopane (T_m) and 17 α (H)-21 β (H)-hopane (H30) were also carried out within the cyclohexane extract and can be found in Appendix E.

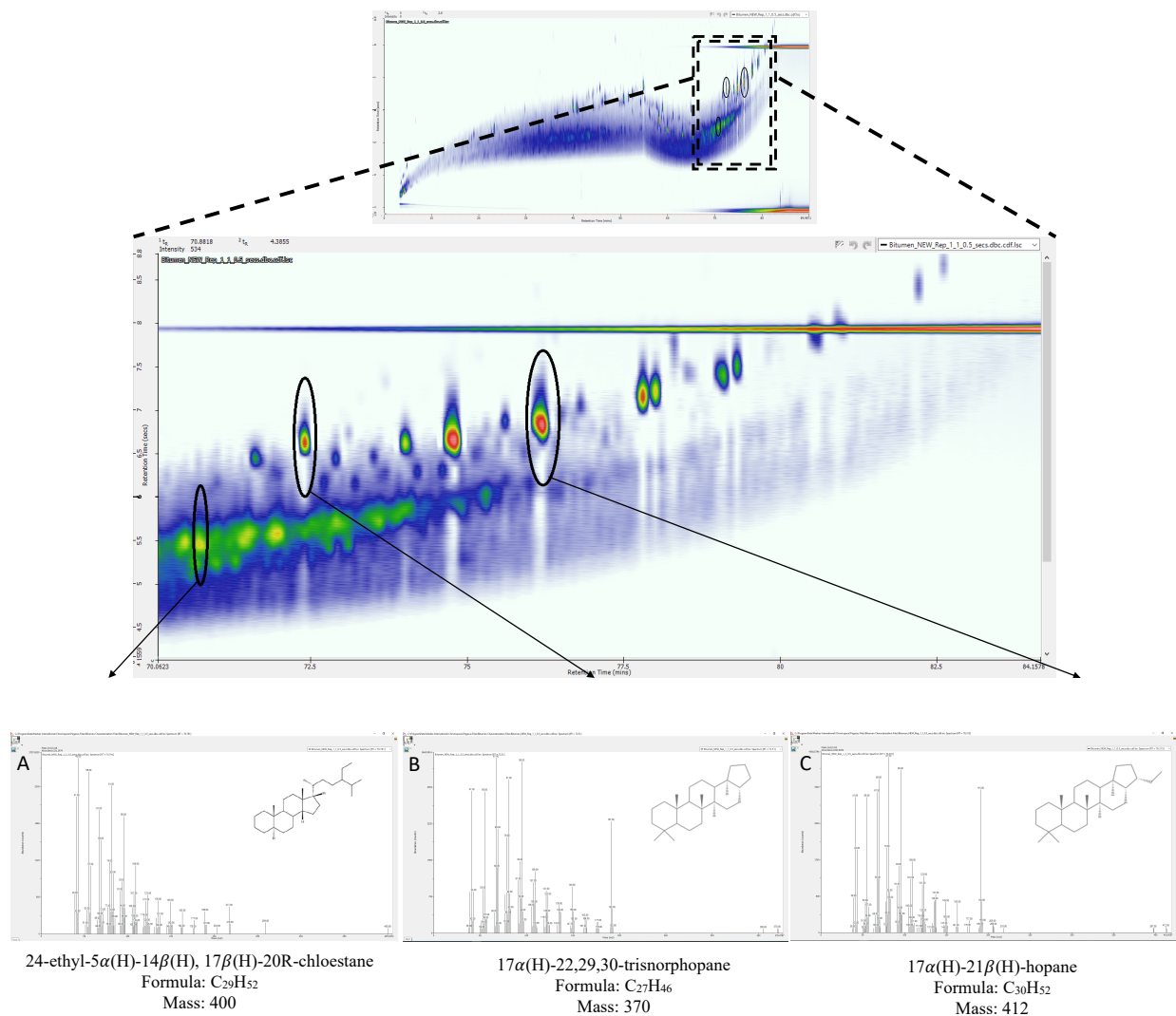


Figure 9.3 Tentative identification of three characteristic biomarkers in the biomarker region of the toluene extract. The compounds (A) 24-ethyl-5 α (H)-14 β (H), 17 β (H)-20R-cholestane (C₂₉ $\alpha\beta\beta$ -20), (B) 17 α (H)-22,29,30-trisnorhopane (T_m), and (C) 17 α (H)-21 β (H)-hopane (H30) were identified by EIC and molecular ion peak.

A noteworthy compound was detected within the methyl hopane region, as seen in Fig. 9.4; however it could not be identified. Initially, the compound was believed to be 2 α -methyl-hopane C31 (2 α MH C31), based on the EIC m/z 205 and identification in the literature [142]. Research shows that 2 α MH is indicative of oxygen producing cyanobacteria and commonly found in samples of marine origin [144, 154]. On the other hand, it has also been shown that

thermally mature oils from carbonate source rocks have the highest 2α MH indices, due to 2α MH requiring cracking from kerogen to be present, which is an uncommon process in immature bitumen [154]. After further assessment, it was clear that the ratio of ions m/z 191 and 205 did not agree with that of 2α MH C31. Furthermore, the bitumen oil sands sample did not contain an m/z 259 ion. With a higher retention in both dimensions than the previously identified hopanes and intense m/z 191 fragment in comparison to the m/z 205 fragment, the compound was tentatively classified as a C31 late-eluting terpane [143].

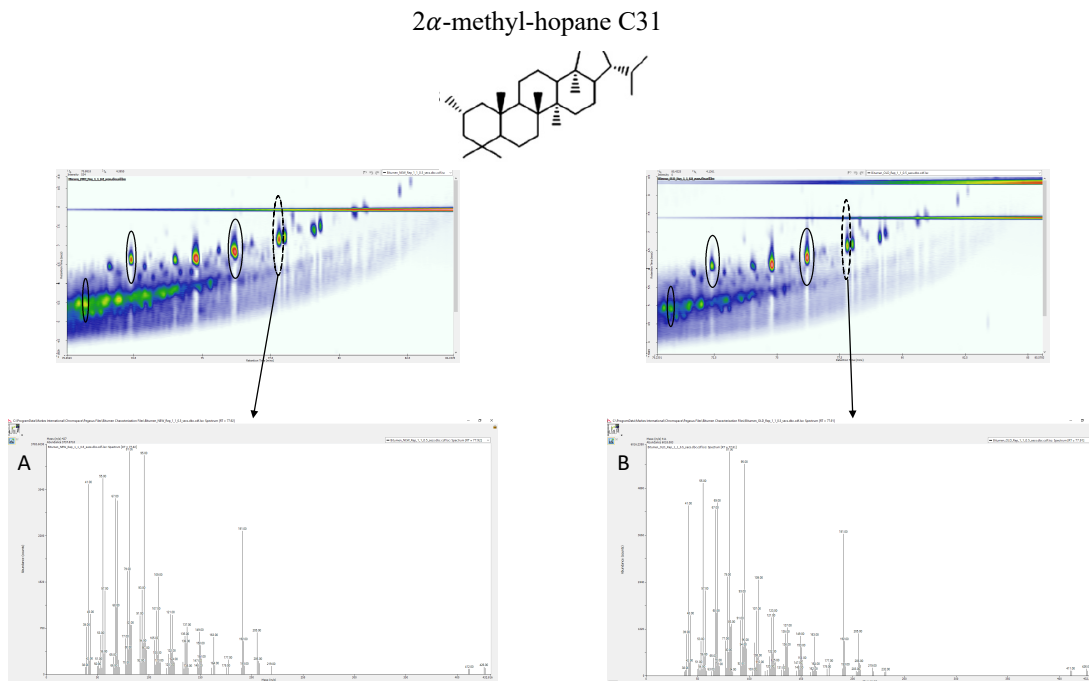


Figure 9.4 Mass spectrum of a C31 late-eluting terpane found in (A) toluene bitumen oil sands extract and (B) cyclohexane bitumen oil sands extract.

9.3.4 Differences between extraction solvents

As previously mentioned, the cyclohexane extract contained more aromatic hydrocarbons than the toluene extract. Monoaromatic and triaromatic steroids based on m/z ions 253 and 231, respectively, were identified in both extracts. Specifically, aromatic species including naphthalenes, phenanthrenes, and polycyclic aromatic hydrocarbons with 4, 5 and 6 rings were only identified in the cyclohexane extract. Since they are typically found in high abundance within crude oils, their identification is of great importance [153]. In order to properly identify these compounds within such a complex mixture, the correct extraction solvent and analytical technique are required. Naphtha has previously been established as a good solvent for separating bitumen from oil sands due to the low toxicity, good quality and high recovery of bitumen [149]. Despite these advantages, naphtha does not extract the heavy compounds, leading to an incomplete extraction [149]. Cyclohexane was a better option as the extraction solvent in comparison to toluene due to the alicyclic structure and non-polar hydrophobic nature. In literature, cyclohexane has proven to be the solvent of choice due to the high recovery, low solid content in the extracted bitumen, low toxicity, and high solvent removal rate [149, 156, 157].

As seen in Fig. 9.5, three aromatic groups have been differentiated based on the characteristic m/z ions [153]. The various diagnostic ions were evaluated in both the cyclohexane and toluene extracts; however, these specific aromatic groups only appeared within the cyclohexane extract. The 4-ring, 5-ring, and 6-ring aromatics were identified by m/z ions 202, 252 and 276, respectively. Late eluting within the secondary dimension, these compounds were present in relatively low abundance. The EIC for each group made their presence more prominent amongst the other highly abundant species. The red, blue and green boxes label the 4-ring, 5-ring and 6-ring aromatics, respectively. Despite only using an EI source, group-type

analysis of the aromatic hydrocarbons present within the bitumen sample was possible. For further identification of individual species, FI or PI would be beneficial additions to the GC×GC separation.

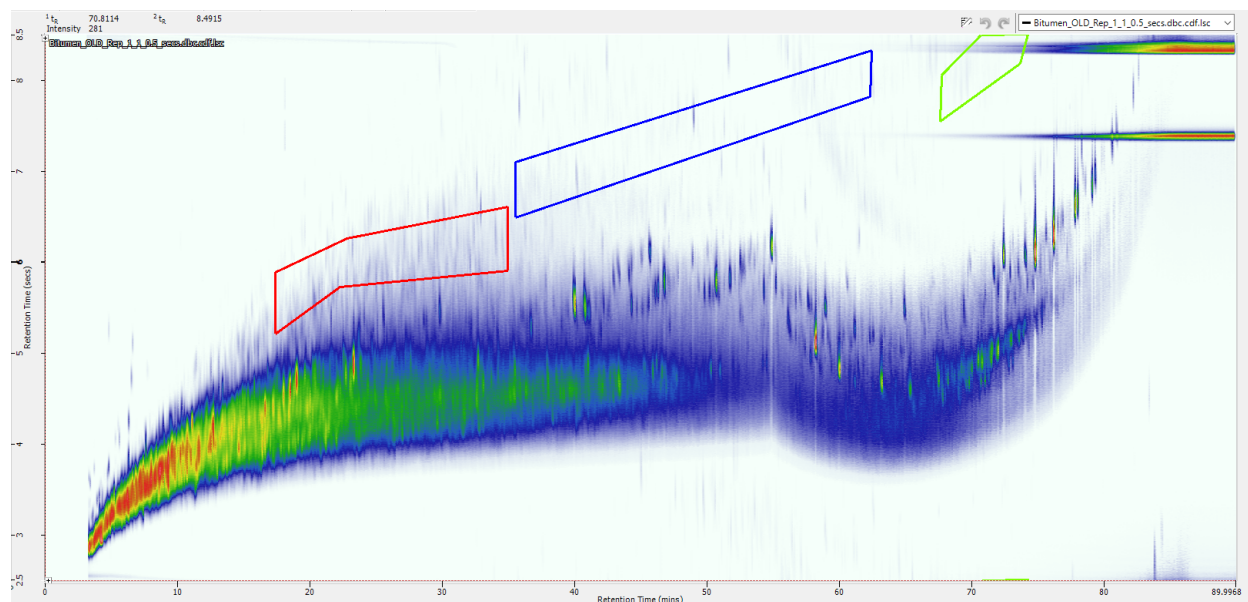


Figure 9.5 Aromatic hydrocarbons found within the cyclohexane extract of bitumen oil sands. The colored boxes correspond to various aromatic groups: 4-ring aromatics (red), 5-ring aromatics (blue) and 6-ring aromatics (green).

9.4 Conclusions

Cryogen-free thermal modulation was successfully used with GC×GC-TOFMS for the analysis of bitumen oil sands for the first time. Without the need for expensive cryogenics, the SSM offers an alternative platform with comparable performance to other commercial thermal interfaces. Total group and biomarker analysis were performed to differentiate classes of homologous compounds within a complex matrix. Detailed characterization of these groups was performed using extracted ion chromatograms for diagnostic m/z ions. Distinguishing biomarkers, including 24-ethyl-5 α (H)-14 β (H), 17 β (H)-20R-cholestane ($C_{29}\alpha\beta\beta$ -20), 17 α (H)-

22,29,30-trisnorhopane (T_m) and $17\alpha(H)$ - $21\beta(H)$ -hopane (H30) were tentatively identified based on EIC and confirmation of the molecular ion. Their determination is vital in evaluating the thermal maturity, source rock and oil origin, and possible precursor bacteria and biodegradation processes involved. Cyclohexane and toluene extracts were compared on their ability to fully characterize the extracted bitumen from oil sands. Toluene was able to extract the majority of the saturated hydrocarbons and aromatics, however, cyclohexane proved to be the more appropriate choice. Cyclohexane allowed full extraction of saturated hydrocarbons as well as all aromatic hydrocarbons including aromatic steroids and polycyclic aromatic hydrocarbons. Overall, GC×GC-TOFMS with an SSM platform can be applied for the analysis of biomarkers in bitumen.

Chapter 10. Summary and future work

10.1 Summary

GC×GC provides superior separation through the use of two orthogonal columns, placed in series to overcome the limitations of 1D GC. To preserve the separation achieved within the ¹D and further separate analytes in the ²D, a modulating interface must be placed between the two columns. As the ‘heart’ of a GC×GC system, modulators have significantly evolved over the years to further enhance the separation power achievable with this analytical technique. With the many commercial and experimental platforms available, it can be challenging to determine which best suits the desired application. It is important to understand the operational capabilities of each platform including modulation volatility range, ²D retention time reproducibility, ²D peak widths and peak capacity. Currently, there is no universal modulator, and each has its advantages and disadvantage. In search of an ideal modulator for GC×GC, various modulator platforms were optimized, evaluated or improved upon if possible.

In the work presented in this thesis the coating within the trapping capillary of the UW single-stage, consumable-free, thermal modulator was optimized. In an attempt to recreate the sorptive surface with carbon-doped silica nanoparticles originally created by Edwards, several Restek stationary phases (MXT-1 #1, #2 and #3) were subjected to various treatment plans. Through chromatographic evaluation, SEM and EDX, it was evident that the starting material that was used by Edwards was different from that of the MXT-1 (#1, #2 and #3) columns that were tested. Due to the change in the manufacturing process of the Restek MXT-1 deactivation layer, an alternative column from a different manufacturer was investigated. DB-PS1 and DB-

PS2887 from Agilent Technologies were initially subjected to a similar treatment plan that was previously established by Edwards. Both phases provided satisfactory separation of diesel. To further optimize the coating within DB-PS1 and DB-PS2887 after treatment, various treatment plans were applied to determine an appropriate range of voltages. A range of 40 V to 50 V were necessary for DB-PS1, while 40 V followed by 35 V were more appropriate for DB-PS2887. It was concluded that treatment of the entire capillary resulted in a strong adsorbent that could not efficiently release the trapped analytes in a quick manner. Various sections of the trapping capillaries were then treated with varying voltages to create a section of the phase that was more adsorbent than the other. Specifically, DB-PS1 #42 was superior to all other phases. The trapping capillary was treated for ten minutes at 45 V followed by two five-minute phases at 40 V on one half, while 40 V was applied for ten minutes followed by two five-minute phases at 35 V on the other half. Configuration B was better because the more adsorbent material effectively focused the trapped analytes and completely released the analytes onto the ²D column in a quick manner. This resulted in a superior separation of a diesel sample without any streaking in the ²D, while also operating at lower modulation voltages. After treatment, nanoparticles were created within DB-PS1 #42. The half that was treated with 45 V had a uniform surface completely covered in spongy nanoparticles, while the half treated with 40 V had a smaller abundance of nanoparticles. In comparison to the DB-PS1 phase, DB-PS2887 performed inferior and was deemed an inferior choice. An optimal set of treatment parameters were obtained for an alternative material for the trapping capillaries within the UW thermal modulator.

Improvements to the UW thermal modulator design were also implemented to prevent hot spots, or poorly cooled areas at the ends of the trapping capillary. Changing the original rectangular shape of the ceramic cooling pads to a new trapezoidal design provided effective

cooling to the entire length of the trapping capillary. With complete coverage, the potential for pyrolysis was vastly reduced. In an effort to eliminate the streaking in the ²D for some capillaries, the adsorbent layer from the portions of the trapping capillary located within the unions was removed. The streaking was not completely eliminated in some cases, but the separation of late eluting compounds was improved due to fewer co-elutions. Despite the improvements, the removal process was not reproducible. Further improvements were required, unless the need for the removal of the adsorbent layer from the unions was not necessary, as was the case for the DB-PS1 #42 trapping capillary.

The separational capabilities of the UW thermal modulator were evaluated through a comparison to a commercially available flow-based platform for the analysis of several conventional and synthetic engine oils of various viscosities and brands. A direct comparison was not possible due to the differing operational parameters of the two modulator platforms. Both platforms were optimized accordingly to their operational parameters. The differences amongst the engine oils was established based on the distribution of hydrocarbons within the UCM. Overall, both platforms achieved an adequate separation of the various engine oils. The thermal modulator produced less wraparound of the isothermal portion of the analysis, which allowed for greater differentiation of analytes from the UCM. The flow modulator could not accommodate a longer ²D column, hindering the elution of a distinct group of substituted ADPAs. Soft ionization was employed to assist in tentatively identifying monononyl and dinonyl diphenylamines in all samples. Neither model was deemed superior as a direct comparison between the thermal and flow platforms was not possible. A comprehensive separation of specific classes of compounds and differentiation of engine oils was achieved with both platforms. The aim is to publish this work in the future to a journal in a related field.

Alteration of a commercial flow modulator was also performed to test a proof of concept hybrid interface. Through the addition of a cryogen-free focusing mechanism, adequate 2D re-injection band widths were achieved for less volatile analytes at 2D flow rates compatible with mass spectrometric detection. The 0.5 μm and 3.0 μm film traps were superior in providing significant focusing in comparison to the 5.0 μm film trap. Too much cooling in combination with a thick film resulted in excessive tailing in the 2D due to analytes not being desorbed efficiently. This would require a hot jet to properly remobilize the strongly trapped analytes. Alternatively, increasing the cooling air temperature with the oven throughout the run would decrease the strong sorption within the thick film. The 3.0 μm film trap provided too much retention in comparison to the 0.5 μm film trap. The 0.5 μm and 3.0 μm traps provided an average decrease in peak width of 43% and 18%, respectively. The uninsulated copper line achieved a substantially narrower peak width for the heavy compounds, emphasizing the benefits of allowing the cooling air to follow the oven temperature during the analysis. The hybrid system employed the advantages of both thermal and flow-based platforms and proved to be a promising design.

Finally, the evaluation of a recently introduced commercial thermal modulator and its ability to analyze bitumen were completed. Previous evaluations of the SSM were expanded upon by determining the operational capabilities to analyze two standard mixtures of different volatilities. The modulator was successful in achieving an adequate separation of a multiresidue pesticide mixture and a fragrance allergens mixture. The 1D retention time reproducibility was sufficient for both mixtures. Irreproducible 2D retention times were caused by the unsynchronized timing of the initiation of the modulation process in regard to the GC analysis. The 2D peak widths at half height were consistent with other thermal platforms on the market.

The ^2D peak widths produced by the fragrance allergen mixture were significantly wider when compared to the multiresidue pesticide mixture. The secondary re-injection band widths were subsequently evaluated at ~ 50 ms. Ultimately, it was concluded that the long ^2D column was the cause of the wider peak widths for the fragrance allergens mixture. A shorter ^2D column would have alleviated the wraparound; however, the direct comparison of both standard mixtures was more important. Overall, the SSM provided an affordable option to achieve acceptable GC \times GC without the need for consumable cryogenes. The evaluation was further expanded upon through the analysis of bitumen, which had not been previously accomplished with the SSM. Total group and biomarker classification were performed to differentiate homologous compounds within a complex matrix. Three distinguishing biomarkers, including 24-ethyl-5 α (H)-14 β (H), 17 β (H)-20R-cholestane ($\text{C}_{29}\alpha\beta\beta$ -20), 17 α (H)-22,29,30-trisnorhopane (T_m) and 17 α (H)-21 β (H)-hopane (H30) were tentatively identified based on their molecular ion and diagnostic fragments. Two different extraction solvents, cyclohexane and toluene, were compared on their ability to extract relevant compounds of bitumen from oil sands. Both solvents extracted the majority of the relevant compound classes; however, cyclohexane proved to be a more appropriate choice. In conclusion, the SSM could be successfully applied for the analysis of biomarkers in bitumen. The intention is to publish this work in journals in related fields.

The work presented in this thesis provides an in-depth examination of various modulators to determine the ideal platforms for GC \times GC. The UW thermal modulator was optimized by determining an appropriate alternative starting material for the trapping capillaries. Through various treatment evaluations, an optimal plan was achieved. The changes which occur to the stationary phase during the treatment process to create an ideal trapping phase were studied in detail. The trapping capillary must not be too adsorbent, otherwise trapped analytes are not

released quickly and completely for further separation. For thin stationary phases, the formation of sorbent nanoparticles is required for proper operation, while for thick stationary phases it is not necessary. Furthermore, the combination of two phases of differing adsorptivity within a single trapping capillary allowed the trapped analytes to be further focused before complete desorption. The comparison, improvement and evaluation of commercial modulators provided a better understanding of the benefits and limitations of these designs. This understanding is critical in the search of an ideal modulator for GC×GC.

10.2 Future work

To improve the treatment process and applicability of the trapping capillaries of the UW thermal modulator, several modifications are needed. First, the evaluation of different treatment gases could be performed. Compressed house air has always been implemented during the treatment process to assist in the proper transformation of the stationary phase to an adsorbent material for trapping and desorption of analytes. Based on the SEM and EDX results obtained for the untreated portion of DB-PS1 #41, it begs the question as to if the oxygen is necessary for transformation. Inert gases such as helium or argon should be investigated to assess the transformation of the stationary phase when supplied during the treatment process. Additionally, constant heating with a laboratory oven should be investigated. Capacitive discharge has always been implemented as the source of heating during the treatment process; however, this method offers an alternative mechanism. Most ovens easy to use and programable up to 1000 °C. As previously mentioned, the process of adsorbent removal from the unions at both ends of the trapping capillary should be improved to achieve consistent results when necessary to improve modulation. Mineral acids and bases could be applied to remove the polysiloxane stationary

phase within these sections of the trapping capillary. Sulfuric and nitric acid and potassium hydroxide are quite damaging to the phase in columns [158]. Other options that cause the least amount of damage to the stationary phase include hydrochloric acid or ammonium hydroxide [158]. By treating the areas of the trapping capillary with an acid or base, the stationary phase could be removed in a more uniform and reproducible fashion. A thorough investigation of the various concentrations of acids and bases, as well as the time applied would have to be performed to obtain the optimal removal of the stationary phase. DB-PS1 #42 produced very promising results when placed in configuration B; however, diesel was the only sample analyzed. To ensure the treatment process applied to create DB-PS1 #42 is the optimal set of parameters, various samples of ranging volatilities and polarities should be analyzed. Finally, a full evaluation of the modulator should be performed. This should include analysis of a wide range of compounds and concentrations to determine the dynamic range of the modulator.

Improvement of commercial modulators could produce an ideal platform for GC×GC. The hybrid interface based on modified flow modulator is a promising proof of concept. Alternative film thicknesses, such as 1.0 μm, should be evaluated. This thickness could be a possible compromise for the proper amount of retention to trap analytes without causing too much broadening during remobilization. Furthermore, a vortex cooler or thermoelectric coolers could be implemented to provide a substantial decrease in cooling temperature to trap the more volatile compounds. These cooling methods could then be programmed to decrease the amount of cooling as the analysis progresses. This should assist in achieving trapping of the more volatile compounds, while also achieving complete desorption of the heavier molecular weight compounds. The final goal is to develop a protocol for the evaluation of various modulators and test all possible varieties. This should include cryogenic platforms, which were not previously

tested. Quantitative comparative measurements between modulator systems could also offer an in-depth understanding of the quality of the modulators. Through the use of standard reference mixtures, such as the Century mix or Mega-Mega mix, various platforms could be directly compared on their ability to identify and quantify compounds within a complex mixture at various concentration ranges. Software platforms could assist in the evaluation of these standard mixtures in terms of the number of compounds separated above a chosen signal-to-noise ratio.

References

- [1] F. J. Santos and M. T. Glaceran, "The application of gas chromatography to environmental analysis," *Trends in Analytical Chemistry*, vol. 21, pp. 672-685, 2002.
- [2] T. Górecki, J. Harynuk and O. Panic, "The evolution of comprehensive two-dimensional gas chromatography (GC×GC)," *Journal of Separation Science*, vol. 27, pp. 359-379, 2004.
- [3] A. Mostafa, M. Edwards and T. Górecki, "Optimization aspects of comprehensive two-dimensional gas chromatography," *Journal of Chromatography A*, vol. 1255, pp. 38-55, 2012.
- [4] J. C. Giddings, "Two-dimensional separations: concept & promise," *Analytical Chemistry*, vol. 56, pp. 1258A-1270A, 1984.
- [5] C. J. Venkatramani, J. Xu and J. B. Phillips, "Separation orthogonality in temperature-programmed comprehensive two-dimensional gas chromatography," *Analytical Chemistry*, vol. 68, pp. 1486-1492, 1996.
- [6] J. Phillips and Z. Liu, "Comprehensive two-dimensional gas chromatography using an on-column thermal modulator interface," *Journal of Chromatographic Science*, vol. 29, pp. 227-231, 1991.
- [7] M. Edwards, A. Mostafa and T. Górecki, "Modulation in comprehensive two-dimensional gas chromatography: 20 years of innovation," *Analytical Bioanalytical Chemistry*, vol. 401, pp. 2335-2349, 2011.
- [8] R. E. Murphy, M. R. Schure and J. P. Foley, "One- and two-dimensional chromatographic analysis of alcohol ethoxylates," *Analytical Chemistry*, vol. 70, pp. 1585-1594, 1998.
- [9] W. Khummueng, J. Harynuk and P. Marriott, "Modulation ratio in comprehensive two-dimensional gas chromatography," *Analytical Chemistry*, vol. 78, pp. 4578-4587, 2006.
- [10] P. Marriott and R. Shellie, "Principles and applications of comprehensive two-dimensional gas chromatography," *Trends in Analytical Chemistry*, vol. 21, pp. 573-583, 2002.
- [11] R. Ong and P. Marriott, "A review of basic concepts in comprehensive two-dimensional gas chromatography," *Journal of Chromatographic Science*, vol. 40, pp. 276-291, 2002.

- [12] T. Górecki, O. Panic and N. Oldridge, "Recent advances in comprehensive two-dimensional gas chromatography (GC×GC)," *Journal of Liquid Chromatography & Related Technologies*, vol. 29, pp. 1077-1104, 2006.
- [13] V. Cuzuel, A. Sizun, G. Cognon, I. Rivals, F. Heulard, D. Thiebaut and J. Vial, "Human odor and forensics. Optimization of a comprehensive two-dimensional gas chromatography method based on orthogonality: How not to choose between criteria," *Journal of Chromatography A*, vol. 1536, pp. 58-66, 2018.
- [14] J. Dallüge, J. Beens and U. T. Brinkman, "Comprehensive two-dimensional gas chromatography: a powerful and versatile analytical tool," *Journal of Chromatography A*, vol. 1000, pp. 69-108, 2003.
- [15] J. A. Murray, "Qualitative and quantitative approaches in comprehensive two-dimensional gas chromatography," *Journal of Chromatography A*, vol. 1261, pp. 58-68, 2012.
- [16] M. S. Klee, J. Cochran, M. Merrick and L. M. Blumberg, "Evaluation of conditions of comprehensive two-dimensional gas chromatography that yield a near theoretical maximum in peak capacity gain," *Journal of Chromatography A*, vol. 1383, pp. 151-159, 2015.
- [17] J. Blomberg, T. Riemersma, M. v. Zuijlen and H. Chaabani, "Comprehensive two-dimensional gas chromatography coupled with fast sulphur-chemiluminescence detector: implications of detector electronics," *Journal of Chromatography A*, vol. 1050, pp. 77-84, 2004.
- [18] R. Ruiz-Guerrero, C. Vendevre, D. Theibaut, F. Bertoncini and D. Espinat, "Comparison of comprehensive two-dimensional gas chromatography coupled with sulfur-chemiluminescence detector to standard methods for speciation of sulfur-containing compounds in middle distillates," *Journal of Chromatographic Science*, vol. 44, pp. 566-573, 2006.
- [19] K. A. Schug, I. Sawicki, D. D. Carlton, Jr., H. Fan, H. M. McNair, J. P. Ninmo, P. Kroll, J. Smuts, P. Walsh and D. Harrison, "Vacuum ultraviolet detector for gas chromatography," *Analytical Chemistry*, vol. 86, no. 8329-8335, 2014.
- [20] T. Gröger, B. Gruber, D. Harrison, M. Saraji-Bozorgzad, M. Mthembu, A. Sutherland and R. Zimmermann, "A Vacuum Ultraviolet Absorption Array Spectrometer as a Selective Detector for Comprehensive Two-Dimensional Gas Chromatography: Concept and First Results," *Analytical Chemistry*, vol. 88, pp. 3031-3039, 2016.
- [21] L. Mondello, P. Q. Tranchida, P. Dugo and G. Dugo, "Comprehensive two-dimensional gas chromatography-mass spectrometry: a review," *Mass Spectrometry Reviews*, vol. 27, pp. 101-124, 2008.

- [22] A. Mostafa, T. Górecki, "Sensitivity of comprehensive two-dimensional gas chromatography (GC×GC) versus one-dimensional gas chromatography (1D GC)," *LC GC Europe*, pp.1-14, 2013.
- [23] J. B. Phillips and E. B. Ledford, "Thermal modulation: a chemical instrumentation component of potential value in improving portability," *Field Analytical Chemistry & Technology*, vol. 1, pp. 23-29, 1996.
- [24] J. B. Phillips, R. B. Gaines, J. Blomberg, F. van der Wielen, J. Dimandja, V. Green, J. Granger, D. Patterson, L. Racovalis, H. Jan de Geus, J. de Boer, P. Haglund, J. Lipsky, V. Sinha and E. B. Ledford Jr, "A robust thermal modulator for comprehensive two-dimensional gas chromatography," *Journal of High Resolution Chromatography*, vol. 22, pp. 3-10, 1999.
- [25] R.B. Gaines and G. S. Frysinger, "Setting the record straight about the capabilities of the rotating thermal heater as a modulator for GC×GC," *Journal of Chromatography A*, vol. 1, pp. 263-264, 2004.
- [26] P. J. Marriott and R. M. Kinghorn, "Longitudinally modulated cryogenic system. A generally applicable approach to solute trapping and mobilization in gas chromatography," *Analytical Chemistry*, vol. 69, pp. 2582-2588, 1997.
- [27] E. Ledford and C. Billesback, "Jet-cooled thermal modulator for comprehensive multidimensional gas chromatography," *Journal of High Resolution Chromatography*, vol. 23, pp. 202-204, 2000.
- [28] J. Beens, M. Adachour, R. Vreuls, K. van Altena and U. T. Brinkman, "Simple, non-moving modulation interface for comprehensive two-dimensional gas chromatography," *Journal of Chromatography A*, vol. 919, pp. 127-132, 2001.
- [29] J. Harynuk and T. Górecki, "Design considerations of a GC×GC system," *Journal of Separation Science*, vol. 25, pp. 304-310, 2002.
- [30] L. Ramos, "Basic Instrumentation for GC×GC," in *Comprehensive two-dimensional gas chromatography*, Oxford, Elsevier Science, 2009, pp. 30-35.
- [31] J. Harynuk and T. Górecki, "New liquid nitrogen cryogenic modulator for comprehensive two-dimensional gas chromatography," *Journal of Chromatography A*, vol. 1019, pp. 53-63, 2003.
- [32] S. Kim, G. Serrano, K. Wise, K. Kurabayahi and E. Zellers, "Evaluation of a microfabricated thermal modulator for comprehensive two-dimensional microscale gas chromatography," *Analytical Chemistry*, vol. 83, pp. 5556-5562, 2011.

- [33] G. Serrano, D. Paul, S.-J. Kim, K. Kurabayahi and E. Zellers, "Comprehensive two-dimensional gas chromatography separations with a microfabricated thermal modulator," *Analytical Chemistry*, vol. 84, pp. 6973-6980, 2012.
- [34] J. Luong, X. Guan, S. Xu, R. Gras and R. Shellie, "Thermal independent modulator for comprehensive two-dimensional gas chromatography," *Analytical Chemistry*, vol. 88, pp. 8428-8432, 2016.
- [35] J&X Technologies, "Principles of SSM," J&X Technologies (Shanghai, China), 2018. [Online]. Available: http://www.jnxtec.com/page111?_l=en. [Accessed May 2019]
- [36] LECO Corporation, "Simply GC×GC," LECO Corporation (St. Joseph, MI, USA), 2017. [Online]. Available: <https://www.leco.com/simply-gcxgc>. [Accessed April 2019]
- [37] LECO Corporation, "GC×GC Methodology - Hot Pulse Time," *Training Class Lab Manual of Pegasus 4D GCxGC Time of Flight Mass Spectrometer*, p. 279, 2009.
- [38] J. Harynuk and T. Górecki, "Flow model for coupled-column gas chromatography systems," *Journal of Chromatography A*, vol. 1086, no. 135-140, 2005.
- [39] J&X Technologies, "Solid State Modulator for Comprehensive Two-Dimensional Gas Chromatography (GC×GC) SSM 1800/1810 Installation and Operation," (Shanghai, China), 2019. [Online]. Available: http://prod87c5f.hkpic1.websiteonline.cn/upload/SSM1800_InstallationandOperation_v3.pdf. [Accessed June 2019]
- [40] J. Seeley, N. Schimmel and S. Seeley, "The multi-mode modulator: A versatile fluidic device for two-dimensional gas chromatography," *Journal of Chromatography A*, vol. 1536, pp. 6-15, 2018.
- [41] J. Seeley, N. Micyus, S. Bandurski, S. Seeley and J. McCurry, "Microfluidic Deans switch for comprehensive two-dimensional gas chromatography," *Analytical Chemistry*, vol. 79, pp. 1840-1847, 2007.
- [42] M. Adahchour, J. Beens, R. Vreuls and U. Brinkman, "Recent developments in comprehensive two-dimensional gas chromatography (GC×GC) II. Modulation and detection," *Trends in Analytical Chemistry*, vol. 25, pp. 540-553, 2006.
- [43] C. Bruckner, B. Prazen and R. Synovec, "Comprehensive two-dimensional high-speed gas chromatography with chemometric analysis," *Analytical Chemistry*, vol. 70, pp. 2796-2804, 1998.
- [44] J. Seeley, F. Kramp and C. Hicks, "Comprehensive two-dimensional gas chromatography via differential flow modulation," *Analytical Chemistry*, vol. 72, pp. 4346-4352, 2000.

- [45] P. Bueno Jr. and J. Seeley, "Flow-switching device for comprehensive two-dimensional gas chromatography," *Journal of Chromatography A*, vol. 1027, pp. 3-10, 2004.
- [46] N. Micyus, J. McCurry and S. Seeley, "Comprehensive two-dimensional gas chromatography with a simple fluidic modulator," *American Laboratory*, pp. 1-10, 2006.
- [47] S. Prebihalo, K. Berrier, C. Freye, N. Bahaghighat, N. Moore, D. Pinkerton and R. Synovec, "Multidimensional gas chromatography: advances in instrumentation, chemometrics and applications," *Analytical Chemistry*, vol. 90, pp. 505-532, 2018.
- [48] D. Deans, "A new technique for heart cutting in gas chromatography," *Chromatographia*, vol. 1, pp. 18-22, 1968.
- [49] K. Sharif, S.-T. Chin, C. Kulsing and P. Marriott, "The microfluidic Deans switch: 50 years of progress, innovation and application," *Trends in Analytical Chemistry*, vol. 82, pp. 35-54, 2016.
- [50] J. Harynuk and T. Górecki, "Comprehensive two-dimensional gas chromatography in stop-flow mode," *Journal of Separation Science*, vol. 27, pp. 431-441, 2004.
- [51] N. Oldridge, O. Panic and T. Górecki, "Stop-flow comprehensive two-dimensional gas chromatography with pneumatic switching," *Journal of Separation Science*, vol. 31, pp. 3375-3384, 2008.
- [52] F.-Y. Wang, "New valve switching modulator for comprehensive two-dimensional gas chromatography," *Journal of Chromatography A*, vol. 1188, pp. 274-280, 2008.
- [53] P. Q. Tranchida, F. A. Franchina, P. Dugo and L. Mondello, "Use of greatly reduced gas flows in flow-modulated comprehensive two-dimensional gas chromatography-mass spectrometry," *Journal of Chromatography A*, vol. 1359, pp. 271-276, 2014.
- [54] F. A. Franchina, M. Maimone, P. Q. Tranchida and L. Mondello, "Flow modulation comprehensive two-dimensional gas chromatography-mass spectrometry using $\sim 4\text{ mL min}^{-1}$ gas flows," *Journal of Chromatography A*, vol. 1441, pp. 134-139, 2016.
- [55] J. F. Griffith, W. L. Winniford, J. Sun, R. Edam and J. C. Luong, "A reversed-flow differential flow modulator for comprehensive two-dimensional gas chromatography," *Journal of Chromatography A*, vol. 1226, pp. 116-123, 2012.
- [56] J. Krupčík, R. Gorovenko, I. Špánik, P. Sandra and M. Giardina, "Comparison of the performance of forward fill/flush and reverse fill/flush modulation in comprehensive two-dimensional gas chromatography," *Journal of Chromatography A*, vol. 1466, pp. 113-128, 2016.

- [57] SepSolve Analytical Ltd., "Insight: Outstanding performance for routine GC×GC," SepSolve Analytical Ltd. (Peterborough, UK), 2018. [Online] <http://www.sepsolve.com/uploads/brochure/2018-06-19-11-11-56-32-INSIGHT%20brochure.pdf> [Accessed May 2019].
- [58] SepSolve Analytical Ltd., "Insight flow modulator user guide," 2018.
- [59] A. Ghosh, . C. T. Bates, S. K. Seeley and J. V. Seeley, "High speed Deans switch for low duty cycle comprehensive two-dimensional gas chromatography," *Journal of Chromatography A*, vol. 1291, pp. 146-154, 2013.
- [60] LECO Corporation, "FLUX GC×GC. The operation, use, and concepts behind a diverting flow technique," LECO Corporation (St. Joseph, MI, USA), 2019. [Online] https://cdn2.hubspot.net/hubfs/2603456/FLUX_MODULATOR_WHITE_PAPER.pdf [Accessed July 2019].
- [61] Agilent Technologies, "Agilent G2855A Deans switching system: installation and operation," Agilent Technologies (Wilmington, DE, USA), 2003. [Online] https://www.agilent.com/cs/library/usermanuals/Public/G2855-90100_031969.pdf [Accessed May 2019].
- [62] C. Duhamel, P. Cardineal, V. Peulon-Agasse, R. Firor, L. Pascaud, G. Semard-Jouset, P. Giusti and V. Livadris, "Comparison of cryogenic and differential flow (forward and reverse fill/flush) modulators and applications to the analysis of heavy petroleum cuts by high-temperature comprehensive two-dimensional gas chromatography," *Journal of Chromatography A*, vol. 1387, pp. 95-103, 2015.
- [63] LECO Corporation, "LECO's GC×GC Utilizing a consumable-free modulator and second column modulation," LECO Corporation (St. Joseph, MI, USA), 2013. [Online]. Available: <https://www.leco.com/component/edocman/?task=document.viewdoc&id=1161&Itemid=1161>. [Accessed June 2019].
- [64] Zoex Corporation, "ZX-2," Zoex Corporation (Houston, TX, USA), 2012. [Online]. Available: <http://zoex.com/wp-content/uploads/2012/07/ZX-2-Product-Specs.pdf>. [Accessed April 2019].
- [65] J&X Technologies, "SSM1800 Solid State Modulator for comprehensive two dimensional gas chromatography (GC×GC) Second Edition," J&X Technologies (Shanghai, China) 2018. [Online]. Available: http://prod87c5f.hkpic1.websiteonline.cn/upload/SSM1800_InstallationandOperation_v3.pdf. [Accessed May 2019].

- [66] G. Semard, C. Gouin, J. Bourdet, N. Bord and V. Livadris, "Comparative study of differential flow and cryogenic modulators comprehensive two-dimensional gas chromatography systems for the detailed analysis of light cycle oil," *Journal of Chromatography A*, vol. 1218, pp. 3146-3152, 2011.
- [67] B. Pollo, G. Alexandrino, F. Augusto and L. Hantao, "The impact of comprehensive two-dimensional gas chromatography on oil & gas analysis: Recent advances and applications in petroleum industry," *Trends in Analytical Chemistry*, vol. 105, pp. 202-217, 2018.
- [68] B. Gruber, B. A. Weggler, R. Jaramillo, K. A. Murrell, P. K. Piotrowski and F. L. Dorman, "Comprehensive two-dimensional gas chromatography in forensic science: A critical review of recent trends," *Trends in Analytical Chemistry*, vol. 105, pp. 292-301, 2018.
- [69] P. Q. Tranchida, G. Purcaro, M. Maimone and L. Mondello, "Impact of comprehensive two-dimensional gas chromatography with mass spectrometry on food analysis," *Journal of Separation Science*, vol. 39, pp. 149-161, 2016.
- [70] E. A. Higgins Keppeler, C. L. Jenkins, T. J. Davis and H. Bean, "Advances in the application of comprehensive two-dimensional gas chromatography in metabolomics," *Trends in Analytical Chemistry*, vol. 109, pp. 275-286, 2018.
- [71] M. S. S. Amaral and P. J. Marriott, "The Blossoming of Technology for the Analysis of Complex Aroma Bouquets - a Review on Flavour and Odorant Multidimensional and Comprehensive Gas Chromatography Applications," *Molecules*, vol. 24, pp. 1-30, 2019.
- [72] T. C. Tran, G. A. Logan, E. Grosjean, D. Ryan and P. J. Marriott, "Use of comprehensive two-dimensional gas chromatography/time-of-flight mass spectrometry for the characterization of biodegradation and unresolved complex mixtures in petroleum," *Geochimica et Cosmochimica Acta*, vol. 74, pp. 6468-6484, 2010.
- [73] M. K. Jennerwein, M. Eschner, T. Gröger, T. Wilharm and R. Zimmermann, "Complete group-type quantification of petroleum middle distillates based on comprehensive two-dimensional gas chromatography time-of-flight mass spectrometry (GC×GC -TOFMS) and visual basic scripting," *Energy and Fuels*, vol. 28, pp. 5670-5681, 2014.
- [74] C. Kulsing, P. Rawson, R. L. Webster, D. J. Evan and P. J. Marriott, "Group-type analysis of hydrocarbons and sulfur compounds in thermally stressed mercox jet fuel samples," *Energy and Fuels*, vol. 31, pp. 8978-8984, 2017.
- [75] B. M. F. Avila, V. B. Pereira, A. O. Gomes and D. A. Azevedo, "Speciation of organic sulfur compounds using comprehensive two-dimensional gas chromatography coupled to time-of-flight mass spectrometry: A powerful tool for petroleum refining," *Fuel*, vol. 126, pp. 188-193, 2014.

- [76] R. K. Nelson, K. M. Gosselin, D. J. Hollander, S. A. Murawski, A. Gracia, C. M. Reddy and J. R. Radovic, "Exploring the complexity of two iconic crude oil spills in the Gulf of Mexico (Ixtoc I and Deepwater Horizon) using comprehensive two-dimensional gas chromatography (GC×GC)," *Energy and Fuels*, vol.33, pp. 3925-3922, 2019.
- [77] T. C. Tran, G. A. Logan, E. Grosjean, J. Harynuk, D. Ryan and P. Marriott, "Comparison of column phase configurations for comprehensive two dimensional gas chromatographic analysis of crude oil and bitumen," *Organic Geochemistry*, vol. 37, pp. 1190-1194, 2006.
- [78] A. Lee, A. Lewis, K. Bartle, J. McQuaid and P. Marriott, "A comparison of modulating interface technologies in comprehensive two-dimensional gas chromatography (GC×GC)," *Journal of Microcolumn Separations*, vol. 12, pp. 187-194, 2000.
- [79] O. Panic, *Development of a Cost-Effective and Consumable-Free Interface for Comprehensive Two-Dimensional Gas Chromatography (GC×GC)* (Unpublished Master Thesis). University of Waterloo, Waterloo, Ontario, Canada, (2007).
- [80] O. Panic, T. Górecki, C. McNeish, A. Goldstein, B. Williams, D. Worton, S. Hering and N. Kreisberg, "Development of a new consumable-free thermal modulator for comprehensive two-dimensional gas chromatography," *Journal of Chromatography A*, vol. 1218, pp. 3070-3079, 2011.
- [81] A. Goldstein, D. Worton, B. Williams, S. Hering, N. Breisbery, O. Panic and T. Górecki, "Thermal desorption comprehensive two-dimensional gas chromatography for in-situ measurements of organic aerosols," *Journal of Chromatography A*, vol. 1186, pp. 340-347, 2008.
- [82] C. McNeish, *Development of a Single-Stage Modulator for Comprehensive Two-Dimensional Gas Chromatography (GC×GC)* (Unpublished Master Thesis). University of Waterloo, Waterloo, Ontario, Canada, (2011).
- [83] M. Edwards, *Development of a New Consumable-free Modulator for Comprehensive Two-Dimensional Gas Chromatography* (Unpublished proposal). University of Waterloo, Waterloo, Ontario, Canada, (2011).
- [84] A. Muscalu, M. Edwards, T. Górecki and E. Reiner, "Evaluation of a single-stage, consumable-free modulator for comprehensive two-dimensional gas chromatography: Analysis of polychlorinated biphenyls, organochlorine pesticides and chlorobenzenes," *Journal of Chromatography A*, vol. 1391, pp. 93-101, 2015.
- [85] D. B. Lewis, "Scanning Electron Microscopy and X-ray Microanalysis," *Transactions of the Institute of Metal Finishing*, vol. 70, pp. 198-202, 1992.

- [86] K. D. Vernon-Parry, "Scanning Electron Microscopy: An introduction," *Analysis*, vol. 13, pp. 40-44, 2000.
- [87] A. V. Girao, G. Caputo and M. C. Ferro, "Application of Scanning Electron Microscopy-Energy Dispersive X-ray Spectroscopy (SEM-EDS)," in *Comprehensive Analytical Chemistry*, 2017, pp. 153-168.
- [88] M. Scimeca, S. Bischetti, H. K. Lamsira, R. Bonfiglio and E. Bonanno, "Energy Dispersive X-ray (EDX) microanalysis: A powerful tool in biomedical research and diagnosis," *European Journal of Histochemistry*, vol. 62, pp. 1-10, 2018.
- [89] P. J. Goodhew, J. Humphreys and R. Beanland, "Electron microscopy and analysis," New York: Taylor & Francis, 2001.
- [90] V. Kazmiruk, "Scanning electron microscopy," Rijeka: InTech, 2012.
- [91] A. J. Garratt-Reed and D. C. Bell, "Energy dispersive x-ray analysis in the electron microscope," Oxford: BIOS Scientific Publishers Limited, 2003.
- [92] J. de Zeeuw, "Deactivation of metal surfaces: applications in gas chromatography (GC) for the past 15 years," *American Laboratory*, 2012.
- [93] D. Wang, S. L. Chong and A. Malik, "Sol-Gel column technology for single-step deactivation, coating, and stationary-phase immobilization in high-resolution capillary gas chromatography," *Analytical Chemistry*, vol. 69, pp. 4566-4576, 1997.
- [94] L. Blomberg, "Deactivation of glass capillary columns for gas chromatography," *Journal of Chromatography A*, vol. 115, pp. 365-372, 1975.
- [95] S. N. Atapattu and C. F. Poole, "Selectivity equivalence of two poly(methylphenylsiloxane) open-tubular columns prepared with different deactivation techniques for gas chromatography," *Journal of Chromatography A*, vol. 1185, pp. 305-309, 2008.
- [96] J. de Zeeuw and J. Luong, "Developments in stationary phase technology for gas chromatography," *Trends in Analytical Chemistry*, vol. 21, pp. 594-607, 2002.
- [97] P. Sandra and M. Verzele, "Surface treatment, deactivation and coating in (GC)² (glass capillary gas chromatography)," *Chromatographia*, vol. 10, pp. 419-425, 1977.

- [98] P. Louette , F. Bodino and J.-J. Pireaux, "Poly(dimethyl siloxane) (PDMS) XPS reference core level and energy loss spectra," *Surface Science Spectra*, vol. 12, pp. 38-43, 2005.
- [99] Restek Corporation, "Frequently Asked Questions: surface treatments," Restek Corporation (Bellefonte, PA, USA) [Online]. Available: www.restek.com. [Accessed June 2019].
- [100] Agilent Technologies , "Capillary DB-ProSteel," Agilent Technologies (Wilmington, DE, USA) [Online]. Available: <https://www.agilent.com/en/products/gas-chromatography/gc-columns/capillary/db-prosteel>. [Accessed June 2019].
- [101] T. H. Thomas and T. C. Kendrick, "Thermal analysis of polydimethylsiloxanes. I. thermal degradation in controlled atmospheres," *Journal of Polymer Science: Part A-2*, vol. 7, pp. 537-549, 1969.
- [102] S. Bello and K. Bello, "Production process of base oils: the prospects and challenges for local industries in Nigeria," *International Journal of Engineering and Technology*, vol. 36, pp. 452-456, 2016.
- [103] S. L. Silva, A. M. Silva, J. C. Ribeiro, F. G. Martins, F. A. Da Silva and C. M. Silva, "Chromatographic and spectroscopic analysis of heavy crude oil mixtures with emphasis in nuclear magnetic resonance spectroscopy: A review," *Analytica Chimica Acta*, vol. 707, pp. 18-37, 2011.
- [104] L. Severa, M. Havlicek and V. Kumbar, "Temperature dependent kinematic viscosity of different types of engine oils," *Acta Universitatis Agriculturae et Silviculturae Mendelianae Brunensis*, vol. 57, pp. 95-102, 2009.
- [105] R. M. Balabin and R. Z. Safieva, "Motor oil classification by base stock and viscosity based on near infrared (NIR) spectroscopy data," *Fuel*, vol. 87, pp. 2745-2752, 2008.
- [106] W. Fortunato de Varvalho Rocha, M. M. Schantz, D. A. Sheen, P. M. Chu and K. A. Lippa, "Unsupervised classification of petroleum Certified Reference Materials and other fuels by chemometric analysis of gas chromatography - mass spectrometry data," *Fuel*, vol. 197, pp. 248-258, 2017.
- [107] C. Vendeuvre, F. Bertoncini, L. Duval, J.-L. Duplan, D. Thiebaut and M.-C. Hennion, "Comparison of conventional gas chromatography (1D-GC) and comprehensive two-dimensional gas chromatography (GC×GC) for the detailed analysis of petrochemical samples," *Journal of Chromatography A*, vol. 1056, pp. 155-162, 2004.

- [108] C. von Muhlen, C. A. Zini, E. B. Caramao and P. J. Marriott, "Applications of comprehensive two-dimensional gas chromatography to the characterization of petrochemical and related samples," *Journal of Chromatography A*, vol. 1105, pp. 39-50, 2006.
- [109] C. Da Costa, M. Turner, J. C. Reynolds, S. Whitmarsh, T. Lynch and C. S. Creaser, "Direct analysis of oil additives by high-field asymmetric waveform ion mobility spectrometry-mass spectrometry combined with electrospray ionization and desorption electrospray ionization," *Analytical Chemistry*, vol. 88, pp. 2453-2458, 2016.
- [110] G. Kreisberger, C. W. Klampfl and W. W. Buchberger, "Determination of antioxidants and corresponding degradation products in fresh and used engine oils," *Energy and Fuels*, vol. 30, pp. 7638-7645, 2016.
- [111] A. Kupareva, P. Maki-Arvela, H. Grenman, K. Eranen, R. Sjöholm, M. Reunanen and D. Y. Murzin, "Chemical characterization of lube oils," *Energy and Fuels*, vol. 27, pp. 27-34, 2013.
- [112] M. R. Djokic, T. Dijmans, G. Yildiz, W. Prins and K. M. Van Geem, "Quantitative analysis of crude and stabilized bio-oils by comprehensive two-dimensional gas-chromatography," *Journal of Chromatography A*, vol. 1257, pp. 131-140, 2012.
- [113] M. K. Jennerwein, A. C. Sutherland, M. Eschner, T. Gröger, T. Wilharm and R. Zimmermann, "Quantitative analysis of modern fuels derived from middle distillates - The impact of diverse compositions on standard methods evaluated by an offline hyphenation of HPLC-refractive index detection with GC×GC-TOFMS," *Fuel*, vol. 187, pp. 16-25, 2017.
- [114] C. Gallacher, R. Thomas, C. Taylor, R. Lord and R. M. Kalin, "Comprehensive composition of Creosote using comprehensive two-dimensional gas chromatography time-of-flight mass spectrometry (GC×GC -TOFMS)," *Chemosphere*, vol. 178, pp. 34-41, 2017.
- [115] C. Lorentz, D. Laurenti, J. L. Zotin and C. Geantet, "Comprehensive GC×GC chromatography for the characterization of sulfur compound in fuels: A review," *Catalysis Today*, vol. 292, pp. 26-37, 2017.
- [116] K. D. Nizio, T. M. McGinitie and J. J. Harynuk, "Comprehensive multidimensional separations for the analysis of petroleum," *Journal of Chromatography A*, vol. 1255, pp. 12-23, 2012.

- [117] R. L. Webster, P. W. Rawson, C. Kulsing, D. J. Evans and P. J. Marriott, "Investigation of the thermal oxidation of conventional and alternate aviation fuels with comprehensive two-dimensional gas chromatography accurate mass quadrupole time-of-flight mass spectrometry," *Energy and Fuels*, vol. 31, pp. 4886-4894, 2017.
- [118] T. C. Tran, G. A. Logan, E. Grosjean, J. Harynuk, D. Ryan and P. Marriott, "Comparison of column phase configurations for comprehensive two-dimensional gas chromatographic analysis of crude oil and bitumen," *Organic Geochemistry*, vol. 37, pp. 1190-1194, 2006.
- [119] H. D. Bahaghighat, C. E. Freye and R. E. Synovec, "Recent advances in modulator technology for comprehensive two-dimensional gas chromatography," *Trends in Analytical Chemistry*, vol. 113, pp. 1-13, 2018.
- [120] H. Cai and S. D. Stearns, "A comprehensive two-dimensional gas chromatography valve modulation method using hold-release ¹D column flow for long ²D separation time with 100% transfer," *Journal of Chromatography A*, vol. 1569, pp. 200-211, 2018.
- [121] M. S. Alam, C. Stark and R. M. Harrison, "Using variable ionization energy time-of-flight mass spectrometry with comprehensive GC×GC to identify isomeric species," *Analytical Chemistry*, vol. 88, pp. 4211-4220, 2016.
- [122] A. Giri, M. Coutriade, A. Racaud, K. Okuda, J. Dane, R. B. Cody and J.-F. Focant, "Molecular characterization of volatiles and petrochemical base oils by photo-ionization GC×GC -TOF-MS," *Analytical Chemistry*, vol. 89, pp. 5395-5403, 2017.
- [123] Markes International, "Select-eV: The next generation of ion source technology (Application Note 528)," Markes International (Llantrisant, UK) 2016.
- [124] R. C. Striebach, L. M. Shafer, R. K. Adams, Z. J. West, M. J. DeWitt and S. Zabarnick, "Hydrocarbon group-type analysis of petroleum-derived and synthetic fuels using two-dimensional gas chromatography," *Energy and Fuels*, vol. 28, pp. 5696-5706, 2014.
- [125] K. Lissitsyna, S. Huertas, L. Quintero and L. Polo, "PIONA analysis of kerosene by comprehensive two-dimensional gas chromatography coupled to time of flight mass spectrometry," *Fuel*, vol. 116, pp. 716-722, 2014.
- [126] L. R. Rudnick, "Lubricant additives: chemistry and applications," Boca Raton: Taylor & Francis Group, 2009.
- [127] Z. Lu, A. O. De Silva, T. E. Peart, C. J. Cook, G. R. Tetreault, M. R. Servos and D. C. Muir "Distribution, partitioning and bioaccumulation of substituted diphenylamine antioxidants and benzotriazole UV stabilizers in an urban creek in Canada," *Environmental Science & Technology*, vol. 50, pp. 9089-9097, 2016.

- [128] E. M. Kristenson, P. Korytár, C. Danielsson, M. Kallio, M. Brandt, J. Mäkelä, R. J. Vreuls, J. Beens and U. A. Brinkman, "Evaluation of modulators and electron-capture detectors for comprehensive two-dimensional gas chromatography of halogenated organic compounds," *Journal of Chromatography A*, vol. 1019, pp. 65-77, 2003.
- [129] G. Semard, M. Adahchour and J.-F. Focant, "Chapter 2 Basic Instrumentation for GC×GC," in *Comprehensive Two Dimensional Gas Chromatography*, Amsterdam, Elsevier, 2009, pp. 15-48.
- [130] LECO Corporation, "Thermal modulation without the hassle of liquid nitrogen," LECO Corporation (St. Joseph, MI, USA), 2008. [Online]. Available: <https://www.leco.com/product/thermomodulator>. [Accessed June 2019].
- [131] P. Q. Tranchida, F. A. Franchina, P. Dugo and L. Mondello, "Flow modulation low-pressure comprehensive two-dimensional gas chromatography," *Journal of Chromatography A*, vol. 1372, pp. 236-244, 2014.
- [132] P. Harvey and R. Shellie, "Factors affecting peak shape in comprehensive two-dimensional gas chromatography with non-focusing modulation," *Journal of Chromatography A*, vol. 1218, pp. 3153-3158, 2011.
- [133] MSP Kofel, "Gas chromatography troubleshooting and reference guide," MSP Kofel (Munchenbuchsee, Switzerland), 2005. [Online]. <https://www.chromacademy.com/troubleshooter-gc/resources/gc-msp-troubleshooting-1.pdf> [Accessed June 2019].
- [134] H. Cortes, B. Winniford, J. Luong and M. Pursch, "Comprehensive two-dimensional gas chromatography review," *Journal of Separation Science*, vol. 32, pp. 883-904, 2009.
- [135] X. Guan, Z. Zhao, S. Cai, S. Wang and H. Lu, "Analysis of volatile organic compounds using cryogen-free thermal modulation based comprehensive two-dimensional gas chromatography coupled with quadrupole mass spectrometry," *Journal of Chromatography A*, vol. 1587, pp. 227-238, 2019.
- [136] O. Amador-Muñoz and P. Marriott, "Quantification in comprehensive two-dimensional gas chromatography and a model of quantification based on selected summed modulated peaks," *Journal of Chromatography A*, vol. 1184, pp. 323-340, 2008.
- [137] O. Amador-Muñoz, R. Villalobos-Pietrini, A. Aragon-Pina, T. Tran, P. Morrison and P. Marriott, "Quantification of polycyclic aromatic hydrocarbons based on comprehensive two-dimensional gas chromatography-isotope dilution mass spectrometry," *Journal of Chromatography A*, vol. 1201, pp. 161-168, 2008.

- [138] M. Zoccali, B. Giocastro, P. Tranchida and L. Mondello, "Use of a recently developed thermal modulator within the context of comprehensive two-dimensional gas chromatography combined with time-of-flight mass spectrometry: Gas flow optimization aspects," *Journal of Separation Science*, vol. 42, pp. 691-697, 2019.
- [139] D. C. Harris, "Quantitative chemical analysis," New York: W. H. Freeman and Company, 2010.
- [140] J. M. K. C. Donev et al., "Energy Education - Bitumen," University of Calgary, 2018. [Online]. Available: <https://energyeducation.ca/encyclopedia/Bitumen>. [Accessed 30 June 2019].
- [141] Canadian Association of Petroleum Producers, "Oil Sands," Canadian Association of Petroleum Producers (Calgary, Alberta, Canada), 2018. [Online]. Available: <https://www.capp.ca/canadian-oil-and-natural-gas/oil-sands>. [Accessed 30 June 2019].
- [142] A. Aguiar, A. I. Silva Junior, D. A. Azevedo and F. R. Aquino Neto, "Application of comprehensive two-dimensional gas chromatography coupled to time-of-flight mass spectrometry to biomarker characterization in Brazilian oils," *Fuel*, vol. 89, pp. 2760-2768, 2010.
- [143] A. Aguiar, H. G. M. Aguiar, D. A. Azevedo and F. R. Aquino Neto, "Identification of Methylhopane and Methylmoretane series in Ceara Basin Oils, Brazil, using comprehensive two-dimensional gas chromatography coupled to time-of-flight mass spectrometry," *Energy and Fuels*, vol. 25, pp. 1060-1065, 2011.
- [144] R. S. Silva, H. G. Aguiar, M. D. Rangel, D. A. Azevedo and F. R. Aquino Neto, "Comprehensive two-dimensional gas chromatography with time of flight mass spectrometry applied to biomarker analysis of oils from Colombia," *Fuel*, vol. 90, pp. 2694-2699, 2011.
- [145] J. C. Forsythe, A. E. Omerantz, D. J. Seifert, K. Wang, Y. Chen, J.Y. Zuo, R. K. Nelson, C. M. Reddy, A. Schimmelmann, P. Sauer, K. E. Peters and O. C. Mullins, "A geological model for the origin of fluid compositional gradients in a large Saudi Arabian oilfield: an investigation by two-dimensional gas chromatography (GC×GC) and asphaltene chemistry," *Energy and Fuels*, vol. 29, pp. 5666-5680, 2015.
- [146] J&X Technologies, "Analysis the Chemical Composition of Kerosene by GC×GC - FID (Document No. E103)," J&X Technologies (Shanghai, China), 2018.
- [147] J&X Technologies, "Group analysis of light cycle oil (LCO) by comprehensive two-dimensional gas chromatography (Document No. E101)," J&X Technologies (Shanghai, China), 2018.

- [148] J&X Technologies, "Group analysis of diesel by comprehensive two-dimensional gas chromatography (Document No. E102)," J&X Technologies (Shanghai, China), 2018.
- [149] T. Wang, C. Zhang, R. Zhao, C. Zhu, C. Yang and C. Liu, "Solvent extraction of bitumen from oil sands," *Energy and Fuels*, vol. 28, pp. 2297-2304, 2014.
- [150] J. Wu and T. Dabros, "Process for solvent extraction of bitumen from oil sand," *Energy and Fuels*, vol. 26, pp. 1002-1008, 2012.
- [151] C. C. Walters, F. C. Wang, M. B. Higgins and M. E. Madincea, "Universal biomarker analysis using GC×GC with dual FID and ToF-MS (EI/FI) detection," *Organic Geochemistry*, vol. 115, pp. 57-66, 2018.
- [152] F. Nardella, N. Landi, I. Degano, M. Colombo, M. Serradimigni, C. Tozzi and E. Ribechini, "Chemical investigations of bitumen from Neolithic archaeological excavations in Italy by GC/MS combined with principal component analysis," *Analytical Methods*, vol. 11, pp. 1449-1459, 2019.
- [153] K. E. Peters, C. C. Walters and J. M. Moldowan, "The biomarker guide: volume 1 biomarkers and isotopes in the environment and human history," Cambridge: Cambridge University Press, 2005.
- [154] K. E. Peters, C. C. Walters and J. M. Moldowan, "The biomarker guide: volume 2 biomarkers and isotopes in petroleum exploration and earth history," Cambridge: Cambridge University Press, 2005.
- [155] A. G. Scarlett, A. I. Despaigne-Diaz, S. A. Wilde and K. Grice, "An examination by GC×GC -TOFMS of organic molecules present in highly degraded oils emerging from Caribbean terrestrial seeps of Cretaceous age," *Geoscience Frontiers*, vol. 10, pp. 5-15, 2019.
- [156] K. Pal, L. da Paz Nogueira Branco, A. Heintz, P. Choi, Q. Liu, P. R. Seidl and M. R. Gray, "Performance of solvent mixtures for non-aqueous extraction of Alberta oil sands," *Energy and Fuels*, vol. 29, pp. 2261-2267, 2015.
- [157] N. Hossein, L. Vagi, P. Choi, Q. Liu and M. R. Gray, "Solvent screening for non-aqueous extraction of Alberta oil sands," *The Canadian Journal of Chemical Engineering*, vol. 91, pp. 1153-1160, 2013.
- [158] D. Rood, "Gas chromatography problem solving and troubleshooting," *Journal of Chromatographic Science*, vol. 34, pp. 305-306, 1996.

APPENDIX

Appendix A

Chapter 3 Supplementary material

Alternative sources for stationary phase within trapping capillary

Various voltage treatments of Agilent columns

Performance results

The various voltages applied to the Agilent trapping capillaries during the treatment process were evaluated by the analysis of diesel. The experimental details were previously discussed in section 3.2. DB-PS1 #27 was treated at 55 V followed by 50 V. The chromatographic results can be seen in Figure 3.A.1. Active (A-C) and passive cooling (D-F) were compared at similar modulation voltages. The greatest difference in chromatographic performance can be seen at the lower voltage of 25 V between active (A) and passive (D) cooling. At a low modulation voltage, the temperature increase applied to the trapping capillary was rather low. Applying a lower modulation voltage, was not necessarily negative, as long as the voltage was sufficient in remobilizing the trapped analytes. When comparing the low modulation voltage separations, it was clear it was especially detrimental to the separation with

active cooling. Due to the lower trapping temperatures achievable with active cooling, a higher modulation voltage would be necessary. With passive cooling, the lower modulation voltage did not present as much of negative effect on the separation. However, it was still inadequate in providing an acceptable separation. The streaking present in the two-dimensional space was caused by strong sorption by select analytes that were not remobilized due to the low modulation voltage. As the oven temperature increased during the analysis, these analytes would elute off the trapping phase as a broad band. These are undesirable in a GC×GC separation due to the large secondary bandwidths that are created, as well as the possible co-elutions that could occur within the secondary space. With a modulation voltage of 40 V, the separation was greatly improved for both modes of cooling, more so for active (B) than passive (E). The streaking within the second dimension caused by poorly remobilized analytes had been nearly eliminated by applying a significantly higher modulation voltage. At a more appropriate voltage, the streaking should theoretically be removed completely. The separation of diesel with active and passive cooling with 40 V applied for modulation provided an adequate separation of the analytes within the second dimension. Visualization of the roof-tile effect, a feature of GC×GC chromatograms beneficial in group analysis, was clear and differentiated. Increasing the modulation voltage to 55 V was unfavorable for both active (C) and passive (F) cooling. In both chromatograms, it was apparent that compounds have disappeared when comparing the separation to that of 40 V. Due to the excessive voltage and corresponding temperature increase, pyrolysis of the sample occurred. Overall, a mid-range modulation of 40 V was appropriate for the DB-PS1 #27 trapping capillary that was treated at 55 V for ten minutes, followed by two five-minute phases at 50 V. Chromatographically, these treatment parameters performed adequately, but further investigation by SEM and EDX was required.

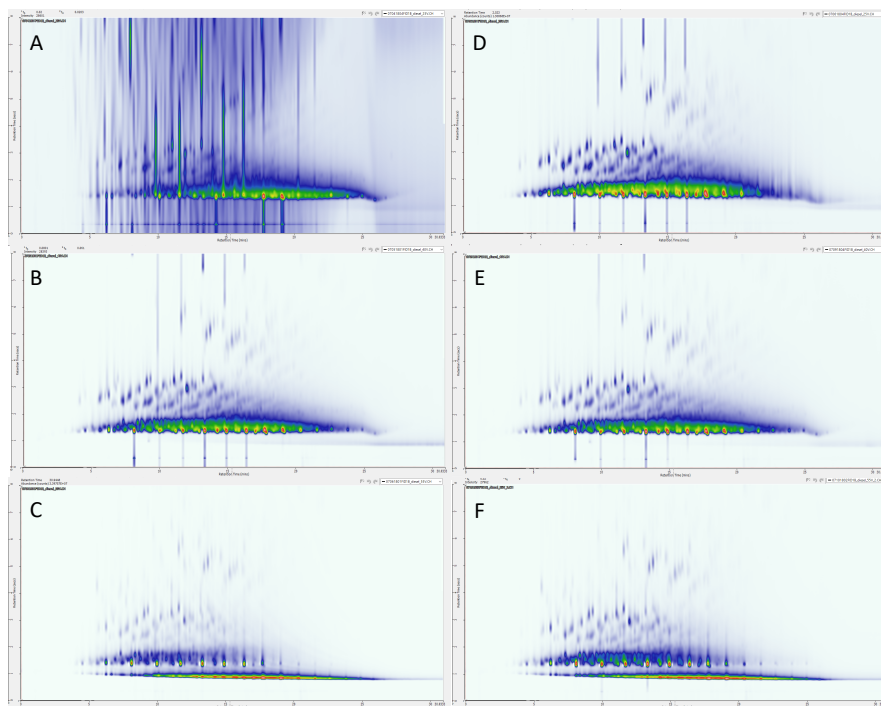


Figure 3.A. 1 Comparison of the performance of the DB-PS1 #27 trapping capillary at various modulation voltages with active (A - C) and passive cooling (D - F) in the analysis of diesel. The deactivation layer was present within the unions at the front and back end of the trapping capillary. Modulation voltages were 25 V (A and D), 40 V (B and E) and 55 V (C and F).

The DB-PS1 column was also treated with a ten-minute phase at 30 V, followed by two five-minute phases at 25 V labeled #11. The separation of diesel with active and passive cooling at various modulation voltages is presented in Fig 3.A.2. A lower voltage of 35 V produced very different results with active (A) and passive cooling (D). Combination of the low treatment voltages and low modulation voltage resulted in very broad bands in the second dimension of poorly remobilized analytes with active cooling. On the other hand, passive cooling achieved a substantially better separation with minimal to no streaking in the second dimension. By increasing the modulation voltage to 50 V, the separation achieved with active cooling (B) was slightly improved; however, broad bands within the second dimension still existed. The separation achieved with passive cooling (E) was contrary to active cooling and provided an

improved separation with no streaking in the second dimension. Further increasing the modulation voltage to 55 V again caused pyrolysis of the sample due to the excessive temperatures applied to the trapping capillary. The treatment parameters applied to DB-PS1 #27 and #11 were deemed inferior to those applied for DB-PS1 #9 and #1 due to insufficient trapping and remobilization of analytes.

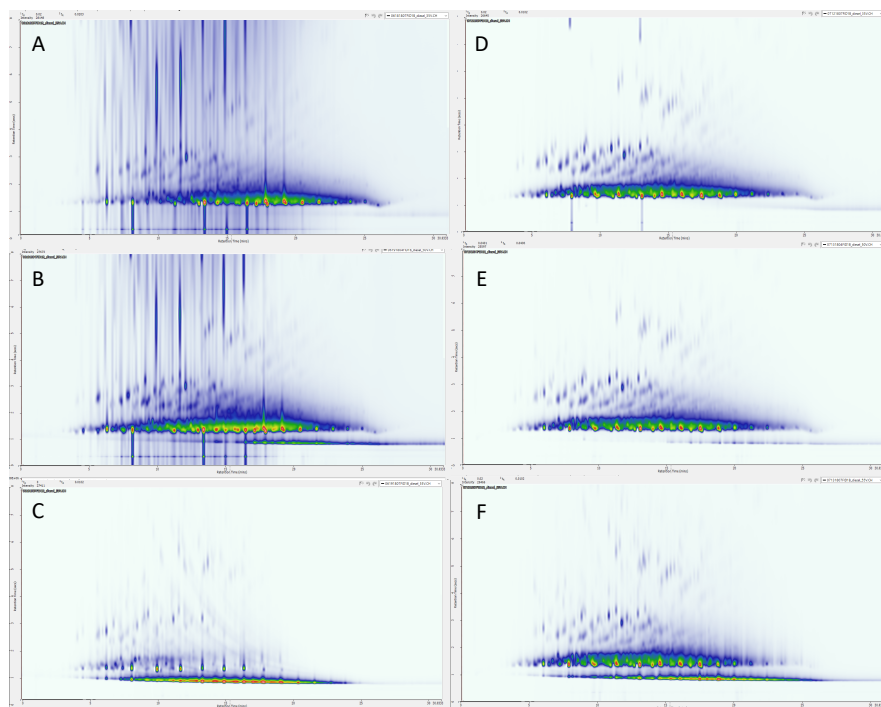


Figure 3.A. 2 Comparison of the performance of the DB-PS1 #11 trapping capillary at various modulation voltages with active (A - C) and passive cooling (D - F) in the analysis of diesel. The deactivation layer was present within the unions at the front and back end of the trapping capillary. Modulation voltages were 35 V (A and D), 50 V (B and E), 55V (C and F).

The analysis of diesel with DB-PS2887 #22, which was treated at 60 V followed by 55 V, at various modulation voltages with active and passive cooling is presented in Fig. 3.A.3.

Initially, the separation appeared drastically different from the previous chromatograms presented with DB-PS1. The lower eluting band within the second dimension presented a larger

unresolved complex mixture when utilizing the DB-PS2887 when compared to DB-PS1. This hindered the separation and identification of the non-polar species of a diesel mixture. A discharge voltage of 35 V presented clearly different separations with active (A) and passive (D) cooling. With active cooling, the low modulation voltage was not sufficient to completely remobilize the trapped analytes. On the other hand, passive cooling provided less of a trapping effect, resulting in less voltage required for remobilization of the analytes. There were minor streaks present from analytes that were more strongly sorbed with passive cooling. An increase in modulation voltage to 40 V greatly improved the separation achieved with active (B) and passive (E) cooling. The broad streaking bands in the secondary space with active cooling were completely eliminated when the higher voltage was applied. Despite the improvement of the second-dimension separation, the lower eluting secondary band did not improve substantially and still remained as a large unresolved mixture. This was due to more analytes being sorbed onto the treated material within the trapping capillary. The analytes were not released in a quick fashion, resulting in tailing and incomplete desorption. These effects resulted in less resolution in the band. The minor streaking that was previously present with passive cooling had also been improved with the increase in modulation voltage. Pyrolysis occurred at a voltage of 45 V and 50 V for active (C) and passive (F) cooling, respectively. Compared to DB-PS1, the pyrolysis was more extreme with the DB-PS2887 at lower voltages.

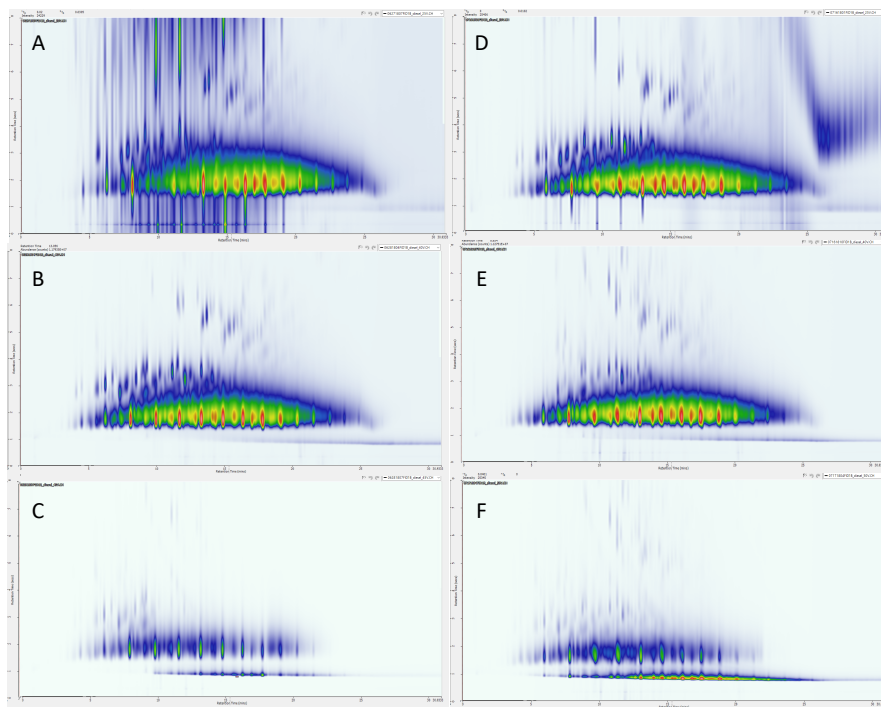


Figure 3.A.3 Comparison of the performance of the DB-PS2887 #22 trapping capillary at modulation voltages with active (A - C) and passive cooling (D - F) in the analysis of diesel. The deactivation layer was present within the unions at the front and back end of the trapping capillary. Modulation voltages were 25 V (A and D), 40 V (B and E), 45 V (C) and 50 V (F).

DB-PS2887 #25 was treated at voltages of 30 V and 25 V, then utilized in the analysis of diesel with active and passive cooling at various modulation voltages, as seen in Fig. 3.A.4. Combination of the lowest treatment voltages and a modulation voltage of 30 V was insufficient in providing adequate chromatographic performance when active cooling was applied (A). The early eluting band was strongly sorbed onto the trapping phase with active cooling and insufficiently remobilized with a low modulation voltage of 30 V. This resulted in intense secondary tailing and poor resolution. On the other hand, with passive cooling, a more adequate separation was achieved (D). A weaker trapping mechanism allowed a lower discharge voltage to more effectively remobilize the analytes onto the second dimension. However, some of the aromatic species that were previously apparent with DB-PS2887 #17 were not separated. By

increasing the modulation voltage to 45 V, the separation with active cooling was slightly improved (B). A small group of analytes were separated at the front end of the unresolved band, but intense tailing still remained. The separation achieved with passive cooling at 45 V (E) was rather similar to that of 30 V. At a modulation voltage of 55 V and 50 V, pyrolysis occurred with active (C) and passive (F) cooling, respectively. This was caused by the excessive temperature increase experienced by the trapping capillary with these applied modulation voltages. As previously seen, the pyrolysis of the diesel sample was extreme in comparison to that of DB-PS1. DB-PS2887 #22 and #25 were found to be inferior compared to DB-PS2887 #17 and #2 since efficient trapping and remobilization could not be achieved. Overall, the best DB-PS2887 trapping capillaries were found to be inferior when compared to the DB-PS1 trapping capillaries. Despite these conclusions, SEM and EDX was performed on all trapping capillaries to characterize the morphology and elemental composition of the phase.

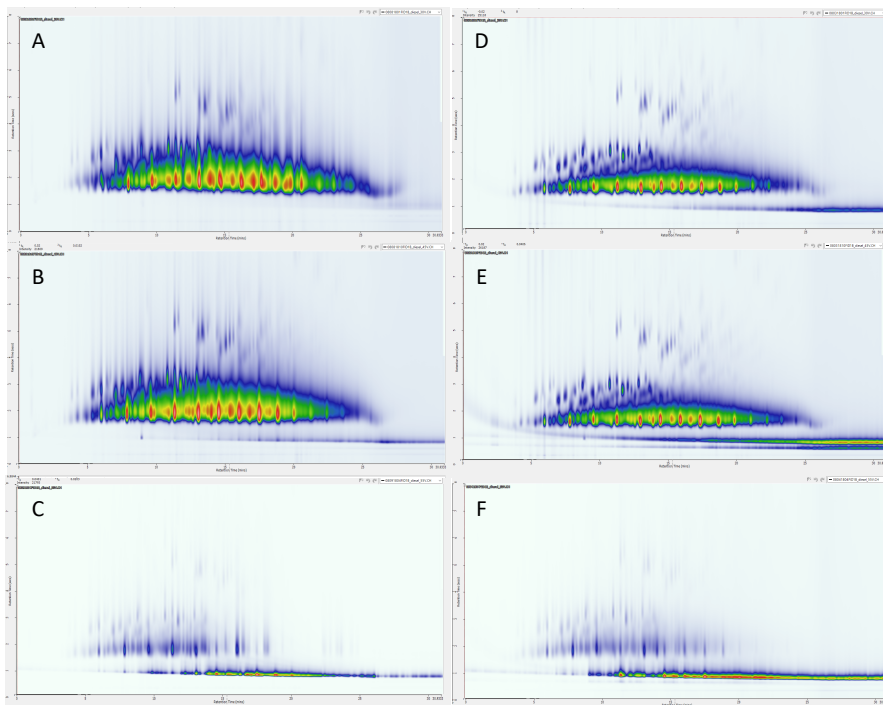


Figure 3.A.4 Comparison of the performance of the DB-PS2887 #25 trapping capillary at modulation voltages with active (A - C) and passive cooling (D - F) in the analysis of diesel. The deactivation layer was present within the unions at the front and back end of the trapping capillary. Modulation voltages were 30 V (A and D), 45 V (B and E), 50 V (F), and 55V (C).

SEM and EDX results

The SEM images for DB-PS1 #27 as seen in Fig. 3.A.5, confirmed the creation of a sorbent material after treatment. At a magnification of ~ 100 times (A), the surface within the capillary was uniform with no large gaps or holes. Under higher magnification, it was evident that the entire stationary phase had adhered to the deactivation layer to create a new porous layer. There were no flakes of decomposed PDMS stationary phase left after treatment and the surface was covered with high surface area nanoparticles.

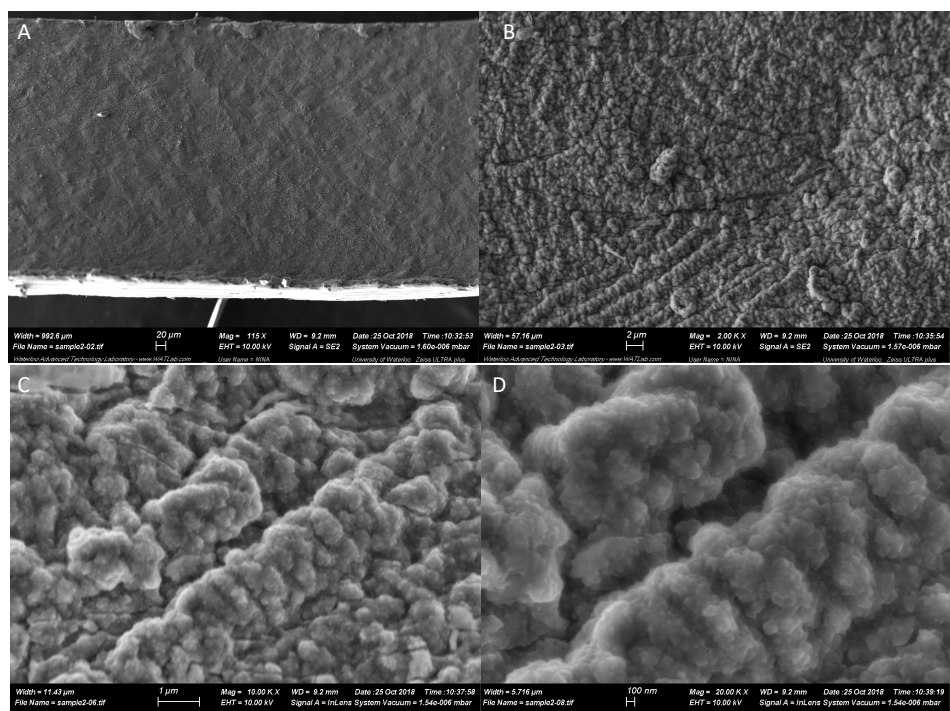


Figure 3.A. 5 SEM images of DB-PS1 #27, (A) ~100x magnification treated, (B) 2,000 magnification treated, (C) 10,000x magnification treated, and (D) 20,000x magnification treated.

Fig 3.A.6 displays the area which was chosen for analysis, as well as the spectra obtained for the untreated and treated DB-PS1 #27. The untreated spectrum was placed above the treated spectrum for direct comparison. It is important to note the different x-axis scales between the untreated and treated spectra. After treatment there was an increase of oxygen relative to silicon when compared to the untreated capillary spectrum. This was consistent with the conversion of PDMS to carbon-doped silica.

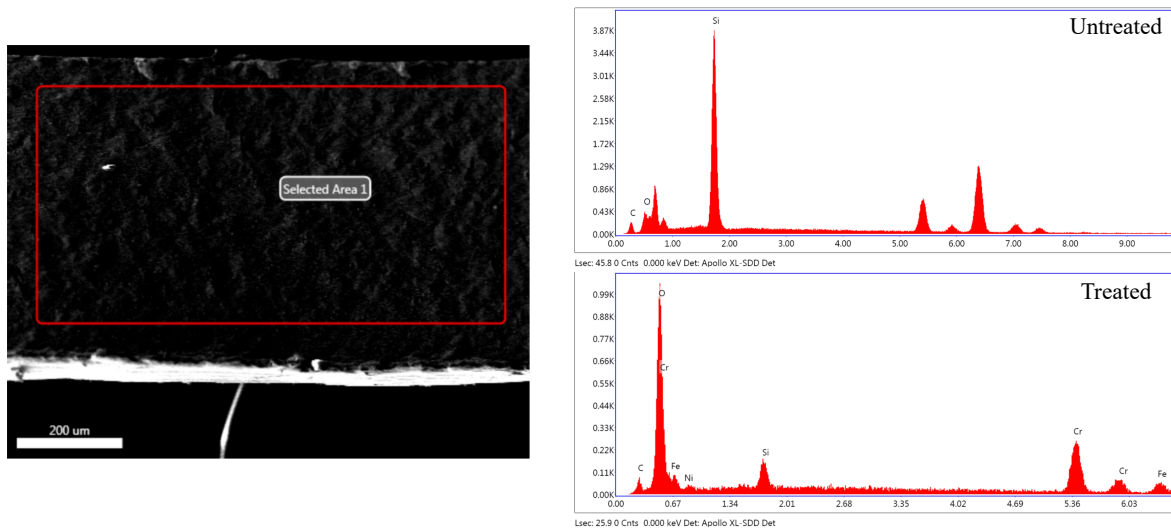


Figure 3.A. 6 EDX results of DB-PS1 #27 compared to the spectra obtained for the untreated DB-PS1.

Fig. 3.A.7 displays the SEM results at various magnifications for DB-PS1 #11. Visually, the appearance of the surface was similar to that of DB-PS1 #9, which was treated at a higher voltage of 40 V followed by 35 V. The stationary phase has been cracked and damaged, as seen in Fig. 3.A.7B with several different surfaces present. At a higher magnification (C), it was easier to visualize each individually. The dark smooth surface was the stationary phase that has been slightly broken down, the bright reflective white flake was the decomposed section of the stationary phase and the nanoparticle present is only partially created. In comparison to the slightly higher treatment process that was previously analyzed, it was clear that with a lower voltage, the same conversion process has begun but not fully completed.

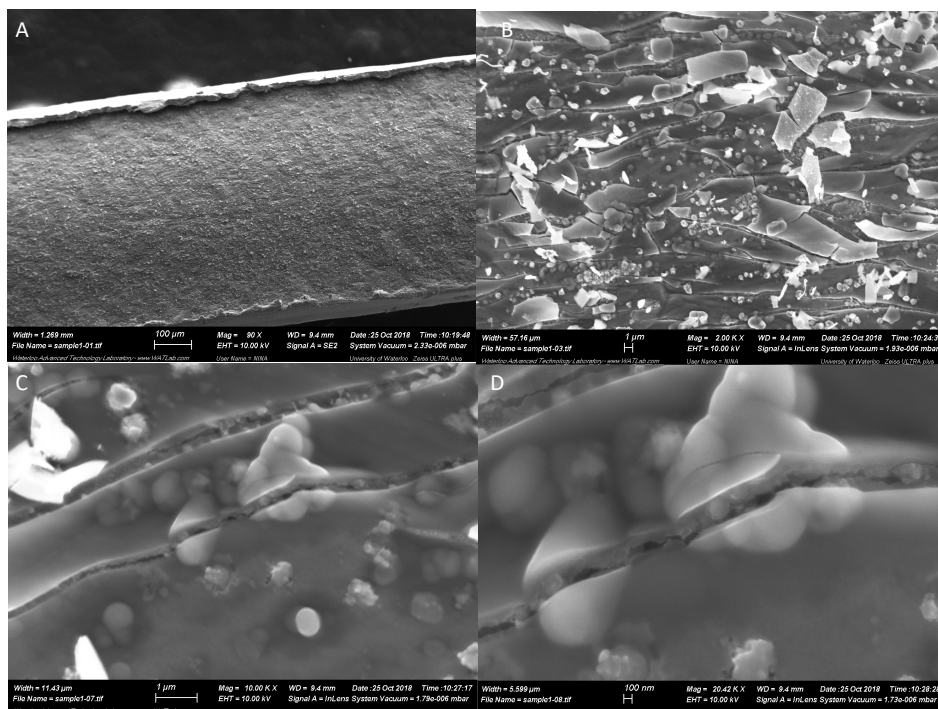


Figure 3.A. 7 SEM images of DB-PS1 #11, (A) ~100x magnification treated, (B) 2,000x magnification treated, (C) 10,000x magnification treated, and (D) 20,000x magnification treated.

The EDX results of DB-PS1 #11 of the area examined, as well as the corresponding spectra are displayed in Fig. 3.A.8. After treatment, the relative intensity of oxygen increased in relation to silicon. This was consistent with conversion of PDMS to silica.

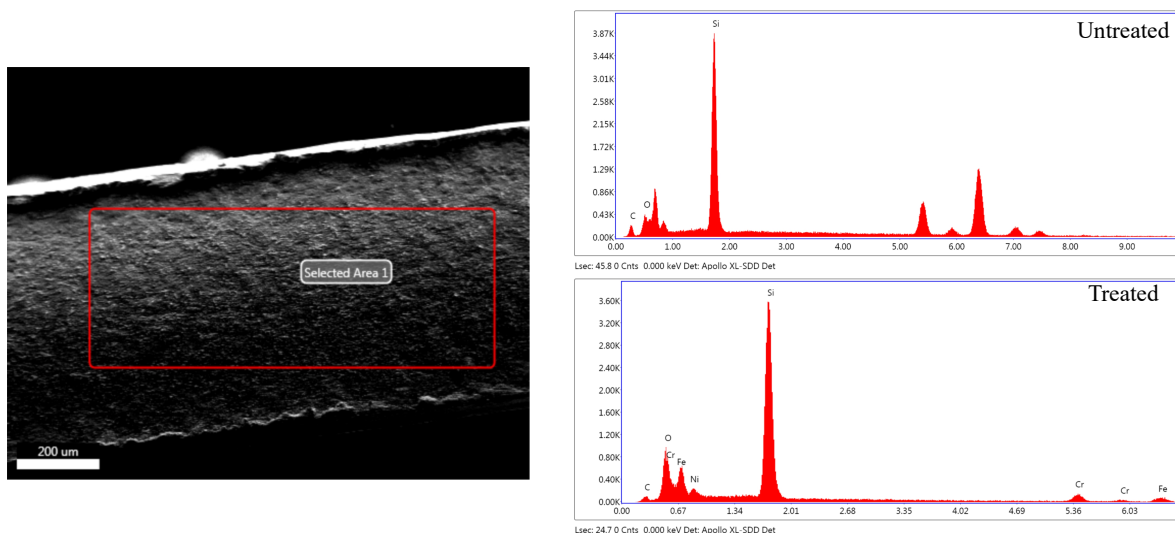


Figure 3.A. 8 EDX results of DB-PS1 #11 compared to the spectra obtained for the untreated DB-PS1.

The SEM images at various magnifications for DB-PS2887 #27 are displayed in Fig. 3.A.9. Under low magnification of 100 times, the surface of the phase appeared uniform with no large gaps or holes. Under closer inspection at 5,000 (C) and 20,000 (D) magnification, the surface appeared rough and cracked with various textures. The stationary phase had been decomposed and adhered to the underlying deactivation layer. The extreme temperature increase that was applied during treatment drastically altered the original material resulting in smaller and less abundant nanoparticles scattered amongst the decomposed phase. This may explain the inferior chromatographic performance of this trapping capillary.

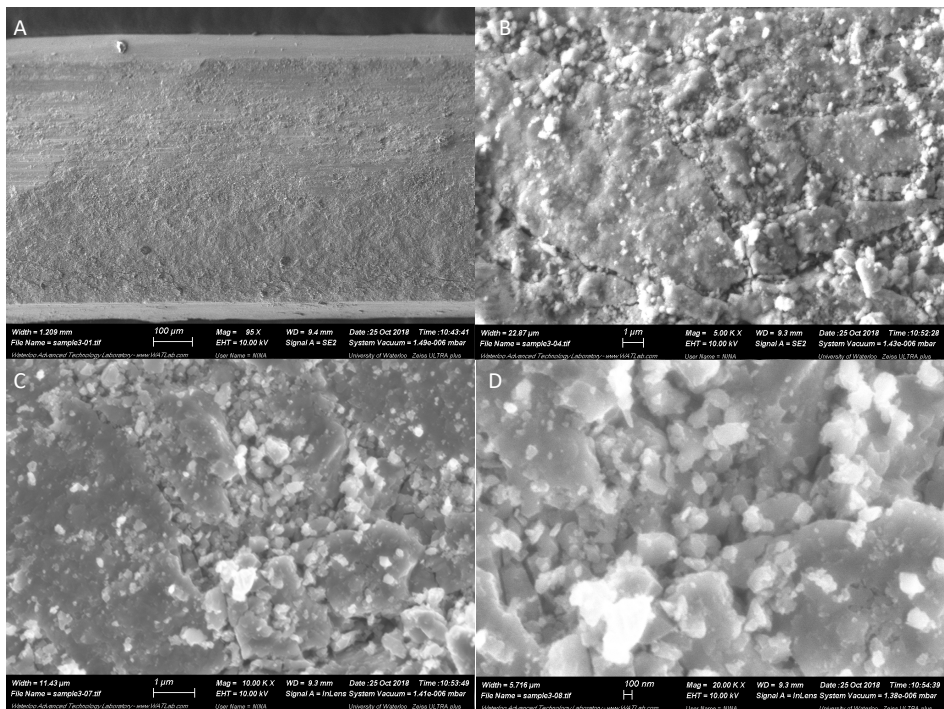


Figure 3.A.9 SEM images of DB-PS2887 #22, (A) ~100x magnification treated, (B) 5,000x magnification treated, (C) 10,000x magnification treated, and (D) 20,000x magnification treated.

EDX analysis was applied to the entire surface area, as seen in Fig. 3.A.10. Compared to the spectrum of the untreated capillary, the presence of chromium and oxygen increased after treatment. Silicon appeared to be non-existent after treatment; however, when the presence of metals was taken into consideration it was considered that silicon was likely present in a higher abundance. The relative increase of oxygen signal was consistent with conversion of PDMS to silica.

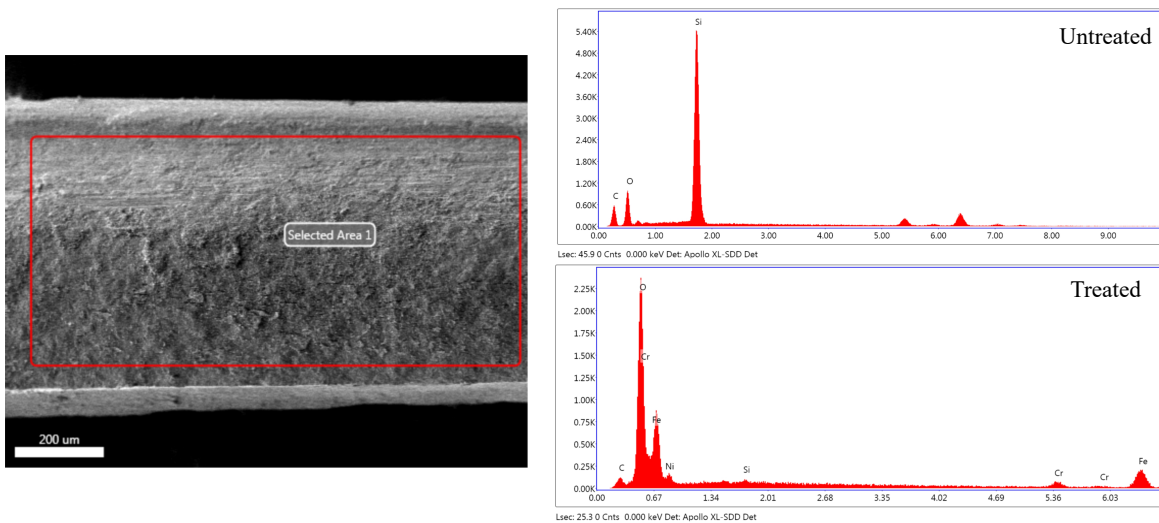


Figure 3.A. 10 EDX results of DB-PS2887 #22 compared to the spectra obtained for the untreated DB-PS2887.

SEM images of the surface's topography of DB-PS2887 # 25 are displayed in Fig. 3.A.11. Gold coating was also applied to this sample to ensure detailed images could be acquired. Amongst all four of the magnifications captured, it was difficult to differentiate the stationary phase from the underlying deactivation layer. Fig. 3.A.11B best displays each of these different surfaces. The stationary phase was the glossy, smooth surface with a reflective appearance and the deactivation layer was the rougher surface with a sand-like appearance. The low voltages applied in this treatment process altered the stationary phase only slightly. The gaps and holes in the phase, which were present before treatment, remained. The areas of stationary phase which did not contain a gap were consistent and smooth. None of the stationary phase had been converted into the sorbent nanoparticle material. The thickness of the stationary phase was clearly seen, similar to that within DB-PS2887 #17, which was treated at a slightly higher set of voltages. Overall, this phase looked very similar to that of the original, untreated DB-PS2887.

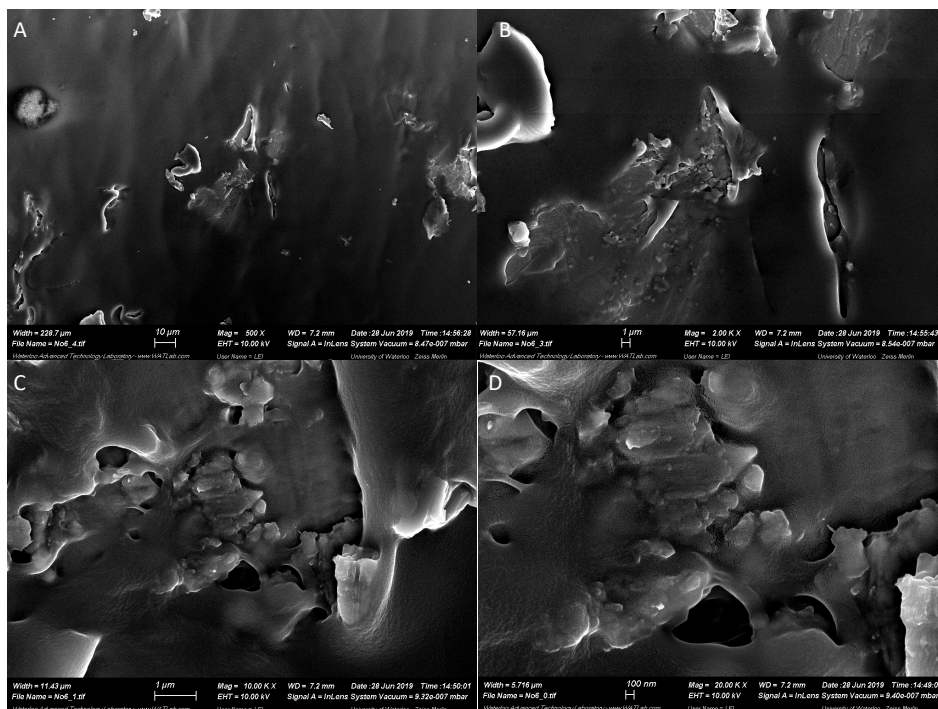


Figure 3.A. 11 SEM images of DB-PS2887 #25, (A) 500x magnification treated, (B) 2,000x magnification treated, (C) 10,000x magnification treated, and (D) 20,000x magnification treated.

EDX was also performed on the two different surfaces within DB-PS2887 #25, as seen in Fig. 3.A.12. Area 1 corresponded to the underlying deactivation layer and area 2 corresponded to the stationary phase that had been barely converted during the treatment process. Relative intensities of the iron and chromium signals in area 2 were higher than in the untreated capillary and area 3, indicating the treatment led to less shielding of the underlying metal capillary. The intensity of oxygen in the two areas was higher than the untreated capillary, indicating the partial decomposition of the stationary phase. The incomplete transformation of the original material to the desired adsorbent with silicon-based nanoparticles was substantiated by the SEM and EDX results.

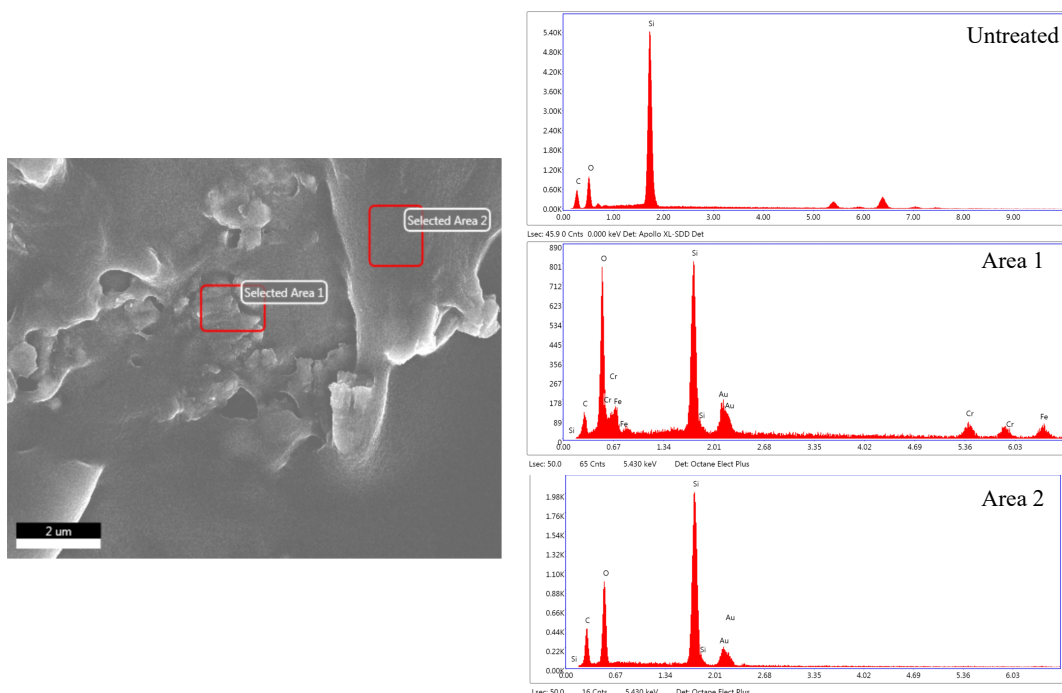


Figure 3.A. 12 EDX results of DB-PS2887 #25 for two separate areas compared to the spectra obtained for the untreated DB-PS2887.

Treatment plan for different portions of the entire trapping capillary

Performance results

DB-PS1 #43 was first analyzed in configuration A. Passive cooling at a range of modulation voltages from 25 V to 50 V was applied, as seen in Fig. 3.A.13. With a lower modulation voltage of 30 V, the overall separation in the ²D was adequate. However, the combination of a strong adsorbent and low modulation voltage resulted in streaking due to poor remobilization of analytes. Increasing the modulation voltage by 10 V eliminated the presence of the majority of streaking in the ²D. An additional 10 V caused pyrolysis of the diesel, decomposing a small portion of the sample. In comparison to the previously acquired GC×GC

chromatograms with the partially treated trapping capillaries, this trap was deemed inferior and not evaluated further.

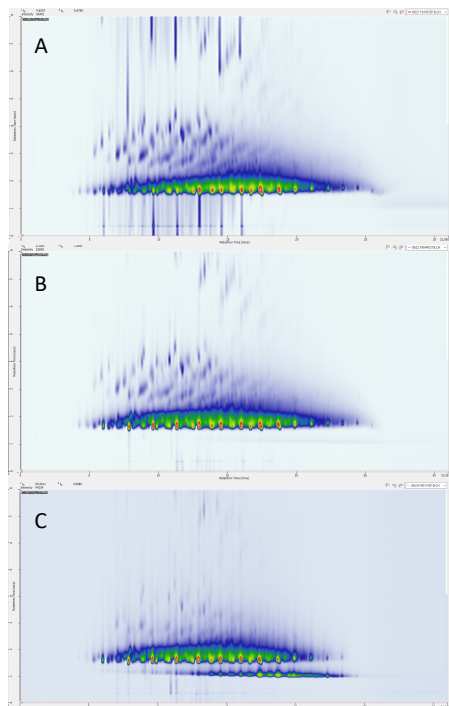


Figure 3.A. 13 Comparison of the performance of the DB-PS1 (Configuration A) trapping capillary at various modulation voltages with passive cooling (A - C) in the analysis of diesel. The deactivation layer was present within the unions at the front and back end of the trapping capillary. Modulation voltages were 30 V (A), 40 V (B) and 50 V (C).

The analysis of diesel at various modulation voltages with active cooling with DB-PS2887 #36 trapping capillary is displayed in Fig. 3.A.14. Separation of various groups from the unresolved mixture was achieved at a low modulation voltage of 25 V (A) without streaking in the ²D. A similar separation was obtained with a modulation voltage of 30 V (B). Increasing the modulation voltage to 40V caused extreme column bleed to occur below the unresolved mixture at the beginning of the ²D. However, pyrolysis of the diesel sample did not occur at this modulation voltage. It was concluded that the center treatment of DB-PS2887 at 40 V and 35 V was another viable option. The combination of a less adsorbent material and more adsorbent

material was beneficial in efficiently trapping analytes and completely releasing them in a quick manner. The smaller portions of the untreated material at the ends of the trapping capillary were beneficial in this process without causing any broad streaks in the ²D. Optimal chromatographic separation of diesel was obtained at lower modulation voltage, prolonging the life of the trapping capillary.

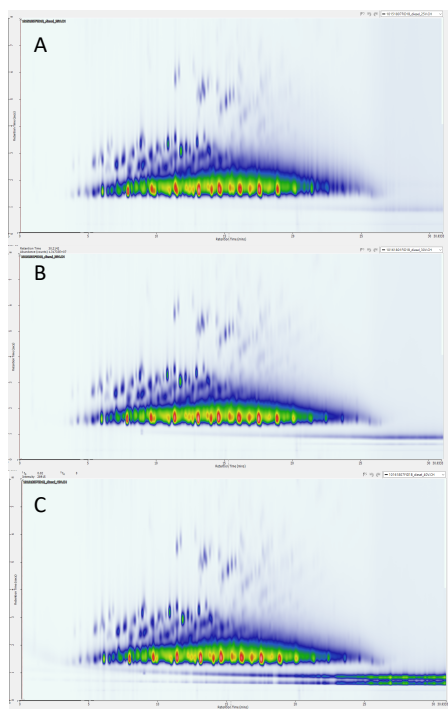


Figure 3.A. 14 Comparison of the performance of the DB-PS2887 #36 trapping capillary at various modulation voltages with active cooling (A - C) in the analysis of diesel. The deactivation layer was present within the unions at the front and back end of the trapping capillary. Modulation voltages were 25 V (A), 30 V (B) and 40 V (C).

SEM and EDX results

The SEM images at various magnifications of DB-PS1 #40 are displayed in Fig. 3.A.15. Magnification of 500 times displayed the overall uneven surface of the phase with two varying colors, as depicted in Fig. 3.A.15A. Under closer examination (B-D), the varying materials of the

phase were identified. The underlying, dark, spongy material corresponded to the altered deactivation layer. The broken, dark and glossy materials were the stationary phase that had been decomposed. The light-colored flakes that appeared to be loose corresponded to the intermediate product of the stationary phase as it adhered to the deactivation layer to create nanoparticles. The porous round particles randomly dispersed along the surface were the nanoparticles. Despite being treated with a higher set of voltages, the surface topography was similar to that of DB-PS1 #9, which was treated at 40 V and 35 V. However, the chromatographic performances of DB-PS1 #9 and #40 were drastically different from one another. The latter produced extreme streaking within the 2D , causing broad bands which co-eluted with other important compounds.

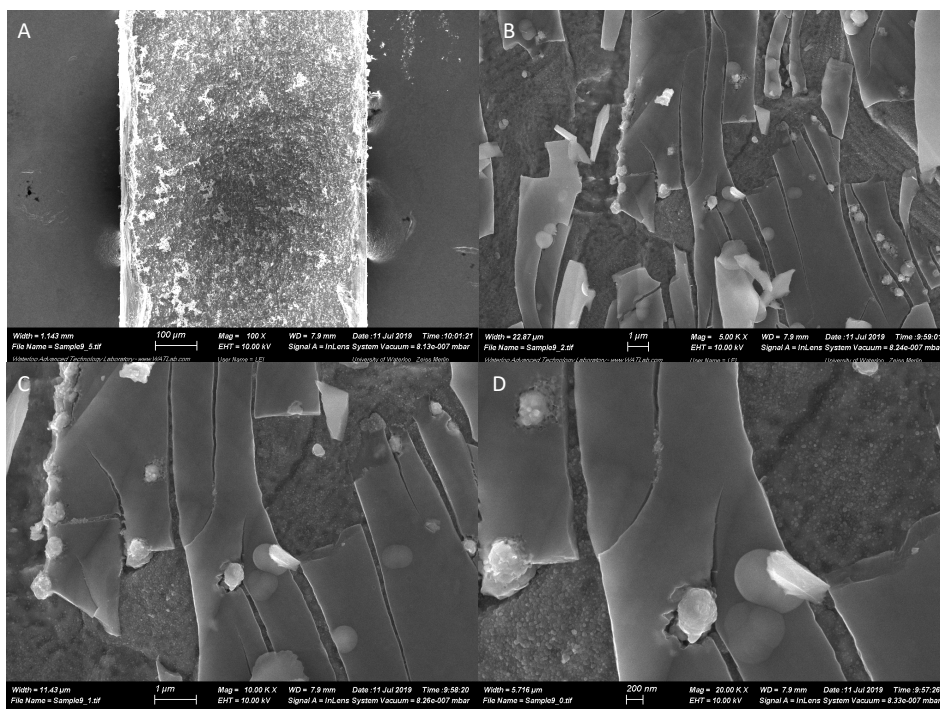


Figure 3.A. 15 SEM images of DB-PS1 #40, (A) 100x magnification treated, (B) 5,000x magnification treated, (C) 10,000x magnification treated, and (D) 20,000x magnification treated.

EDX analysis was performed on the three distinctive materials to characterize the elemental composition of DB-PS1 #40, as seen in Fig. 3.A.16. The nanoparticle composition was noted by Spot 1, while areas 1 and 2 corresponded to the underlying deactivation layer and intermediate decomposed stationary phase, respectively. Relative intensities of the iron and chromium signals in Spot 1 and area 2 were lower than the untreated capillary and area 1, indicating that the treatment process led to slightly better shielding of the metal capillary. The intensity of iron and chromium signals was comparable between the untreated capillary and area 1. Significant increase of oxygen in area 1 compared to spot 1 and area 2 pointed to the conversion of PDMS to silica.

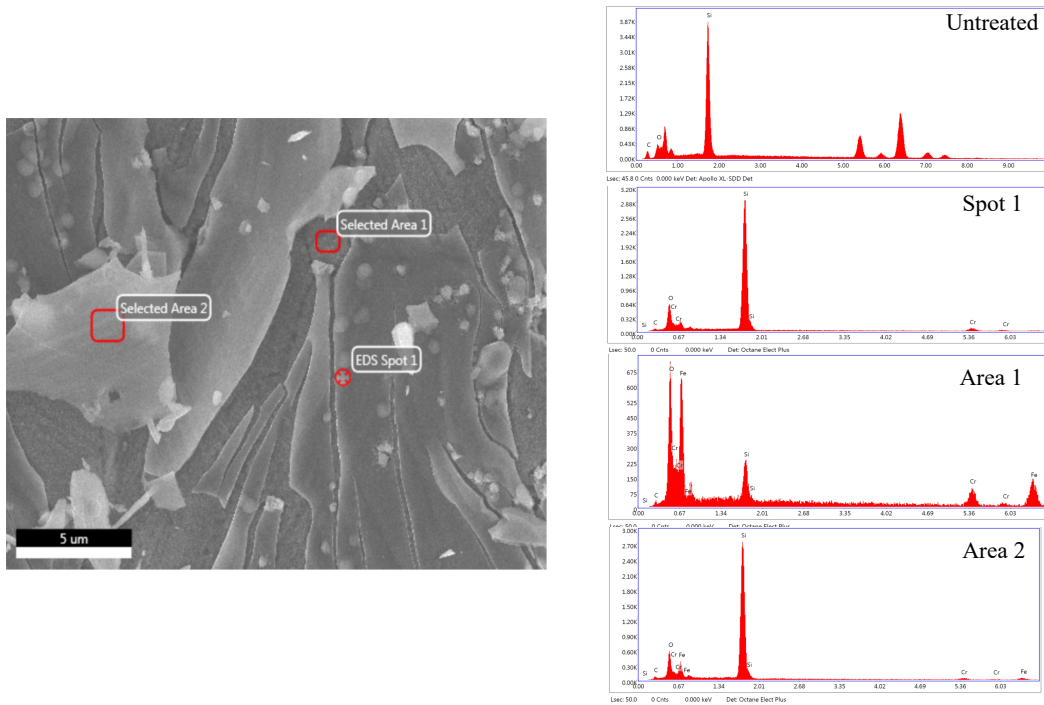


Figure 3.A. 16 EDX results of DB-PS1 #40 for two separate areas compared to the spectra obtained for the untreated DB-PS1.

Before performing SEM and EDX analysis, DB-PS2887 #39 was gold coated to ensure the results obtained were not unsatisfactory due to the excess charging on the surface. SEM images of DB-PS2887 #39 are displayed in Fig 3.A.17. Lower magnification (A) displayed the consistent surface across the phase that contained various textures but was not severely cracked and broken down. Under closer magnification, nanoparticles of various sizes were present over large sections of the surface, while the other areas were smooth and intact. The areas that were cracked contained various size nanoparticles all along the edges of the crack. The stationary phase was completely removed, only leaving the underlying deactivation phase with nanoparticles.

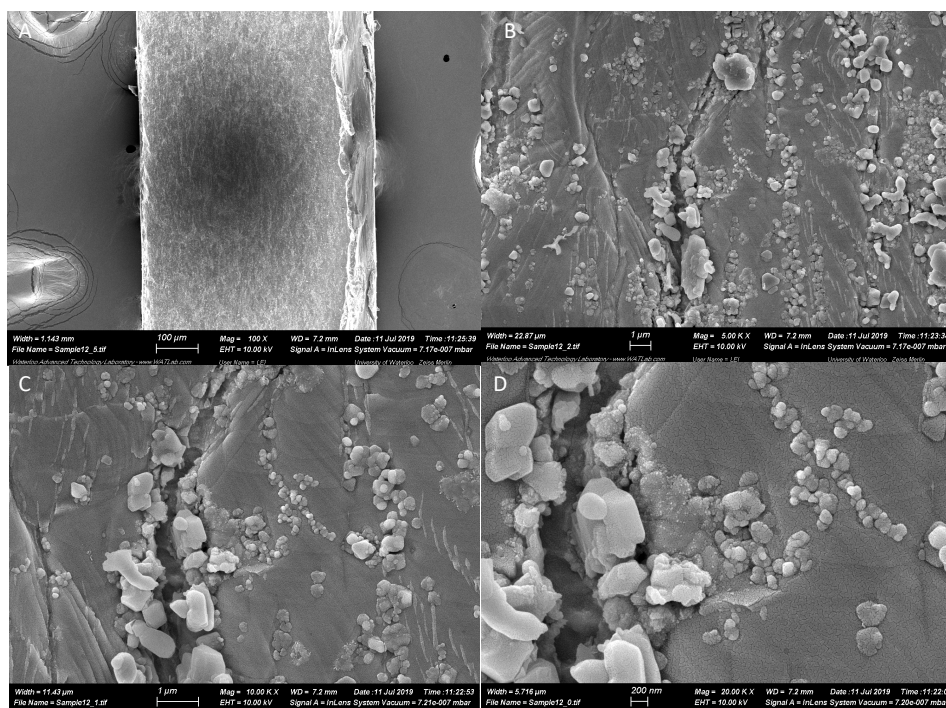


Figure 3.A. 17 SEM images of DB-PS2887 #39, (A) 100x magnification treated, (B) 5,000x magnification treated, (C) 10,000x magnification treated, and (D) 20,000x magnification treated.

EDX results of DB-PS2887 #39 are seen in Fig. 3.A.18. Area 1 corresponded to a large nanoparticle along the surface. Area 2 corresponded to the smooth underlying deactivation layer

where no nanoparticles were located. Area 3 contained to an area with several smaller nanoparticles on the surface. The intensities of iron and chromium were also higher than in the untreated capillary, indicating the treatment produced less shielding of the underlying metal capillary. The relative intensity of oxygen in all three areas were higher than in the untreated capillary, indicating the treatment process decomposed the stationary phase. Furthermore, this also indicated the conversion of PDMS to silica.

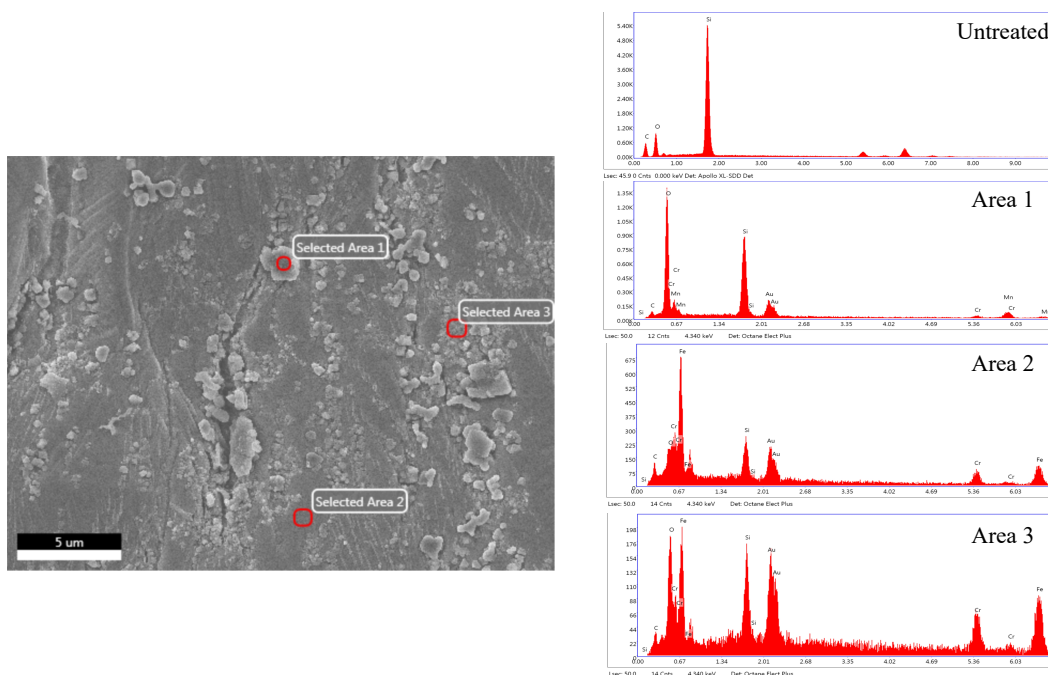


Figure 3.A. 18 EDX results of DB-PS2887 #39 for three separate areas compared to the spectra obtained for the untreated DB-PS2887.

The untreated portion of DB-PS1 #41 was also analyzed by SEM to visualize the topography of the phase, as seen in Fig. 3.A.19. It was evident that the untreated material had been altered during the consecutive modulation periods which occurred during the analyses due to the cracked and uneven surface, as seen in Fig. 3.A.19A. Under closer examination, the appearance of the material was similar to that of the treated portion of the trap (Fig. 3.27). The

stationary phase had been cracked and began to decompose, as seen in Fig. 3.A.19B. The same crystal-like structures were also created on the entire surface, as previously seen in the treated portion of the trapping capillary. However, in comparison to the treated portion, the surface appeared to be more intact and less decomposed. There were fewer flakes of stationary phase present in the untreated portion. A combination of crystal-like structures on the loose, decomposed stationary phase and nanoparticles on the underlying deactivation layer were present. This may suggest that oxygen was not necessary for the transformation of the stationary phase to an adsorbent material.

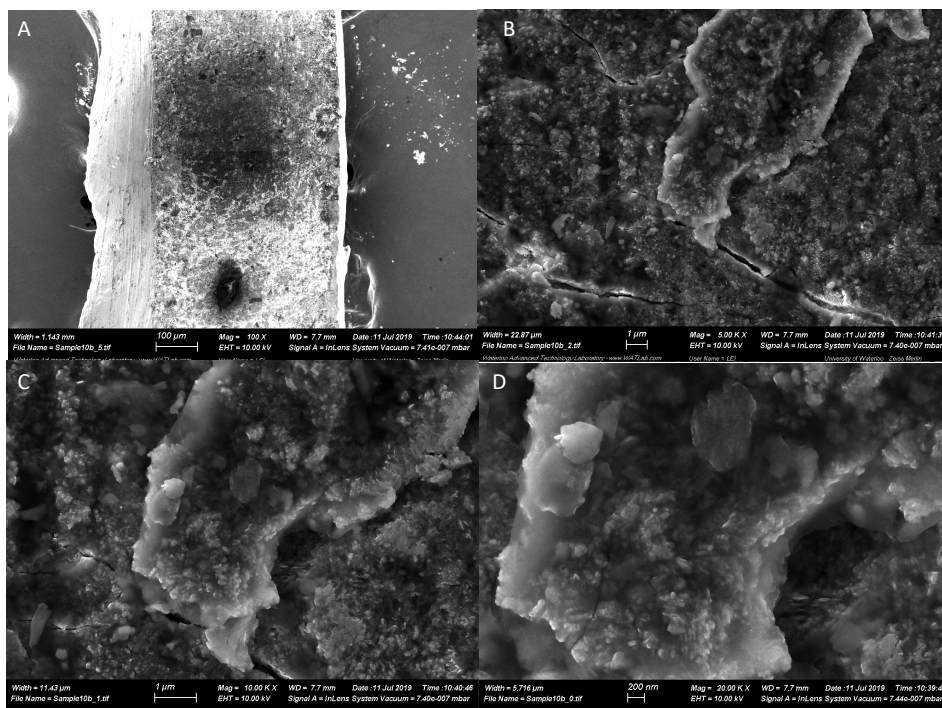


Figure 3.A. 19 SEM images of DB-PS1 #41 (Untreated Half), (A) 100x magnification treated, (B) 5,000x magnification treated, (C) 10,000x magnification treated, and (D) 20,000x magnification treated.

The EDX results for the untreated section of DB-PS1 #41 are displayed in Fig. 3.A.20. Area 1 corresponded to a smooth flake of stationary phase that was light in color. Area 2

corresponded to an underlying layer which had small nanoparticles present. Area 3 corresponded to a flake of stationary phase that had crystal-like structures. The relative intensity of oxygen in all three areas was higher than the untreated capillary, indicating the treatment process decomposed the stationary phase. Iron and chromium were higher in all three areas, indicating the treatment process resulted in less shielding of the underlying metal capillary.

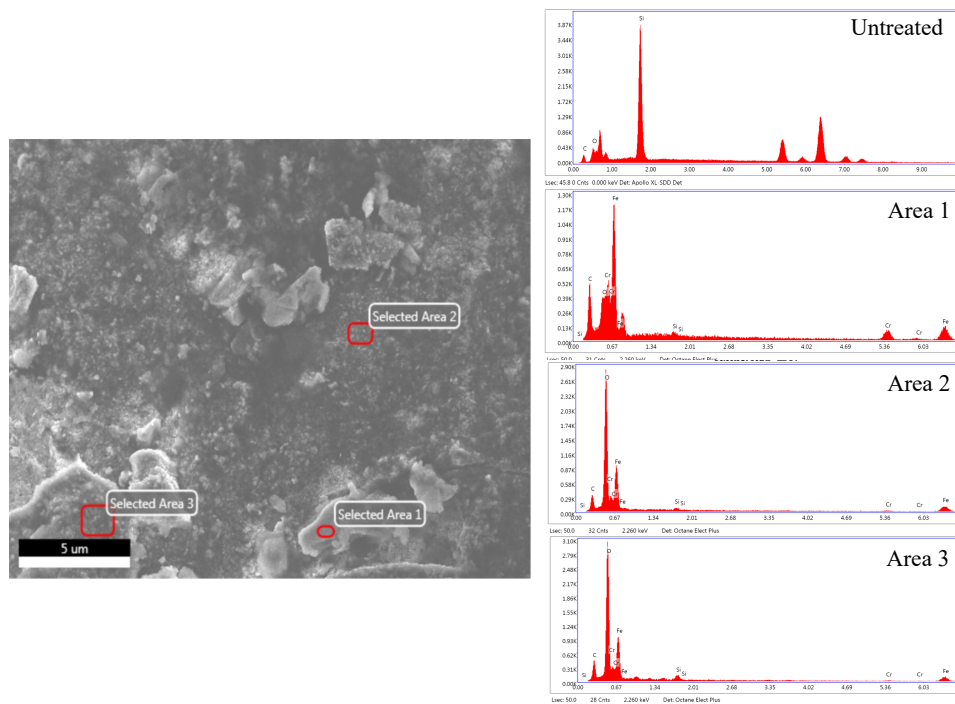


Figure 3.A. 20 EDX results of DB-PS1 #41 (Untreated Half) for three separate areas compared to the spectra obtained for the untreated DB-PS1.

DB-PS1 #43 was treated for the entire length of the trapping capillary, but one half was treated with 50 V followed by 45 V, while the other half was treated at 40 V followed by 35 V. SEM images of the half treated with higher voltages of 50 V and 45 V are displayed in Fig. 3.A.21. Under lower magnifications of 500 (A) and 2,000 (B), it was apparent that the surface was completely cracked and broken down. Closer magnifications of 10,000 (C) and 20,000 (D) displayed a surface which was cracked, exposing the underlying deactivation layer and covered with irregularly shaped crystal-like nanoparticles. The cracks did not appear as deep as those

created in DB-PS1 #32. The surface after treatment was very similar to that of DB-PS1 #41 and DB-PS1 #32. This was to be expected due to the same treatment process utilized for all three trapping capillaries.

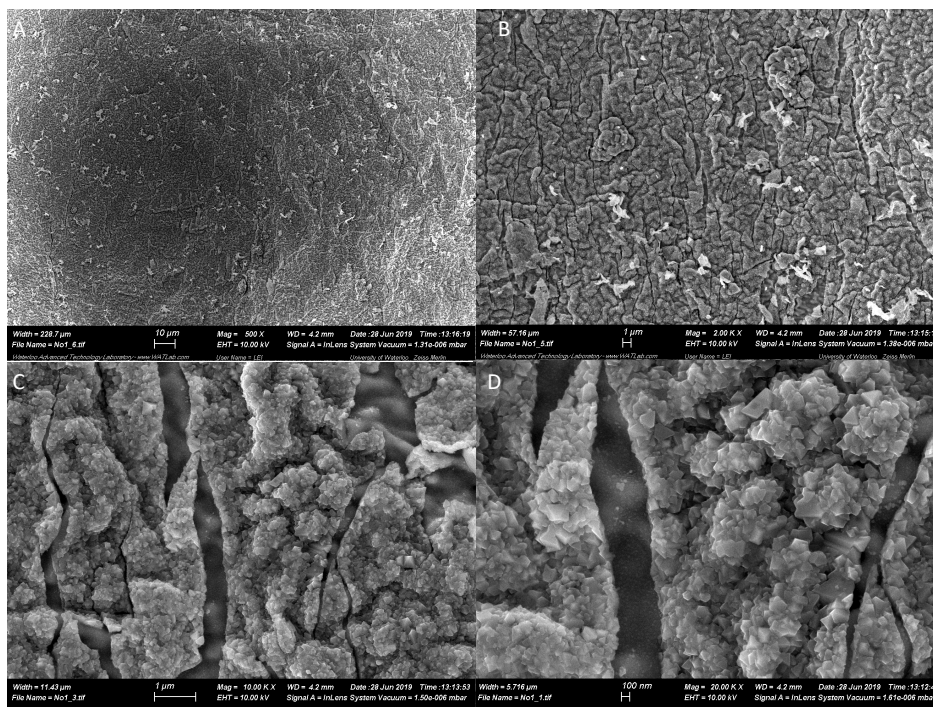


Figure 3.A. 21 SEM images of DB-PS1 #43 (Half 50 V/45 V), (A) 500x magnification treated, (B) 2,000x magnification treated, (C) 10,000x magnification treated, and (D) 20,000x magnification treated.

EDX was performed on the half of DB-PS1 #43 that was treated at 50V followed by 45V, as seen in Fig. 3.A.22. Area 1 included the crystal-like structures. Area 2 corresponded to the light colored, smooth flake of stationary phase. Areas 1 and 2 had an increase in relative abundance of oxygen, indicating the conversion of PDMS to silica. The apparent difference between the spectra for areas 1 and 2 was the abundance of silicon. However, due to the higher abundance of metals in area 1, the relative intensity of silicon was most likely comparable between areas 1 and 2.

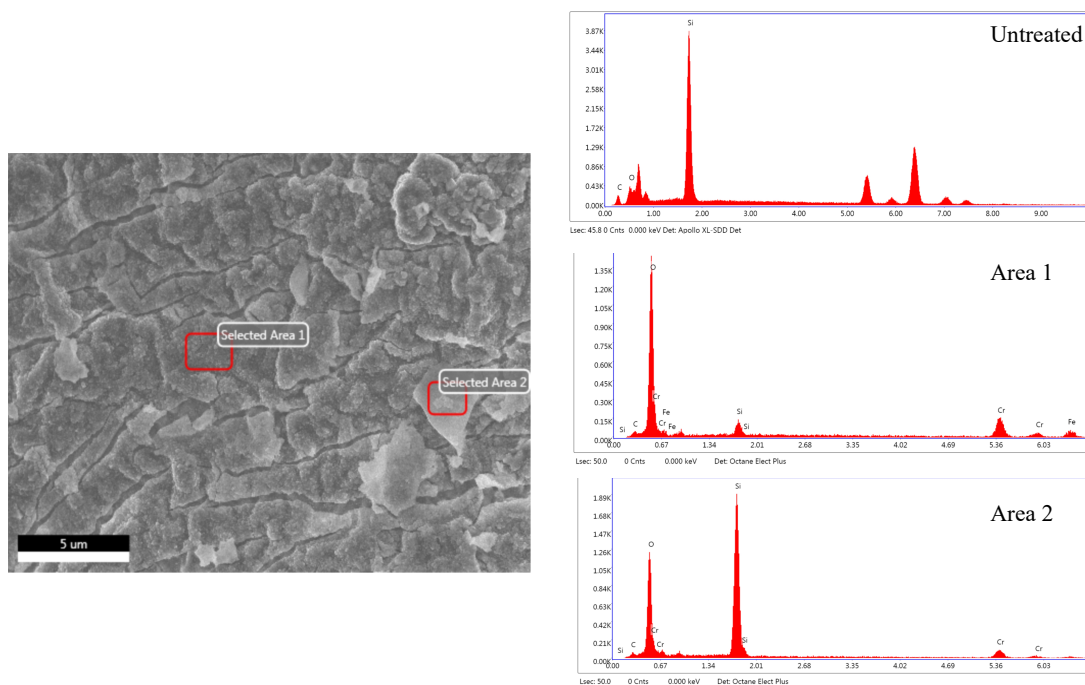


Figure 3.A. 22 EDX results of DB-PS1 #43 (Half 50 V/45 V) for two separate areas compared to the spectra obtained for the untreated DB-PS1.

SEM images of the other half of DB-PS1 #43, which was treated at 40 V followed by 35 V, are displayed in Fig. 3.A.23. Under lower magnifications of 500 (A) and 2,000 (B), the surface was uneven and cracked with small flakes of light-colored stationary phase loosely attached. With higher magnifications of 10,000 (C) and 20,000 (D) it was clear the stationary phase had been cracked and decomposed, exposing the underlying deactivation layer. Flakes of stationary phase were separated, and nanoparticles were created by the decomposed stationary phase adhering to the underlying deactivation layer. Within the cracks of the stationary phase, the nanoparticles were clearly visible. The nanoparticles present within a small section differed in appearance and size. Some appeared smooth and large, while others were smaller in size and spongier-like in appearance. The surface's topography was extremely similar to that of DB-PS1 #9, which was also treated under the same voltages of 40 V and 35 V.

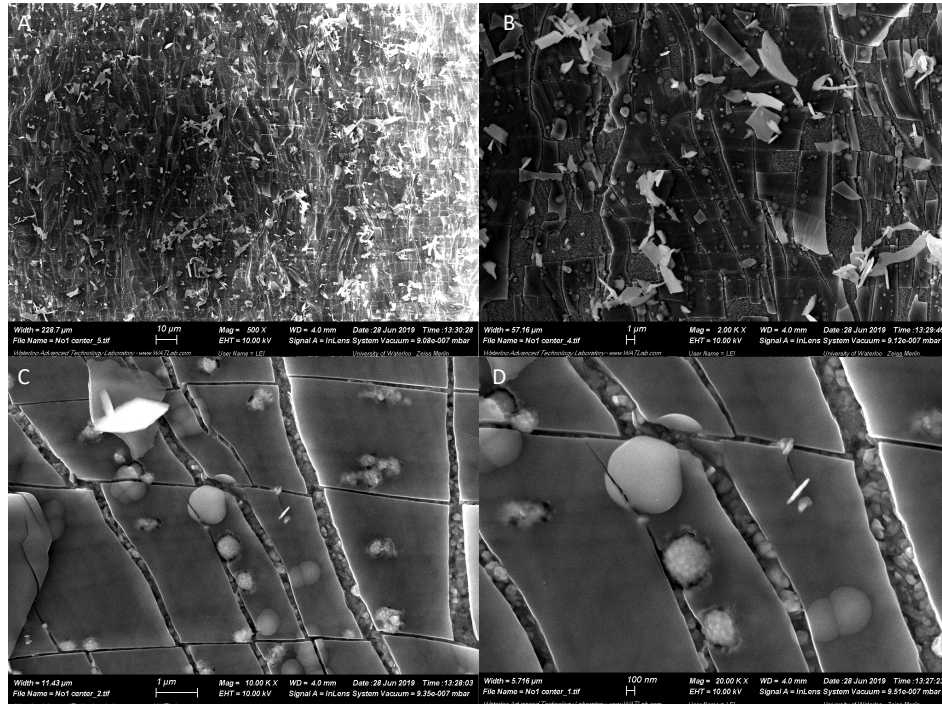


Figure 3.A.23 SEM images of DB-PS1 #43 (Half 40 V/35 V), (A) 500x magnification treated, (B) 2,000x magnification treated, (C) 10,000x magnification treated, and (D) 20,000x magnification treated.

EDX was also performed on the half of DB-PS1 #43 that was treated with 40 V and 35 V, as seen in Fig. 3.A.24. Area 1 evaluated a large, smooth surfaced nanoparticle. Area 2 corresponded to the smooth stationary phase that remained intact on top of the underlying deactivation layer, with no nanoparticles present. Area 3 corresponded to the underlying deactivation layer which contained small nanoparticles. Compared to the untreated spectrum, the relative abundance of iron and chromium decreased significantly for areas 1 and 2. The material formed after treatment must have shielded the underlying metal capillary better, as the signals for metals decreased relative to that of silicon. The increase in the abundance of silicon could have been due to better shielding of the underlying metal, or to more of the silicon-based deactivation

layer being exposed. The relative intensities of iron, chromium and oxygen increased in area 3 due to the conversion of PDMS to silica.

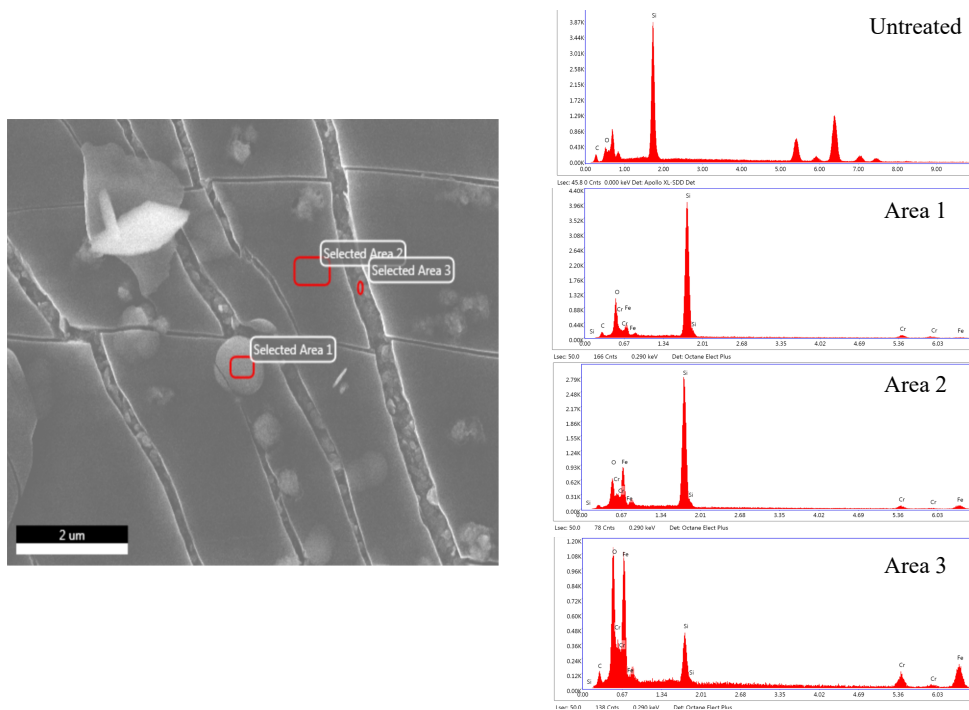


Figure 3.A. 24 EDX results of DB-PS1 #43 (Half 40 V/35 V) for three separate areas compared to the spectra obtained for the untreated DB-PS1.

Appendix B

Chapter 6 Supplementary information

Comparison of thermal and flow-based modulation in comprehensive two-dimensional gas chromatography –time-of-flight mass spectrometry (GC×GC -TOFMS) for the analysis of base oils

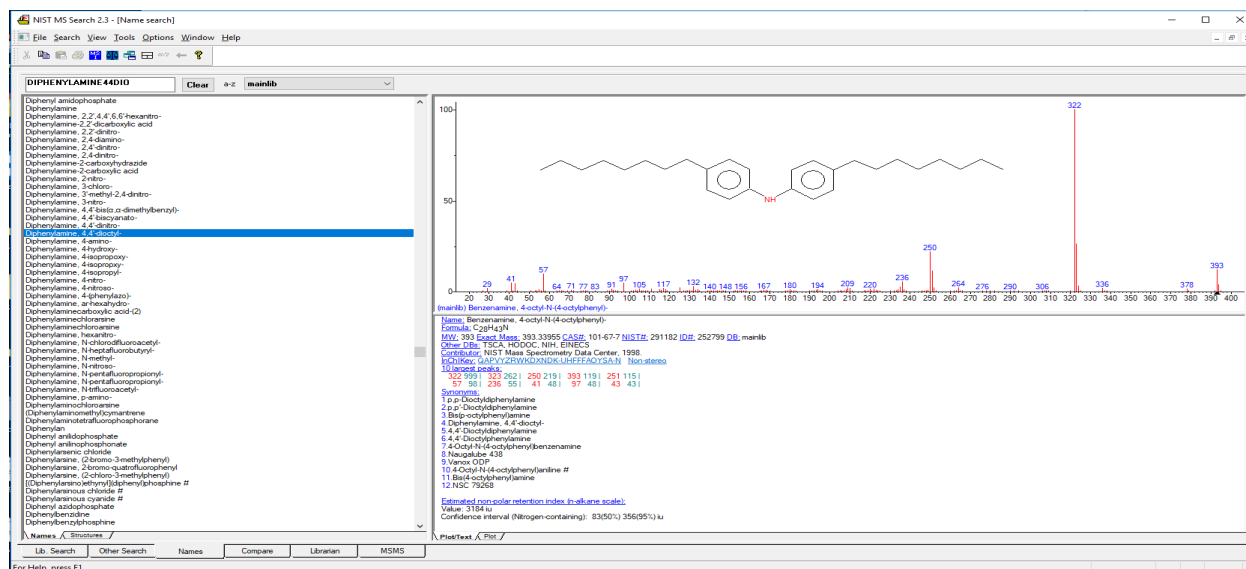
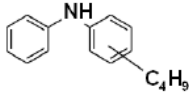
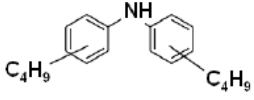
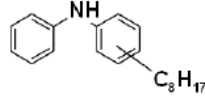
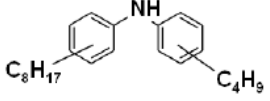
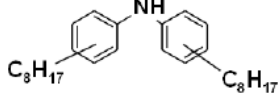
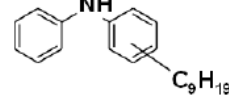
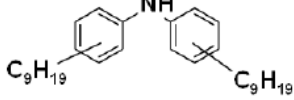
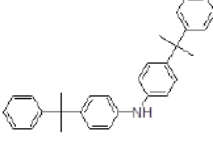
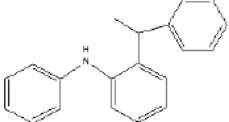


Figure 6.B. 1 NIST database search of dioctyl substituted diphenylamine.

Table 6.B. 1 Multiple reaction monitoring diagnostic transitions. Reprinted with permission from [128].

Analyte	Structure	MRM Transitions (*quantifier)
Monobutyl Diphenylamine (C4)		226→134* 226→106 226→93
Dibutyl Diphenylamine (C4C4)		282→134* 282→106 282→93
Monooctyl Diphenylamine (C8)		282→134* 282→106 282→93
Monobutyl monooctyl Diphenylamine (C4C8)		338→134* 338→94 338→106
Dioctyl Diphenylamine (C8C8)		394→134* 394→106 394→93
Monononyl Diphenylamine (C9)		296→134* 296→106 296→210
Dinonyl Diphenylamine (C9C9)		422→336 422→148 422→106 422→134*
Dimethyl-distyrenated Diphenylamine (diAMS)		406→196* 406→119 406→103
Monostyrenated Diphenylamine MS (two isomers)		274→182*(peak 1) 274→180*(peak 2) 274→105

Appendix C

Chapter 7 Replicate data

Modified flow modulator: A proof of concept hybrid interface

Table 7.C. 1 Reproducibility of peak width at half height (ms) with 0.5 μm cooling trap in the absence and presence of cooling (2000 ms)

Peak Width at Half Height (ms)								
	Jet Off				2000 ms cooling			
Compound	Rep 1	Rep 2	Rep 3	%RSD	Rep 1	Rep 2	Rep 3	%RSD
C7	275	287	281	2.2	270	276	271	1.2
C8	526	518	516	1.0	532	538	531	0.8
C9	539	519	525	1.9	484	501	504	2.2
C10	308	309	301	1.5	231	228	235	1.6
C11	537	549	550	1.3	649	663	676	2.0
C12	374	349	366	3.5	211	209	216	1.6
C13	551	624	602	6.4	530	505	512	2.5
C14	676	719	690	3.2	618	619	622	0.3
C15	324	309	318	2.3	593	578	565	2.4
C16	593	549	561	4.0	182	178	177	1.4
C17	724	738	679	4.3	361	315	353	7.1
C18	563	538	533	3.0	161	165	163	1.0
C19	419	391	394	3.8	282	301	291	3.3
C20	611	598	603	1.0	292	269	280	4.2
C21	743	690	728	3.8	250	249	253	0.9
C22	759	704	715	4.0	224	224	233	2.4
C23	643	618	570	6.1	242	240	239	0.7
C24	578	602	552	4.3	243	250	258	2.9
C25	727	740	773	3.2	240	224	220	4.5
C26	728	739	742	1.0	239	255	241	3.4
C27	634	603	580	4.5	271	258	259	2.7
C28	710	732	742	2.3	251	260	256	1.7
C29	715	762	755	3.4	257	253	252	1.1
C30	775	738	734	3.0	271	269	272	0.7
C31	766	794	797	2.2	350	344	326	3.8
C32	274	779	787	47.9	392	388	388	0.5
C33	777	796	809	2.1	475	466	444	3.5
C34	806	790	824	2.1	548	535	543	1.2
Avg	595	610	608	4.6	345	341	342	2.2

Table 7.C. 2 Reproducibility of ¹D retention time (min) with 0.5 μm cooling trap in the absence and presence of cooling (2000 ms)

Primary Retention Time								
	Jet Off				2000 ms cooling			
Compound	Rep 1	Rep 2	Rep 3	%RSD	Rep 1	Rep 2	Rep 3	%RSD
C7	3.23	3.23	3.23	0.00	3.23	3.23	3.23	0.00
C8	4.37	4.37	4.37	0.00	4.37	4.37	4.37	0.00
C9	5.88	5.88	5.88	0.00	5.88	5.88	5.88	0.00
C10	7.53	7.53	7.53	0.00	7.53	7.53	7.53	0.00
C11	9.10	9.10	9.10	0.00	9.10	9.10	9.10	0.00
C12	10.68	10.68	10.68	0.00	10.68	10.68	10.68	0.00
C13	12.11	12.11	12.11	0.00	12.10	12.10	12.10	0.00
C14	13.47	13.47	13.47	0.00	13.47	13.47	13.47	0.00
C15	14.84	14.84	14.84	0.00	14.76	14.76	14.76	0.00
C16	16.05	16.05	16.05	0.00	16.03	16.05	16.05	0.07
C17	17.20	17.20	17.20	0.00	17.19	17.19	17.19	0.00
C18	18.35	18.35	18.35	0.00	18.35	18.35	18.35	0.00
C19	19.42	19.42	19.42	0.00	19.35	19.35	19.35	0.00
C20	20.43	20.43	20.43	0.00	20.38	20.39	20.35	0.09
C21	21.36	21.36	21.36	0.00	21.35	21.35	21.35	0.00
C22	22.29	22.29	22.29	0.00	22.28	22.28	22.28	0.00
C23	23.22	23.22	23.22	0.00	23.17	23.17	23.17	0.01
C24	24.08	24.08	24.08	0.00	24.02	24.02	24.02	0.01
C25	24.86	24.86	24.86	0.00	24.85	24.85	24.85	0.01
C26	25.65	25.65	25.64	0.03	25.64	25.64	25.64	0.01
C27	26.43	26.44	26.43	0.00	26.41	26.41	26.41	0.00
C28	27.16	27.16	27.16	0.00	27.14	27.14	27.14	0.00
C29	27.87	27.87	27.87	0.00	27.86	27.86	27.85	0.00
C30	28.59	28.59	28.59	0.00	28.57	28.57	28.57	0.01
C31	29.37	29.38	29.37	0.03	29.34	29.34	29.34	0.01
C32	30.32	30.23	30.23	0.17	30.20	30.20	30.20	0.01
C33	31.22	31.22	31.22	0.01	31.15	31.18	31.15	0.04
C34	32.36	32.36	32.39	0.06	32.29	32.31	32.29	0.03
Avg				0.01				0.01

Table 7.C. 3 Reproducibility of ²D retention time (s) with 0.5 μm cooling trap in the absence and presence of cooling (2000 ms)

Secondary Retention Time								
	Jet Off				2000 ms cooling			
Compound	Rep 1	Rep 2	Rep 3	%RSD	Rep 1	Rep 2	Rep 3	%RSD
C7	1.16	1.17	1.16	0.56	1.17	1.18	1.17	0.61
C8	1.36	1.39	1.37	0.91	1.41	1.42	1.39	1.1
C9	1.51	1.55	1.52	1.1	1.76	1.76	1.62	4.7
C10	1.80	1.81	1.80	0.27	1.88	1.88	1.87	0.27
C11	1.19	1.20	1.20	0.27	1.47	1.44	1.41	2.1
C12	1.70	1.72	1.71	0.50	1.89	1.89	1.88	0.25
C13	1.17	1.18	1.17	0.43	1.81	1.82	1.80	0.61
C14	1.16	1.16	1.16	0.31	1.82	1.83	1.80	0.9
C15	1.71	1.73	1.71	0.83	1.83	1.83	1.82	0.18
C16	1.41	1.46	1.42	1.8	1.88	1.92	1.91	1.15
C17	1.14	1.14	1.14	0.27	1.86	1.86	1.88	0.58
C18	1.42	1.44	1.45	1.1	1.96	1.97	1.94	0.72
C19	1.60	1.60	1.62	0.83	1.90	1.92	1.88	1.1
C20	1.29	1.35	1.34	2.5	1.94	1.95	1.89	1.7
C21	1.12	1.12	1.12	0.28	1.95	1.95	1.92	1.0
C22	1.12	1.11	1.11	0.32	1.99	1.98	1.98	0.28
C23	1.29	1.29	1.35	2.4	2.01	2.04	2.00	0.9
C24	1.39	1.33	1.37	2.3	2.04	2.05	2.04	0.35
C25	1.10	1.11	1.11	0.22	2.04	2.05	2.03	0.43
C26	1.10	1.10	1.10	0.36	2.07	2.08	2.05	0.8
C27	1.11	1.09	1.10	0.79	2.08	2.09	2.09	0.28
C28	1.10	1.11	1.10	0.33	2.09	2.10	2.11	0.31
C29	1.10	1.09	1.10	0.54	2.12	2.13	2.13	0.14
C30	1.12	1.15	1.13	1.2	2.21	2.21	2.18	0.62
C31	1.18	1.33	1.17	7.3	2.32	2.32	2.30	0.49
C32	1.78	1.25	1.26	21.1	2.47	2.45	2.44	0.75
C33	1.34	1.35	1.34	0.20	2.64	2.62	2.62	0.52
C34	1.47	1.47	1.60	5.1	2.80	2.81	2.78	0.53
Avg				1.9				0.83

Table 7.C. 4 Reproducibility of peak height with 0.5 μm cooling trap in the absence and presence of cooling (2000 ms)

Peak Height: Tallest Slice								
	Jet Off				2000 ms cooling			
Compound	Rep 1	Rep 2	Rep 3	%RSD	Rep 1	Rep 2	Rep 3	%RSD
C7	27568600	25776900	26400100	3.4	26154300	26126600	26492900	0.78
C8	15930900	15691600	15935000	0.88	15051100	15055400	15534100	1.8
C9	13633000	13443500	13409700	0.89	12820900	12798800	12593400	1.0
C10	11386100	11037100	11218500	1.6	9857360	10552100	10610600	4.05
C11	15621000	15208000	15132000	1.7	11911500	12024000	12229900	1.3
C12	11891800	11803900	11691000	0.85	11267200	12020300	12385500	4.8
C13	15092100	14010900	14385000	3.8	13559000	14671600	14005500	4.0
C14	11969800	11617700	11281600	3.0	14020100	14180300	14198700	0.70
C15	11724900	10501300	11203200	5.5	12309700	13382900	13368600	4.73
C16	11558000	11637500	11913300	1.6	19124400	17993100	19181800	3.6
C17	13007500	12832100	13816700	4.0	17611500	19665500	18608200	5.5
C18	11668600	11689000	11603300	0.38	14077100	14648300	16934000	9.9
C19	11520000	11697500	11042400	3.0	22183000	20986500	21054500	3.14
C20	11619500	11397600	11326100	1.3	17504900	17870100	18114200	1.72
C21	9865970	10292900	9986980	2.2	25266600	26349200	26639200	2.77
C22	9270060	10458700	10856100	8.1	27581400	29215700	29130700	3.21
C23	11095000	11228800	11419600	1.5	23115500	23095800	22441400	1.7
C24	11215800	10531700	11115000	3.4	24979100	25219400	24172000	2.2
C25	11037700	10597100	10159700	4.1	23256200	24158700	25755800	5.2
C26	9714440	9203580	9448010	2.7	23738900	24249600	24954200	2.5
C27	12798700	13555500	13588000	3.4	16367300	16443900	17051700	2.3
C28	10362300	9442190	10186000	4.9	22346900	22399400	22765200	1.0
C29	11014500	9590750	10322300	6.9	20169200	20773300	20318000	1.5
C30	9151140	9686600	10220800	5.5	16571200	18136300	17434500	4.5
C31	9475320	8789870	8946310	4.0	13668400	13304100	15156400	7.0
C32	7251430	6912920	7162370	2.5	10979400	11095900	11851100	4.2
C33	7049490	6038070	6628620	7.7	10350800	10650300	11639200	6.2
C34	5222870	5241320	5357190	1.4	8108120	8060140	9354620	8.6
Avg				3.2				3.6

Table 7.C. 5 Reproducibility of total peak area with 0.5 μ m cooling trap in the absence and presence of cooling (2000 ms)

Peak Area: Total								
	Jet Off				2000 ms cooling			
Compound	Rep 1	Rep 2	Rep 3	%RSD	Rep 1	Rep 2	Rep 3	%RSD
C7	839142000	822685000	826498000	1.0	790431000	799208000	799289000	0.64
C8	851369000	830585000	837564000	1.3	792408000	801940000	809846000	1.1
C9	920071600	905128500	907710500	0.88	855629700	879026600	874465200	1.4
C10	959038000	942398000	947747000	0.89	895695000	906658400	910126000	0.83
C11	948238600	933222600	936349500	0.84	855775200	1011435000	910554900	8.5
C12	961955000	954518000	948034600	0.73	903624000	865971600	867168000	2.4
C13	954866000	939957000	942390400	0.85	898225600	914431400	919807400	1.2
C14	942208600	930986300	959609700	1.5	842652000	915701600	906974000	4.5
C15	970657000	956975000	955881000	0.86	877074400	883633600	891847200	0.84
C16	965233000	951200000	950960000	0.86	968123900	917029900	922147800	3.0
C17	965180900	880776007	951557400	4.9	946489000	917670100	893902000	2.9
C18	963139000	950030000	949060000	0.82	891398000	904485000	926285000	1.9
C19	968504000	956714000	955176000	0.76	856128100	888653500	901241200	2.6
C20	968308000	961645000	957075000	0.59	897930700	897053000	908572000	0.71
C21	847606000	964574000	961821000	7.2	895369000	904843900	881485000	1.3
C22	975725000	913677000	920897100	3.6	896095000	901123000	912413000	0.93
C23	963205100	956503300	948881100	0.75	883171000	936197000	952230000	3.9
C24	965116400	970836200	956504100	0.75	883598000	1035780000	1040330000	9.0
C25	847313500	910153800	945030600	5.5	884974000	888075000	900107000	0.90
C26	827512000	963388000	949713000	8.2	872161000	883601000	896605000	1.4
C27	933640400	926839100	917411200	0.88	879964000	863166000	881375000	1.2
C28	957806000	962694000	948085000	0.78	893782000	881220000	907617000	1.5
C29	895261000	944857000	930311800	2.8	871185000	870620000	885946000	1.0
C30	900309800	953342000	944468200	3.0	876130000	875994000	891107000	1.0
C31	924033400	963939200	927436500	2.4	854812000	853150000	868605000	1.0
C32	937228600	938562300	933728200	0.27	878809000	880399000	888553000	0.59
C33	913271100	911976800	907583800	0.33	854015000	840923000	869906000	1.7
C34	903714200	901953600	851851900	3.3	848048000	846422000	862808700	1.1
Avg				2.0				2.1

Table 7.C. 6 Reproducibility of peak width at half height (ms) with 3.0 μm cooling trap in the absence and presence of cooling (2600 ms)

Peak Width at Half Height (ms)								
	Jet Off				2600 ms cooling			
Compound	Rep 1	Rep 2	Rep 3	%RSD	Rep 1	Rep 2	Rep 3	%RSD
C7	407	386	384	3.1	1235	1191	1222	1.9
C8	729	620	626	9.3	607	582	593	2.1
C9	720	721	717	0.3	616	653	659	3.6
C10	495	489	491	0.6	882	878	895	1.0
C11	767	770	744	1.9	480	486	470	1.7
C12	1008	955	1023	3.6	532	540	552	1.9
C13	709	679	680	2.5	424	412	410	1.7
C14	724	711	747	2.5	430	433	440	1.2
C15	953	933	897	3.1	452	452	454	0.3
C16	509	502	914	36.7	493	479	492	1.6
C17	806	732	763	4.8	464	458	456	0.8
C18	977	976	1038	3.6	484	489	499	1.6
C19	993	977	947	2.4	522	515	505	1.7
C20	520	517	521	0.4	533	500	503	3.6
C21	783	754	787	2.4	513	515	503	1.3
C22	852	780	794	4.7	518	542	554	3.4
C23	581	526	968	34.8	516	537	524	2.0
C24	547	527	972	36.8	551	524	523	2.9
C25	881	772	800	7.0	576	557	627	6.2
C26	869	767	785	6.8	609	528	588	7.3
C27	841	708	666	12.4	573	567	576	0.8
C28	981	848	810	10.2	598	593	557	3.9
C29	987	808	755	14.3	549	627	576	6.8
C30	947	824	852	7.4	674	668	649	2.0
C31	890	875	825	3.9	747	772	775	2.0
C32	1018	910	902	6.9	901	897	1427	28.4
C33	1189	1189	1128	3.0	1173	1108	1507	16.9
C34	1342	1230	1272	4.4	1387	1380	1502	4.8
Avg	822	767	814	8.2	644	639	680	4.0

Table 7.C. 7 Reproducibility of ¹D retention time (min) with 3.0 μm cooling trap in the absence and presence of cooling (2600 ms)

Primary Retention Time								
	Jet Off				2600 ms cooling, 0.05 min delay			
Compound	Rep 1	Rep 2	Rep 3	%RSD	Rep 1	Rep 2	Rep 3	%RSD
C7	3.23	3.23	3.23	0.00	3.20	3.15	3.15	0.91
C8	4.30	4.30	4.30	0.00	4.30	4.30	4.30	0.00
C9	5.81	5.81	5.81	0.00	5.81	5.81	5.81	0.00
C10	7.45	7.45	7.45	0.00	7.38	7.38	7.38	0.00
C11	9.03	9.03	9.03	0.03	9.03	9.03	9.03	0.00
C12	10.54	10.54	10.54	0.00	10.55	10.55	10.55	0.01
C13	12.04	12.04	12.04	0.00	12.02	12.02	12.02	0.00
C14	13.40	13.40	13.40	0.02	13.40	13.40	13.39	0.04
C15	14.69	14.69	14.69	0.00	14.69	14.69	14.69	0.01
C16	15.98	15.98	15.91	0.26	15.94	15.94	15.94	0.01
C17	17.12	17.13	17.13	0.04	17.11	17.11	17.11	0.01
C18	18.20	18.20	18.20	0.00	18.23	18.23	18.24	0.01
C19	19.28	19.28	19.28	0.00	19.36	19.37	19.32	0.14
C20	20.35	20.35	20.35	0.00	20.39	20.39	20.35	0.10
C21	21.28	21.28	21.28	0.00	21.35	21.35	21.35	0.00
C22	22.21	22.21	22.21	0.01	22.29	22.28	22.28	0.02
C23	23.15	23.15	23.08	0.18	23.19	23.22	23.19	0.07
C24	24.01	24.01	23.94	0.17	24.05	24.05	24.08	0.07
C25	24.79	24.79	24.80	0.02	24.86	24.87	24.87	0.02
C26	25.59	25.58	25.58	0.02	25.66	25.67	25.67	0.02
C27	26.36	26.37	26.37	0.03	26.45	26.45	26.44	0.02
C28	27.09	27.08	27.08	0.02	27.16	27.18	27.18	0.05
C29	27.80	27.81	27.80	0.02	27.87	27.89	27.89	0.03
C30	28.52	28.51	28.51	0.01	28.60	28.60	28.61	0.03
C31	29.29	29.31	29.31	0.04	29.37	29.37	29.37	0.01
C32	30.15	30.17	30.17	0.05	30.23	30.23	30.34	0.20
C33	31.21	31.16	31.16	0.10	31.32	31.29	31.32	0.06
C34	32.30	32.29	32.29	0.01	32.43	32.41	32.47	0.08
				0.04				0.07

Table 7.C. 8 Reproducibility of ²D retention time (s) with 3.0 μm cooling trap in the absence of cooling

Secondary Retention Time (s)	Jet Off						
	Original			Corrected for Wraparound			
Compound	Rep 1	Rep 2	Rep 3	Corrected Rep 1	Corrected Rep 2	Corrected Rep 3	%RSD
C7	2.63	2.70	2.69	2.63	2.70	2.69	1.3
C8	2.44	2.44	2.44	2.44	2.44	2.44	0.0
C9	2.72	2.78	2.78	2.72	2.78	2.78	1.3
C10	3.24	3.26	3.26	3.24	3.26	3.26	0.4
C11	2.89	2.89	2.91	2.89	2.89	2.91	0.4
C12	2.89	2.88	2.88	2.89	2.88	2.88	0.1
C13	3.09	3.12	3.14	3.09	3.12	3.14	0.9
C14	2.90	2.89	2.89	2.90	2.89	2.89	0.3
C15	2.94	2.97	2.94	2.94	2.97	2.94	0.5
C16	3.35	3.38	2.94	3.35	3.38	2.94	7.5
C17	2.99	3.03	3.04	2.99	3.03	3.04	1.0
C18	2.97	2.96	2.94	2.97	2.96	2.94	0.6
C19	2.99	2.99	2.98	2.99	2.99	2.98	0.2
C20	3.33	3.36	3.35	3.33	3.36	3.35	0.5
C21	3.00	2.96	2.94	3.00	2.96	2.94	1.1
C22	3.00	3.00	2.95	3.00	3.00	2.95	1.0
C23	3.31	3.34	3.00	3.31	3.34	3.00	6.0
C24	3.30	3.37	2.97	3.30	3.37	2.97	6.5
C25	3.02	2.97	3.01	3.02	2.97	3.01	0.9
C26	3.03	2.98	2.97	3.03	2.98	2.97	1.0
C27	2.99	3.16	3.18	2.99	3.16	3.18	3.3
C28	3.03	3.02	3.01	3.03	3.02	3.01	0.4
C29	3.04	3.05	2.96	3.04	3.05	2.96	1.5
C30	3.25	3.19	3.17	3.25	3.19	3.17	1.2
C31	3.55	3.71	3.79	3.55	3.71	3.79	3.3
C32	4.10	4.18	4.21	4.10	4.18	4.21	1.4
C33	0.44	0.41	0.37	4.74	4.71	4.67	0.8
C34	1.12	1.06	1.11	5.42	5.36	5.41	0.5
							1.6

Table 7.C. 9 Reproducibility of ²D retention time (s) with 3.0 μm cooling trap in the presence of cooling (2600 ms)

Secondary Retention Time (s)	2600 ms cooling						
	Original			Corrected for Wraparound			
Compound	Rep 1	Rep 2	Rep 3	Corrected Rep 1	Corrected Rep 2	Corrected Rep 3	%RSD
C7	3.15	3.03	3.02	3.15	3.03	3.02	2.4
C8	2.63	2.61	2.61	2.63	2.61	2.61	0.4
C9	3.34	3.31	3.32	3.34	3.31	3.32	0.5
C10	3.53	3.56	3.54	3.53	3.56	3.54	0.4
C11	3.70	3.71	3.69	3.70	3.71	3.69	0.4
C12	3.86	3.84	3.84	3.86	3.84	3.84	0.2
C13	3.94	3.94	3.93	3.94	3.94	3.93	0.1
C14	4.02	3.98	4.01	4.02	3.98	4.01	0.5
C15	4.13	4.11	4.10	4.13	4.11	4.10	0.4
C16	4.19	4.19	4.17	4.19	4.19	4.17	0.3
C17	4.22	4.23	4.21	4.22	4.23	4.21	0.2
C18	4.25	4.26	4.26	4.25	4.26	4.26	0.1
C19	0.05	0.02	3.09	4.35	4.32	3.09	18.3
C20	0.11	0.07	0.06	4.41	4.37	4.36	0.6
C21	0.13	0.15	0.10	4.43	4.45	4.40	0.5
C22	0.14	0.16	0.16	4.44	4.46	4.46	0.2
C23	0.22	0.14	0.21	4.52	4.44	4.51	1.0
C24	0.26	0.23	0.16	4.56	4.53	4.46	1.1
C25	0.32	0.20	0.29	4.62	4.50	4.59	1.3
C26	0.30	0.31	0.33	4.60	4.61	4.63	0.3
C27	0.29	0.30	0.34	4.59	4.60	4.64	0.7
C28	0.39	0.34	0.37	4.69	4.64	4.67	0.5
C29	0.39	0.36	0.37	4.69	4.66	4.67	0.3
C30	0.68	0.75	0.73	4.98	5.05	5.03	0.7
C31	1.10	1.09	1.07	5.40	5.39	5.37	0.4
C32	1.45	1.41	1.09	5.75	5.71	5.39	3.5
C33	1.67	1.72	1.55	1.67	1.72	1.55	5.1
C34	2.26	2.18	2.16	2.26	2.18	2.16	2.4
							1.5

Table 7.C. 10 Reproducibility of peak height with 3.0 μm cooling trap in the absence and presence of cooling (2600 ms)

Peak Height: Tallest Slice								
Compound	Jet Off				2600 ms cooling, 0.05 min delay			
	Rep 1	Rep 2	Rep 3	%RSD	Rep 1	Rep 2	Rep 3	%RSD
C7	13682200	8940270	9039680	25.7	7261830	3746440	7509790	34.1
C8	11278400	12917000	13002200	7.8	13698700	14469600	14664600	3.6
C9	11220200	10649600	10847000	2.7	11329400	11401200	11668700	1.6
C10	8021860	7406600	7462600	4.5	8125100	8096020	8095490	0.21
C11	10303200	9767200	10177800	2.8	14055200	14450700	15050100	3.5
C12	6561800	6637200	6850470	2.2	13574900	14238900	14399100	3.1
C13	9420640	9299400	9286530	0.79	13916300	14202700	14830400	3.3
C14	11083700	10756500	10643200	2.1	17766300	17643000	18124400	1.4
C15	9099670	8858680	9519060	3.6	18159900	18858600	19272600	3.0
C16	6905060	6326950	6212310	5.7	11329100	12471600	11822600	4.8
C17	8936860	9333470	9186900	2.2	15043100	15344000	16267700	4.1
C18	6105610	6193460	6102440	0.84	11532000	11800600	10954000	3.8
C19	7508830	7513200	8245360	5.5	13744600	13578600	13503300	0.91
C20	6816100	6653420	6297370	4.0	9613360	9949190	9824330	1.7
C21	10219900	10104900	9943950	1.4	16035100	16289800	17026700	3.1
C22	9484730	9909070	9573700	2.3	16005500	15289800	15585600	2.3
C23	7487390	6474980	6222120	10.0	9986740	10258700	10903800	4.5
C24	7323240	6109560	6480090	9.4	9696260	9856930	10418400	3.8
C25	9471790	9254980	9012430	2.5	14063200	15075500	13742700	4.9
C26	9259540	9811390	9542790	2.9	12331600	13373600	11733700	6.7
C27	7851700	7907340	8272720	2.9	12777750	12996400	13696400	3.6
C28	8314960	9000040	9814310	8.3	10926800	10924000	10777400	0.79
C29	7791930	9124310	9586470	10.5	11705900	10761800	11414500	4.3
C30	7961290	8275250	8070090	2.0	9176310	9182770	8579350	3.9
C31	6631590	6259660	6216870	3.6	7264720	6596110	6558280	5.8
C32	5391940	5001810	4579400	8.1	3375240	4093780	2737170	19.9
C33	3436370	3883840	4931250	18.8	2931470	2942760	3510900	10.6
C34	3530890	3895960	3864110	5.4	2317180	2450240	2560060	5.0
				5.7				5.3

Table 7.C. 11 Reproducibility of peak area with 3.0 μm cooling trap in the absence and presence of cooling (2600 ms)

Peak Area: Total								
	Jet Off				2600 ms cooling, 0.05 min delay			
Compound	Rep 1	Rep 2	Rep 3	%RSD	Rep 1	Rep 2	Rep 3	%RSD
C7	904315000	577993000	883206000	23.2	702835000	911241000	920783000	14.6
C8	889506000	862977000	877456000	1.5	902394000	925737000	945428000	2.3
C9	841482000	793586000	809929000	3.0	927939000	959092000	978890000	2.7
C10	824712000	771846000	788228000	3.4	969426000	994524000	1028071000	3.0
C11	937070000	778754000	825384000	9.6	972465000	995096000	1026580000	2.7
C12	947705000	909450000	938755000	2.1	957204000	984339000	1015170000	2.9
C13	699523000	791571000	819380000	8.1	972222900	999680000	1035660000	3.2
C14	845958000	806804000	847488000	2.8	971643000	1001021000	1036350000	3.2
C15	879751000	847075000	874748000	2.0	969801000	998094000	1030965600	3.1
C16	959878000	913756000	949246000	2.6	966634000	993580000	1027480000	3.1
C17	949314000	712152000	857384000	14.2	984729000	999552000	1045350000	3.1
C18	941758000	915479000	937793000	1.5	974985000	998802000	1033600000	2.9
C19	921166000	894075000	809424000	6.7	982481000	974258000	1016700000	2.3
C20	950182000	924749000	949586000	1.5	1002110000	1012010000	1047759000	2.4
C21	878903000	843420000	865852000	2.1	988040000	1005560000	1041130000	2.7
C22	875336000	851921000	864860000	1.4	991979400	1008300000	1005580000	0.87
C23	941589000	925708000	946853000	1.2	986211000	1008296000	1030730000	2.2
C24	939462000	996692000	1029480000	4.6	989283000	1016660000	1049138000	2.9
C25	863449000	843387000	745722000	7.7	992937600	995910000	1191300000	10.7
C26	837327000	859066000	866343000	1.8	993911000	997310200	1027100000	1.8
C27	908666000	907878000	930948000	1.4	974170000	977467000	992824000	1.0
C28	859325000	858472000	977991000	7.7	1007183000	999485400	1055090000	3.0
C29	825473000	766408000	855972000	5.6	759208000	1335000000	1513980000	32.8
C30	854914000	917481000	935829000	4.7	995167000	995971500	1024480000	1.7
C31	886318000	1044560000	1114652000	11.5	973992000	982871000	979178000	0.46
C32	895436000	886062000	881880000	0.78	1005160000	1002710000	1037325000	1.9
C33	782643000	899286000	909065000	8.1	917147000	983002400	1155110000	12.1
C34	764666000	893328000	913311000	9.4	701756000	1218970000	901840000	27.7
				5.4				5.5

Appendix D

Chapter 8 Supplementary data

Evaluation of the operational capabilities of a solid-state thermal modulator in comprehensive two-dimensional gas chromatography-time-of-flight mass spectrometry (GC×GC -TOFMS)

Table 8.D. 1 Identified compound list of total MRP standards mixture using the SSM platform.

MRP Std. Mix	Standard	Average Retention Time		CAS	Formula	Average Match Factor	
		¹ D (min)	² D (s)			Forward	Reverse
Phosmet	1	15.45	2.01	732-11-6	C11H12NO4PS2	898	900
Pyridaphenthion	1	15.35	1.59	119-12-0	C14H17N2O4PS	883	891
EPN	1	15.54	1.37	2104-64-5	C14H14NO4PS	912	925
Azinphos methyl	1	16.20	2.24	86-50-0	C10H12N3O3PS2	878	895
Pyrazophos	1	16.70	1.35	13457-18-6	C14H20N3O5PS	874	877
Pyraclofos	1	16.96	1.56	89784-60-1	C14H18ClN2O3PS	787	788
Diazinon	1	9.35	0.42	333-41-5	C12H21N2O3PS	928	940
Isazophos	1	9.58	0.78	42509-80-8	C9H17ClN3O3PS	872	873
Chloropyrifos methyl	1	10.25	0.82	5598-13-0	C7H7Cl3NO3PS	853	878
Pirimiphos methyl	1	10.87	0.65	29232-93-7	C11H20N3O3PS	867	871
Fenitrothion	1	10.90	0.92	122-14-5	C9H12NO5PS	863	865
Chlorpyrifos	1	11.22	0.66	2921-88-2	C9H11Cl3NO3PS	813	833
Pirimiphos ethyl	1	11.67	0.53	23505-41-1	C13H24N3O3PS	743	743
Quinalphos	1	12.17	0.92	13593-03-8	C12H15N2O3PS	864	873

Phosalone	1	16.15	1.48	2310-17-0	C12H15ClNO4PS2	733	786
Azinphos ethyl	1	16.80	2.06	2642-71-9	C12H16N3O3PS2	897	899
Chloroneb	2	6.12	0.65	2675-77-6	C8H8Cl2O2	901	904
cis-Chlordane	2	12.71	0.76	5103-71-9	C10H6Cl8	767	785
trans-Chlordane	2	12.75	0.73	5103-74-2	C10H6Cl8	805	836
Chlorfenson (Ovex)	2	12.92	1.10	80-33-1	C12H8Cl2O3S	673	910
Chlorbenside	2	12.45	0.91	103-17-3	C13H10Cl2S	751	802
Delta - BHC	2	9.04	0.82	319-86-8	C6H6Cl6	902	940
Hexachlorobenzene	2	8.41	0.53	118-74-1	C6Cl6	859	865
gamma-BHC (Lindane)	2	8.34	0.70	319-85-7	C6H6Cl6	912	924
Alpha BHC	2	9.60	1.15	319-84-6	C6H6Cl6	916	927
Heptachlor	2	10.53	0.49	76-44-8	C10H5Cl7	821	831
Pentachlorobenzene	2	6.29	0.41	608-93-5	C6HCl5	863	867
Pentachloroanisole	2	8.55	0.51	1825-21-4	C7H3Cl5O	869	889
Pentachlorothioanisole	2	10.95	0.75	1825-19-0	C7H3Cl5S	864	879
Aldrin	2	11.25	0.51	309-00-2	C12H8Cl6	907	907
4,4'-Dichlorobenzophenone	2	11.49	0.83	90-98-2	C13H8Cl2O	941	961
Fenson	2	11.58	1.15	80-38-6	C12H9ClO3S	862	870
Isodrin	2	11.80	0.69	465-73-6	C12H8Cl6	868	869
Heptachlor epoxide	2	12.00	0.73	1024-57-3	C10H5Cl7O	832	885
4,4'-DDE	2	13.15	0.76	72-55-9	C14H8Cl4	913	927
2,4'-DDE	2	12.54	0.76	3424-82-6	C14H8Cl4	892	907
cis-Nonachlor	2	13.90	0.90	5103-73-1	C10H5Cl9	779	784
trans-Nonachlor	2	12.80	0.60	39765-80-5	C10H5Cl9	823	826
Dieldrin	2	13.22	0.87	60-57-1	C12H8Cl6O	905	906
2,4'-DDD	2	13.28	0.93	53-19-0	C14H10Cl4	756	833
Endrin	2	13.60	1.05	72-20-8	C12H8Cl6O	826	831
Ethylan (Penthane)	2	13.65	0.79	72-56-0	C18H20Cl2	897	920
B-Endosulfan (Endosulfan II)	2	13.80	1.22	33213-65-9	C9H6Cl6O3S	896	898
2,4'-DDT	2	13.96	0.95	789-02-6	C14H9Cl5	652	798
Endrin aldehyde	2	14.09	1.38	7421-93-4	C12H8Cl6O	868	895
2,4'-Methoxychlor	2	14.76	1.27	30667-99-3	C16H15Cl3O2	768	770
4,4'-Methoxychlor olefin	2	14.45	1.11	2132-70-9	C16H14Cl2O2	787	796
Endosulfan ether	2	9.97	0.67	3369-52-6	C9H6Cl6O	842	847
Endosulfan sulfate	2	14.53	1.35	1031-07-8	C9H6Cl6O4S	831	836
4,4'-DDT	2	14.65	0.97	50-29-3	C14H9Cl5	898	905

Endrin ketone	2	15.39	1.76	53494-70-5	C12H8Cl6O	904	911
Tetradifon	2	16.05	1.48	116-29-0	C12H6Cl4O2S	845	845
Mirex	2	16.55	1.24	2385-85-5	C10Cl12	817	880
2,6-Dichlorobenzonitrile (Dichlobenil)	3	4.20	0.67	1194-65-6	C7H3Cl2N	906	917
Biphenyl	3	4.71	0.42	92-52-4	C12H10	928	947
3,4-Dichloroaniline	3	5.23	0.82	95-76-1	C6H5Cl2N	946	948
THPI (Tetrahydrophthalimide)	3	5.94	1.15	1469-48-3	C8H9NO2	939	941
Tetrachloronitrobenzene (Tecnazene)	3	7.10	0.64	117-18-0	C6HCl4NO2	895	907
2,3,5,6-Tetrachloroaniline	3	7.50	0.68	3481-20-7	C6H3Cl4N	899	901
Pentachloroaniline	3	9.95	0.87	527-20-8	C6H2Cl5N	846	886
Pendimethalin	3	11.86	0.68	40487-42-1	C13H19N3O4	856	862
Diphenylamine	3	7.50	0.78	122-39-4	C12H11N	864	941
Pentachloronitrobenzene (Quintozene)	3	8.95	0.72	82-68-8	C6Cl5NO2	761	784
Pentachlorobenzonitrile	3	9.00	0.85	20925-85-3	C7Cl5N	690	724
Chlorothalonil	3	9.37	1.34	1897-45-6	C8Cl4N2	886	891
Ethalfuralin	3	7.80	1.02	55283-68-6	C13H14F3N3O4	900	900
Trifluralin	3	7.97	1.96	1582-09-8	C13H16F3N3O4	891	895
Benfluralin	3	8.04	1.26	1861-40-1	C13H16F3N3O4	869	874
Profluralin	3	9.14	1.01	26399-36-0	C14H16F3N3O4	846	848
Fluchloralin	3	9.40	0.13	33245-39-5	C12H13ClF3N3O4	868	870
Prodiamine	3	10.95	0.25	29091-21-2	C13H17F3N4O4	907	911
Dichlofluanid	3	11.01	0.96	1085-98-9	C9H11Cl2FN2O2S2	851	868
Isopropalin	3	11.76	0.39	33820-53-0	C15H23N3O4	871	873
Tolyfluanid	3	12.03	0.93	731-27-1	C10H13Cl2FN2O2S2	790	812
Oxyfluorfen	3	13.30	0.58	42874-03-3	C15H11ClF3NO4	799	801
Nitralin	3	15.09	1.07	1836-75-5	C13H19N3O6S	786	790
Pebulate	4	5.60	0.16	1114-71-2	C10H21NOS	900	905
N-(2,4-Dimethylphenyl)formamide	4	5.80	0.90	60397-77-5	C9H11NO	889	896
Propachlor	4	7.30	0.67	1918-16-7	C11H14ClNO	922	933
Cycloate	4	7.65	0.38	1134-23-2	C11H21NOS	895	897
Diallate (cis & trans)	4	8.27	0.37	2303-16-4	C10H17Cl2NOS	891	903
Diallate (cis & trans)	4	8.45	0.38	2303-16-4	C10H17Cl2NOS	882	893
Triallate	4	9.68	0.39	2303-17-5	C10H16Cl3NOS	880	902
Propyzamide	4	9.26	0.40	23950-58-5	C12H11Cl2NO	878	879
Dimethachlor	4	10.15	0.76	50563-36-5	C13H18ClNO2	928	938
Propanil	4	10.18	0.93	709-98-8	C9H9Cl2NO	877	895

Acetochlor	4	10.25	0.58	34256-82-1	C14H20ClNO2	915	915
Alachlor	4	10.43	0.62	15972-60-8	C14H20ClNO2	906	906
Metolachlor	4	11.15	0.63	51218-45-2	C15H22ClNO2	916	919
Linuron	4	11.00	0.80	330-55-2	C9H10Cl2N2O2	863	863
Diphenamid	4	11.65	1.24	957-51-7	C16H17NO	857	876
Metazachlor	4	11.88	1.06	67129-08-2	C14H16ClN3O	860	897
Flutolanil	4	12.95	0.79	66332-96-5	C17H16F3NO2	848	860
Pretilachlor	4	13.05	0.58	51218-49-6	C17H26ClNO2	881	881
Oxadiazon	4	13.20	0.53	19666-30-9	C15H18Cl2N2O3	894	896
Norflurazon	4	14.45	1.48	27314-13-2	C12H9ClF3N3O	796	845
Methoxychlor	4	15.26	1.28	72-43-5	C16H15Cl3O2	818	823
Fenpropathrin	4	15.74	0.91	39515-41-8	C22H23NO3	870	874
Tebufenpyrad	4	15.84	0.89	119168-77-3	C18H24ClN3O	816	817
Fluquinconazole	4	17.45	1.87	136426-54-5	C16H8Cl2FN5O	693	701
Prochloraz	4	17.50	1.49	67747-09-5	C15H16Cl3N3O2	778	778
Pyridaben	4	17.45	1.40	96489-71-3	C19H25ClN2OS	777	830
Etridiazole	5	5.45	0.47	2593-15-9	C5H5Cl3N2OS	907	912
Atrazine	5	8.90	0.73	1912-24-9	C8H14ClN5	874	893
Terbutylazine	5	9.19	0.62	5915-41-3	C9H16ClN5	923	926
Pyrimethanil	5	9.40	0.74	53112-28-0	C12H13N3	867	870
Terbacil	5	9.55	1.14	5902-51-2	C9H13ClN2O2	898	925
Vinclozoline	5	10.35	0.54	50471-44-8	C12H9Cl2NO3	908	909
Triadimefon	5	11.43	0.57	43121-43-3	C14H16ClN3O2	933	934
Tebuconazole	5	14.89	1.01	107534-96-3	C16H22ClN3O	876	876
Propargite	5	14.96	0.81	2312-35-8	C19H26O4S	787	789
MGK-264	5	11.94	0.61	113-48-4	C17H25NO2	827	841
Cyprodinil	5	11.87	0.85	121552-61-2	C14H15N3	832	855
Penconazole	5	11.95	0.77	66246-88-6	C13H15Cl2N3	876	878
Fipronil	5	12.00	0.37	120068-37-3	C12H4Cl2F6N4OS	810	812
Triflumizole	5	12.30	0.45	68694-11-1	C15H15ClF3N3O	846	846
Triadimenol	5	12.25	0.66	552	C14H18ClN3O2	900	909
Procymidone	5	12.25	0.80	55219-65-3	C14H18ClN3O2	815	816
Captan	5	12.16	1.44	133-06-2	C9H8Cl3NO2S	898	898
Folpet	5	12.28	1.44	133-07-3	C9H4Cl3NO2S	850	868
Paclobutrazol	5	12.60	0.75	76738-62-0	C15H20ClN3O	881	882
Flutriafol	5	12.80	1.16	76674-21-0	C16H13F2N3O	782	840
Fludioxonil	5	12.99	1.51	131341-86-1	C12H6F2N2O2	873	877

Triacyclazole (Beam)	5	12.99	2.33	41814-78-2	C9H7N3S	910	922
Chlorfenapyr	5	13.49	0.72	122453-73-0	C15H11BrClF3N2O	856	859
Myclobutanil	5	13.20	1.07	88671-89-0	C15H17ClN4	777	797
Lenacil	5	14.55	1.81	2164 08 1	C13H18N2O2	873	916
Hexazinone (Velpar)	5	14.70	1.95	51235-04-2	C12H20N4O2	862	862
Captafol	5	15.01	1.75	2425 06 1	C10H9Cl4NO2S	891	891
Iprodione	5	15.39	1.06	2164 08 1	C13H18N2O2	811	818
Pyriproxyfen	5	16.35	1.32	95737-68-1	C20H19NO3	838	877
Fenarimol	5	16.68	1.67	60168-88-9	C17H12Cl2N2O	864	915
Etofenprox	5	18.49	1.70	80844-07-1	C25H28O3	883	887
Fluridone	5	18.69	1.04	59756-60-4	C19H14F3NO	795	821
Transfluthrin	6	10.54	0.21	118712-89-3	C15H12Cl2F4O2	878	878
Tefluthrin	6	9.65	0.98	79538-12-0	C17H14ClF7O2	886	886
Anthraquinone	6	11.25	1.29	84-61-1	C14H8O2	919	923
Bioallethrin	6	12.17	0.33	584-79-2	C19H26O3	920	930
Resmethrin	6	15.13	0.74	10453-86-8	C22H26O3	843	864
Bifenthrin	6	15.57	0.61	82657-04-3	C23H22ClF3O2	884	622
Tetramethrin	6	15.60	1.15	7696-12-0	C19H25NO4	862	887
Phenothrin (cis & trans)	6	16.11	0.89	26002-80-2	C23H26O3	903	913
Lambda-Cyhalothrin	6	16.55	0.79	91465-08-6	C23H19ClF3NO3	889	889
trans-Permethrin	6	17.31	1.28	61949-77-7	C21H20Cl2O3	851	857
cis-Permethrin	6	17.45	1.31	61949-76-6	C21H20Cl2O3	774	796
Cyfluthrin	6	18.00	1.34	68359-37-5	C22H18Cl2FNO3	710	747
Cypermethrin	6	18.25	1.50	52315-07-8	C22H19Cl2NO3	776	776
Flucythrinate	6	18.35	1.50	70124-77-5	C26H23F2NO4	808	809
tau-Fluvalinate	6	19.23	1.51	102851-06-9	C26H22ClF3N2O3	846	849
Fenvalerate	6	19.05	1.93	51630-58-1	C25H22ClNO3	886	886
2-Phenylphenol	7	6.26	0.66	90-43-7	C12H10O	933	968
Bromopropylate	7	15.58	0.98	18181-80-1	C17H16Br2O3	800	803
Chloropropham	7	7.88	0.43	101-21-3	C10H12ClNO2	880	881
Metalaxyl	7	10.55	0.85	57837-19-1	C15H21NO4	867	870
DCPA methyl ester (Chlorthal-dimethyl)	7	11.30	0.63	1861-32-1	C10H6Cl4O4	851	852
Chlozolinate	7	12.05	0.58	84332-86-5	C13H11Cl2NO5	855	855
Fluazifop-p-butyl	7	13.65	0.43	79241-46-6	C19H20F3NO4	860	869
Chlorobenzilate	7	13.79	0.78	510-15-6	C16H14Cl2O3	912	914
Carfentrazone ethyl	7	14.40	0.76	128639-02-1	C15H14Cl2F3N3O3	752	755

2-Decanoylhydrazino-1,4-naphthoquinone	7	18.50	1.18	57960-19-7	C20H26N2O3	669	725
Methacrifos	8	6.02	0.51	62610-77-9	C7H13O5PS	896	897
Sulfotepp	8	8.06	0.55	3689-24-5	C8H20O5P2S2	882	886
Terbufos	8	9.17	0.44	13071-79-9	C9H21O2PS3	901	926
Tolclofos-methyl	8	10.39	0.94	57018-04-9	C9H11Cl2O3PS	781	792
Fenchlofos (Ronnell)	8	10.60	0.67	299-84-3	C8H8Cl3O3PS	849	856
Malathion	8	11.10	0.75	121-75-5	C10H19O6PS2	924	925
Fenthion	8	11.30	0.97	55-38-9	C10H15O3PS2	839	882
Bromophos methyl	8	11.63	0.80	2104-96-3	C8H8BrCl2O3PS	820	847
Bromfenvinphos-methyl	8	12.06	1.12	13104-21-7	C10H10BrCl2O4P	696	706
Chlorfenvinphos	8	12.10	0.80	470-90-6	C12H14Cl3O4P	854	860
Tetrachlorvinphos	8	12.57	0.96	22248-79-9	C10H19Cl4O4P	700	807
Bromfenvinphos	8	12.82	0.92	33399-00-7	C12H14CBrCl2O4P	670	701
Profenofos	8	13.07	0.87	41198-08-7	C11H15BrClO3PS	784	792
Prothiofos	8	13.00	0.70	34643-46-4	C11H15Cl2O2PS2	873	873
Sulprofos	8	14.25	1.04	35400-43-2	C12H19O2P2S3	891	892
Carbophenothion	8	14.40	1.07	786-19-6	C11H16ClO2PS3	819	830
Edifenphos	8	14.46	1.59	17109-49-8	C14H15O2PS2	784	819
Leptophos	8	16.20	1.42	21609-90-5	C13H10BrCl2O2PS	804	817
Coumaphos	8	17.40	1.86	56-72-4	C14H16ClO5PS	715	779
Mevinphos	9	5.15	0.63	7786-34-7	C7H13O6P	903	903
Phorate	9	8.26	0.56	298-02-2	C7H17O2PS3	897	911
Fonofos	9	9.23	0.72	944-22-9	C10H15OPS2	875	898
Disulfoton	9	9.52	0.59	298-04-4	C8H19O2PS3	924	927
Methyl parathion	9	10.35	0.89	298-00-0	C8H10NO5PS	834	848
Parathion (Ethyl parathion)	9	11.35	0.74	56-38-2	C10H14NO5PS	880	892
Triazophos	9	14.21	1.59	24017-47-8	C12H16N3O3PS	879	885
Piperonyl butoxide	9	15.08	0.73	51-03-6	C19H30O5	788	860

Table 8.D. 2 Unidentified and co-elutions in MRP mixture

Compound	Std	CAS	Unidentified	Co-elution	Co-elution Replicate	Compound (s) causing Co-elution
4,4'-DDD	2	72-54-8	Y	N	N/A	N/A
Endosulfan I	2	959-98-8	Y	N	N/A	N/A
trans-Chlordane	2	5103-74-2	N	Y	1 & 2	Chlordane
Dichloran	3	99-30-9	Y	N	N/A	N/A
Nitrofen	3	1836-75-5	Y	N	N/A	N/A
Pentachlorobenzonitrile	3	20925-85-3	N	Y	3	delta- BHC
Allidochlor	4	93-71-0	Y	N	N/A	N/A
Clomazone	4	81777-89-1	Y	N	N/A	N/A
Propisochlor	4	86763-4705	Y	N	N/A	N/A
Tebufenpyrad	4	119168-77-3	Y	N	N/A	N/A
Buprimate	5	41483-43-6	Y	N	N/A	N/A
Flusilazole	5	85509-19-9	Y	N	N/A	N/A
Acrinathrin	6	101007-06-1	Y	N	N/A	N/A
Deltamethrin	6	52918-63-5	Y	N	N/A	N/A
Acequinocyl	7	57960-19-7	Y	N	N/A	N/A
Bromfenvinfos	8	33399-00-7	N	Y	3	Clofenvinfos
Bromophos-ethyl	8	4824-78-6	Y	N	N/A	N/A
Chlorothiophos	8	60238-56-4	Y	N	N/A	N/A
Ethion	8	563-12-2	Y	N	N/A	N/A
Iodofenphos	8	563-12-2	Y	N	N/A	N/A
Tetrachlorvinphos	8	22248-79-9	N	Y	1	2,4'-DDE
Methyl Parathion	9	298-00-0	N	Y	1 & 3	Tolclofos-methyl

Table 8.D. 3 Identified compound list of total FA standards mixture using the SSM platform.

FA Std Mix	Standard	Average Retention Time		CAS	Formula	Average Match Factor	
		¹ D (min)	² D (s)			Forward	Reverse
1-Fluoronaphthalene	Internal	14.87	0.55	321-38-0	C10H7F	908	908
Citral	A	17.91	1.47	5392-40-5	C10H16O	892	892
3,7-dimethyl-7-hydroxyoctanal	A	18.58	1.53	107-75-5	C10H20O2	886	887
Cinnamal	A	17.94	1.55	104-55-2	C9H8O	932	932
Lilial	A	26.06	0.44	80-54-6	C14H20O	909	909
α -amylcinnamaldehyde	A	29.47	0.56	122-40-7	C18H18O	909	909
Lylal	A	30.00	0.77	31906-04-4	C13H22O2	842	842
Phenylacetaldehyde	A	10.07	0.87	122-78-1	C8H8O	949	956
α -hexyl-cinnamaldehyde	A	28.53	0.47	101-86-0	C15H20O	898	898
Benzyl alcohol	B	9.76	0.62	100-51-6	C7H8O	914	914
Linalool	B	12.07	3.40	78-70-6	C10H18O	864	864
Citronellol	B	16.54	3.57	106-22-9	C10H20O	903	903
Geraniol	B	17.36	2.46	106-24-1	C10H18O	864	864
4-methoxybenzyl alcohol	B	18.34	1.52	105-13-5	C8H10O2	915	915
Cinnamyl alcohol	B	19.14	1.29	104-54-1	C9H10O	906	906
Eugenol	B	20.67	0.70	97-53-0	C10H12O2	924	924
Methyl eugenol	B	22.29	0.92	93-15-2	C11H14O2	880	881
Isoeugenol	B	23.67	0.90	97-54-1	C10H12O2	914	914
α -amylcinnamic alcohol	B	30.57	0.54	101-85-9	C14H20O	848	848
Farnesol	B	30.84	2.52	4602-84-0	C15J26O	864	864
d-limonene	C	9.57	3.17	5989-27-5	C10H16	940	940
Camphor	C	13.58	1.51	76-22-2	C10H16O	932	946
4-allylanisole	C	15.51	0.26	140-67-0	C10H12O	951	952
Methyl 2-octynoate	C	15.67	0.32	111-12-6	C9H14O2	952	956
Safrole	C	18.59	0.56	94-59-7	C10H10O2	942	947
Methyl 2-nonynoate	C	19.00	1.52	111-80-8	C10H16O2	927	927
Coumarin	C	23.08	2.90	91-64-5	C9H6O2	954	954
iso- α -methylionone	C	24.42	2.53	127-51-5	C14H22O	905	909
Benzyl benzoate	C	32.68	1.57	120-51-4	C14H22O2	926	926
Benzyl salicylate	C	35.28	1.42	118-58-1	C14H12O3	928	935
Benzyl cinnamate	C	40.74	1.82	103-41-3	C16H14O2	895	895

1,8-Cineole	C	9.61	3.27	470-82-6	C ₁₀ H ₁₈ O	894	894
-------------	---	------	------	----------	-----------------------------------	-----	-----

Table 8.D. 4 Retention time reproducibility for MRP mixture

MRP Std Mix		Primary Retention Time Reproducibility				Secondary Retention Time Reproducibility						
Compound	Standard	Rep 1 (min)	Rep 2 (min)	Rep 3 (min)	%RSD	Rep 1 (s)	Corrected Rep 1 (s)	Rep 2 (s)	Corrected Rep 2 (s)	Rep 3 (s)	Corrected Rep 3 (s)	%RSD with wraparound correction
Phosmet	1	15.46	15.45	15.45	0.02	2.07	2.07	1.94	1.94	2.03	2.03	3.2
Pyridafenthion	1	15.35	15.35	15.35	0.00	1.64	1.64	1.51	1.51	1.61	1.61	4.4
EPN	1	15.55	15.54	15.55	0.02	1.42	1.42	1.29	1.29	1.39	1.39	4.9
Azinphos methyl	1	16.20	16.20	16.20	0.01	2.30	2.30	2.16	2.16	2.25	2.25	3.2
Pyrazophos	1	16.71	16.70	16.70	0.03	1.40	1.40	1.25	1.25	1.38	1.38	6.0
Pyraclufos	1	16.96	16.96	16.96	0.02	1.61	1.61	1.49	1.49	1.58	1.58	4.2
Diazinone	1	9.35	9.35	9.35	0.01	0.47	3.47	0.35	3.35	0.45	3.45	1.9
Isazophos	1	9.58	9.57	9.58	0.07	0.82	3.82	0.71	3.71	0.81	3.81	1.7
Chlorpyrifos-methyl	1	10.26	10.25	10.25	0.02	0.87	3.87	0.74	3.74	0.86	3.86	1.8
Pirimiphos methyl	1	10.88	10.86	10.87	0.08	0.69	3.69	0.59	3.59	0.68	3.68	1.6
Fenitrothion	1	10.90	10.89	10.90	0.04	0.97	3.97	0.85	3.85	0.95	3.95	1.7
Chlorpyrifos	1	11.22	11.21	11.22	0.05	0.71	3.71	0.58	3.58	0.70	3.70	1.9
Pirimiphos ethyl	1	11.69	11.65	11.68	0.18	0.57	3.57	0.46	3.46	0.56	3.56	1.7
Quinalphos	1	12.18	12.17	12.18	0.06	0.96	3.96	0.85	3.85	0.96	3.96	1.6
Phosalone	1	16.15	16.15	16.15	0.00	1.53	1.53	1.40	1.40	1.50	1.50	4.8
Azinphos ethyl	1	16.80	16.80	16.80	0.01	2.11	2.11	1.97	1.97	2.10	2.10	3.7
Chloroneb	2	6.12	6.11	6.12	0.11	0.69	3.69	0.57	3.57	0.68	3.68	1.8
cis-Chlordane	2	12.72	12.70	12.70	0.07	0.80	3.80	0.69	3.69	0.80	3.80	1.6
trans-Chlordane	2			12.75						0.73	3.73	
Chlorfenson (Ovex)	2	12.92	12.91	12.92	0.06	1.14	4.14	1.03	4.03	1.13	4.13	1.4
Chlorbenside	2	12.45	12.45	12.45	0.01	0.96	3.96	0.83	3.83	0.94	3.94	1.8
D-BHC	2	9.05	9.05	9.03	0.12	0.86	3.86	0.73	3.73	0.86	3.86	2.0
Hexachlorobenzene	2	8.41	8.40	8.41	0.04	0.57	3.57	0.45	3.45	0.56	3.56	1.9
gamma-BHC (Lindane)	2	8.34	8.33	8.34	0.07	0.75	3.75	0.62	3.62	0.73	3.73	1.8
Alpha-BHC	2	9.60	9.60	9.60	0.01	1.20	4.20	1.07	4.07	1.20	4.20	1.8
Heptachlor	2	10.54	10.53	10.54	0.06	0.53	3.53	0.41	3.41	0.52	3.52	1.9
Pentachlorobenzene	2	6.29	6.28	6.29	0.09	0.46	3.46	0.33	3.33	0.44	3.44	2.0
Pentachloroanisole	2	8.55	8.55	8.55	0.03	0.56	3.56	0.43	3.43	0.55	3.55	2.0
Pentachlorothioanisole	2	10.95	10.95	10.95	0.00	0.81	3.81	0.67	3.67	0.78	3.78	1.9
Aldrin	2	11.25	11.24	11.25	0.06	0.56	3.56	0.44	3.44	0.54	3.54	1.9
4,4'-Dichlorobenzophenone	2	11.49	11.48	11.49	0.05	0.88	3.88	0.76	3.76	0.87	3.87	1.7

Fenson	2	11.59	11.57	11.58	0.06	1.19	4.19	1.07	4.07	1.18	4.18	1.6
Isodrin	2	11.80	11.80	11.80	0.01	0.74	3.74	0.60	3.60	0.72	3.72	2.0
Heptachlor Epoxide	2	12.00	12.00	12.00	0.00	0.77	3.77	0.65	3.65	0.76	3.76	1.8
4,4'-DDE	2	13.15	13.15	13.15	0.00	0.80	3.80	0.68	3.68	0.79	3.79	1.8
2,4'-DDE	2	12.54	12.53	12.54	0.03	0.80	3.80	0.69	3.69	0.80	3.80	1.7
cis-Nonachlor	2	13.90	13.90	13.90	0.00	0.96	3.96	0.84	3.84	0.94	3.94	1.7
trans-Nonachlor	2	12.80	12.80	12.80	0.00	0.65	3.65	0.52	3.52	0.63	3.63	1.9
Dieldrin	2	13.23	13.20	13.22	0.12	0.91	3.91	0.79	3.79	0.90	3.90	1.7
2,4'-DDD	2	13.30	13.25	13.28	0.19	0.95	3.95	0.88	3.88	0.94	3.94	1.0
Endrin	2	13.60	13.60	13.60	0.00	1.10	4.10	0.98	3.98	1.08	4.08	1.6
Ethylan (Perthane)	2	13.65	13.65	13.65	0.02	0.84	3.84	0.71	3.71	0.82	3.82	1.9
B-Endosulfan (Endosulfan II)	2	13.80	13.80	13.80	0.01	1.27	4.27	1.15	4.15	1.25	4.25	1.5
2,4'-DDT	2	13.95	13.95	13.97	0.10	1.01	4.01	0.88	3.88	0.97	3.97	1.7
Endrin Aldehyde	2	14.10	14.08	14.10	0.04	1.43	1.43	1.30	1.30	1.42	1.42	5.0
2,4'-Methoxychlor	2	14.77	14.76	14.76	0.04	1.31	4.31	1.19	4.19	1.29	4.29	1.5
4,4'-Methoxychlor olefin	2	14.45	14.45	14.45	0.00	1.16	4.16	1.03	4.03	1.14	4.14	1.7
Endosulfan ether	2	9.97	9.96	9.97	0.06	0.72	3.72	0.60	3.60	0.70	3.70	1.8
Endosulfan sulfate	2	14.54	14.53	14.54	0.05	1.39	1.39	1.27	1.27	1.38	1.38	4.9
4,4'-DDT	2	14.65	14.64	14.65	0.02	1.02	4.02	0.89	3.89	1.00	4.00	1.7
Endrin ketone	2	15.39	15.39	15.39	0.03	1.81	1.81	1.67	1.67	1.79	1.79	4.2
Tetradifon	2	16.05	16.04	16.05	0.02	1.52	1.52	1.41	1.41	1.51	1.51	4.2
Mirex	2	16.55	16.55	16.55	0.01	1.29	4.29	1.16	4.16	1.26	4.26	1.6
2,6-Dichlorobenzonitrile (Dichlobenil)	3	4.20	4.20	4.20	0.00	0.72	3.72	0.59	3.59	0.70	3.70	1.9
Biphenyl	3	4.71	4.71	4.71	0.10	0.47	3.47	0.34	3.34	0.45	3.45	2.0
3,4-Dichloroaniline	3	5.24	5.23	5.24	0.13	0.87	3.87	0.74	3.74	0.86	3.86	1.9
THPI (Tetrahydrophthalimide)	3	5.94	5.94	5.94	0.07	1.20	4.20	1.06	4.06	1.19	4.19	1.8
Tetrachloronitrobenzene (Tecnazene)	3	7.10	7.10	7.10	0.01	0.68	3.68	0.56	3.56	0.67	3.67	1.8
2,3,5,6-Tetrachloroaniline	3	7.50	7.50	7.50	0.02	0.73	3.73	0.60	3.60	0.71	3.71	1.9
Pentachloroaniline	3	9.95	9.95	9.95	0.02	0.91	3.91	0.79	3.79	0.90	3.90	1.7
Pendimethalin	3	11.85	11.85	11.87	0.09	0.73	3.73	0.61	3.61	0.69	3.69	1.7
Diphenylamine	3	7.51	7.50	7.50	0.03	0.83	3.83	0.71	3.71	0.81	3.81	1.8

Pentachloronitrobenzene (Quintozene)	3	8.95	8.95	8.95	0.00	0.77	3.77	0.64	3.64	0.75	3.75	1.8
Pentachlorobenzonitrile	3	9.00	9.00		0	0.91	3.91	0.78	3.78			2.5
Chlorothalonil	3	9.39	9.35	9.38	0.22	1.39	1.39	1.28	1.28	1.37	1.37	4.0
Ethalfuralin	3	7.81	7.76	7.82	0.42	0.06	3.06	2.94	2.94	0.05	3.05	2.2
Trifluralin	3	8.00	7.95	7.95	0.36	0.01	3.01	2.89	2.89	3.00	3.00	2.2
Benfluralin	3	8.07	8.01	8.05	0.39	0.02	3.02	2.89	2.89	0.86	3.86	16.1
Profluralin	3	9.16	9.10	9.16	0.36	0.06	3.06	2.94	2.94	0.05	3.05	2.2
Fluchloralin	3	9.40	9.40	9.40	0.01	0.18	3.18	0.05	3.05	0.16	3.16	2.2
Prodiamine	3	10.95	10.95	10.95	0.01	0.30	3.30	0.17	3.17	0.28	3.28	2.1
Dichlofluanid	3	11.01	11.00	11.01	0.05	1.00	4.00	0.89	3.89	1.00	4.00	1.6
Isopropalin	3	11.77	11.76	11.76	0.05	0.43	3.43	0.31	3.31	0.41	3.41	1.9
Tolyfluanid	3	12.03	12.02	12.03	0.05	0.96	3.96	0.86	3.86	0.96	3.96	1.6
Oxyfluorfen	3	13.30	13.30	13.30	0.00	0.63	3.63	0.50	3.50	0.61	3.61	1.9
Nitralin	3	15.09	15.08	15.09	0.03	1.11	4.11	0.99	3.99	1.10	4.10	1.6
Pebulate	4	5.60	5.59	5.60	0.06	0.21	3.21	0.09	3.09	0.19	3.19	2.2
N-(2,4-Dimethylphenyl)formamide	4	5.80	5.80	5.80	0.01	0.95	3.95	0.81	3.81	0.94	3.94	1.9
Propachlor	4	7.30	7.29	7.30	0.04	0.72	3.72	0.59	3.59	0.71	3.71	1.9
Cycloate	4	7.65	7.65	7.65	0.02	0.43	3.43	0.30	3.30	0.41	3.41	2.1
Diallate (cis & trans)	4	8.28	8.26	8.27	0.09	0.41	3.41	0.29	3.29	0.40	3.40	1.9
Diallate (cis & trans)	4	8.45	8.45	8.45	0.00	0.42	3.42	0.30	3.30	0.41	3.41	2.0
Triallate	4	9.70	9.64	9.70	0.35	0.44	3.44	0.31	3.31	0.42	3.42	2.1
Propyzamide	4	9.26	9.25	9.26	0.05	0.44	3.44	0.32	3.32	0.43	3.43	2.0
Dimethachlor	4	10.15	10.15	10.15	0.02	0.80	3.80	0.68	3.68	0.79	3.79	1.8
Propanil	4	10.18	10.17	10.18	0.06	0.97	3.97	0.84	3.84	0.96	3.96	1.8
Acetochlor	4	10.25	10.25	10.25	0.01	0.63	3.63	0.49	3.49	0.61	3.61	2.0
Alachlor	4	10.44	10.42	10.43	0.08	0.67	3.67	0.55	3.55	0.65	3.65	1.8
Metolachlor	4	11.15	11.15	11.15	0.00	0.67	3.67	0.56	3.56	0.66	3.66	1.8
Linuron	4	11.00	11.00	11.00	0.00	0.85	3.85	0.73	3.73	0.83	3.83	1.7
Diphenamid	4	11.65	11.65	11.65	0.00	1.29	4.29	1.15	4.15	1.27	4.27	1.9
Metazachlor	4	11.89	11.87	11.88	0.06	1.11	4.11	0.98	3.98	1.09	4.09	1.7
Flutolanil	4	12.95	12.94	12.95	0.04	0.83	3.83	0.72	3.72	0.82	3.82	1.7
Pretilachlor	4	13.05	13.05	13.05	0.00	0.63	3.63	0.50	3.50	0.61	3.61	2.0
Oxadiazon	4	13.20	13.20	13.20	0.01	0.58	3.58	0.45	3.45	0.56	3.56	2.0
Norflurazon	4	14.45	14.45	14.45	0.00	1.53	1.53	1.40	1.40	1.51	1.51	4.5

Methoxychlor	4	15.65	15.67	14.45	4.57	1.42	4.42	1.27	4.27	1.14	4.14	3.2
Fenpropathrin	4	15.74	15.74	15.74	0.03	0.96	3.96	0.83	3.83	0.94	3.94	1.7
Tebufenpyrad	4	15.84	15.83	15.84	0.03	0.94	3.94	0.82	3.82	0.92	3.92	1.7
Fluquinconazole	4	17.45	17.45	17.45	0.00	1.92	1.92	1.79	1.79	1.88	1.88	3.6
Prochloraz	4	17.50	17.50	17.50	0.00	1.54	1.54	1.42	1.42	1.53	1.53	4.5
Pyridaben	4	17.45	17.45	17.45	0.00	1.46	1.46	1.33	1.33	1.41	1.41	4.5
Etridiazole	5	5.45	5.45	5.45	0.01	0.52	3.52	0.39	3.39	0.51	3.51	2.0
Atrazine	5	8.90	8.90	8.90	0.01	0.78	3.78	0.65	3.65	0.77	3.77	1.9
Terbutylazine	5	9.20	9.19	9.19	0.06	0.67	3.67	0.55	3.55	0.66	3.66	1.9
Pyrimethanil	5	9.40	9.39	9.40	0.03	0.79	3.79	0.66	3.66	0.77	3.77	1.9
Terbacil	5	9.55	9.54	9.55	0.02	1.18	4.18	1.06	4.06	1.17	4.17	1.7
Vinclozoline	5	10.35	10.35	10.35	0.00	0.58	3.58	0.46	3.46	0.57	3.57	1.9
Triadimefon	5	11.44	11.42	11.43	0.07	0.62	3.62	0.50	3.50	0.60	3.60	1.8
Tebuconazole	5	14.90	14.89	14.89	0.03	1.06	4.06	0.93	3.93	1.04	4.04	1.8
Propargite	5	14.96	14.95	14.96	0.03	0.86	3.86	0.74	3.74	0.84	3.84	1.7
MGK-264	5	11.95	11.91	11.95	0.20	0.64	3.64	0.54	3.54	0.63	3.63	1.5
Cyprodinil	5	11.88	11.86	11.87	0.07	0.89	3.89	0.78	3.78	0.88	3.88	1.7
Penconazole	5	11.95	11.95	11.95	0.00	0.81	3.81	0.69	3.69	0.80	3.80	1.8
Fipronil	5	12.00	12.00	12.00	0.02	0.42	3.42	0.30	3.30	0.40	3.40	2.0
Triflumizole	5	12.31	12.30	12.30	0.03	0.50	3.50	0.38	3.38	0.49	3.49	1.9
Triadimenol	5	12.25	12.25	12.25	0.01	0.70	3.70	0.58	3.58	0.68	3.68	1.8
Procymidone	5	12.25	12.25	12.25	0.00	0.85	3.85	0.73	3.73	0.83	3.83	1.7
Captan	5	12.16	12.15	12.16	0.03	1.49	1.49	1.36	1.36	1.47	1.47	5.0
Folpet	5	12.29	12.27	12.28	0.06	1.48	1.48	1.36	1.36	1.47	1.47	4.5
Pacloutrazol	5	12.60	12.60	12.60	0.00	0.80	3.80	0.67	3.67	0.79	3.79	1.9
Flutriafol	5	12.80	12.80	12.80	0.02	1.21	4.21	1.07	4.07	1.19	4.19	1.9
Fludioxonil	5	12.99	12.99	13.00	0.02	1.55	1.55	1.44	1.44	1.55	1.55	4.3
Tricyclazole (Beam)	5	13.00	12.99	13.00	0.04	2.38	2.38	2.26	2.26	2.36	2.36	2.7
Chlorfenapyr	5	13.50	13.49	13.50	0.04	0.76	3.76	0.64	3.64	0.74	3.74	1.8
Myclobutanil	5	13.20	13.20	13.20	0.00	1.11	4.11	0.99	3.99	1.10	4.10	1.6
Lenacil	5	14.55	14.55	14.55	0.01	1.86	1.86	1.73	1.73	1.84	1.84	3.7
Hexazinone (Velpar)	5	14.70	14.70	14.71	0.04	2.01	2.01	1.87	1.87	1.97	1.97	3.7
Captafol	5	15.01	15.00	15.01	0.03	1.80	1.80	1.67	1.67	1.78	1.78	3.9
Iprodione	5	15.40	15.39	15.40	0.03	1.11	4.11	0.98	3.98	1.09	4.09	1.7
Pyriproxyfen	5	16.35	16.34	16.35	0.03	1.38	1.38	1.24	1.24	1.35	1.35	5.6
Fenarimol	5	16.69	16.68	16.68	0.03	1.72	1.72	1.59	1.59	1.69	1.69	4.0
Etofenprox	5	18.50	18.49	18.49	0.02	1.76	1.76	1.61	1.61	1.71	1.71	4.3

Fluridone	5	18.70	18.65	18.72	0.19	0.11	3.11	2.97	2.97	0.06	3.06	2.3
Transfluthrin	6	10.54	10.53	10.54	0.07	0.25	3.25	0.13	3.13	0.23	3.23	2.0
Tefluthrin	6	9.68	9.61	9.67	0.37	0.02	3.02	2.90	2.90	0.01	3.01	2.2
Anthraquinone	6	11.25	11.25	11.25	0.01	1.34	1.34	1.22	1.22	1.33	1.33	5.1
Bioallethrin	6	12.17	12.17	12.18	0.02	0.38	3.38	0.25	3.25	0.36	3.36	2.0
Resmethrin	6	15.15	15.10	15.15	0.19	0.79	3.79	0.67	3.67	0.76	3.76	1.7
Bifenthrin	6	15.58	15.56	15.57	0.04	0.66	3.66	0.54	3.54	0.65	3.65	1.9
Tetramethrin	6	15.60	15.60	15.60	0.01	1.20	4.20	1.07	4.07	1.19	4.19	1.7
Phenothrin (cis & trans)	6	16.12	16.11	16.11	0.03	0.94	3.94	0.82	3.82	0.91	3.91	1.7
Lambda-Cyhalothrin	6	16.55	16.55	16.55	0.01	0.84	3.84	0.71	3.71	0.81	3.81	1.7
trans-Permethrin	6	17.32	17.31	17.31	0.03	1.35	4.35	1.20	4.20	1.29	4.29	1.8
cis-Permethrin	6	17.45	17.45	17.45	0.00	1.36	1.36	1.24	1.24	1.34	1.34	4.8
Cyfluthrin	6	18.03	18.00	17.96	0.22	1.41	1.41	1.28	1.28	1.35	1.35	4.8
Cypermethrin	6	18.29	18.27	18.20	0.27	1.56	1.56	1.43	1.43	1.50	1.50	4.2
Flucythrinate	6	18.35	18.35	18.35	0.00	1.56	1.56	1.42	1.42	1.52	1.52	4.8
tau-Fluvalinate	6	19.23	19.22	19.25	0.07	1.56	1.56	1.42	1.42	1.54	1.54	4.9
Fenvalerate	6	19.05	19.05	19.05	0.01	1.99	1.99	1.86	1.86	1.94	1.94	3.4
2-Phenylphenol	7	6.25	6.26	6.27	0.15	0.71	3.71	0.58	3.58	0.69	3.69	1.9
Bromopropylate	7	15.59	15.57	15.58	0.04	1.02	4.02	0.90	3.90	1.01	4.01	1.7
Chloroprotham	7	7.89	7.87	7.89	0.10	0.48	3.48	0.35	3.35	0.46	3.46	2.0
Metalaxyl	7	10.55	10.55	10.55	0.00	0.90	3.90	0.77	3.77	0.88	3.88	1.8
DCPA methyl ester (Chlorthal-dimethyl)	7	11.31	11.30	11.30	0.04	0.68	3.68	0.56	3.56	0.67	3.67	1.8
Chlozolinate	7	12.05	12.05	12.05	0.00	0.62	3.62	0.50	3.50	0.62	3.62	1.9
Fluazifop-butyl	7	13.65	13.65	13.65	0.01	0.47	3.47	0.35	3.35	0.46	3.46	2.0
Chlorobenzilate	7	13.79	13.78	13.79	0.05	0.83	3.83	0.71	3.71	0.81	3.81	1.7
Carfentrazone ethyl	7	14.40	14.40	14.40	0.00	0.81	3.81	0.69	3.69	0.79	3.79	1.8
2-Decanoylhydrazino-1,4-naphthoquinone	7	18.50	18.50	18.50	0.00	1.24	4.24	1.10	4.10	1.21	4.21	1.7
Methacrifos	8	6.02	6.01	6.02	0.13	0.55	3.55	0.43	3.43	0.54	3.54	2.0
Sulfotepp	8	8.06	8.05	8.06	0.06	0.60	3.60	0.48	3.48	0.58	3.58	1.9
Terbufos	8	9.17	9.16	9.17	0.07	0.48	3.48	0.36	3.36	0.47	3.47	2.0
Tolclofos-methyl	8	10.39	10.40	10.39	0.05	0.99	3.99	0.85	3.85	0.98	3.98	1.9
Fenchlophos (Ronnell)	8	10.60	10.60	10.60	0.02	0.72	3.72	0.59	3.59	0.71	3.71	1.9
Malathion	8	11.10	11.10	11.10	0.00	0.79	3.79	0.66	3.66	0.79	3.79	2.0
Fenthion	8	11.30	11.29	11.30	0.02	1.02	4.02	0.89	3.89	1.00	4.00	1.8
Bromophos methyl	8	11.64	11.62	11.63	0.06	0.85	3.85	0.72	3.72	0.83	3.83	1.8
Bromfenvinphos-methyl	8	12.06	12.05	12.06	0.03	1.15	4.15	1.05	4.05	1.16	4.16	1.5

Chlorfenvinphos	8	12.10	12.10	12.10	0.00	0.85	3.85	0.73	3.73	0.84	3.84	1.8
Tetrachlorvinphos	8		12.56	12.57	0.05			0.90	3.90	1.02	4.02	2.1
Bromfenvinphos	8	12.84	12.80		0.22	0.98	3.98	0.85	3.85			2.3
Profenofos	8	13.08	13.06	13.08	0.06	0.91	3.91	0.80	3.80	0.90	3.90	1.6
Prothiofos	8	13.00	13.00	13.00	0.00	0.75	3.75	0.62	3.62	0.74	3.74	1.9
Sulprofos	8	14.25	14.24	14.25	0.02	1.09	4.09	0.96	3.96	1.07	4.07	1.8
Carbophenothion	8	14.40	14.40	14.40	0.00	1.12	4.12	0.99	3.99	1.09	4.09	1.7
Edifenphos	8	14.46	14.45	14.46	0.05	1.62	1.62	1.52	1.52	1.62	1.62	3.7
Leptophos	8	16.20	16.20	16.20	0.00	1.48	1.48	1.35	1.35	1.44	1.44	4.9
Coumaphos	8	17.40	17.40	17.40	0.00	1.91	1.91	1.78	1.78	1.88	1.88	3.7
Mevinphos	9	5.15	5.15	5.15	0.03	0.67	3.67	0.54	3.54	0.66	3.66	1.9
Phorate	9	8.27	8.26	8.26	0.06	0.60	3.60	0.48	3.48	0.59	3.59	1.9
Fonofos	9	9.24	9.22	9.23	0.06	0.76	3.76	0.64	3.64	0.75	3.75	1.8
Disulfoton	9	9.52	9.51	9.52	0.07	0.64	3.64	0.51	3.51	0.62	3.62	1.9
Methyl parathion	9		10.35					0.89	3.89			
Parathion (Ethyl parathion)	9	11.36	11.35	11.35	0.03	0.79	3.79	0.67	3.67	0.77	3.77	1.8
Triazophos	9	14.22	14.21	14.21	0.04	1.63	1.63	1.51	1.51	1.62	1.62	4.2
Piperonyl butoxide	9	15.08	15.05	15.10	0.17	0.77	3.77	0.65	3.65	0.76	3.76	1.8
Avg					0.08							2.4

Table 8.D. 5 Retention time repeatability of FA mixture

FA Std Mix		Primary Retention Time Reproducibility				Secondary Retention Time Reproducibility						
Compound	Standard	Rep 1 (min)	Rep 2 (min)	Rep 3 (min)	%RSD	Rep 1 (s)	Corrected Rep 1 (s)	Rep 2 (s)	Corrected Rep 2 (s)	Rep 3 (s)	Corrected Rep 3 (s)	%RSD with wraparound correction
1-Fluoronaphthalene	Internal	14.87	14.87	14.87	0.00	0.31	4.31	0.31	4.51	0.82	4.82	5.6
Citral	A	17.87	17.94	17.94	0.22	3.88	3.88	3.88	4.11	0.42	4.42	6.5
3,7-dimethyl-7-hydroxyoctanal	A	18.53	18.60	18.60	0.20	3.94	3.94	3.94	4.18	0.47	4.47	6.3
Cinnamal	A	17.95	17.93	17.93	0.04	1.29	1.29	1.29	1.53	1.83	1.83	17.6
Lilial	A	26.06	26.06	26.06	0.00	0.19	4.19	0.19	4.42	0.72	4.72	6.0
α -amylcinnamaldehyde	A	29.47	29.47	29.47	0.00	0.30	4.30	0.30	4.55	0.84	4.84	5.9
Lylal	A	30.00	30.00	29.99	0.02	0.52	4.52	0.52	4.73	1.05	5.05	5.6
Phenylacetaldehyde	A	10.07	10.07	10.07	0.01	0.61	4.61	0.84	4.84	1.15	5.15	5.5
α -hexyl-cinnamaldehyde	A	32.20	32.20	32.20	0.00	0.21	4.21	0.21	4.45	0.75	4.75	6.0
Benzyl alcohol	B	9.73	9.80	9.76	0.35	0.38	4.38	0.38	4.59	0.89	4.89	5.5
Linalool	B	12.07	12.08	12.08	0.05	3.15	3.15	3.15	3.37	3.67	3.67	7.7
Citronellol	B	16.54	16.54	16.54	0.00	3.32	3.32	3.32	3.55	3.86	3.86	7.6
Geraniol	B	17.33	17.34	17.40	0.22	3.55	3.55	3.55	3.76	0.07	4.07	6.9
4-methoxybenzyl alcohol	B	18.33	18.36	18.33	0.08	1.26	1.26	1.26	1.48	1.81	1.81	18.2
Cinnamyl alcohol	B	19.13	19.14	19.14	0.01	1.03	1.03	1.03	1.27	1.57	1.57	21.0
Eugenol	B	20.67	20.67	20.67	0.00	0.44	4.44	0.44	4.67	0.99	4.99	5.8
Methyl eugenol	B	22.28	22.33	22.27	0.16	0.67	4.67	0.67	4.87	1.22	5.22	5.7
Isoeugenol	B	23.67	23.67	23.67	0.00	0.64	4.64	0.64	4.87	1.18	5.18	5.5
α -amylcinnamic alcohol	B	30.57	30.57	30.57	0.00	0.29	4.29	0.29	4.51	0.81	4.81	5.7
Farnesol	B	30.81	30.82	30.88	0.13	3.60	3.60	3.60	3.82	0.12	4.12	6.8
d-limonene	C	9.60	9.53	9.56	0.35	2.92	2.92	2.92	3.12	3.45	3.45	8.4
Camphor	C	13.53	13.60	13.60	0.28	3.90	3.90	0.15	4.15	0.48	4.48	7.0
4-allylanisole	C	15.52	15.51	15.51	0.00	0.01	4.01	0.01	4.24	0.54	4.54	6.2
Methyl 2-octynoate	C	15.67	15.67	15.67	0.01	0.18	4.18	0.18	4.25	0.54	4.54	4.4
Safrole	C	18.60	18.58	18.58	0.05	0.29	4.29	0.29	4.54	0.85	4.85	6.1
Methyl 2-nonynoate	C	18.93	19.07	19.00	0.35	3.94	3.94	3.94	4.14	0.47	4.47	6.3
Coumarin	C	23.09	23.07	23.09	0.05	2.62	2.62	2.62	2.90	3.17	3.17	9.5
iso- α -methylionone	C	24.40	24.40	24.47	0.16	3.60	3.60	3.60	3.84	0.14	4.14	7.1
Benzyl benzoate	C	32.68	32.68	32.67	0.02	1.32	1.32	1.32	1.54	1.86	1.86	17.5
Benzyl salicylate	C	35.27	35.29	35.29	0.04	1.18	1.18	1.18	1.39	1.69	1.69	18.0
Benzyl cinnamate	C	40.74	40.74	40.74	0.00	1.56	1.56	1.56	1.80	2.09	2.09	14.7

1,8-Cineole	C	9.62	9.62	9.60	0.10	3.02	3.02	3.02	3.25	3.53	3.53	7.9
AVG					0.09							8.6

Table 8.D. 6 Peak area reproducibility MRP mixture

MRP Std Mix		Peak Area Reproducibility			
Compound	Standard	Rep 1	Rep 2	Rep 3	%RSD
Phosmet	1	2058370	2138520	1644650	13.6
Pyridafenthion	1	181092	175999	162169	5.7
EPN	1	2063360	2191170	1561040	17.2
Azinphos methyl	1	2024370	2072370	1551180	15.3
Pyrazophos	1	150560	173563	119569	18.3
Pyraclufos	1	1046730	1143210	793750	18.1
Diazinone	1	2905450	3954710	2750290	20.5
Isazophos	1	163000	219267	140858	23.2
Chloropyrifos-methyl	1	3551770	4795480	4005700	15.3
Pirimiphos methyl	1	93399	131979	81019	26.0
Fenitrothion	1	2282940	3147380	2048270	23.2
Chlorpyrifos	1	4491250	4350560	3610250	11.4
Pirimiphos ethyl	1	147392	178254	117323	20.6
Quinalphos	1	2458840	3361470	2059710	25.4
Phosalone	1	2546810	3273640	2213180	20.2
Azinphos ethyl	1	273752	279339	202628	17.0
Chloroneb	2	8197110	10013200	7288660	16.3
cis-Chlordane	2	8928860	9920510	11654800	13.6
trans-Chlordane	2			3933380	
Chlorfenson (Ovex)	2	4660370	6414300	4288520	22.2
Chlorbenside	2	4729390	6456400	4096910	24.0
D-BHC	2	10999200	9700080	15680800	25.9
Hexachlorobenzene	2	9037040	9758340	8302550	8.1
gamma-BHC (Lindane)	2	11348000	13996700	10134800	16.7
Alpha-BHC	2	10330500	12157100	9176360	14.2
Heptachlor	2	9411410	13020100	9113530	20.7
Pentachlorobenzene	2	8773080	10149100	8167130	11.2
Pentachloroanisole	2	6699630	7741870	6055790	12.5
Pentachlorothioanisole	2	5430980	6693040	5039940	15.1
Aldrin	2	7786830	10975500	7118460	23.9
4,4'-Dichlorobenzophenone	2	3336640	4303820	3029700	18.7
Fenson	2	3612230	4281730	3071250	16.6

Isodrin	2	8381210	9843880	7830250	12.0
Heptachlor Epoxide	2	6573520	7762530	6914060	8.6
4,4'-DDE	2	5090020	6625620	4895160	17.1
2,4'-DDE	2	6184840	9005750	6817290	20.2
cis-Nonachlor	2	167826	230555	142794	25.1
trans-Nonachlor	2	5696130	5862050	4989430	8.4
Dieldrin	2	853783	1051035	764415	16.5
2,4'-DDD	2	5744830	8859590	4892410	32.1
Endrin	2	6329500	8593070	6574390	17.3
Ethylan (Perthane)	2	2614710	3143730	2484060	12.7
B-Endosulfan (Endosulfan II)	2	4582590	5817660	4023970	19.1
2,4'-DDT	2	7808060	6913130	10734500	23.6
Endrin Aldehyde	2	3388740	3391810	2574220	15.1
2,4'-Methoxychlor	2	3483320	4307480	2825080	21.0
4,4'-Methoxychlor olefin	2	3900870	3617290	3364440	7.4
Endosulfan ether	2	7570440	8973370	6381250	17.0
Endosulfan sulfate	2	3269570	3674080	2763500	14.1
4,4'-DDT	2	4389800	4677350	3816470	10.2
Endrin ketone	2	4759290	5808870	3815070	20.8
Tetradifon	2	2443340	1618330	2054610	20.2
Mirex	2	6346650	7318230	5828470	11.6
2,6-Dichlorobenzonitrile (Dichlobenil)	3	9840140	9082490	8003280	10.3
Biphenyl	3	10855300	11506800	8694120	14.2
3,4-Dichloroaniline	3	3716100	4578470	3430260	15.3
THPI (Tetrahydrophthalimide)	3	2479020	3478420	2373730	22.0
Tetrachloronitrobenzene (Tecnazene)	3	3638390	4539220	3329700	16.4
2,3,5,6-Tetrachloroaniline	3	530027	583414	447128	13.2
Pentachloroaniline	3	5469880	4096690	4965380	14.3
Pendimethalin	3	1719350	2258340	2562280	19.6
Diphenylamine	3	970713	1185930	799737	19.6
Pentachloronitrobenzene (Quintozene)	3	6510570	8040070	6166230	14.4
Pentachlorobenzonitrile	3	518201	595275		9.8
Chlorothalonil	3	4328040	2715800	3790450	22.7
Ethalfuralin	3	218951	301335	460424	37.5
Trifluralin	3	136521	185748	121724	22.6

Benfluralin	3	2570500	3335620	2254880	20.4
Profluralin	3	2245410	3175030	2012890	24.8
Fluchloralin	3	2372210	3382190	2178200	24.4
Prodiamine	3	1975990	2576040	1777730	19.7
Dichlofluanid	3	4920370	6330790	4528950	18.0
Isopropalin	3	2461920	3300780	2131540	22.9
Tolylfluanid	3	3940810	4507000	3238190	16.3
Oxyfluorfen	3	1269800	1488320	1101060	15.1
Nitralin	3	1237450	1349120	932497	18.4
Pebulate	4	2083130	2743090	2050190	17.1
N-(2,4-Dimethylphenyl)formamide	4	1514700	2326620	1572900	25.1
Propachlor	4	2391210	3577630	2417800	24.2
Cycloate	4	2868330	3837610	2794150	18.4
Diallate (cis & trans)	4	2174300	3094180	1977070	24.7
Diallate (cis & trans)	4	95675	137686	80910	28.1
Triallate	4	3815850	4975150	3539730	18.5
Propyzamide	4	2628340	3571700	2524650	19.8
Dimethachlor	4	2132540	2896130	1675880	27.6
Propanil	4	326135	454091	255521	29.2
Acetochlor	4	2069430	2780470	2324410	15.1
Alachlor	4	2065420	2762550	1856760	21.3
Metolachlor	4	528286	733204	451354	25.5
Linuron	4	1229200	1399960	1072260	13.3
Diphenamid	4	2879940	3335670	2631850	12.1
Metazachlor	4	439372	517728	380366	15.5
Flutolanil	4	1561920	1841240	1270330	18.3
Pretilalchlor	4	1885420	2025980	1615240	11.3
Oxadiazon	4	1704910	2145300	1585170	16.3
Norflurazon	4	98623	237812	164955	41.7
Methoxychlor	4	622046	781193	480008	24.0
Fenpropathrin	4	1768370	1888210	1302360	18.7
Tebufenpyrad	4	1687570	1835990	1132180	23.9
Fluquinconazole	4	107882	169480	108434	27.5
Prochloraz	4	62746	68075	44091	21.6
Pyridaben	4	486360	537206	409763	13.4
Etridiazole	5	3497630	4285180	3204320	15.3

Atrazine	5	206134	280484	177308	24.1
Terbuthylazine	5	274390	317526	263653	10.0
Pyrimethanil	5	2867030	3893000	2707180	20.4
Terbacil	5	1588760	2302070	1559580	23.1
Vinclozoline	5	3069100	4456920	2879690	24.8
Triadimefon	5	82522	107380	68207	23.0
Tebuconazole	5	1392080	1514000	1140570	14.1
Propargite	5	2031410	2024870	1583980	13.6
MGK-264	5	83965	100620	69901	18.1
Cyprodinil	5	1782000	1966450	1613140	9.9
Penconazole	5	132429	268493	125301	46.0
Fipronil	5	1162740	1531910	1070960	19.4
Triflumizole	5	817981	985343	662026	19.7
Triadimenol	5	288987	327989	222373	19.1
Procymidone	5	696559	1011971	655322	24.8
Captan	5	4302760	5398090	3552650	21.0
Folpet	5	3942490	4882590	3286380	19.9
Pacllobutrazol	5	1185110	971264	888707	15.1
Flutriafol	5	1678960	1821270	1405690	12.9
Fludioxonil	5	216391	221322	163844	15.9
Tricyclazole (Beam)	5	1103820	1191260	849625	16.9
Chlorfenapyr	5	1581330	1758490	1269720	16.1
Myclobutanil	5	175353	214748	67176	50.1
Lenacil	5	575469	667115	442833	20.1
Hexazinone (Velpar)	5	232287	193398	201759	9.8
Captafol	5	2528030	2756690	2165060	12.0
Iprodione	5	779680	886438	606423	18.7
Pyriproxyfen	5	1881650	1981130	1548160	12.6
Fenarimol	5	1957960	2037610	1454290	17.4
Etofenprox	5	499273	441920	357771	16.4
Fluridone	5	246282	385010	214865	32.1
Transfluthrin	6	2883560	3870180	2519350	22.6
Tefluthrin	6	2978880	4164260	2720580	23.4
Anthraquinone	6	2920230	3802950	2726600	18.2
Bioallethrin	6	1640460	1860540	1364700	15.3
Resmethrin	6	207696	222372	162650	15.8
Bifenthrin	6	2015280	2195300	1547580	17.4

Tetramethrin	6	1746140	1618330	1366370	12.3
Phenothrin (cis & trans)	6	1476550	1602040	1191600	14.8
Lambda-Cyhalothrin	6	1575470	1675360	1271930	13.9
trans-Permethrin	6	327267	365495	264090	16.1
cis-Permethrin	6	680991	360080	490516	31.6
Cyfluthrin	6	37372	31021	18694	32.7
Cypermethrin	6	42061	42697	44920	3.5
Flucythrinate	6	79448	81353	56044	19.5
tau-Fluvalinate	6	129883	265468	169046	37.1
Fenvalerate	6	1099960	1094510	791656	17.7
2-Phenylphenol	7	4005000	5148740	3893930	16.0
Bromopropylate	7	1540750	1661730	1193890	16.6
Chloroprotham	7	2588280	3528230	2323870	22.5
Metalaxyl	7	103264	113296	87493	12.8
DCPA methyl ester (Chlorthal-dimethyl)	7	2825110	3856960	2763890	19.5
Chlozolate	7	966720	631872	647918	25.2
Fluazifop-butyl	7	1196980	1437310	1023600	17.0
Chlorobenzilate	7	2380900	2803340	1981660	17.2
Carfentrazone ethyl	7	945594	1128000	776586	18.5
2-Decanoylhydrazino-1,4-naphthoquinone	7	826685	831914	565149	20.6
Methacrifos	8	3343640	4785210	3178080	23.5
Sulfotepp	8	112602	158290	104660	23.1
Terbufos	8	3060180	3577270	2650240	15.0
Tolclofos-methyl	8	7549520	7503260	6999720	4.1
Fenchlofos (Ronnel)	8	352117	504567	347682	22.3
Malathion	8	2704490	3731360	2440730	23.0
Fenthion	8	3790080	4581830	3529130	13.8
Bromophos methyl	8	2830770	3660040	2487900	20.1
Bromfenvinphos-methyl	8	2658750	3031390	2217540	15.5
Chlorfenvinphos	8	54425	86599	81055	23.2
Tetrachlorvinphos	8		125000	85378	26.6
Bromfenvinphos	8	111273	145987		19.1
Profenofos	8	1342470	1640900	1027900	22.9
Prothiofos	8	2609450	3059320	2339410	13.6
Sulprofos	8	2232680	2421270	1828110	14.0
Carbophenothion	8	275649	312694	219364	17.5

Edifenphos	8	502808	750632	570705	21.1
Leptophos	8	1729070	1309020	1224810	19.0
Coumaphos	8	38602	144651	102793	56.0
Mevinphos	9	1085390	1494790	1067930	19.9
Phorate	9	3874930	5411380	3454640	24.3
Fonofos	9	6816920	5489800	4552160	20.2
Disulfoton	9	799852	1146104	668843	28.3
Methyl parathion	9		2784420		
Parathion (Ethyl parathion)	9	2560020	2808600	2037540	15.9
Triazophos	9	1532290	1841190	1207570	20.7
Piperonyl butoxide	9	358664	402097	272488	19.2
Avg					19.2

Table 8.D. 7 Peak area reproducibility of FA mixture

FA Std Mix		Peak Area Reproducibility			
Compound	Standard	Rep 1	Rep 2	Rep 3	%RSD
1-Fluoronaphthalene	Internal	672899	744359	647864	7.3
Citral	A	421508	463131	398166	7.7
3,7-dimethyl-7-hydroxyoctanal	A	495984	573544	505840	8.0
Cinnamal	A	1382949	1328220	1376790	2.2
Lilial	A	620371	860721	739473	16.2
α -amylcinnamaldehyde	A	867819	1058829	870331	11.8
Lyrar	A	305740	330073	316372	3.8
Phenylacetaldehyde	A	1421370	1577520	1299370	9.7
α -hexyl-cinnamaldehyde	A	783093	925365	797334	9.4
Benzyl alcohol	B	1720863	1826362	1543547	8.4
Linalool	B	1253990	1168080	1161383	4.3
Citronellol	B	565314	677040	558695	11.1
Geraniol	B	365319	445130	405239	9.8
4-methoxybenzyl alcohol	B	751874	911339	769422	10.8
Cinnamyl alcohol	B	938852	1053800	920698	7.4
Eugenol	B	887863	1000090	857337	8.2
Methyl eugenol	B	1468405	1726295	1460952	9.7
Isoeugenol	B	266668	304296	313882	8.5
α -amylcinnamic alcohol	B	477742	599999	370544	23.8
Farnesol	B	163570	185761	165267	7.2
d-limonene	C	973765	980419	873721	6.3
Camphor	C	68554	42993	55189	23.0
4-allylanisole	C	1394740	1158320	1263350	9.3
Methyl 2-octynoate	C	1322800	1474890	1216434	9.7
Safrole	C	1559058	2692364	2324016	26.4
Methyl 2-nonynoate	C	730144	978689	810911	15.1
Coumarin	C	734208	576597	1413969	49.0
iso- α -methylionone	C	1220620	1405230	1151330	10.4
Benzyl benzoate	C	813425	694335	918557	13.9
Benzyl salicylate	C	705613	818339	745449	7.6
Benzyl cinnamate	C	660714	736039	670153	6.0

1,8-Cineole	C	1863750	1984250	1653730	9.1
AVG					11.5

Table 8.D. 8 Summary of evaluation criteria for both MRP and FA mixtures

Evaluation Criteria	MRP Mixture	FA Mixture
1t_R %RSD	0.08%	0.09%
2t_R %RSD	2.4%	8.6%
Avg. difference between maximum and minimum 2t_r (msec)	129	528
Peak Area %RSD	19.2%	11.5%
$^2w_{1/2}$ (msec)	104	196
$^2w_{1/2}$ %RSD	3.9%	2.5%
Second dimension Peak Capacity	17	12

Appendix E

Chapter 9 Supplementary data

Evaluation of the operational capabilities of a solid-state thermal modulator in comprehensive two-dimensional gas chromatography-time-of-flight mass spectrometry (GC×GC -TOFMS)

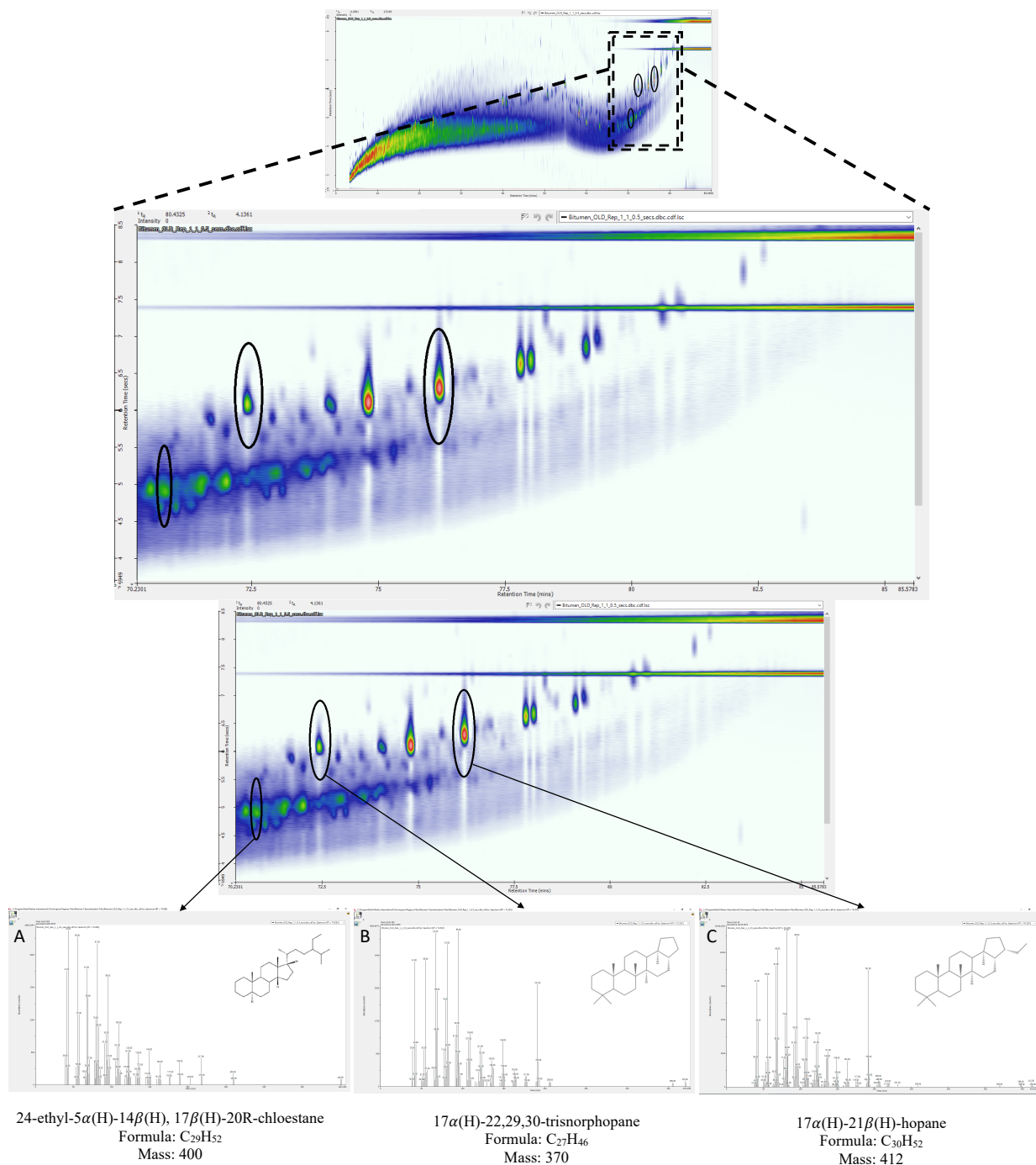


Figure 9.E. 1 Tentative identification of three characteristic biomarkers in the biomarker region of the cyclohexane extract. The compounds (A) 24-ethyl-5 α (H)-14 β (H), 17 β (H)-20R-cholestane (C₂₉ $\alpha\beta\beta$ -20), (B) 17 α (H)-22,29,30-trisnorhopane (T_m) and (C) 17 α (H)-21 β (H)-hopane (H30) were identified by EIC and molecular ion peak.